

Surfactant-Based Separations

Surfactant-Based Separations

Science and Technology

John F. Scamehorn, EDITOR
University of Oklahoma

Jeffrey H. Harwell, EDITOR
University of Oklahoma



American Chemical Society, Washington, DC

American Chemical Society
Library

1155 16th St., N.W.

In Surfactant-Based Separations, Scamehorn, J., et al.;
ACS Symposium Series; American Chemical Society: Washington, DC, 1999.

Surfactant-based separations
: science and technology



Library of Congress Cataloging-in-Publication Data

Surfactant-based separations : science and technology / John F. Scamehorn, editor, Jeffrey H. Harwell, editor.

p. cm.—(ACS Symposium series. ISSN 0097-6156 : 740)

Includes bibliographical references and index.

ISBN 0-8412-3618-6

1. Separation (Technology) Congresses. 2. Surface active agents Congresses.

I. Scamehorn, John F., 1953- . II. Harwell, Jeffrey H., 1952- . III. Series.

TP156.S45S876 1999
660'.2842—dc21

99-33716
CIP

The paper used in this publication meets the minimum requirements of American National Standard for Information Sciences—Permanence of Paper for Printer Library Materials, ANSI Z39.48-94 1984.

Copyright © 2000 American Chemical Society

Distributed by Oxford University Press

All Rights Reserved. Reprographic copying beyond that permitted by Sections 107 or 108 of the U.S. Copyright Act is allowed for internal use only, provided that a per-chapter fee of \$20.00 plus \$0.50 per page is paid to the Copyright Clearance Center, Inc., 222 Rosewood Drive, Danvers, MA 01923, USA. Replication or reproduction for sale of pages in this book is permitted only under license from ACS. Direct these and other permissions requests to ACS Copyright Office, Publications Division, 1155 16th Street, N.W., Washington, DC 20036.

The citation of trade names and/or names of manufacturers in this publication is not to be construed as an endorsement or as approval by ACS of the commercial products or services referenced herein; nor should the mere reference herein to any drawing, specification, chemical process, or other data be regarded as a license or as a conveyance of any right or permission to the holder, reader, or any other person or corporation, to manufacture, reproduce, use, or sell any patented invention or copyrighted work that may in any way be related thereto. Registered names, trademarks, etc., used in this publication, even without specific indication thereof, are not to be considered unprotected by law.

PRINTED IN THE UNITED STATES OF AMERICA

American Chemical Society
Library

1155 16th St., N.W.

Washington, D.C. 20036

Advisory Board

ACS Symposium Series

Mary E. Castellion
ChemEdit Company

Arthur B. Ellis
University of Wisconsin at Madison

Jeffrey S. Gaffney
Argonne National Laboratory

Gunda I. Georg
University of Kansas

Lawrence P. Klemann
Nabisco Foods Group

Richard N. Loepky
University of Missouri

Cynthia A. Maryanoff
R. W. Johnson Pharmaceutical
Research Institute

Roger A. Minear
University of Illinois
at Urbana-Champaign

Omkaram Nalamasu
AT&T Bell Laboratories

Kinam Park
Purdue University

Katherine R. Porter
Duke University

Douglas A. Smith
The DAS Group, Inc.

Martin R. Tant
Eastman Chemical Co.

Michael D. Taylor
Parke-Davis Pharmaceutical
Research

Leroy B. Townsend
University of Michigan

William C. Walker
DuPont Company

Foreword

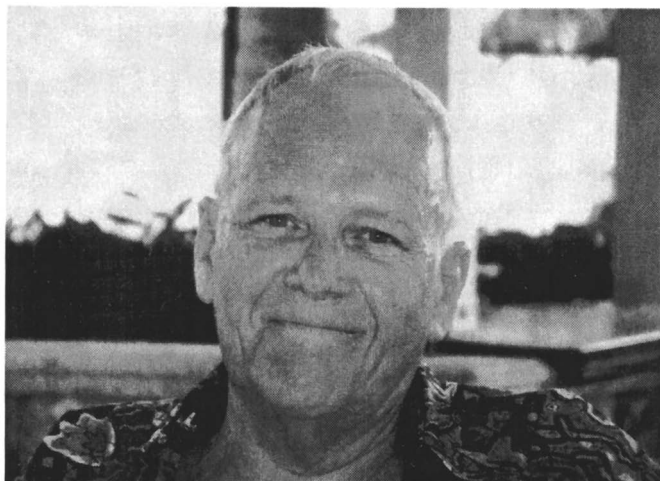
THE ACS SYMPOSIUM SERIES was first published in 1974 to provide a mechanism for publishing symposia quickly in book form. The purpose of the series is to publish timely, comprehensive books developed from ACS sponsored symposia based on current scientific research. Occasionally, books are developed from symposia sponsored by other organizations when the topic is of keen interest to the chemistry audience.

Before agreeing to publish a book, the proposed table of contents is reviewed for appropriate and comprehensive coverage and for interest to the audience. Some papers may be excluded in order to better focus the book; others may be added to provide comprehensiveness. When appropriate, overview or introductory chapters are added. Drafts of chapters are peer-reviewed prior to final acceptance or rejection, and manuscripts are prepared in camera-ready format.

As a rule, only original research papers and original review papers are included in the volumes. Verbatim reproductions of previously published papers are not accepted.

ACS BOOKS DEPARTMENT

Dedication



**To the Memory of
William H. Wade
(1930–1998)
Colleague, Mentor, and Friend**

Preface

This volume is based on the symposium “Surfactant-Based Separations” at the National American Chemical Society (ACS) meeting in Dallas, Texas in March–April 1998. This two and one-half day symposium was sponsored by the Separation Science and Technology Subdivision of the ACS Division of Industrial and Engineering Chemistry, Inc.

Surfactant-based separation processes represent some of the most promising new separation techniques to emerge over the past few decades with potential for breakthrough improvements in industrial and analytical separations. Surfactant-based separations have the general advantages of using a separating agent, which can be green (biodegradable and nontoxic), often having low energy requirements, and being capable of treating easily degraded materials such as biochemicals. The unique tendency for surfactants to adsorb at interfaces and to form aggregates in solution lead to separation methods that have unifying basic principles. The chapters in this book are classified into four major categories: surfactant-enhanced soil remediation; membrane-based separations; adsorption and flotation separations; and extraction and deinking processes. Physical phenomena that are exploited include solubilization into micelles and other surfactant aggregates, surfactant adsorption at solid–liquid or vapor–liquid surfaces, microemulsion formation, emulsion and dispersion formation, foaming behavior, wetting, surfactant precipitation, and liquid crystal formation. Applications include remediation of contaminated soil (in-situ or ex-situ), wastewater and groundwater cleanup, bioseparations, removal of ink to permit recycling of plastic or paper, analytical chemistry, and ore flotation.

The only other book (*1*) dedicated to this topic was published in 1989. The use of surfactants to induce separation processes has been one of the most active areas of research in separation science in the decade since that volume appeared. Techniques such as paper recycling after surfactant-induced deinking has increased dramatically in commercial importance. Methods like micellar-enhanced ultrafiltration have reached the point of field demonstration and even early commercial utilization. Traditional techniques such as ore flotation continue to be widely used. Finally, many new processes have been proposed and are being developed.

Financial support for this symposium was supplied by the Asahi Glass Foundation, the Petroleum Research Fund of the ACS, and the Separation Science and Technology Subdivision of the ACS Division of Industrial and Engineering Chemistry, Inc. We thank Denae Athay for her diligent attention to detail in handling all the administrative aspects of putting the volume together

and Rick Wheeler for drafting the cover art. We also acknowledge Kelly Dennis and Anne Wilson of ACS Books for their help and advice in editing this volume. Professor Scamehorn holds the Asahi Glass Chair in Chemical Engineering and Professor Harwell holds the Conoco/DuPont Professorship in Chemical Engineering at the University of Oklahoma and we thank the organizations that endowed these positions for their financial support.

1. *Surfactant-Based Separation Processes*; Scamehorn, J. F.; Harwell, J. H., Eds.; Marcel Dekker: New York; 1989.

JOHN F. SCAMEHORN
Institute of Applied Surfactant Research
University of Oklahoma
100 East Boyd Street, T-335
Norman, OK 73019

JEFFREY H. HARWELL
School of Chemical Engineering
University of Oklahoma
Norman, OK 73019

Chapter 1

Current Trends and Future Developments in Surfactant-Based Separations

John F. Scamehorn ¹ and Jeffrey H. Harwell ²

¹ Institute for Applied Surfactant Research and ² School of Chemical Engineering,
University of Oklahoma, Norman, OK 73019

Surfactant-based separation processes represent some of the most promising new separation techniques to emerge over the past few decades with potential for breakthrough improvements in industrial and analytical separations. The unique tendency for surfactants to adsorb at interfaces and to form aggregates in solution lead to separation methods that have unifying basic principles. Some major classes of surfactant-based separations discussed in this chapter include those based on ultrafiltration, extraction, flotation, surfactant adsorption, fractionation, surfactant precipitation, and microemulsion formation. Applications include remediation of contaminated soil (in-situ or ex-situ), wastewater and groundwater clean-up, bioseparations, removal of ink to permit recycling of plastic or paper, analytical chemistry, and ore flotation. This chapter gives a brief overview of some of the most exciting directions where developments in surfactant-based separations are heading.

Surfactant-based separations have the general advantages of using a separating agent which can be green (biodegradable and nontoxic), of often having low energy requirements, and of being capable of treating easily degraded materials such as biochemicals. This has been one of the most active areas of research in separation science over the past decade. Techniques such as paper recycling after surfactant-induced deinking has increased dramatically in commercial importance; methods like micellar-enhanced ultrafiltration have reached the point of field demonstration and even early commercial utilization; traditional techniques such as ore flotation continue to be widely used; and new processes have been proposed and are being developed.

The purpose of this chapter is to give the authors' perspective on the status of progress in the field of surfactant-based separations. This is not designed to be a review of the field, but the focus is on what we perceive to be exciting directions of research in the area, particularly as illustrated by chapters in this volume. References are only representative of

the literature; a thorough literature survey is not attempted, nor is it required--it is not necessary to reproduce the many hundreds of references given in the chapters in this book.

Surfactant-Enhanced Ultrafiltration

The first surfactant-enhanced ultrafiltration process studied was micellar-enhanced ultrafiltration or MEUF (1-4, Chapters 7-12). The basic concept is that organic solutes and/or multivalent ions will solubilize and counterions bind, respectively, to micelles. The micelles are then ultrafiltered from solution. There are some major technological limitations to the technology or opportunities to improve the separation: leakage of surfactant monomer through the membrane into the permeate stream; the need to separate surfactant from solutes in the retentate or concentrated stream from the process; the need for selectivity to specifically remove targeted solutes; the possibilities of using surfactant aggregates in solution other than micelles to sequester solutes and be ultrafiltered; and a need to develop scale-up and design capabilities.

Monomer Leakage: Surfactant monomer passes through the membrane into the permeate stream. The resulting surfactant concentration can be high enough to be environmentally unacceptable (even though the surfactant is biodegradable) or economically prohibitive. Several approaches are being taken by researchers to solve this problem. Polymeric surfactants (polymers with hydrophobic regions and hydrophilic regions) can form micelles with hydrophobic microdomains which solubilize organic solutes (5), yet the polymer is large enough to be ultrafiltered from solution, eliminating the monomer leakage problem. Chapters 7 and 8 in this volume report studies using nonionic triblock polymers to remove naphthalene and p-cresol from water. One problem is that nonionic surfactants generally exhibit low flux (or low gel points) compared to ionic surfactants, presumably because the micelles lack the electrostatic repulsion from each other in the gel layer next to the membrane (6). Low flux is unattractive because it increases the capital investment in membrane modules, reducing the economic viability. For example, work has been done with polyethoxylated nonionic surfactants with moderate molecular weight with low critical micelle concentration (CMC) and the expected low monomer leakage is observed (7), although the low flux makes this alternative unattractive. Future advances may be made with the use of polymeric surfactants which are charged, for example, polysoaps (8).

If only multivalent ions are to be removed from water (e.g., CrO_4^{2-} , Cu^{2+}), counterion binding of solute to micelle is the operative phenomena and a hydrophobic domain is not necessary. In this case, a polyelectrolyte of opposite charge to the target ion can be used to bind the ion, then ultrafiltered from solution if the molecular weight is high enough. This process is known as polyelectrolyte-enhanced ultrafiltration (9,10) and solves the surfactant leakage problem.

Polymer/surfactant complexes can solubilize organic solutes similar to micelles, but the surfactant monomer concentration in equilibrium with the complexes (sometimes called micelles on a string) can be substantially below the CMC, leading to about an order of magnitude reduction in monomer leakage in MEUF compared to micelles alone (11,12). However, flux is also reduced.

Finally, another approach to this problem is to remove the surfactant from the permeate stream in a downstream process. A polishing ultrafiltration step with a very small pore size membrane (requiring the use of a moderately large molecular weight surfactant) (6) or foam fractionation treatment of the water (13), or sequestering of the surfactant by an oppositely charged polyelectrolyte (12) are three options for downstream treatment.

Surfactant Regeneration: It is necessary to recover and reuse the surfactant from MEUF, as in many surfactant-based separations, for economical operation. If the solute is valuable, as in bioseparations, this could also make solute/surfactant separation necessary.

In (14) and Chapters 7 and 8 in this volume, the advantage of the block copolymer surfactants in MEUF is discussed. The surfactant exists as micelles or multimer with excellent solubilization under some conditions, but as extended monomers without substantial hydrophobic domains at other conditions, such as lower temperature. So, lowering the temperature results in desolubilization of the organics in the concentrated retentate. This can then permit separation of solute from surfactant; for example, in Chapter 7, a second ultrafiltration step is proposed after cooling the retentate to effect this regeneration. The lack of surfactant monomer leakage with these surfactants has already been discussed, as well as the disadvantage of relatively low fluxes. In general, the use of polymeric surfactants seems to be an extremely promising approach to solve some limitations of MEUF.

As has been reviewed elsewhere (15), there are other regeneration methods, often highly system specific. For removal of volatile organic solutes, the solute can be stripped (vacuum, air, steam, pervaporation) from the retentate - see Chapter 5 and (16). For ionic surfactants, the surfactant can be precipitated from the retentate by addition of a counterion (17) or reduction in temperature (18) for recycle. If the solute is an ion like chromate, a counterion to this target ion can be added to precipitate it from solution, leaving the surfactant in solution to be reused (19). Use of an organic solvent to extract the solute from the retentate is another option as discussed in Chapter 6, although the extractant needs to be chosen so that it does not solubilize highly in micelles itself and so that the surfactant does not extract significantly into the solvent. To date, the toughest problem is when the solute is a nonionic organic solute of low volatility, with surfactant precipitation and liquid-liquid extraction showing the most promise for these systems.

Selectivity in Solute Removal: Traditional MEUF relies on hydrophobic bonding and surfactant head group/solute interactions to solubilize organics and on electrostatic forces to bind counterions. As a result, selective removal of organics of similar structure or of ions of the same charge is not efficient. In order to introduce selectivity in MEUF, a ligand can be added to the system which selectively complexes the solute of interest and is designed to solubilize well into micelles. For metal ion removal, Chapter 10 and (20) discusses the use of ligands to specifically complex multivalent ions and solubilize into micelles in a process sometimes referred as ligand-modified micellar-enhanced ultrafiltration. For example, divalent cations copper or nickel can be removed very

efficiently compared to divalent cation calcium. Ligands can also be electrostatically attached to polyelectrolytes to give selective removal without surfactant monomer leakage (21,22). Recently, it has been shown that commercially available ligands designed for solvent extraction of metals can be very effective in this separation technique (23), the greatly reduced cost of these accessible chemicals making the process more feasible.

In an exciting new development, in Chapter 9, the use of enantioselective micelles composed of optically active surfactants have been shown to be able to selectively remove enantiomers in MEUF. This has great potential for use in biotechnology. This also points out the potential use of MEUF in process applications, in addition to the substantial work on application to environmental problems focused on over the years. Chapter 22 discusses another surfactant-based separation (extraction into reverse micelles) not involving membranes, which also has great potential in bioseparations (24).

Use of Surfactant Aggregates other than Micelles: Recent work has expanded MEUF to utilize other solution aggregates than micelles to sequester solutes and be ultrafiltered from solution. Chapter 13 discusses the use of vesicles to solubilize organic solutes in vesicle-enhanced ultrafiltration where the vesicle can be more effective at solubilization than micelles. The nonequilibrium nature of the vesicles makes the preparation and age of the solutions critical, unlike micellar solutions. The more structured nature of the hydrophobic region of the vesicle may improve selectivity.

Chapter 10 reviews the use of various aggregates in surfactant-based separations, including micelles, microemulsions, polymerized micelles, and vesicles. Polymerized micelles use polymerizable surfactant monomer to freeze the micelle structure and are different than micelles formed from polymeric surfactants. This research may solve the monomer leakage problem without lowering flux. Chapter 12 shows that flux in MEUF can be very poor when liquid crystals, instead of micelles, are present in MEUF. Since the vast majority of work on surfactant aggregates being ultrafiltered has used micelles, the potential for these other aggregated structures being even more useful in some applications is great and will probably prove a fruitful venue for extension of research in the field over the next decade or two.

Ultrafiltration Device Design Considerations: Typical industrial ultrafiltration units would be spiral wound, hollow fiber, or plate and frame. Many laboratory studies have involved a stirred cell because it is convenient to run and requires a relatively low solution volume. The stirred cell is run on a batch or semi-batch basis, whereas industrial units are often run in a steady state configuration. Chapter 11 shows that the rejection and flux on a unit area basis are quite similar between the spiral wound units and the stirred cells, justifying the use of the latter to generate data, which can be used for large scale designs. This robustness is present even though the geometry and dynamics (steady state vs. batch) of the systems are quite different.

Chapter 12 shows that one can observe good rejection of micelles using pore sizes larger than that of the micelles if the ultrafiltration is permitted to run for a long enough time to allow a gel layer of surfactant to build up next to the membrane. The gel layer acts as the filtering agent at this point. This provides opportunities for higher flux in MEUF.

As MEUF approaches wide-scale industrial usage, design techniques will be needed to incorporate these units into plants. Chapter 9 and (6,23,25) show some techniques for staging calculations of MEUF since often more than one stage is required to attain a required degree of separation or because concentration and regeneration ultrafiltration stages need to be integrated in one overall process.

Surfactant-Enhanced Soil and Aquifer Remediation

The most exciting, new surfactant-based separation of the last decade has been the rapidly developing use of surfactants for environmental remediation. This application is also further driving the development of new surfactant regeneration and recovery processes, as the re-use of the surfactant is critical to the economics of surfactant-enhanced remediation processes.

The use of surfactants in environmental remediation has been driven by the problem of contaminated soils and ground water aquifers. Solvents or fuels through spills, leaks, or improper disposal of used solvents can contaminate aquifers. Fuel leaks are frequent around older gasoline, diesel and aircraft fuel storage and distribution facilities. Solvents such as toluene may also be released from leaking storage tanks or transfer lines. Hydrocarbon fuels or solvents float on the water in the aquifer because they are less dense than water. Dissolution of the hydrocarbon in the ground water contaminates the aquifer. Since ground water flows "downhill" in the subsurface, the same way water in rivers and creeks flows downhill, contaminated ground water will spread "down gradient" from the site of the original release. Wells and even streams and lakes miles from the original contamination may become contaminated as the contaminated ground water moves down gradient from the source of the contamination. It is critical, therefore, that the spread of the contaminant be stopped, either by hydraulic control of the gradient or by removal of the contaminant liquid. The difficulty of removing the hydrocarbon liquid (called a LNAPL, or Light Non-Aqueous Phase Liquid) from the subsurface is greater than it might first appear. Even if a well is used to pump the LNAPL directly to the surface, droplets of the LNAPL become trapped in the pore structure of the solid matrix of the aquifer by capillary forces. These trapped droplets become a long-term source of slowly dissolving contamination.

If the LNAPL spill is close to the surface, as in the case of a shallow aquifer, it is often possible to dig down to the aquifer and directly remove the contaminated soil. Even in this case, however, the seasonal rise and fall of the aquifer level may distribute the contamination below the water table. For deeper aquifers (30 to 40 feet or more), excavation becomes prohibitively expensive.

While LNAPL contaminated aquifers are a major problem, technologies like in situ air sparging or soil-vapor extraction can address the residual contamination, at least to a large extent. For the case of chlorinated solvents, however, the situation is much worse. Common solvents like methylene chloride, trichloroethylene and dichlorobenzene are more dense than water. When a release of such dense non-aqueous phase liquids (DNAPLS) occurs, the solvent does not pool at the water table—it penetrates the water table and continues to migrate downward. Downward migration stops only when the volume of the spill has been taken-up by the pore structure of the soil and aquifer medium, or when the solvent reaches the confining layer of the aquifer—generally a shale or clay layer. The DNAPL is trapped below the water table. This greatly increases the difficulty of removing it from the aquifer. Excavation now requires pumping down the aquifer, which greatly increases the expense even when it is possible. The limited solubility of the solvent in water greatly increases the mass transfer resistance to removing the solvent as a vapor. Using air or steam to “strip” the solvent from the aquifer is difficult because of the non-uniform flow-paths that quickly develop for gases through the complex, heterogeneous soil matrix.

The conventional approach to remediating NAPL contaminated aquifers is called “pump-and-treat”: The NAPL has some solubility in water. If enough contaminated water is pumped to the surface, all the NAPL is eventually brought to the surface. The problems with this are the time required and the enormous volume of water involved. All the contaminated water produced from the aquifer must be treated. Even relatively small volumes of NAPL require water many thousand times their volume to dissolve them, even at equilibrium solubility levels, which are seldom achievable. Since the heterogeneous distribution of the NAPL together with the flow of the ground water keeps the NAPL from ever reaching an equilibrium concentration in the water, a still greater volume of water than predicted by equilibrium solubility levels is required. The rate of pumping from an aquifer is limited by the ability to treat the produced contaminated water plus the drawdown rate of the aquifer. Consequently, if the volume of NAPL is even a few percent of the volume of the water in the aquifer, pump-and-treat remediation may require decades or even centuries. During this entire period contaminated water is being produced and must be treated. It is important to acknowledge, however, that pump-and-treat can still be used to reverse the flow of the ground water, so that the plume of dissolved contaminant stops moving, even if the actual remediation rate is slow. In many cases it may be found that containing the contaminant by pump-and-treat is the only economically viable option. In still other cases a risk-based analysis of the situation may lead to the conclusion that natural attenuation of the contaminant plume will prevent elevated levels of contaminant from reaching any potential users of the ground water.

Surfactants have been proposed for remediating NAPL contaminated aquifers by two mechanisms. These are referred to as “solubilization” and “mobilization”. Surfactants are attractive remediation agents because they are active at low concentrations, are non-toxic to mammals, and are even edible. They also are highly biodegradable with a properly designed molecular structure.

When the solubilization mechanism is used, micelles are circulated through the contaminated zone. Each micelle takes up some contaminant, thereby increasing the contaminant removal rate. For very low solubility contaminants, such as tetrachloroethylene, the remediation rate may be increased by two or more orders of magnitude when solubilization is used. For higher solubility contaminants, like dichlorobenzene, the increase in solubility may be only a factor of 2 or 3, which is unlikely to be sufficient to justify the expense of using surfactants.

Mobilization is based on a very different mechanism. In mobilization, the surfactant system is carefully designed to produce a low interfacial tension between the NAPL and the water. If the interfacial tension reduction is sufficient, the capillary forces trapping the NAPL droplets are reduced sufficiently to allow the NAPL droplets to be released from the soil. They can then be pumped directly to the surface. This technology can increase the NAPL removal rate by three or more orders of magnitude, changing the time for remediation from centuries to months. Success of a mobilization process requires designing the surfactant system so that it produces a Winsor Type III microemulsion with the NAPL at the conditions in the aquifer. Not only must the surfactant system produce a Type III microemulsion, the microemulsion must have a low viscosity, so that the microemulsion phase is not trapped in the aquifer, and so that injection rates remain high. Further, effective removal of the NAPL from the heterogeneous aquifer matrix is facilitated by rapid equilibration rates between the NAPL and surfactant solution. Chapter 4 examines these design criteria.

In both the solubilization and the mobilization mechanisms, care must be taken to assure that the surfactant remains active in the environment of the subsurface. Failure to account for the change in surfactant solubility in the cold water of an aquifer or the elevated dissolved solids content (electrolyte levels) of the ground water may result in loss of the surfactant through precipitation or phase separation and subsequent failure of the process to produce an enhanced remediation rate. Adsorption of the surfactant onto the soil in the aquifer also can result in a substantial loss of surfactant and become a major expense, causing an economic if not a technical failure of the process. The requirements of high solubilization, low interfacial tension, low adsorption, and robustness at aquifer ground water conditions must be met simultaneously. This places considerable constraints on surfactant selection.

Both mobilization and solubilization have been tested successfully in the field at actual contaminated sites. The economics of the process have been refined to where the components of a successful remediation can be implemented at a cost significantly less than the cost of a pump-and-treat system, with the added advantage of actually having the site clean in a reasonable period of time. However, keeping the cost to an affordable level requires recovery and reinjection of the surfactant. Field tests have now demonstrated that volatile contaminants, including PCE and TCE, can be removed from an aqueous surfactant stream by air stripping without the use of defoamers. This requires designing the strippers to avoid continuous flow of water through the stripper; rather, the volume of liquid flow per unit of cross-sectional area must stay in a dripping-flow

regime. As alternative, membrane pervaporation is currently being examined as discussed in Chapter 5. Membrane air stripping has also been demonstrated to be a technically feasible alternative.

Ultrafiltration of the surfactant flush solution (MEUF) to concentrate the surfactant prior to reinjection (see Chapter 3) may be crucial to an economical subsurface remediation operation. The solute may be separated from the surfactant either before the ultrafiltration (as in Chapter 3) or after it by techniques such as pervaporation of volatile solutes (Chapter 5) or liquid-liquid extraction (Chapter 6). Either way, the problem of separation of solute from surfactant is exactly the same one as faced in treating retentate streams in MEUF as already discussed in detail in the previous section using a number of techniques.

While the components of surfactant-based aquifer remediation have been demonstrated separately, an integrated injection, recovery, and reinjection system has not been successfully demonstrated before now. Chapter 3 examines the difficulties encountered in designing the surfactant formulation so that the surfactant remains active in the aquifer, NAPL recovery rates are high (which keeps the remediation time short), injection rates remain high, yet the surfactant recovery system remains effective! The sometimes-conflicting requirements of the subsurface and the surface recovery systems demand flexibility and creativity for a remediation to be both economical and successful.

Surfactant enhanced aquifer remediation is moving quickly from a promising experimental technology to a full-scale commercial process. Field demonstrations underway during the time that this book is being written will be completed within the year, and will take the technology to the early commercialization stage. Over the subsequent 5-10 years it is likely to expand into a business approaching \$100 M/yr. in sales and consuming \$20 M to \$30 M of surfactant per year.

Another promising use of surfactants is in the *ex situ* decontamination of soils. Many industrial locations have soil that has been contaminated by spilled crude oil, petroleum products, wood treating chemicals, or other contaminants. These spills may or may not reach the water table beneath the site, but they still produce tons of contaminated soil. If the contaminant is water soluble, rain may eventually carry it into the aquifer, contaminating the aquifer. Even if the water solubility is negligible, the soil itself becomes a hazard. *Ex situ* surfactant soil washing uses surfactants as the remediating agents to decontaminate excavated soils. As with the *in situ* surfactant aquifer remediation process, surfactant recovery and reuse dramatically improve the economics of the soil washing process.

There are existing approaches to dealing with contaminated soils. The most common is excavation and disposal in a secure landfill. For contaminants with low toxicity this is often the most inexpensive choice, even if somewhat esthetically unsatisfactory. Even in this case, however, excavation and hauling cost can exceed landfilling costs if the soil is far from a satisfactory landfill. Other alternatives to landfilling include thermal

destruction of the contaminants inside what are essentially large, rotating furnaces or washing the soil with a chemical solution. Surfactants again offer a promising alternative. When a suitable surfactant system can be design to remove the contaminant from the soil surface, it is possible to wash the soil on-site and return it to the excavated hole. Sometimes it is even possible to recycle and reuse the surfactant and the wash water. This results in substantial savings over landfilling costs, and has the additional advantage of permanently removing the contaminant from the environment. Chapter 2 looks at a variation of this, where a microemulsion system is used to decontaminate the soil.

Adsorption, Fractionation, and Flotation Based Processes

Surfactant aggregates such as micelles and vesicles are the obvious mass separating agents in a process like MEUF. Surfactants adsorbed at the solid-liquid interface also form aggregates. These surface aggregates, commonly called admicelles or hemimicelles (26), solubilize organics in almost exactly the same manner as micelles and vesicles; this phenomenon is commonly referred to as adsolubilization or surface solubilization (26), and has been proposed as the basis for new, surfactant-based separation processes. The accumulation of surfactants at the air/water interface, and the resulting lowering of the excess Gibbs free energy of the interface, is the principal phenomenon in formation of stable foams. When the surfactants adsorbed on the surface of a solid are also adsorbed at the air interface, the surfactant-treated solid can demonstrate improved adhesion to the surface of a bubble. The adhesion of a particulate material to a bubble rising through a liquid is the basis of the froth flotation process. A layer of surfactants adsorbed at the air-water interface will solubilize organics and bind with counterions just as will surfactants in a micelle. This phenomenon is the basis of foam fractionation processes.

Flotation and fractionation processes both involve bubbling an insoluble gas (usually air) into an aqueous stream. Materials to be removed adhere to the bubbles as they rise through the process unit and are concentrated in the foam (called a froth in this case), which is skimmed off overhead. Surfactant is useful to both facilitate adhesion of target material to the bubble surface and to as a froth promoter/stabilizer. We use the common convention that flotation operations involve removal of separate phases, such as ore particles or insoluble oil droplets, while fractionation operations involve removal of dissolved materials, such as heavy metal ions.

Froth flotation to remove emulsified oil from water requires surfactant to produce foam, if for no other reason. However, the surfactant also increases adherence of the oil droplets to the air bubbles for reasons which are not well understood. Since reduction in interfacial tension at both the air/water and oil/water interfaces is probably one of the causes of the surfactant's synergism, a research project which we have ongoing is to investigate the advantages of performing a flotation at a composition of surfactant which will produce a microemulsion between the oil and water phases. Results indicate that if the system forms a "Winsor Type III microemulsion", flotation efficiency increases (27). Since this condition also corresponds to minimal interfacial tensions between the water

and oil phases (28), the general idea of improving flotation efficiency by choosing conditions where interfacial tensions are substantially reduced appears to be a promising approach. Of course, since froth stability, air/water interfacial tensions, and other factors also contribute, optimizing these systems is probably going to be much more complex.

Particularly in the 1960's and 1970's, there was a great interest in fractionation operations to remove dissolved solutes like heavy metals from water (29-31). In these processes, surfactant was added to the water and air sparged into the solution. The solute would coadsorb with the surfactant at the air-water interface and accumulate into the foam coming overhead. While there is still activity in this application (32), the processes have not gained significant commercial usage. The basic phenomena involved are well understood, but have not been applied in processes that are fully countercurrent or, in most cases, even staged. Surfactant recovery and reuse will be critical to the economics of many applications of this phenomenon in separations; thus, progress in regeneration of surfactants from environmental separations will improve the viability of fractionation process. An essential element in commercialization of technologies based on fractionation is implementation in a counter-current mode. The use of air-sparged hydrocyclones (33) is a promising route to fully counter-current fractionation processes, which has not, to our knowledge, been explored.

As environmental regulations have become more severe, there has been recent interest in another application of foam fractionation: removal of surfactant itself from aqueous streams. Despite their relative benign nature, allowable surfactant concentrations in wastewater has been declining, leading to a number of streams containing low surfactant concentrations requiring treatment for even further surfactant removal. Foam fractionation has been shown to be effective at achieving this for both anionic and cationic surfactants (13) in single stage studies. Current research in our laboratory is focused on scaling this process up in a multitray fractionation device.

The flotation process is currently the most commercially important application of surfactants in separations. Surfactants adsorbed on the surface of a particle can--at proper adsorption densities--dramatically enhance the adhesion of a particulate to a rising bubble of air being sparged into a slurry. The level of surfactant adsorption on a specific solid surface can be readily controlled by choice of surfactant concentration, pH of the slurry, addition of counterions, and choice of the type of surfactant. This allows one to design the surfactant system so that one particulate component of a slurry is preferentially floated, while other particulate materials do not adhere to the rising bubbles. This is a very important operation in the mining industry and has been the focus of decades of research (Chapter 14). This important process, which has been developed to a high degree of sophistication in the mining industry, should receive serious attention as a low cost option for environmental remediation of contaminated soils and sediments (Chapter 15). A closely related application (from a fundamental point of view) is the use of surfactants to enhance particulate removal from surfaces. This application of surfactants in separations may play an important role in identifying alternative solvent systems for industrial cleaning operations (Chapter 21).

The phenomenon of adsolubilization has been proposed as an alternative to processes such as carbon adsorption (34). This process has attracted little attention and suffers from the need to recover the surfactant from the effluent stream in order to be economical. Another potential application of adsolubilization is in the area of adsorbing barriers for prevention of the migration of ground water contaminants (35,36). This process is very promising and deserves significant attention, which it has yet to receive. In fact, the phenomenon of adsolubilization itself is little understood and is the focus of ongoing research (Chapters 16 and 19).

One of the most active areas of research in surfactant-based separations is the use of surfactants to enhance analytical separations. The area of micellar liquid chromatography has developed into an area of study of its own (Chapters 17 and 18). Here, segregation of compounds between the micellar pseudo-phase and carrier phase is used to modify the retention time of the solubilized compounds; properly manipulated, this can dramatically improve an analytical separation based on liquid chromatography. Similarly, a layer of adsorbed surfactant can be used to modify the relative retention times of compounds in capillary electrophoresis (Chapter 20). The use of surfactants in analytical separations hints at the possible selectivity enhancements possible by modification of adsorption-based separations by use of surfactants. The analytical uses, however, do not require the recovery and reuse of the surfactant in order to be viable. The degree of cross-fertilization between the use of surfactants in analytical separations and the use of surfactants in industrial separations could increase enormously with significant progress in the area of surfactant regeneration and recycling.

Extraction and Deinking Processes

Extraction: There are currently two primary processes phase being intensively studied in which surfactants are used to cause extraction of dissolved materials into a second liquid. Chapter 22 outlines new developments in the use of reverse micelles to extract proteins into a nonaqueous phase, prior to extraction back into an aqueous phase to concentrate the protein. One remarkable advance in this process is the finding that proteins can renature upon dissolution into reverse micelles. To reactivate biological agents as well as separate them is a useful synergism.

Another process, which has been intensively studied, is a cloud point extraction (37) or coacervate extraction (38). In this process, an aqueous solution of a nonionic surfactant above its cloud point separates into two phases; a concentrated phase called the coacervate, and a dilute phase. Organic materials tend to distribute themselves to a high degree into the coacervate phase due to solubilization into the "micelle-like" surfactant aggregates there. This is a specific example of an aqueous biphasic separation (39). Separation factors can be extremely high, but removal of solute from the coacervate phase can be difficult. Many of the methods mentioned under the Surfactant-Enhanced Ultrafiltration section for regeneration of surfactants are only useful for ionic surfactants. Therefore, in our own research group, work has focused on volatile organic removal from

water using cloud point extractions because of the potential for stripping (e.g., vacuum) the organic solute from the coacervate phase following the extraction, permitting recycle of surfactant. We feel that this method has tremendous potential if the surfactant regeneration problem can be solved.

Deinking: In order to reuse paper fibers or printed plastic, the ink must often be removed from the surface and separated from paper or plastic (deinking). Since paper constitutes the largest single component of consumer solid waste, there is considerable political pressure to recycle paper for waste minimization. Due to concerns about air pollution, water-based inks are increasingly popular. Chapter 23 is an extensive overview of the state of the art in paper deinking with water-based inks by both washing and flotation processes. Changes in printing processes (e.g., laser printing in the last ten years), paper characteristics (e.g., more recycled paper used in printed paper), increased pressure to use less water in paper processing, and a desire to use less bleach to produce white paper due to environmental concerns about bleach are just a few of the issues in this technology. New surfactant types and synergistic use of dissimilar surfactants have potential for improving efficiency. For example, the exact mechanism by which air bubbles, ink particles, surfactant, and activator (e.g., calcium) interact in flotation deinking are controversial. As mechanistic studies increase understanding, new generations of processes may result.

Plastic must often have ink removed from the surface prior to reextrusion and reuse. Clear plastic films are one example. Surfactants are environmentally attractive alternatives to organic solvents to achieve deinking and have been shown to be effective in this application.

Acknowledgements

Financial support for continuing research by us in this area was received from the industrial sponsors of the Institute for Applied Surfactant Research including Akzo Nobel, Albemarle, Amway, Colgate-Palmolive, Dial, Dow, DowElanco, DuPont, Halliburton, Henkel, Huntsman, ICI, Kerr-McGee, Lubrizol, Nikko Chemical, Phillips Petroleum, Pilot Chemical, Procter and Gamble, Reckitt and Coleman, S.C. Johnson Wax, Schlumberger, Shell, Sun, Unilever, and Witco. Dr. Scamehorn holds the Asahi Glass Chair and Dr. Harwell holds the Conoco/DuPont Professorship in chemical engineering at the University of Oklahoma.

Literature Cited

1. Leung, P. S. In *Ultrafiltration Membranes and Applications*; Cooper, A. R., Ed.; Plenum: New York, 1979; p 415.
2. Dunn, R. O.; Scamehorn, J. F.; Christian, S. D. *Sep. Sci. Technol.* **1985**, *20*, p 257.
3. Christian, S. D.; Scamehorn, J. F. In *Surfactant-Based Separation Processes*; Scamehorn, J. F.; Harwell, J. H., Eds.; Marcel Dekker: New York, 1989; Ch 1.

4. Scamehorn, J. F.; Christian, S. D.; Ellington, R. T. In *Surfactant-Based Separation Processes*; Scamehorn, J. F.; Harwell, J. H., Eds.; Marcel Dekker: New York, 1989; Ch 2.
5. Hurter, P. N.; Alexandridis, P.; Hatton, T. A. In *Solubilization in Surfactant Aggregates*; Christian, S. D.; Scamehorn, J. F., Eds.; Marcel Dekker: New York, 1995; Ch 6.
6. Roberts, B. L., PhD Dissertation, University of Oklahoma, 1993.
7. Scamehorn, J. F., private communication.
8. Strauss, U. P. In *Interactions of Surfactants with Polymers and Proteins*; Goddard, E.D.; Ananthapadmanabhan, K. P., Eds.; CRC Press: Boca Raton, Florida, 1993; Ch 6.
9. Sasaki, K. J.; Burnett, S. L.; Christian, S. D.; Tucker, E. E.; Scamehorn, J. F. *Langmuir* **1989**, *5*, p 876.
10. Sriratana, S.; Scamehorn, J. F.; Chavedej, S.; Saiwan, C.; Haller, K. J.; Christian, S. D.; Tucker, E. E. *Sep. Sci. Technol.* **1996**, *31*, p 2493.
11. Uchiyama, H.; Christian, S. D.; Tucker, E. E.; Scamehorn, J. F. *J. Colloid Interface Sci.* **1994**, *163*, p 493.
12. Guo, W.; Uchiyama, H.; Tucker, E. E.; Christian, S. D.; Scamehorn, J. F. *Colloid Surf.* **1997**, *123*, p 695.
13. Tharapiwattananon, N.; Scamehorn, J. F.; Osuwan, S.; Harwell, J. H.; Haller, K. J. *Sep. Sci. Technol.* **1996**, *31*, p 1233.
14. Hurter, P. N.; Hatton, T. A. *Langmuir* **1992**, *8*, p 1291.
15. O'Haver, J. H.; Christian, S. D.; Harwell, J. H.; Sabatini, D. A.; Scamehorn, J. F.; Hasagawa, M. A. In *Handbook of Detergents: Volume 5 – Applications*; Mehretea, A., Ed.; Marcel Dekker: New York, In Press.
16. Choori, U. N.; Scamehorn, J. F.; O'Haver, J. H.; Harwell, J. H. *Ground Water Remed. Monitoring* **1998**, *18*, p 157.
17. Brant, L. W.; Stellner, K. L.; Scamehorn, J. F. In *Surfactant-Based Separation Processes*; Scamehorn, J. F.; Harwell, J. H., Eds.; Marcel Dekker: New York, 1989; Ch 12.
18. Wu, B.; Christian, S. D.; Scamehorn, J. F. *Prog. Colloid Polym. Sci.* **1998**, *109*, p 60.
19. Tucker, E. E.; Christian, S. D.; Scamehorn, J. F.; Uchiyama, H.; Guo, W. *ACS Symp. Ser.* **1992**, *491*, p 84.
20. Klepac, J.; Simmons, D. L.; Taylor, R. W.; Scamehorn, J. F.; Christian, S. D. *Sep. Sci. Technol.* **1991**, *26*, p 165.
21. Tuncay, M.; Christian, S. D.; Tucker, E. E.; Taylor, R. W.; Scamehorn, J. F. *Langmuir* **1994**, *10*, p 4688.
22. Tuncay, M.; Christian, S. D.; Tucker, E. E.; Taylor, R. W.; Scamehorn, J. F. *Langmuir* **1994**, *10*, p 4693.
23. Fillippi, B. R.; Scamehorn, J. F.; Taylor, R. W.; Christian, S. D. *Sep. Sci. Technol.* **1997**, *32*, p 2401.
24. Hatton, T. A., In *Surfactant-Based Separation Processes*; Scamehorn, J. F.; Harwell, J. H., Eds.; Marcel Dekker: New York, 1989; Ch 3.
25. Markels, J. H.; Lynn, S.; Radke, C. J. *Ind. Eng. Chem. Res.* **1995**, *34*, p 2436.

26. *Surfactant Adsorption and Surface Solubilization*; Sharma, R., Ed.; American Chemical Society: Washington, 1995.
27. Pondstabodee, S. P.; Scamehorn, J. F.; Chavedej, S.; Harwell, J. H. *Sep. Sci. Technol.* **1998**, *33*, p 591.
28. Bourrel, M.; Schechter, R. S. *Microemulsions and Related Systems: Formulation, Solvency, and Physical Properties*; Marcel Dekker: New York, 1988.
29. Lemlich, R., Ed. *Adsorptive Bubble Separation Techniques*; Academic Press, New York, 1972.
30. Clarke, A. N.; Wilson, D. J. *Foam Flotation: Theory and Applications*; Marcel Dekker: New York, 1983.
31. Okamoto, Y.; Chou, E. J. In *Handbook of Separation Techniques for Chemical Engineers, 2nd Ed.*; Schweitzer, P. A., Ed.; McGraw Hill: New York, 1979; Sec. 2.5.
32. Wungrattanasopon, P.; Scamehorn, J. F.; Chavedej, S.; Saiwan, C.; Harwell, J. H. *Sep. Sci. Technol.* **1996**, *31*, p 1523.
33. Das, A.; Miller, J. D. *Int. J. Mineral Proc.* **1996**, *47*, p 251.
34. Harwell, J. H.; O'Rear, E. A. In *Surfactant-Based Separation Processes*; Scamehorn, J. F.; Harwell, J. H., Eds.; Marcel Dekker: New York, 1989; Ch 7.
35. West, C. C.; Harwell, J. H. *Environmental Sci. Technol.* **1992**, *26*, p 2324.
36. Nayyar, S. P.; Sabatini, D. A.; Harwell, J. H. *Environmental Sci. Technol.* **1994**, *28*, p 1874.
37. Hinze, W. L.; Pramauro, E. *Crit. Rev. Anal. Chem.* **1993**, *24*, p 133.
38. Gullickson, N. D.; Scamehorn, J. F.; Harwell, J. H. In *Surfactant-Based Separation Processes*; Scamehorn, J. F.; Harwell, J. H., Eds.; Marcel Dekker: New York, 1989; Ch 6.
39. *Aqueous Biphasic Separations: Biomolecules to Metal Ions*; Rogers, R. D.; Eiteman, M. A., Eds.; Plenum: New York, 1995.

Chapter 2

Phase Behavior of Perchloroethylene with Mixtures of Sulfosuccinate Surfactants

V. Weerasooriya¹, W. H. Wade¹, and G. A. Pope²

¹ Department of Chemistry and ² Department of Petroleum and Geosystems Engineering, University of Texas at Austin, Austin, TX 78712

Thermodynamically stable Winsor Type I (oil-in-water), Type II (water-in-oil), and Type III (middle phase) phase behavior systems have been identified for perchloroethylene, with a mixture of sodium sulfosuccinate surfactants in the presence of isopropyl alcohol and appropriate electrolyte concentrations. The surfactant mixture is composed of 65% sodium dihexyl sulfosuccinate (Aerosol MA) and 35% sodium dioctyl sulfosuccinate (Aerosol OT) by weight. All experiments were done at 25 °C. The results presented are the electrolyte concentrations and solubilization parameters for the optimum formulations.

In recent years, researchers have witnessed an increase in the number of sites contaminated with organic solvents (*1*). These compounds, generally known as NAPL (non-aqueous phase liquids) due to their very low solubility in water, can be further categorized into two main groups, DNAPLs (dense non aqueous phase liquids) and LNAPLs (light non aqueous phase liquids). Hydrocarbons such as hexane and octane are common examples of LNAPLs. In this research we are interested in a DNAPL known as perchloroethylene (PCE) that is denser than water.

Several decades ago, people used chlorinated hydrocarbons as very efficient degreasers. When these molecules reached the soil's surface, their high density allowed them to sink deep into the ground and reach the aquifers, thus contaminating the potable water supply. A portion of the DNAPL also remained in the soil pores as immovable ganglia held by capillary forces at high interfacial tension (*2*).

Surfactant Enhanced Aquifer Remediation (SEAR) has been shown by several field demonstrations to be a highly effective method for removing chlorinated hydrocarbons (3). Two demonstrations of SEAR have been completed at a DNAPL site known as Operable Unit 2 at Hill Air Force Base in Utah (4,5). The major component of DNAPL this site was trichloroethylene (TCE). The surfactant flood consisted of the injection of 8wt. % sodium dihexyl sulfosuccinate (Aerosol MA), 4wt. % isopropyl alcohol, and 0.7wt. % NaCl. About 99% of the DNAPL was removed after injecting 2.4 pore volumes of surfactant solution. The surfactant, co-surfactant selection, and optimization were done according to a process similar to the one established initially for enhanced oil recovery (6).

The systematics of forming oil-in-water (Winsor Type I), water-in-oil (Winsor Type II), and middle phase (Winsor Type III) microemulsions have been demonstrated by the studies done in our (UT-Austin) laboratory (7-15) and elsewhere (16-22). The phase behavior studies for perchloroethylene were done by using a mixture of dihexyl and dioctyl sulfosuccinate (Aerosol MA and Aerosol OT) surfactants. The ideal mass balance for a given salinity was determined by mixing the two surfactants at different mass ratios. Isopropyl alcohol was used as a co-solvent in this study mainly to reduce the viscosity of the microemulsion for field application processes. CaCl_2 and NaCl were used as the electrolytes. The optimum salinity (S^*) and optimum solubilization parameter (σ^*) were measured for each system studied. The solubilization parameter is defined as the ratio of the volume of oil (or water) solubilized in the microemulsion to the volume of surfactant in the microemulsion (6). At optimum salinity, the microemulsion contains equal volumes of oil and water. The solubilization parameter at that salinity is denoted as the optimum solubilization parameter.

Research Description

Aerosol MA and Aerosol OT were obtained from the Cytec Corporation. The aqueous phase consisted of the surfactant mixtures, isopropyl alcohol, CaCl_2 , and various concentrations of NaCl. The oleic phase (PCE) and aqueous phase were mixed in equal volumes. These formulations were carried out in 5 ml graduated borosilicate glass pipettes that were modified by flame sealing their narrow ends to hold liquid mixtures. All systems were shaken once and allowed adequate time to reach equilibrium at 25 °C. Once equilibrated, the solubilization parameters were determined volumetrically.

Results and Discussion

From the salinity scan with Aerosol MA 8%, IPA 4%, and CaCl_2 0.1% (all by weight), the optimum salinity and optimum solubilization parameter were 3.9 wt. % NaCl and 2.26 ml PCE per ml of surfactant, respectively. The optimum salinity was higher than desirable, so sodium dioctyl sulfosuccinate (Aerosol

OT) was mixed with Aerosol MA to lower it. The lipophilicity of a surfactant increases with an increase in alkyl chain length (15), so Aerosol OT has a greater lipophilicity than Aerosol MA (Figure 1) and thus would be expected to lower the optimum salinity.

The solubilization parameter as a function of the mass fraction of Aerosol OT is shown in Figure 2. In this mass scan, the aqueous phase concentrations were a total surfactant concentration of 4 wt%, IPA of 4% and NaCl of 1.5%. The oil and water solubilization parameters were equal to 3.68 ml/ml for 65% Aerosol MA, 35% Aerosol OT. Thus, at this ratio of surfactants, the optimum salinity has been reduced from 3.9 to 1.5 wt% NaCl. These data can also be represented in a volume fraction diagram (21) as shown in Figure 3.

The studies were then concentrated on the 65/35 Aerosol MA/OT mixture. The effect of Ca^{++} and IPA co-solvent on the optimum salinity and solubilization ratio are tabulated in Table I. The optimum solubilization ratio showed a slight increase as the CaCl_2 concentration increased from 0 to 0.05 wt% and then remained almost constant for higher concentrations. The optimum solubilization parameter decreased from about 5.4 to 3.3 when 8 wt% IPA was added. Although the IPA lowers the solubilization parameter and thus the efficiency of the surfactant, on balance it is still highly beneficial because it also lowers the viscosity and promotes more rapid solubilization of the PCE. Without any co-

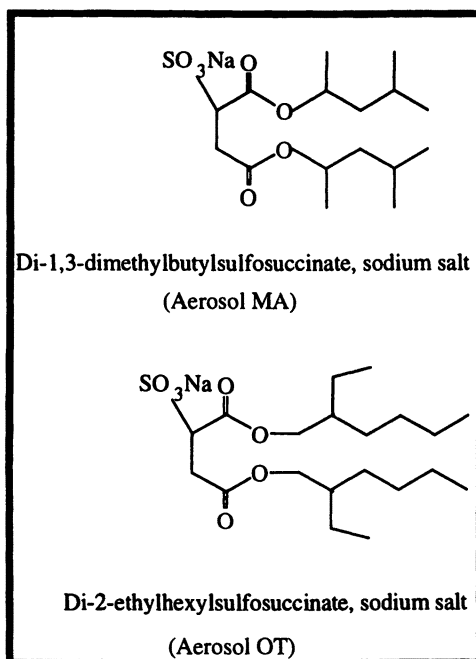


Figure 1. Structures of Surfactants Used

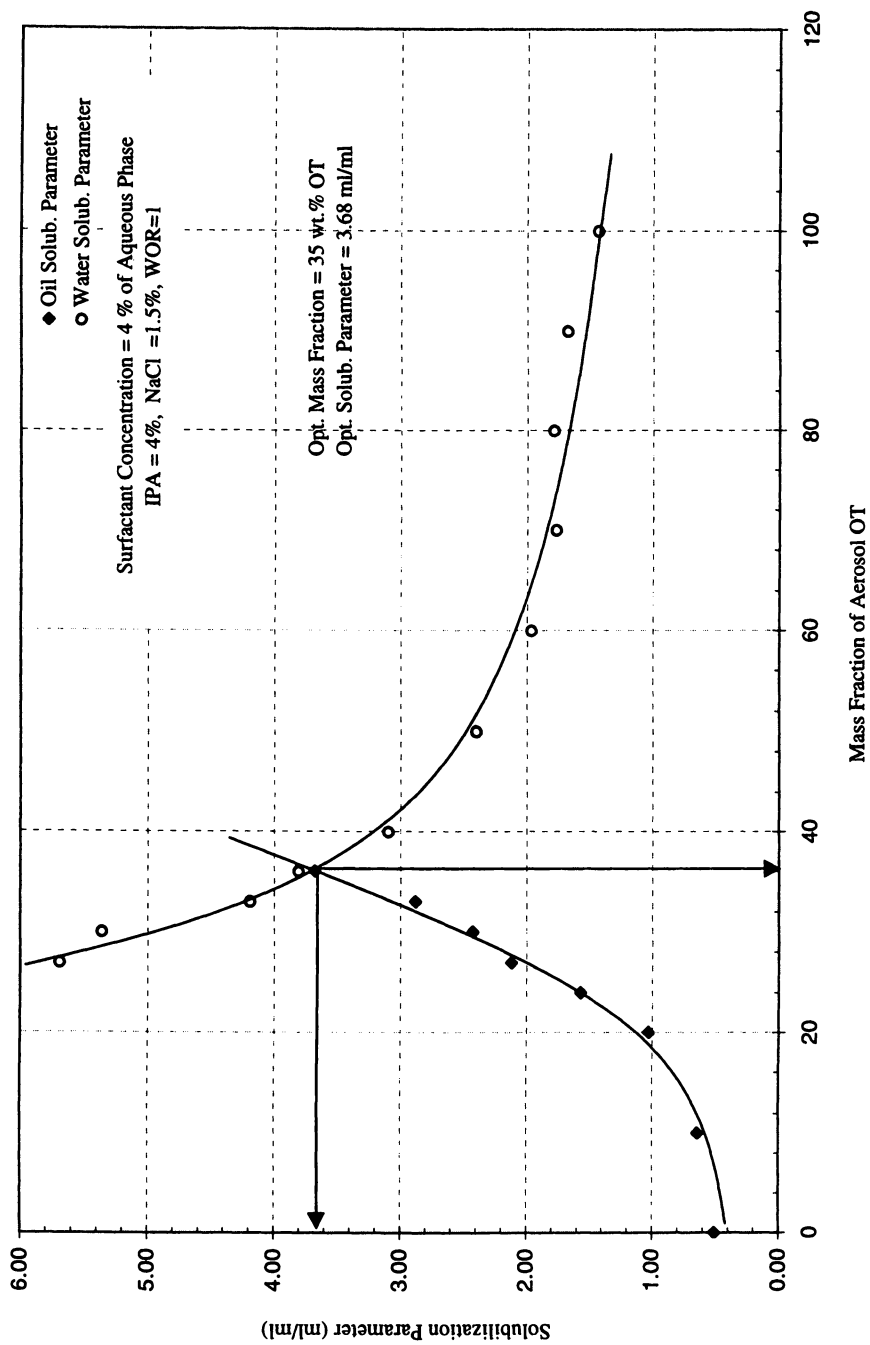


Figure 2. Solubilization parameter vs. mass fraction for Aerosol MA/OT with PCE at 25oC

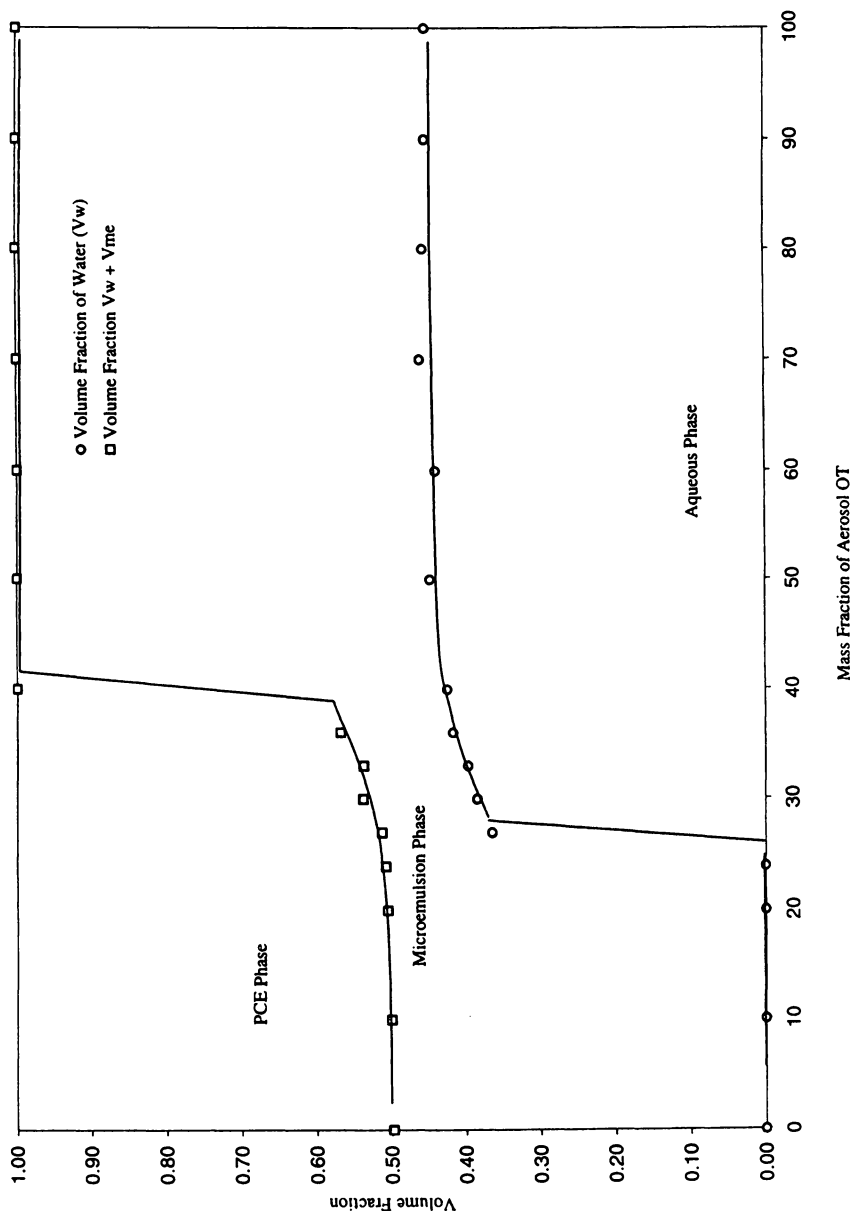


Figure 3. Volume fraction diagram for Aerosol MA/OT mixture with PCE at 25°C

Table I. Experimental Parameters for 8 wt.% MA/OT (65/35) with PCE at 25 °C

IPA (wt.%)	CaCl ₂ (wt.%)	S* (wt.%)NaCl	σ* (ml/ml)
0	0.00	1.41	5.29
0	0.05	1.23	5.45
0	0.10	1.10	5.45
0	0.20	0.86	5.40
8	0.00	1.46	3.16
8	0.05	1.33	3.29
8	0.10	1.20	3.30
8	0.20	0.96	3.30

solvent, the Aerosol MA/OT aqueous mixture forms a highly viscous gel after several days and thus is not suitable for use in remediation without co-solvent.

Acknowledgments

The authors wish to thank the U.S. Naval Facilities Engineering Service Center in collaboration with United States Environmental Protection Agency National Risk Management Research Laboratory for funding this research project. The authors also wish to acknowledge Cytec Corporation for providing surfactants for this study. We would also like to thank Meng Lim and Taimur Malik for their assistance with the laboratory measurements.

Literature Cited

1. MacKay, D. M.; Cherry, J. A. *Environ. Sci. and Technol.*, **1989**, *23* (6), p. 630.
2. Morrow, N. R.; Songkran, B. In *Surface Phenomena in Enhanced Oil Recovery*, Shah, D.O., Ed.; Plenum Press: New York, NY, 1981; p. 387.
3. Fountain, J.C.; Starr, R.C.; Middleton, T.; Beikirch, M.; Taylor, C.; Hodge, D. *Ground Water*, **1996**, *34*, 910-916.
4. Brown, C.L.; Delshad, M.; Dwarakanath, V.; McKinney, D.C.; Pope, G.A.; Jackson, R.E.; Londergan, J.T.; Meinardus, H.W.; Wade, W.H., In *Innovative Subsurface Remediation: Field Testing of Physical, Chemical, and Characterization Technologies*, M. Brusseau, M. Annable, and J. Gierke (eds.) ACS Symposium Series 725, **1998**.
5. Hirasaki, G.J.; Miller, C.A.; Szafranski, R.; Tanzil, D.; Lawson, J.B.; Meinardus, H.W.; Jin, M.; Londergan, J.T.; Jackson, R.E.; Pope, G.A. and Wade, W.H., Submitted to *Journal of Contaminant Hydrology*, **1998**.
6. Bourrel, M. and Schechter, R.S. "*Microemulsions and Related Systems*"; Surfactant Science Series, Marcel Dekker, Inc., New York, NY, **1988**.

7. Baran, J. R. Jr.; Pope, G. A.; Wade, W. H.; Weerasooriya, V. *Langmuir*, **10**(4), **1994**, pp. 1146-1150.
8. Cash, R.L.; Cayias, J.L.; Fournier, G.R.; Jacobson, J.K.; LeGear, C.A.; Schares, T.; Schechter, R.S.; Wade, W.H. *Soc. Pet. Eng. J.*, **17**, **1977**, p. 122.
9. Salager, J.L.; Vasquez, E.; Morgan, J.C.; Schechter, R.S.; Wade, W.H. *Soc. Pet. Eng. J.*, **19**, **1979**, p. 107.
10. Vasquez, E.; Salager, J.L.; El-Emary, M.; Koukounis, C.; Schechter, R.S.; Wade, W.H. *Solution Chemistry of Surfactants*, **2**, **1979**, p. 801.
11. Salager, J.L.; Bourrel, M.; Schechter, R.S.; Wade, W.H. *Soc. Pet. Eng. J.*, **19**, **1979**, p. 271.
12. Graciaa, A.; Schechter, R.S.; Wade, W.H.; Yiv, S.H.; Barakat, Y. *J. Colloid and Interface Sci.*, **89**, **1982**, p.217. Graciaa, A.; Fortenoy, L.; Schechter, R.S.; Wade, W.H.; Yiv, S. *Soc. Pet. Eng. J.*, **22**, **1982**, p. 743.
13. Barakat, Y.; Fortney, L.N.; Schechter, R.S.; Wade, W.H.; Yiv, S.H. *J. Colloid and Interface Sci.*, **92** (2), **1983**, p. 561.
14. Abe, M.; Schechter, D.; Schechter, R.S.; Wade, W.H.; Weerasooriya, U.; Yiv, S. *J. Colloid Interface Sci.*, **114** (2), **1986**, p. 343.
15. Lalanne-Cassou, C.; Carmona, I.; Fortney, L.; Samii, A.; Schechter, R.S.; Wade, W.H.; Weerasooriya, U.; Weerasooriya, V.; Yiv, S. *J. Dispersion Sci. and Tech.*, **8** (2), **1987**, 137.
16. Healy, R. N.; Reed, R.L. *Soc. Pet. Eng., J.*, **17**, **1977**, p. 129.
17. Healy, R. N.; Reed, R.L. *Soc. Pet. Eng., J.*, **16**, **1976**, p. 147.
18. Puerto, M. C.; Reed, R.L. *Soc. Pet. Eng., J.*, **23**, **1983**, p. 669.
19. Nelson, R. C. *Soc. Pet. Eng. J.*, **22**, **1982**, p. 259.
20. Winsor, P. A. In *Solvent Properties of Amphiphilic Compounds*; Butterworths, London, UK, 1954.
21. Shiau, B.; Rouse, J.D.; Sabatini, D.A.; Harwell, J.H.; In *Surfactant-Enhanced Subsurface Remediation: Emerging Technologies*, D.A. Sabatini, R.C.Knox and J.H. Harwell (eds) ACS Symposium Series 594, **1995**.
22. Fountain, J. C. "Transport and Remediation of Subsurface Contaminants", Sabatini, D. A.; Knox, R. C., Eds.; American Chemical Society Symposium Series 491; **1992**.

Integrated Demonstration of Surfactant-Enhanced Aquifer Remediation with Surfactant Regeneration and Reuse

V. Weerasooriya¹, S. L. Yeh², G. A. Pope³, and W. H. Wade¹

Departments of ¹ Chemistry and ³ Petroleum and Geosystems Engineering,
The University of Texas at Austin, Austin, TX 78712

² Naval Facilities Engineering Service Center, Port Hueneme, CA 93043

This paper summarizes a laboratory study to select a suitable surfactant for a surfactant-enhanced aquifer remediation (SEAR) process that integrates surfactant recovery and reinjection. Several anionic, nonionic, and anionic/nonionic mixtures of surfactants with and without co-solvent have been evaluated. Most of these systems showed unacceptable phase behavior with PCE and/or high viscosity and were thus eliminated from further study. The Aerosol MA-80I surfactant demonstrated high solubilization of PCE and low viscosity with PCE; however, due to its high CMC, it is not considered an optimum surfactant for recovery by ultrafiltration. A new surfactant was synthesized especially for this project and found to be the best overall choice due to its excellent solubilization of PCE, low viscosity with PCE and good recovery by filtration due to its low CMC.

In recent years, surfactants have been receiving increasing attention for the enhanced removal of Dense Non-Aqueous Phase Liquids (DNAPLs), such as trichloroethylene (TCE) and perchloroethylene (PCE), which have become trapped in the aquifer as a separate organic phase. Due to the low aqueous solubility and slow rates of dissolution and biodegradation of most DNAPL contaminants, DNAPLs can persist as a long-term source of contamination to surrounding soils and groundwater. Pump and treat systems have proven to be inefficient and costly for addressing the mass transfer limitations of DNAPLs. Surfactants provide a means to overcome these barriers (1), and as recent field results bear out (2-5), they can be used successfully in accomplishing the rapid removal of DNAPL contaminants. While surfactants are applicable to other NAPLs, they have a special niche in the remediation of DNAPLs in

that these compounds, being denser than water, tend to sink to depths that make them less amenable to removal by other methods.

By greatly increasing the effective aqueous solubilities of the DNAPL contaminants, surfactant enhancements allow the time for remediation to be dramatically reduced from decades to months, with attendant cost savings. However, the surfactant test must be carefully designed to control the movement of surfactants and DNAPL in the subsurface, both vertically and laterally, to avoid aggravating existing contamination conditions. In addition, the selection of a surfactant that is optimum for the site DNAPL and hydrogeologic conditions is imperative to successful and cost-effective implementation of the technology. Finally, recent studies have shown that the capacity of the surfactant to be recovered for reuse may become an important criteria in designing a full-scale cleanup effort (6-8).

To date, investigation of subsurface surfactant treatment and aboveground surfactant recovery processes has been pursued independently of each other, and there has been no effort to optimize surfactant selection for a coordinated treatment train which includes surfactant recycle. Thus, upon the completion of several surfactant-enhanced subsurface remediation projects funded under the Department of Defense's (DoD) Strategic Environmental Research and Development Program (SERDP) at Hill AFB in 1996, the idea was conceived to conduct an integrated demonstration which incorporated subsurface remediation and surfactant recycle processes. Reinjection of recovered surfactants would be an integral part of the demonstration, not only to show the technical feasibility of surfactant recycle, but also to prove the regulatory acceptability of this concept. The objective was to bring together groups with expertise in both surfactant-enhanced subsurface remediation and surfactant separations processes at the very outset to optimize the selection of surfactant for both parts of the remediation.

The concept of an integrated surfactant-enhanced aquifer remediation (SEAR) project was submitted and subsequently funded under the DoD's Environmental Security Technology Certification Program (ESTCP). The demonstration site is the base dry-cleaning facility at the Marine Corps Base Camp Lejeune, North Carolina., which has aquifer contamination by PCE, still in use as a dry-cleaning solvent. PCE has been detected as free-phase (mobile) and residual (immobile) DNAPL at the site. Site characterization and test design in preparation for the ESTCP SEAR demonstration has been progress for the past year. Participating organizations on this project include: the Naval Facilities Engineering Service Center (NFESC), the U.S. Environmental Protection Agency (EPA), National Risk Management Research Laboratory (NRMRL), the University of Texas at Austin (UT), the University of Oklahoma at Norman (OU), and Duke Engineering & Services. The phase behavior studies discussed herein were performed by UT.

In order to regenerate surfactant laden with DNAPL for reuse, it is necessary not only to remove DNAPL from the surfactant, but also water, since surfactants will become diluted at least two-fold in the subsurface. Based on prior field successes in processing solutions of similar composition to what has been anticipated for this

project (9-11), pervaporation was chosen for the DNAPL removal step and micellar-enhanced ultrafiltration (MEUF) was selected for the water removal or concentration step. Pervaporation is a membrane process which uses a nonporous membrane to separate feed components based on their volatility. Volatile organic contaminants (VOCs) such as TCE and PCE permeate and evaporate across the membrane, while non-volatile components, such as surfactants are retained. Micellar-enhanced ultrafiltration uses porous membranes with a molecular weight cut-off or MWCO between 1,000 to 50,000 Daltons (12) to filter out surfactants that are aggregated as micelles. Since surfactants will leak across the membrane at their critical micelle concentration or CMC (12), the filtration efficiency, defined here as the mass of surfactant retained by the membrane per mass of surfactant filtered, is highly dependent on the CMC of the surfactant.

Criteria and Factors Influencing Surfactant Selection

Initial surfactant candidates for this study were selected based on prior successful experiences of both the subsurface treatment designers as well as surfactant recovery process designers. Although discussed in more detail elsewhere (1,7-9,11,13-18), some of the basic performance criteria set forth for the surfactant were:

- excellent solubilization for PCE under site temperature and pH conditions;
- ease of removing PCE from surfactant; and
- readily filterable with minimum surfactant losses.

In addition to the requisite of environmental acceptability, i.e. non-toxicity and biodegradability of surfactant residuals, the following were identified as desirable qualities:

- a surfactant that had been previously field-tested;
- a single surfactant rather than a surfactant mixture; and
- one which required no co-solvent or minimum co-solvent for acceptable phase behavior.

These latter considerations were driven by a tight project schedule, field operation concerns, and surfactant recycle economics. It was expected that obtaining regulatory approval for a surfactant that had been previously field-tested would be much quicker than for one that had not. More effort was anticipated to reconstitute a surfactant mixture as compared to a single surfactant, particularly if the individual surfactants did not filter with comparable efficiency through the membranes. Finally, the economics of using a co-solvent, which would not be recoverable by the processes designed to recover surfactant, would certainly be poorer than a system that did not require co-solvent.

Yet, perhaps the single largest driver in surfactant selection that has emerged as this work has progressed is the overall impact of the surfactant on the economics of implementing SEAR. Notwithstanding efforts to give subsurface performance

(DNAPL removal efficiency) and surface performance (surfactant recovery efficiency) equal weight in the surfactant selection process, there were two factors, both unexpected, which have tended to skew the surfactant selection process towards the efficient subsurface performer rather than the easily recoverable one. These were: a scarcity of surfactants which showed acceptable phase behavior, i.e., acceptable solubilization, viscosity, and phase stability, with PCE; and the low permeability aquifer solids containing the PCE DNAPL at the Lejeune dry-cleaning site (avg. hydraulic conductivity = 0.0005 cm/sec). These two conditions indeed had a compound effect, since, for SEAR to be cost-competitive at a site with low permeability soils, a surfactant that is highly efficient in solubilizing PCE is demanded. To illustrate further, a comparison may be made to the site conditions at Hill AFB OU2, the location of a very successful surfactant demonstration conducted in 1996. The average hydraulic conductivity at this site was 0.01 cm/sec(2), or approximately 20 times higher than at the Lejeune site. Thus, while the surfactant demonstration at Hill AFB OU2 was completed in only about one month including the time required for a final PITT for performance assessment, the surfactant demonstration at Lejeune is expected to require 5 months of field time. This assumes the use of a surfactant system which gives high PCE solubilization (on the order of 200,000 mg/l).

Surfactant Screening: Phase Behavior Studies

This section is intended to provide a general discussion of the phase behavior results obtained for the surfactants investigated by the project team; a more comprehensive treatment of the results will be undertaken in other publications. Table 1 summarizes the properties for all of the surfactants evaluated and discussed in this paper. The initial surfactants selected were: Aerosol MA-80I (sodium dihexylsulfosuccinate), Dowfax 8390 (sodium n-hexadecyl diphenyloxide disulfonate), Tween 80 (polyoxyethylene (20) sorbitan monooleate), and DNP-18 (dinonyl phenol polyoxyethylene (18)). Aerosol MA-80I, an anionic surfactant, was chosen as a baseline surfactant since there was considerable data available on its phase behavior with TCE, including field test data (2-5,16,17); however, due to its high CMC, (5,17) MA-80I was not considered to be an optimum surfactant from a recovery viewpoint. Dowfax 8390, another anionic surfactant, was selected because it had also been previously field-tested, and bench-scale data showed that excellent surfactant recovery (>90%) could be obtained using ultrafiltration membranes. The Tween 80 and DNP-18 are both nonionic surfactants, which have been noted for their unfavorable tendency to sorb to aquifer solids (1,14-15); however, they were selected for their low CMC, which would maximize surfactant retention during filtration. Earlier investigations with pervaporation (18) have shown that the surfactant type, whether anionic or nonionic, does not significantly influence the efficiency of VOC removal; therefore, in this initial surfactant selection process, the potential impacts of these various surfactants on VOC removal was not a consideration.

The protocol used for screening these surfactants has been described elsewhere by Pope and Wade (14). Preliminary experiments were conducted to examine the phase

Table 1. Surfactants Investigated In This Study

Name	Type ^a	MW	CMC (mM)
Aerosol MA-80I (sodium dihexylsulfosuccinate)	A	388	5.2 ^b , 20.9-52.3 ^c
Aerosol OT-100 (sodium dioctylsulfosuccinate)	A	445	1.12 ^d , 2.5 ^d
Dowfax 8390 (sodium n-hexadecyl diphenyloxide disulfonate)	A	643 (avg)	0.09-0.4 ^e , 0.66 ^f
DNP-18 (dinonyl phenol polyoxyethylene (18))	N	1138	NA
Tween 80 (polyoxyethylene (20) sorbitan monooleate)	N	1310	0.034 ^f
Tween 21 (polyoxyethylene (4)sorbitan monolaurate)	N	540	NA
Glucopon 625FE (alkyl polyglycoside, avg. alkyl chain =12.8)	N	441 (avg)	0.032 ^f
Isalchem 145- propylene oxide (3.8) sulfate	A	580	0.1 ^g

NA = not available

^a A = anionic, N = nonionic^b Ref. 16^c Ref. 5^d Ref. 15^e Ref. 21^f CMC values from manufacturer^g Ref. 20

behavior of the selected surfactant in the presence of the site DNAPL. Because DNAPL samples collected during the initial site characterization investigation revealed the DNAPL composition to be approximately 98% PCE, phase behavior studies were conducted with PCE. Surfactant solutions were prepared in distilled water, with an average pH of 6.8. Experiments were conducted at room temperature (approx. 25 °C) since groundwater temperatures were measured to average 26 °C in the test zone. With both Aerosol MA-80I and Tween 80, Aerosol OT-100 (sodium dioctylsulfosuccinate), was added to lower the required salinity for optimum solubilization of PCE. For example, earlier work with Tween 21, which has a lower HLB (hydrophilic lipophilic balance) value than that of Tween 80, indicated that greater than 8 wt% NaCl is needed to form an optimum system with PCE (17). With the Aerosol MA-80I, approximately 4 wt% NaCl is needed to form an optimum system (16,17). These salinity values are approximately four times (by wt%) of that required for TCE (14). Concern with high salinity lies with the impurities present in food-grade sodium chloride, such as arsenic, for which groundwater concentrations are strictly regulated. Finally, isopropyl alcohol (IPA) was added to the Aerosol MA-80I/OT-100 and Tween 80/Aerosol OT-100 system in anticipation of unacceptably high viscosities which would occur without it. It should be noted that with chlorinated solvents, the addition of alcohol uniformly decreases contaminant solubilization by the surfactant, although the amount of solubilization reduction will vary with surfactant, alcohol and other additives present.

Of these first four surfactant systems evaluated, only the Aerosol MA-80I/OT-100 (65/35) demonstrated acceptable solubilization phase behavior with PCE. Solubilization data for this system and a comparison to Aerosol MA-80I without OT-100 (the latter discussed in more detail below), is provided in Figure 1. Phase behavior results for each of the surfactant systems screened is provided in Table 2. The DNP-18 surfactant did not form microemulsions with PCE. A 4 wt% Dowfax 8390 solution, which was investigated with NaCl concentrations between 0 and 3 wt% NaCl showed poor solubilization of PCE; at 1.5 wt% NaCl, PCE solubilization by 4 wt% Dowfax 8390 (~15,000 mg/l) was about an order of magnitude less than 4wt% Aerosol MA-80I/OT-100 (65/35) (~250,000 mg/l), with both systems measured without alcohol for comparison. Even in a highly permeable geosystem, this low efficiency of PCE uptake would be highly undesirable from an economic viewpoint. A 4 wt% Tween 80/Aerosol OT-100 system, which was examined in the range of 0-70% Aerosol OT-100 with 4% IPA added, did not equilibrate within several days in the presence of PCE, which was considered unacceptable.

Owing to new results with MEUF which showed poor filtration of MA-80I using 10,000 MWCO membranes, additional surfactant systems were investigated: Tween 21(polyoxyethylene (4) sorbitan monolaurate)/Aerosol OT-100, Glucocon 625FE/Aerosol OT-100, Glucocon 625FE/Aerosol MA-80I, and Glucocon 625FE. Aerosol OT-100 was added to the Tween 21 and Glucocon 625FE for the same reasons discussed earlier; Glucocon 625FE was also investigated with MA-80I to reduce the viscosity. With each surfactant system, IPA was again used to keep the viscosity in an acceptable range. Also, beginning with the Glucocon 625FE studies,

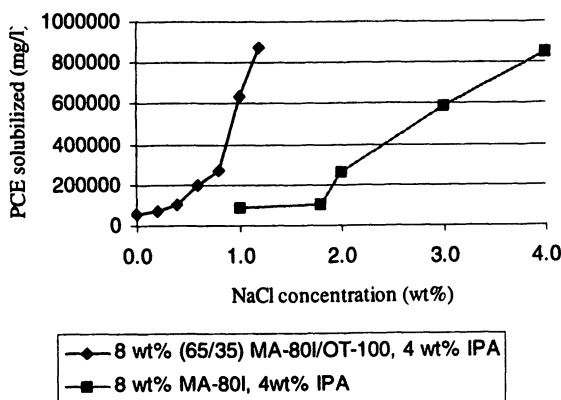


Figure 1. The Effect of Aerosol OT-100 on PCE solubilization by Aerosol MA-80I

Table 2. Summary of Phase Behavior Studies

Surfactant System	Result
Aerosol MA-80I	Good solubilization of PCE at 16% active surfactant; requires 4% IPA for acceptable viscosity
Aerosol MA-80I/Aerosol OT-100	Good solubilization of PCE, but 8% IPA required with 8% active surfactant for acceptable viscosity
Dowfax 8390	Poor solubilization of PCE
DNP-18	Does not form Type I microemulsions
Tween 80/Aerosol OT-100	Equilib. not reached with PCE after several days
Tween 21/Aerosol OT-100	Forms gels
Glucopon 625FE/Aerosol OT-100	Good solubilization of PCE but too viscous
Glucopon 625FE/Aerosol MA-80	Good solubilization of PCE but too viscous
Glucopon 625FE	Equilib. not reached with PCE after several days
Isalchem 145- PO(3.8) sulfate	Excellent solubilization, requires 16 wt% IPA for acceptable viscosity

which followed the investigation of Tween 21/Aerosol OT-100, a minimum of 0.1 wt% calcium chloride was used in all surfactant formulations. This was due to newly available soil column testing data which revealed that without this minimum concentration of calcium chloride, soil fines would be mobilized.

The Tween 21/Aerosol OT-100 system, which was scanned with up to 50% Aerosol OT-100 added, showed gel formations and was therefore not pursued further. The 2 wt% Glucopon 625FE/Aerosol OT-100 (90/10) and 2% Glucopon 625FE/Aerosol MA-80I (90/10 and 80/20) systems showed excellent solubilization of PCE, but even with 8 wt% IPA added, the viscosity of the solutions, which were investigated carefully over a range of PCE concentrations, were too high. Figure 2 shows PCE solubilization data for the 80/20 system. The Glucopon 625FE system did not equilibrate with PCE in a reasonable amount of time and even with 16 wt% IPA had viscosity problems. The Aerosol MA-80I/OT (65/35) system required 8% IPA to lower the microemulsion viscosities to less than 5 cp and was also undesirable since it contained two surfactants rather than one. Viscosity data for the Glucopon 625FE/MA-80I and Aerosol MA-80I/OT-100 systems is provided in Table 3. At this juncture, although a surfactant that came closer to meeting the original project objectives was still desired, no alternatives presented themselves; as such, despite unfavorable filterability characteristics, the Aerosol MA-80I became the exclusive surfactant under investigation.

Aerosol MA-80I Studies

The phase behavior of two Aerosol MA-80I systems have been investigated in detail: an 8 wt% MA-80I, 1.8 wt% NaCl, 0.1 wt% CaCl₂, and 4 wt% IPA system, as well as a 16wt% MA-80I, 1.5 wt% NaCl, 0.1% CaCl₂, and 4 wt% IPA system. With respect to the formation of an optimum Winsor Type III middle-phase system, both of these are both sub-optimum systems. In fact, the first system is a Winsor Type I system with a PCE solubilization of only 105,400 mg/l. The 16 wt% MA-80I system with 1.5 wt% salt (PCE solubilization 262,000 mg/l) is comparable to an 8 wt% MA-80I system with 2.5 wt% NaCl which was initially studied; (all other constituents being the same); however extended studies with the aged 8 wt% MA-80I/2.5 wt% NaCl solutions revealed phase instabilities which were objectionable. With the formulations above, these instabilities are avoided. Preliminary soil column tests performed with the 8wt% Aerosol MA-80I surfactant formulation at 2.5 wt% NaCl, 0.1 wt% CaCl₂ and 4 wt% IPA indicate good soil column test performance when flushed through the aquifer soils containing DNAPL. Preliminary performance criteria included high removal of the PCE in three pore volumes and a low hydraulic gradient, which indicates low in-situ viscosity of the microemulsion that forms as the surfactant solubilizes the PCE. A low hydraulic gradient is even more critical in this project than usual because of the low hydraulic conductivity at the site, especially the bottom two feet of the saturated zone containing the highest saturations of DNAPL just above the clay aquitard, where the hydraulic conductivity is only about 0.0002 cm/s.

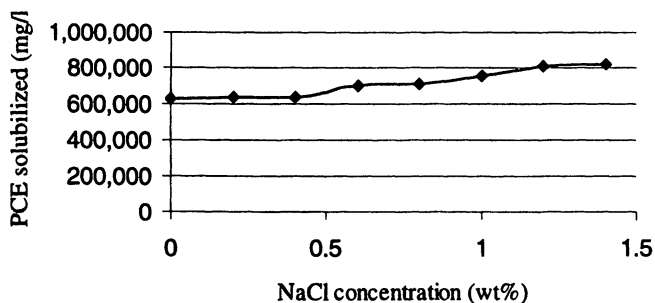


Figure 2. PCE Solubilization vs. Salinity for
4 wt% (80/20) Glucopon 625FE/Aerosol MA-80I,
0.3 wt% CaCl₂, 8 wt% IPA

Table 3. Comparison of Viscosity Measurements for Selected Surfactant Systems

Surfactant System	IPA (wt%)	NaCl (wt%)	CaCl ₂ (wt%)	PCE (vol%)	Equilibrium Viscosity (cp)
Aerosol MA-80I/Aerosol OT-100 (65/35) – 8% active	8	1.20	0.1	0.00	2.16
	8	1.20	0.1	1.00	2.10
	8	1.20	0.1	10.00	4.86
	8	1.20	0.1	25.00	3.83
	8	1.20	0.1	50.00	5.11
Glucopon 625FE/Aerosol MA-80I (90/10) – 4% active	8	1.00	0.4	0.00	2.63
	8	1.00	0.4	1.00	7.03
	8	1.00	0.4	5.00	7.77
	8	1.00	0.4	10.00	17.64
	8	1.00	0.4	25.00	6.54
	8	1.00	0.4	50.00	6.71
Glucopon 625FE/Aerosol MA-80I (80/20) – 4% active	8	0.5	0.3	1.00	37.06
	8	0.5	0.3	5.00	7.70
Isalchem 145- PO (3.8) sulfate – 4% active	16	0.6	0.1	0.00	2.04
	16	0.6	0.1	1.00	2.44
	16	0.6	0.1	10.00	6.08
	16	0.6	0.1	25.00	5.99
	16	0.6	0.1	50.00	7.14

While higher extracted surfactant concentrations resulting from an injectate consisting of 16 wt% Aerosol MA-80I would improve the relative filtration efficiency of the MA-80I in comparison to an 8 wt% injected solution, Aerosol MA-80I recovery using a UF membrane with a reasonable flux, e.g. as would be obtained with a nominal 5-10K MWCO membrane, is still poor. Increasing the surfactant concentration also has the undesirable effect of making PCE removal from the surfactant more difficult. Thus, a vigorous search for an alternative surfactant was undertaken once more. Being the only system that had been identified to have acceptable subsurface performance thus far, the Aerosol MA-80I was set aside as a backup surfactant.

New propoxylated sulfate surfactant results

Recently, a new surfactant with promising phase behavior in the presence of PCE and a low CMC (0.1 mM (20)) has been synthesized by Condea Vista especially for these University of Texas phase behavior studies. General surfactant information and phase behavior results are provided in Tables 1 and 2 respectively. The new surfactant was made by propoxylating and sulfating a branched alcohol known as Isalchem 145 with an average carbon number of about 14. The average number of propylene oxide (PO) groups is 3.8. Phase behavior and viscosity studies indicated that 16 wt.% IPA is required to give low viscosity microemulsions. However, the solubilization ratio is about 8 times higher than Aerosol MA-80I; in addition, testing with the pervaporation and ultrafiltration membranes has shown that VOC removals in the presence of the Isalchem 145- 3.8 PO sulfate are comparable to the Aerosol MA-80I and the filtration efficiency is > 90% using a 5-10K MWCO membrane. A 4 wt% active solution with 0.1 wt% CaCl₂, 0.6 wt% NaCl and 16 wt% IPA at pH=4 solubilizes 490,000 mg/l of PCE. The viscosity ranges from about 2 to 7 cp depending on the PCE concentration (see Table 3). Additional studies, including column experiments, are in progress to further evaluate this new surfactant, but at this time it appears to be the best choice of all of the candidates studies for this project. A comprehensive treatment of the phase behavior and soil column studies performed with Isalchem 145-3.8 PO sulfate will be provided in another paper.

Summary and Conclusions

Many challenges have been encountered thus far in the selection of a surfactant for the MCB Camp Lejeune site that has optimum properties for both PCE removal and surfactant regeneration. The results of the phase behavior studies stress the necessity of a successful surfactant system to be robust with respect to pH, groundwater electrolytes, and alcohol. Furthermore, this study shows that the fast equilibration of the mixtures to low viscosity microemulsions over a large range of organic contaminant concentrations can be as important as the surfactant's capacity for solubilization. Since most of the surfactants investigated have required the addition of alcohol as co-solvent for satisfactory viscosity characteristics, it seems inevitable that methods for co-solvent recovery will need to be included alongside processes for surfactant recovery to provide the full cost benefit of material recycle in SEAR.

As the SEAR technology moves toward commercialization, the economics of the surfactant remediation process, which is closely tied to the fieldtime required to accomplish site remediation is evermore significant. Sites with low permeability formations, such as the Lejeune site, are clearly pushing the performance boundaries of available surfactant systems. Thus, the long-term viability of the technology will rely on the continuation of ongoing efforts to expand the performance of already-identified surfactants as well as to explore the potential of new classes of surfactants. This paper shows how a systematic laboratory investigation can be used to overcome very difficult problems and identify an excellent surfactant candidate for the site specific conditions.

Acknowledgements

The authors wish to thank the U.S. Naval Facilities Engineering Service Center in collaboration with United States Environmental Protection Agency National Risk Management Research Laboratory for funding this research project. The authors would also like to acknowledge the invaluable contributions of the project team members: Leland Vane with the U.S. EPA NRMRL, Cincinnati, OH for his expertise on pervaporation and the overall treatment train for surfactant recovery; Lynn Wood at the U.S. EPA NRMRL, Ada, OK for his assistance with the subsurface design and field analyses; Jeff Harwell, John Scamehorn, and Edwin Tucker at the University at Oklahoma, Norman, OK for their soil column testing, MEUF design and general input on all issues; and John Londergan and Fred Holzmer at Duke Engineering & Services, Austin, TX, for their excellent field support and superior understanding of the site hydrogeology. We especially wish to thank Larry Britton of Condea Vista for synthesizing and providing to us in a very short time period several batches of new surfactant for this laboratory investigation.

Literature Cited

- (1) West, C.C. Harwell, J.H. *Environ. Sci. and Technol.* **1992**, *26*, 2324-2330.
- (2) Brown, C.K., Pope, G.A., Delshad, M. et al. *J. Am. Chem. Soc.*, in press.
- (3) Dwarakanath, V., Pope, G.A., Shotts, D. et al. *J. of Contaminant Hydrology*, in press.
- (4) *Demonstration of Surfactant-Enhanced Aquifer Remediation of Chlorinated Solvent DNAPL at Operable Unit 2, Hill AFB, Utah*, Air Force Center for Environmental Excellence, Technology Transfer Division, Brooks Air Force Base, San Antonio, Texas and OO-ALC/EMR, Hill Air Force Base, Ogden, Utah, January **1998**.
- (5) *AATDF Surfactant/Foam Process for Aquifer Remediation*, DOD Grant No. DACA39-93-1-001, Advanced Applied Technology Demonstration Facility, Rice University, Houston, TX, **1997**.
- (6) Krebs-Yuill, B., Harwell, J.H., Sabatini, D.A., Knox, R.C. Chap. 19, In *Surfactant-Enhanced Subsurface Remediation, Emerging Technologies*, Sabatini, D.A., Knox, R.C., Harwell, J.H. Eds. American Chemical Society Symposium Series 594, Washington D.C., **1995**.

- (7) Sabatini, D.A., Knox, R.C., Harwell, J.H. "Surfactant-Enhanced DNAPL Remediation: Surfactant Selection, Hydraulic Efficiency, and Economic Factors", U.S. Environmental Protection Agency, EPA/600/S-96/002, Ada, OK, August 1996.
- (8) *AATDF Technology Practices Manual for Surfactants and Cosolvents: Second Edition*, Advanced Applied Technology Demonstration Facility Program, Rice University, Houston, Texas, December 1997.
- (9) Jiang, J-S., Vane, L.M., Sikdar, S.K. *J. Membr. Sci.* **1997**, *136*, 233-247.
- (10) Vane, L.M. Section 7.5, In *Standard Handbook of Hazardous Waste Treatment & Disposal, 2nd edition*, Freeman H. Ed. McGraw Hill, New York, 1998.
- (11) Christian, S.D., Tucker, E.E., Scamehorn, J.F. "Colloid-enhanced ultrafiltration in remediating wastewater and groundwater", published in the *Proceedings of Chemical Specialities USA 94 Symposium*.
- (12) Harwell, J.H., unpublished work.
- (13) Christian, S.D., Scamehorn J.F. Chap. 1, In *Surfactant-Based Separation Processes*, Scamehorn, J.F., Harwell, J.H. Eds. Surfactant Science Series, Vol. 33, New York, 1989.
- (14) Pope, G.A., Wade, W.H. Chap. 11, In *Surfactant-Enhanced Subsurface Remediation, Emerging Technologies*, Sabatini, D.A., Knox, R.C., Harwell, J.H. Eds. American Chemical Society Symposium Series 594, Washington D.C., 1995.
- (15) Shiau, B-J., Sabatini, D.A., Harwell, J.H. *Environ. Sci. Technol.* **1995**, *29*, 2929-2935.
- (16) Dwarakanath, V. Ph.D. Dissertation, The University of Texas at Austin, TX, 1997.
- (17) Baran Jr., J.R., Pope, G.A., Wade, W.H., Weerasooriya, V. *Prog. Colloid Polym. Sci.* **1998**, *109*, 74-84.
- (18) Choori, U.N. M.S. Thesis, The University of Oklahoma, Norman, OK, 1994.
- (19) Vane, L.M., Alvarez, F.R., Hitchens, L., Jiang, J-S. "Separation of Volatile Organic Compounds from Surfactant Solutions By Pervaporation", ACS Symposium Series, in press.
- (20) Tucker, E.E., unpublished work.
- (21) Kumpabooth, K., Scamehorn, J.F., Osuwan, S., Harwell, J.H., "Surfactant Recovery from Water Using Foam Fractionation: Effect of Temperature and Added Salt", in press.

Chapter 4

Soil Remediation with Microemulsions: Basic Properties

F.-H. Haegel, F. Dierkes, S. Kowalski, K. Mönig, M. J. Schwuger,
G. Subklew, and P. Thiele

Forschungszentrum Jülich, Institut für Chemie und Dynamik der Geosphäre,
Institut 7: Angewandte Physikalische Chemie, D-52425 Jülich, Germany

Soil remediation with microemulsions requires various separation procedures including solid/liquid extraction, solid/liquid separation, liquid/liquid extraction, and liquid/liquid separation for removal of the contaminant and reuse of the microemulsion. Bicontinuous microemulsions with 39-45 % of rape oil methyl ester (RME) and O/W microemulsions with < 1 % RME content were used to extract polycyclic aromatic hydrocarbons (PAH) or polychlorinated biphenyls (PCB) from soil material. Bicontinuous microemulsions with nonionic surfactants may preferably be used for *ex situ* treatment of contaminated fine fractions of soil, whereas O/W microemulsions or bicontinuous microemulsions with mixed nonionic and anionic surfactants were found to be suitable for *in situ* application. Extraction is complete with bicontinuous microemulsions and fairly good with O/W microemulsions. The temperature-dependent phase behavior allows the partial separation of the contaminant from bicontinuous microemulsions and the reuse of the major part of the surfactant. O/W microemulsions loaded with pollutants can be recycled by liquid/liquid extraction with excess oil.

Soil remediation is a classical separation process. Pollutants which have penetrated the soil or were mixed into it are to be removed from the solid matrix. They may be present as phase, dissolved in water, evaporated in air, or adsorbed at the surface of particles. Separation is achieved by using differences in the chemical and physical behavior of pollutant and matrix. Degradability, volatility, adsorptiveness, and solubility may be used to remove hazardous organic compounds from soil.

Thermal and biological remediation techniques are used to degrade organics by pyrolysis and combustion or by microorganisms, respectively. Pneumatic techniques are based on the volatility of pollutants. The classical soil washing process uses the adsorptiveness of pollutants. Due to the large interfacial area fine particles strongly

adsorb the pollutants. Separation of the highly contaminated fine fraction from coarse grains enables the partial reuse of soil.

Often combinations of different techniques must be used. Soil washing for example is only possible at relatively low cost for soils with a fine particle content of lower than 35 % (1). A process which is able to further decontaminate the fine fraction can help to increase this value. Attempts to remove hydrophobic contaminants with volatile organic solvents (2) and surfactants (3) are known from the literature. However they are often not effective enough, are ecologically critical or too expensive. The unique properties of microemulsions may help to overcome these shortcomings.

Besides the use for *ex situ* treatment of soil material (4), microemulsions may be used for *in situ* application, too (5, 6). However, such a process is much less controlled and additional needs have to be fulfilled. Stability of the microemulsion and complete biodegradation of the components under the conditions in the soil is required. Legislative restrictions may also influence the economics of the process.

Fundamentals

Properties of Microemulsions. Microemulsions are thermodynamically stable, optically isotropic dispersions of two non-miscible liquids, liquid mixtures or solutions that are stabilized by at least one amphiphilic component. They are different from emulsions and ordinary solutions and exhibit the useful properties of both types of liquid systems.

Whereas the production of emulsions needs a high level of mechanical or thermal energy, microemulsions usually form spontaneously by mixing the components. The process may be sometimes inhibited by the slow dissolution of solids or liquid crystals used as starting materials or formed in the mixture. This problems can, however, be overcome by proper premixing of the components or a gentle temperature increase.

Microemulsions have a microscopic structure consisting of domains of the non-miscible liquids, e.g. water and oil, separated by an amphiphilic layer. According to the fast dynamic changes of the structure, there is no long-range interaction of the domains and amphiphilic layers. Thus microemulsions are not liquid crystalline and show no optical birefringence. They usually exhibit moderate Newtonian viscosity.

Due to their microscopic structure microemulsions with water and oil are good solvents for hydrophilic and hydrophobic compounds. They show excellent wetting of hydrophobic and hydrophilic surfaces. The dynamics of the system usually enable high mass transfer rates. All these properties make microemulsions interesting for extraction processes in general and for soil remediation in particular.

Partial separation of extracted non-volatile compounds from the microemulsion can be achieved by temperature change (7) or liquid/liquid extraction with excess oil (8). Both possibilities will be discussed in detail later on. Volatile compounds may be separated by evaporation techniques, like air stripping. Foaming of surfactant containing systems, however, makes these separation processes difficult. Suppression of foaming is the key to more effective soil remediation processes with surfactant systems. Technological progress in this field is urgently required.

Phase Behavior of Microemulsion Systems. According to their definition microemulsions contain at least three components, e.g. water, oil and surfactant. The phase behavior of these ternary mixtures at constant pressure and temperature is described by a Gibbs triangle showing the one-, two- and three-phase regions depending on composition. Two independent variables are needed to determine the composition in the Gibbs triangle. It is most convenient to use the mass fraction α of oil in the binary oil-water mixture and the mass fraction γ of surfactant in the ternary system.

A stack of Gibbs triangles at different temperatures forms a prism (Figure 1). Vertical sections through the prism result in pseudobinary phase diagrams. Planes which include the edge representing the pure surfactant will cut an area from the prism which shows the phase behavior at constant α . Sections parallel to the oil-water area result in pseudobinary phase diagrams at constant γ .

Microemulsions with Nonionic Surfactants. Microemulsion-forming systems with sufficient amount of nonionic surfactant will have a phase behavior which is shown schematically in Figure 2. Two different two-phase areas are separated by a single-phase region, for which the structure is schematically inserted into the diagram. At low oil content and low temperature oil droplets in water are formed resulting in an O/W microemulsion. Vice versa, a W/O microemulsion is formed at low water content and high temperatures. In between a gradual change of structure is observed resulting in a sponge-like structure at comparable amounts of oil and water. This type of microemulsion is called bicontinuous.

For many purposes the most suitable type of phase diagram is obtained by a vertical section at constant α . The phase boundaries of systems forming bicontinuous microemulsions have the shape of a fish (Figure 3), whose body represents a three-phase region 3ϕ and the tail the single phase microemulsion 1ϕ . For systems with nonionic surfactants the "fish" is surrounded by two different two-phase regions 2ϕ at lower and 2ϕ at higher temperatures. In 2ϕ the surfactant is much more soluble in the aqueous phase. If the temperature is increased the surfactant becomes more oil-soluble. In 2ϕ most of the surfactant is dissolved in the oil phase.

The position of the "fish" on the temperature scale can be expressed by the transition temperature \bar{T} from 3ϕ to 1ϕ . It depends on the chemical nature of the components chosen (9). The more hydrophobic the oil for a given surfactant, the higher is the position of the fish on the temperature scale. Enhanced hydrophobicity of the surfactant for a given oil, however, shifts 3ϕ to lower temperatures. In such systems liquid crystalline phases (LC) often appear in 1ϕ and reduce its extension or sometimes even prevent its existence.

After extraction of the soil material with a microemulsion of composition α and γ_{ex} at temperature T_{ex} an excess oil phase can be separated by cooling to the splitting temperature T_{sp} . The surfactant will preferably be dissolved in the aqueous phase, whereas hydrophobic contaminants can be removed with the oil phase. The microemulsion can be reformed by increasing the temperature to T_{ex} and adding the lacking components.

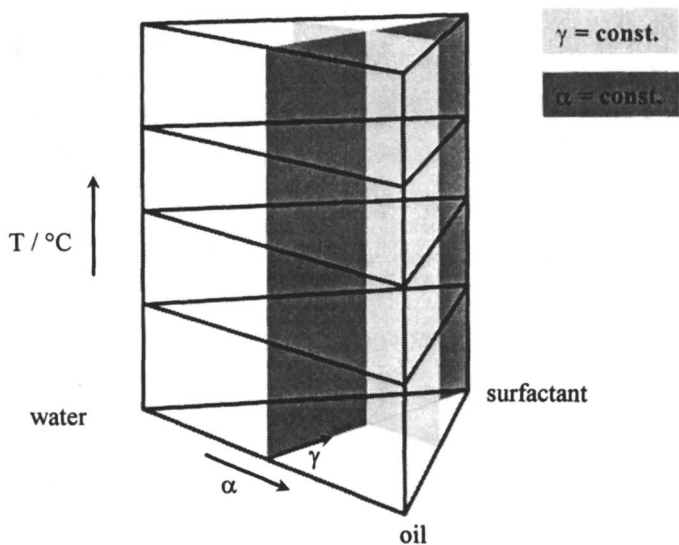


Figure 1. Phase prism of a microemulsion system with vertical sections at constant α and γ .

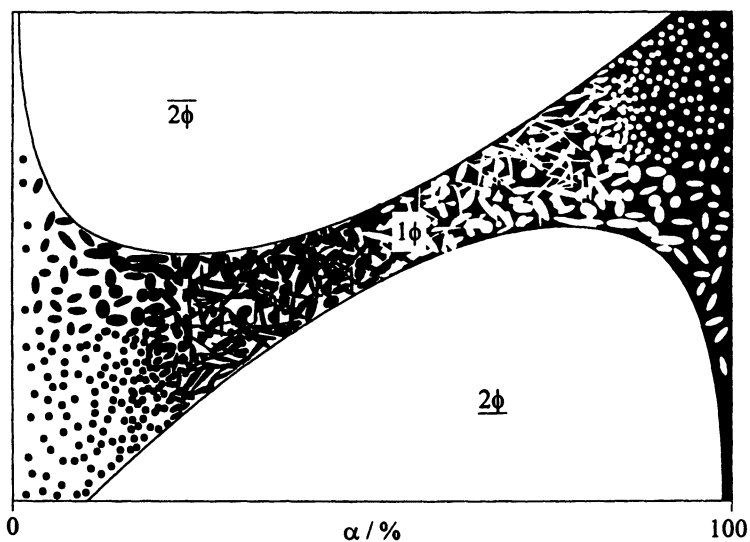


Figure 2. Pseudobinary phase diagram of a microemulsion with nonionic surfactant at constant γ .

Microemulsions with Ionic Surfactants. Microemulsions with ionic surfactants show the reverse phase behavior. In this case the surfactant is more soluble in oil at lower temperatures and more soluble in water at higher temperatures. The influence of the hydrophilicity and hydrophobicity of oil and surfactant are also reverse, e.g. using more hydrophobic oils results in a decrease of \tilde{T} . Most important for the phase behavior of ionic microemulsion systems is the strong influence of electrolyte. Increase of salt concentration results in a shift of \tilde{T} to higher temperatures and in a reduction of liquid crystals. The salt content is best expressed as the mass fraction of salt ϵ in its binary aqueous solution. Usually brine is used as a pseudocomponent instead of water in the phase diagrams.

Splitting of ionic microemulsion systems into an excess oil phase and an aqueous surfactant-rich phase is achieved by increasing the temperature. This behavior makes those systems interesting for *in situ* remediation. Since the temperature in the soil of temperate latitudes is about 10 °C, heating of the microemulsion is much more convenient than cooling.

Microemulsions with Mixtures of Nonionic and Ionic Surfactants. The fundamental behavior of mixed systems of brine, oil, nonionic surfactant and ionic surfactant has been described by Kahlweit et al. (10) (Figure 4). The surfactant mixtures show either ionic or nonionic behavior depending on the mixing ratio. The mass fraction of the ionic component in the binary surfactant mixture is expressed as δ . At low δ the system forms a microemulsion of the nonionic type. Increasing δ leads to higher \tilde{T} . The increase of the transition temperature becomes steeper and steeper. At some δ the behavior changes to an ionic type. \tilde{T} rises very steeply from low temperatures and increases less and less with increasing δ .

Choice of Components. A microemulsion used as an extraction medium in soil remediation should be stable in an adequate temperature and concentration range. Its components must be biodegradable, readily available and cheap. Most surfactants used today in commercial detergents fulfill these requirements in aqueous solution. The degradation behavior in soil is much less familiar. Additional investigations under aerobic and anaerobic conditions are therefore needed for the system of choice before its application in soil.

Surfactants. Nonionic surfactants of the polyethoxylate type are suitable for forming biodegradable bicontinuous microemulsions for the *ex situ* treatment of contaminated soil. For *in situ* application attention has to be paid to further requirements. The temperature range is fixed at about 10°C and extensive separation of the pollutant is required to reuse the microemulsion. O/W microemulsions can be formed by most types of surfactant. Degradation in soil was shown for C_{12/14}E₁₀ (11). Bicontinuous microemulsions can be obtained with mixtures of anionic and nonionic branched and double chain surfactants (6) in order to suppress liquid crystal formation. Ethoxylated castor oil and dialkyl sulfosuccinates have been found suitable. However, nothing is known about the biodegradation of the components in soil.

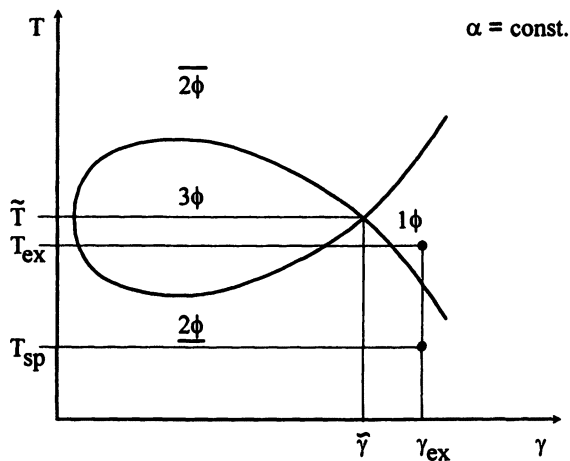


Figure 3. Pseudobinary phase diagram of a microemulsion with nonionic surfactant at constant α .

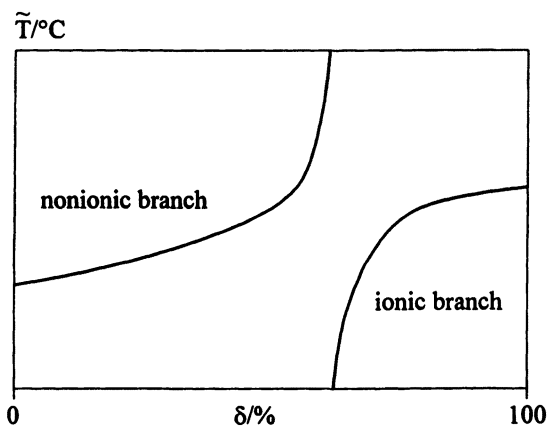


Figure 4. Schematic representation of \tilde{T} for microemulsions with mixed nonionic and ionic surfactants.

Oils. Liquid crystals are preferentially formed in systems composed of long-chained oils (12). Therefore triglycerides are less suitable. Besides, they form bicontinuous microemulsions only at high temperature and high surfactant content (7). Rape oil methyl ester (RME), which is produced in large amounts as a diesel substitute, is an ideal oil. It combines good degradability, economy and solvent properties. Other fatty acid esters or essential oils may be used instead.

Remediation Processes with Microemulsions. The process, schematically shown in Figure 5, can be used for the *ex situ* remediation of soils, silt and clay fractions contaminated with non-volatile pollutants (13). Within this concept, the contaminated soil is intensively mixed with a microemulsion of biodegradable components. The extraction process is followed by a solid/liquid separation yielding a decontaminated soil and the microemulsion containing the contaminants. After phase separation by lowering the temperature, the aqueous surfactant-rich phase is recycled for further extraction. The contaminated oil phase has to be degraded, incinerated or disposed of. In the case of PAH, degradation by microorganisms is possible (11). The residual components of the microemulsion on the soil can be removed by rinsing and biodegradation.

The *in situ* application of O/W microemulsions for non-volatile contaminants requires a different process (Figure 6). The microemulsion is infiltrated into the soil and takes up the contaminant during transport to the extraction well. After passing through the soil the O/W microemulsion is mixed with excess oil. The emulsion formed is separated by using a centrifuge. The oil phase loaded with the pollutant can be treated in the same manner as for the *ex situ* process.

Experimental

Materials. Triply distilled water was used for the studies on bicontinuous microemulsions with nonionic surfactants. Microemulsions with mixed nonionic and anionic surfactants were prepared with water of ultrapure grade produced in our own laboratory by electrodeionization (14). O/W microemulsions were formed with deionized water in our laboratory or with tap water at the laboratory of Westfalia Separator GmbH, Oelde.

Pyrene of 99 % purity was purchased from Janssen Chimica; Brueggen-Bracht. PCB were obtained from Promochem, Wesel. Single PCB of 99 % purity were used for doping the soil. Standard mixture N 0813 with $10 \text{ ng } \mu\text{l}^{-1}$ of each PCB in isooctane was chosen for calibration and doping of RME for liquid/liquid separation. The purity of the single components was 99 %. Hexachlorobenzene (Aldrich, Steinheim) of 99 % purity was used as the internal standard for GC-ECD of PCB.

Alkyl polyethoxylates (C_iE_j ; i = chain length, j = degree of ethoxylation) were used as surfactants for nonionic systems. Synperonic 91/ j surfactants ($\text{C}_9/11\text{E}_j$) were supplied by ICI Surfactants, Essen. Marlipal 24/ x $\text{C}_{12/14}\text{EO}_j$ ($j = 0.1 \cdot x$) were a gift from Hüls, Marl. AOT (sodium bis (2-ethylhexyl) sulfosuccinate) and Tergitol TMN 6 (hexaoxyethylene 2,5,8-trimethylnonanol) were obtained from Fluka, Buchs. The ethoxylated castor oil Emulan EL was supplied by BASF, Ludwigshafen.

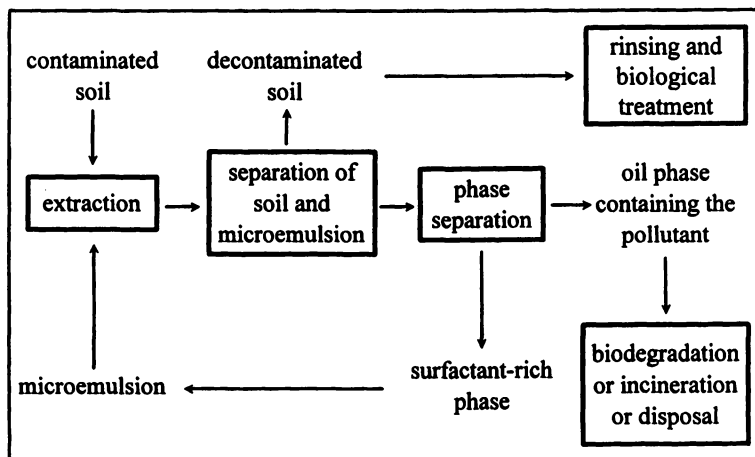


Figure 5. Schematic representation of *ex situ* treatment of contaminated soil with bicontinuous microemulsion.

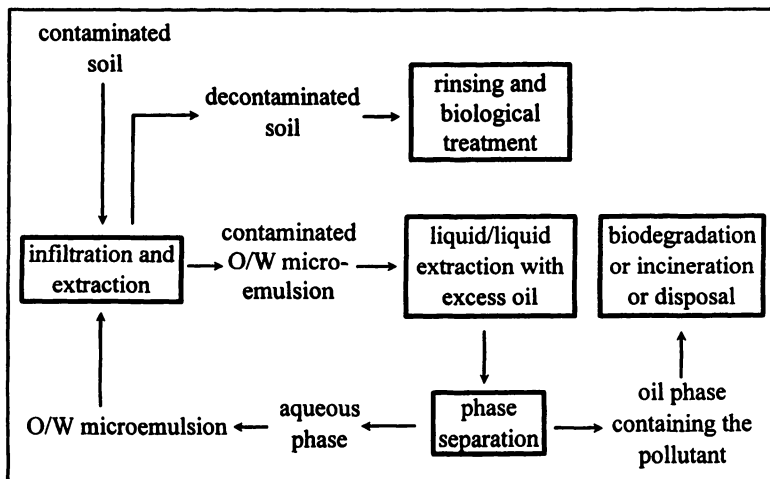


Figure 6. Schematic representation of *in situ* remediation of contaminated soil with O/W microemulsion.

Rape oil methyl ester (RME) produced by base-catalyzed transesterification of rape oil with methanol was supplied by GET, Jülich. RME of technical grade from a gas station in Düren was used for liquid/liquid extraction with O/W microemulsion and for the formation of microemulsions with mixed nonionic and anionic surfactants.

Extraction experiments with nonionic bicontinuous microemulsions were performed with an air-dried fine silt fraction from the hydrocyclone outlet of a soil washing plant. It was contaminated with more than 3000 mg PAH per kg soil (16 EPA PAH). The content of pyrene was about 400 mg kg⁻¹. Furthermore the material contained about 13.5 % (w/w) of organic carbon. Extraction experiments with O/W microemulsions were performed on an air-dried sandy soil sample (85 % < 500 µm) from a PAH contaminated site in Düsseldorf-Heerdt. The silt fraction (< 63 µm) was about 13 %. The content of pyrene was 160 ± 20 mg kg⁻¹. For the extraction with microemulsions of mixed nonionic/anionic type an orthic luvisol (A-horizon) was dried on air, fractionated by sieving (< 200 µm) and doped with the six Ballschmitter PCB, no. 28 (4.12 mg/kg soil), no. 52 (2.79 mg/kg soil), no. 101 (3.66 mg/kg soil), no. 153 (2.56 mg/kg soil), no. 138 (6.78 mg/kg soil), no. 180 (3.83 mg/kg soil); nomenclature according to (15). The size of the particles was very small. More than 95 % (w/w) of the particles were smaller than 63 µm. The water content was between 3-4 % (w/w).

Methods.

Determination of Phase Diagrams. Samples with different compositions of water or brine, surfactant and oil were weighed into test tubes with volume scale and thermostatted in a water bath. After reaching bath temperature the samples were shaken and remained in the water bath until equilibrium. The number of coexisting phases was detected visually. LC phases were identified by crossed polarizers. This procedure was performed at different temperatures, in steps of 2 °C (nonionic systems) and 2.5 °C (anionic/nonionic systems) near the phase boundaries.

Doping of Soil with PCB. 500 g of an orthic luvisol fraction with particle size < 200 µm was suspended in 500 g of hexane. 10 ml of a doping solution of the six Ballschmitter PCB was added to the mixture. The suspension was stirred for 15 min and left for 2 h. The solvent was evaporated on air in a hood. During this procedure, which took several days, the mixture was occasionally homogenized. Doping had been performed about 3 years before extraction.

Extraction with Nonionic Bicontinuous Microemulsion. 5 g of the contaminated fine soil material was treated with 30 g of the microemulsion in a glass vessel with a mechanical stirrer at 200 rpm in a water bath at 43 °C. In order to avoid considerable evaporation of water, the container was mounted with a cover which had a bore as narrow as possible for the shaft of the stirrer. After two hours stirring was stopped and the vessel was left in the water bath overnight in order to achieve complete sedimentation of the soil. The pyrene concentration was determined in the supernatant.

Extraction with O/W Microemulsion. 5g of the air-dried PAH-contaminated soil from Düsseldorf-Heerdt was extracted with 30 ml of different O/W microemulsions. The samples were shaken for 24 h at 10 °C and 250 rpm in an incubator shaker from New Brunswick Scientific, Edison, N.J.. After centrifugation with a Centrikon T-324 from Kontron Instruments, Munich, at 10 °C and 20,000 rpm the pyrene content in the supernatant was determined.

Extraction with Anionic/Nonionic Bicontinuous Microemulsion. 3.3 g of soil and 10 g of microemulsion were weighed into Duran bottles (50 ml) equipped with a Teflon-coated magnetic stirrer. The bottles were tightly closed and placed into a water bath at 10 °C. The dispersion was stirred at 400 rpm for 3 hours. After this time the stirrer was switched off and the soil started to sediment. After about 12 hours the Duran bottle was opened and a few milliliters of the microemulsion was filtered through a 0.45µm filter (type Spartan 13/20 from CS-Chromatographieservice, Langerwehe) with a Hamilton syringe (2.5 ml, gastight).

Distribution of Pyrene after Splitting. For the determination of the distribution of pyrene between the polar and the non-polar phase after splitting bicontinuous microemulsions the same procedures were chosen as described under "Phase Diagrams". The only differences were:

- i The oil was artificially doped with a certain amount of pyrene or PCB.
- ii Initially, an appropriate temperature was chosen to form a microemulsion, then the samples were cooled or heated for phase separation.
- iii In order to reach complete demulsification under gravity and equilibration the samples were stored for periods ranging from one day up to two weeks at constant temperature.

Determination of Pyrene. The determination of pyrene on soil was performed by a kind of Soxhlet extraction with toluene. The soil was filled into a glass cylinder with frit at the bottom, so that only the solvent could pass the frit. The soil was extracted for 4 h. The pyrene concentration was determined by means of UV derivative spectroscopy (Kontron Uvikon 860) at 333 nm. The samples were diluted by a factor of 100 with propane-2-ol and measured in 10 mm QS cuvettes from Hellma.

Determination of PCB. PCB were extracted in the same manner as pyrene. The soil was extracted for 8 hours and the extract was cleaned up and analyzed by gas chromatography with ECD detection as described below.

The filtered microemulsion was analyzed by a special analytical procedure. The internal standard (hexachlorobenzene dissolved in n-hexane) and 200 µl of boron trifluoride etherate were added to 100 µl of microemulsion. The vial was closed and after about 12 hours the solution was cleaned up by column chromatography with an 8 cm glass column using silica gel. The PCB were eluted with 4 ml n-hexane. Then 5 µl n-dodecane was added to the eluate and n-hexane was removed by a light argon stream (purity: 5.0). The analytes were taken up in 100 µl toluene and analyzed by a gas chromatograph (Carlo Erba, GC 6000 Vega series 2) equipped with an ECD detector and an on-column injector. A 60 m × 0.32 mm i.d. DB-5 column from J&W

was used for the separation of PCB with the following temperature program: 80 °C (2 minutes) → 10 °C/min → 170 °C → 3 °C/min → 270 °C → 5 °C/min → 320 °C (5 minutes). Helium (purity: 5.6) was used as the carrier gas (150 kPa) and nitrogen (purity: 5.0) as the make-up gas (175 kPa). In addition, the carrier gas was purified by a moisture trap obtained from Fisons.

Determination of Surfactants and Oil. Surfactants and RME were analyzed by HPLC. For the determination of the surfactants a Nucleosil column (CS-Chromatographieservice, Langerwehe) with 10 cm × 4 mm i.d. was used. The analytes were eluted with a mixture of methanol/water (70/30 v/v) and a flow rate of 0.6 ml/min using a Merck-Hitachi L-6200A pump. A differential refractometer (ERC 7512) was used as the detector. RME was also determined with the same type of column and the same flow rate, but the eluent was a mixture of methanol/water (90/10 v/v). In this case the chromatographic system consisted of a Gynkotec M480 pump and a differential refractometer (Shodex RI-71).

Results and Discussion

Microemulsion Formulation. Three different systems were used to extract PAH or PCB from different soil materials. A bicontinuous microemulsion with nonionic surfactant was used to simulate *ex situ* treatment. An O/W microemulsion and a bicontinuous microemulsion with a mixture of anionic and nonionic surfactants were prepared for experiments under *in situ* conditions. All types of surfactants used in these studies are degradable according to OECD standards. Rape oil methyl ester (RME) was used throughout as the oil component. Purity of water and source of RME were not found to affect the phase behavior of the microemulsions used in these studies.

Bicontinuous Microemulsions with Nonionic Surfactants. Two alkyl polyethoxylates C_{9/11}E_j with an average degree of ethoxylation *j* of 4 and 5 were chosen for microemulsion formation. Figure 7 shows the phase diagrams obtained for α = 50 %. The phase boundaries are considerably skewed compared to the nearly ideal features found for pure surfactants. The deviations are due to the presence of more and less hydrophobic components in the technical mixtures (16).

The behavior typical of C_iE_j is found. The less *j*, i.e. the more hydrophobic the surfactant, the lower the temperature range for 3φ and 1φ. Extended liquid crystalline phases (LC) cover parts of 1φ. C_{9/11}E₅ forms microemulsions with RME and water in a suitable temperature range between 39 and 60 °C. The crossing of the phase boundaries is found at $\tilde{T} = 60$ °C and $\tilde{\gamma} = 20$ %. C_{9/11}E₄ makes even more moderate temperatures between 30 and 47 °C available. For this ternary system the values of $\tilde{T} = 47$ °C and $\tilde{\gamma} = 20$ % are obtained. Further reduction of *j* results in a growing liquid crystalline phase compared to the extension of 1φ, thus restricting the use for extraction more and more.

Lowering the temperature range can also be achieved by decreasing the oil content (Figure 8). For α = 30 % the bicontinuous microemulsion already forms at

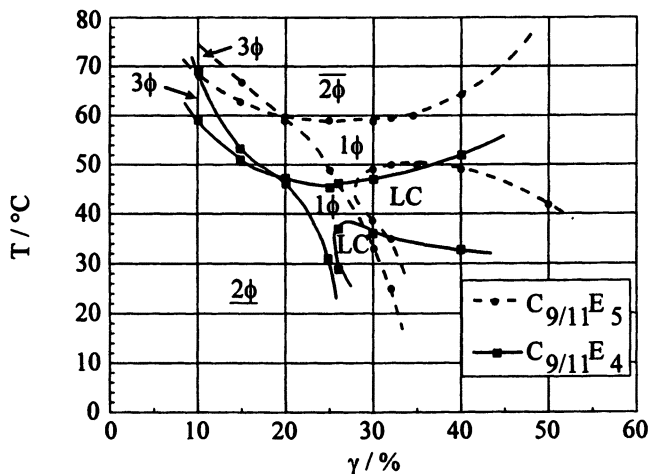


Figure 7. Pseudobinary phase diagram for two microemulsions with two different alkyl polyethoxylates at constant α .

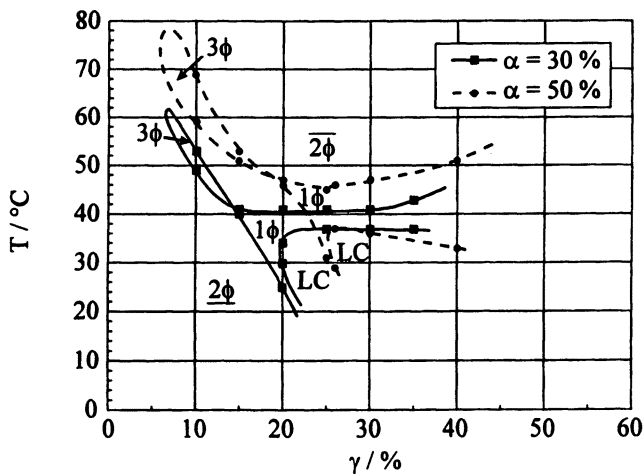


Figure 8. Pseudobinary phase diagram for microemulsions with $C_{9/11}E_5$ at two different α .

$\tilde{T} = 40\text{ }^{\circ}\text{C}$ and $\tilde{\gamma} = 15\%$ with $\text{C}_{9/11}\text{E}_4$. Reduction of temperature and surfactant content both favor the use of lower oil content, as long as the extraction capacity is not affected.

O/W Microemulsions with Nonionic Surfactants. This type of microemulsion was formed by adding RME to a solution of $\text{C}_{12/14}\text{E}_j$. Exact values of the composition are given later in Tables I and III together with results for the extraction of soil and the separation of the pollutant from the microemulsion. The oil content for extraction was below the saturation value. After liquid/liquid extraction with excess RME saturation is achieved and small amounts of the oil remain in the phase as emulsion droplets. They may be removed by filtration through a sand column. Since during *in situ* processes the microemulsion is diluted, it must be concentrated by membrane filtration for reuse.

Other nonionic or anionic surfactants and surfactant mixtures may be used for O/W microemulsions. The system should be optimized for maximum contaminant extraction, minimum adsorption on soil and minimum solubility in RME. The optimum surfactant depends on the contaminant, on the soil and on the groundwater properties. In particular the influence of calcium ions on anionic surfactants has to be taken into consideration.

Microemulsions with Mixed Nonionic and Anionic Surfactants. Figure 9 shows the phase behavior of a microemulsion formed by water, calcium chloride, RME, AOT and Tergitol TMN 6 with two different concentrations of calcium chloride. Small changes of the salt concentration yield large changes of \tilde{T} . With increasing calcium chloride concentration 3ϕ is shifted to higher temperatures. More surfactant is necessary to achieve 1ϕ at lower temperature. In order to split the microemulsion into two phases of type 2ϕ the system must be heated to higher temperatures. Therefore the addition of salt is unfavorable for splitting the microemulsion after extraction. On the other hand, increasing salt concentration suppresses the formation of liquid crystals. At $\epsilon = 0.3\%$ no liquid crystals are formed.

Complete suppression of liquid crystals for $\epsilon = 0.25\%$ can be achieved by replacing 10% (w/w) of the nonionic surfactant Tergitol TMN 6 by the very bulky castor oil ethoxylate Emulan EL. Since only small amounts of Tergitol TMN6 were replaced, the phase behavior was not changed significantly. The efficiency in forming 1ϕ and the phase boundary $1\phi/2\phi$ is not appreciably affected. Reduction of oil content does not result in favorable phase behavior of this microemulsion, but leads to the formation of liquid crystals.

Soil Extraction. Extraction with the nonionic bicontinuous microemulsion was performed with a highly contaminated fine fraction from a soil washing plant. The material was contaminated with PAH. Pyrene was determined as a representative PAH. O/W microemulsion was chosen to extract a soil from a contaminated site. The anionic/nonionic microemulsion was used for the extraction of PCB from a doped arable soil of orthic luvisol type.

Extraction with a Nonionic Bicontinuous Microemulsion. Extraction was performed at $\gamma = 22\%$ and $43\text{ }^\circ\text{C}$. Figure 10 shows the results of a multistep extraction of a fine soil fraction. The total amount of pyrene removed from the soil after each extraction step is presented. In the first extraction step about 10 % more pyrene was extracted than with a Soxhlet extraction using toluene as the solvent. For the second extraction step half the extraction liquid was replaced by fresh microemulsion. After this extraction step, within the error limits, significantly more pyrene was not removed from the soil. In the third and fourth steps 83 % of the liquid was replaced. No further dissolution of pyrene was observed.

Even if the extraction results are excellent multiple extraction will be necessary. Since the loaded microemulsion cannot be completely removed or flushed out from the solid, the pollutant content can only be reduced by dilution. The number of steps required depends mainly on the effectiveness of solid/liquid separation and will be discussed later on.

Extraction with an O/W Microemulsion. A real soil contaminated with PAH was extracted at $10\text{ }^\circ\text{C}$ with different systems containing alkyl polyethoxylates of type C_{12/14}E_j. The surfactant concentration was 50 g l^{-1} . The RME concentration was dependent on the surfactant and near the saturation limit. Extraction results for pyrene are listed in Table I.

Table I. Extraction Results for O/W Microemulsions

Surfactant	RME concentration / g l^{-1}	amount of extracted pyrene / mg kg^{-1}	extracted pyrene relative to toluene extraction / %
C _{12/14} E ₇	5	107	67
C _{12/14} E ₉	4	114	71
C _{12/14} E ₂₀	1.7	111	69

No significant difference was found for the three surfactants. The extraction yield was about 69 % relative to hot extraction with toluene. This value is considerably lower than the results obtained for the fine fraction with a bicontinuous microemulsion. It is nearly identical to extraction by surfactant solutions on the same material. Whether the extraction is sufficient or not depends on the actual situation. On this soil PAH were mainly in an adsorbed state. In such a case any reduction may result in a decrease of contaminant release from the site.

Since the addition of RME has no influence on the removal of the pollutant, surfactant solution may be used instead. However, saturation with RME will take place anyway in the successive liquid/liquid extraction. The uptake of the oil by surfactant solution may therefore decrease the separation of pollutant from the surfactant solution.

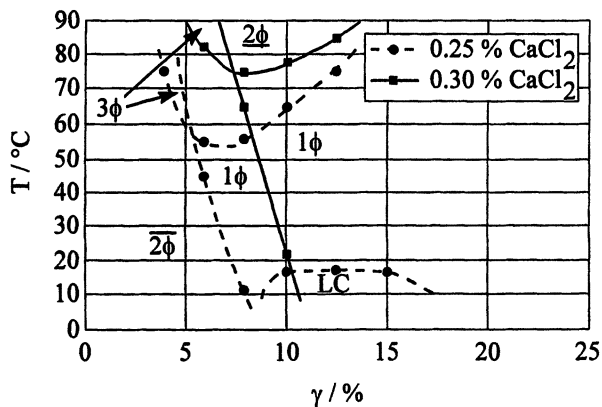


Figure 9. Pseudobinary phase diagram for a microemulsion with a nonionic and an anionic surfactant at constant α , δ and two different constant salinities ϵ .

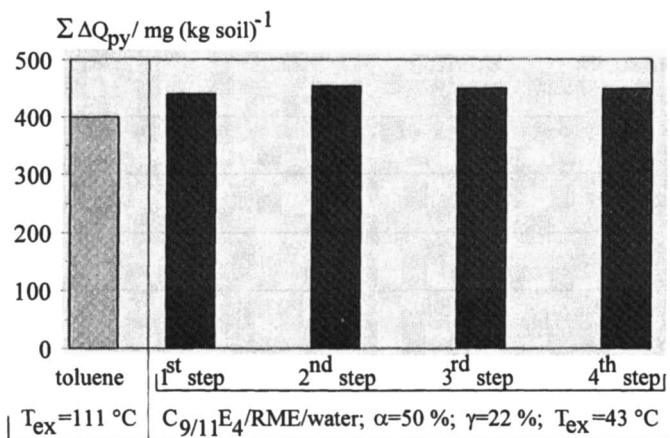


Figure 10. Extraction result for a PAH-contaminated fine fraction from the outlet of a soil washing plant.

Extraction with Anionic/Nonionic Bicontinuous Microemulsion. The extraction properties of the above-mentioned system with $\alpha = 50\%$, $\gamma = 10\%$, $\delta = 70\%$ (with 10% of Tergitol TMN 6 replaced by Emulan EL), and $\epsilon = 0.25\%$ CaCl_2 were investigated with a PCB-doped soil at 10 °C. The results of the batch experiment are listed in Table II and compared with the results obtained by hot extraction with toluene for 8 hours. Three independent extractions were performed in each case.

The results show that the extraction efficiency varies more or less for each PCB. It can be seen that the extraction efficiency of the sum of PCB is higher compared to toluene extraction. Comparing the sum of PCB with the sum of PCB doped on the soil, extraction was nearly complete. The relative deviation is between 2-6% for the determination of PCB in the batch experiment, whereas the relative deviations for the toluene extraction are higher and the deviations were larger with increasing chlorine content of PCB.

The PCB remaining in the soil were determined by toluene extraction after washing with water. Between 3-7% of the PCB remained on the soil. Adding the amounts of the batch extraction and the amounts on the soil, more than 100% was found for the total of PCB. Balancing the amount of PCB does not seem useful in this case. The problem is that part of the microemulsion system cannot be removed by flushing with water and remains on the soil. The adsorption of AOT was determined by the difference in the microemulsion after contact with the soil. It was found to be 14 g kg^{-1} . Adsorption of the nonionic surfactant was so low that it could not be detected. The batch extraction demonstrates the efficiency of microemulsions as extraction media for PCB. Flushing with water, however, will not be sufficient for the removal of microemulsion components remaining in the soil. Surfactant solution should be used instead.

Table II. Extraction Results for Anionic/Nonionic Microemulsion

PCB no.	doped amount / mg kg^{-1}	amount extracted by toluene / mg kg^{-1}	amount extracted by microemulsion / mg kg^{-1}	extraction relative to toluene / %	extraction relative to doping / %
28	4.12	3.85 ± 0.24	4.35 ± 0.20	113 ± 8	106 ± 5
52	2.79	2.81 ± 0.20	3.57 ± 0.21	127 ± 8	128 ± 8
101	3.66	3.79 ± 0.36	3.98 ± 0.12	105 ± 10	109 ± 3
153	2.46	2.56 ± 0.40	2.98 ± 0.09	116 ± 16	116 ± 4
138	6.78	5.16 ± 1.26	5.07 ± 0.16	98 ± 25	75 ± 2
180	3.83	3.00 ± 0.69	3.41 ± 0.06	114 ± 23	89 ± 2
sum	23.74	21.17 ± 1.57	23.37 ± 0.37	110 ± 12	98 ± 2

Solid/Liquid Separation. Solid/liquid separation is mainly needed for *ex situ* treatment. However, fine particles flushed out of the soil may also disturb the *in situ* process. Only preliminary experiments have been performed thus far. Pressure filtration of the fine fraction failed. However, those materials are usually treated in a chamber filter press. The water content can be reduced by this means to about 30 % (w/w) of the total mass of the soil material. Similar results can be expected for microemulsions.

Extraction of soil columns yielded only slightly enhanced turbidity for different soils. The particle content does not seem critical for the process. Experiments for the O/W microemulsion with a decanting centrifuge were not successful. This problem has to be further investigated.

Separation of the Pollutant. Whereas the contaminant can be separated partially from bicontinuous microemulsions by temperature change, O/W microemulsions must be extracted with excess oil. The economy of the process is strongly dependent on the part of contaminant which shall be removed. Since at the end of the process the contamination of the soil material can be controlled for *ex situ* treatment, this parameter is mainly determined by technical needs. For *in situ* remediation legislative regulations play an important role, if the microemulsion is to be reused.

Separation from a Nonionic Bicontinuous Microemulsion. Splitting of the nonionic bicontinuous microemulsion by temperature decrease yields partial separation of pyrene with the oil phase. The results obtained for model systems are shown in Figure 11. That part of pyrene $m_{py}/m_{py,0}$ which can be removed from the microemulsion is closely connected to the volume of the oil phase V_{OP} which separates from a microemulsion with the initial oil volume V_0 . With increasing temperature difference the separated amount of pollutant increases approximating to a certain limit (17). A temperature difference of about 20-25 K is sufficient to reduce the contaminant concentration in the microemulsion to about half of its initial value. The loss of surfactant by separation of the oil phase is nearly constant for all temperatures. About 10 % of $C_{9/11}E_4$ is dissolved in RME and must be replaced.

This reduction of contaminant concentration will be sufficient in a multiple step process as shown in Figure 12. After each extraction of the soil the surfactant is recovered separately by temperature-induced splitting and separation of the excess oil phase. The contaminant concentration in the recovered microemulsions of the successive extraction steps will be lower and lower, thus leading in the end to a considerable reduction of the pollutant remaining in the soil. A reduction to about 3 % of the initial amount of contaminant within three steps might be possible (17).

Separation from an O/W Microemulsion. Results obtained for the multiple extraction of pyrene with RME for an O/W microemulsion of RME in $C_{12/14}E_9$ aqueous solution doped with 51.3 mg l^{-1} pyrene are listed in Table III. Oil and microemulsion were intensively mixed for extraction. Phase separation was achieved by a centrifugal separator.

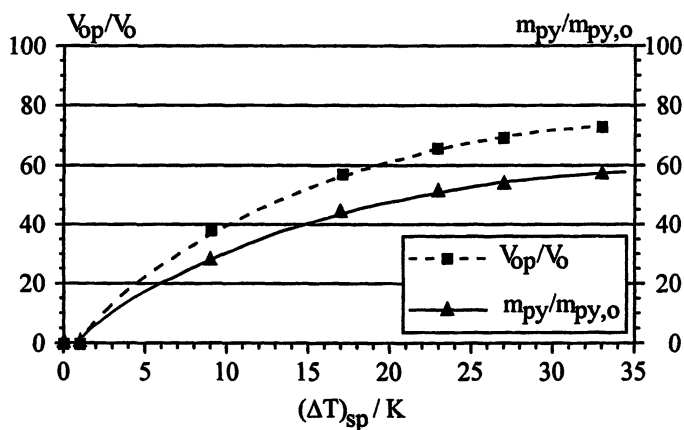


Figure 11. Temperature-induced separation of RME and pyrene from a doped microemulsion.

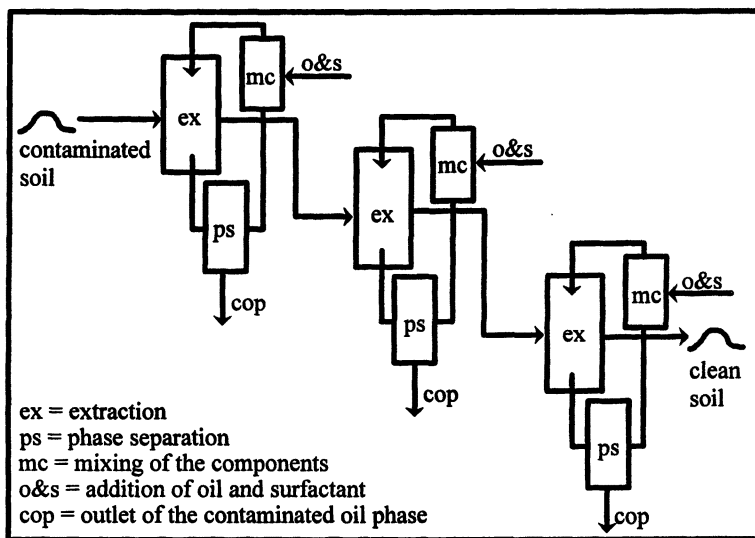


Figure 12. Schematic representation of a multiple-step *ex situ* extraction with microemulsion.

The results show that the contaminant can be effectively removed with an excess of oil. However, the use of the oil twice in a ratio $V(\mu E)/V(\text{oil}) = 10$ will cost about the same as the surfactant which can be recovered. The effectiveness of the process will be strongly influenced by the value of contaminant load which must be achieved. Therefore legislative and administrative regulations will be very important.

From the technical point of view an 88 % removal achieved in the second step will be sufficient. According to the Nernst distribution law this value could also be realized by extracting 5 times with $V(\mu E)/V(\text{oil}) = 100$. However, a continuous process would require the use of 5 separators. From the effectiveness of the first step it can be concluded that RME is a better solvent than the microemulsion. The mass ratio of organic compounds in the microemulsion and in the RME phase is about 5, whereas the concentration ratio of pyrene in both phases is about 2. More hydrophilic surfactants may exhibit even better results.

Table III. Parameters and Results for the Liquid/Liquid Extraction of an O/W Microemulsion (°Initial Solution; * First Extraction; ** Second Extraction; * Third Extraction)**

surfactant concentration in the aqueous phase / g l ⁻¹	RME concentration in the aqueous phase / g l ⁻¹	outlet flux of the aqueous phase / l h ⁻¹	outlet pressure of the aqueous phase / MPa	$V(\mu E)/V(\text{oil})$	$m_{\text{py}}/m_{\text{py},0}$
49.0	4.42	-	-	-	1.00 °
48.3	4.63	34	0.34	100	0.67*
45.5	6.31	34	0.24	10	0.12 **
43.4	6.50	64	0.35	10	0.03 ***

Separation from an Anionic/Nonionic Bicontinuous Microemulsion. Temperature-induced splitting and separation of the PCB contaminated oil phase has been performed on a doped model system with $\gamma = 10\%$ (with 10 % of Tergitol TMN 6 replaced by Emulan EL), $\delta = 70\%$, $\varepsilon = 0.25\%$ CaCl₂. Results are shown in Table IV.

The values which can be obtained for the separation of RME are similar to those of nonionic microemulsions. However, since the phase boundary for this microemulsion to $\underline{2}\phi$ is at 62 °C the temperature difference from the extraction at 10 °C is much higher. The separation of PCB was found to be more efficient, whereas only small amounts of the surfactants are lost with the oil phase. There is only a slight preference for the nonionic surfactant in RME. The system behavior is clearly of an anionic type.

Table IV. Separation of an Oil Phase by Temperature-Induced Splitting of an Anionic/Nonionic Microemulsion

T / °C	relative amount of RME in the oil phase / %	relative amount of PCB in the oil phase / %	relative amount of AOT in the oil phase / %	relative amount of TMN6 in the oil phase / %
70	35.3	40.2	1.10	5.1
80	48.1	61.4	0.35	6.0
90	58.2	62.4	0.35	4.0

Whether mere phase separation by temperature increase may play a role in surfactant recovery is not yet clear. The contaminant load of the recovered microemulsion seems to be too high to allow reinjection. For this reason its use for non-volatile pollutants is very restricted or even impossible. Volatile contaminants can be removed by evaporation. Phase separation may improve the process because there are few foaming problems for the oil phase. A combination with repeated liquid/liquid extraction of the surfactant-containing phase by recovered oil is possible.

Conclusions

Appropriate microemulsions consisting of biodegradable components were found for application in soil remediation. These microemulsions are excellent extraction media for removing hydrophobic pollutants from soil. The contaminants can be dissolved in bicontinuous microemulsion in one extraction step. O/W microemulsions are not as effective, although fairly good. The separation of pyrene with the oil phase is satisfactory in an *ex situ* process and sufficient for application in a technical multistep process. For *in situ* remediation the separation from O/W microemulsions might become economic if the system is optimized and the legislative restrictions are not too severe. Bicontinuous microemulsions with mixed nonionic and anionic surfactants will always contain high amounts of pollutant after phase separation. This type of microemulsion is therefore restricted to volatile contaminants which can be removed by stripping or similar techniques.

Legend of Symbols and Abbreviations

1ϕ = one-phase region

2ϕ = two-phase region with the surfactant in the oil phase

$\underline{2\phi}$ = two-phase region with the surfactant in the aqueous phase

3ϕ = three-phase region

α = mass fraction of oil in the binary oil/water mixture

γ = mass fraction of surfactant in the microemulsion system

$\tilde{\gamma}$ = minimum mass fraction of surfactant necessary to form a one-phase bicontinuous microemulsion at given α (and given α , δ , ϵ respectively)

γ_{ex} = mass fraction of surfactant in the ternary mixture used for extraction

δ = mass fraction of anionic surfactant in an anionic/nonionic surfactant mixture

$(\Delta T)_{\text{sp}}$ = difference between extraction and splitting temperature

ϵ = mass fraction of salt in the binary water/salt mixture

$\Sigma \Delta Q_{\text{py}}$ = sum of the mass of pyrene removed from soil in multiple steps

LC = liquid crystals

m_{py} = mass of pyrene separated with the excess oil phase

$m_{\text{py},0}$ = initial mass of pyrene in the microemulsion

RME = rape oil methyl ester

\tilde{T} = temperature at $\tilde{\gamma}$

T_{ex} = extraction temperature

T_{sp} = splitting temperature

$V(\mu\text{E})$ = volume of an O/W microemulsion

$V(\text{oil})$ = volume of oil added for liquid/liquid extraction of an O/W microemulsion

V_{O} = initial volume of oil in a bicontinuous microemulsion

V_{op} = volume of oil phase after splitting a bicontinuous microemulsion

Acknowledgement

Sponsoring of the studies on liquid/liquid extraction of O/W microemulsions by Stadtwerke Düsseldorf is gratefully acknowledged. Further we are grateful to ICI, Hüls and BASF for supplying us with the surfactants.

References

1. Pearl, M.; Wood, P. In *Contaminated Soil '95*; van den Brink, W. J.; Bosman, R.; Arendt, F., Eds.; Kluwer Academic Publishers, Dordrecht, The Netherlands, 1995, vol. II; pp 1113-1122
2. Noordkamp, E. R.; Grotenhuis, J. T. C.; Rulkens, W. H. In *Contaminated Soil '95*; van den Brink, W. J.; Bosman, R.; Arendt, F., Eds.; Kluwer Academic Publishers, Dordrecht, The Netherlands, 1995, vol. II; pp 1317-1318.
3. Tiehm, A.; Stieber, M.; Werner, P.; Frimmel, F. H. In *Contaminated Soil '95*; van den Brink, W. J.; Bosman, R.; Arendt, F., Eds.; Kluwer Academic Publishers, Dordrecht, The Netherlands, 1995, vol. II; pp 1371-1372.
4. Mönig, K.; Clemens, W.; Haegel, F.-H.; Schwuger, M. J. In *Proceedings of the International Symposium on Micelles, Microemulsions and Monolayers*; Shah, D.O., Ed.; Marcel Dekker, New York, NY, 1997; pp 215-231.
5. Bonkhoff, K.; Wittmann, M.; Haegel, F.-H.; Subklew, G. In *Contaminated Soil '95*; van den Brink, W. J.; Bosman, R.; Arendt, F., Eds.; Kluwer Academic Publishers, Dordrecht, The Netherlands, 1995, vol. II; pp 959-967..
6. Dierkes, F.; Haegel, F.-H.; Schwuger, M. J. *Colloids Surfaces A*, **1998**, *141*, 217-225
7. Mönig, K.; Haegel, F.-H.; Schwuger, M. J. *Tenside Surf. Det.* **1996**, *33(3)*, 228-232.
8. Bonkhoff, K.; Haegel, F.-H.; Kowalski, S.; Subklew, G. *WO 97/37742* (priority: April 4, 1996).

9. Kahlweit, M.; Strey, R.; Firman, P. *J. Phys. Chem.* **1986**, *90*, 671-677.
10. Kahlweit, M.; Strey, R.; *J. Phys. Chem.* **1987**, *91*, 1553-1557.
11. Ludwig, S.; Pavlus, S.; Eschner, C.; Kneifel, H.; Webb, L.; Bonkhoff, K.; Haegel, F.-H.; Subklew, G. In *In-situ-Sanierung von Böden*, Kreysa, G.; Wiesner, J., Eds.; DECHEMA, Frankfurt am Main, Germany, 1996; pp 223-227.
12. Friberg, S. E.; Gan-Zuo, L. *J. Soc. Cosmet. Chem.* **1983**, *34*, 73-81.
13. Clemens, W.; Haegel, F.-H.; Schwuger, M. J.; Soeder, C.; Stickdorn, K.; Webb, L. *WO 94/04289*, 3. 3. 1994 (priority: August, 22, 1992).
14. Neumeister, H.; Fürst, L.; Flucht, R.; Nguyen, V. D. *Ultrapure water 1996*, *13(7)*, 60-64.
15. Ballschmiter, K.; Zell, M. *Fresenius Z. Anal. Chem.* **1980**, *302*, 20-31.
16. Kunieda, H.; Yamagata, M. *Langmuir* **1993**, *9*, 3345-3351.
17. Bonkhoff, K.; Haegel, F.-H.; Mönig, K.; Schwuger, M. J.; Subklew, G. In *Contaminated Soil '95*; van den Brink, W. J.; Bosman, R.; Arendt, F., Eds.; Kluwer Academic Publishers, Dordrecht, The Netherlands, 1995, vol. II; pp 1157-1158.

Chapter 5

Separation of Volatile Organic Compounds from Surfactant Solutions by Pervaporation

L. M. Vane, E. L. Giroux, F. R. Alvarez, and L. Hitchens

National Risk Management Research Laboratory, U.S. Environmental Protection Agency, 26 West Martin Luther King Drive, Cincinnati, OH 45268

Pervaporation is gradually becoming an accepted and practical method for the recovery of volatile organic compounds (VOCs) from aqueous process and waste streams. As the technology has matured, new applications for pervaporation have emerged. One such application is the separation of VOCs from surfactant solutions, such as those used to remediate soils contaminated with chlorinated solvents, thereby enabling the reuse of the surfactant solution. In pervaporation, a nonporous hydrophobic membrane separates the surfactant solution from a vapor phase (vacuum) which extracts the VOC. As a result, pervaporation does not suffer from foaming problems commonly encountered with conventional separation processes. In this paper, the effect of surfactants on process fundamentals and recent experimental results with surfactant solutions will be discussed.

Motivation

In 1994, the U.S. Environmental Protection Agency's National Risk Management Research Laboratory (EPA-NRMRL) initiated research to determine if volatile organic compounds (VOCs) could be recovered from surfactant solutions by pervaporation. The initial focus was on surfactant solutions generated during a surfactant enhanced aquifer remediation (SEAR) project in which the contaminants were dense non-aqueous phase liquids (DNAPLs), such as chlorinated solvents. In SEAR processes, the surfactants are added at concentrations above that required to create surfactant self-aggregates (micelles), in other words, the concentrations are higher than the critical micelle concentration (CMC). These micelles act as high capacity reservoirs where organic compounds can accumulate, thereby creating a high apparent solubility of the organic compounds in the surfactant solution. Thus,

a dramatically smaller volume of surfactant solution would be required to "solubilize" the same amount of organic as compared to water without additives. Months or years would be needed to remove residual organic from a soil with surfactants rather than decades or centuries for standard pump & treat systems.

SEAR researchers have found that efficient surfactant recovery and reuse is essential for the cost effectiveness of this soil remediation technology (1). Such a recycling process would most likely involve a contaminant removal step and a separate surfactant recovery step. Unfortunately, foaming problems may develop when conventional technologies, such as vacuum, steam, or air stripping, are used to remove the VOCs. Other processes, like carbon adsorption of VOCs, may not be technically or economically feasible when surfactants are present or at the concentrations of VOCs which may be achieved during a SEAR project.

Background

Pervaporation is a process in which a liquid stream containing VOCs is placed in contact with one side of a non-porous polymeric membrane while a vacuum or gas purge is applied to the other side. The components in the liquid stream sorb into the membrane, permeate through the membrane, and evaporate into the vapor phase (hence the word **pervaporate**). A schematic diagram of a pervaporation cell is shown in Figure 1. The permeate vapor is then condensed. By using a membrane which is VOC-selective, the material on the vapor permeate side of the membrane will contain VOCs with concentrations significantly higher than those on the liquid side of the membrane. Further, the permeate composition may differ widely from that of the vapor evolved after a free vapor-liquid equilibrium process (2). A concentration factor of 1,000 is not uncommon. For example, in EPA-NRMRL experiments, a 100 μm thick silicone membrane was used to concentrate a 100 ppm (0.01 wt%) 1,1,1-trichloroethane (TCA) aqueous stream to over 10 wt% TCA in the permeate (3). Under these conditions, the permeate consists of a TCA phase and a TCA-saturated water phase, allowing easy recycle or disposal of the TCA. The permeate water phase would be returned to the feed stream for further treatment. As a result, the only two streams leaving this process would be a TCA permeate stream and a VOC-free water residual stream. A schematic diagram of a pervaporation system is shown in Figure 2.

In the authors' experience, when first exposed to pervaporation, individuals often develop two misconceptions about pervaporation. First, the pervaporation membrane is sometimes erroneously pictured as an adsorbent which becomes saturated and must be regenerated in a separate cycle - in the same manner as sorbents used to remove VOCs from air or water. Actually, the vacuum or purge gas continuously "regenerates" the membrane. Pervaporation is, therefore, a continuous and steady state process. Another misconception is that pervaporation is a filtration process - as are many environmental membrane processes. Pervaporation is not used to separate particulates from water, rather it removes soluble VOCs from a liquid solution. Further, since the pervaporation membrane is non-porous, the

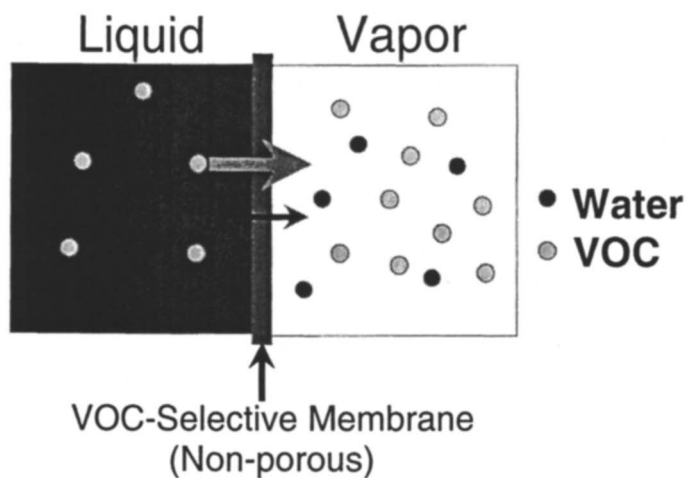


Figure 1. Schematic Diagram of Pervaporation Cell.

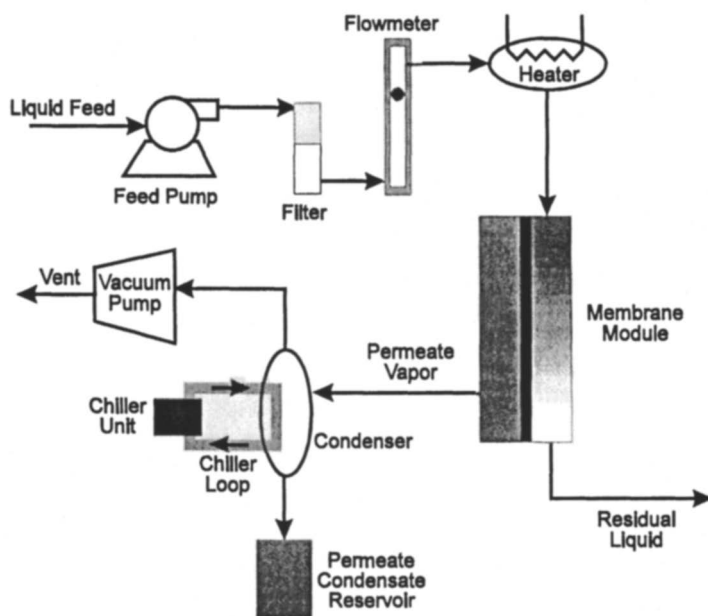


Figure 2. Schematic Diagram of Pervaporation System.

bulk feed liquid flows past the membrane, not through it. Only a small fraction of the feed permeates through the membrane.

Current Uses of Pervaporation. Pervaporation processes have found use in the chemical industry to break azeotropic water/alcohol mixtures and to perform separations which are highly energy intensive when distillation is used (4). For the azeotropic systems, a hydrophilic membrane is used allowing water to be preferentially transported, thereby dehydrating the alcohol feed solution. Over the past decade, a growing amount of attention has been paid to the application of pervaporation to environmental problems (5-12). In many of these instances, small amounts of a VOC must be removed from a large amount of water. Conventionally, air stripping or activated carbon treatment are used, however, air stripping is susceptible to fouling and merely turns a water pollution problem into an air pollution problem and activated carbon treatment involves costly regeneration steps and may not be suitable for VOCs which are easily displaced by other organic compounds. Several advantages of pervaporation are: no fugitive emissions, no regeneration costs (VOCs are continuously removed on vacuum side), compact/modular systems, and low operating costs. An additional advantage of pervaporation is the potential to recycle/reuse the recovered VOC.

To date, a small number of pervaporation demonstrations for VOC recovery from groundwater have been performed, including an EPA SITE demonstration in San Diego by Zenon Environmental (13) and a demonstration in Florida by Lockheed-Martin with a Membrane Technology Research pilot unit (6). Published reports on process economics for VOC recovery from water streams indicate that pervaporation is more cost effective for VOC concentrations greater than 10 ppm than activated carbon adsorption or air stripping with vapor phase carbon adsorption (14,15). Hybrid technologies which combine pervaporation with conventional separation processes have also been considered. In one example of a hybrid process, pervaporation is used to reduce the higher concentrations while activated carbon is used as a polishing step.

Application of Pervaporation to Surfactant Solutions. Since a non-porous membrane separates the liquid and vapor phases in pervaporation, no foam should be generated when the feed stream contains a surfactant. In EPA-NRMRL experiments, foaming was not observed during pervaporation unless a membrane or module defect was present. As a result, pervaporation may have a significant technical advantage over some competing conventional processes. Liquid-liquid extraction, most likely with a membrane contactor, should also be effective for removal of organic contaminants from surfactant solutions, especially non-volatile or semi-volatile contaminants (16-19). EPA-NRMRL is currently (1998) participating in an integrated surfactant soil remediation and surfactant recycling demonstration sponsored by the Department of Defense. A schematic diagram of the proposed field system is shown in Figure 3. As proposed, pervaporation will be used to separate VOCs from the surfactant solutions and ultrafiltration will be used to reconcentrate the surfactant prior to reinjection.

In 1995, EPA-NRMRL initiated pilot and bench-scale tests of pervaporation for removing VOCs such as TCA and toluene from surfactant solutions (3). These experiments showed that pervaporation could effectively remove all of the studied VOCs from surfactant solutions. However, the presence of the surfactant did diminish removal efficiencies. For a typical set of operating conditions (1 gpm feed flow rate, 50°C feed temperature, 50 torr permeate pressure, 4 m² membrane area), the EPA-NRMRL pilot unit removed 99% of the TCA and 98% of the toluene when no surfactant was present. Under the same conditions, but with 1.7 wt% of an anionic surfactant (DowFax 8390) present, 91% of the TCA and 82% of the toluene were removed (20). The relative removals are shown in Figure 4. Clearly, toluene removal was more effected by the surfactant than was TCA removal.

Pervaporation Theory

Typically, the removal of VOCs from water by pervaporation is controlled by the mass transport resistance in the liquid boundary layer next to the membrane (7,21-25). The other resistances; diffusion through the membrane, membrane support, and permeate boundary layer are usually small compared to that of the liquid boundary layer. Although the membrane may not present a significant resistance to VOC transport, it is the most significant resistance for water transport. Thus, VOC transport is generally controlled by boundary layer resistance while water transport is controlled by membrane permeability to water and membrane thickness. This simplification is not true for other organic compounds, such as alcohols, which have lower Henry's constants and lower membrane permeabilities. Membrane module designers and users strive to reduce the thickness of the VOC boundary layer. Unfortunately, high shear rates are required to reduce the boundary layer resistance to even the order of the other resistances. Much effort has been expended in the membrane community to model these various mass transport resistances. The most simplistic model for the liquid-side resistance is that of a stagnant or laminar boundary layer through which VOCs must diffuse in order to reach the membrane surface. Thus, mass transport is a direct function of the diffusivity of the VOC in water as well as the thickness of the boundary layer. Empirical relationships have been developed to estimate the mass transport coefficients for liquid boundary layers (k^L) in various membrane configurations. These relationships usually take the following form (26,27):

$$k^L = \frac{D}{d_h} a_1 Re^{a_2} Sc^{a_3} \left(\frac{d_h}{L} \right)^{a_4} [=] \frac{\text{length}}{\text{time}} \quad (1)$$

where the dimensionless Reynolds (Re) and Schmidt (Sc) numbers are defined as:

$$Re = \frac{u\rho d_h}{\eta} \quad Sc = \frac{\eta}{\rho D} \quad (2)$$

where D (diffusivity), ρ (density), and η (viscosity) are physical properties of the fluid, u is the superficial velocity of the fluid in the liquid flow channel, d_h and L are

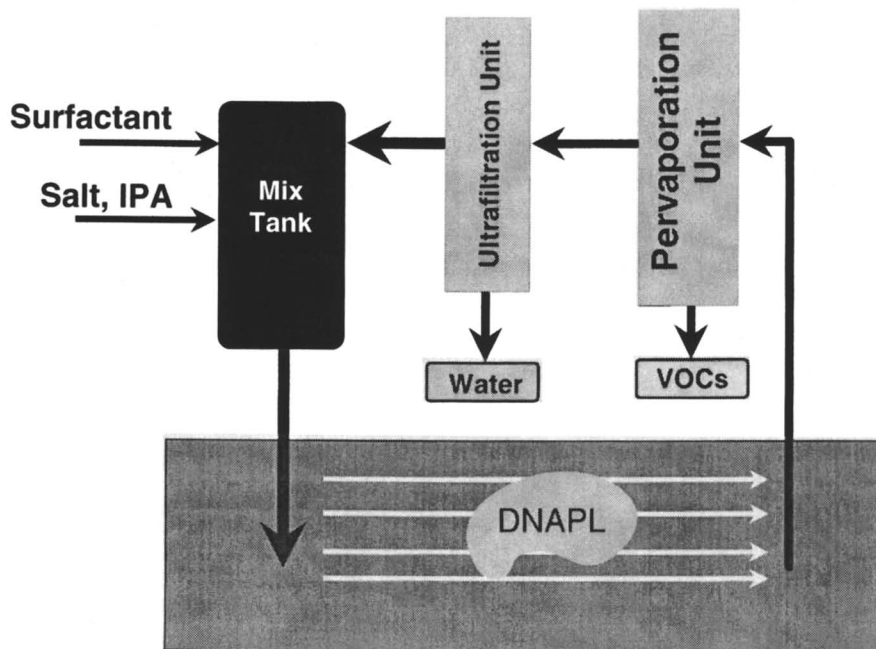


Figure 3. Schematic Diagram of Proposed Integrated Field Demonstration of Surfactant Remediation and Recovery/Reuse.

VOC Removal from Surfactant Solution by Pervaporation

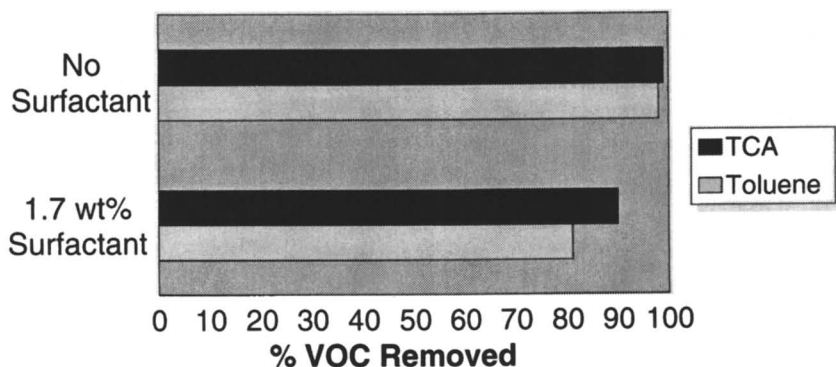


Figure 4. Performance of EPA-NRMRL Pervaporation Pilot Unit Equipped with Spiral Wound Membrane Modules for Removal of Selected VOCs in the Presence and Absence of Surfactant. (Conditions: 50°C, 1 gpm, 4 m² membrane area, DowFax 8390 Surfactant, 1.7wt% surfactant = 40xCMC).

hydraulic diameter and length of the cell, respectively, and a_1, a_2, a_3, a_4 are constants. One common form of equation 1 is L ev eque's correlation:

$$k^L = 1.6 \frac{D}{d_h} Re^{1/3} Sc^{1/3} \left(\frac{d_h}{L} \right)^{1/3} = 1.6 \left(\frac{uD^2}{d_h L} \right)^{1/3} \quad (3)$$

which applies in the laminar flow regime in open channels during the development of the concentration boundary layer (28).

The rate material is transported through the membrane is proportional to the concentration difference between the liquid and permeate phases and the overall mass transport coefficient, k , as follows:

$$J_{voc} = k \left[C_{voc}^L - C_{voc}^V \right] [=] \frac{\text{mass}}{\text{time} \times \text{area}} \quad (4)$$

where J_{voc} is the flux of VOC and C_{voc}^L and C_{voc}^V are the bulk liquid phase and permeate phase concentrations. As described earlier, for VOCs in water, k can often be approximated as k^L . Further, these systems are often operated such that C_{voc}^V is negligible compared to C_{voc}^L . In such cases, equation 4 can be integrated over a given membrane module to yield:

$$\ln \left(\frac{C_r}{C_f} \right) = \frac{-k^L A}{Q} \quad (5)$$

where C_r , C_f , A , and Q are the residual (module outlet) VOC concentration, feed concentration, membrane area, and liquid flow rate, respectively. Thus, the fraction of VOC remaining after passing through a membrane module, C_r/C_f , varies exponentially with k^L , A , and Q .

Impact of Surfactants on Removal of VOCs.

The introduction of surfactants into the liquid phase affects several parameters and assumptions which were used to develop equations 1 through 5 and, therefore, the performance of a pervaporation system. First, the surfactants tend to increase the intrinsic viscosity (η/ρ) of the solutions (3). The increase in viscosity is a function of both the type of surfactant, the surfactant concentration, and the VOC concentration. In solutions above the CMC of the surfactant, concentrations of VOC far above the water solubility of the VOC can be obtained. Much of the VOC is solubilized in the micelles, thereby swelling these domains. This tends to raise the viscosity, sometimes dramatically, especially if the presence of the VOC causes phase separation to occur. However, a viscosity increase of 10-20% would be typical at the VOC and surfactant concentrations generally seen in the fluid extracted during SEAR applications. This should only marginally impact pervaporation performance.

The second, and most significant, effect of surfactants on pervaporation performance also arises from the partitioning of the VOC into the micelles. In equation 4, the concentration driving force is more accurately represented by the activity driving force. For surfactant solutions, this can be expressed by the

concentration of VOC which is not sequestered in the micelles. This “extramolecular” VOC may only be a small fraction of the total VOC in the system as shown pictorially in Figure 5. Only limited information is available for the partitioning of VOCs in surfactant solutions (29-34). Methods for determining this partitioning include vapor pressure and headspace measurements, which are referenced to systems without surfactant. EPA-NRMRL has used the equilibrium partitioning in closed systems (EPICS) headspace method to determine the micellar partitioning of VOCs for several VOCs in a variety of surfactants over a range of temperatures (article in preparation by the authors of this chapter).

Headspace Method for Determining Henry’s Law Constants. Briefly, in the EPICS procedure, VOC was added to vials containing either deionized water or a surfactant solution in six replicates of each of two volumes. A methanol solution (30 – 50 μL) of a mixture of TCA, trichloroethylene (TCE), toluene, and tetrachloroethylene (PCE) was added to each vial, which was immediately sealed with a crimp cap fitted with a Teflon-surfaced septum. Under management by a headspace autosampler (CombiPAL, LEAP Technologies, Carrboro, NC), vials were incubated at the desired temperature with agitation for 15 minutes, then 1 mL of headspace was withdrawn into a heated syringe and directly submitted to GC analysis (Tremetrics 9001 GC equipped with FID detector). By using complementary volumes in two-vial trials (16 mL liquid, 5.7 mL vapor in one vial and 5.7 mL liquid, 16 mL vapor in the other) and by adding equal masses of VOCs to vials, the expression provided for data analysis by Gossett (35) was simplified to:

$$H_c = \frac{v-r}{vr-1} = \frac{C_g}{C_L} \quad (6)$$

where v is the ratio of vapor-phase volumes in the two vials (V_{g1}/V_{g2} in Gossett’s notation), r is the ratio of vapor-phase analyte concentrations (C_{g1}/C_{g2} in Gossett’s notation) and H_c is the “dimensionless” Henry’s law constant representing the ratio of the gas phase concentration (C_g) of a VOC to that in the liquid phase (C_L), both in the same units. Estimates of H_c were made from results of all combinations of pairs of vials (35). With six each of small and large liquid volumes, there were 36 estimates. The median of the estimates was taken to characterize that trial. Estimates which ranked 12th and 25th in the ordered group were taken to define a 67% confidence interval (36,37). Confidence intervals of 95% were similarly calculated and used to assign statistically significant differences in H_c values at the 5% level. Error bars shown in Figures 6 and 7 correspond to the 67% confidence interval.

Not surprisingly, the surfactant greatly impacts the magnitude of H_c as shown in Figure 6 for DowFax 8390 surfactant and TCA. The CMC of the DowFax was reported by the vendor (Dow Chemical) to be 0.426 g-active/L. As surfactant is added above the CMC, micelles form, creating hydrophobic zones to which the VOCs partition. The more surfactant present, the more hydrophobic regions available to take up VOC and less VOC is available to partition into the headspace. Sub-CMC quantities of the surfactant did not alter H_c since no separate hydrophobic

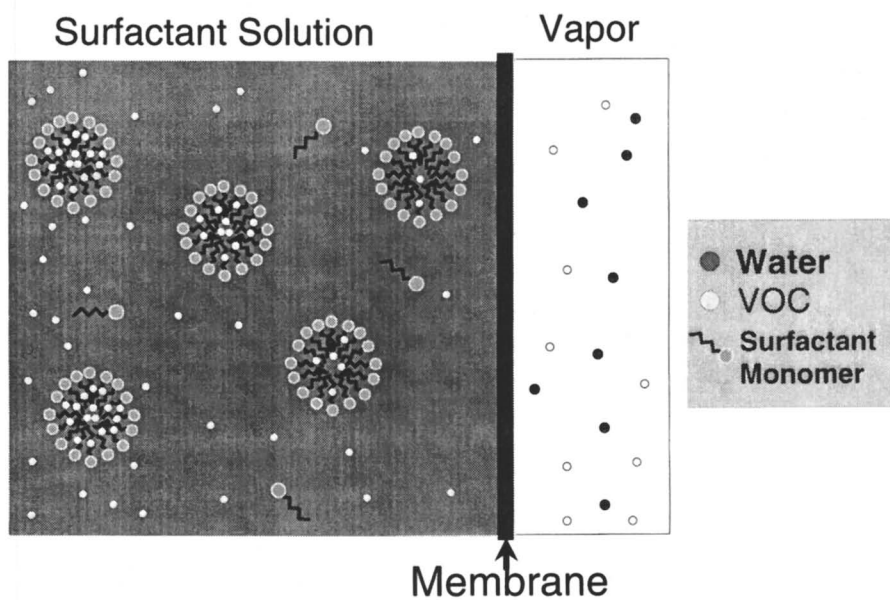


Figure 5. Pictorial Representation of the Partitioning of VOC Between Surfactant Micelles and the Extramicroemulsion Region.

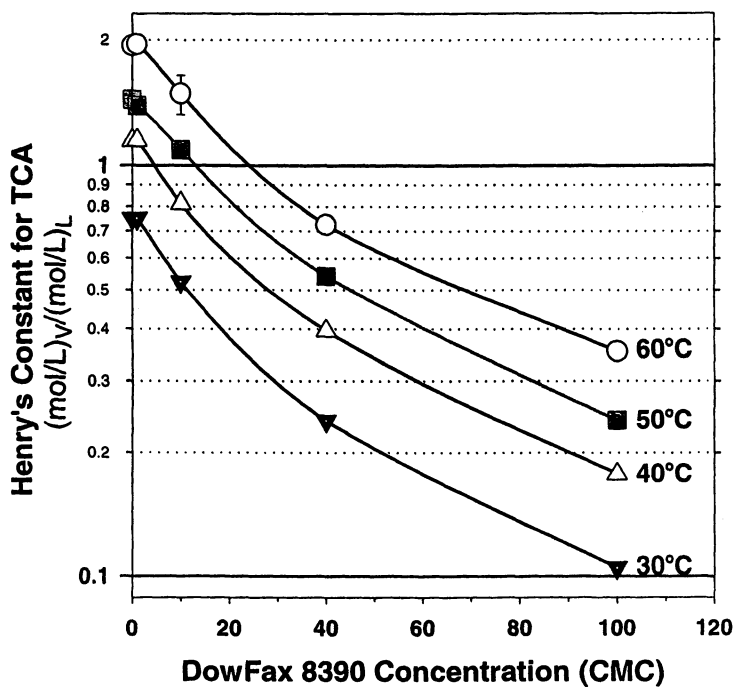


Figure 6. Effect of Temperature and Surfactant Concentration on Vapor-Liquid Partitioning of 1,1,1-trichloroethane (TCA). DowFax 8390 Surfactant.

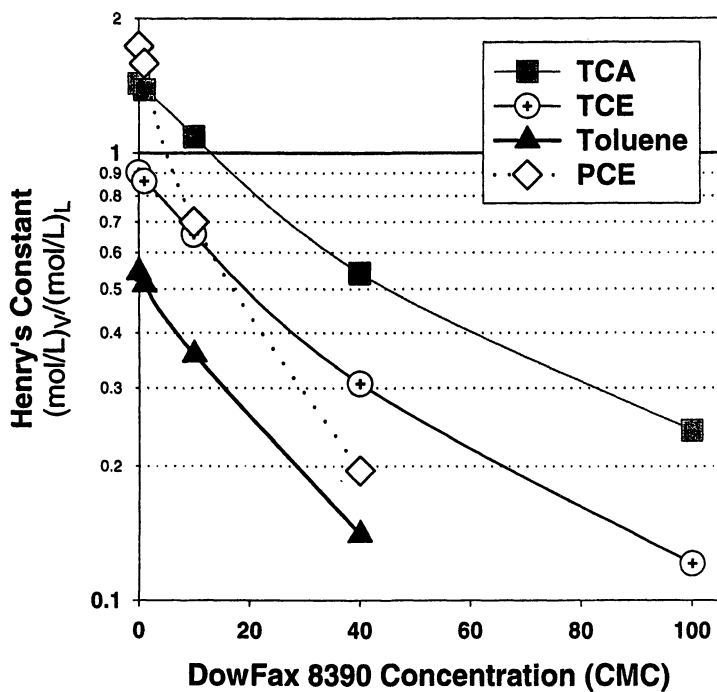


Figure 7. Magnitude of Impact of Surfactant on Henry's Constant Varied with type of VOC. Conditions: 50°C, DowFax 8390 Surfactant.

zone is available. The drop in H_c caused by the addition of surfactant can be quite dramatic. In Figure 6, H_c for TCA drops almost an order of magnitude upon the addition of 100 times the CMC of the DowFax. Similar trends were observed for Triton X-100 (nonionic), Cytec MA 80-I (anionic), and Sodium Dodecyl Sulfate (anionic). As expected, higher temperatures yielded higher values of H_c , although the shapes of the curves in Figure 6 were not affected by temperature.

Theoretically, the more hydrophobic the VOC, the more readily it will partition into the micelles. This is clearly the case for DowFax 8390 with TCA, TCE, Toluene, and PCE, as displayed in Figure 7. The curves for TCA and TCE exhibit similar shapes while H_c for toluene responds more rapidly to the addition of surfactant. PCE, the most hydrophobic of the four VOCs studied, displays the most dramatic response to increased surfactant levels. In fact, of the four VOCs studied, PCE is the easiest to remove from water by vapor-liquid stripping, but can become the most difficult to remove upon addition of surfactant because of its micellar partitioning.

Calculation of Extramolecular Fraction of VOC. Actually, H_c for surfactant solutions might best be described as an “apparent H_c ” since the liquid concentration in the denominator of equation 6 is the total concentration of VOC solubilized in the surfactant solution, both in the micelles and in the extramolecular water region. Unless significant amounts of non-surfactant materials, such as alcohols or salts, have been added to the solution, the H_c of a VOC in the extramolecular water is not affected by the surfactant. Thus, the extramolecular concentration of VOC can be calculated from the headspace concentration above a given surfactant solution and the H_c for the VOC in water void of surfactant (or appropriate background solution). Likewise, the fraction of VOC in the solution which is extramolecular can be calculated from the H_c measured with surfactant and that measured without:

$$f_{ex} = \frac{H_c \text{ [with surfactant]}}{H_c \text{ [no surfactant]}} \quad (7)$$

where f_{ex} is the extramolecular fraction of VOC in the system. The calculated values for f_{ex} for data in Figures 6 and 7 are shown in Figures 8 and 9, respectively. The f_{ex} data in Figure 9 more clearly shows the impact of VOC hydrophobicity on micellar partitioning. In the presence of 40xCMC DowFax 8390, slightly more than 10% of PCE is extramolecular while almost 40% of the TCA is outside the micelles. In addition, while temperature has a marked impact on the magnitude of H_c (as seen in Figure 6), it does not dramatically impact f_{ex} as evidenced by the overlapping curves in Figure 8. As a result, a surfactant solution at 30°C will have approximately the same fraction of VOC in micellar form as a solution at 60°C.

Impact of Surfactant on Traditional Pervaporation Mass Transport Model.

The process of removing VOCs from water by pervaporation is often modeled as the diffusion of VOC from the bulk liquid phase through a stagnant or laminar boundary layer to the membrane surface. As a result, a steep concentration gradient develops on the liquid side of the membrane, referred to as “concentration polarization”. At

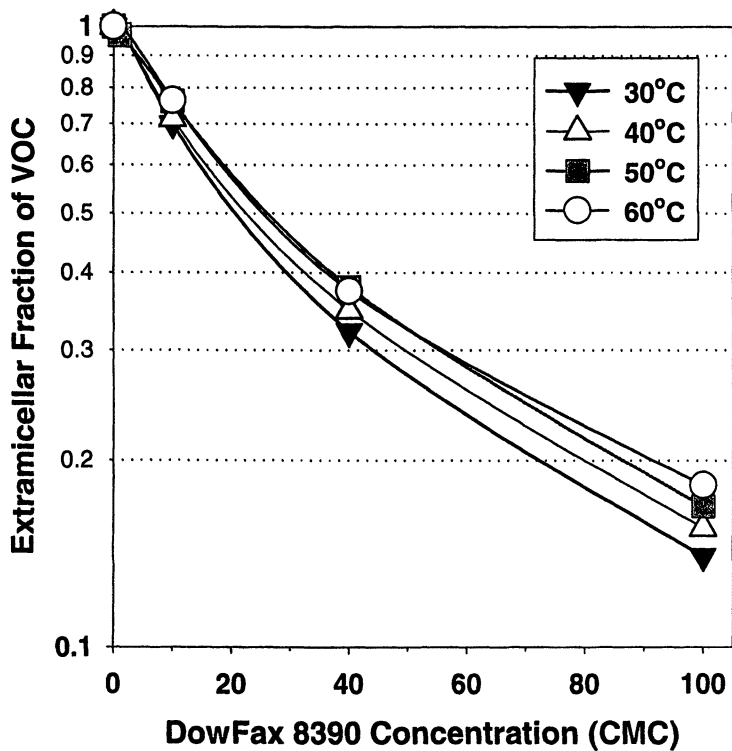


Figure 8. Extramicellar Fraction of TCA as Function of Temperature and Surfactant Concentration.

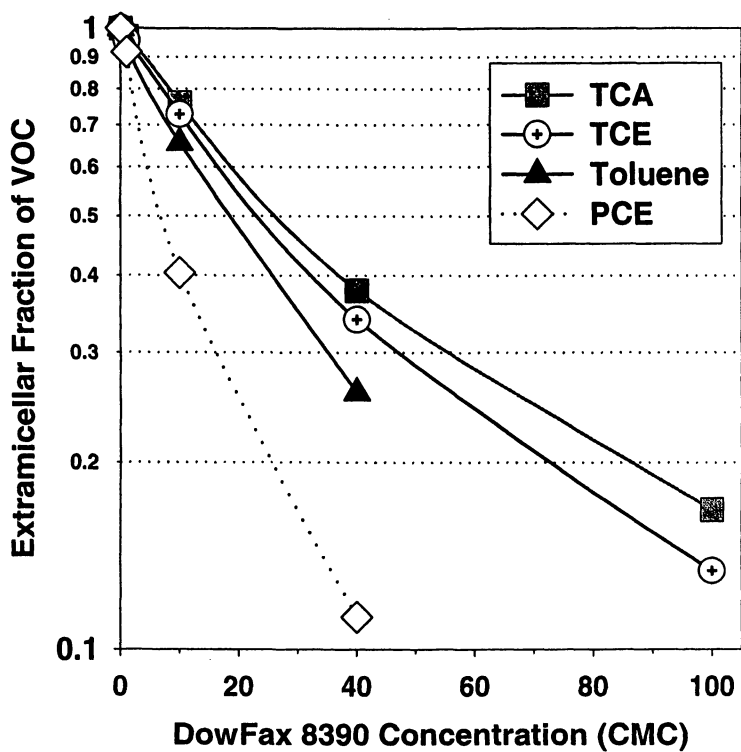


Figure 9. Extracellular Fraction of VOC Varies with Nature of VOC and Surfactant Concentration. (all data obtained at 50°C)

the liquid-side of the membrane, the membrane is in equilibrium with the VOC in the water. The VOC then diffuses through the membrane and desorbs on the vacuum side. Equation 4 could be rewritten to describe the flux in terms of the concentration of VOC in the membrane material at the liquid and vapor surfaces (C_M^L and C_M^V) and the membrane mass transport coefficient (k^M):

$$J_{voc} = k^M [C_M^L - C_M^V] \quad (8)$$

If surfactant were added to this system, keeping constant the total VOC concentration at the membrane surface, then the net effect would be to reduce the amount of VOC the membrane “sees” by a factor f_{ex} , thus reducing C_M^L by the same factor. In essence, the activity of the VOC is reduced due to the partitioning of the VOC into the micelle. In many cases the vapor concentration is small compared to the liquid concentration ($C_M^L \gg C_M^V$), therefore, the flux of VOC through the membrane would also be reduced by a factor f_{ex} . This would result in a modification to equation 5 as shown below:

$$\ln\left(\frac{C_r}{C_f}\right) = \frac{-f_{ex} k^L A}{Q} \quad (9)$$

Thus, in order to remove the same fraction of total VOC from the feed stream, the membrane area, A , would have to be multiplied by a factor of $(1/f_{ex})$. Similarly, if the same amount of area were used for both systems, then the fraction of VOC remaining should be altered via equation 5 as if A were reduced by a factor f_{ex} .

Comparison of Predicted to Observed Pervaporation Performance. In Figure 4, the performance of a pervaporation system with TCA and toluene with and without DowFax 8390 was reported. The fraction TCA remaining (C_r/C_f) without surfactant was 0.01 (99% removed). According to Figure 9, for TCA in 40xCMC DowFax 8390 at 50°C, $f_{ex} = 0.38$. Thus, by introducing these values of f_{ex} and C_r/C_f into equation 9, C_r/C_f with surfactant should be 0.17, indicating 83% TCA removal as opposed to the 91% removal observed in the actual tests. Similarly, toluene f_{ex} data suggest only 61% removal with 40xCMC DowFax vs. the 82% removal observed. The fraction removed reported in the figure was found to be independent of the feed concentration of VOC over several decades of concentration. For example, TCA removal from the DowFax solution was found to be 91±1% for TCA concentrations ranging from 20 to 3000 mg/L. Toluene removal from the same solution was 82±1% for concentrations ranging from 15 to 800 mg/L. VOC concentrations were typically below 20 mg/L for experiments with no surfactants due to the limited solubilities. Even in the absence of surfactant, however, the fraction of VOC removed was independent of the VOC concentration in the feed fluid. This concentration independence is predicted by equation 4 in which the fraction remaining is only a function of the mass transport coefficient (which is generally independent of concentration), membrane area, and flow rate.

The difference between observed performance and that predicted from a simple application of the extramolecular fraction to existing pervaporation models

was observed for bench and pilot scale experiments with a variety of membrane configuration. Fortunately, the experiments show that actual pervaporation performance is not diminished as much as equilibrium measurements and current theory might suggest. Unfortunately, pervaporation performance is affected noticeably by surfactants and standard models for pervaporation cannot account for micellar partitioning. EPA-NRMRL researchers are in the process of modeling the pervaporation of VOCs from a surfactant system. The current focus of the modeling effort is describing the effect of surfactant micelles on the transport of VOCs through the liquid boundary layer. Early indications are that the micelles act as a source of VOC in the boundary layer, yielding a less steep concentration gradient in the boundary layer and a higher concentration of VOC at the membrane surface than predicted from current models. This higher membrane surface concentration translates into higher VOC flux (per equation 8) and greater % VOC removal in surfactant systems than might be predicted from the overly simplistic relationship shown in equation 9. A pictorial representation of the VOC concentration in the liquid boundary layer in the presence and absence of surfactants is shown in Figure 10.

Conclusions

In this paper, a headspace method was used to measure the Henry's constants of several VOCs in surfactant solutions at a variety of temperatures and surfactant concentrations. Measurements of Henry's constants for VOCs in surfactant solutions indicate that the magnitude of micellar partitioning is a direct function of the hydrophobicity of the VOC. The tendency of the four VOCs studied in this project to partition to surfactant micelles increased in the order: TCA < TCE < Toluene < PCE. Although previous authors have used a similar method, this paper reported Henry's constants for the DowFax 8390 system, described how the extracellular fraction of VOC could be directly calculated from observed Henry's constants, and extended the range of temperatures for which data were determined. The partitioning information was then used to show how surfactants reduce the concentration of VOC available to the pervaporation membrane. Comparison of the partitioning data to pilot scale pervaporation results with and without anionic DowFax 8390 indicated that current pervaporation models do not adequately account for micellar partitioning of VOCs and the effect this partitioning will have on boundary layer and membrane transport. This analysis supported previous observation for bench scale pervaporation with a non-ionic surfactant. In general, pervaporation pilot unit performance was significantly affected by the presence of the surfactant, although not as significantly as suggested by equilibrium partitioning measurements and current models. Nevertheless, pervaporation can be used to remove VOCs from surfactant solutions without foaming problems which can plague separation processes relying on direct vapor-liquid contact, like air stripping. However, new models are needed to assist in predicting pervaporation performance when surfactants are present.

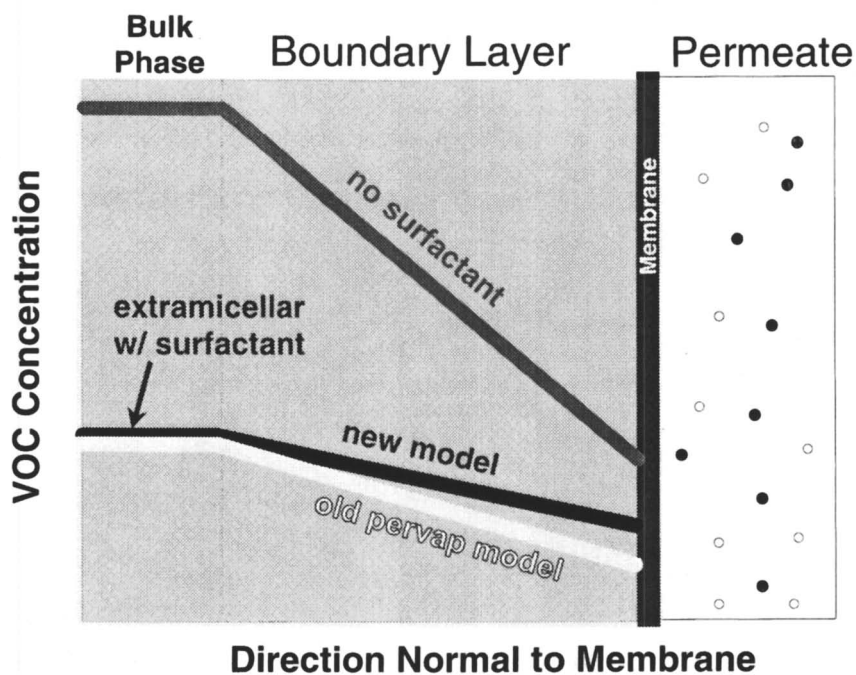


Figure 10. Qualitative Illustration of the Effect of Surfactants on the VOC Concentration in the Liquid Boundary Layer and at the Membrane Surface.

Literature Cited

1. Krebs-Yuill, B., Harwell, J.H., Sabatini, D.A., and Knox, R.C. *ACS Symposium Series* **1995**, *594*, pp 265-278.
2. Fleming, H.L.; Slater, C.S. In *Membrane Handbook*; Winston, H.W.S., Sirkar, K.K., Eds.; Van Nostrand Reinhold: New York, 1992; pp 105-159.
3. Jiang, J.-S., Vane, L.M., and Sikdar, S.K. *J. Mem. Sci.* **1997**, *136*, pp 233-247.
4. Schehlmann, M.S., Wiedemann, E., and Lichtenthaler, R.N. *J. Mem. Sci.* **1995**, *107*, pp 277-282.
5. Baker, R., Kaschemekat, J., Wijmans, H., and Simmons, V. *Adv. Filtr. Sep. Technol.* **1990**, *1*, pp 330-335.
6. Baker, R. W., Athayde, A. L., Daniels, R., Le, M., Pinnau, I., Ly, J. H., Wijmans, J. G., Kaschemekat, J. H., and Helm, V. D. Development of Pervaporation to Recover and Reuse Volatile Organic Compounds from Industrial Waste Streams. DOE/AL/98769--1. 1997. U.S. Department of Energy.
7. Baker, R.W., Wijmans, J.G., Athayde, A.L., Daniels, R., Ly, J.H., and Le, M. *J. Mem. Sci.* **1997**, *137*, pp 159-172.
8. Blume, I., Wijmans, J.G., and Baker, R.W. *J. Mem. Sci.* **1990**, *49*, pp 253-286.
9. Blume, I. and Baker, R. W. Process for Recovering Organic Components from Liquid Streams. Membrane Technology & Research, Inc. 359,739(5,030356). 1991. U.S. 1989.
10. Kaschemekat, J., Wijmans, J.G., Baker, R.W., and Blume, I. *Proceedings Third International Conference of Pervaporation Processes Chemical Industries* **1988**, pp 405-412.
11. Kaschemekat, J., Wijmans, J.G., and Baker, R.W. *Proceedings Fourth International Conference of Pervaporation Processes Chemical Industries* **1989**, pp 321-331.
12. Wijmans, J.G., Kaschemekat, J.E., Davidson, J.E., and Baker, R.W. *Environmental Progress* **1990**, *9*, pp 262-268.
13. Zenon Environmental, Inc. Cross-Flow Pervaporation System. EPA/540/R-95/511a. 1995. Cincinnati, Ohio, USEPA-ORD.
14. Lipski, C. and Cote, P. *Environmental Progress* **1990**, *9*, pp 254-261.
15. Losin, M. S. and Miller, B. D. Pervaporation Technology: Fundamentals and Industrial Applications. 1993.
16. Hasegawa, M.A., Sabatini, D.A., and Harwell, J.H. *J. Env. Eng.* **1997**, *123*, pp 691-697.
17. Hutter, J.C., Vandegrift, G.F., Nunez, L., and Redfield, D.H. *AIChE Journal* **1994**, *40*, pp 166-177.
18. Clarke, A.N., Mutch, R.D., Jr., Wilson, D.J., and Oma, K.H. *Wat. Sci. Tech.* **1992**, *26*, pp 127-135.
19. Oma, K.H., Clarke, A.N., Megehee, M.M., and Wilson, D.J. *Separation Science and Technology* **1993**, *28*, pp 2319-2349.
20. Vane, L.M. In *Standard Handbook of Hazardous Waste Treatment and Disposal*; Freeman, H.M., Ed.; 1998; pp 7.60-7.72

21. Dotremont, C., Van den Ende, S., Vandommele, H., and Vandecasteele, C. *Desalination* **1994**, *95*, pp 91-113.
22. Pereira, C.C., Habert, A.C., Nobrega, R., and Borges, C.P. *J. Mem. Sci.* **1998**, *138*, pp 227-235.
23. Psaume, R., Aptel, Ph., Aurelle, Y., Mora, J.C., and Bersillon, J.L. *J. Mem. Sci.* **1988**, *36*, pp 373-384.
24. Raghunath, B. and Hwang, S.-T. *J. Mem. Sci.* **1992**, *75*, pp 29-46.
25. Raghunath, B. and Hwang, S.-T. *J. Mem. Sci.* **1992**, *65*, pp 147-161.
26. Karlsson, H.O.E. and Tragardh, G. *J. Mem. Sci.* **1993**, *76*, pp 121-146.
27. Nijhuis, H.H., Mulder, M.H.V., and Smolders, C.A. *J. Mem. Sci.* **1991**, *61*, pp 99-111.
28. Rautenbach, R. and Helmus, F.P. *J. Mem. Sci.* **1994**, *87*, pp 171-181.
29. Anderson, M.A. *Environ. Sci. Technol.* **1992**, *26*, pp 2186-2191.
30. Smith, G.A., Christian, S.D., and Scamehorn, J.F. *J. Colloid and Interface Science* **1989**, *130*, pp 254-265.
31. Tucker, E.E. and Christian, S.D. *J. Colloid and Interface Science* **1985**, *104*, pp 562-568.
32. Uchiyama, H., Tucker, E.E., Christian, S.D., and Scamehorn, J.F. *Journal of Physical Chemistry* **1994**, *98*, pp 1714-1718.
33. Uchiyama, H., Christian, S.D., Tucker, E.E., and Scamehorn, J.F. *AICHE Journal* **1994**, *40*, pp 1969-1975.
34. Valsaraj, K.T., Gupta, A., Thibodeaux, L.J., and Harrison, D.P. *Water Research* **1988**, *22*, pp 1173-1183.
35. Gossett, J.M. *Environ. Sci. Technol.* **1987**, *21*, pp 202-208.
36. Cornish-Bowden, A., Porter, W.R., and Trager, W.F. *J. Theor. Bio.* **1978**, *74*, pp 163-175.
37. Sillitto, G.P. *Biometrika* **1947**, *34*, pp 36-40.

The Use of Liquid-Liquid Extraction in Hollow Fiber Membrane for the Removal of Organic Contaminants from Aqueous Surfactant Streams

B. Kitiyanan ¹, J. H. O'Haver ², Jeffrey H. Harwell ¹, and D. A. Sabatini ³

¹Schools of Chemical Engineering and Materials Science and ³Civil Engineering and Environmental Science, University of Oklahoma, Norman, OK 73019

²Department of Chemical Engineering, University of Mississippi, University, MS 38677

Liquid-liquid extraction in a hollow-fiber membrane contactor is examined as a means to remove organic contaminants from an aqueous surfactant stream. The effect of flow rate and the presence of the micellar pseudophase on the liquid-liquid extraction process are determined. Laboratory studies with the model contaminants perchloroethylene and isobutylbenzene in aqueous solutions of Dowfax 8390 or Igepal CO-880 surfactants are discussed. Squalane is utilized as the extracting fluid and a Hoechst-Celanese Corporation membrane module as the contactor. Results shows that (1) higher aqueous flow rates result in lower removal efficiencies, (2) high surfactant concentrations lower the removal efficiencies, (3) hollow fiber contactors help prevent emulsion formation, and (4) liquid-liquid extraction is a viable option for the removal of contaminants from aqueous surfactant streams.

The use of a surfactant solution can expedite the pump-and-treat process in ground water remediation, a process called Surfactant Enhanced Subsurface Remediation (1). Several field tests have shown very promising results for this process (2). However, the cost of implementing the technology will be prohibitively high unless methods are developed for recovering and recycling the surfactant (3).

There are various processes which might be effective for the removal of volatile and/or non-volatile organic components from surfactant solutions (4-7). Each of these methods usually involves contacting the contaminated aqueous surfactant stream with an additional phase (air or some other liquid) which provides a lower chemical potential

environment for the organic contaminant, but not for the surfactant. Hence, only the contaminants will transfer from the aqueous phase due to the chemical potential difference.

Several separation methods based on the above idea have been implemented in laboratory scale. They are: air-stripping in both packed column and hollow fiber membrane contactors (5), vacuum-stripping in packed column (6), and liquid-liquid extraction in a hollow fiber membrane contactor (7). Recently, both packed column and hollow fiber membrane air-stripping processes were implemented in pilot scale (Walk, R. D., The University of Oklahoma, MS thesis, 1997.). Their high removal efficiencies show the ability of these processes to go to the field. Nevertheless, more information of the effects of surfactants on pilot plant design and operation is still essential.

This work will examine the effect of flow rate and the presence of the micellar pseudophase on the liquid-liquid extraction process utilizing a hollow-fiber membrane contactor similar to that used in previous work (7). The driving force for this work was to evaluate whether or not to implement this process at a field test of surfactant-enhanced remediation.

Background

Liquid-Liquid Extraction. Liquid-liquid extraction, sometimes referred to as solvent extraction, is basically the separation process resulting from the distribution of some constituent between two immiscible liquids when they are in contact. In this work, an organic pollutant will be extracted from a surfactant aqueous stream by contacting it with a solvent phase. If the organic contaminant in the original solution distribute themselves differently between the two liquid phases, a certain degree of separation will result. To understand the contaminant distribution between the two phases, the solvent-water partition coefficient is defined as

$$K_d = \frac{C_{oil}}{C_w^*} \quad (1)$$

where C_{oil} = oil (solvent) phase contaminant concentration and C_w^* = equilibrium water phase contaminant concentration.

Liquid-liquid extraction may be highly effective for removal of hydrophobic, nonvolatile contaminants that cannot be economically removed by air stripping. Since the separation is determined by the solubility of the organic pollute into the solvent, high removal efficiency can be obtained by proper solvent selection. Moreover, the volumetric flowrate of the extracting solvent can be greatly reduced without significant loss of extraction efficiency when the solvent phase has a high capacity for the contaminant. As a result, the operating costs and solvent cost—including the solvent regeneration costs—are potentially diminished with good solvent selection. Equally important, however, is consideration of the back contamination of the surfactant stream by micellar solubilization of the stripping solvent; this consideration drastically reduces the options available for selecting the solvent.

Removing the contaminant from the spent solvent is necessary and will probably be an expensive component of the overall process. For example, distillation could be used to recover the spent solvent, but will have high-energy costs associated with it. It has been suggested that steam stripping in a hollow fiber membrane may be more effective for this purpose (8).

Surfactant Properties. Surfactants are molecules that consist of hydrophilic and hydrophobic parts referred to as head and tail group respectively. The hydrophilic portion of the surfactant is attracted to water while the hydrophobic portion of the surfactant is repelled by water. This molecular structure causes the surfactant's molecules to aggregate into micelles when its concentration reaches the critical micelle concentration (CMC). The micelle interior can be envisioned as a pseudo-oil phase. Organic compounds preferentially partition into the interior of the micelles, thereby increasing the solubility of the organic in a aqueous surfactants solution relative to its water solubility.

The micellar partition coefficient is typically used to describe the extent to which a specific compound will solubilize into a given surfactant micelle. The micellar partition coefficient, K_m , is defined as (9):

$$K_m = \frac{X_m}{X_{aq}} \quad (2)$$

where X_m = mole fraction of the contaminant in the micellar phase and X_{aq} = mole fraction of the contaminant in the water phase. If the concentration of surfactant is much greater than the concentration of contaminant ($C_{surf,m} \gg C_m$), then X_m can be shown as

$$X_m = \frac{C_m}{C_{surf,m} + C_m} \cong \frac{C_{tot} - C_{aq}}{C_{surf,m}} \quad (3)$$

when C_{tot} = total concentration of contaminant in surfactant solution, C_{aq} = molar concentration of contaminant in aqueous phase (and can be approximated as the concentration of contaminant in pure water); $C_{surf,m}$ = molar concentration of surfactant in micellar form. The mole fraction of contaminant in the aqueous phase (the extra-micellar contaminant concentration) can also be written as:

$$X_{aq} = C_{aq} \cdot \bar{v}_w \quad (4)$$

when \bar{v}_w = molar volume of water. The micellar partition coefficient, then, can be simplified as

$$K_m \cong \frac{C_{tot} - C_{aq}}{C_{surf,m} \cdot C_{aq} \cdot \bar{v}_w} \quad (5)$$

Effect of Micellar Surfactant in Liquid-Liquid Extraction. In environmental remediation applications, surfactants are typically applied at concentrations well above their CMC in order to increase washing or flushing solution capacity to remove contaminants. Contaminant partitioning into the hydrophobic interior of the micelles will significantly increase their solubility in the aqueous phase. The surfactant enhancement in contaminant extraction also causes increased difficulty in decontaminating these surfactant solutions. By selecting a stripping solvent that offers a high contaminant distribution coefficient, the solvent phase will act as a chemical potential sink for the organic contaminant.

Additionally, back contamination of the solvent into surfactant micelles and transfer of valuable surfactant to the solvent stream must be avoided. Therefore, the solvent has to be carefully selected so that it will neither be solubilized by the surfactant micelles nor absorb the surfactant into itself. Back contamination could prevent the reinjection of the surfactant stream.

In conventional liquid-liquid extraction, it is necessary to separate the phases between solvent and oil; with surfactant, the formation of stable emulsions must also be avoided (10). Unfortunately, the ability of surfactants to reduce the interfacial tension between water and oil phases can cause stable emulsions if the phases are directly contacted.

Hollow Fiber Membrane Contactor. A hollow fiber membrane unit may be utilized to allow the two liquid phases to intimately contact without formation of a dispersion/emulsion. One fluid will flow inside the hollow fibers, which have hydrophobic porous walls, while the second fluid phase will flow outside the fibers. Analogous to a shell-and-tube heat exchanger, the fluid that flows inside the hollow fiber membrane will be referred to as the tube-side fluid, and the fluid that flows outside the membrane will be referred to as the shell-side fluid. In addition, high mass transfer rates will be achieved due to the high surface area per volume in the hollow fiber units, which is much greater than that in conventional contacting equipment, and because of the porous nature of the membrane (11) (See Figure 1). Moreover, the effect of membrane on the overall mass transfer coefficient is also negligible (12). In the hollow fiber membrane contactor, the liquid-liquid interface is immobilized by the pressure difference between the phases in the pores of the microporous hydrophobic membrane as shown in Figure 1.

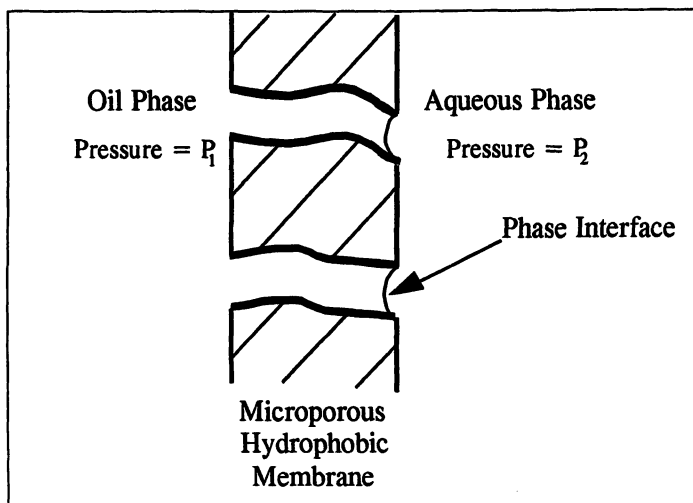


Figure 1. Interface immobilized in the pores of a hydrophobic membrane.

In liquid-liquid extraction, the solvent (oil) phase will wet the membrane because the membrane is hydrophobic. To achieve dispersion-free operation, the liquid interface has to be stabilized by applying a higher pressure on the aqueous side ($P_2 > P_1$). Aqueous liquid does not enter the pore unless a certain critical pressure is exceeded (13). The maximum allowable value of differential pressure for entering the hydrophobic pore of membrane is called the break-through pressure.

The presence of surfactants in the aqueous phase will drastically decrease the interfacial tension and increase the ability of the aqueous phase to wet the membrane. As a result, the value of the break-through pressure could be quite low. Surfactants that sufficiently lower the break-through pressure could allow transfer of the aqueous through the pores, which would negate the benefits of using the membrane to keep the phases separate. For such surfactants, a non-porous membrane could potentially be utilized; the membrane would need to be selected so that the contaminant had good solubility in the membrane material. Membranes with small pore sizes are preferable so that a comfortable value of pressure difference between the phases is obtainable in operation¹¹.

There is also the concern about mass transfer retardation from this pressure differential. The effect of this pressure difference is negligible on the total chemical potential driving force since the contribution of pressure difference is much less than the contribution of the concentration difference on the total chemical potential (11, 14).

Model. In the study of air stripping and liquid-liquid extraction processes, the pseudo-phase equilibrium model of micellar surfactant is applied to sizing the height or length of the unit (5, 7). This model is developed from a mass flux balance around the aqueous liquid phase integrated with the equilibrium expression by assuming that the partitioning of the contaminant between the micellar pseudophase and the extracellular aqueous phase is always at equilibrium (5). This assumption is practical since the micellar "life-time" is very short—on the order of millisecond—and solubilization can

rapidly reach equilibrium with the contaminant already dissolved in the aqueous phase (15). The driving force for mass transfer is based on the concentration difference between contaminant dissolved only in aqueous phase (excluding all contaminant in the micellar pseudophase) and the associated contaminant concentration in the solvent phase (path A in Figure 2). Contaminant that is only dissolved in the aqueous phase will transfer to the solvent phase and contaminant in surfactant aggregates will simultaneously adjust to the new equilibrium.

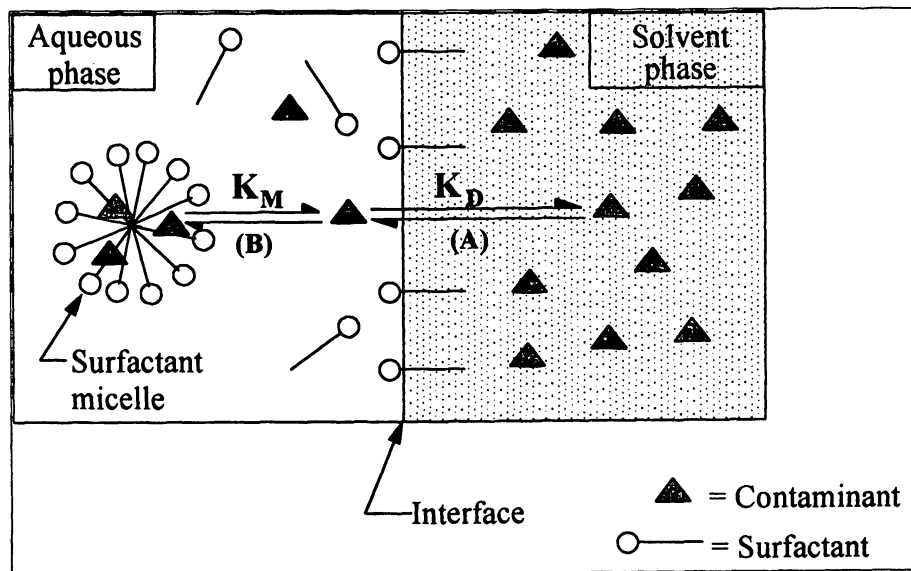


Figure 2. The Pseudophase separation model of liquid-liquid extraction. Path (A) contaminant equilibrium between oil and water represented by the oil/water partition coefficient. Path (B) contaminant equilibrium between the micellar pseudophase and extramellar aqueous solution represented by the micellar partition coefficient.

Materials and Methods

Materials. Tetrachloroethylene (PCE) and iso-butylbenzene (IBB) were the two contaminants studied in this research because their vapor pressures differ by an order of magnitude (Table I). PCE is a dense non-aqueous phase liquid (DNAPL) while IBB is a light non-aqueous phase liquid (LNAPL). Both PCE and IBB were purchased from Aldrich Chemical Co., Milwaukee, WI with 99%+ purity and used as received.

Table I. Properties of contaminants

Contaminant	PCE (Tetrachloroethylene)	IBB (iso-Butyl benzene)
Type	Chlorinated Hydrocarbon	Hydrocarbon
Formula	C ₂ Cl ₄	C ₁₀ H ₁₄
Formula Weight	165.83	134.22
Water Solubility at 25 °C	150 mg/L	14 mg/L
Vapor Pressure at 25 °C	20 mm Hg (0.3837 psia)	2.06 mm Hg (0.0398 psia)
Boiling point	121.2 °C	170 °C
Specific Density	1.63 at 20/4 °C	0.86 at 20/4 °C
log K _{ow} *	≈ 2.5	≈ 4.1
Henry's law constant	≈ 1.5 × 10 ⁻² (atm m ³ /mol)	1.09 × 10 ⁻² (atm m ³ /mol)

*The K_{ow} is the *n*-octanol/Water partition coefficient.

Dowfax 8390, a commercial mixture of sodium mono- and dihexadecyl diphenyl oxide disulfonates, (DPDS) and IGEPAL CO-880, a commercial polyethoxylated nonylphenol (ENP), were the surfactants used. DPDS was received from Dow Chemical Co., Midland, MI. IGEPAL CO 880 was obtained from Rhone-Poulenc, Cranbury, NJ. DPDS is a twin-head anionic surfactant while ENP is a nonionic surfactant. The properties of DPDS and IGEPAL CO 880 are shown in Table II.

Table II. Properties of surfactant

	DPDS	ENP
Ingredients	disodium Hexadecyl diphenyl oxide disulfonate, and Disodium dihexadecyl diphenyl oxide disulfonate	nonylphenol polyethyleneoxide ethanol (branched) (C ₂ H ₄ O) _n C ₁₅ H ₂₄ O
% active (by wt.)	40 % maximum	100 %
CMC (mM)	0.3	0.275
Formula Weight	642	1540
Appearance	light-brown liquid	waxy solid

Squalane (2, 6, 10, 15, 19, 23 hexamethyltetracosane, C₃₀H₆₂) was received from Pfaltz & Bauer, Inc., Waterbury, CT. Squalane was chosen as a solvent for extracting the solubilized contaminants from surfactant solution because it provides high partition coefficients, does not harm the environment, is non-toxic, and does not measurably solubilize in surfactant solutions⁷. The properties of squalane are shown in Table III.

Table III. Properties of squalane

Solvent Name	Squalane
Chemical Name	2,6,10,15,19,23-Hexamethyltetracosane
Formula	$C_{30}H_{62}$
Formula Weight	422.8
Boiling point	350 °C at 760 mm Hg
Specific Density	0.81 at 15/4 °C
Specific heat at 20°C	0.62
Appearance	Clear, oily liquid

The membrane column for the liquid-liquid extraction experiments was a Liqui-Cel Extra-Flow, a commercially available hollow fiber membrane contactor purchased from Hoechst-Celanese Corporation. The membrane column was 6 cm. in diameter and 20 cm. in length. The unit contained a Celgard X30 hollow-fiber membrane; the membrane material was polypropylene and with an estimated specific surface area of $1465 \text{ m}^2/\text{m}^3$. Each hollow fiber was 300 μm outside diameter with the wall thickness of 30 μm . The membrane wall is porous with an average pore diameter of 0.03 μm ; pores cover 40% of the fiber's surface. The effective surface area for mass transfer within the 20 cm column was 1.4 m^2 . An internal baffle, located at the middle of the column, ensured good liquid-fiber contact; the shell-side flow regime was intermediate between parallel and cross-flow.

Methods. Squalane-water-contaminant equilibrium experiments were conducted to determine equilibrium oil-water partition coefficient (K_D). The experiment for PCE was performed in 40 ml (EPA) vials. Each vial was sealed with a Teflon-coated septum. For IBB, the one liter glass bottles were used due to the lower water solubility of IBB. The samples were prepared with no headspace, and left to equilibrium at least 72 hrs with shaking twice a day. The partition coefficient (K_D) of PCE and IBB for water and squalane system were determined by analyzing the concentration of the aqueous phase (16). The maximum solubility of contaminants in surfactant measured using the maximum additivity method.

For the liquid-liquid extraction experiments, the samples were prepared by mixing 4 liters of water containing surfactant and contaminant at desired the concentration in amber glass bottles. The sealed bottles were stirred at least 4 hours.

To establish the counter-current flow of oil and the aqueous phase in the column, deionized water was first pumped into the column, and the desired flowrate set. Squalane was then introduced into the column. March orbital magnetic drive pumps delivered both oil and aqueous phases. Because the membrane was hydrophobic, squalane wet and filled the pores. To stabilize the contacting surface of oil and aqueous phase within the membrane's pores, a 5 psi higher pressure on the aqueous phase was maintained by adjusting a back pressure valve on the aqueous side. The aqueous phase was then switched from deionized water to surfactant solution. Both inlet and outlet of aqueous solutions were sampled; at least four outlet samples were taken at different times for each run.

A high performance liquid chromatograph (HPLC) equipped with a SHIMADZU SIL-10A auto injector and Water-486 tunable absorbance detector was used to analyze the aqueous samples. Typical mobile phases ranged from 70% to 80% acetonitrile depending upon the type of surfactant and contaminant.

Results and Discussion

The partition coefficients for PCE and IBB are shown in Table IV. The K_D for IBB is greater than for PCE, as expected based on its higher K_{ow} value (see Table I).

Table IV. The partition coefficient (K_D) between squalane and water, and the micellar partition coefficient (K_m) at maximum solubility

	The partition coefficient (K_D) between squalane and water	
	PCE	IBB
Coil/Cwater	1 509	12 000
Xoil/Xwater	~40 000	~310 000
	The micellar partition coefficient (K_m) at maximum solubility	
	PCE	IBB
Xs/Xwater for Dowfax 5×CMC	17 899	187 790
Xs/Xwater for IGEPAL 5×CMC	14 955	201 535

Figure 3 and Table V show the effect of the presence of the micellar pseudophase on contaminant removal in the liquid-liquid extraction unit. In Figure 3, the percent contaminant removal in 5×CMC surfactant solution is considerably less than the case of 0.8×CMC of the same type surfactant solution at 500 ml/min of aqueous flowrate. The percent contaminant removal is less for the 5×CMC case because the micellar pseudophase competes with the squalane phase to solubilize the contaminants. However, at a lower aqueous flowrate of 100 ml/min, the percent contaminant removal at 5×CMC increases and approaches the removal efficiency of the 0.8×CMC case, as shown in Table V.

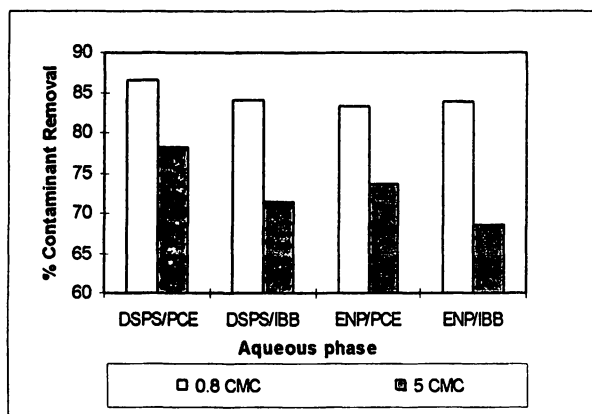


Figure 3. The effect of surfactant concentration on percent contaminant removal at aqueous flowrate 500 ml/min and squalane flowrate 5 ml/min.

Table V. The effect of surfactant concentration on contaminant removal from surfactant solution at squalane flowrate 5 ml/min.

Surfactant	Contaminant	Aqueous Flowrate (ml/min)	Average percent contaminant removal	
			0.8×CMC	5×CMC
DPDS	PCE	100	98.5	97.2
DPDS	PCE	500	86.5	78.1
DPDS	IBB	100	99.2	97.1
DPDS	IBB	500	84.0	71.4
ENP	PCE	100	97.7	97.6
ENP	PCE	500	83.2	73.6
ENP	IBB	500	83.9	68.5

In general, higher aqueous flowrates will lower removal efficiencies. This is due to the contaminant having a shorter time to transfer from the aqueous phase to the squalane phase at higher aqueous flowrates (Figure 4 and Figure 5). However, the squalane flowrate has little effect on percent removal due to the high contaminant-squalane partition coefficient.

Moreover, it can be noticed that IBB has a lower percent removal at 5×CMC from both surfactant solutions. This is because IBB has a micellar partition coefficient much greater than that of PCE (see Table IV). However, IBB may still be effectively removed from surfactant solution because of its very high partition coefficient into squalane, even though IBB's micellar partition coefficient is greater than PCE's micellar partition coefficient by an order of magnitude.

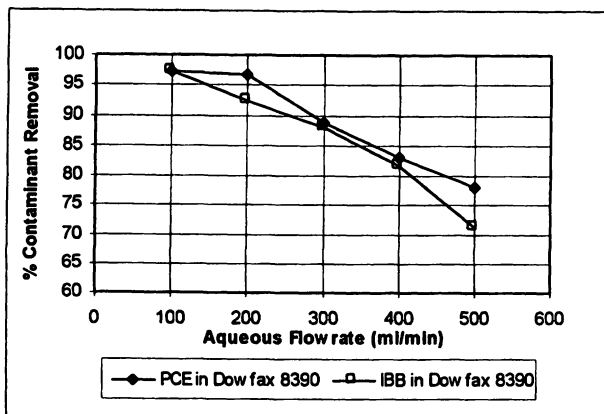


Figure 4. The percent contaminant removal from $5\times$ CMC DPDS solution at oil flowrate 5 ml/min.

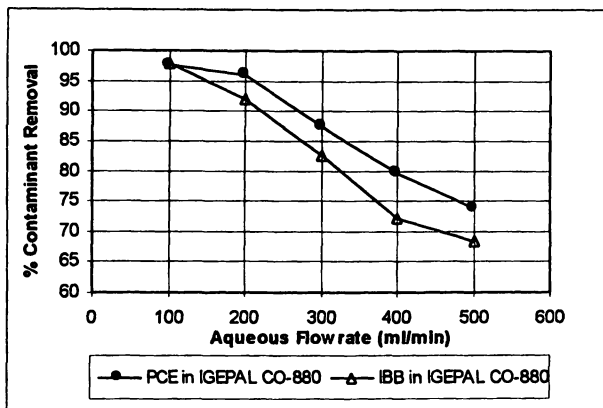


Figure 5. The percent contaminant removal from $5\times$ CMC ENP solution at oil flowrate 5 ml/min.

Table VI and Table VII contain the results of contaminant removal at different aqueous flowrate and squalane flowrate for $0.8\times$ CMC and $5\times$ CMC surfactant solution. Each set of results represents the average of the % removals for multiple runs.

Table VI. Contaminant removal from $0.8\times$ CMC surfactant

Flowrate (ml/min)		Average percent contaminant removal			
Aqueous	Squalane	DPDS		ENP	
		PCE	IBB	PCE	IBB
100	5	98.5	99.2	97.7	NA
500	5	86.5	84.0	83.2	83.9
100	30	99.4	99.3	99.9	99.9
500	30	NA	90.6	87.0	NA

NA = Not applicable

Table VII. The conclusion of percent contaminant removal from 5×CMC surfactant

Flowrate (ml/min)		Average percent contaminant removal			
		DPDS		ENP	
Aqueous	Squalane	PCE	IBB	PCE	IBB
100	5	97.2	97.1	97.6	97.9
200	5	96.7	92.2	96.0	91.9
300	5	88.8	88.1	87.3	82.6
400	5	83.0	81.6	79.6	72.1
500	5	78.1	71.4	73.6	68.45
100	30	99.7	99.3	97.1	NA
500	30	79.6	NA	NA	68.5

NA = Not applicable

The overall mass transfer coefficient

Hasegawa, et al. (7) demonstrated that the surfactant liquid-liquid extraction model (SLLEM) was corroborated by experimental results. This model was derived from mass balance calculations combined with the partition coefficients of contaminant between water and both the micellar pseudophase and the solvent phase. For continuous counter-current flow, the required length of contact for liquid-liquid extraction is given by:

$$Z = \frac{Q_w}{K_w a \cdot A_c} \frac{1}{\alpha} \ln \left[\left(\frac{S}{S\alpha + 1} \right) \left(\frac{C_{in}}{C_{out}} \cdot \alpha + \frac{1}{S} \right) \right] \quad (6)$$

where $\alpha = \frac{1}{K_m \cdot C_{surf,m} \cdot \bar{v}_w + 1} - \frac{1}{S}$ and $S = \frac{Q_{oil} \cdot K_d}{Q_w}$; Q_w is the aqueous phase volumetric flowrate and Q_{oil} the solvent phase volumetric flowrate. K_w is the overall mass transfer coefficient based on aqueous side. A_c and a are, respectively the cross-sectional areas of the column perpendicular to flow and the specific surface area of the hollow fiber membrane for mass transfer.

The overall mass transfer coefficient can be calculated from the above equation; the results are shown in Figure 6. Obviously, the K_w value at 100 ml/min aqueous flow rate has the lowest value for the same contaminant/surfactant system. This indicates that there is a tradeoff between flow rate and removal; i.e., to get a very high percent recovery you must lower the aqueous flow rate. A lower rate appears to be more than offset by a longer contact time. It is interesting that the value of K_w levels off at higher flow rates. This suggests that the designing engineers should perform optimization studies on the impact of the mass transfer coefficient for the full-scale implementation of the process.

For systems containing IBB as a contaminant, the K_w value is higher than the value for PCE. From the equilibrium results, both the oil-water partition coefficient

about an order of magnitude. It can be seen in the model that the oil-water partition coefficient (K_D) plays a more important role than the micellar partition coefficient K_m .

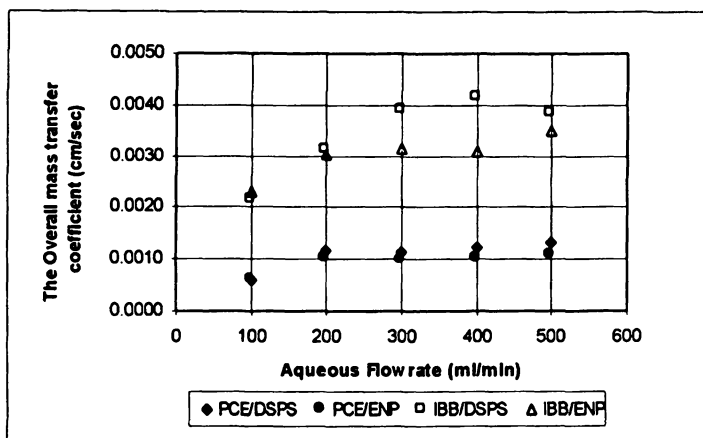


Figure 6. The overall mass transfer coefficient as varied aqueous flowrate at oil flowrate 5 ml/min

Ideally, the mass transfer coefficients from equation 6 should be compared to values from empirical equations in dimensionless form. For instance, the mass transfer coefficients in air-stripping packed column can be obtained from Onda's equation (17). By analogy to a shell and tube heat exchanger, the mass transfer coefficients in hollow fiber membrane can be related to equations developed for heat transfer. The flow patterns on the shell side of the membrane module can be in parallel flow, crossflow or semi-crossflow (as used in this study). Furthermore, the shellside flow in the membrane module is influenced by backmixing, bypassing, and channeling. In general, the empirical equations developed in the literature seemingly reflect the specific system and conditions studied. Further studies are suggested to correlate and explain the mass transfer coefficient data (11).

Conclusion.

The liquid-liquid extraction process is capable of removing a high percentage of contaminants from aqueous surfactant streams, even when contaminant activities are reduced by the presence of the micellar pseudophase. The use of a hollow fiber membrane contactor helps prevent the formation of emulsions during operation. As expected, longer contact times (i.e., lower aqueous flow rates) improve contaminant removal, but the overall process will be more expensive due to the larger hollow fiber membrane contactor required. The overall mass transfer coefficient is constant at higher flow rates but decreases with lower flow rates. All of these factors should be considered and optimized for a pilot scale application of this process.

Literature Cited.

1. Sabatini, D. A.; Knox, R. C.; Harwell, J. H. In *Surfactant Enhanced Subsurface Remediation: Emerging Technologies*; Sabatini, D. A.; Knox, R. C., Harwell, J. H. Ed.; ACS Symposium Series 594; American Chemical Society: Washington, DC, 1995, Chapter 1, pp 1.
2. Harwell, J. H.; Sabatini, D. A.; Knox, R. C. In *Annual Surfactants Review: New Products and Applications in Surfactant Technology*; D.R. Karsa, Ed.; Sheffield Academic Press, Sheffield, England, 1998, Volume 1; pp 30-58.
3. Krebs-Yuill, B.; Sabatini, D. A.; Knox, R. C.; Harwell, J. H. In *Surfactant Enhanced Subsurface Remediation: Emerging Technologies*, Sabatini, D. A., Knox, R. C., Harwell, J. H. Ed.; ACS Symposium Series 594; American Chemical Society: Washington, DC, 1995, Chapter 19, pp. 265.
4. Yeufeng, Y.; Scamehorn J. F.; Christian, S. D. In *Surfactant Enhanced Subsurface Remediation: Emerging Technologies*, Sabatini, D. A., Knox, R. C., Harwell, J. H. Ed.; ACS Symposium Series 594; American Chemical Society: Washington, DC, 1995, Chapter 17, pp. 231.
5. Lipe, K. M.; Sabatini, D. A.; Hasegawa, M. A.; Harwell, J. H. *Ground Water Monitoring and Remediation*, 1996, 16, 85.
6. Choori, U. N.; Scamehorn, J. F.; O'Haver, J. H.; Harwell, J. H. *Ground Water Monitoring and Remediation*, 1998, 18, 157.
7. Hasegawa, M. A.; Sabatini, D. A.; Harwell, J. H. *J. Envir. Eng.* 1997, 123, 691.
8. Hutter, J. C.; Vandegrift, G. F. In *Environmental Remediation: Removing Organic and Metal Ion Pollutants*, Vandegrift, G. F., Reed, D. T., Tasker, I. R. Ed.; ACS Symposium Series 509; American Chemical Society: Washington, DC, 1992, Chapter 4, pp 47.
9. Rouse, J. D.; Sabatini, D. A.; Deeds, N. E.; Brown, R. E. *Environ. Sci. Technol.*, 1995, 29, 2484.
10. Treybal, R. E. *Mass-Transfer Operations*, 3rd edition, McGraw-Hill, New York, 1980.
11. Prasad, R.; Sirkar, K. K. In *Membrane Handbook*, Ho, W. S., Sirkar, K. K. Ed.; Van Nostrand Reinhold, New York, 1992, Chapter 47, pp. 727.
12. Yang, M. C.; Cussler, E. L. *AIChE Journal*, 1986, 32, 1910.
13. Kim, B. S.; Harriott, P. *J. Colloid Interface Sci.*, 1987, 115, 1.
14. Prasad, R.; Bhave, R. R.; Kiani, A. K.; Sirkar, K. K. *J. Membr. Sci.*, 1986, 26, 79.
15. Ward A. J. In *Solubilization in surfactant aggregates*, Christian, S. D., Scamehorn, J. F. Ed.; Marcel Dekker, New York, 1995, Chapter 7, pp. 237.
16. Zander, A. K.; Qin, R.; Semmens, M. J. *J. Envir. Eng.*, 1989, 115, 768.
17. Onda, K.; Takeuchi, H.; Okumoto, Y. *J. Chem. Eng. Japan*, 1968, 1, 56.

Chapter 7

Block Copolymer Micelles for Water Remediation

Jos T. F. Keurentjes

Department of Chemical Engineering, Process Development Group, Eindhoven
University of Technology, P.O. Box 513, 5600 MB Eindhoven, Netherlands

In this study aqueous solutions of block copolymers of the PEO-PPO-PEO type have been used for the extraction of organic pollutants from aqueous streams. For a proper description of this system, and hence for a description of the solubilization of organic components, the use of a modified Flory Huggins model is required. Saturation experiments have shown that above a certain transition temperature the solubilization of naphthalene in a 10 wt% solution can increase to up to 135 times the solubility in water. This corresponds with a value of the normalized partition coefficient (PPO core/water) in excess of 2000. This transition takes place over a temperature interval of about 15 °C. The predominant effect causing this solubilization increase is an increase in micelle radius, while the change in polarity of the micelle core is of minor importance. Process options are described, based on the use of ultrafiltration membranes. As the solubilization process has shown to be reversible, the saturated micelle solution can easily be regenerated by a moderate decrease in temperature.

For the remediation of polluted water streams several technologies are currently being applied. Biotreatment can be regarded as the simplest method to deal with water pollution, however, it can only be used for the removal of biodegradable compounds. Many water streams originating from industrial activity contain one single or a limited group of related compounds. Provided these compounds are volatile, steam or air stripping are usually considered the most effective technologies to be applied, despite the energy consumption involved. For non-volatile pollutants, however, liquid-liquid extraction will be the appropriate technique to be used, as for almost every compound an efficient extractant can be found. Nevertheless, several drawbacks of L-L extraction can be identified. Firstly, a liquid that is an effective extractant for a specific pollutant

usually is difficult to regenerate. Secondly, and this is especially valid for the removal of low concentrations of pollutant, there will always be an equilibrium concentration of the extractant dissolved in the water stream to be treated, how ever small this concentration will be. Nevertheless, for many practical cases this concentration will exceed the concentration of the pollutant to be removed, so that the original problem has been replaced by a new one. In this study we have used aqueous solutions of amphiphilic block copolymers as an extractant for organic pollutants from aqueous streams. It will be shown that the two drawbacks commonly associated with the use of liquid extractants as described above can effectively be overcome.

In this study we use amphiphilic block copolymers of the poly(ethylene oxide)-poly(propylene oxide)-poly(ethylene oxide) type, commercially known as Pluronics or Synperonics. These have found important applications in the field of detergency, foaming and antifoaming and as an additive to many products to improve wetting properties (1). A broad range is commercially available with different molecular weights, different block lengths and varying block ratios, so that it is possible to use a polymer with the characteristic properties required for a specific application. Due to their aggregation behavior in water, these block copolymers can effectively be used for increasing the solubility of hydrocarbons (2-7).

From a process engineering point of view, it appears extremely attractive to combine the extraction properties of these polymer aggregates with the capability of ultrafiltration membranes to retain the polymers, while being permeable for small molecules (8). Several routes have been proposed in the literature to make this a feasible combination of techniques. Scamehorn and coworkers (9) developed a micellar enhanced ultrafiltration (MEUF) technique in which the micelle solution is directly added to the polluted stream. Subsequently, the micelle solution is filtered over an ultrafiltration membrane to separate the micelles from the purified water stream. More recently, the same principle has been used for the separation of enantiomeric mixtures, using entioselective surfactants (10). In a different approach, a hollow fiber membrane has been used to provide a semi-permeable barrier between the block copolymer solution and the polluted stream, a process often referred to as pertraction. This barrier is permeable to the compounds to be extracted, but impermeable to the block copolymers (7).

For an effective application of these solutions as an extraction medium, it is important to have a basic insight in the processes governing the transformations occurring in these aqueous block copolymer solutions. In this paper the effect of temperature and concentration on the extraction of naphthalene has been investigated.

Theory

In figure 1 a generalized phase diagram of the poly(ethylene oxide)-poly(propylene oxide)-poly(ethylene oxide) block copolymers is depicted. At low temperature and concentration the molecules form a stable solution in water. By increasing the temperature or concentration to values above the CMT (critical micellization temperature) or CMC (critical micellization concentration) an intermediate transition region exists in which both free molecules and micelles can be found. In this region, the free molecule-micelle equilibrium will shift toward the micelles with increasing temperature and polymer concentration. Upon a further increase of temperature or

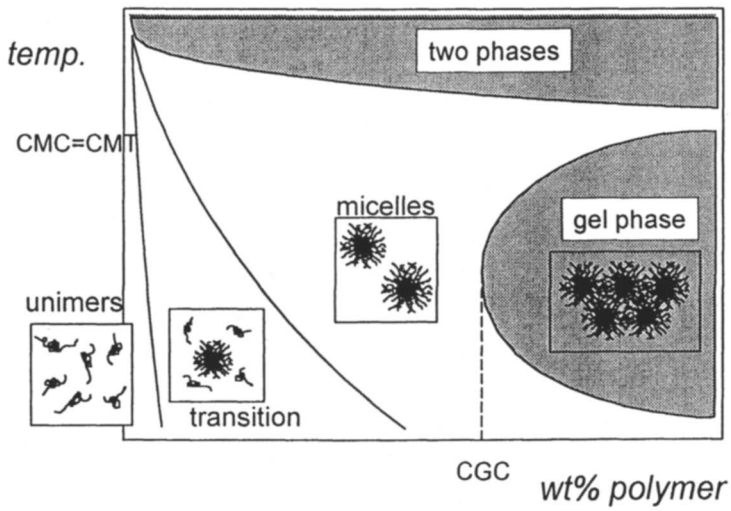


Figure 1. Generalized phase diagram for aqueous solutions of PEO-PPO-PEO block copolymers

concentration a region can be defined in which all molecules are found in micelles (11-13).

The solubilization properties of these PEO-PPO block copolymer solutions can only be calculated when a proper model of the micelle solution can be defined. For this purpose, we compared three different models: UNIFAC, the "normal" Flory Huggins, and a modified Flory Huggins model. In addition to the models evaluated here, the self-consistent lattice theory can provide a powerful means to evaluate the solubilization behavior of block-copolymer micelles (14-16)

UNIFAC. The simplest description of the thermodynamic properties of a polymer solution as a function of temperature and composition is based on activity coefficients:

$$\mu_i^* = kT \ln \frac{f_i}{f_i^0} = kT \ln a_i \quad (1)$$

in which μ_i^* is the reduced chemical potential of component i , and f_i and f_i^0 are the fugacities of component i in the mixture and in its pure liquid state, respectively. In order to estimate the activity coefficients a_i , UNIFAC (Uniquac Functional group Activity Coefficients) can be used (17). The activity coefficients are split up into a combinatorial part (γ_i^c) and a residual part (γ_i^r). The combinatorial part is related to the shape and the size of the molecules, whereas the residual part comprises interactions between the different groups in a molecule:

$$\ln \gamma_i = \ln \gamma_i^c + \ln \gamma_i^r \quad (2)$$

In polymer solutions, however, changes in free volume may occur upon mixing. In order to compensate for these effects, Oishi and Prausnitz (18) proposed an additional third term (γ_i^{FV}) for eq. 2:

$$\ln \gamma_i = \ln \gamma_i^c + \ln \gamma_i^r + \ln \gamma_i^{FV} \quad (3)$$

Flory Huggins. A common way to describe the behavior of polymer solutions is the Flory Huggins model. In this model the polymer is divided into m equivalent segments, usually the degree of polymerization. Each segment of the polymer and each solvent molecule occupy a volume element of a lattice. Assumptions of this model are:

1. Solvent molecules and polymer segments occupy one single site of the lattice
2. The lattice is homogeneous; each site is surrounded by the same number of neighboring sites
3. Volume effects associated with mixing are neglected
4. Interactions between segments is limited to neighboring segments only

Based on statistics, expressions for the enthalpy and entropy of mixing can be derived (19):

$$S_{mix} = -kM_0 \left(v_1 \ln v_1 + \frac{v_2}{m} \ln v_2 \right) \quad (4)$$

$$H_{mix} = kT\chi_{12}M_0v_1v_2 \quad (5)$$

In these expressions M_0 , v_1 and v_2 are defined as

$$M_0 = n_1 + n_2 \cdot m \quad (6)$$

$$v_1 = \frac{n_1}{M_0} \quad (7)$$

$$v_2 = \frac{mn_2}{M_0} \quad (8)$$

where v_1 and v_2 are the volume fraction solvent and polymer, respectively; m is the degree of polymerization; n_1 and n_2 are the number of solvent and polymer molecules, respectively; M_0 is the total number of segments and χ_{12} is the Flory Huggins interaction parameter between solvent and polymer. This χ -parameter only depends on the properties of the two interacting segments ($kT\chi$ =constant).

Modified Flory Huggins. Specifically for PEO-water and PPO-water systems, a modification of the Flory Huggins approach has been proposed by Karlström and coworkers (20,21). As a result of rotational freedom, the polymer segments are assumed to be in a polar or a non-polar conformation. The polar and nonpolar states have degeneration factors f_p and f_n , respectively, and are assumed to be in equilibrium with each other. The two conformations exhibit a different interaction with water, which is expressed in the polymer-water interaction parameters (χ_{pw} and χ_{nw}) that increase when the polymer becomes more hydrophobic. The derivation of the Gibbs free energy can now be performed similar to the ordinary Flory Huggins expression and results in

$$\frac{H}{kTM_0} = v_1v_2(P\chi_{pw} + (1-P)\chi_{nw}) + v_2^2P(1-P)\chi_{pn} + v_2(1-P)\alpha \quad (9)$$

$$-\frac{S}{M_0k} = v_1 \ln v_1 + \frac{v_2}{m} \ln v_2 + v_2(P \ln P + (1-P) \ln \frac{(1-P)}{F}) \quad (10)$$

in which P is the probability that a polymer segment will be in the polar state; F is the degeneration ratio (f_p/f_n), and α is the energy difference between the polar and nonpolar conformation. The equilibrium composition of the two phases can now be determined by calculating the two points with the same tangent on the Gibbs free energy curve. In these points, the chemical potentials of both components in both phases are equal.

Addition third component. When a third component is added to the water-polymer system, it will be distributed between the two phases. Hydrophilic components will preferentially dissolve in the water phase, while hydrophobic components will prefer

the polymer phase, provided the polymer forms hydrophobic microdomains. The effect of the added component on the Gibbs free energy results in one additional term in the entropy equation and two additional terms in the enthalpy equation:

$$\frac{H}{kTM_0} = v_1 v_2 (P \chi_{pw} + (1-P) \chi_{nw}) + v_2^2 P(1-P) \chi_{pn} + v_2(1-P) \alpha + v_1 v_3 \chi_{w3} + v_2 v_3 \chi_{p3} \quad (11)$$

$$-\frac{S}{M_0 k} = v_1 \ln v_1 + \frac{v_2}{m} \ln v_2 + v_3 \ln v_3 + v_2 (P \ln P + (1-P) \ln \frac{(1-P)}{F}) \quad (12)$$

The additional terms in the enthalpy equation represent the interaction of the third component with water (χ_{w3}) and with the polymer (χ_{p3}), respectively. It is important to note, however, that it is assumed that the interactions between the additional component and the polar and nonpolar states of the polymer are equal. The calculation of the partitioning of the third component is similar to the calculation of the polymer-water system, except that now a tangent plane instead of a tangent has to be calculated.

Experimental

To study the effect of block length and block ratio of the block copolymers on hydrocarbon solubilization capacity, three different block copolymers were used: L64, P103, and P104. The basic properties of these three polymers, obtained from BASF (Ludwigshafen, Germany) are given in Table I. For the application investigated here, it is important that micellization, and hence solubilization of the organic, occurs around room temperature. As it is known from literature that P104 forms stable micelles (12) and is capable of solubilizing significant amounts of hydrocarbons at room temperature (7), this polymer was used as the starting material. Also, P103, a polymer with a different block ratio and L64, a polymer with a different length but a block ratio similar to P104 were used.

As the focus of this study was on the effect of block length and block ratio of the polymer, only one single organic solute has been used. The solubilization of naphthalene in different polymer solutions at different temperatures was determined in the setup depicted in figure 2. Saturation was obtained by circulating 200 mL of the polymer solution over a column (length and diameter of 15 and 2.5 cm, respectively) packed with pure naphthalene crystals. The naphthalene was p.a. quality and was obtained from Aldrich. The circulation velocity was varied between 10 and 20 cm/min. The temperature, measured at the top of the column using a Pt-100 thermocouple, was controlled by a Braun FrigoMix-S/ThermoMix-S combination. To minimize heat losses, the column was isolated with glass wool and tin foil. Samples were taken at the top of the column and were diluted using a Microlab 1000 diluter prior to analysis. The concentration of naphthalene was measured spectrophotometrically using a Beckman DU-500 UV/VIS apparatus at a wavelength of 276 nm. Polymer concentrations were determined by refractive index measurements. DSC analysis of pure polymer samples was performed on a Seiko RDSC 220 apparatus. DSC analysis of aqueous polymer solutions was performed on a Perkin Elmer 7 Series thermal analysis system.

Table I. Basic physical properties of the block copolymers used

property	L64	P103	P104
MW (g/mol)	2900	4950	5900
% PEO	40	30	40
γ (mN/m, 25 °C, 0.1%)	43	34	33
cloud point (°C)			
1 wt% polymer	58	86	81
10 wt% polymer	60	52	78
HLB	12-18	12-18	12-18

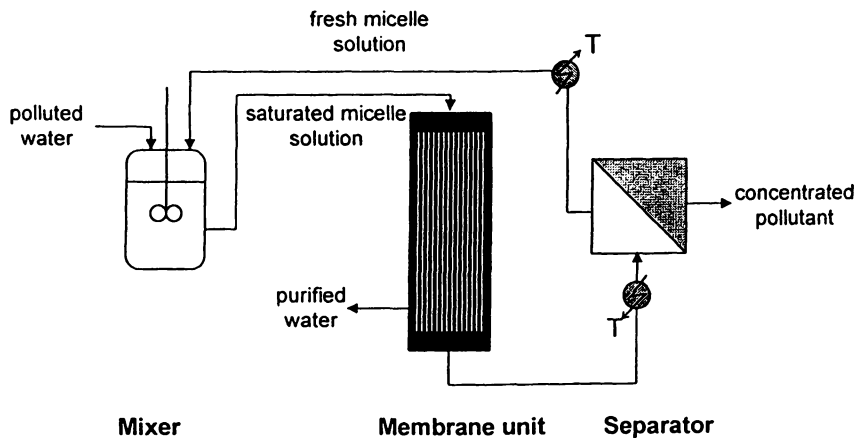


Figure 2. Experimental setup for the determination of naphthalene solubility in various block copolymer solutions

Results and Discussion

Modeling PEO-PPO systems. The three different models described in the Theory section have been compared with experimental data. The phase diagrams for PEO-water and PPO-water have been constructed using these models. In figure 3 phase diagrams for PEO-water are depicted. From the experimental values (22) it appears that these systems possess both a lower and an upper critical solution temperature, LCST and UCST, respectively. This results in an “egg-shape” demixing region. UNIFAC only describes UCST, due to the fact that the additional non-combinatorial entropy contributions are absent, and due to the fact that the interaction parameters are temperature-independent. Essentially the same applies for the “normal” Flory Huggins model. From figure 3 it can also be concluded that the UNIFAC prediction hardly shows any correlation with the experimental data. Improvement of these calculations by adjusting interaction parameters by making them temperature-dependent, or by correcting for free volume appears to be impossible (23).

The “normal” Flory Huggins model does not predict any demixing above 0 °C for the PEO-water system. Values for $\chi_{\text{EO-water}}$ found in the literature range from 0.2-0.4 at 25 °C (5,24), whereas from the Flory Huggins model a value in excess of 0.5 is required (for $m=\infty$):

$$\chi_{T_c} = \lim(m \rightarrow \infty) \frac{1}{2} \left(1 + \frac{1}{\sqrt{m}} \right)^2 = 0.5 \quad (13)$$

Assuming a UCST of 227 °C at $m=50$, an adjusted χ -parameter of 1.1 can be calculated. Using this value of 1.1, it is possible to describe the lower demixing behavior of PEO-water. This is shown in figure 4 for $m=50$ and 182, respectively. Although the Flory-Huggins description yields a better approximation of the phase behavior, it still does not adequately describe the experimental data. Moreover, the adjustment of the χ -parameter according to equation (13) is undesired, as it is treated more as a fit parameter instead of a physical quantity. From figure 3 it can be concluded that the composition of the aqueous as well as the PEO phase are reasonably well predicted using the modified Flory-Huggins model. Also, it is the only model predicting UCST and LCST values corresponding with experimental data.

In figure 5 the phase diagrams for the PPO-water system are depicted. Like for the PEO-water system, the modified Flory-Huggins model is the only model describing the data reasonably well. The change in polarity of the PPO and PEO blocks and their interaction with water upon a change in temperature will be of great importance for the formation and growth of the micelles. Upon a change in temperature from 70 to 90 °C the fraction polymer in the polar configuration will decrease strongly, thus forcing the water out of the core of the micelle. This will cause growth and compaction of the PPO core. It has been shown by Wanka et al. (12) that the aggregation number of different PEO-PPO block copolymers (P104, P123 and P127) strongly increases with increasing temperature, while the hydrodynamic radius remains constant. When the phase diagrams are calculated for different chain lengths of PPO, it appears that the differences between demixing curves decrease upon an increase of the molecular weight, so that it can be concluded that the cores of the micelles formed by L64

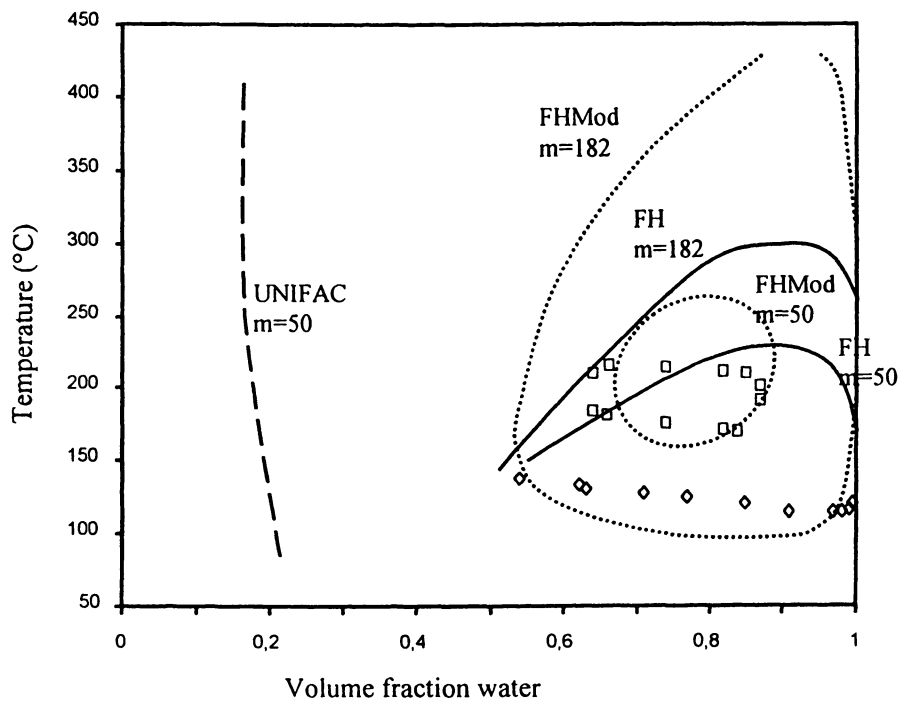


Figure 3. Phase diagram for the system PEO-water. Experimental data are from (19); □ represents data for $m=50$ and ◇ represents data for $m=182$. $\chi_{EO-water}=1.1$ (25 °C).

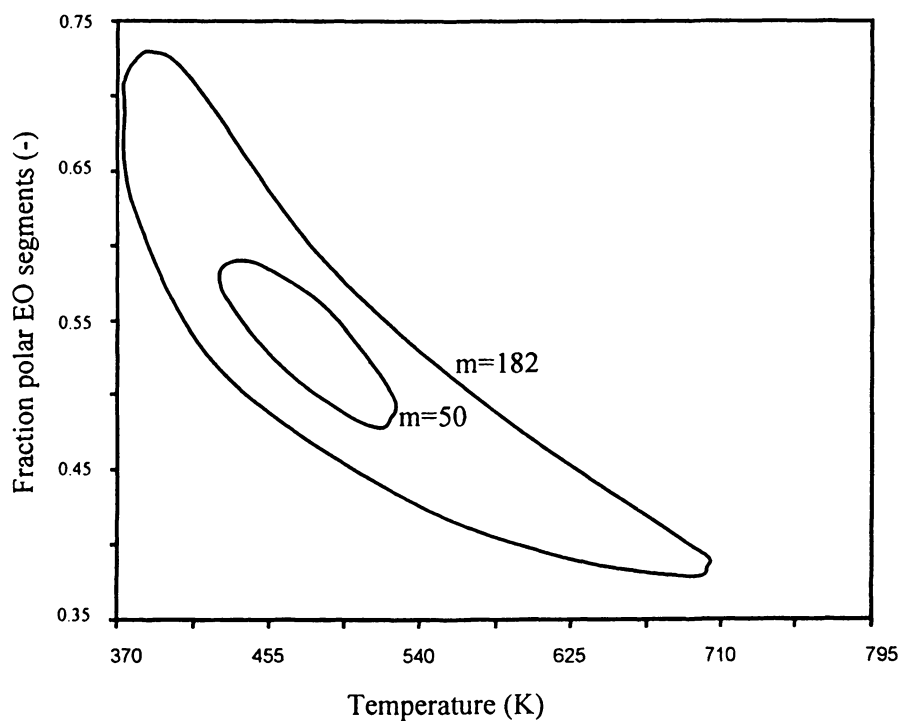


Figure 4. Fraction polar polymer at demixing at different temperatures.

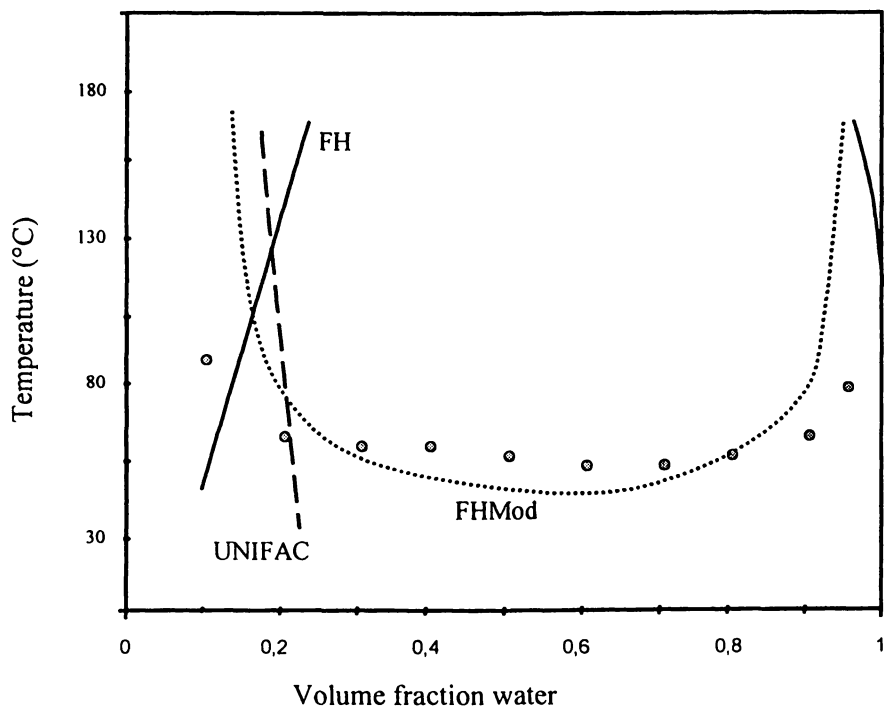


Figure 5. Phase diagram for the system PPO-water. Experimental data are from (21) for $m=400$; $\chi_{\text{PO-water}}=2.0$ (25 °C).

($m_{\text{PPO}}=30$), P103 and P104 (both with $m_{\text{PPO}}=58$) will approximately have the same composition.

Solubilization of hydrocarbons. The solubilization of naphthalene has been established by measuring the saturation concentration with varying polymer concentrations at different temperatures. The results are depicted in figures 6-8, in which the ratio between the concentration in the micelle solution and the concentration in pure water is plotted as a function of the polymer concentration (figure 6), or temperature (figures 7 and 8). From figure 6 it can be concluded that the saturation concentration increases approximately linearly with an increase in polymer concentration, a result in agreement with earlier work (7,25). As in the transition region the number of micelles will increase proportionally with an increase in the polymer concentration, it seems likely that all data of figure 6 are located in the transition region. In Table II, the normalized saturation ratios are given. This ratio K_{PPO} is defined as

$$K_{\text{PPO}} = \frac{c_{\text{polymer}} / c_{\text{water}}}{\text{wt}\%_{\text{polymer}} * \text{wt}\%_{\text{PPO}}} \quad (14)$$

where $\text{wt}\%_{\text{polymer}}$ is the weight fraction polymer in the solution and $\text{wt}\%_{\text{PPO}}$ is the weight fraction PPO in the polymer. From Table II it will be obvious that the normalized saturation of L64 is the most dependent on the polymer concentration. For P103 and P104 normalized partition coefficients in excess of 2000 have been established, indicating that the micelle core represents an effective extraction medium for naphthalene. The solubilization of naphthalene in the micelle solution is probably determined by the PPO block, although an increase in the length of the PEO block may result in better stabilization of the core, so that the partition coefficient can increase slightly (26).

From figure 8 it can be seen that the transition temperature is a polymer characteristic depending on block lengths and ratios. The transition temperature appears to increase upon a decrease in polymer length. From the literature (12,27,28), it is known that L64 hardly forms any micelles at 25 °C, while P104 forms stable aggregates at this temperature.

Modeling hydrocarbon solubilization. The saturation experiments have been described using the modified Flory Huggins model. The parameters used are listed in Table III. From these calculations it appears that the normalized distribution coefficient for naphthalene over the PPO core and water decreases upon an increase in temperature. Since the polarity of the PPO blocks does not change over the entire temperature interval (15), it is obvious that the model in this form is not capable to describe the measured effects.

For this reason, the curvature of the micelles has been taken into account for the calculation of the partial Gibbs free energy of the solute. The same phenomenon has been observed in emulsion polymerization, where particles are swollen with monomer (29). The contribution of the surface tension (σ) and core radius R_0 to the partial Gibbs free energy can be calculated according to the Gibbs-Thomson equation:

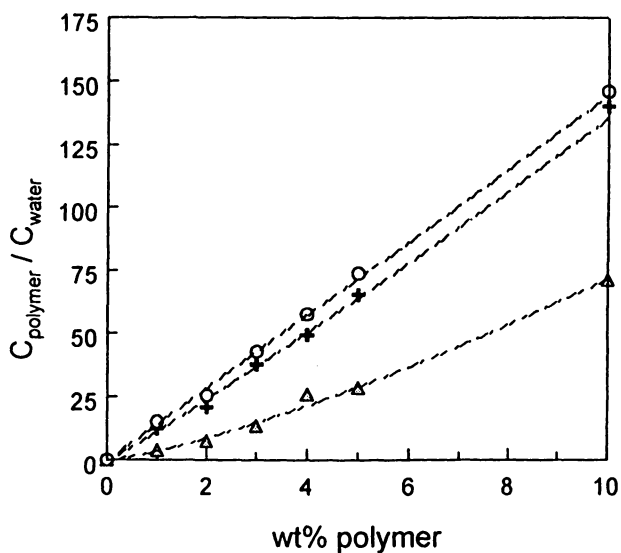


Figure 6. Solubility of naphtalene in the polymer solution relative to the solubility in pure water for different polymer concentrations (+, P104; Δ, L64; o, P103; T=30°C).

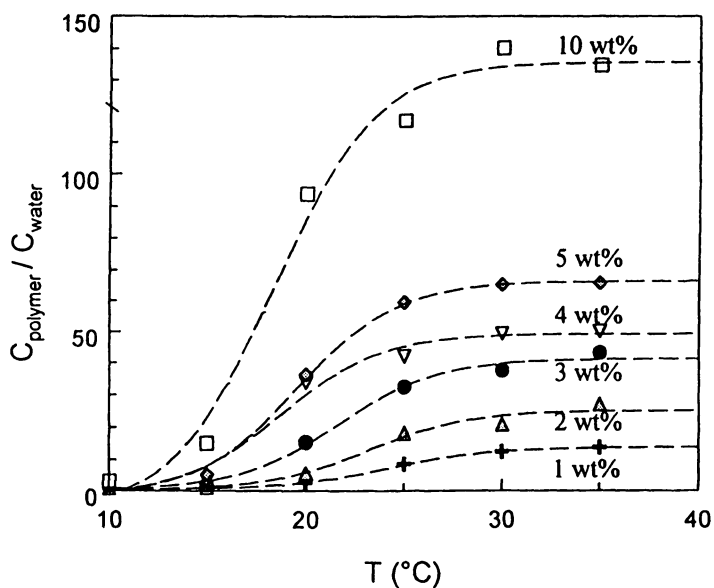


Figure 7. Solubility of naphtalene in P104 solutions as a function of the temperature for different polymer concentrations.

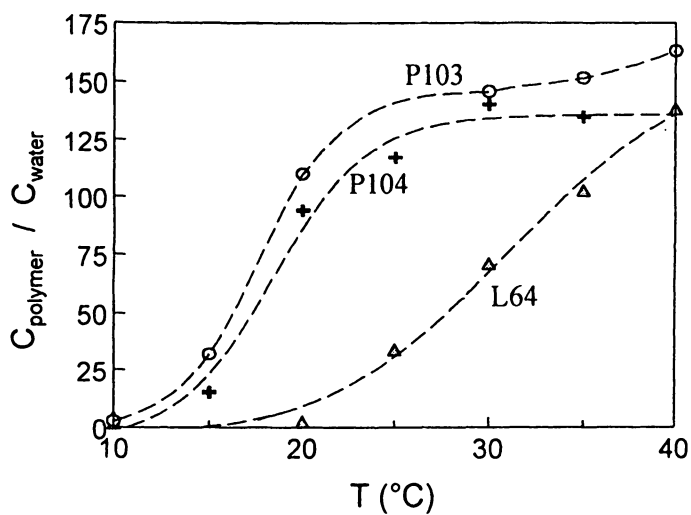


Figure 8. Solubility of naphthalene in 10 wt% solutions of different polymers (+, P104; Δ , L64; o, P103).

Table II. Normalized partition coefficients for L64, P104, and P103 solutions at 30 °C and varying polymer concentrations

wt% polymer	L64	P104	P103
1	648	2064	2165
2	625	1734	1821
3	756	2091	2038
4	1080	2058	2060
5	953	2176	2112
10	1184	2336	2084

Table III. Parameters used in the modified Flory Huggins model for the calculation of the distribution of naphthalene over the PPO core and the surrounding aqueous phase.

$RT\chi_{pw}^{(17)}$	1.7	kJ/mol
$RT\chi_{nw}^{(17)}$	8.5	kJ/mol
$RT\chi_{pn}^{(17)}$	1.4	kJ/mol
$RT\alpha^{(17)}$	11.5	kJ/mol
$RT\chi_{p3}^{(10)}$	$24.8 \cdot 10^{-2}$	kJ/mol
$RT\chi_{w3}^{(10)}$	13.6	kJ/mol
$F^{(17)}$	60	
$\sigma^{(5)}$	25.9	mN/m

$$\mu_s = \frac{2V_m \sigma (1 - v_m)^{1/3}}{R_0} \quad (15)$$

with V_m as the molar volume of the solute, v_m as the volume fraction of the solute, and R_0 as the radius of the unswollen micelle core. The calculated results are depicted in figure 9, from which it can be concluded that an increase of the core radius from 1 nm to approximately 4 nm is sufficient to explain the measured normalized partition coefficients. A core radius of 4 nm appears reasonable when compared with data found in the literature, where micelle radii of about 7 nm are reported (11,13). From figure 9 it can also be seen that the solubility increase caused by the composition change of the micelle at a constant radius is of minor importance, while growth of the core represents the predominant effect.

Although a shift in the ratio polar and nonpolar PO segments in the micelle core is the driving force for phase separation, it is remarkable that it plays a minor role in the solubilization process. It seems plausible, however, that the polarity change of the PPO blocks induces micelle growth due to the fact that this is determined by the interaction between water and the PPO segments.

DSC experiments. DSC experiments have been performed on pure polymers and on 10 wt% aqueous solutions. In figure 10 the results for polypropylene glycol (MW=3000) and P104 are shown. The curve for PPG does not show any heat effect in the range between 10 and 40 °C. Hence, melting of the core does not seem a likely mechanism for the solubilization transition taking place. The DSC curve for P104, however, does show an endothermic peak at 35 °C. This peak is most likely the result of melting of the PEO blocks, as it exactly corresponds with the melting temperature of PEG with a similar molecular weight (for P104 $MW_{PEO} \approx 800$; $T_{melt} = 32-36$ °C). It can also be seen from the P104 curve that the PPO blocks in this polymer show the same glass transition as observed in PPG at -70 °C.

The DSC curves of 10 wt% solutions of P104 and L64 (figure 11) show an endothermic peak, which is similar to the melting peak of the pure polymer, although it occurs at somewhat lower temperature. It can also be seen that the transition temperature exactly corresponds with the transition found in the solubilization experiments. The heat effect observed is of the same order of magnitude (66 J/g for the melting of P104 and 55 J/g for L64, respectively). This value, however, is one order of magnitude higher than the standard enthalpy for micellization (30). The heat effect, which is probably the result of a transformation of the PEO blocks in the micelle from an ordered to a disordered state, seems to be dependent on the aggregation behavior of the polymer. Subsequently, this is reflected in the solubilization of naphtalene.

Concept process design. As can be seen from figures 7 and 8, the solubility of naphtalene in a micelle solution strongly depends on the temperature. In contrast to the solubility of naphtalene in pure water, which increases almost linearly with temperature, the saturation concentration in a micelle solution shows a stepwise increase above a certain transition temperature. Even more important, this phenomenon appears to be reversible. When a saturated solution of P104 is cooled down from 30 to 10 °C, this results in crystallization of the naphtalene. After filtration over a Whatman

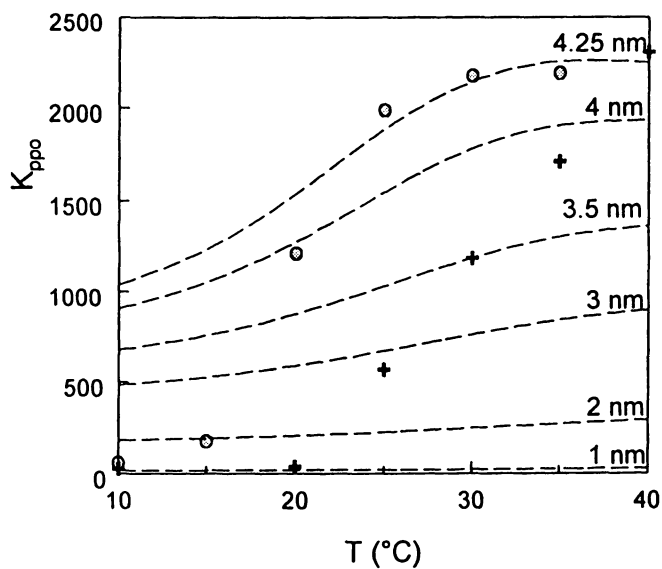


Figure 9. Calculated and experimental normalized partition coefficients at different temperatures for different core radii (nm) ($m_{\text{PPG}}=58$; +, L64; •, P104).

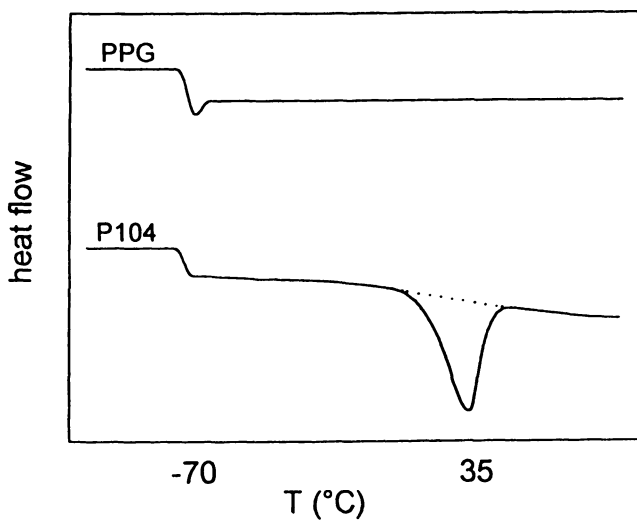


Figure 10. DSC diagram of pure PPG and P104.

No. 5 filter, more than 99% of the naphtalene has been recovered from the polymer solution without any measurable loss of polymer.

Now it is possible to describe in general terms possible processes for the removal of organic pollutants from an aqueous stream (figure 12). At elevated temperatures, the amphiphilic block copolymers will form micelles capable of extracting the organics. This can effectively be performed in a hollow fiber membrane unit (figure 12a), in which the molecular weight cut off value of the membrane should be smaller than the molecular weight of the polymer, but *significantly larger* than the molecular weight of the pollutant, thus allowing easy passage through the membrane (7). Regeneration of the pollutant-free micelle solution can easily be accomplished by cooling down the loaded micelle solution. The micelle solution will be rearranged, so that the pollutant will be forced to separate from the polymer solution, forming a second phase. This second phase can then easily be separated from the polymer solution using a simple separator. To overcome potential mass transfer limitations in this system, a more favorable set-up could be a system in which the polluted aqueous stream is mixed with the micelle solution, followed by UF to concentrate the micelle solution (figure 12b) (9). The micelle solution can then be regenerated in a similar fashion as described for the pertraction system. Another, probably more complicated option for the regeneration of the micelle solution has been proposed using supercritical carbon dioxide (31).

Conclusions

It has been shown that aqueous solutions of block copolymers of the PEO-PPO-PEO type are capable of extracting organic pollutants (e.g. polyaromatics) from aqueous streams. For a proper description of the PEO-PPO-PEO system, and hence for the solubilization of organic components, a modified Flory Huggins model is required. Saturation experiments have shown that above a certain transition temperature the solubilization of naphtalene in a 10 wt% solution can increase up to 135 times the solubility in water. This corresponds with a value of the normalized partition coefficient in excess of 2000. The predominant effect causing this solubilization increase is an increase in micelle radius, while the change in polarity of the micelle core is of minor importance. A process has been proposed based on pertraction with an ultrafiltration membrane. As the solubilization process is reversible, the saturated micelle solution can easily be regenerated.

Nomenclature

a_i	activity component i [-]
F	degeneration ratio between polar and nonpolar state [-]
f_i	fugacity component i [Pa]
f_i^0	fugacity pure i [Pa]
f_n	degeneration factor nonpolar state [-]
f_p	degeneration factor polar state [-]
G	Gibbs free enthalpy [J/mol]
H_{mix}	enthalpy of mixing [J/mol]
k	Boltzmann constant [J/K]

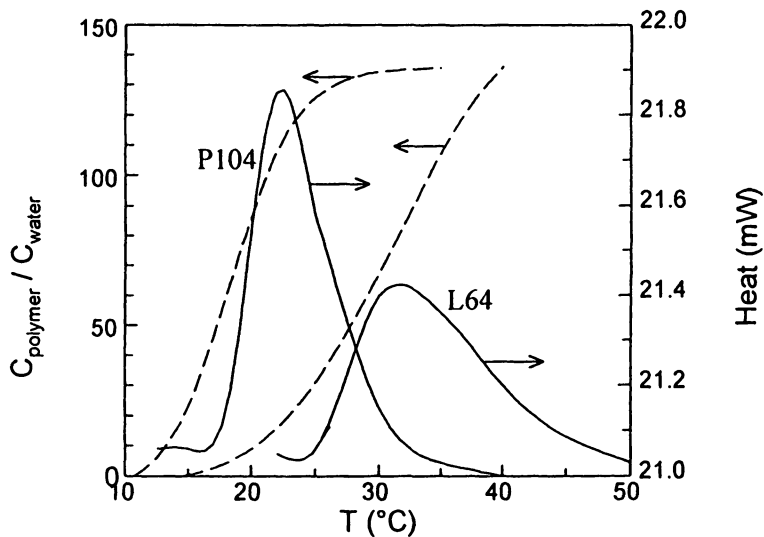


Figure 11. Solubilization transition and DSC experiments for 10 wt% solutions of P104 and L64.

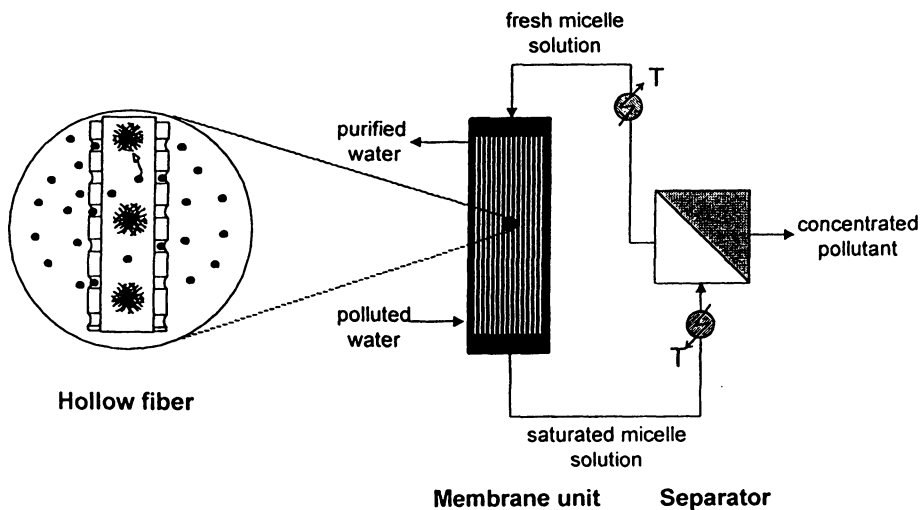


Figure 12. Process options for the removal of organic pollutants from aqueous streams (a) pertraction-based process (b) micellar enhanced ultrafiltration process

K_{PPO}	normalized partition coefficient [-]
m	degree of polymerization [-]
M_0	total number of segments [-]
n_i	number of molecules component i [-]
P	fraction polar segments [-]
R_0	radius unswollen particle [m]
S_{mix}	entropy of mixing [J/mol.K]
T	temperature [K]
v_i	volume fraction component i [-]
V_m	molar volume [m ³ /mol]
α	energy difference between polar and nonpolar segments [J/mol]
γ	activity coefficient [-]
μ_i	reduced chemical potential component i [J/mol]
μ_s	surface partial Gibbs free enthalpy [J/mol]
σ	surface tension [N/m]
	Flory Huggins interaction parameter [-]

Acknowledgment

This work has been carried out by P.J.M. Lebens for his MSc thesis, and was performed at Akzo Nobel Central Research, Arnhem, The Netherlands.

Literature cited

1. BASF Wyandotte Corp., Product data sheet Pluronics
2. Smith, G.A.; Christian, S.D.; Tucker, E.E.; Scamehorn, J.F. *Am. Chem. Soc. Symp. Ser.* **1986**, *342*, 184
3. Calvert, T.L.; Philips, J.P.; Dungon, S.R. *Am. Inst. Chem. Eng. J.* **1994**, *40*, 1449
4. Noolandi, J.; Hong, K.M.; *Macromolecules* **1983**, *16*, 1443
5. Nagarajan, R.; Ganesh, K. *J. Chem. Phys.* **1989**, *90*, 5843
6. Nagarajan, R.; Barry, M.; Ruckenstein, E. *Langmuir* **1986**, *1*, 210
7. Hurter, P.N.; Hatton, T.A.; *Langmuir* **1992**, *8*, 1291
8. Lebens, P.J.M.; Keurentjes, J.T.F. *Ind. Eng. Chem. Res.* **1996**, *35*, 3415
9. Christian, S.D.; Scamehorn, J.F.; in *Surfactant-based Separation Processes*, Scamehorn, J.F.; Harwell, J.H., Eds., Surfactant Science Series vol. 33, Marcel Dekker, New York, 1989, 3
10. Overdeest, P.E.M.; Van der Padt, A.; Keurentjes, J.T.F.; Van 't Riet, K. *in preparation* **1998**
11. Zhou, Z.; Chu, B. *J. Colloid Interface Sci.* **1988**, *126*, 171
12. Wanka, G.; Hoffman, H.; Ulbricht, W. *Colloid Polymer Sci.* **1990**, *268*, 101
13. Brown, W.; Schillen, K.; Almgren, M.; Hvidt, S.; Bahadur, P. *J. Phys. Chem.* **1991**, *95*, 1850
14. Hurter, P.N.; Scheutjens, J.M.H.M.; Hatton, T.A.; *Macromolecules* **1993**, *26*, 5592
15. Hurter, P.N.; Scheutjens, J.M.H.M.; Hatton, T.A.; *Macromolecules* **1993**, *26*, 5030
16. Linse, P.; Malmsten, M.; *Macromolecules* **1992**, *25*, 5434
17. Fredenslund, A.; Gmehling, J.; Michelsen, J.; Rasmussen, M.L.; Prausnitz, J.M. *Ind. Eng. Chem. Proc. Des. Dev.* **1977**, *16*, 450

18. Oishi, T.; Prausnitz, J.M. *Ind. Eng. Chem. Proc. Des. Dev.* **1978**, *17*, 333
19. Hill, T.L. *Introduction to Statistical Thermodynamics*, Addison-Wesley, Reading, MA, 1960
20. Karlström, G. *J. Phys. Chem.* **1985**, *89*, 4962
21. Björling, M.; Linse, P.; Karlström, G. *J. Phys. Chem.* **1990**, *94*, 471
22. Saeki, S.; Kuwahara, N.; Kaneko, M. *Polymer* **1976**, *17*, 685
23. Rasmussen, D.; Rasmussen, P. *Chem. Eng. Progress* **1987**, 50
24. Malcolm, G.N.; Rowlinson, J.S. *Trans. Faraday Soc.* **1957**, *53*, 921
25. Hurter, P. N., PhD Thesis, Massachusetts Institute of Technology, Cambridge, MA, 1992
26. Nagarajan, R.; Ganesh, K. *J. Colloid Interface Sci.* **1996**, *184*, 489
27. McDonald, C.; Wong, C. *J. Pharm. Pharmac.* **1974**, *26*, 556
28. Al-Saden, A.A.; Whateley, T.L.; Florence, A.T. *J. Colloid Interface Sci.* **1982**, *90*, 303
29. Maxwell, I.A.; Kurja, J.; Van Dormaele, G.H.J.; German, A.L. *Makromol. Chem.* **1992**, *193*, 2049
30. Yu, G.; Deng, Y.; Dalton, S.; Wang, Q.; Attwood, D.; Price, C.; Booth, C. *J. Chem. Soc. Faraday Trans.* **1992**, *88*, 2537
31. McFann, G.J.; Johnston, K.P.; Hurter, P.N.; Hatton, T.A.; *Ind. Eng. Chem. Res.* **1993**, *32*, 2336

Chapter 8

Wastewater Remediation: Utilization of Environmentally Responsive Polymeric Surfactants for the Sequestration of *p*-Cresol

R. Scott Armentrout, Michael F. Richardson, and Charles L. McCormick¹

University of Southern Mississippi, Department of Polymer Science,
Hattiesburg, MS 39406

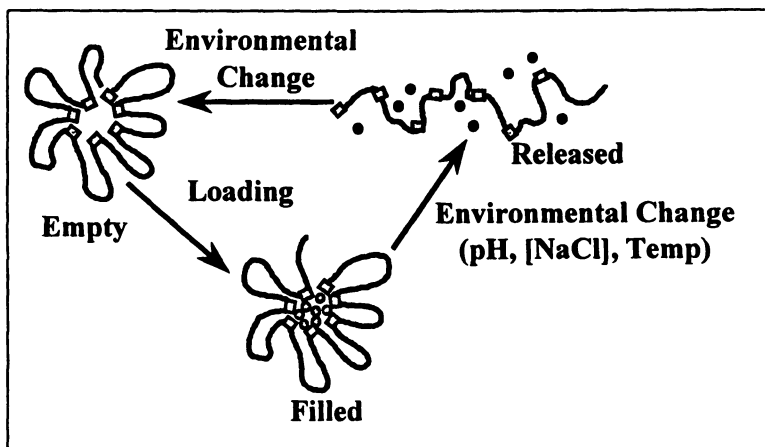
It is well known that hydrophobically-modified water soluble polymers form ordered hydrophobic microdomains in aqueous media and may serve as sequestration sites for various water foulants including surfactants and hydrocarbons. In this work, equilibrium dialysis experiments are utilized to determine the binding isotherms of *p*-cresol to the triblock surfactant, Pluronic F127, as a function of polymer concentration and temperature. Binding of the model water foulant to the polymeric surfactant occurs when the polymer resides in a multimeric conformation that is temperature dependent. At 5°C the polymer resides in a monomeric conformation, but the presence of the foulant facilitates a unimer to multimer transition that leads to increased foulant binding. Positive cooperativity is shown to exist through Scatchard analysis of the data. Ultrafiltration experiments utilizing hollow fiber membranes indicate that the polymer-foulant interactions are increased by the shear forces commonly utilized in ultrafiltration applications.

Micellar-enhanced ultrafiltration (MEUF) has been shown to be an effective method of removing organic solutes from aqueous streams (1). This method is characterized by the addition of a surfactant to the aqueous stream containing the organic foulant, thus causing the foulant to be solubilized within the micellar hydrophobic core. The stream is then passed through a microporous membrane, such that most of the organic solute and surfactant remain in the retentate. Although this method often achieves high efficiencies of removing a foulant, monomeric surfactant continuously crosses the membrane into the permeate.

¹ Corresponding author.

Therefore, added surfactant is required as time progresses to maintain a critical micelle concentration.

In order to circumvent this problem, polymeric surfactants may be utilized as the solubilization agent. In this case, the size of the monomeric surfactant is sufficiently large to prevent passage through the membrane into the permeate. In addition, if appropriate functionality is designed along the polymer backbone, the aggregation behavior of the polymeric surfactant may be controlled by changes in environmental conditions such as pH or temperature (2-9). This can allow facile separation of the organic solute from the polymer surfactant, thus leading to a recyclable remediation process as is illustrated in Scheme 1.



Scheme 1. Idealized remediation cycle for a stimuli-responsive polymeric surfactant.

In this work, MEUF is first modeled by equilibrium dialysis experiments utilizing the commercially available polymeric surfactant, Pluronic F127, as the solubilization agent. F127 is a PEO-PPO-PEO triblock copolymer that has been shown to exhibit temperature dependent aggregation behavior in aqueous media (10). This polymer exists in a monomeric state (unimer) at low temperatures and low polymer concentrations since both blocks (PEO and PPO) are soluble at low temperatures ($<15^{\circ}\text{C}$). However, increasing the temperature causes microphase separation of the hydrophobic PPO blocks and thus leads to the formation of micelle-like structures (multimer). It is thought that this temperature responsiveness may be utilized to control the binding of an organic solute in a MEUF process. It is the objective of this endeavor to probe the nature of the temperature responsive associations of F127 and its efficiency to sequester p-cresol, a model water foulant.

Experimental

Materials. p-Cresol was purified by vacuum sublimation. Pluronic F127 was obtained as a gift from BASF Corporation and used as received.

Instrumentation. UV-vis measurements were conducted with a Hewlett-Packard 8452A diode array spectrophotometer. Right-angle dynamic light scattering measurements were performed with a Brookhaven Instruments 128-channel BI-2030 AT digital correlator using a Spectra Physics He-Ne Laser operating at 632.8 nm at 5 and 25°C. Samples were clarified for light scattering measurements by centrifugation. Hydrodynamic diameters were obtained from the cumulants analysis method.

Equilibrium Dialysis Experiments. Equilibrium dialysis experiments were performed utilizing equilibrium dialysis cells (5ml) from Bel-Art Products and regenerated cellulose membranes having a nominal molecular weight cutoff of 6000. Solutions containing the polymeric surfactant, F127, and p-cresol of known concentrations ($[F127]=0.4\text{g/dl}$, 0.6g/dl and 0.8 g/dl ; $[Cresol]_{\text{feed}}=7\text{mM}-70\text{mM}$) were placed in one side of each dialysis cell (retentate) and deionized water was placed in the other side (permeate). The cells were thermostated at 25°C in a Napco incubator or at 5°C in a water bath regulated with a Lauda RM6 water circulator. The concentration of p-cresol in the retentate, $[Cresol]_{\text{ret}}$ and permeate, $[Cresol]_{\text{per}}$ were determined by UV spectroscopy. Dialysis experiments in the absence of F127 indicated that equilibrium concentrations of p-cresol were obtained in 24 hr. Dynamic light scattering data indicated that the polymeric surfactant was quantitatively retained within the retentate compartment.

Analysis of Equilibrium Dialysis Experiments. From $[Cresol]_{\text{ret}}$ and $[Cresol]_{\text{per}}$, the concentration of p-cresol bound within the hydrophobic microdomains of F127, $[Cresol]_{\text{bnd}}$, was calculated from Equation 1.

$$[Cresol]_{\text{bnd}} = [Cresol]_{\text{ret}} - [Cresol]_{\text{per}} \quad (1)$$

Equation 1 remains valid if the concentration of cresol in the permeate is equivalent to the free concentration of cresol (unbound cresol) in the retentate. From the concentration of bound cresol the ratio of moles of foulant bound per mole of F127, r , is then calculated from equation 2:

$$r = \frac{[Cresol]_{\text{bnd}}}{[F-127]} \quad (2)$$

where $[F127]$ is the concentration of F127 in the retentate. Binding isotherms were prepared by plotting r as a function of free cresol in the retentate, $[Cresol]_{\text{per}}$

(11, 12). The experimental results were analyzed by employing the Scatchard method (13). The Scatchard equation, based on a simple site-binding model (binding of ligand models to independent, indistinguishable binding sites), is

$$\frac{r}{[\text{Cresol}]_{per}} = nK - rK \quad (3)$$

where n =total number of binding sites, and K represents the intrinsic binding constant. Efficiency of foulant sequestration is analyzed by monitoring rejection ratios, a term commonly used in membrane applications which is given in equation 4:

$$\text{Rejection Ratio} = \left(1 - \frac{[\text{Cresol}]_{per}}{[\text{Cresol}]_{ret}} \right) \times 100 \quad (4)$$

Ultrafiltration Experiments. Ultrafiltration of solutions containing Pluronic F127 and p-cresol were performed with an A/G Technology QuixStand[™] Benchtop System coupled with a MasterFlex peristaltic pump (Cole Palmer). Polysulfone hollow membranes with 1.0 mm inside diameter lumen and a 10K MWCO were utilized. Retentate recirculation rates were varied from 100 to 300 ml min⁻¹. Experiments were carried out at 25 and 5°C (cold room). Clean water flux for this membrane was measured to be 23.1±0.2 liter m⁻² hr⁻¹. The concentration of p-cresol in the permeate was determined by UV absorbance measurements.

Results and Discussion

Binding isotherms for F127 and p-cresol and the corresponding hydrodynamic diameters for the F127/p-cresol complexes at 25°C for [F127]=0.4, 0.6, and 0.8 g/dl are shown in Figure 1. At this temperature, F127 exhibits a monomeric conformation at [F127]=0.4 g/dl, whereas a multimeric conformation should be realized for [F127]=0.6 and 0.8 g/dl since the cmc of F127 at 25°C is 0.6 g/dl (10). The binding isotherms indicate that sequestration of p-cresol occurs throughout the range of [Cresol] investigated. The hydrodynamic diameter, as determined from dynamic light scattering, agrees well with data shown previously for the multimer of F127 (10). Therefore, the multimer of F127 acts as the solubilization agent for the organic solute. It is interesting to point out that even at [F127]=0.4 g/dl (a concentration of F127 below the cmc at 25°C), a multimeric state exists. Therefore, the presence of the organic foulant facilitates the formation of multimers of F127 in solution thus leading to binding of the organic solute.

Binding isotherms for F127 and p-cresol and the corresponding hydrodynamic diameters for the F127/p-cresol complexes at 5°C for [F127]=0.4, 0.6, and 0.8 g/dl are shown in Figure 2. Under these conditions in the absence of organic solutes, F127 exists in a monomeric state as shown previously (10).

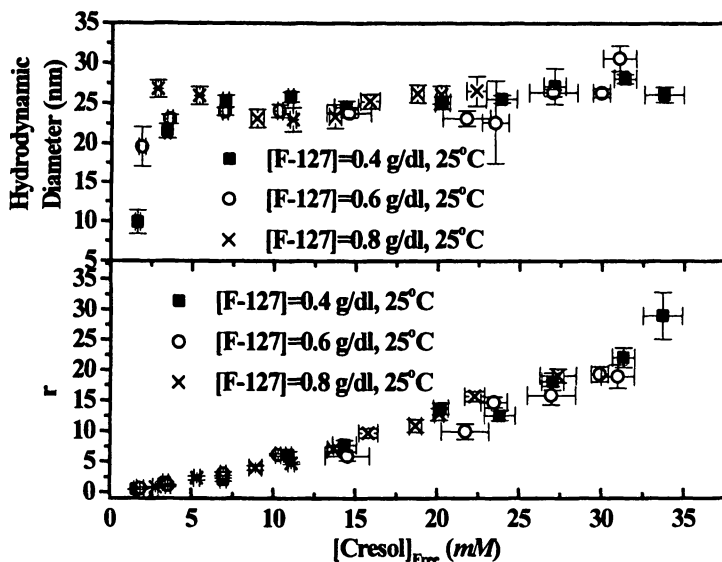


Figure 1. Binding isotherms for F127 and p-cresol at 25°C for [F127]=0.4, 0.6, and 0.8g/dl and the corresponding hydrodynamic diameter of the polymer-foulant complex as a function of p-cresol concentration.

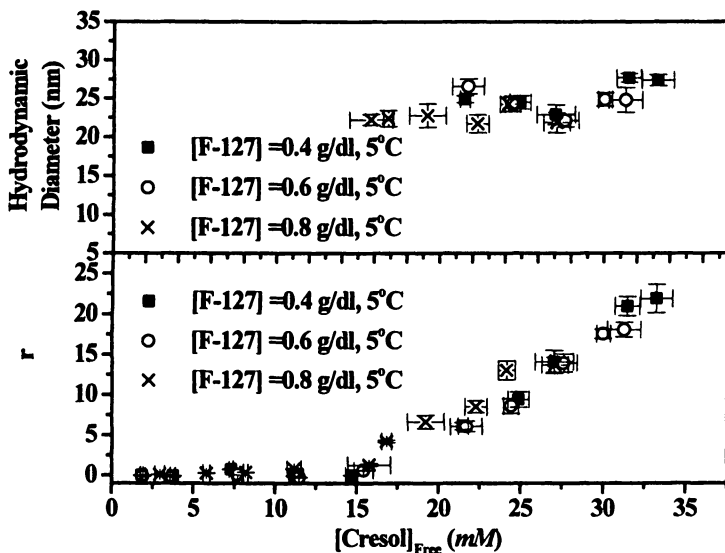


Figure 2. Binding isotherms for F127 and p-cresol at 5°C for [F127]=0.4, 0.6, and 0.8g/dl and the corresponding hydrodynamic diameter of the polymer-foulant complex as a function of p-cresol concentration.

Therefore, one would not expect a large interaction between F127 and p-cresol. Figure 2 confirms that there is minimal binding of the foulant to the polymer at low concentrations of p-cresol. However, as the concentration of the foulant is increased, significant binding does occur. This binding seems to occur at a critical concentration of p-cresol. As the concentration of p-cresol increases within the system, it is postulated that a unimer-to-multimer transition occurs facilitating capture of the hydrocarbon foulant as is confirmed from dynamic light scattering data.

In order to further determine whether or not binding of the foulant to the polymeric surfactant is enhanced by the presence of the foulant, a Scatchard analysis was employed. Figure 3 shows a Scatchard plot for the F127/p-cresol system at 5°C. For a system with no cooperativity (that is the binding of a cresol molecule to the polymer is not influenced by the presence of other cresol molecules bound to the polymer chain) the shape of a Scatchard plot should be a straight line with a negative slope. However, this is not the case in our system. The plots shown in Figure 3 contain two distinct regions, initially a steep vertical portion followed by one with a small positive slope. This shape indicates that the foulant molecules bind initially with a high degree of cooperativity but later with a less degree (12). This agrees well with the hypothesis that the foulant molecules are nucleating a unimer-to-multimer transition at a critical foulant concentration. Note that the shape of the plot remains the same regardless of polymer concentration. This again indicates that the polymer conformation is the same for each system.

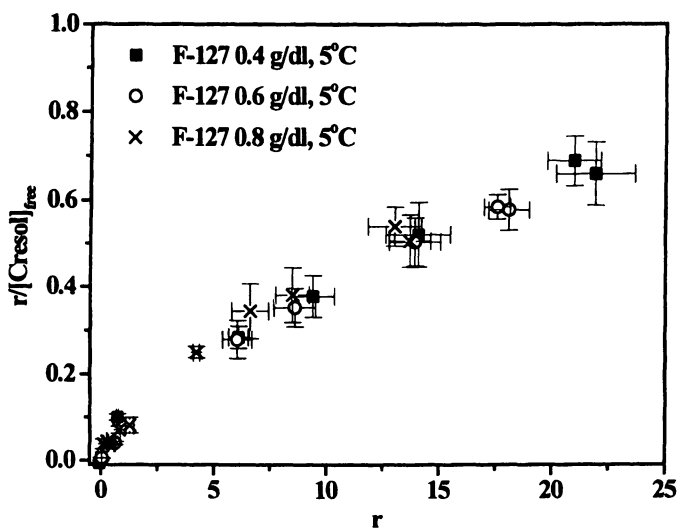


Figure 3. Scatchard plots for [F127]=0.4, 0.6 and 0.8g/dl at 5°C.

Table I. Rejection Ratios as a function of $[\text{Cresol}]_{\text{feed}}$, [F127], and Temperature

$[\text{Cresol}]_{\text{feed}}$ (mM)	0.4 g/dl, 5°C	0.6 g/dl, 5°C	0.8 g/dl, 5°C	0.4 g/dl, 25°C	0.6 g/dl, 25°C	0.8 g/dl, 25°C
7	<1%	<1%	2.4±0.4%	8.1±0.9%	14±4%	15±2%
14	<1	<1	2.7±0.2	13±2	13±2	21±3
21	<1	<1	2.5±0.1	9±1	17±2	22±2
28	<1	<1	4.3±0.3	15±1	22±1	22±1
35	<1	1.9±0.1	4.9±0.7	15±2	16±2	25±1
42	8±1	12±1	14±1	18±1	18±2	28±2
49	11±1	14±2	18±2	14±1	23±1	27±3
56	14±1	19±2	19±2	18±1	22±2	29±2
63	18±1	22±1	25±2	18±1	24±2	31±2
70	17±1	22±1	24±2	21±3	23±2	31±2

In order to determine the remediation efficiency of F127 (ability to sequester p-cresol), rejection ratios were determined for each of the systems investigated and are shown in Table 1. Note that the rejection ratios for the 5°C samples are much lower than those at 25°C for $[\text{Cresol}]_{\text{feed}} \leq 35 \text{ mM}$. One may also note that the rejection ratios are quite low when compared to the solubilization of organics in small molecule surfactants. (Christian found rejection ratios >97% for 1-hexadecylpyridinium chloride/p-cresol systems (14).) This could be due to the differences in packing and dynamics of the small molecule and polymeric surfactants, thus controlling the equilibrium between bound and unbound organic solutes. Despite these low rejection ratios, the utilization of this system in a micellar enhanced ultrafiltration process might still be effective since loss of the solubilizing agent (surfactant) does not occur.

Although equilibrium dialysis experiments are typically utilized to approximate the micellar enhanced ultrafiltration process, the shear forces experienced by the retentate within the membrane lumen during ultrafiltration applications utilizing cross-flow geometries, are not present. These shear forces may lead to lower rejection ratios in an ultrafiltration application since intra- and intermolecular hydrophobic associations in water-soluble polymers can be disrupted in a shear field (15). Therefore, in order to evaluate shear effects on the remediation efficiency of F127, ultrafiltration experiments were conducted utilizing a hollow fiber membrane system.

Figure 4 illustrates the rejection ratio as a function of time at three recirculation rates. This ultrafiltration experiment was initially carried out at 25°C with a recirculation rate of 100 ml/min. As indicated in the figure, Note that the rejection ratio increases as the polymer is concentrated in the retentate. This agrees with data from the equilibrium dialysis experiments. As indicated in the figure, the rejection ratio for this regime is ~50, indicating that 50% of the foulant is retained within the polymeric micelles. It is interesting to note that the rejection ratio is higher in the ultrafiltration experiment than in the equilibrium dialysis experiments. This indicates that the shear forces developed within the lumen of

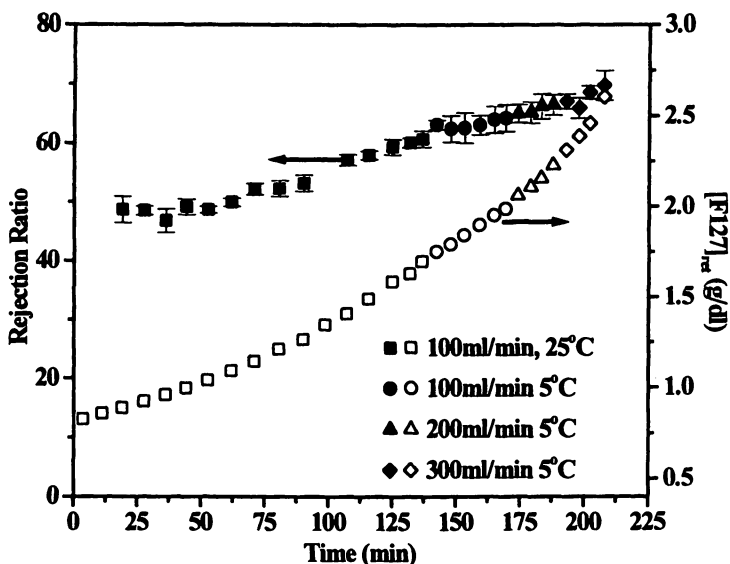


Figure 4. Rejection ratio and $[F127]_{ret}$ as a function of time at specified recirculation rates and temperatures for an ultrafiltration experiment. $[Cresol]_{feed}=50$ mM, $[F127]=0.8$ g/dl.

the hollow fiber do not destroy the polymer-foulant interactions. On the contrary, it appears that within the shear field, the polymer-foulant interactions are increased. This may occur by the disruption of a fraction of the polymer-polymer associations allowing for a larger percentage of the organic solute to penetrate into the hydrophobic microdomains.

The apparatus was then placed in a cold room (5°C) and after an equilibrium temperature was established, the experiment was continued. As seen in Figure 4, the rejection ratio increases as the concentration of F127 increases. This is projected from the equilibrium dialysis and dynamic light scattering experiments which show at this concentration of F127 (>1.5 g/dl), the polymer maintain a multimeric conformation. The recirculation rate was then increased to discern whether the increased shear forces would disrupt the associative domains responsible for sequestration. Figure 4 shows that the surfactant-foulant interactions are sufficiently strong such that the rejection ratio does not decrease.

Finally, the normalized flux (flux at a given time divided by the clean water flux) is plotted as a function of time (Figure 5) for the ultrafiltration experiment discussed above. As expected, the flux decreases as the experiment proceeds due to the development of concentration polarization along the membrane surface. The flux also decreases as the temperature is lowered. However, as the recirculation rate is increased, the increased shear forces within the membrane lumen act to remove the concentration polarization layer and thus, an increase in the flux is observed.

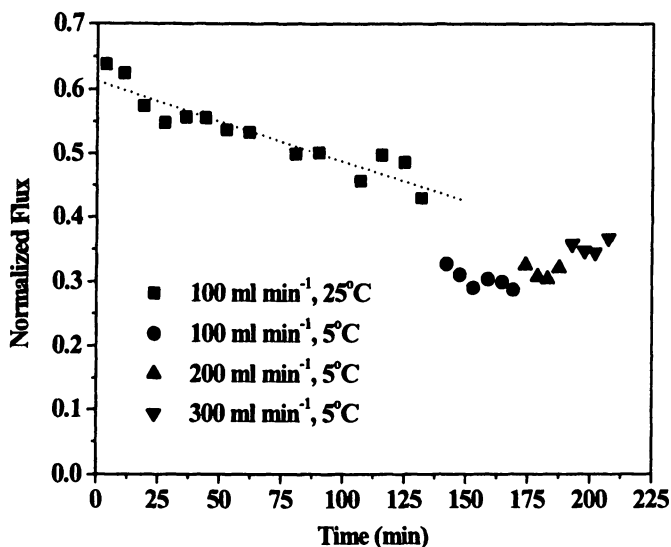


Figure 5. Normalized flux as a function of time for specified recirculation rates and temperatures for an ultrafiltration experiment. $[\text{Cresol}]_{\text{feed}}=50 \text{ mM}$, $[\text{F127}]=0.8\text{g/dl}$.

Conclusions

The solubilization of a model water foulant, p-cresol, by the polymeric surfactant, Pluronic 127, has been studied via equilibrium dialysis, dynamic light scattering and ultrafiltration experiments. It has been shown that at 25°C p-cresol is readily solubilized by F127 since the polymeric surfactant exists in a multimer conformation. It has also been shown that, in the monomeric state (5°C), the binding of the foulant by F127 does not occur below a critical foulant concentration. However, above a critical concentration of p-cresol, F127 undergoes a unimer-to-multimer transition which leads to sequestration of the foulant. It has been shown through a Scatchard analysis that the system exhibits positive cooperativity in the mechanism of binding the foulant to the polymeric surfactant. Ultrafiltration experiments have demonstrated that the polymer-foulant binding interactions are largely unaffected by shear in a hollow fiber membrane.

Acknowledgements

The authors of this paper would like to thank the Office of Naval Research for financial support of this research.

References

1. Christian, S. D.; Scamehorn, J. F. (Eds.) *Solubilization in Surfactant Aggregates*; Marcel Dekker, Inc.: New York City, New York, 1995 and references therein.
2. Hu, Y.; Armentrout, R. S.; McCormick, C. L. *Macromolecules* **1997**, *30*, 3538.
3. Hu, Y.; Smith, G. L.; Richardson, M. F.; McCormick, C. L. *Macromolecules* **1997**, *30*, 3526.
4. Kramer, M. C.; Steger, J. R.; Hu, Y.; McCormick, C. L. *Macromolecules* **1996**, *29*, 1992.
5. Kramer, M. C.; Steger, J. R.; Hu, Y.; McCormick, C. L. *Polymer* **1996**, *37*, 4539.
6. Aota, H.; Araki, S.; Morishima, Y.; Kamachi, M.; *Macromolecules* **1997**, *30*, 4090.
7. Morishima, Y.; Nomura, S.; Ikeda, T.; Seki, M.; Kamachi, M. *Macromolecules* **1995**, *28*, 2894.
8. Strauss, U. P.; Gershfeld, N. L.; Cook, E. J. *J. Physical Chemistry* **1956**, *60*, 577.
9. Strauss, U. P.; Gershfeld, N. L. *J. Physical Chemistry* **1954**, *58*, 747.
10. Wu, C.; Liu, T.; Chu, B.; Schneider, D. K.; Graziano, V. *Macromolecules* **1997**, *30*, 4574.
11. Anthony, O.; Zana, R. *Langmuir* **1996**, *12*, 1967.
12. Maruthamuthu, M.; Subramanian, E. *Colloid and Polymer Science* **1990**, *268*, 256.
13. Scatchard, G. *Annals of the New York Academy of Sciences* **1949**, *51*, 660.
14. Bhat, S. N.; Smith, G. A.; Tucker, E. E.; Christian, S. D.; Scamehorn J. F.; Smith, W. *Industrial Engineering Chemical Research* **1987**, *26*, 1217.
15. Chang, Y.; McCormick, C. L. *Polymer* **1994**, *35*, 3503.

Resolution of Enantiomers Using Enantioselective Micelles in Ultrafiltration Systems

P. E. M. Overdeest¹, Jos T. F. Keurentjes², A. van der Padt¹, and K. van 't Riet¹

¹ Department of Food Science, Food and Bioprocess Engineering Group,
Wageningen Agricultural University, P. O. Box 8129, 6700 EV
Wageningen, Netherlands

² Department of Chemical Engineering, Process Development Group, Eindhoven
University of Technology, P.O. Box 513, 5600 MB Eindhoven, Netherlands

Since it has been recognized that the demand for enantiopure compounds will increase, more and more effort is put in the development of resolution technology. The traditional route to obtain homochiral products is enantiomer separation using diastereoisomer crystallization. Disadvantages of this resolution processes are costly scale-up and a high energy requirement. An alternative is ultrafiltration of enantioselective micelles, which is an easily scalable process with a low energy requirement. In this system, the enantioselective micelles preferentially form a complex with one of the enantiomers. Only free enantiomers can pass the membrane.

The objective of this research is to describe the complexation of phenylalanine enantiomers by enantioselective micelles (cholesteryl-L-glutamate anchored in nonionic micelles). It is concluded that straightforward multicomponent Langmuir isotherms can describe the enantiomer complexation by these micelles.

The applied science of enantiomer separation, chirotechnology, is a fast developing research field with applications in the pharmaceutical, agrochemical and food industries. The main reasons for the increasing demand for enantiomerically pure compounds are (1):

- enantiomers can have different biological activities;
- enantiomers can counteract one another's effect, so-called antagonism;
- the unwanted enantiomer is seen as an impurity as a consequence of registration constraints in certain countries; and
- production costs can decrease significantly as a consequence of an increased production capacity or a decreased use of other expensive achiral intermediates.

Since not all optically pure products are available from the chiral pool (2), enantiomers have to be produced from (a)chiral substrates or have to be separated

from their racemic mixture (equimolar mixture of the two enantiomers). Diastereoisomer crystallization, the conventional separation method, is often a batchwise operation (3) and requires relatively inflexible multi-step processing (1). In many cases a low product yield is observed in one single batch operation, due to a generally low selectivity.

The use of membranes for the resolution of racemates can result in a continuous and energy efficient multi-stage separation process at an industrial scale. Chiral discrimination is the basis of enantiomer separation (4). This chiral discrimination can take place in the membrane matrix itself or in the liquid phases separated by the membrane. Selective membranes have been applied as an enantioselective barrier retaining one enantiomer more than the other. Examples thereof are membrane matrices made of chiral polymers (5–7), molecular imprinted membranes (3,8,9), supported liquid membranes (10–12), emulsion liquid membranes (13,14) and membranes containing proteins (15,16). Non-selective membranes have been used to separate two (im)miscible phases of which at least one is chiral, similar to liquid/liquid extraction where two immiscible phases are used to separate enantiomers (17–19). The performance of conventional liquid/liquid extraction equipment is often limited by backmixing and flooding (20). These limitations are eliminated in hollow-fiber membrane extraction, where non-selective membranes separate both phases (21,22). For an efficient process design, it is mandatory that the chiral selector molecules from one phase are insoluble in the other phase. Moreover, if there is a demand for both enantiomers in their optically pure form, the partition of the enantiomers over both phases should not be too far from unity, since at a high partition coefficient one of the enantiomers will become extremely diluted. This results in losses of valuable product (23). Alternatively, membranes are used to separate a miscible enantioselective microheterogeneous phase from the aqueous bulk. Membrane rejection of the enantioselective phase is guaranteed by using molecules or colloidal particles larger than the pore size of the membrane, e.g. BSA (24,25) or enantioselective micelles as demonstrated by our group (26). Micellar-enhanced ultrafiltration (MEUF) has proven its potential to preconcentrate heavy metals and organic compounds from aqueous streams (27–29). In addition, micelles are used in micellar electrokinetic capillary chromatography (MEKC) to separate enantiomers on an analytical scale (30–32).

Figure 1 shows the investigated MEUF system in which a chiral selector molecule (cholesteryl-L-glutamate) preferentially forms a ternary complex with one of the enantiomers (phenylalanine, Phe) using a Cu(II) ion. The D,L notation is used to distinguish between both phenylalanine enantiomers. The chiral selector molecules (CS) are anchored in micelles of the nonionic surfactant, nonyl-phenyl polyoxyethylene [E10] ether. Nonionic surfactants are used to eliminate undesired electrostatic interactions between enantiomers, Cu(II) ions and micelles (33,34). The MEUF system results in enantiomer separation as a consequence of:

- selective complexation of enantiomers by chiral selectors;
- rejection of micelles by the membrane and consequently of complexed enantiomers; and
- permeation of uncomplexed enantiomers.

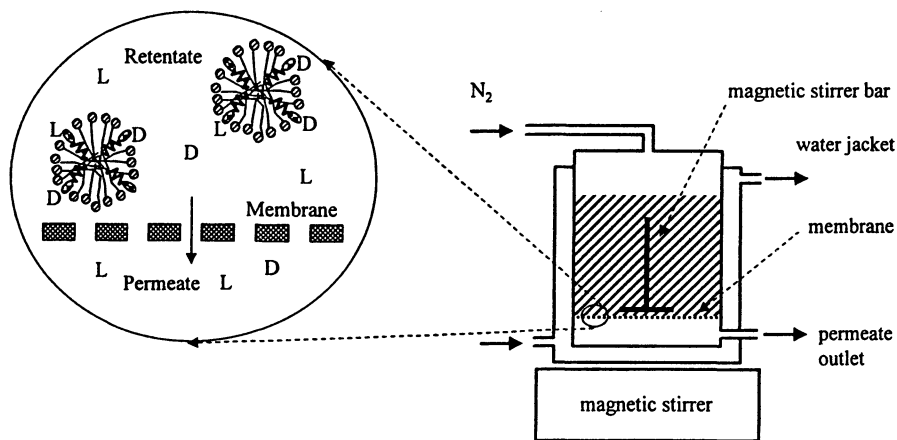


Figure 1. Experimental set-up of the Amicon cell and an impression of the enantiomer separation at the membrane.

The objective of this study is to describe the complexation of enantioselective micelles and Phe enantiomers in an ultrafiltration system. These complexation isotherms are required to design a system based upon MEUF for the complete resolution of a racemic mixture.

Theory

Analogous to Langmuir adsorption isotherms, the binding of enantiomers by chiral selector molecules can be described assuming reversible one-to-one complexations.

Single- and Multicomponent Langmuir Complexation Isotherms. Langmuir has derived the classical equilibrium isotherm for localized nonlinear monolayer adsorption, considering equilibrium at equal adsorption and desorption rates (35). It is proposed for single gas adsorption and based on the following assumptions (36):

- adsorbate molecules are held at a defined number of sites;
- each site can accommodate one single adsorbate molecule;
- the adsorption energy is equal for all sites; and
- neighboring adsorbate-adsorbate interactions do not occur.

The Langmuir isotherm has been adapted to describe multicomponent solute adsorption from dilute solutions by simple replacement of the adsorbate pressure by the solute concentration (37). Competitive adsorption takes place, since two enantiomers strive for complexation with the same site. Both single- and multicomponent Langmuir isotherms are used to describe enantiomer complexation (25,38,39). The single-component isotherms are given by equations 1 and 2, respectively:

$$q_D = \frac{q_s K_D c_D}{1 + K_D c_D} \quad (\text{mM}) \quad (1)$$

$$q_L = \frac{q_s K_L c_L}{1 + K_L c_L} \quad (\text{mM}) \quad (2)$$

and the multicomponent isotherms are given by equations 3 and 4, respectively:

$$q_D = \frac{q_s K_D c_D}{1 + K_D c_D + K_L c_L} \quad (\text{mM}) \quad (3)$$

$$q_L = \frac{q_s K_L c_L}{1 + K_D c_D + K_L c_L} \quad (\text{mM}) \quad (4)$$

where q_s is the Langmuir capacity concentration (mM), c_D and c_L are the equilibrium free concentrations (mM), q_D and q_L are the equilibrium complexed concentrations (mM), and K_D and K_L are the Langmuir affinity constants (mM^{-1}) for D and L enantiomers, respectively. The complexed concentrations (q_D , q_L) are calculated from the measured permeate concentrations (c_D , c_L):

$$q_D = c_{D,\text{tot}} - c_D \quad (\text{mM}) \quad (5)$$

$$q_L = c_{L,\text{tot}} - c_L \quad (\text{mM}) \quad (6)$$

where the index 'tot' specifies the total concentrations at the start of an experiment.

Enantioselectivity. The enantioselectivity ($\alpha_{D/L}$) of the mixed micelles is defined as the ratio of the complexed concentrations (q_D / q_L) over the ratio of the free concentrations (c_D / c_L) (36):

$$\alpha_{D/L} = \frac{q_D / q_L}{c_D / c_L} \quad (-) \quad (7)$$

Based on this definition the intrinsic ($\alpha_{D/L,\text{int}}$) and apparent ($\alpha_{D/L,\text{app}}$) enantioselectivity are calculated. According to Langmuir complexation (36):

$$\alpha_{D/L,\text{int}} = \frac{K_D}{K_L} \quad (-) \quad (8)$$

and using equations 5 and 6:

$$\alpha_{D/L,\text{app}} = \frac{c_L (c_{D,\text{tot}} - c_D)}{c_D (c_{L,\text{tot}} - c_L)} \quad (-) \quad (9)$$

By definition an enantioselectivity larger than one indicates a complexation preference of the selector for the D-enantiomer.

Experimental

Materials. Analytical grade D-,L-, and DL-Phenylalanine (Phe), $\text{CuCl}_2 \cdot 2\text{H}_2\text{O}$, KCl, and KOH were obtained from Merck (Darmstadt, Germany) and used without further purification. The surfactant, Serdiox NNP 10 (nonyl-phenyl polyoxyethylene [E10] ether), was a generous gift by Servo Delden b.v. (Delden, The Netherlands). An average molecular weight of 644 g/mol was assumed, since the surfactant is most

probably a mixture of different NNPs. The chiral selector, cholesteryl-L-glutamate, was synthesized at the Department of Organic Chemistry of the Wageningen Agricultural University. Throughout the study distilled and RO filtered water was used.

Ultrafiltration Experiments. To determine the adsorption isotherms of D- and L-Phe the total concentrations of both enantiomers were varied, whereas all other solute concentrations remained the same (Table I).

Table I. Total solute concentrations and conditions as used in the ultrafiltration experiments.

Component	Concentration (mM)
NNP 10	7.8
LCG	0.3
D-Phe	0, 0.075, 0.15, 0.30, 0.45, 0.80 or 1.0
L-Phe	0, 0.075, 0.15, 0.30, 0.45, 0.80 or 1.0
CuCl ₂ ·2H ₂ O	0.3
KCl	100
Conditions:	
T	25 °C
pH	11

Batches of 50 mL solution, which were used in complexation experiments, were prepared as follows. The chiral selector, which is insoluble in pure water, was dispersed in a concentrated surfactant solution to yield a stable and transparent solution, which indicates that the selector was completely dissolved. Final solutions were obtained by mixing stock solutions: 5 mL 1.0 M KCl, 5.0 mL 3.0 mM CuCl₂·2H₂O, 2.5 mL 0 - 20 mM D-Phe, 2.5 mL 0 - 20 mM L-Phe and 35 mL of the concentrated selector and surfactant solution. The mixtures were set at pH 11 and stirred overnight. Cu(II) ions were added as the chelating agent and KCl was added to maintain a constant ionic strength. Using this method the selector solubility in the nonionic micelles was found to be optimal.

Ultrafiltration experiments were performed in a thermostated 300-mL Amicon cell at 25 °C placed on a magnetic stirrer adjusted to 400 rpm to minimize concentration polarization of micelles and foam production, Figure 1. An Amicon regenerated cellulose membrane (YM3) was used with a 3 kDa MWCO (Amicon Inc., USA). Part of the bulk liquid permeated through the membrane driven by 3 bar N₂. The initial 4 mL of permeate were discarded and the following three fractions of 1 mL were collected and analyzed. All experiments were at least done in triplicate.

Analytical Methods. Phenylalanine enantiomers present in permeate samples were analyzed by HPLC using a 4 mm I.D. \times 150 mm Crownpak CR (+) chiral crown ether column (Daicel) operated at 15°C. Concentrations were measured by UV absorbance at 254 nm (Applied Biosystems). Between each series of analysis a five-point calibration was used to obtain concentrations based upon peak area. A solution of perchloric acid in water (pH 2.0) was used as the mobile phase (0.8 mL/min) and was filtered before use through a 0.2 μ m membrane filter (Sartopore 300).

Results and Discussion

Measured Concentrations. The measured permeate concentration remains approximately the same during each complexation experiment. Independent experiments indicate that membrane rejection can be neglected, so that it can be concluded that the equilibrium concentration does not change during the UF process (26). Therefore, in the following average permeate concentrations will be used.

During the UF process both the selector and complexed concentrations increase proportionally with a decrease in retentate volume. As a consequence, equations 1 – 4 can still be used to describe complexation. To keep the notation simple, q_D , q_L and q_s refer to the concentrations at the start of an experiment and not to the actual concentrations during the experiment.

Fitting the Single-component Complexation Isotherms. Figure 2 shows the results of single-component complexation experiments with D- and L-Phe. Conditions and concentrations are given in Table I, given $c_{L,tot} = 0$ in case of D-Phe complexation and $c_{D,tot} = 0$ in case of L-Phe complexation. Equations 1 and 2 can be rewritten into explicit expressions of the free enantiomer concentrations using equations 5 and 6. For the D-enantiomer:

$$\hat{c}_D = \frac{-B + \sqrt{B^2 + 4c_{D,tot}K_D}}{2K_D} \quad (\text{mM}) \quad (10)$$

here $B = K_D(q_s - c_{D,tot}) + 1$. This explicit equation has been fitted on the measured permeate concentrations (dependent variables) of single-component experiments. A weighted least-squares method has been used, since the measured concentrations have a heterogeneous error variance, Figure 3. Error variances are calculated using the average permeate concentrations of the repeated experiments. Root and logarithm transformations have turned out to be unsuitable. Residuals are weighed with the inverse of the estimated error variances of the measured concentrations (s_D^2). For the D-enantiomer:

$$RSS = \sum \left(\frac{(c_D - \hat{c}_D)^2}{s_D^2} \right) \quad (-) \quad (11)$$

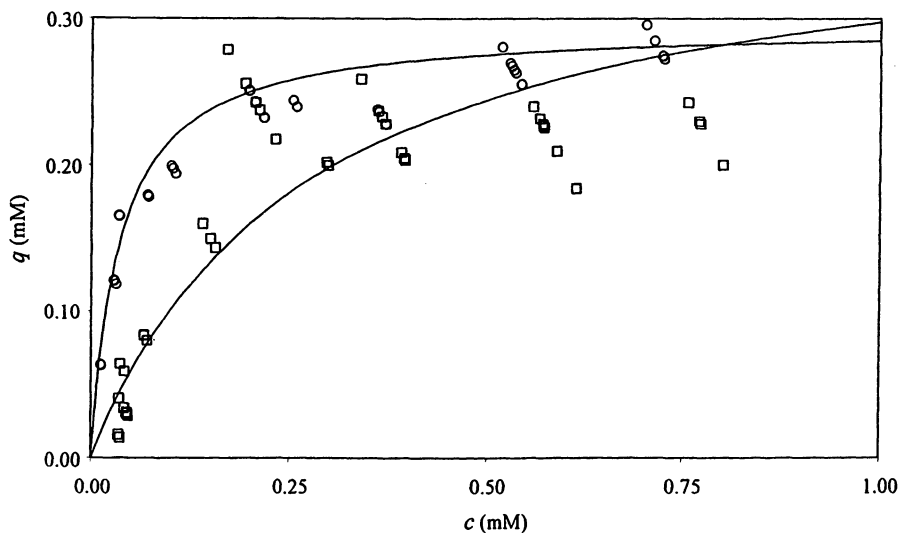


Figure 2. Single-component complexation isotherms of D-Phe (O) and L-Phe (□), fitted with equations 1 and 2 (solid lines).

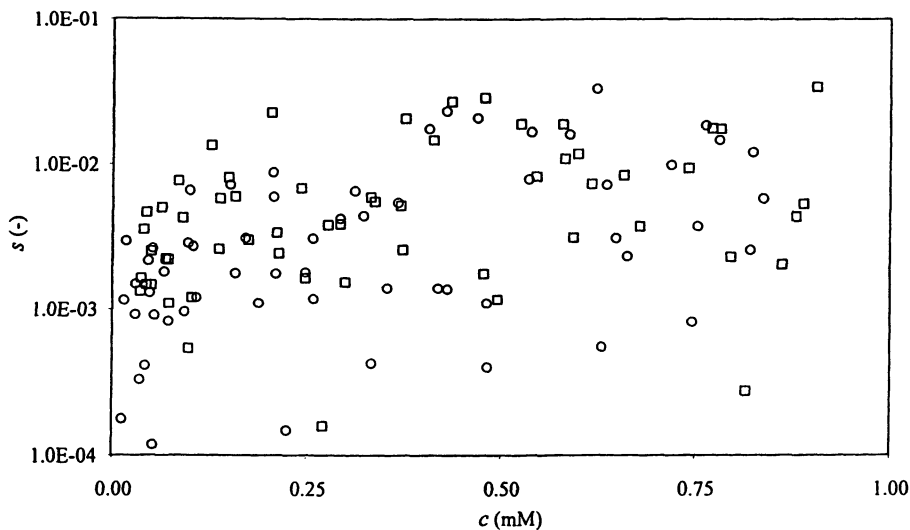


Figure 3. Standard error of the average measured D-Phe (O) and L-Phe (□) permeate concentrations (resp. s_D and s_L) as a function of the average measured permeate concentration (c).

The same procedure is followed for the L-enantiomer. An algorithm based on the Levenberg-Marquardt method is used to minimize the residual sums of squares (RSS).

Single-Component Langmuir parameters and 95% Confidence Intervals. The lines in Figure 2 represent the least-squares fitted curves of the complexation results. The estimated Langmuir capacity concentration (q_s) and affinity constants (K_D and K_L) of the two single-component fits are shown in Table II.

Table II. Langmuir constants (q_s , K_D and K_L), intrinsic selectivity ($\alpha_{D/L,int}$) and 95% confidence intervals (c.i) are estimated by fitting single- (equations 1 and 2) and multicomponent (equations 3 and 4) isotherms.

eq.	n	q_s	K_D	K_L	$\alpha_{D/L,int}$	c.i. $\alpha_{D/L,int}^{(i)}$	c.i. $\alpha_{D/L,int}^{(ii)}$
(1)	34	0.30 ± 0.013	28 ± 0.067		7.7	± 3.1	$+ 5.2$ $- 2.2$
(2)	41	0.38 ± 0.078		3.7 ± 1.5			
(3,4)	218	0.28 ± 0.004	28 ± 1.3	20 ± 0.76	1.4	± 0.081	$+ 0.083$ $- 0.080$

(i) using equation 14; (ii) using a Monte-Carlo method and s_{K_D} and s_{K_L} .

The confidence intervals of these estimated parameters (\hat{b}) are calculated using the estimated standard error of these parameters (s_b):

$$b = \hat{b} \pm s_b t_{\alpha/2, \nu} \quad (12)$$

where $t_{\alpha/2, \nu}$ is the upper $\alpha/2$ percent point of the t -distribution with $\nu = n - p$ degrees of freedom, where n is the number of data, and p the number of parameters. The squared standard error equals the corresponding diagonal element of the $p \times p$ variance-covariance matrix of the estimated parameters (40):

$$\text{variance-covariance matrix} = \left(\frac{RSS}{n-p} \right)^2 (J'J)^{-1} \quad (-) \quad (13)$$

where J is the $n \times p$ Jacobian matrix, which is a result of the fitting procedure.

The estimated Langmuir capacity concentrations (q_s) are equal to the chiral selector and Cu(II) ion concentration. Independent experiments show that non-selective complexation plays an insignificant role compared to selective complexation by the selector (Overdeest, P.E.M., to be published). This guarantees a high efficiency of the chiral selector molecules and supports the assumption that the CS:Cu(II) complex can be regarded as a localized complexation site. It is concluded that the single-component complexations of D- and L-Phe are adequately described, Figure 2.

Intrinsic Enantioselectivity and 95% Confidence Intervals Based upon Single-Component Isotherms. The intrinsic enantioselectivity ($\alpha_{D/L,int}$) can be calculated using K_D , K_L and equation 8. Based upon the single-component isotherms a remarkable value of 7.7 is estimated. In order to determine the 95% confidence interval of $\alpha_{D/L,int}$ equation 8 is expanded by a Taylor series to obtain the standard error of $\alpha_{D/L,int}$ ($s_{\alpha_{D/L,int}}$) (41):

$$\frac{s_{\alpha_{D/L,int}}^2}{\alpha_{D/L,int}^2} \approx \frac{s_{K_D}^2}{K_D^2} + \frac{s_{K_L}^2}{K_L^2} = C_{K_D}^2 + C_{K_L}^2 \quad (-) \quad (14)$$

here, $s_{K_D}^2$ and $s_{K_L}^2$ are elements of the variance-covariance matrix and C_{K_D} and C_{K_L} are the relative variances of K_D and K_L , respectively. This approximation is valid for values of C lower than 0.15 (-) (41). This approximation results in $\alpha_{D/L,int} = 7.7 \pm 3.1$ (-), Table II. Error distributions of parameters in nonlinear models are not necessarily symmetric (42–44). However, the calculated confidence interval of $\alpha_{D/L,int}$ using equation 14 is symmetric. Assuming that the effects of covariance between pairs of parameters can be ignored and that the distributions of parameters are normal can lead to significant errors, up to 2- and 3-fold in the calculated uncertainties (45). As a consequence, a Monte Carlo method is additionally used to calculate the confidence interval of $\alpha_{D/L,int}$, which consisted of the following steps (45):

- a new set of K_D and K_L is simulated using the estimated K_D , K_L , s_{K_D} and s_{K_L} and the normal distribution;
- $\alpha_{D/L,int}$ is calculated using the simulated K_D and K_L and equation 8;
- the first and second steps are repeated many times (2000); and
- the 95% confidence interval is obtained from the increasingly ordered list by eliminating the upper and lower 2.5% of the simulations.

This results in $5.5 < \alpha_{D/L,int} = 7.7 < 13$ (-), Table II. Note that the asymmetry of the confidence interval is caused by the non-linearity of equation 8 and $C_{K_L} = 0.20$ (-), hence the use of the Monte-Carlo method is compulsory.

Fitting the Multicomponent Complexation Isotherms. Complexation experiments with both D- and L-enantiomers have been done to determine if Langmuir's assumptions are valid for multicomponent complexation. Typical results are shown in

Figure 4. Conditions and concentrations are given in Table I. For the multicomponent isotherms an iterative procedure has been developed from a dependent set of equations to estimate the free concentrations (\hat{c}_D, \hat{c}_L) using equations 3 – 6. For the D-enantiomer this is:

$$c_{D,\text{tot}} - \hat{c}_D = \frac{q_s K_D \hat{c}_D}{1 + K_D \hat{c}_D + K_L \hat{c}_L} \quad (\text{mM}) \quad (15)$$

A similar equation can be derived for the L-enantiomer. The total concentrations ($c_{D,\text{tot}}, c_{L,\text{tot}}$) are the independent variables. In both the single- and multicomponent isotherms the same fitting procedure is followed. However, for the residual sum of squares equation 16 has been used:

$$RSS = \sum \left(\frac{(c_D - \hat{c}_D)^2}{s_D^2} + \frac{(c_L - \hat{c}_L)^2}{s_L^2} \right) \quad (-) \quad (16)$$

The results on which the multicomponent isotherms are fitted (equation 15 and the analogous equation for the L-enantiomer) include both series of single-component results.

Multicomponent Langmuir Parameters. The lines in Figure 4 represent the least-squares fitted curves for complexation results. The estimated Langmuir capacity concentration (q_s) and affinity constants (K_D and K_L) of the multicomponent fit are given in Table II. Confidence intervals have been calculated using equation 12. Again, the estimated Langmuir capacity concentration (q_s) is close to the chiral selector and Cu(II) ion concentration. In the case of multicomponent complexation the CS:Cu(II) complex can be considered as one single complexation site.

When we compare the estimated Langmuir affinity constants of single- and multicomponent isotherms, it appears that the affinity for D-Phe is the same in both cases (28 mM⁻¹), Table II. However, this is not true for the affinity constants of L-Phe (3.7 vs. 20 mM⁻¹). This would suggest that Langmuir isotherms are not valid, since the value of K_L should be independent of the presence of D-Phe. To further investigate the difference in K_L we have made parity-plots. These plots are made by plotting the measured concentrations against the corresponding predicted concentrations using equations 3 and 4 and the multicomponent parameters, Figure 5. From these figures it can be concluded that straightforward multicomponent Langmuir isotherms are very well capable of predicting the free enantiomer concentrations. Only at a low L-enantiomer concentration ($c_L < 0.035$ mM) deviations cannot be explained by the related measurement error. Nevertheless, L-enantiomer concentrations below 0.035 mM can be regarded not to be part of the relevant concentration window.

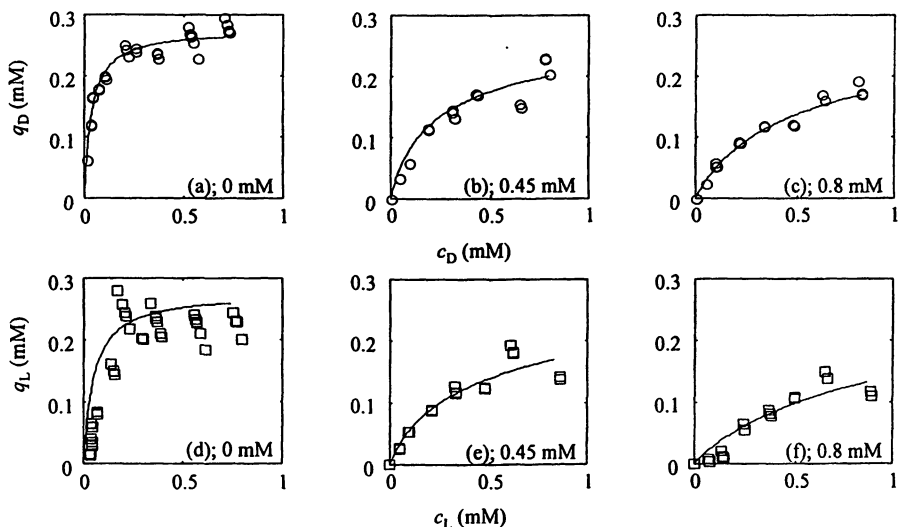


Figure 4. Single- and multicomponent complexation isotherms of D-Phe (O) and L-Phe (□) simultaneously fitted with equations 3 and 4 (solid lines).

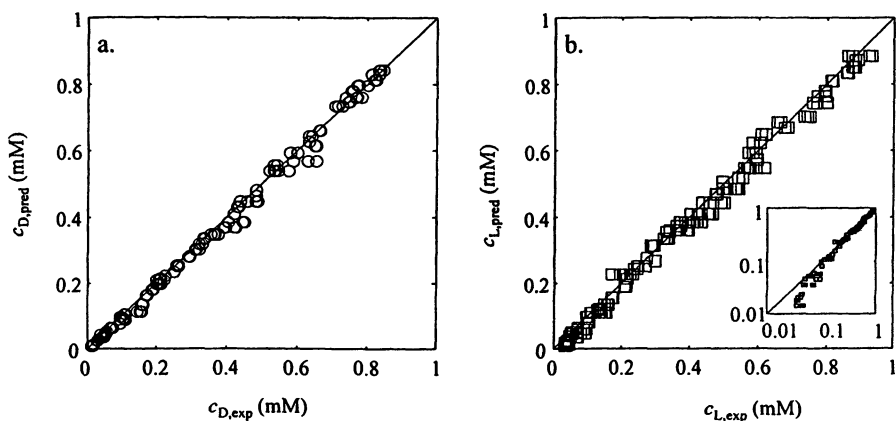


Figure 5. Parity-plots of all measurements (c_{exp}) and predictions (c_{pred}) for D-Phe (a) and L-Phe (b). Predictions are based upon equations 3 and 4 and multicomponent parameters of Table II.

Intrinsic Enantioselectivity Based upon Multicomponent Isotherms. An intrinsic enantioselectivity of 1.4 is calculated, based upon the multicomponent isotherms and equation 8. Both equation 14 and the Monte Carlo method yield similar confidence intervals, $1.3 < \alpha_{D/L,int} = 1.4 < 1.5$ (-). This is caused by the fact both values of CK_D and CK_L are lower than 0.15 (-), which makes equation 14 a better approximation. Both methods indicate that the difference between $\alpha_{D/L,int}$ based upon single- and multicomponent isotherms are significant. Therefore, the apparent enantioselectivity is calculated.

Apparent Enantioselectivity. In order to study the difference in $\alpha_{D/L,int}$ based on single- and multicomponent isotherms the apparent enantioselectivity ($\alpha_{D/L,app}$) is calculated for each multicomponent experiment using equation 9. The 95% confidence interval of $\alpha_{D/L,app}$ is determined by a Monte Carlo method:

- a new set of c_D and c_L is simulated using the average c_D and c_L , the calculated s_D and s_L and the normal distribution;
- $\alpha_{D/L,app}$ is calculated using the simulated c_D and c_L and equation 9;
- the first and second steps are repeated many times (2000); and
- the 95% confidence interval is obtained from the increasingly ordered list by eliminating the upper and lower 2.5% of the simulations.

Figure 6 shows the apparent enantioselectivity and 95% confidence intervals as function of the total enantiomer concentration ($c_{D,tot} + c_{L,tot}$). For simplicity the error bars at higher concentrations are replaced by a gray rectangle. Error bars of data indicated by an arrow included zero, caused by a low c_L . The uncertainty in $\alpha_{D/L,int}$ and $\alpha_{D/L,app}$ is always larger at the upper part of the interval. At $c_{D,tot} + c_{L,tot} > 0.5$ mM the apparent enantioselectivity and the 95% confidence intervals equal the intrinsic selectivity as is predicted by equations 3 and 4. However, the apparent selectivity increases significantly to a value of 4.5 (-) at decreasing $c_{D,tot} + c_{L,tot}$, which cannot be predicted by multicomponent Langmuir isotherms, but is related to the model error in L-Phe prediction at $c_L < 0.035$ mM. From the results in Figure 6 it is tempting to conclude that $\alpha_{D/L,app}$ will approach $\alpha_{D/L,int}$ at infinitely low concentrations of $c_{D,tot} + c_{L,tot}$ (see solid line).

Conclusions

A separation process, based on ultrafiltration of nonionic enantioselective micelles containing cholesterol-L-glutamate, can be applied for the resolution of D,L-phenylalanine enantiomers. Using this system, apparent enantioselectivities of 1.4 to 4.5 have been measured. This paper is focused on the description of the selective complexation of the enantioselective micelles and D,L-phenylalanine. It is shown that competitive multicomponent Langmuir isotherms can be used to describe the enantiomer complexation accurately. The estimated affinity constants (K_D and K_L) are 28 mM^{-1} and 20 mM^{-1} for D- and L-Phe, respectively. The capacity concentration (q_s) is 0.28 mM and nearly equals the chiral selector and Cu(II) ion concentration (95%). This guarantees a high efficiency of these selector and Cu(II) molecules and supports

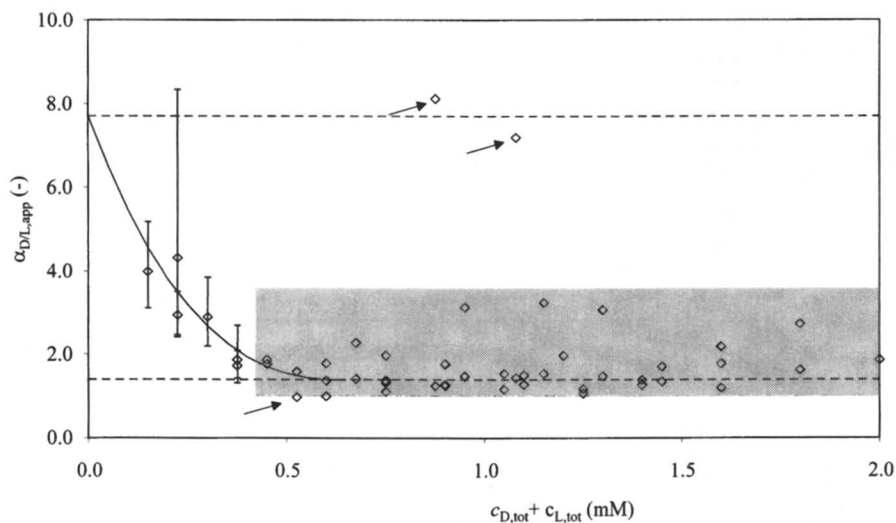


Figure 6. Apparent enantioselectivity for all UF experiments. The dotted lines represent the intrinsic enantioselectivity based on single- ($\alpha_{D/L,int} = 7.7$) and multicomponent ($\alpha_{D/L,int} = 1.4$) isotherms, Table II.

the assumption that the selector:Cu(II) complex can be regarded as a localized complexation site. Since the differences between D- and L-Phe complexation are subtle, a multi-stage separation process is needed in order to fulfill 99.9 % resolution of a racemate. To obtain a cost effective separation system an increase in both enantiomer and selector concentration is mandatory.

Acknowledgments

Financial support for this work was provided by the Dutch Technology Foundation (grant no. WCH44.3380), Akzo Nobel, and DSM. The authors are grateful to drs. T.J.M. de Bruin for synthesis of cholesteryl-L-glutamate.

Literature Cited

- (1) Crosby, J. *Tetrahedron* **1991**, *47*, 4789.
- (2) Sheldon, R. A. *Chiral technology: industrial synthesis of optically active compounds*; Marcel Dekker: New York, 1993.
- (3) Yoshikawa, M.; Izumi, J. I.; Kitao, T.; Sakamoto, S. *Macromolecules* **1996**, *29*, 8197.
- (4) Davankov, V. A. *Chirality* **1997**, *9*, 99.
- (5) Aoki, T.; Ohshima, M.; Shinohara, K. I.; Kaneko, T.; Oikawa, E. *Polymer* **1997**, *38*, 235.
- (6) Tone, S.; Masawaki, T.; Eguchi, K. *J. Membr. Sci.* **1996**, *118*, 31.
- (7) Masawaki, T.; Sasai, M.; Tone, S. *J. Chem. Eng. Japan* **1992**, *25*, 33.
- (8) Yoshikawa, M.; Izumi, J. I.; Kitao, T. *Polym. J.* **1997**, *29*, 205.
- (9) Allender, C. J.; Brain, K. R.; Heard, C. M. *Chirality* **1997**, *9*, 233.
- (10) Ersoz, M.; Vural, U. S.; Okdan, A.; Pehlivan, E.; Yildiz, S. *J. Membr. Sci.* **1995**, *104*, 263.
- (11) Bryjak, M.; Kozlowski, J.; Wiczorek, P.; Kafarski, P. *J. Membr. Sci.* **1993**, *85*, 221.
- (12) Shinbo, T.; Yamaguchi, T.; Yanagishita, H.; Sakaki, K.; Kitamoto, D.; Sugiura, M. *J. Membr. Sci.* **1993**, *84*, 241.
- (13) Pickering, P. J.; Chaudhuri, J. B. *J. Membr. Sci.* **1997**, *127*, 115.
- (14) Pickering, P. J.; Chaudhuri, J. B. *Chirality* **1997**, *9*, 261.
- (15) Higuchi, A.; Hashimoto, T.; Yonehara, M.; Kubota, N.; Watanabe, K.; Uemiya, S.; Kojima, T.; Hara, M. *J. Membr. Sci.* **1997**, *130*, 31.
- (16) Lakshmi, B. B.; Martin, C. R. *Nature* **1997**, *388*, 758.
- (17) Kellner, K. H.; Blasch, A.; Chmiel, H.; Lammerhofer, M.; Lindner, W. *Chirality* **1997**, *9*, 268.
- (18) Pickering, P. J.; Chaudhuri, J. B. *Chem. Eng. Sci.* **1997**, *52*, 377.
- (19) Takeuchi, T.; Horikawa, R.; Tanimura, T. *Sep. Sci. Technol.* **1990**, *25*, 941.
- (20) Keurentjes, J.; Voermans, F. J. M. In *Chirality in industry II: Development in the manufacture and applications of optically active compounds*; Collins, A. N.; Sheldrake, G. N.; Crosby, J., Eds.; John Wiley & Sons: Chichester, 1997.
- (21) Ding, H. B.; Carr, P. W.; Cussler, E. L. *AIChE J.* **1992**, *38*, 1493.

- (22) Pirkle, W. H.; Bowen, W. E. *Tetrahedron: Asymm.* **1994**, *5*, 773.
- (23) Keurentjes, J.; Nabuurs, L. J. W. M.; Vegter, E. A. *J. Membr. Sci.* **1996**, *113*, 351.
- (24) Poncet, S.; Randon, J.; Rocca, J. L. *Sep. Sci. Technol.* **1997**, *32*, 2029.
- (25) Itoh, T.; Saura, Y.; Tsuda, Y.; Yamada, H. *Chirality* **1997**, *9*, 643.
- (26) Creagh, A. L.; Hasenack, B. B. E.; Van der Padt, A.; Sudhölter, E. J. R.; Van 't Riet, K. *Biotechnol. Bioeng.* **1994**, *44*, 690.
- (27) Scamehorn, J. F.; Christian, S. D.; Ellington, R. T. In *Surfactant-based separation processes*; Scamehorn, J. F.; Harwell, J. H., Eds.; Marcel Dekker: New York, 1989.
- (28) Hong, J. J.; Yang, S. M.; Lee, C. H. *J. Chem. Eng. Japan* **1994**, *27*, 314.
- (29) Akita, S.; Yang, L.; Takeuchi, H. *J. Membr. Sci.* **1997**, *133*, 189.
- (30) Nishi, H. *J. Chromatogr. A* **1997**, *780*, 243.
- (31) Swartz, M. E.; Mazzeo, J. R.; Grover, E. R.; Brown, P. R. *J. Chromatogr. A* **1996**, *735*, 303.
- (32) Dalton, D. D.; Taylor, D. R.; Waters, D. G. *J. Chromatogr. A* **1995**, *712*, 365.
- (33) Yagi, H.; Uenishi, K.; Kushijima, H. *J. Ferment. Bioeng.* **1993**, *76*, 306.
- (34) Scamehorn, J. F.; Ellington, R. T.; Christian, S. D. *Rec. Adv. Sep. Techniq.* **1996**, *82*, 48.
- (35) Langmuir, I. *J. Am. Chem. Soc.* **1918**, *40*, 1361.
- (36) Ruthven, D. M. *Principles of adsorption and adsorption processes*; John Wiley & Sons: New York, 1984.
- (37) Guiochon, G.; Shirazi, S. G.; Katti, A. M. *Fundamentals of preparative and nonlinear chromatography*; Academic Press: Boston, 1994.
- (38) Lim, B. G.; Ching, C. B.; Tan, R. B. H. *Sep. Technol.* **1995**, *5*, 213.
- (39) Charton, F.; Jacobsen, S.; Guiochon, G. *J. Chromatogr.* **1993**, *630*, 21.
- (40) Myers, R. H. *Classical and modern regression with applications*; PWS-Kent: Boston, 1989.
- (41) Chatfield, C. *Statistics for technology*; Chapman and Hall: New York, 1983.
- (42) Van Boekel, M. A. J. S. *J. Food Sci.* **1996**, *61*, 477.
- (43) Press, W. H.; Flannery, B. P.; Teukolsky, S. A.; Vetterling, W. T. *Numerical recipes, the art of scientific computing*; Cambridge: New York, 1986.
- (44) Straume, M.; Johnson, M. L. *Methods Enzymol.* **1992**, *210*, 117.
- (45) Alper, J. S.; Gelb, R. I. *J. Phys. Chem.* **1990**, *94*, 4747.

Chapter 10

Surfactant-Based Colloidal Particles as the Extracting Phase for the Removal of Metal Ions from Aqueous Environments: Kinetic and Applied Aspects

Christian Tondre

Laboratoire de Chimie Physique Organique et Colloïdale, Université Henri Poincaré-Nancy I, Unité Mixte de Recherche CNRS-UHP (UMR 7565), B.P. 239, 54506 Nancy-Vandoeuvre Cedex, France

The hydrophobic core of surfactant micelles, which is hydrocarbon-like, can be used to solubilize lipophilic complexing agents, which in turn can extract metal ions. The coupling of micellar extraction with ultrafiltration has opened the way to extraction processes taking place in almost totally aqueous media. Research conducted in our laboratory during the past few years, has focused on the kinetics and mechanisms of complex formation in different kinds of surfactant-based colloidal particles (micelles, mixed micelles, microemulsion, polymerized micelles, vesicles) and on the effective removal of metal ion pollutants using membrane processes. The present review concerns more specifically the complexation/extraction of transition metal ions with different types of complexing agents, either from industrial origin or obtained from original synthesis. The stopped-flow technique with spectrophotometric detection has been used to characterize the kinetics of complex formation. Special attention is given to the following points: factors influencing the rate of complexation, parameters affecting the efficiency of metal extraction by micellar ultrafiltration, the part played by the rate of complexation (kinetic separations), and efficacy of micellar extraction compared to standard solvent extraction.

The role played by "micelles" (taken here in a large sense including microemulsion particles for instance) in separation processes has become more and more recognized over the last decade. Not only can micelles act as an extracting phase for a variety of compounds susceptible of interacting either hydrophobically or electrostatically with them (1), but they can also be responsible for different phenomena observed in solvent extraction, as for instance the spectacular increases of the extraction rates associated with the formation of w/o microemulsions (2) or the splitting of the

organic phase (third phase formation) related to the existence of inter-aggregate interactions (3). The interest of micellar particles is especially well illustrated in separation methods such as cloud-point extraction (4), micellar-enhanced ultrafiltration (MEUF) (5), micellar electrokinetic chromatography (MEKC) (6) or hollow-fiber membrane extraction (7). Many applications can be found, which can help solve analytical problems as well as environmental ones. The present paper will specifically address the question of the removal of metal ions from aqueous environments using ultrafiltration. The use of micelles for this purpose can be considered in two different ways: either the metal ions to be removed are electrostatically bound to the charged surface of the micelles (ion-exchange process) or a lipophilic extractant/metal complex is solubilized in the hydrophobic core of the micelles. Only the second method will be considered here. It is the only one permitting selective separations.

To the best of my knowledge the first report of surfactant enhanced ultrafiltration was due to P.S. Leung (8), who had mentioned the possibility of using the differences in retention of various chelating agents to separate two metallic ions in a mixture. However the real advances in the field of micellar enhanced ultrafiltration were due to Scamehorn and coworkers who have done pioneering work (9) (see also ref. (10) and references therein) and who have edited the first book on this topic (1). Several other groups over the world have also been involved to a lesser extent in the investigation of metal extraction studies using micellar systems and ultrafiltration (only the most recent references are cited here) (10-15). The research conducted in my group since 1989 has focused on both the kinetic and thermodynamic aspects of the complexation of metal ions by micelle-solubilized lipophilic extractants (16) and on its practical application to the elimination of metal ions from aqueous solutions (17-21). Our main concerns were the following: i) to analyze the importance of the different parameters controlling the micellar extraction of metal ions in order to optimize the extraction yields; ii) to understand the part played by the kinetic effects and see how these effects can be used to perform selective separations; iii) to evaluate the advantages and drawbacks of micellar extraction compared to standard solvent extraction.

It is the aim of this chapter to review some of the major results which have been obtained during the past few years concerning the above mentioned aspects of micellar extraction. For this purpose a large number of extracting agents have been used with varying chemical structure, hydrophobicity, complexing groups and ionization states. Some information concerning these extractants, including abbreviations used below, have been collected in Table I. Different types of surfactant-based colloidal particles have also been considered as the extracting phase: ionic and nonionic micelles, mixed micelles, microemulsions, polymerized micelles, and vesicles. A schematic representation of these particles is given in Table II, where the type of extractant which was solubilized in each type of particle and the parameters that we intended to investigate are also indicated. These parameters included not only the surface characteristics of the micelles, but also the nature of the hydrophobic domain and the rigidity of the amphiphilic membrane.

Table I - Extractants solubilized in micelles

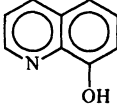
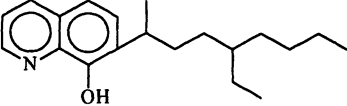
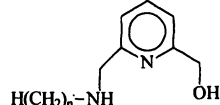
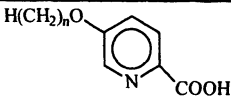
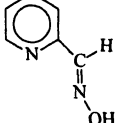
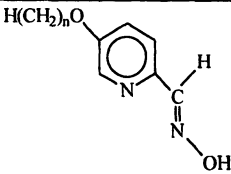
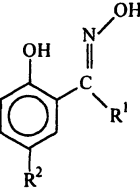
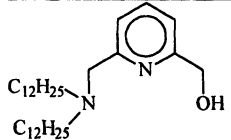
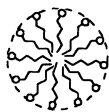
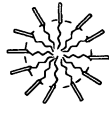
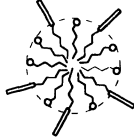
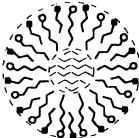
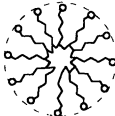
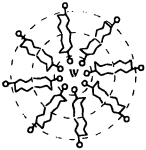
Chemical formula and name	Origin	Abbreviation	Collaboration and [ref]
 8-hydroxyquinoline	Commercial product	HQ	
 7-(4-ethyl-1-methyloctyl)-8-hydroxyquinoline	Purification of industrial extractant Kelex 100	C ₁₁ -HQ	
 6-(alkylamino)methyl-2-(hydroxymethyl)pyridines	Original Synthesis	C _n NHMePyr n=1,4,8,10,12,14,16	P. SCRIMIN P. TECILLA (Univ. Padua, Italy) [17], [27]
 5-alkoxypicolinic acids	Original Synthesis	C _n -PIC n=12,15,18	A. BREMBILLA P. LOCHON (ENSIC-INPL Nancy, France) [19], [24]
 Pyridine aldoxime	Commercial product	PAX	-id-
 5-alkoxypyridine aldoxime	Original synthesis	C _n -PAX n=12,15	-id-
 (E)-1-(2'-hydroxy-5'-alkylphenyl)1-alkanone oximes 2-hydroxy-5-alkylbenzophenone oximes	Original synthesis	Hydroxyoximes R ¹ =H, phenyl, -C ₆ H ₁₃ R ² =-CH ₃ , -C(CH ₃) ₃ , -(CH ₂) ₂ CH ₂ C(CH ₃) ₃ , -C ₆ H ₁₃	J. SZYMANOWSKI (Institute of Chem. Technol. & Eng., Poznan, Polgone) [20], [34]
 6-(di-n-dodecylaminomethyl)-2-(hydroxymethyl)pyridine	Original synthesis	diC ₁₂ NMePyr	P. SCRIMIN P. TECILLA (Univ. Padua, Italy) [30]

Table II - Types of surfactant-based colloidal particles and parameter investigated

<i>type of colloidal particle</i>	<i>schematic structure</i>	<i>extractant type and characteristics</i>	<i>parameter investigated and [ref]</i>
ionic micelles (CTAB, SDS)		ionizable extractants with varying HLB	nature of the electric charge HLB of extractant [17], [25], [27]
non-ionic micelles (C ₁₂ EO ₆ , Triton X-100, Brij 35)		highly lipophilic extractant	no electric charge; effect of the thickness of the hydrophilic layer [28]
mixed micelles (CTAB/C ₁₂ EO ₆)		negatively charged extractant (ion-pair formation with CTAB)	effect of surface electrostatic potential [19], [24]
microemulsions (CTAB/butanol/alkane/water)		extractant with oily nature (ex: Kelex 100)	microemulsification of the extractant; effect of the oil content; slow rate of complexation [18]
polymerized micelles poly-(undec-10-enylTAB)		ionizable extractants with varying HLB	static micelles (no dynamic of monomer exchange) [28]
vesicles (DODAB, DHAB, DDAB)		double chain extractant	thickness and rigidity of the bilayer; gel-fluid transition [30]

CTAB = cetyltrimethylammonium bromide, SDS = sodium dodecylsulfate, DODAB, DHAB, DDAB = dioctadecyl, dihexadecyl, didodecyl [dimethyl ammonium bromide]

II - Chemical Factors Affecting the Rate of Rejection of Metal Ions

In this paragraph we will only consider the part played by the factors which are of strictly chemical nature. It is obvious that, when ultrafiltration is used, there are a number of technical parameters which can affect the rate of rejection of metal ions (type of ultrafiltration device, nature of the membrane, pore size, applied pressure, etc); these parameters will not be considered here. All the experiments mentioned here have been carried out with a stirred-cell of small volume, using cellulosic membranes of molecular weight cut off 10,000 Da. We will show below that the yield of metal extraction by micellar particles is affected by the same parameters as in standard solvent extraction, such as for instance the HLB of the extractant or its ionization state. But in addition, the yield of recovered metal may be influenced by the nature of the micellar surface and especially its electric charges. The values given in the following for this yield has been defined as

$$Y(\%) = \frac{[Me]_0 - [Me]_{per}}{[Me]_0} \times 100$$

where $[Me]_0$ and $[Me]_{per}$ are the total metal concentration and the concentration in the permeate respectively.

a) Lipophilicity of the extractant. Copper extraction has been investigated using a series of 6-[(alkylamino)methyl]-2-(hydroxymethyl) pyridines, $C_nNHMePyr$, (see Table I) with alkyl chain lengths varying from 4 to 16 carbon atoms, solubilized in different kinds of micellar systems. Figure 1 shows the results that have been obtained at pH 5.0 for different values of the initial ratio between the extractants and the copper ions, when the extracting phase was CTAB micelles (17). Such a pattern of curves can be easily predicted, at least qualitatively, from simple equilibrium and mass balance considerations, assuming that the amount of copper extracted is directly related to the partitioning of the metal/extractant complex between the aqueous phase and the micellar pseudo-phase. The results clearly demonstrate the part played by both the hydrophobic character of the complexing agent and its concentration.

b) Ionization state of the extractant. In standard solvent extraction the metal extraction yield usually drops when the pH becomes acidic enough, due to a competition between protons and the metal ions for the complexing site. This is also observed in micellar extraction, as shown in Figure 2 for the extraction of Cu^{2+} by 7-(4-ethyl-1-methyloctyl)-8-hydroxyquinoline (C_{11} -HQ) solubilized in CTAB/butanol (21). As for its more hydrophilic homologue, 8-hydroxyquinoline (HQ), in solvent extraction (22), the release of copper from its complex takes place in a more acidic region than the release of nickel (18). The results presented in Figure 2 illustrate the drastic effect of pH on the yield of copper extraction.

c) Micellar surface charge. Another factor which can influence the rate of rejection of metal ions, is the electrostatic potential at the surface of the micelles, since the partitioning coefficient of the extracting agent (or of its complex with a metal ion) will depend on its proper electric charge (23). For the extraction of Cu^{2+} by

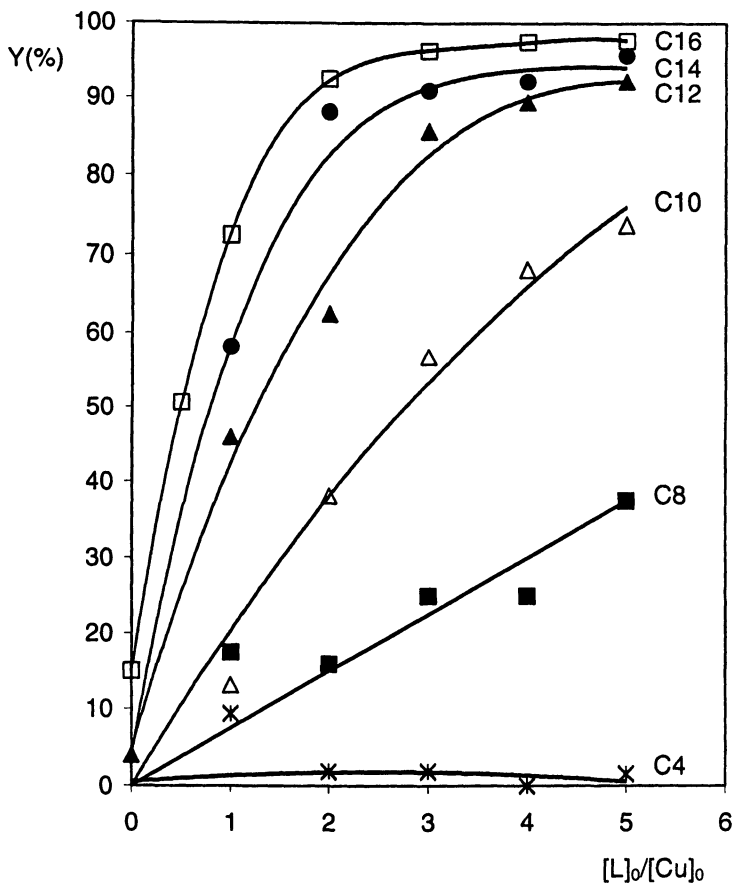


Figure 1. Extraction in CTAB micelles: yield of copper(II) extraction Y versus the ligand to metal ratio for extractants with varying alkyl chain length. $[CTAB]=2.5 \times 10^{-2}$ M; $[Cu^{2+}]_0=10^{-4}$ M; $pH=5.0$. Reproduced from ref 17. Copyright American Chemical Society 1993.

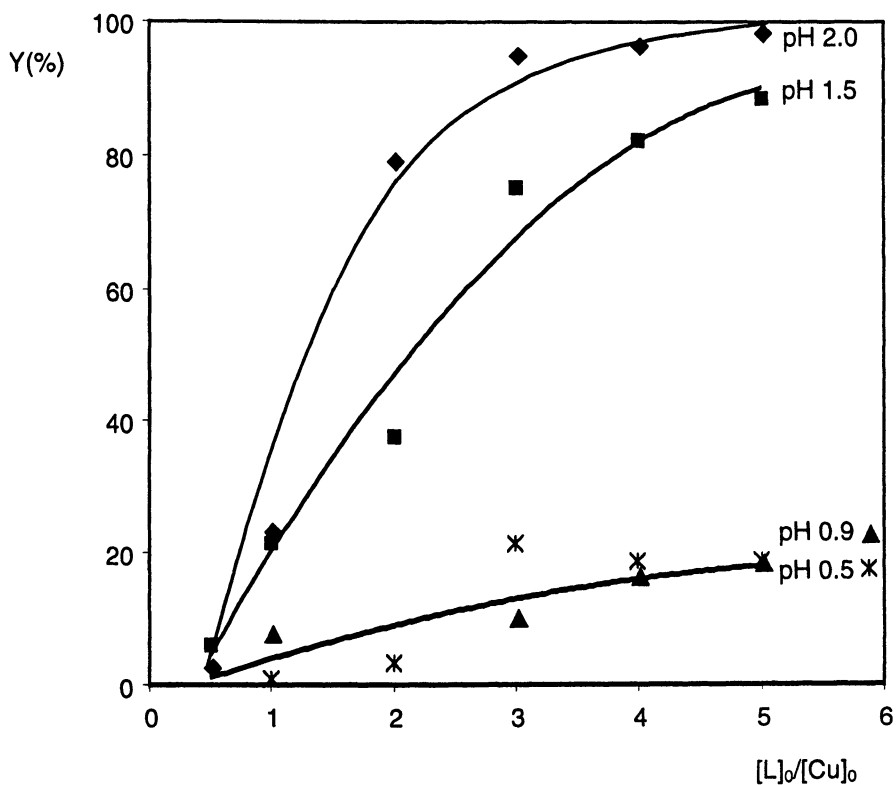


Figure 2. Yield of copper extraction (from ultrafiltration experiments) vs extractant to metal ratio. CTAB 0.45 %/n-butanol 0.45 %/water (0.1 M NaBr) 99.1 %; $[Cu^{2+}] = 3.34 \times 10^{-4}$ M; $[C_{11}\text{-HQ}] = 3.34$ to 16.7×10^{-4} M. Reproduced from ref 21. Copyright American Chemical Society 1997.

C_n NHMePyr, it has been shown that the yields of extraction measured in similar conditions are larger for $C_{12}EO_6$ micelles than with CTAB micelles, especially at low ligand/metal ratios (17). Other results have been obtained for the extraction of Ni^{2+} by a series of long chain derivatives of alkoxypicolinic acid (C_n -Pic) solubilized either in pure CTAB micelles or in CTAB/ $C_{12}EO_6$ mixed micelles (19, 24). The increase of the proportion of the nonionic surfactant is associated in this case with a decrease of the electrostatic potential of the micellar particles, which obviously facilitates the metal extraction. The yield of metal removal can thus be improved by adapting the type of micellar systems used. In the latter case, the effect observed may be attributed to the ion-pairing interaction between the carboxylic group of C_n -Pic and the polar head of CTAB.

III - Kinetic Separation and Factors Influencing the Kinetics of Complex Formation

The kinetic aspects of metal ion extraction have a special significance in the case of micellar systems. These systems appear perfectly isotropic, although their intimate nature is microheterogeneous, and for this reason they are especially convenient to investigate extractant/metal ion reactions, which normally take place in highly heterogeneous biphasic conditions. Stopped-flow kinetic experiments involving different kinds of more or less hydrophobic extractants showing a UV absorbance spectrum, have been conducted in a large number of microheterogeneous systems. The results of a few of them have been collected in Table III in order to show how the apparent rate constant for complex formation can be considerably reduced when a water soluble (at least partly) complexing agent is replaced by a hydrophobic analogue. Reduction factors ranging from about 10 to 100 were measured depending on the reaction medium and experimental conditions. These rate reduction effects have different possible origins and they can be exploited in some cases to perform kinetic separations of metal ions. Several explanations have been put forward to account for the fact that the interfacial reaction is slower than the bulk reaction in micellar solutions (25): effects of local concentrations of reagents, electrostatic repulsions inducing a spatial separation of the reagents, local H^+ concentration different from the macroscopic one (16a), reduction of the probability of collisions due to limitation of diffusion, steric hindrances to the approach of reagents, or unfavorable orientation increasing the activation energy barrier.

a) Kinetic separations. An example of kinetic separation (18) of a mixture of Ni^{2+} and Co^{2+} ions is shown in Figure 3. The large difference in the kinetics of complex formation involving either Ni^{2+} or Co^{2+} ions is well known (26), but in most instances a separation on a kinetic basis is not possible because both metal ions react very rapidly. In the case presented here, if the ultrafiltration immediately follows the introduction of the metal ions, only the fastest reacting ions (cobalt in this example) will be removed. The shorter the time allotted between reaction and ultrafiltration, the better the separation is. Cationic micelles of CTAB are more effective than nonionic micelles because of the contribution of electrostatic repulsion.

Table III - Rate of extractant/metal complex formation (k_f^{app}) in microheterogeneous systems at 25° C. Rate reduction with highly hydrophobic extractants

Extractants/ metal	Medium and Experimental Conditions	$k_f^{app}(M^{-1}s^{-1})$		Reduction factor	[Ref]
		Complexing agent	Hydrophobic analog		
HQ and $C_{11}HQ/Ni^{2+}$	Microemulsion (CTAB/butanol/ C_{16}/H_2O) pH 7.5 (0.1 M TEA buffer)	196	5.6	35	[16a]
	Microemulsion ($C_{12}EO_6$ /decane/ H_2O) pH 7.5 (0.1 M TEA buffer)	230	9.25	25	[16a]
$C_1NHMePyr$ and $C_{16}NHMePyr/Cu^{2+}$	CTAB $2.5 \times 10^{-2}M$ pH 3.5	2744	128	21	[27]
	$C_{12}EO_6$ $2.0 \times 10^{-2}M$ pH 3.5	2539	280	9	[27]
PAX and $C_{12}PAX/Ni^{2+}$	CTAB $2.5 \times 10^{-2}M$ pH 6.5	1030	2.95	349	[19]
	$C_{12}EO_6$ $2.0 \times 10^{-2}M$ pH 6.5	2010	19.3	104	[19]
Salicylaldoxime and C_7 , (phenyl)- analog/ Cu^{2+}	CTAB $7.5 \times 10^{-2}M$ pH 4.35 (acetate buffer $2.5 \times 10^{-2}M$)	2270	44.4	51	[34]

See the significance of abbreviations used in Tables I and II

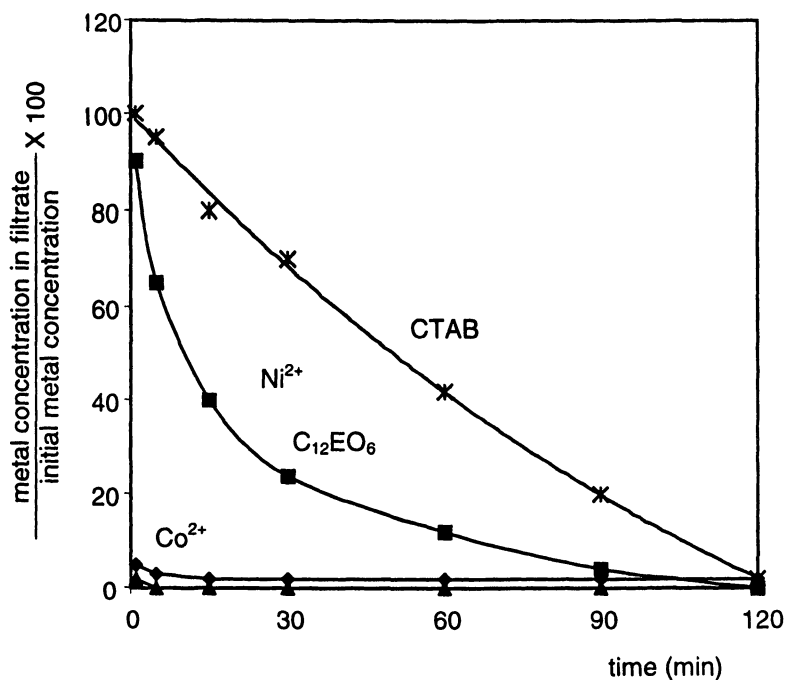


Figure 3. Ultrafiltration following complexation: percent of metal ion concentration in filtrate relative to initial concentration, versus time allotted between the start of reaction and ultrafiltration. Analytical concentrations before ultrafiltration: $[\text{CoCl}_2]=[\text{NiCl}_2]=1.7 \times 10^{-4}$ M; $[\text{C}_{11}\text{-HQ}]=3.34 \times 10^{-3}$ M. CTAB/butanol micelles: (X): Ni^{2+} ; (Δ): Co^{2+} . C_{12}EO_6 micelles: (\blacksquare): Ni^{2+} ; (\blacklozenge): Co^{2+} . Reproduced with permission from ref 18. Copyright 1993 Academic Press, Inc.

b) Ways of affecting the kinetics of complex formation. Very little has been done so far in view of developing the use of such kinetic effects for separation purposes. We will briefly review here some of the possible ways that can be thought of to further reduce the kinetics of complex formation.

i) Increase the partition coefficient of the complexing agent: This can be achieved by adding an oil in the micellar core (o/w microemulsion) (18). Figure 4 shows the variation of the observed rate constant characterizing the reaction of Co^{2+} with $\text{C}_{11}\text{-HQ}$ in CTAB/butanol micelles in the presence of increasing amounts of different added oils. (Note that obtaining a significant solubilization of these n-alkanes required the presence of 0.04 to 0.08 M of NaBr in the aqueous phase). The rate reduction in the best case was only by a factor on the order of two.

ii) Stabilize the complexing agent inside the micelles: This can be done through ion-pairing interactions between the surfactant and the complexing agent. This effect is demonstrated in Figure 5 in which is represented the variation of the observed rate constant for the kinetics of complexation of Ni^{2+} ions with $\text{C}_{12}\text{-PIC}$ at $\text{pH } 7.0 \pm 0.5$ and 4.5 ± 0.5 versus the mole fraction of CTAB in mixtures of CTAB and C_{12}EO_6 . In the pure nonionic micelles the reaction is very fast and it becomes slower by more than three orders of magnitude in the pure cationic micelles. This is clearly the effect of the association of the carboxylate group of the extractant with the positively charged surfactant polar heads, since it was reported earlier that, with a positively charged extractant, the measured rate constants (27) have quite similar values in CTAB or C_{12}EO_6 , respectively. Note however, that the negative charge on the extractant molecule would imply a faster rate of complexation in an homogeneous aqueous phase, compared to a neutral or cationic extractant.

iii) Increase the separation between complexing agent and metal ion: Nonionic surfactants of the alkyl polyethyleneoxide type offer a way to test the effect of the separation distance, by changing the number of ethylene oxide (EO) units constituting the hydrophilic moiety of the surfactant. Provided that a very lipophilic extractant is used ($\text{C}_{16}\text{NHMePyr}$ was chosen for these experiments (28), see Table I), we expect it to reside essentially in the hydrophobic core of the micelles and the metal ion to have to find its way through the hydrophilic palisade. Changing the number of EO units from 6 to 23 did not show the expected decrease of the observed rate constant and no direct correlation could be observed between this rate and the thickness of the hydrophilic layer.

iv) Use of polymerized micelles or vesicles: Another way to make a lipophilic extractant more strongly bound to surfactant-based colloidal particles (apart from attaching it through a covalent bond) could be to rigidify the amphiphilic layer in order to decrease the exchange dynamics between the free and bound extractants. This effect added to the electrostatic repulsions on the approaching metal ion has been tested in two different ways, using polymerized micelles or vesicles.

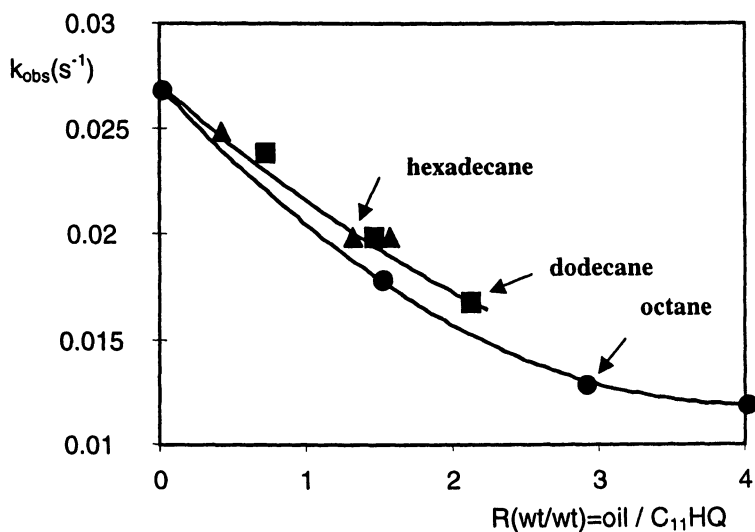


Figure 4. Variation of the observed rate constant with the ratio of oil to $\text{C}_{11}\text{-HQ}$ for the complexation reaction of Co^{2+} . (●): octane; (■): dodecane; (▲): hexadecane. Reproduced with permission from ref 18. Copyright 1993 Academic Press, Inc.

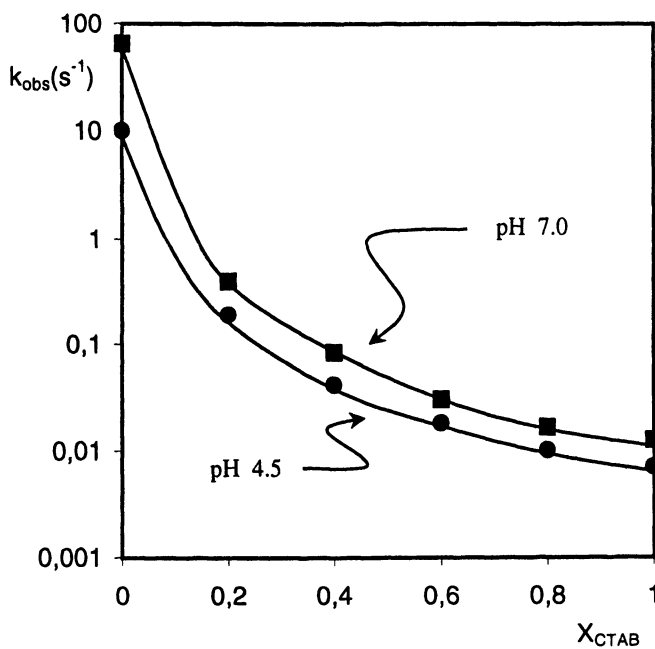


Figure 5. Effect of the mole fraction of CTAB in mixtures of CTAB and C_{12}EO_6 on the kinetics of complexation of Ni^{2+} ions with $\text{C}_{12}\text{-PIC}$. Overall surfactant concentration 2×10^{-2} M; $[\text{C}_{12}\text{-PIC}] = 10^{-4}$ M; $[\text{Ni}^{2+}]_0 = 10^{-3}$ M. Reproduced with permission from ref 24. Copyright 1995 Steinkopff Verlag.

The polymerized micelles were obtained from undec-10-enyltrimethylammonium bromide (28), a surfactant analogous to CTAB or DTAB, except that the alkyl chain was shorter (with only eleven carbon atoms) and contained a terminal double bond. The kinetics of copper complexation with the same series of extractants as those considered in paragraph IIa ($C_n\text{NHMePyr}$ with n varying this time from 1 to 16) were investigated. The variation of the observed rate constants as a function of n is compared in Figure 6 with the results relative to CTAB and DTAB. The decrease of the reaction rate associated with an increase of the number of carbon atoms of the extracting agents is less important with the polymerized micelles than with CTAB or DTAB. We can conclude that in this case, the shorter surfactant chain length for the polymerized micelles is not compensated by the freezing of the micelle dynamics. However, further efforts will have to be made with polymerized micelles having longer hydrophobic tails.

The use of vesicular systems offers another way to reduce the mobility of a solubilized extractant. It is indeed well known that bilayers are more rigid than conventional micelles and in addition they show, when varying the temperature, a gel to fluid transition (29) which could also affect the mobility. The observed rate constants characterizing the complexation of Cu^{2+} with the extractant $\text{diC}_{12}\text{NMePyr}$ (see Table I) have been determined in different types of vesicles (DODAB, DHAB and DDAB), varying the temperature (30). The results obtained at pH 3.5 are shown in Figure 7. They were interpreted as demonstrating the existence of two distinct kinetic behaviors depending whether the alkyl chains in the vesicles are in a gel state or in a fluid state. This behavior was only observed with a ligand having a double alkyl chain and not with single-chain ligands and it has appeared to be practically unaffected by the type of vesicles considered, except that the change in the kinetics of complex formation was satisfactorily well correlated with the critical transition temperature. In the case of DHAB, the observation of two relaxation times in a temperature domain close to the critical temperature, has suggested that the two states of the bilayer are coexisting when approaching the transition. An important conclusion of these experiments was that, very unexpectedly, the gelification of the amphiphilic layer is associated with an increase of the rate of complex formation and not with its decrease. This was attributed to the fact that the complexing site is more easily accessible than in the fluid state because the alkyl chains of the extractant cannot penetrate as deeply in the bilayer.

IV - Advantages and Drawbacks of Micellar Extraction Compared to Solvent Extraction

After the kinetic aspects discussed above, let's return to equilibrium conditions in order to examine how micellar extraction can be compared to solvent extraction. A systematic comparison of both processes has recently been carried out using different complexing agents which were either solubilized in micelles (CTAB and $C_{12}\text{EO}_6$) or in an organic solvent (31). In each case the yield of extraction was measured as a function of pH, when strictly comparable quantities of the extractants were used. All the extraction curves were fitted with theoretical models assuming different

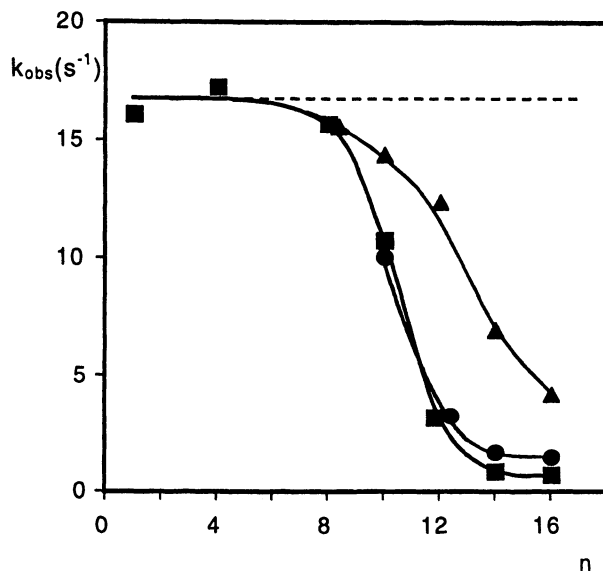


Figure 6. Variation of k_{obs} for copper complexation versus n in different reaction media. (■) $[CTAB]=2.5 \times 10^{-2}$ M, (●) $[DTAB]=4 \times 10^{-2}$ M; (▲) $[polymer]=2 \times 10^{-2}$ M. $pH=3.5 \pm 0.2$, $[C_nNHMePyr]=10^{-4}$ M, $[Cu^{2+}]=5 \times 10^{-3}$ M. Reproduced with permission from ref 28. Copyright 1996 Steinkopff Verlag.

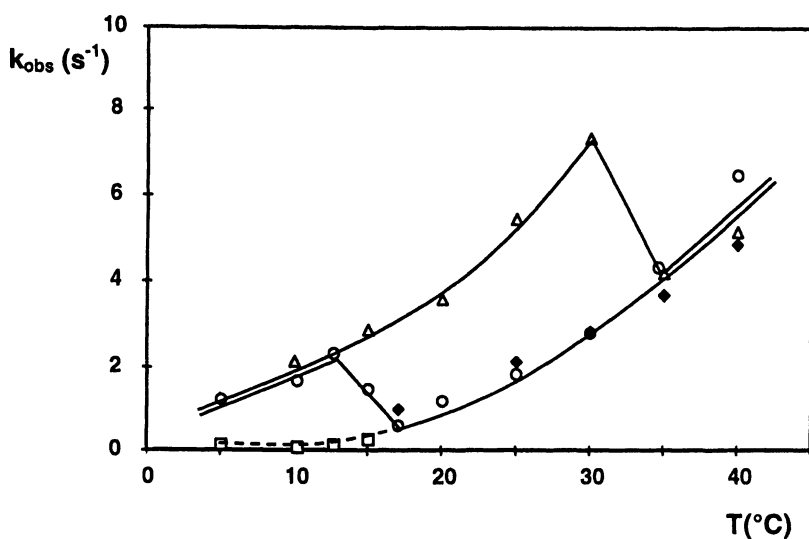


Figure 7. Observed rate constants versus temperature for the complexation of Cu^{2+} by $diC_{12}NMePyr$ solubilized in vesicles of DODAB (Δ), DHAB (slow \square , fast O), DDAB (\blacklozenge). $[Cu^{2+}]=5$ mM, $[Surf.]=1.5$ mM, $[ligand]=0.1$ mM, $pH=3.5 \pm 0.1$, $\lambda=320$ nm. Reproduced from ref 30. Copyright American Chemical Society 1997.

stoichiometries for the extractant/metal complexes. Figure 8 represents such curves for the case of copper extraction by C_{11} -HQ: i) in water/isooctane biphasic systems with variable phase volumes ($v_{\text{org}}/v_{\text{aq}}=1; 0.1; 0.033; 0.01$) and ii) in nonionic $C_{12}EO_6$ micelles using ultrafiltration. In the first cases, the curves were correctly predicted by the model when assuming a 2:1 complex of the type L_2Cu (where L is the unprotonated extractant, LH representing the acidic extractant C_{11} -HQ), in agreement with the work of Stary (22), which concerned 8-hydroxyquinoline (HQ), the non-alkylated analogue of C_{11} -HQ. The experimental points measured in the $C_{12}EO_6$ micelles are falling quite nicely on the curve obtained when the $v_{\text{org}}/v_{\text{aq}}$ ratio was equal to 0.01. This observation is especially interesting since it demonstrates that when the $v_{\text{org}}/v_{\text{aq}}$ ratio becomes of the same order as the volume fraction of the micellar pseudo-phase (about 0.01 in the present case), both processes lead to very similar results, at least when nonionic micelles are concerned.

Such comparisons are necessary to evaluate the advantages and drawbacks of micellar extraction. To start with the negative points, the following disadvantages can be mentioned: the process is restricted to low metal content (concentrations up to millimolar can be treated but problems may arise for larger values); the leakage of monomeric surfactant at concentrations of the order of the cmc or greater cannot be ignored (32); ion expulsion effects due to Donnan equilibria may complicate the process (9c, 31); the problem of recycling of the micellar phase is far from being completely solved (21); due to the Laplace pressure effect, the solubilization capacity of micelles for complexing agents should in any case remain lower than that of hydrocarbons (33). Turning now to the positive points: no organic solvents are required and the process operates in 99 % aqueous media; membrane processes are easy to implement and they are convenient for continuous flow treatments; the counterions of the micelles can contribute to the formation of a neutral extractant/metal complex (31); in favorable cases, selective separations can be achieved on kinetic criteria (18).

The first part of this chapter has highlighted the main chemical factors to be considered in order to optimize the rejection of metal ions by ultrafiltration when surfactant-based colloidal particles are used as the extracting phase. The domain of kinetic separations which was approached in the second part is a largely open field of investigation, where new inventive contributions could bring some breakthrough leading to further developments and applications. Only some of the possible paths by which such separations could be improved have been explored and those only in a very preliminary fashion. The last part demonstrated that micellar extraction and solvent extraction may lead to very similar results. Each specific problem will require a careful examination of the advantages and disadvantages of micellar ultrafiltration using the guidelines briefly suggested in this chapter.

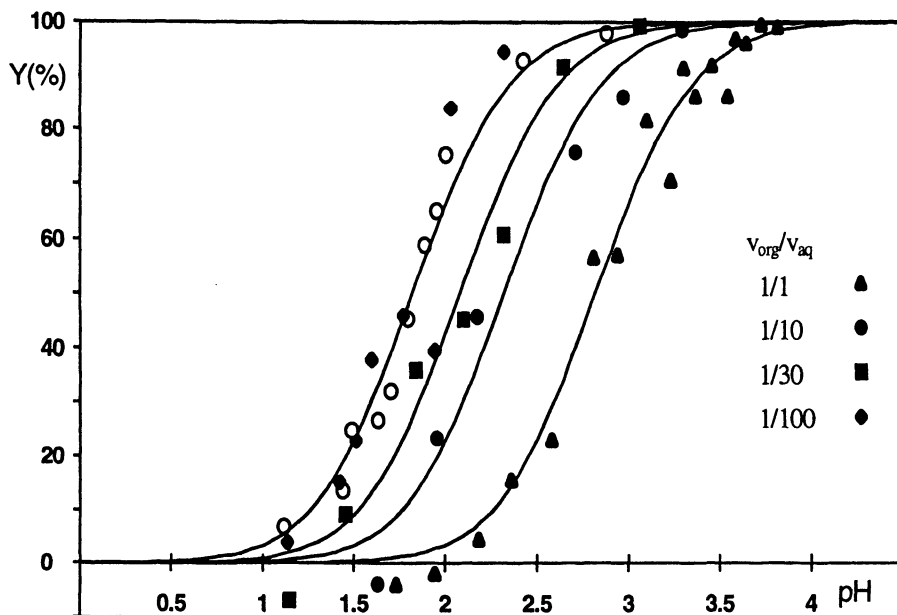


Figure 8. Yields of extraction of Cu^{2+} ions versus pH for C_{11} -HQ in C_{12}EO_6 micelles (O) and in biphasic water/isooctane systems with $v_{\text{org}}/v_{\text{aq}}$ as indicated; $[\text{Cu}^{2+}]_0 = 10^{-4}$ M; $[\text{C}_{11}\text{-HQ}] = 5 \times 10^{-4}$ M (micellar solution) or $(v_{\text{aq}}/v_{\text{org}}) \times 5 \times 10^{-4}$ M (isooctane). The full lines are theoretical fits of the solvent extraction data. Adapted from ref 31.

Acknowledgments

The author wants to acknowledge the contributions of the people cited in the references, who at one moment or another, have been involved in the works reviewed here: M. Boumezioud, A. Bouraine, N. François, M. Hébrant, M. Ismael, H.-S. Kim, S.-G. Son, C. Toumi, P. Tounissou. He is also indebted to P. Scrimin and P. Tecilla (Padua University, Italy), J. Szymanowski (Poznan Technical University, Poland), P. Lochon and A. Brembilla (ENSIC - National Polytechnic Institute of Nancy, France), J.P. Roque (Montpellier University, France), who, through different kinds of cooperative programs, have been involved in the synthesis of the various extracting agents or of the polymerized micelles.

The participation of the author in the 215th American Chemical Society (ACS) Dallas Meeting (1998) was made possible due to the support of the Petroleum Research Fund of the ACS, which is also greatly appreciated.

Literature Cited

1. *Surfactant-Based Separation Processes*, Surfactant Science Series Vol. 33, J.F. Scamehorn and J.H. Harwell, Eds., Marcel Dekker, New York 1989.
2. Bauer, D., Komornicki, J. *Proc. Int. Solvent Extr. Conf.* 1983, 315; Fourre, P., Bauer, D. *C.R. Acad. Sci. Paris, Ser. 2* 1981, 292, 1077.
3. Osseo-Asare, K. *Adv. Colloid Interface Sci.* 1991, 37, 123; Erlinger, C.; Gazeau, D.; Zemb, T.; Madic, C.; Lefrançois, L.; Hébrant, M.; Tondre, C., *Solv. Extr. Ion Exch.* 1998, 16, 707.
4. Pramauro, E.; Pelizzetti, E. *Trends Anal. Chem.* 1988, 7, 260.
5. Christian, S.D.; Scamehorn, J.F. in ref. 1 p. 3; Scamehorn, J.F.; Christian, S.D.; Ellington, R.T. in ref. 1 p. 29.
6. Watarai, H. *J. Chromatogr. A* 1997, 780, 93; Haddad, P.R.; Macka, M.; Hilder, E.F.; Bogan, D.P. *J. Chromatogr. A* 1997, 780, 329; Tani, H.; Kamidate, T.; Watanabe, H. *J. Chromatogr. A* 1997, 780, 229.
7. Hurter, P.N.; Hatton, T.A. *Langmuir* 1992, 8, 1291.
8. Leung, P.S. in *Ultrafiltration Membranes and Applications*, A.R. Cooper, Ed., Plenum, New York 1980 p. 415-421.
9. a) Klepac, J.; Simmons, D.L.; Taylor, R.W.; Scamehorn, J.F.; Christian, S.D. *Sep. Sci. Technol.*, 1991, 26, 165; b) Christian, S.D.; Tucker, E.E.; Scamehorn, J.F.; EL-Sayed, D.A.; *AIChE J.* 1988, 34, 189; c) Dharmawardana, U.R.; Christian, S.D.; Taylor, R.W.; Scamehorn, J.F. *Langmuir* 1992, 8, 414; d) Scamehorn, J.F.; Christian, S.D.; El-Sayed, D.A.; Uchiyama, H.; Younis, S.S. *Sep. Sci. Technol.* 1994, 29, 809.
10. Fillipi, B.R.; Scamehorn, J.F.; Taylor, R.W. Christian, S.D. *Sep. Sci. Technol.* 1997, 32, 2401.
11. Pramauro, E.; Bianco Prevot, A. *Pure Appl. Chem.* 1995, 67, 551.
12. Reiller, P.; Lemordant, D.; Moulin, C.; Beaucaire, C. *J. Colloid Interface Sci.* 1994, 163, 81.

13. Paulenova, A.; Rajec, P.; Jezikova, J. *Radioanal. Nucl. Chem* **1998**, *228*, 119; Paulenova, A.; Rajec, P.; Adamcik, P.; *J. Radioanal. Nucl. Chem.* **1998**, *228*, 115.
14. Keskinler, B.; Danis, U.; Cakici, A.; Akay, G. *Sep. Sci. Technol.* **1997**, *32*, 1899.
15. Ahmadi, S.; Huang, Y.-C.; Batchelor, B.; Koseoglu, S.S. *J. Environment. Eng.* **1995**, *121*, 645.
16. a) Tondre, C.; Boumezioud, M. *J. Phys. Chem.* **1989**, *93*, 846; b) Boumezioud, M.; Kim, H.S.; Tondre, C. *Colloids Surfaces* **1989**, *41*, 255.
17. Tondre, C.; Son, S.-G.; Hébrant, M.; Scrimin, P. Tecilla, P. *Langmuir* **1993**, *9*, 950.
18. Ismael, M.; Tondre, C. *J. Colloid Interface Sci.* **1993**, *160*, 252.
19. Hébrant, M.; Bouraine, A.; Tondre, C.; Brembilla, A.; Lochon, P. *Langmuir* **1994**, *10*, 3994.
20. Richmond, W.; Tondre, C.; Krzyzanowska, E., Szymanowski, J. *J. Chem. Soc. Faraday Trans.* **1995**, *91*, 657.
21. Tondre, C.; Hébrant, M.; Perdicakis, M.; Bessière, J. *Langmuir* **1997**, *13*, 1446
22. Sary, J.; *Anal. Chim. Acta* **1969**, *28*, 132.
23. Hébrant, M.; Tondre, C. *J. Coll. Interface Sci.* **1992**, *154*, 378.
24. Hébrant, M.; Bouraine, A.; Brembilla, A.; Lochon, P.; Tondre, C. *Colloid Polym. Sci.* **1995**, *273*, 598.
25. Tondre, C.; Hébrant, M. *J. Phys. Chem.* **1992**, *96*, 11079.
26. Eigen, M. *Pure Appl. Chem.* **1963**, *6*, 97; Eigen, M., Wilkins, R.G in *Mechanism of Inorganic Reactions*, Advances in Chemistry Series, Am. Chem. Soc., Washington D.C. **1965**, *49*, 55.
27. Son, S.-G.; Hébrant, M.; Tecilla, P.; Scrimin, P.; Tondre, C. *J. Phys. Chem.* **1992**, *96*, 11072.
28. Hébrant, M.; Toumi, C.; Tondre, C.; Roque, J.P.; Leydet, A.; Boyer, B. *Colloid Polym. Sci.* **1996**, *274*, 453.
29. Kunitake, T. *Angew. Chem. Int. Ed. Engl.* **1992**, *31*, 709.
30. Hébrant, M.; Tecilla, P.; Scrimin, P.; Tondre, C. *Langmuir* **1997**, *13*, 5539.
31. Hébrant, M.; François, N.; Tondre, C. *Colloids Surfaces A* **1998**, in press.
32. Tounissou, P.; Hébrant, M.; Rodehüser, L.; Tondre, C. *J. Colloid Interface Sci.* **1996**, *183*, 484; Tounissou, P.; Hébrant, M.; Tondre, C. *J. Colloid Interface Sci.* **1996**, *183*, 491.
33. Mukerjee, P. in *Solution Chemistry of Surfactants*, K.L. Mittal, Ed., Plenum Publish Corp., *Vol. 1* **1979** p. 153.
34. Cierpiszewski, R.; Hébrant, M.; Szymanowski, J.; Tondre, C. *J. Chem. Soc. Faraday Trans.* **1996**, *92*, 249.

Chapter 11

Micellar-Enhanced Ultrafiltration in a Spiral Wound Ultrafiltration Module and Comparison with Stirred Cell Performance

Bruce L. Roberts ¹, John F. Scamehorn ², and Sherril D. Christian ²

¹ Kerr-McGee Technical Center, 3301 Northwest 150th Street,
Oklahoma City, OK 73134

² Institute for Applied Surfactant Research, University of Oklahoma,
Norman, OK 73019

Micellar-enhanced ultrafiltration, utilizing anionic or cationic surfactants with a spiral-wound membrane module, is shown to be effective in separating dissolved tert-butylphenol, divalent copper cation, and divalent chromate anion from aqueous streams. Membranes having molecular weight cutoffs of 5,000 to 20,000 Daltons are used. Large rejections and high fluxes are observed until large retentate surfactant concentrations are attained; rejections range from 98% to 99.9%. Reasonable agreement of both rejection and flux results among stirred cell, semi-equilibrium dialysis, and spiral wound devices indicates that the solutes in the permeate are present at near-equilibrium concentrations and that results from the stirred cell and semi-equilibrium dialysis experiments can be scaled-up to commercial spiral wound units. The former methods require smaller volumes of fluid and they are faster and less expensive to operate than full-scale ultrafiltration equipment.

Ultrafiltration is a useful separation process for removing and recovering solute species having molecular weights of 1,000 Daltons or more. However, traditional ultrafiltration is not effective in removing solutes having molecular weights less than about 500 Daltons.

In micellar-enhanced ultrafiltration (MEUF), aqueous pollutant molecules which are too small to be removed by direct ultrafiltration become attached to these micelles and the micelles are ultrafiltered from solution, resulting in purified water. The economic advantages of MEUF are that it is a low-energy process, it may be staged to achieve any desired degree of separation, it can simultaneously remove both nonionic organic molecules and charged ions (inorganic or organic), and it uses a nontoxic, biodegradable separating agent (surfactant).

Dissolved organic solutes (1-14,25,26,27) or multivalent ions (6,7,9-11,15-24,28,29,30,31) can be removed from water using MEUF. This is illustrated in Figure 1 for removal of multivalent cations and organic solutes. In this example, an anionic surfactant is first added to the water at concentrations well above the CMC (i. e., the concentration at which aggregates of surfactant molecules called micelles begin to form in significant amounts).

The interior of a micelle is hydrocarbon-like and capable of 'solubilizing' organic solutes. When anionic surfactants are used in MEUF, the head group regions of the micelle are negative, and the micelle surface has a highly-negative electrical potential. Therefore, multivalent metal ions in solution (e. g., copper, lead, or thorium) preferentially bind to the oppositely charged micellar surface by electrostatic attraction. Conversely, when cationic surfactants are used, negative ions like chromate will bind to the positively-charged micellar surface. If a feed solution containing the added surfactant is forced through an ultrafiltration membrane having pore diameters small enough to block the passage of the micelles, the organic molecules and metal ions bound to the micelles are also prevented from entering the stream that passes through the membrane (the permeate). The concentrations of the organic molecules, metal ions, and surfactants in the permeate correspond very nearly to their uncomplexed species concentrations in the solution retained by the membrane (the retentate) (1,2,5,6,8,16).

Assuming that the concentrations of uncomplexed (monomeric) solutes is equal to the concentrations of these species in the permeate, information about the equilibrium solubilization of organic solutes by surfactant micelles can be used to predict *a priori* the efficiency of MEUF in removing these solutes from aqueous streams (1,2,4-8). A recent book summarizes the current state of knowledge of the phenomenon of solubilization (32) and a review article summarizes methods of measuring solubilization (33). One such method, semi-equilibrium dialysis (SED) (5,8,16,34-42), can measure solubilization isotherms for volatile or nonvolatile solutes and binding isotherms for ions attached to surfactant micelles.

MEUF can be used to remove either anionic or cationic multivalent ionic species that bind to surfactant micelles (6,7,9,10,11,15-24). For example, we have investigated the removal of a number of cations, including zinc, nickel, copper, lead, and calcium, and several anions, including chromate, and the cyano-complexes of iron and nickel. The equilibrium assumption mentioned above, which has been valuable in predicting the efficiency of MEUF in removing dissolved organic species, seems to apply equally well in estimating the concentrations of ionic species passing through the ultrafiltration membrane. SED experiments produce results in essential agreement with MEUF data for several aqueous ionic solute/ionic surfactant systems (15-17).

Both rejection of target solutes and concentration polarization effects have been studied in detail for stirred cell ultrafiltration units, and gel points have been determined for a number of types of surfactants (1,2,17,14,24). However, most commercial ultrafiltration operations use spiral wound or hollow fiber devices.

The purpose of this study is to compare results of MEUF obtained from a stirred cell or from a dialysis cell and from a pilot scale spiral wound device for removal of nonionic organic solutes and of multivalent cations and anions. Both rejections (indicating concentrations of solutes in the permeate stream passing through the membrane) and flux behavior are compared. The stirred cell is operated in batch mode while the pilot plant

spiral wound unit used here is capable of operating in a total recycle mode with all of the permeate and retentate recycling back to the feed, permitting attainment of an unambiguous steady state. This study indicates scale-up effects for MEUF and the value of laboratory experiments using stirred cells or dialysis cells to prediction of the performance of MEUF on a commercial scale.

Experimental

Methods

A flow diagram of the ultrafiltration apparatus used for this study is shown in Figure 2. The pump (P1) was a Burks stainless steel booster pump powered by a one-fourth horsepower Franklin 120 volt motor. The temperature of the feed tank was held constant by pumping refrigerated coolant through a heat exchanger made of 1/4 inch stainless steel tubing in a 4 inch diameter coil in the feed tank. A temperature probe and controller were used to control the coolant pump (P2) to provide the desired temperature in the feed tank. The feed pressure to the membrane was held constant at 60 psig. The retentate flow rate was held constant at 400 mL/min. The apparatus start-up was done with the coarse adjustment pressure control valve (V1), a ball valve, completely open. The feed pressure to the membrane was then set at 60 psig. The retentate and permeate flow rate were measured by actuating two electromagnetic three way valves (V3 and V4) that diverted the retentate and permeate streams into collection beakers. The beakers with their solutions were weighed on an Ohaus triple beam balance and the weight of the empty beakers was subtracted to arrive at mass flow rates for the two streams. The electromagnetic sampling valves (V3 and V4) were controlled by a microprocessor controller that energized the valves for fifteen seconds. Using an iterative process of adjusting the retentate flow rate valve (V6) and the fine adjustment pressure control valve (V2) and measuring the mass flow rate of the retentate stream, the 60 psig feed pressure and 400 mL/min retentate flow rate were established. The three-way system drain valve (V5) was used to drain permeate from the apparatus to increase the concentration of surfactant in the feed tank. The membrane, shown in Figure 3, was a five square foot cellulose acetate spiral wound membrane manufactured by Spectrum Medical Products. In the stirred cell experiments, similar cellulose acetate membranes were used. In general, the permeate flow rate was 440 mL/min for distilled and deionized water at a pressure of 60 psig on the retentate side of the membrane. The system reached steady state within a few minutes, attainment of steady state being indicated by a constant permeate flux, within a precision of one percent. Therefore, all the data presented are at steady state.

Materials

The following compounds were all used as received from the vendor: cetyl pyridinium chloride (CPC) from Hexcel; cupric chloride dihydrate 99% from Fisher; sodium chromate, Certified, from Fisher; and 4-tert-butylphenol (TBP) 99% from Aldrich. Commercial grade dodecyl sodium sulfate (SDS) of stated 70% purity was obtained from Aldrich; this industrial quality material was used to simulate the operation of large-scale MEUF processes, in which the cost of surfactant will play a major role in determining whether economical separations can be performed.

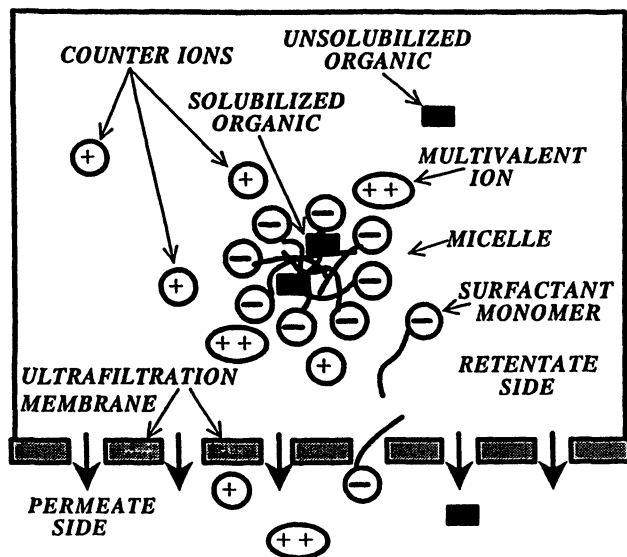
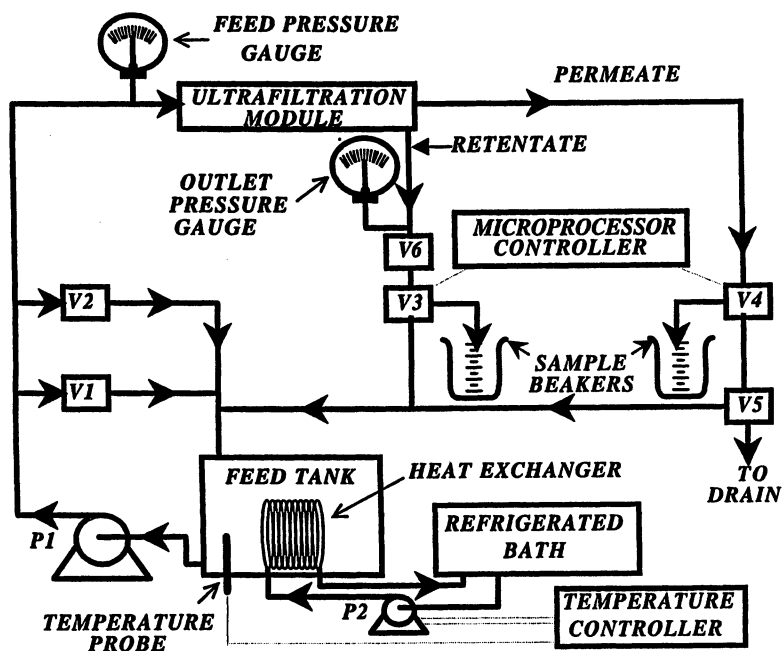


Figure 1. Illustration of Micellar-Enhanced Ultrafiltration (MEUF) Applied to the Removal of a Target Organic and a Target Multivalent Cationic Metal in an Aqueous Solution



Results

The spiral wound unit was used to separate the nonionic organic solute (TBP) using either the anionic surfactant (SDS) or the cationic surfactant (CPC). The separation of anionic chromate (CrO_4^{2-}) was studied using the cationic surfactant CPC, and cationic copper (Cu^{+2}) removal was studied using the anionic surfactant SDS. Direct comparisons of permeate concentrations using the regenerated cellulose spiral wound membrane and either stirred cell or dialysis studies are discussed.

The fluxes and permeate concentrations are shown in Figures 4 through 6 for CPC and TBP for the spiral wound membrane. A direct comparison between the stirred cell (1) and spiral wound membrane flux results for CPC and TBP using 5K molecular weight cutoff (MWCO) membranes is shown in Figure 7 through 9. The effect of membrane MWCO on TBP, CPC, and SDS permeate concentrations are shown in Figure 9 through Figure 13. Cellulose acetate membranes were used in all experiments.

The permeate surfactant concentrations for SDS in the presence of a target metal for the spiral wound membrane module are shown in Figure 14. The rejection of copper for the spiral wound 10,000 MWCO membrane is shown in Figure 15. Figure 16 compares the permeate copper concentration from stirred cell and spiral wound membranes. Figure 17 compares results of a previous semi-equilibrium dialysis study of permeate chromate concentrations (16) with data obtained here with the spiral wound apparatus.

Discussion

Flux

Fluxes were studied at four different outlet retentate flow rates using CPC as the surfactant and TBP as the target organic. Relative flux is defined as flux divided by the flux of the pure solvent under the same conditions. As shown in Figures 4 and 7 both flux and relative flux decrease monotonically as surfactant concentration increases.

Increasing the linear velocity of flow across the surface of the membrane (increasing the outlet retentate flow rate) minimizes the laminar sub-layer thickness, reducing the effects of concentration polarization. The reduction of the thickness of the laminar sub-layer region increases the concentration gradient across the region, thus increasing the molar flux of rejected species away from the membrane surface to the bulk solution. This decreases the concentration of rejected species near the membrane surface, thus increasing the permeate flux.

There is no appreciable increase in the permeate flux caused by increasing the outlet retentate flowrate from 1600 mL/min to 3400 mL/min. The permeate concentrations of TBP and CPC decrease with increasing outlet retentate flowrate for a given average retentate concentration as shown in Figure 5 and Figure 6. At very low flowrates, ultrafiltration results become more like semi-equilibrium results, possibly owing to the fact that micelle formation in the permeate can lead to increased concentrations of both the surfactant and the organic solute in the effluent stream. The 1600 mL/min and 3400 mL/min outlet retentate flowrates resulted in the minimum permeate concentrations; there is no further significant reduction of the concentration polarization effect when the outlet retentate flowrate exceeds 1600 mL/min. After considering the flux results in Figure 4 and

THE MAJOR COMPONENTS OF A SPIRAL WOUND ULTRAFILTRATION MEMBRANE

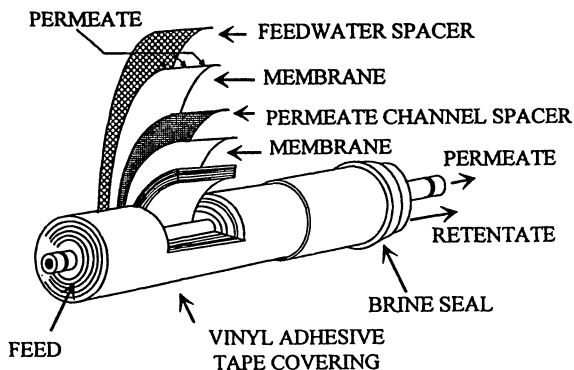


Figure 3. Illustration of the Major Components of an Ultrafiltration Spiral Wound Membrane

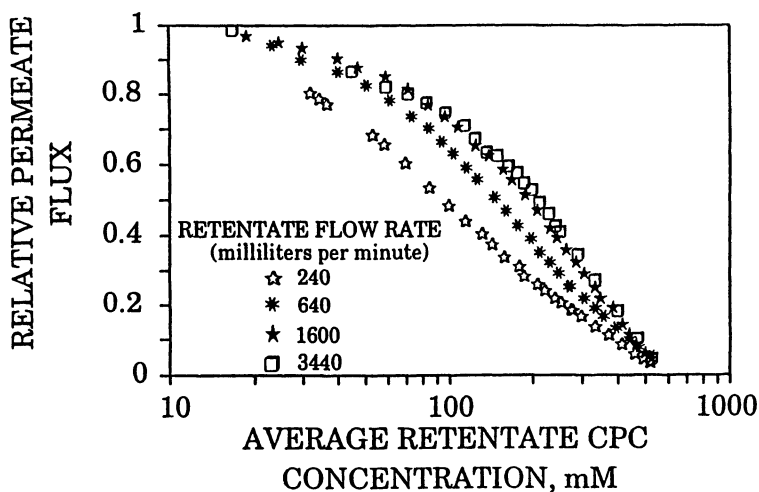


Figure 4. Relative Permeate Flux Using CPC and 5,000 MWCO Spiral Wound Membrane

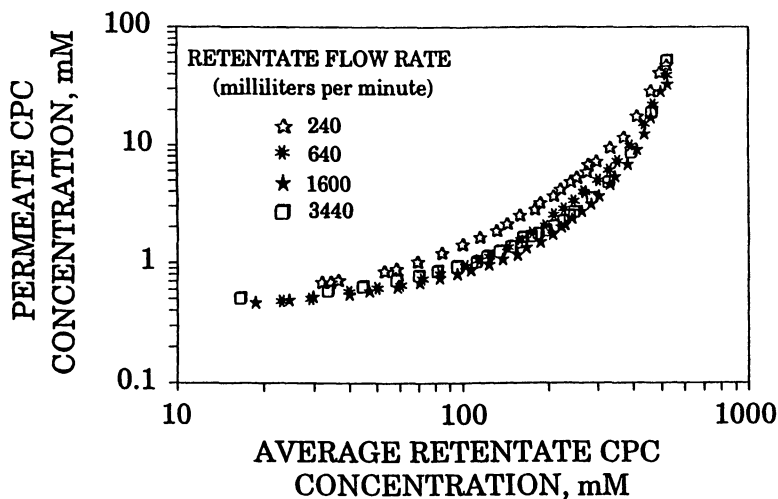


Figure 5. Permeate CPC Concentrations Using CPC and 5,000 MWCO Spiral Wound Membrane

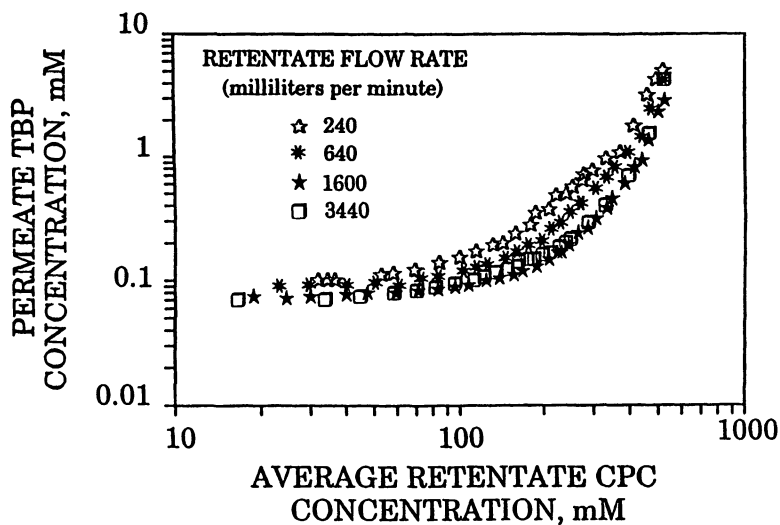


Figure 6. Permeate TBP Concentration Using CPC and 5,000 MWCO Spiral Wound Membrane

the permeate concentration values in Figures 5 and 6, all subsequent experiments were performed at a outlet retentate flowrate of 1600 mL/min.

The gel concentration or gel point is the retentate concentration at which permeate flux becomes zero. The gel concentration in Figure 4 is near an average retentate CPC concentration of 600 mM and does not vary with changes in the outlet retentate flowrate. Previous stirred cell work has shown that the relative permeate flux and surfactant permeate concentration are dependent on stirrer speed or the linear velocity of the retentate solution near the membrane and that there is a stirrer speed for the stirred cell (2) above which rejection does not decrease further, just as there is a linear flow rate for the spiral wound membrane above which rejection does not decrease further. The comparison of flux for stirred cell (1) and spiral wound 5,000 MWCO membranes (this work) is shown in Figure 7. The gel concentration, near 600 mM, in Figure 7 is nearly the same for both the stirred cell and the spiral wound membrane. The permeate flux for the spiral wound membrane compares very well with the stirred cell permeate flux on a per unit area basis, especially considering that membrane surface area for the stirred cell is at least two orders of magnitude smaller than the spiral wound membrane surface area. A comparison of Figure 4 with Figure 7 shows a striking similarity in the curve shapes. The difference in permeate flux values are more prominent in the midrange retentate concentrations. The stirred cell has a severe retentate linear velocity gradient ranging from zero directly in the center of the membrane to a maximum velocity at the outer edges of the membrane. In contrast, the linear retentate velocity in the spiral wound unit varies only moderately between the inlet and outlet.

Comparison of Stirred Cell and Spiral Wound Permeate Concentrations for Organic Solute with a 5,000 MWCO Membrane

The permeate concentrations shown in Figure 8 and 9 for the stirred cell and the spiral wound membrane are very similar. The stirred cell has slightly lower permeate CPC and TBP concentrations when the retentate CPC concentration is above 200 mM while the spiral wound membrane has a slightly lower permeate CPC concentration below 90 mM retentate CPC concentration. Overall, the performance (flux and permeate purity) of the stirred cell and spiral wound membranes are very similar and suggest that data collected from the stirred cell is adequate for the initial design and evaluation of an MEUF process for application to a industrial process stream when the target solute is a dissolved nonionic organic. Similar results have been obtained by Tounissou, et al. (25,26); these authors have compared MEUF behavior in stirred-cell and tangential ultrafiltration experiments.

Comparison of SDS, CPC and TBP Permeate Concentrations for Different Spiral Wound Molecular Weight Cutoff Membranes

The permeate concentrations of CPC and TBP in Figure 10 and Figure 11 for the spiral wound unit follow the same general trend observed for a stirred cell of increasing permeate concentrations with increasing MWCO (2). However, a minimum for the permeate CPC concentrations for the 10,000 MWCO membrane was observed in the stirred cell (2) but not in the spiral wound results. The spiral wound permeate TBP concentrations increase with increasing membrane MWCO while smaller changes in permeate TBP concentrations with changing membrane MWCO was observed in stirred cell results. One can speculate that

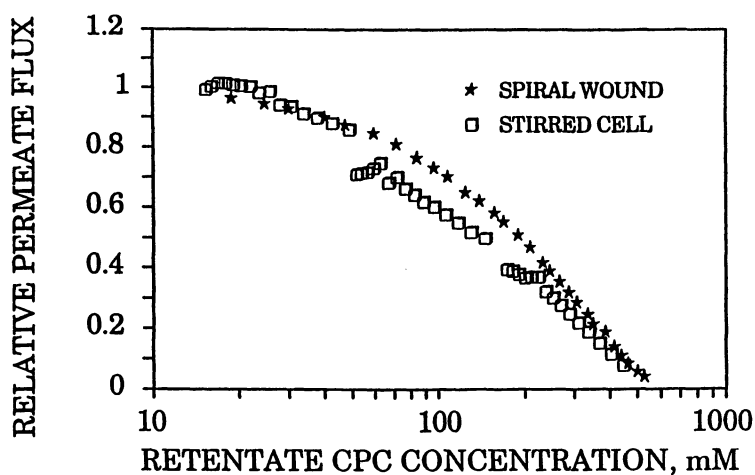


Figure 7. Comparison of Stirred Cell and Spiral Wound Membrane Relative Permeate Fluxes for a 5,000 MWCO Membrane

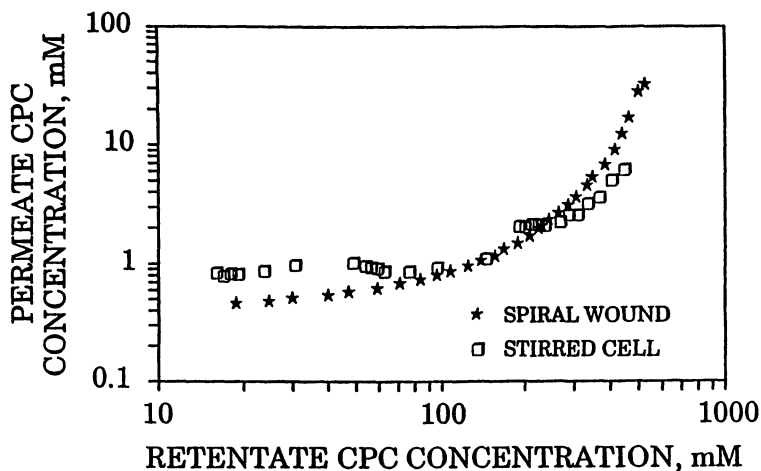


Figure 8. Permeate CPC Concentration for Stirred Cell and Spiral Wound Membranes with TBP, 5,000 MWCO Membrane

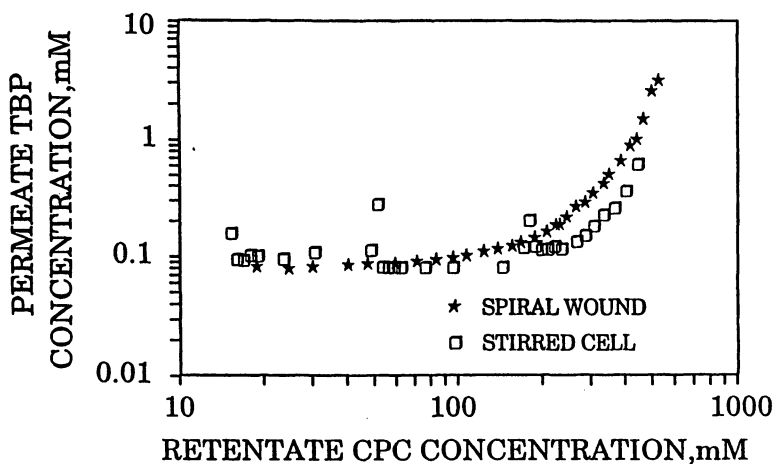


Figure 9. Permeate TBP Concentration for Stirred Cell and Spiral Wound Membranes with CPC, 5,000 MWCO Membrane

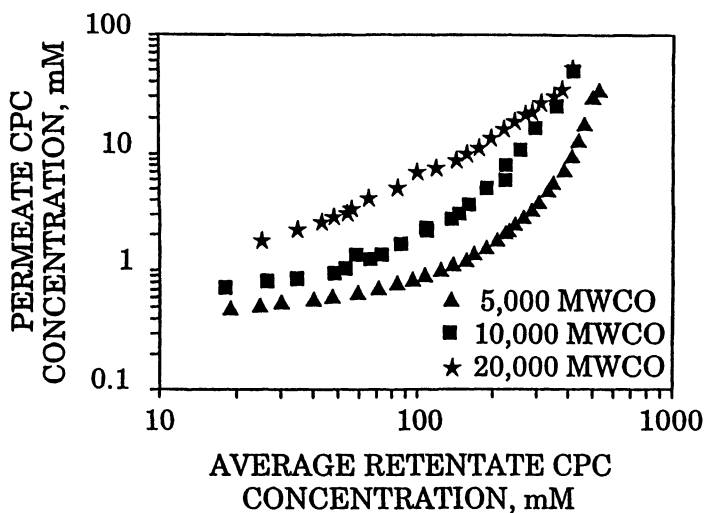


Figure 10. Comparison of CPC Permeate Concentration for Different Molecular Weight Cutoff Spiral Wound Membranes

the screen next to the surface of the membrane in the spiral wound configuration is more effective at suppressing the development of the laminar sub-layer region than the stirring mechanism in the stirred cell. A thinner laminar sub-layer would be characteristic of enhanced mixing near the surface and less presieving. The reduced presieving may be causing the increasing TBP concentrations with increasing MWCO membranes observed using the spiral wound configuration.

Figure 12 and Figure 13 show permeate concentrations of SDS and TBP. Changing spiral wound membrane MWCO does not effect the permeate concentration of TBP as observed for a stirred cell unit for the CPC/TBP system (2). There is also a minimum in the permeate SDS concentration for the 20,000 MWCO spiral wound membrane which is similar to that observed from 10,000 MWCO stirred cell experiments (2).

The Effect of Added Electrolyte on Surfactant Permeate Concentration

The effect of added electrolyte (target metals) on the surfactant permeate concentration is shown in Figure 13. In general, the permeate surfactant concentration decreases as the target metal concentration increases, as is illustrated by Figure 14. The ratio of surfactant concentration to metal concentration for the feed remains constant for the duration of the experiment even though additional surfactant/metal solution concentrate is incrementally added to the system and permeate solution is incrementally removed from the system in order to concentrate the surfactant and metal remaining in the system. However, the higher metal concentration to surfactant concentration ratio does illustrate the effect added electrolyte has on the surfactant CMC of anionic surfactants and therefore, on permeate surfactant concentrations. The permeate SDS concentrations shown in Figure 14 illustrates that an increase in the ratio of metal concentration to surfactant concentration causes a decrease in the permeate SDS concentration. The permeate SDS and CPC concentrations for experiments with added electrolyte are all significantly below their respective pure surfactant solution CMC values of 0.8 mM and 8.2 mM over a large range of average surfactant retentate concentrations. These results are not unexpected since the CMC of an ionic surfactant solution is depressed by added electrolyte (25,43). The depression of the CMC means the monomer concentration of the ionic surfactant is reduced and therefore, the equilibrium surfactant monomer concentration in the permeate is also reduced.

Spiral Wound/Semi-equilibrium Dialysis Systems with Metal Ions/Metal Complexes.

The spiral wound membrane rejection ranges between 99 and 100 percent for copper as shown in Figure 15. Increasing the feed copper to surfactant concentration ratio causes an increase in the permeate copper concentration at a given surfactant feed concentration.

Figure 16 shows a comparison of spiral wound MEUF and stirred cell permeate copper concentration. The stirred cell permeate copper concentration is approximately three times that observed for the spiral wound chromate permeate. While this may appear to be a large difference, it is due in part to the fact that almost all of the copper is being removed by the separation, making the permeate concentrations quite low. The copper rejection is 99.97 % vs. 99.99 %, so considering that there is a reduction in concentration of approximately 10,000 fold, agreement within a factor of 3 is reasonable.

Dialysis experiments using the semi-equilibrium dialysis technique yield the equilibrium concentration of target organic and target metal in the permeate (1,2,4-8,15-17).

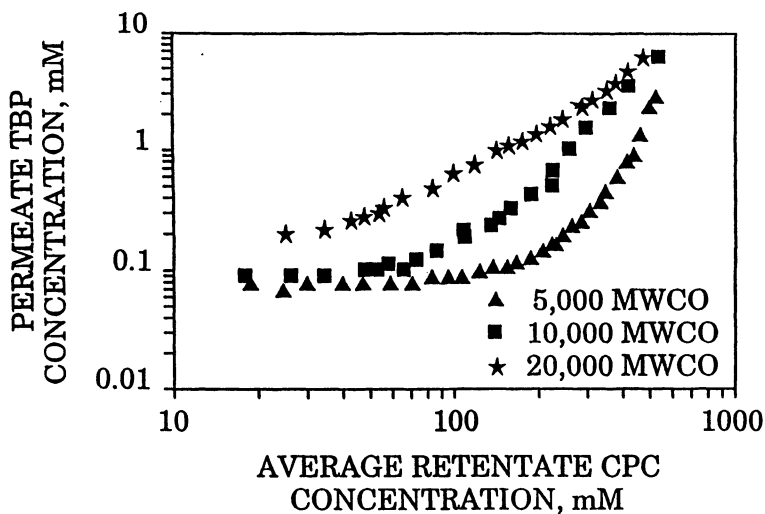


Figure 11. Comparison of TBP Concentrations for Different Molecular Weight Cutoff Spiral Wound Membranes

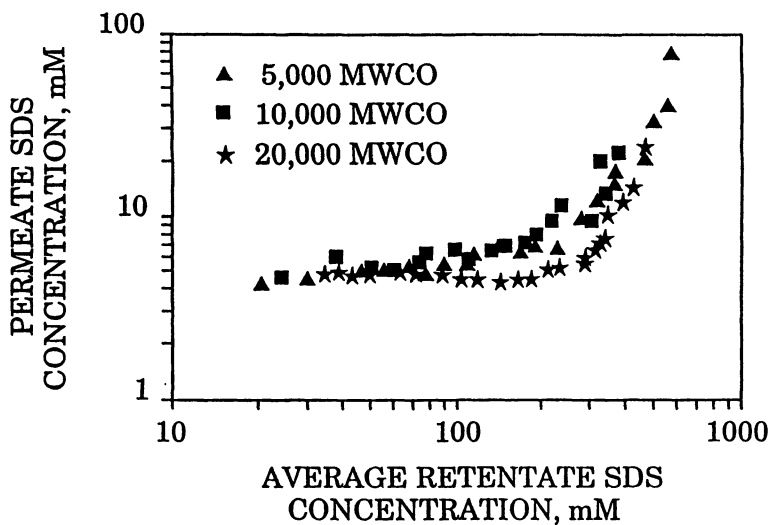


Figure 12. Comparison of SDS Permeate Concentration for Different Molecular Weight Cutoff Spiral Wound Membranes

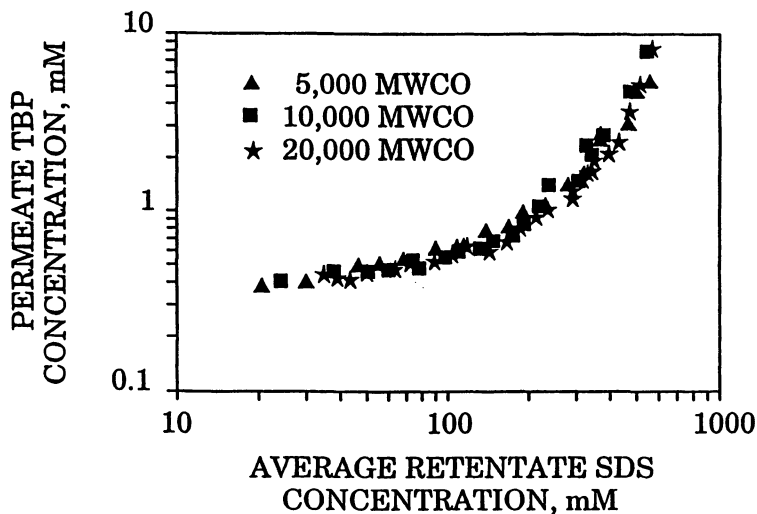


Figure 13. Comparison of TBP Permeate Concentration for Different Molecular Weight Cutoff Spiral Wound Membranes

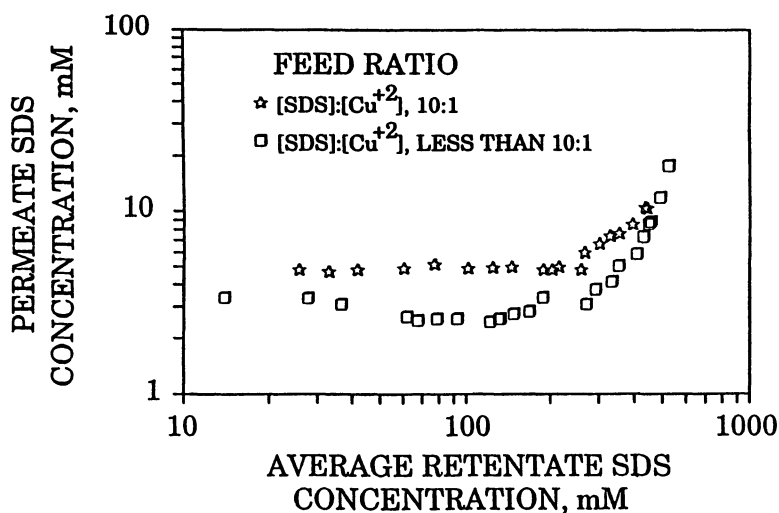


Figure 14. Comparison of the SDS Permeate Concentrations at Different Copper Feed Concentrations for a 10,000 MWCO Spiral Wound Membrane

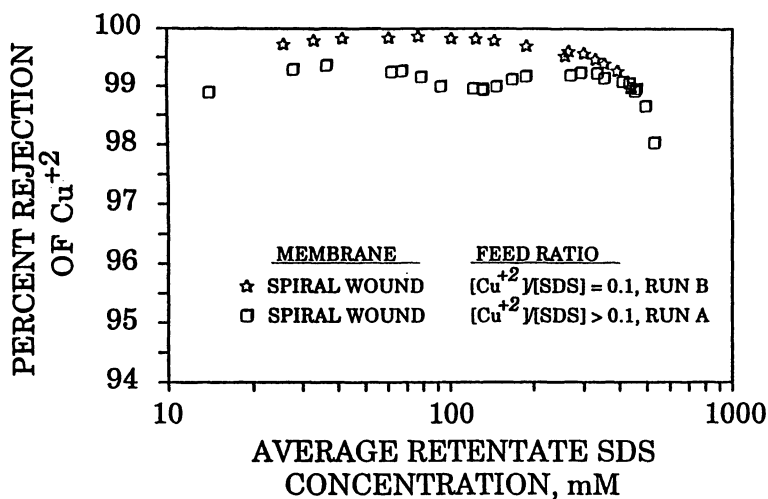


Figure 15. Rejection of Cu^{+2} for Spiral Wound 10,000 MWCO Membrane

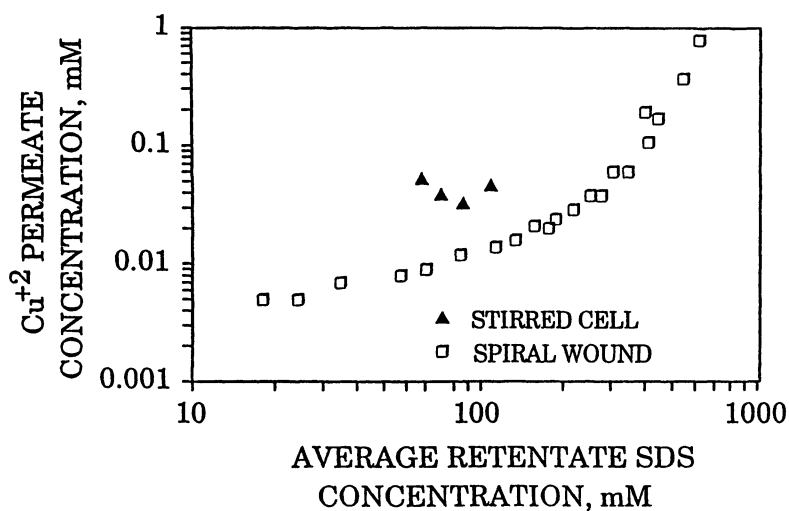


Figure 16. Comparison of the Permeate Cu^{+2} Concentration for Stirred Cell and Spiral Wound Membranes, 20,000 MWCO

Figure 17 shows a comparison of spiral wound MEUF and semi-equilibrium dialysis permeate chromate concentration and chromate rejection, for a cationic surfactant (cetylpyridinium chloride or CPC). The semi-equilibrium dialysis permeate chromate concentration is approximately one half the permeate chromate concentration observed for the spiral wound chromate permeate. The chromate rejection is 99.86 % vs. 99.93 %, so considering that there is a reduction in concentration of approximately 1,000 fold, agreement within a factor of 2 is reasonable.

Conclusions

MEUF has been shown to effectively remove either a dissolved organic solute or divalent cationic heavy metal in a spiral wound membrane with high flux and rejection until high retentate surfactant concentrations are attained.

A comparison of results from stirred cell, semi-equilibrium dialysis and spiral wound studies validates the use of stirred cell and semi-equilibrium data to do initial design and evaluation of the application of MEUF for an industrial process stream containing a nonionic organic pollutant.

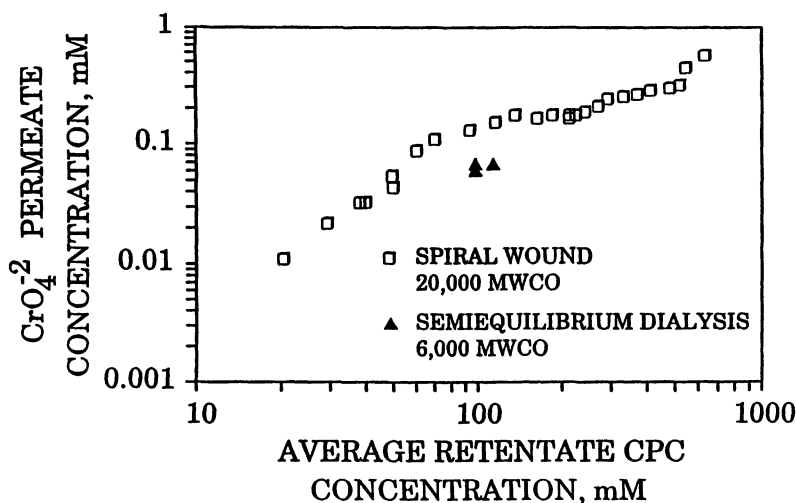


Figure 17. Comparison of the Permeate CrO_4^{2-} Concentration for a Semi-equilibrium Dialysis Cell Membrane and Spiral Wound Membrane

Acknowledgments

Financial support for this work was provided by National Science Foundation Grant CBT 8814147. In addition, support was received from the industrial sponsors of the Institute for Applied Surfactant Research including Akzo Nobel, Amway Colgate-Palmolive, Dial, Dow, DowElanco, DuPont, Henkel, ICI, Kerr-McGee, Lubrizol, Nikko Chemical Phillips Petroleum, Pilot Chemical, Reckitt and Coleman, Schlumberger, Shell, Sun, Unilever, and Witco. Dr. Scamehorn holds the Asahi Glass Chair in chemical engineering at the University of Oklahoma.

References

1. Dunn, R. O.; Scamehorn, J. F.; Christian, S. D. *Sep. Sci. Technol.* **1985**, *20*, pp 257-284.
2. Dunn, R. O.; Scamehorn, J. F.; Christian, S. D. *Sep. Sci. Technol.* **1987**, *22*, pp 763-789.
3. Gibbs, L. L.; Scamehorn, J. F.; Christian, S. D. *J. Membrane Sci.* **1987**, *30*, pp 67-74.
4. Smith, G. A.; Christian, S. D.; Tucker, E. E.; Scamehorn, J. F. *ACS Symp. Ser.* **1987**, *342*, pp 184-198.
5. Bhat, S. N.; Smith, G. A.; Tucker, E. E.; Christian, S. D.; Smith, W.; Scamehorn, J. F. *Ind. Eng. Chem. Res.* **1987**, *26*, pp 1217-1222.
6. Scamehorn, J. F.; Harwell, J. H. In *Surfactants in Chemical/Process Engineering*; Wasan, D. T.; Shah, D. O.; Ginn, M. E., Eds.; Marcel Dekker: New York, 1988; pp 77-125.
7. Scamehorn, J. F.; Harwell, J. H. In *Surfactants in Emerging Technologies*; Rosen, M. J., Ed.; Marcel Dekker: New York, 1987; pp 169-185.
8. Christian, S. D.; Scamehorn, J. F. In *Surfactant-Based Separation Processes*; Scamehorn, J. F.; Harwell, J. H., Eds.; Marcel Dekker: New York, 1989; pp 3-28.
9. Harwell, J. H.; Scamehorn, J. F. In *Management of Hazardous and Toxic Wastes in the Process Industries*; Kolaczowski, S. T.; Crittenden, B. D., Eds.; Elsevier: London, 1987; pp 352-361.
10. Dunn, R. O.; Scamehorn, J. F.; Christian, S. D. *Colloid Surf.* **1989**, *35*, pp 49-56.
11. Christian, S. D.; Tucker, E. E.; Scamehorn, J. F. *Am. Environ. Lab.* **1990**, *February*, pp 13-20.
12. Leung, P. S. In *Ultrafiltration Membranes and Applications*; Cooper, A. R., Ed.; Plenum Press: New York, 1979; pp 415-421.
13. Kandori, K.; Schechter, R. S. *Sep. Sci. Tech.* **1990**, *25*, pp 83-108.
14. Roberts, B. R., A Study of Surfactant-Based Separation Processes, Ph.D. Dissertation, University of Oklahoma, Norman, 1993.
15. Scamehorn, J. F.; Ellington, R. T.; Christian, S. D.; Penney, B. W.; Dunn, R. O.; Bhat, S. N. *AIChE Symp. Ser.* **1986**, *250*, pp 48-58.
16. Christian, S. D.; Bhat, S. N.; Tucker, E. E.; Scamehorn, J. F.; El-Sayed, D. A. *AIChE J.* **1988**, *34*, pp 189-194.
17. Scamehorn, J. F.; Christian, S. D.; Ellington, R. T. In *Surfactant-Based Separation Processes*; Scamehorn, J. F.; Harwell, J. H., Eds.; Marcel Dekker: New York, 1989; pp 29-51.
18. Scamehorn, J. F.; Christian, S. D. In Proceedings of the Ninth AESF / EPA Conference on Environmental Control for the Metal Finishing Industry, Chapter N. **1988**.

19. Klepac, J.; Simmons, D. L.; Taylor, R. W.; Christian, S. D. *Sep. Sci. Tech.* **1991**, *26*, pp 165-173.
20. Dharmawardana, U. R.; Christian, S. D.; Taylor, R. W.; Scamehorn, J. F. *Langmuir* **1992**, *8*, pp 414-419.
21. Tucker, E. E.; Christian, S. D.; Scamehorn, J. F.; Uchiyama, H.; Guo, W. *ACS Symp Ser.* **1992**, *491*, pp 86-98.
22. Christian, S. D.; Scamehorn, J.F.; Tucker, E. E.; O'Rear, E. A.; Harwell, J. H. In *Handbook on Removal of Heavy Metals from Industrial Wastewater*; Peters, R. W., Ed.; CRC Press: Boca Raton, Florida, in press.
23. Simmons, D. L.; Schovanec, A. L.; Scamehorn, J. F.; Christian, S. D.; Taylor, R. W. *ACS Symp Ser.* **1992**, *509*, pp 180-193.
24. Scamehorn, J. F.; Christian, S. D.; El-Sayed, D. A.; Uchiyama, H. *Sep. Sci. Tech.* **1994**, *29*, pp 809-830.
25. Tounissou, P.; Hebrant, M.; Rodehuser, L.; Tondre, D. *J. Coll. Interface Sci.* **1996**, *183*, pp 484-490.
26. Tounissou, P.; Hebrant, M.; Tondre, C. *J. Coll. Interface Sci.* **1996**, *183*, pp 491-497.
27. Gelinas, S.; Weber, M. E. *Sep. Sci. Technol.* **1998**, *33*, pp 1241-1254.
28. Huang, Y-C.; Batchelor, B.; Koseoglu, S. S. *Sep. Sci. Technol.* **1994**, *29*, pp 1979-1998.
29. Pramauro, E.; Bianco, A.; Viscardi, G.; Hinze, W. L. *Colloid. Surf.* **1992**, *63*, pp 291-300.
30. Reiller, P.; Lemordant, D.; Hafiane, A.; Moulin, C.; Beaucaire, C. *J. Coll. Interface Sci.* **1996**, *177*, pp 519-527.
31. Charbit, F.; Steinchen, A.; Sadaoui, Z.; Charbit, G. *J. Membrane Sci.* **1997**, *133*, pp 1-13.
32. *Solubilization in Surfactant Aggregates*; Christian, S. D.; Scamehorn, J. F., Eds.; Marcel Dekker: New York, 1995.
33. Nguyen, C. M.; Christian, S. D.; Scamehorn, J. F. *Tenside Surfactant Deterg.* **1988**, *25*, pp 328-336.
34. Smith, G. A.; Christian, S. D.; Tucker, E. E.; Scamehorn, J. F. *J. Solution Chem.* **1986**, *15*, pp 519-529.
35. Christian, S. D.; Smith, G. A.; Tucker, E. E.; Scamehorn, J. F. *Langmuir* **1985**, *1*, pp 564-567.
36. Lee, B. H.; Christian, S. D.; Tucker, E. E.; Scamehorn, J. F. *Langmuir* **1991**, *7*, pp 1332-1336.
37. Mahmoud, F. Z.; Christian, S. D.; Tucker, E. E.; Scamehorn, J. F. *J. Phys. Chem.* **1989**, *93*, pp 5903-5908.
38. Lee, B. -H.; Christian, S. D.; Tucker, E. E.; Scamehorn, J. F. *J. Phys. Chem.* **1991**, *95*, pp 360-365.
39. Uchiyama, H.; Christian, S. D.; Scamehorn, J. F.; Abe, M.; Ogino, K. *Langmuir* **1991**, *7*, pp 95-100.
40. Lee, B. H.; Christian, S. D.; Tucker, E. E.; Scamehorn, J. F. *Langmuir* **1990**, *6*, pp 230-235.
41. Uchiyama, H.; Christian, S. D.; Tucker, E. E.; Scamehorn, J. F. *J. Phys. Chem.* **1993**, *97*, pp 10868-10871.
42. Christian, S. D.; Tucker, E. E.; Scamehorn, J. F.; Uchiyama, H. *Colloid Polym. Sci.* **1994**, *272*, pp 745.
43. Rosen, M. J. *Surfactants and Intefacial Phenomena*; Second Edition; Wiley: New York, 1988; Ch. 3.

Chapter 12

Crossflow Microfiltration Characteristics of Surfactants

The Effects of Membrane Physical Chemistry and Surfactant Phase Behavior on Gel Polarization and Rejection

G. Akay¹, P. T. Odirile¹, B. Keskinler¹, and R. J. Wakeman²

¹ Centre for Process Intensification and Innovation, Department of Chemical and Process Engineering, University of Newcastle, Newcastle-upon-Tyne NE1 7RU, United Kingdom

² Department of Chemical Engineering, Loughborough University, Loughborough LE11 3TU, United Kingdom

The crossflow microfiltration behaviour of surfactants are studied using a double chain cationic surfactant and membranes of differing chemical structure or alternatively, using several types of surfactants and a single type of membrane. In all cases, the membrane pore size ratings and crossflow velocity are identical. The transient filtration characteristics for each membrane / surfactant system are evaluated through the measurement of permeate flux and rejection as a function of time. It is shown that the development of rejection as a consequence of the surfactant deposition on the membrane can be described in terms of the van der Waals forces as quantified by the Hamaker constant for the membrane / water / surfactant system. The electrostatic forces appear to have no significant effect for the cationic surfactant. The steady-state microfiltration characteristics indicate that the rejection and permeate flux are not significantly affected by the type of membrane. For a given surfactant/membrane system, gel concentration (C_g) is determined using the steady state data. It is shown that C_g increases with increasing

phase boundary surfactant concentration when the surfactant phase is transformed from L to L + L_v phase where L is the isotropic phase and L_v is a viscous phase such as lamellar, hexagonal or cubic phases.

Introduction

Because of their unique ability to form well ordered molecular aggregates and structures, ranging from a few nanometers to several hundred microns, surfactants can be used as carriers for the removal of organic contaminants from water or they can be used as nano-reactors in which the surfactant assembly takes the form of a semi-permeable membrane separating the reacting species. The smallest surfactant aggregate used for such purposes is the micellar state of the surfactant which can encapsulate organics within the hydrocarbon tails (solubilisation) while the ionic species can be bound to the micelle surface formed by the ionic head groups. Using a crossflow ultra-filtration technique, micelles and the contaminants are concentrated and clean water is harnest as permeate. This is the basis for the Micellar Enhanced Ultrafiltration (MEUF) which has been studied extensively and periodical reviews are available (1).The efficiency and selectivity of organic and metal ion removal of the surfactants can be further enhanced by incorporating polyelectrolytes and / or ligands in the surfactant assembly (2,3). More recently, mathematical modelling of MEUF has also been published (4-6).

The removal of surfactants from water is also important in the recovery of such molecules for re-cycling in detergent manufacturing or for environmental reasons. Surfactants can also be recovered through crossflow filtration using ultrafiltration or microfiltration membranes. In the latter case, the membrane pore size is several orders of magnitude greater than the size of the molecular assemblies formed by the surfactant. Recent experimental studies by the present authors (7-9) indicate that during the crossflow filtration of surfactants, a secondary membrane is formed within the pores and over the primary membrane. The secondary membrane is in a highly viscous surfactant phase and consequently, a very steep surfactant concentration gradient can be sustained across the secondary membrane and permeate. The primary membrane physical and physico-chemical characteristics are dominant in affecting the permeate flux and solute rejection during the early stages of the crossflow filtration while the steady state behaviour of the process is predominantly dictated by the nature of the surfactant and the interaction between the surfactant / membrane / water. The establishment of the steady state conditions is dependent on the process parameters (feed concentration, C_F ; crossflow velocity, u; transmembrane pressure drop, ΔP ; temperature, T ; and membrane pore size, d) as well as the physico-chemical characteristics of the surfactant (i.e., head group charge, zeta-potential, phase of the surfactant, hydrophile-lipophile balance, HLB) and that of the membrane (hydrophobicity, zeta-potential). The effects of process parameters on the transient and steady state

permeate flux characteristics and surfactant rejection have been evaluated for a number of surfactant / membrane systems (7-13).

Secondary Membrane Formation and Transient Permeate Flux: The qualitative mechanism of the crossflow membrane filtration of surfactant can be deduced from the studies in references (7-13). As the surfactant aggregates deposit on the membrane and within the pores, they undergo phase change due to increased concentration and immobilisation as a result of surfactant / membrane interactions. Unlike many other solutes, the capture of the surfactants by the membrane is relatively easy due to the existence of hydrophobic and hydrophilic moieties on the same molecule which allows the membrane to capture the surfactant through the tail or head. The rate of surfactant capture will increase under the attractive electrostatic interactions. However, such interactions will only be important initially until a monolayer surfactant coverage of the membrane is completed. Subsequent surfactant deposition will result in the formation of the secondary membrane. The structure of the secondary membrane in lamellar phase forming surfactants reveals that the surfactant molecules are anchored on the surface and pores of the primary membrane and grown outwards as lamellar strands thus forming a new porous structure (8). However, due to the presence of permeate flux through the developing secondary membrane, the macroscopic structure of the lamellar phase in the secondary membrane differs from the freely grown lamellar phase. As the filtration proceeds, the increased surfactant concentration results in the reduction of the porosity and pore size of the secondary membrane which in turn reduces the transient permeate flux $J(t)$, where t is time and J is flux. However, both crossflow and permeate flow over and across the secondary membrane results in the erosion of the surfactant phase and therefore the steady state represents a balance between the surfactant deposition and removal.

Transient Rejection: In MEUF as in the filtration of particulate suspensions, the primary membrane pore size can be similar to micelle size and consequently, the steady state conditions are reached rapidly and the surfactant rejection can approach 100 %. However, when the membrane pore size is several orders of magnitude larger than the micelle size, the establishment of the steady state is delayed. Although the permeate flux is very high, the transient solute rejection $R(t)$ is correspondingly very low, where R is transient solute rejection. Several studies indicate that high surfactant rejection is obtained only after the permeate flux reaches steady state (7-13)

Steady State: Under steady state conditions, the physico-chemical nature of the primary membrane does not appear to be very important in dictating the steady state permeate flux (J^*) and steady state surfactant rejection (R^*) except at very high rejections exceeding 99 %. The membrane physico-chemistry is also important at very high feed surfactant concentrations when it approaches or

exceeds the so-called gel concentration (C_g) or pseudo-gel concentration (C'_g) which are obtained by extrapolating the linear part of the curves J^* vs $\ln(C_F)$ as $J^* \rightarrow 0$. Gel concentration C_g refers to the case when there is no residual flow as $C_F \rightarrow C_g$. In some cases, flux never becomes zero and therefore the gel concentration is termed as pseudo-gel concentration (8).

Estimation of Surfactant Concentration in Secondary Membrane: It was found that the surfactant in the secondary membrane is in a highly viscous state (such as lamellar phase) which may be deduced from the phase diagram of the surfactant / water binary system (8). It was also postulated that the surfactant concentration in the secondary membrane is related to the pseudo-gel concentration (or gel concentration) through (8):

$$C_m = A[C'_g]^N \quad (1)$$

where (A) and (N) are two constants. Assuming that $N \approx 1$, the value of $A \approx 10$ for dioctadecyldimethylammonium chloride (DODDMAC) / polystyrene (8), and $A \approx 13$ for cetyltrimethylammonium bromide (CTAB) / cellulose acetate membrane (12) systems. The significance of these findings is that, the surfactant concentration C_m in the secondary membrane is far in excess of the gel (or pseudo-gel) concentration which is often taken as the solute concentration over the membrane. Therefore, this assumption is not correct and this boundary condition should be re-examined. It is also necessary to examine the validity of eq.1 for other surfactants and membrane systems.

Gel (or pseudo-gel) concentration has some unique properties since it is independent of membrane physical properties (i.e., pore size) and all of the process variables (1,14). However, it is found that for the cationic DODDMAC, C_g increases with increasing hydrophobicity of the membrane as characterised by the membrane solubility parameter (δ_m) (10).

Surfactant Phase Diagrams: According to the present description of the secondary membrane, the surfactant should be in a viscous state. Let us represent this viscous state of the surfactant by L_v (i.e., lyotropic liquid crystalline phases such as lamellar, hexagonal or cubic phases), in the surfactant / water binary system, then such a state is usually reached through a dispersion state, ($L + L_v$) in which the viscous phase (L_v) is dispersed in an isotropic liquid phase, (L) representing the micellar solution. In some cases, micellar solution may only exist over a very small concentration range as in DODDMAC. The viscous phase L_v extends over a large surfactant concentration range. As the surfactant concentration is increased, defects in the lyotropic liquid crystalline (LLC) phase decreases and the mechanical strength of the LLC increases. Defects in LLCs are occupied by the isotropic phase and hence they can be regarded as the pores of the secondary

membrane. It can be assumed that the “strength” and “morphology” of the viscous phase, L_v should dictate the permeate flux and surfactant rejection (15).

Effects of Organics and Electrolytes: In the presence of organics and electrolytes (especially high valency ions) changes in the permeation and rejection behaviour of the secondary membrane should be expected since such constituents alter the phase diagrams of the surfactant / water binary systems. Although the phase diagrams of some surfactant /water binary systems and surfactant /water /organic ternary systems are available, those of surfactant /water /electrolyte system are almost non-existent. Some recent studies using pulsed field gradient NMR (16) and dead-end filtration (13) have indicated the importance of heavy metal ions on the mechanical strength of the surfactant phases. It is found (13) that even at very low concentrations (≈ 0.1 mM) metal ions can lead the formation of the viscous phase at very low surfactant concentrations which subsequently results in the increased permeate flux and reduced surfactant rejection due to the increased porosity and reduced mechanical strength of the viscous surfactant phase in the secondary membrane.

The effect of the single valency metal ions (i.e., Na^+) on the surfactant phase is only apparent at very high concentrations (i.e., ≈ 100 mM) when the salting out of the surfactant takes place. In this case, packing and the hydrodynamic resistance of the surfactant phase increase (13) thus lowering the permeate flux.

Theoretical

Development of the Secondary Membrane: Referring to Figure 1, in which the crossflow filtration of a suspension is illustrated with respect to a set of Cartesian co-ordinates (x_i ; $i = 1, 2, 3$), we can assume that the most important forces acting on a particle are due to the continuous phase flow (drag), particle-flow field interactions (i.e., flow induced diffusion) and external field (such as electric field). The particle fluxes generated by the these forces are represented by $J_i^{(\alpha)}$ where $\alpha = 1, 2, 3$ respectively (11). It can be shown that the translational convective diffusion equation for the particle number density (n) is given by

$$\frac{Dn}{Dt} + \sum_{\alpha=1}^3 J_{i,\alpha}^{(\alpha)} = Q \quad (2)$$

where t is time, Q is a sink (or source) term and Dn/Dt is the material derivative

$$\frac{Dn}{Dt} = \frac{\partial n}{\partial t} + V_i n_{,i} \quad (3)$$

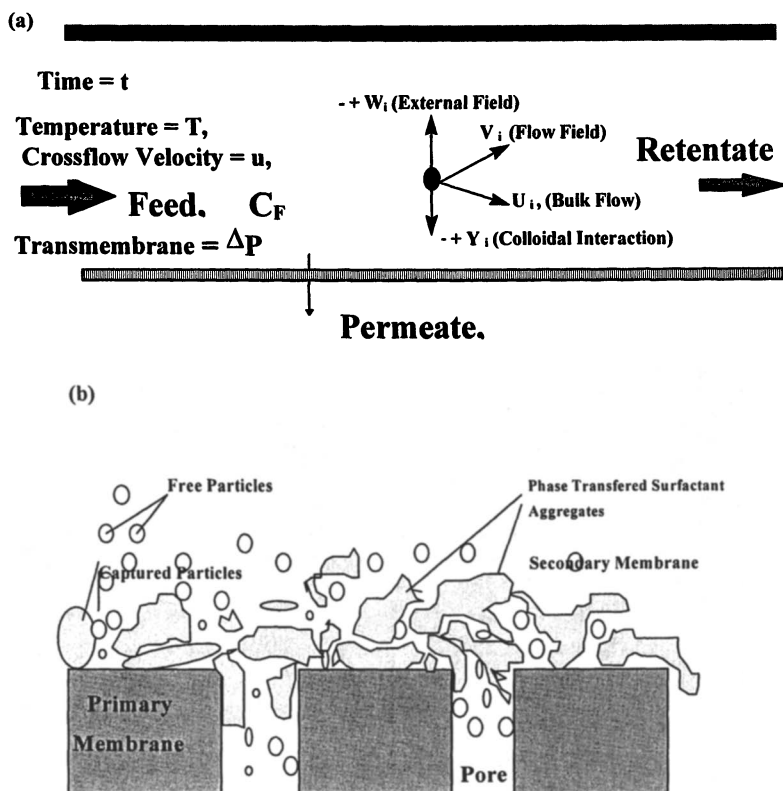


Figure 1. Crossflow membrane separation of surfactant dispersions. (a) Flow geometry and the components of the particle velocity due to various forces acting on a particle (surfactant aggregate). (b) Diagrammatic illustration of surfactant particle capture and the formation of secondary membrane by phase transformation as the surfactant concentration on the primary membrane increases.

where V_i is the velocity vector of the fluid. In the above equations Cartesian tensor notation is used; summation over a repeated vector (or tensor) index (i) is assumed and co-variant differentiation is represented by a comma (,). The particle flux vectors $J_i^{(\alpha)}$ ($\alpha = 1, 2, 3$) can be expressed in terms of the gradients of scalar fields as discussed by Akay and Wakeman (11). The components of the particle flux vector can be written as:

$$J_i^{(1)} = -D_o n_{,i} \quad (\text{Fickean particle flux}) \quad (4)$$

$$J_i^{(2)} = -n D_o t_R^2 \Gamma_{,i}^m \quad (\text{Flow field induced particle flux}) \quad (5)$$

$$J_i^{(3)} = \frac{D_o n}{kT} F_i \quad (\text{Interaction force field induced particle flux}) \quad (6)$$

where D_o is the particle diffusion constant, t_R is a relaxation time constant associated with the stress (or flow) induced particle diffusion, m is a constant and Γ is the second invariant of the rate of deformation tensor given by:

$$\Gamma = e_{ij} e_{ij} \quad (7)$$

where e_{ij} is the rate of deformation tensor given by

$$e_{ij} = \frac{1}{2} (V_{i,j} + V_{j,i}). \quad (8)$$

Equation (5) is a simplified form of the stress induced particle flux vector proposed by Tirrell and Malone, (17) , and have been given by Akay, (18,19) to account for the flow induced diffusion in macromolecules. Note that the reference (19) is also useful for the background of eq.2 and the notation used here. Zydney and Colton, (20), used the experimentally determined form of stress induced diffusion flux in order to account for the hydrodynamic lift encountered in crossflow filtration.

Our main concern in this study is the particle flux generated by the force field between a particle and membrane as a consequence of various processes which are available in the literature (21-23). The important components of the interaction force fields are due to London-van der Waals and double layer forces. The non-zero component of the interaction force normal to the membrane surface between a spherical particle and a flat surface can be written as (23),

$$F_1 = - \left[\frac{2}{3} \frac{H\lambda}{\beta^2 (\beta + 2)^2 a} \right] + \frac{\epsilon a (\zeta_p^2 + \zeta_m^2) \kappa \exp(-\kappa h)}{2(1 - \exp(-2\kappa h))} \left[2 \frac{\zeta_p \zeta_m}{\zeta_p^2 + \zeta_m^2} - \exp(-\kappa h) \right] \quad (9)$$

In the above equation, the first term represents the London-van der Waals forces. Here H is the Hamaker constant for the surfactant / water / membrane system, β is the dimensionless separation distance ($\beta = h/a$), (a) is particle radius and λ is the retardation factor (23). The second term in eq. 9 is the particle / membrane interaction term arising from double layer forces. Here ϵ is the dielectric constant of the fluid, ζ_p and ζ_m are the surface potentials of the surfactant particle and membrane respectively which are approximated by the zeta-potentials. κ is the Debye-Huckel reciprocal double layer thickness. The eq. 9 is valid when the absolute value of the zeta-potentials is less than 60 mV and $\kappa a > 10$. The Hamaker constant H for the surfactant / water / membrane system can be calculated from (24,10)

$$H = H_{mws} = (H_{mm}^{0.5} - H_{ww}^{0.5})(H_{ss}^{0.5} - H_{ww}^{0.5}) \quad (10)$$

where H_{mm} , H_{ww} and H_{ss} are the Hamaker constants for the membrane, water and surfactant respectively. In eq. 10, we use the Hamaker constant for the surfactant, rather than surfactant assembly as suggested by Wakeman and Akay (10) when the surfactant is in a lamellar phase.

The inclusion of the reaction (source or sink) term, Q in the mass balance equation is important for two reasons. Firstly particle breakup can occur during flow over and through the membrane, thus increasing the number density of the particles, (n) and secondly, as the particles are deposited on the membrane their behaviour changes due to: (i) increased particle /particle interactions which essentially lead to a phase transformation in surfactant systems and close packing in the case of solid particles, and (ii) particle / membrane interactions which can be attractive (particle immobilisation / capture) or repulsive as in particle detachment. The immobilisation reaction model for particle collectors (i.e., membrane) has been treated by Adamczyk et al (25). The reaction term can be written as

$$Q = Q_r - Q_f \quad (11)$$

where Q_r is the reverse reaction (removal) rate and Q_f is the forward reaction (capture) rate. The growth rate of the gel layer is

$$\frac{\partial C_m}{\partial t} = -Q \quad (12)$$

where C_m is the immobilised surfactant concentration in the gel layer. The particle removal rate Q_r from the gel layer is increased as a result of crossflow and

permeate flux. Removal by crossflow is important on the membrane surface while the detachment by permeate is important within the pores and it has implications in surfactant rejection mechanism as discussed later. The experimental results (8) indicate that the capture rate increases with increasing bulk surfactant concentration and membrane / surfactant interactions. The rate of particle deposition / capture during crossflow filtration is reflected by the decay of permeate and development of surfactant rejection. Therefore, the transient behaviour of surfactant crossflow filtration is a useful tool in this respect also. The effect of membrane physical chemistry on the capture of surfactant particles can therefore be analysed in terms of the eq. 12 in which it is assumed that the forward reaction Q_f is dependent on the process variables (C_f , T , ΔP) as well as the interaction force as given by eq. 9. Due to the complexity of the hydrodynamics and interactions we adopt an empirical approach and analyse the results in terms of dimensionless parameters which are given by van de Ven, (22).

$$\text{The Adhesion number, } A_d = H_{mws}/6kT \quad (13)$$

$$\text{Double layer number, } D_l = 4\pi\epsilon\epsilon_0\zeta_p\zeta_m a/kT \quad (14)$$

$$\text{Double-layer asymmetry number, } D_a = (\zeta_p - \zeta_m)^2 / 2\zeta_p\zeta_m \quad (15)$$

$$\text{Dimensionless double-layer thickness, } \tau = \kappa a \quad (16)$$

The form of eq. 9 suggests that the double-layer asymmetry number could also be defined as:

$$D'_a = 2\zeta_p\zeta_m / (\zeta_p^2 + \zeta_m^2). \quad (17)$$

In these equations, k is the Boltzman constant, ϵ is the dielectric constant of the medium, ϵ_0 is the permittivity of the vacuum. Since ζ_m and ζ_p can be highly dependent on pH, dimensionless numbers associated with the zeta-potentials can be changed over a wide range.

Experimental

Equipment: A computer-controlled crossflow equipment (7-9) shown in Fig 2, was used to carry out experiments at constant temperature (either 30 or 60 °C) with the controller maintaining a constant transmembrane pressure drop (ΔP) of 204 kPa (30 psi) and crossflow velocity (u) of either 1.5 or 4.0 m/s. The dimensions of the separation cell are: Length 60 mm, width 40 mm and thickness 3 mm. With the crossflow velocities and surfactant concentrations used in the experiments, the

Reynolds number in the flow cell ranged from $\approx 2 \times 10^3$ to $\approx 2 \times 10^4$. The membrane was used in flat sheet form, and a new membrane was used for each experiment. Both the retentate and permeate were recycled back into the feed tank to keep the feed surfactant concentration constant. The transient permeate flux $J(t)$ and transient permeate concentration $C(t)$ were monitored during the filtration. Small amounts of permeate samples were removed for surfactant concentration determination. Details of the experimental technique, including surfactant concentration determination can be found in (7,8)

Surfactants: The following surfactants are used in the experiments: Dioctadecyldimethylammonium chloride (DODDMAC), with an average molar mass of 585Da, is supplied by Sherex Chemical Company Inc. (See reference (7-10)) for details. Didecyldimethylammonium bromide (DDAB), cationic; Sodium dioctylsulphosuccinate, Aerosol-OT, anionic are supplied by Aldrich. Sodium linear alkyl (C_{10} - C_{13}) benzene sulphonate (Marlon A390) with average molar mass 346 ± 2 Da, is supplied by Hüls. Alcohol ethoxylate, $C_{13}E_7$, non-ionic (Synperonic A7) with average molar mass of 530Da, is supplied by ICI.

Membranes: All the membranes have the same nominal pore size rating of 0.2 μm . Polytetrafluoroethylene (PTFE), Nylon 6,6, cellulose nitrate (CN) and cellulose acetate (CA) membranes are supplied by Sartorius; track-etched polycarbonate (PC) membranes (Nuclepore) are supplied by Costar Corp., polyethersulphone (PES) membranes are supplied by Xflow, and Zirconia (ZrO_2) membranes are supplied by Ceramesh.

Results for Dioctadecyldimethylammonium Chloride (DODDMAC)

Zeta-Potential: The variation of zeta-potential as a function pH of DODDMAC dispersion and zirconia and cellulose nitrate membranes are shown in Fig. 3. The zeta-potential for cellulose nitrate is reproduced from Bowen and Cooke (26). The natural pH range of DODDMAC is also indicated. Caution must be exercised here since zeta - potential is dependent on the ionic environment. The experimental conditions of Bowen and Cooke (26) are different than those of ours.

Transient Flux and Surfactant Rejection: The variation of the transient permeate flux $J(t)$ at pH = 5.2 (natural pH of DODDMAC dispersion) with time is shown in Fig.4 for various membranes which have nominally similar pore size ratings (0.2 μm). However, the actual average pore sizes are considerably different as shown in Table 1. In all cases, the process conditions are identical with $u = 4$ m/s, $\Delta P = 204$ kPa (30 psi) and $T = 60$ $^{\circ}\text{C}$. As seen in Fig. 4, the behaviour of transient permeate flux decay is highly dependent on the membrane. In the case of highly hydrophobic PTFE membrane, permeate flux initially increases before decaying to its 'steady state' level, while for hydrophilic membranes, the rate of decay is slow as

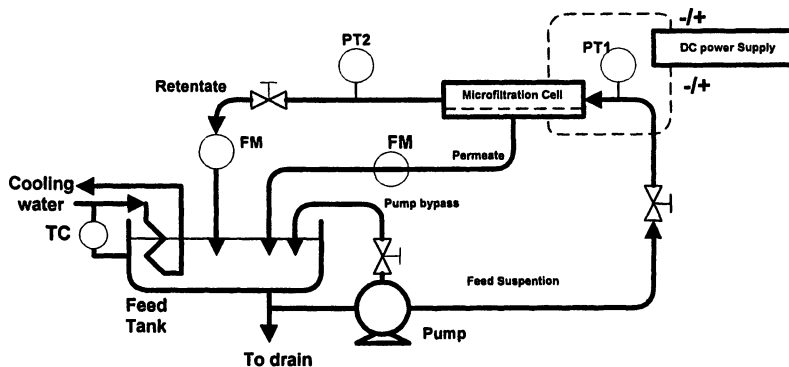


Figure 2. Crossflow filtration equipment. FM=Flow meter; PT=Pressure transducer; TM=Temperature control.

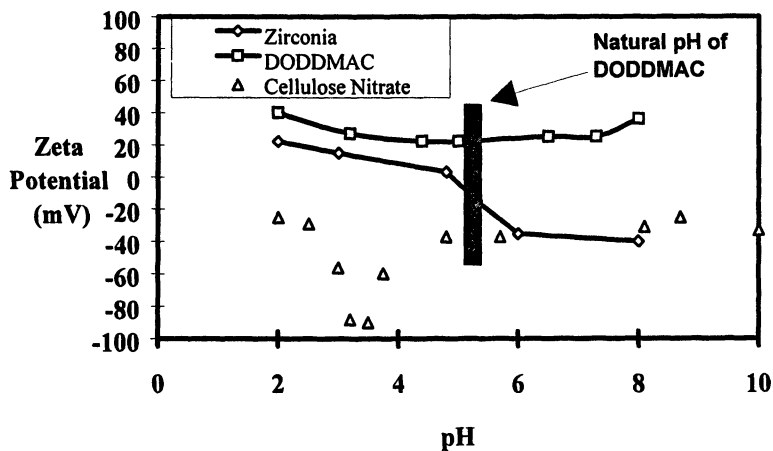


Figure 3. Zeta-potential of the cationic surfactant DODDMAC and zirconia and cellulose nitrate (CN) membranes. Data for CN membranes is adopted with permission from reference (26).

illustrated by cellulose nitrate membrane. The permeate flux decay for the zirconia membrane is the fastest. When the membranes are relatively hydrophilic, the initial flux level indicates the pore surface area available for flow. Steady state flux levels appear to reflect the membrane pore size. The effect of pH on the flux decay is shown in Fig. 5 which indicates that the flux decay becomes faster with decreasing pH. When $\text{pH} \geq 7$, flux decay is not significantly affected by pH within experimental error. The variation of transient rejection $R(t)$ is shown in Fig. 6 for the membranes illustrated in Fig. 4. The rejection increases rapidly if the rate of permeate flux decay is high as most clearly illustrated by the behaviour of zirconia and cellulose nitrate membranes; 80 % rejection is achieved by zirconia within 100 seconds while 3000 seconds of filtration is required in the case of cellulose nitrate membranes. In all cases a base-line rejection of $\approx 15\%$ is present. The development of rejection for PTFE is highly different than the others; initially, the base-line rejection is lower than the other membranes and rejection increases more gradually.

Table 1. Physico- chemical and Physical Characteristics of Membranes

Chemical Name	Mean Pore Size (μm)	Solubility Parameter δ (MPa)	Surface Energy γ (mJ/m^2)	Hamaker Constant $H_{11} \times (10^{-20}\text{J})$
Polytetrafluoroethylene, PTFE	0.36	13.9	18.5	3.5
Polyethersulphone, PES	0.31	21.1	-	-
Polycarbonate, PC	0.25	19.1	42	8.6
Polystyrene, PS	1.20	19.7	40.7	6.4
Nylon 6,6	0.46	22.9	35.9	7.4
Zirconia, ZrO_2	0.16	200	73	15
Cellulose Acetate, CA	0.36	-	38	7.8
Water	47.8	4.8	72.9	4.3
DODDMAC	-	17.9	-	4.7

Steady State Permeate Flux and Surfactant Rejection: The variation of steady state permeate flux, J^* with feed concentration, C_F for zirconia and PES membranes are shown in Figs. 7 and 8. These are typical of all the membranes investigated in this study. When $C_F \rightarrow 0$, $J^* \rightarrow J_0^*$ where, J_0^* is the steady state clean water permeate flux. From the variation of J^* with $\log C_F$, we estimate the gel concentration C_g . Note that this is a true gel concentration as opposed to a pseudo-gel concentration encountered in some systems especially when metal ions are present in the dispersions. As shown previously (7), gel concentration C_g is independent of temperature for DODDMAC. The variation of the steady state rejection, R^* with feed surfactant concentration C_F for zirconia and PES membranes are shown in Figs. 9 and 10 respectively. In both cases, very high rejections approaching 99.9 % are observed as $C_F \rightarrow C_g$. Rejections at 30°C are slightly better than the rejection above the Kraft temperature of $\approx 45.7^\circ\text{C}$ for this surfactant.

Results for Anionic and Non-Ionic Surfactant: The variation of the steady permeate flux J^* and surfactant rejection for the ionic surfactants

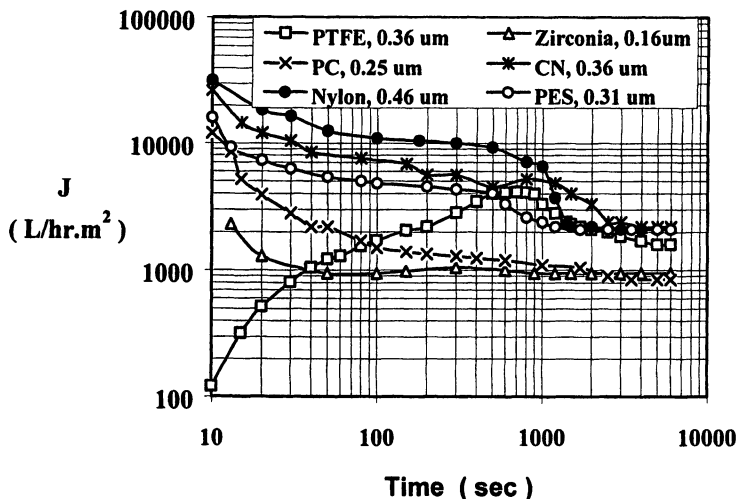


Figure 4. Development/decay of transient permeate flux $J(t)$ with time for various membranes during crossflow filtration of DODDMAC when $\Delta P=204$ kPa, $u=4$ m/s, and $T=60^{\circ}\text{C}$.

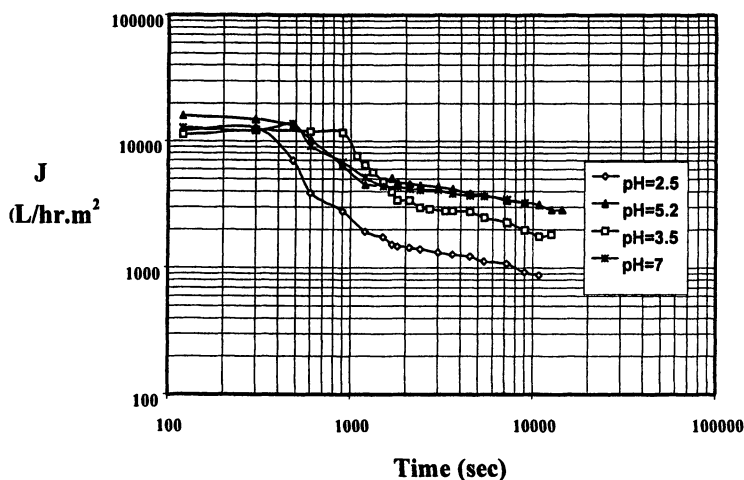


Figure 5. Decay of transient permeate flux $J(t)$ with time for cellulose nitrate membrane at different pH values during crossflow filtration of DODDMAC when $\Delta P=204$ kPa, $u=4$ m/s, and $T=60^{\circ}\text{C}$.

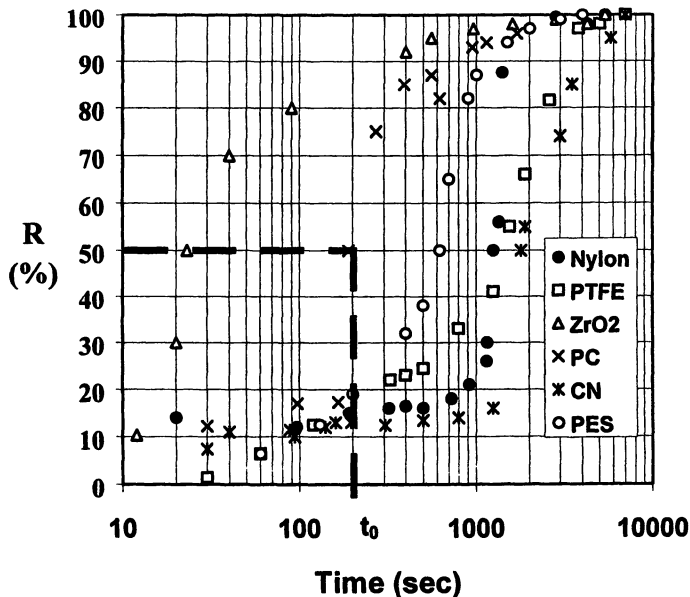


Figure 6. Development of transient rejection, $R(t)$ with time for various membranes during crossflow filtration of DODDMAC when $\Delta P=204$ kPa, $u=4$ m/s and $T=60^\circ\text{C}$. The corresponding fluxes are shown in Fig.5.

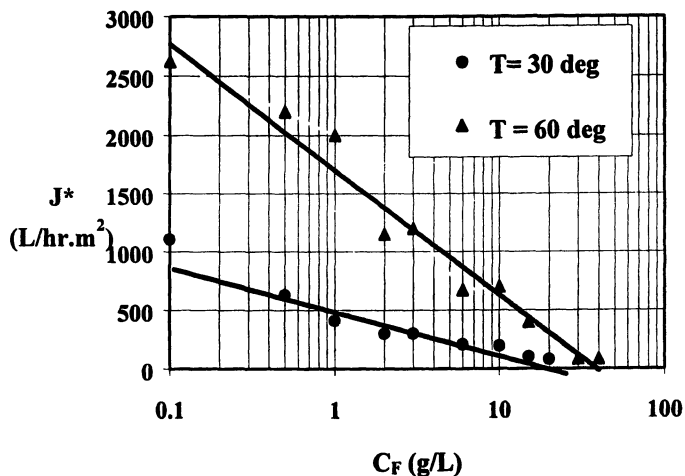


Figure 7. The variation of steady state permeate flux, J^* with feed concentration C_F for DODDMAC using PES membranes at two different temperatures when $\Delta P=204$ kPa, and $u=4$ m/s.

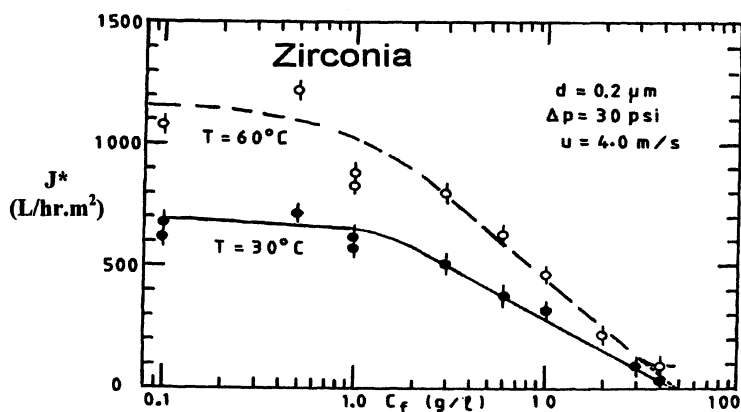


Figure 8. The variation of steady state permeate flux, J^* with feed concentration, C_F , for DODDMAC using zirconia (Ceramesh) membranes at two different temperatures when $\Delta P=204$ kPa, and $u=4$ m/s.

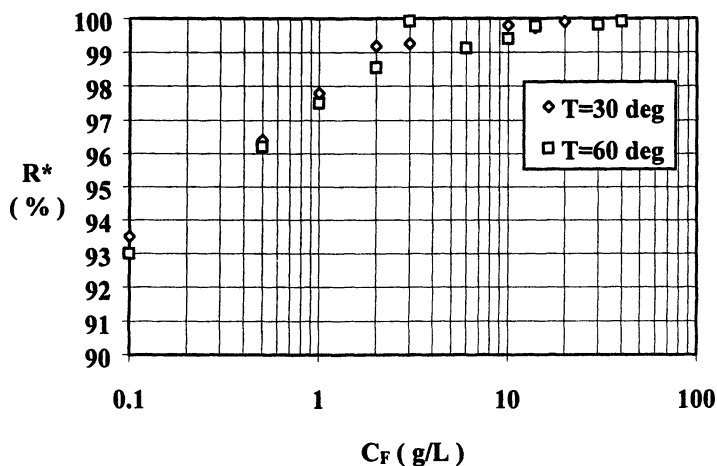


Figure 9. The variation of steady state surfactant rejection R^* with feed concentration for DODDMAC using PES membranes under the conditions of Fig. 8.

dioctylsulphosuccinate (Aerosol OT) and sodium linear alkyl benzene sulphonate (Marlon A390) are shown in Figs. 11 and 12 respectively. The corresponding steady state rejection data are shown in Figs. 13 and 14. Figs. 11 and 12 also illustrate respectively the effects of crossflow velocity and temperature on the permeate flux. In line with previous results, permeate flux is enhanced with increasing crossflow velocity and temperature. From these figures, gel concentration can be calculated. As seen in Figs. 13 and 14, unlike the previous case of DODDMAC, crossflow velocity and temperature do not appear to influence the steady state rejection within the experimental error. Furthermore, the rejection increases slowly with increasing feed concentration and reaches a maximum when $C_F \approx 10$ g/L for Aerosol OT and $C_F \approx 7.0$ g/L for Marlon A390 . In both cases the peak steady state rejection is reached at $C_F \approx 20$ mM.

Discussions

Surfactant Deposition, Formation and Structure of Secondary Membrane

Surfactant-Water -Membrane Interactions: Previously, the present authors (10,27) have examined the type of surfactant orientation at the membrane surface and subsequent phase behaviour of the surfactant as the surfactant concentration increases with time. Akay and Wakeman (10,27) used solubility parameter (single or three component solubility parameters (28)) in order to quantify the surfactant-water-membrane interactions. They also proposed that the thickness of the water layer could be calculated by considering the equilibrium force between the membrane and the surfactant assembly. In the present study we assume that the surfactant rejection is proportional to the amount of surfactant deposited. An examination of Figs. 4 and 6 indicates that this assumption is valid while the shape of the rejection curves suggests that a master curve can be obtained by using a time-shift parameter. The shift parameter, t_0 , is defined as the time required to reach 50 % rejection, as shown in Fig. 6. The data in Fig. 6 is re-plotted using a dimensionless time scale t/t_0 as shown in Fig. 15. As seen in this figure, all data can be reduced to a single curve although the data for zirconia and PTFE show some deviation. The deviation of the data for PTFE can be explained on the bases of marked differences of permeate flux development for this membrane as shown in Fig. 4.

As discussed previously, in the absence of any external field, it can be assumed that the rate of deposition of surfactant is proportional to the total interaction force, F_1 (e.g., eq. 9), which can be decomposed into van der Waals forces (attractive) and electrostatic forces which may be attractive or repulsive depending on the magnitude and signs of the zeta-potentials of the membrane and surfactant. Accordingly, an inspection of the zeta-potential data given in Fig. 3 indicates that at the natural pH of DODDMAC dispersion (pH = 5.2), cellulose nitrate membranes should yield faster surfactant deposition than the zirconia membrane and therefore the rate of decay of permeate flux (and hence the

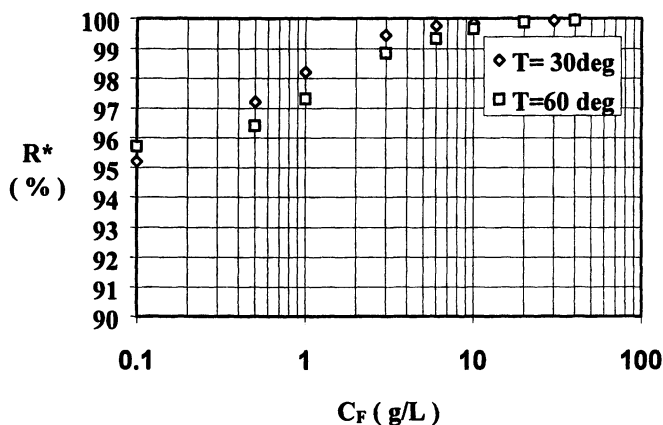


Figure 10. The variation of steady state surfactant rejection R^* with feed concentration for DODDMAC using zirconia (Ceramesh) membranes under the conditions of Fig. 7.

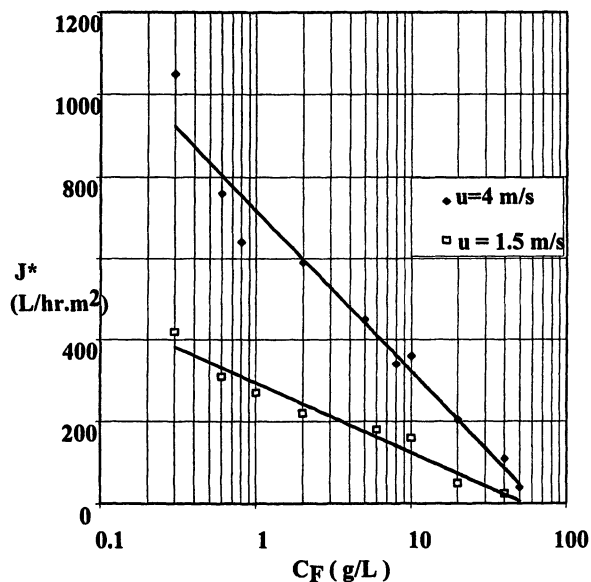


Figure 11. The variation of the steady state permeate flux J^* with surfactant feed concentration C_F for sodium dioctylsulphosuccinate (Aerosol OT) using PES membranes at two different crossflow velocities ($u=1.5$ or 4 m/s) when $\Delta P=204$ kPa and $T=30^\circ\text{C}$.

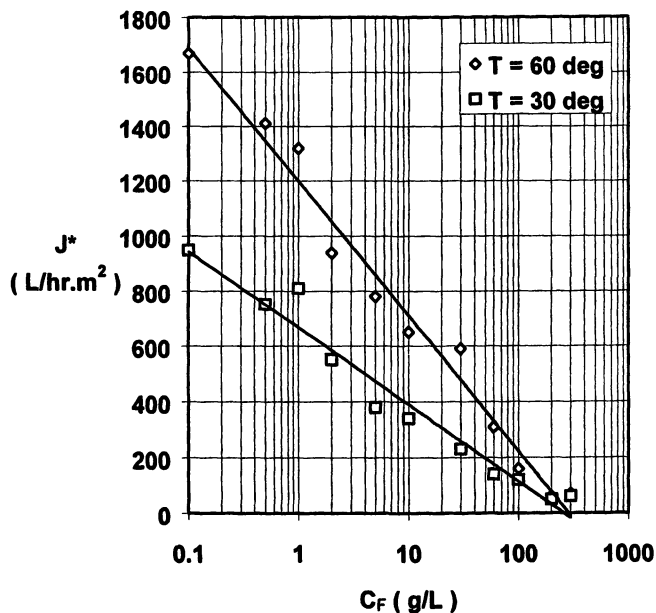


Figure 12. The variation of the steady state permeate flux J^* with surfactant feed concentration, C_F for sodium linear alkyl (C_{10} - C_{13}) benzene sulphonate (Marlon A390) using PES membranes at two different temperatures (30 and 60°C) when $\Delta P=204$ kPa and $u=4$ m/s.

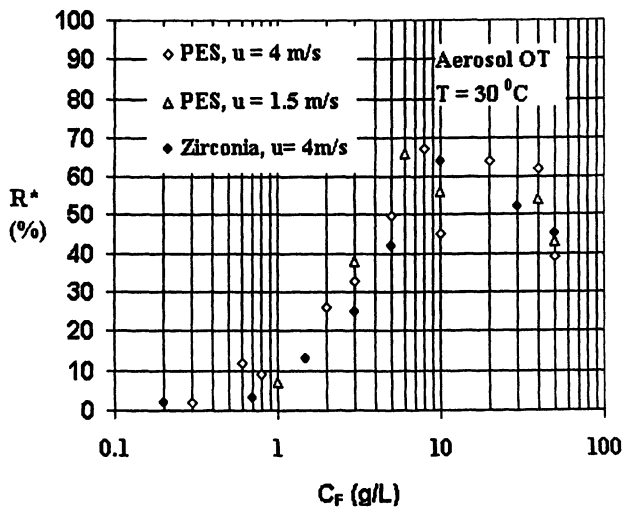


Figure 13. The variation of the steady state surfactant rejection R^* with feed surfactant concentration for sodium dioctylsulposuccinate (Aerosol OT) using PES and zirconia membranes at two different crossflow velocities ($u=1.5$ or 4 m/s) when $T=30^\circ\text{C}$ and $\Delta P=204$ kPa.

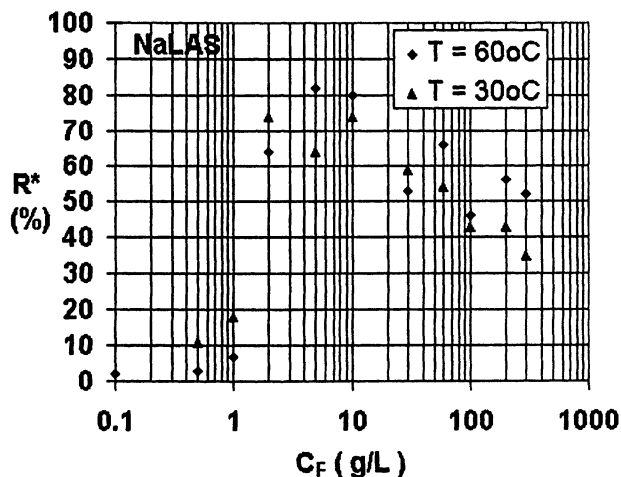


Figure 14. The variation of the steady state surfactant rejection R^* with feed surfactant concentration, C_F for sodium linear alkyl ($C_{10} - C_{13}$) benzene sulphonate (Marlon A390) using PES membranes at two different temperatures (30 or 60°C) when $\Delta P = 204$ kPa and $u = 4$ m/s.

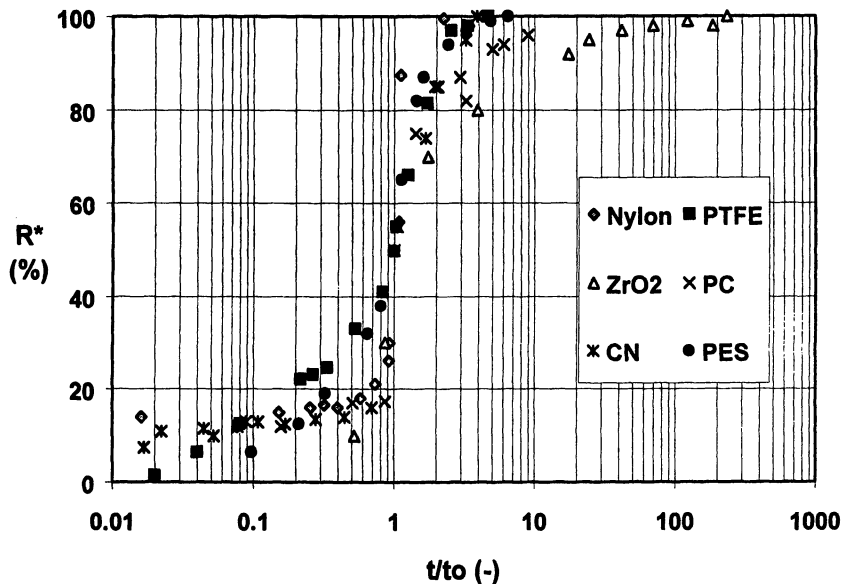


Figure 15. The variation of the steady state surfactant rejection R^* for DODDMAC as a function of dimensionless time t/t_0 for several membranes when $\Delta P = 204$ kPa, $u = 4$ m/s and $T = 60^\circ\text{C}$. Original data is shown in Fig.5.

surfactant rejection) should be higher for cellulose nitrate than zirconia membrane. However, on both accounts, the reverse is true as shown in Figs. 4 and 6. Steady state flux is established only after 50 seconds for zirconia while 1500 seconds is required for cellulose nitrate. Similarly, the rejection data indicates that while $t_0 = 25$ seconds for zirconia, $t_0 = 1800$ seconds for cellulose nitrate. These results indicate that the electrostatic attractions are only important initially until a monolayer surfactant coverage of the membrane is completed. Subsequent surfactant deposition results in the formation of the secondary membrane in which the van der Waals forces become dominant.

The Effect of Electrostatic Forces on Flux Decay and Rejection: The variation of zeta-potential with pH for the cellulose nitrate membrane also indicates that if the electrostatic forces were to be important in the rate of deposition of DODDMAC, then the crossflow experiments at pH = 3.5 (where the zeta-potential of CN-membrane reaches minimum) should yield the fastest flux decay compared with the crossflow experiments at say pH = 2.5 or pH = 5.2 or pH = 7.0. However, as shown in Fig. 5, this is not the case and permeate flux decays faster and the steady state flux is lower if the pH is low. These results can be explained in terms of corrosion of the metallic pipes and fittings in the crossflow equipment resulting in the accumulation of metal ions in the feed. It has been shown that even at very low metal ion concentration, the rate of flux decay accelerates and steady state permeate flux is reduced (12,13). In the presence of high valence metal ions, gel concentration is also reduced but due to the low levels of surfactant in the gel (forming the secondary membrane), gel porosity is increased and there is always a relatively high residual permeate flux even after the feed concentration C_F is far in excess of the pseudo-gel concentration C'_g . These results are also confirmed by dead-end filtration (13) and pulsed field gradient nuclear magnetic resonance experiment (16). It is therefore important to minimise the leaching of metal ions into the feed stream especially at low levels of surfactant concentrations.

Effects of van der Waals Forces on Flux Decay and Rejection: In order to explain the variation of t_0 evaluated for various membranes as a measure of rate of surfactant deposition during crossflow membrane filtration, we now consider the contribution of the van der Waals forces through the adhesion number $A_d = H_{mws}/6kT$. The variation of t_0 (time to reach 50% rejection) with the Hamaker constant for the membrane-water-surfactant system is shown in Fig. 16. It can be seen that as the adhesion force increases (i.e., increasing H_{mws}) t_0 decreases as expected. Note that H_{mws} is negative for PTFE. Negative Hamaker constants and its interpretation have been discussed by Visser (29). It may be concluded that if H_{mws} is negative, the initial flux is very low until the surface coverage of the membrane by the surfactant increases its wetting characteristics and the flux increases. When the surfactant concentration is sufficient to form a gel layer, permeate flux starts to decrease.

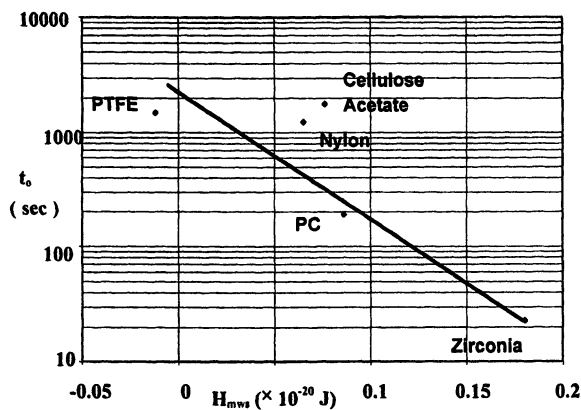


Figure 16. The variation of the time shift parameter t_0 with Hamaker constant for the membrane- water-surfactant system, H_{mws} for several membranes and DODDMAC at $T=60^\circ\text{C}$.

Steady State Filtration Characteristics of Surfactants

Phase Behaviour of Surfactant / Water System: The steady state filtration characteristics (concentration dependence of flux, rejection and gel concentration) can be interpreted by considering the phase behaviour of surfactant / water system (8). The phase diagram of Aerosol OT is typical of the surfactants used in the present study. This phase diagram adopted from (30) is shown in Fig. 17 in which the phase boundaries are drawn as a function of temperature and surfactant concentration. Here, L represents the isotropic liquid phase (i.e., micellar solution), L_α represents the viscous phase L_v (in this case lamellar phase) and $L + L_\alpha$ is the lamellar dispersion phase.

Table 2. Surfactant Phase Behaviour and Gel Concentration at 30°C.

Surfactant Name	Type	Average Formula Weight (Da)	CMC (g/L)	C_1 (g/L)	C_2 (g/L)	Type of L_v	Ref	C_g (Membrane) g/L
Diocetadecyl-dimethyl chloride (DODDMAC)	Cationic	586	0.0	0.0	320	L_β	7, 8, 31, 34	16 (PTFE) 20(PC) 28(PES) 33(PES) 47(ZrO ₂)
Didecylidimethyl ammonium bromide (DDAB)	Cationic	407	0.0	0.0	50	L_α	32	20 (CA)
Sodium dioctyl sulphosuccinate (Aerosol OT)	Anionic	444	0.7	40	150	L_α	30, 33	90 (PES) 100(ZrO ₂)
Sodium linear alkyl benzene sulfonate (Marlon A390)	Anionic	346	0.42	255	680	L_α	27	180 (PES)
Sodium dodecyl sulfonate (SDS)	Anionic	288	2.25	405	405	H_1	34, 35	202 (CA)
Alcohol ethoxylate (Synperonic A7)	Non-ionic	530	0.0	380	380	H_1	36	220 (PES)

At a given temperature, the concentrations at which phase boundaries appear are denoted by C_1 and C_2 as shown in Fig. 17. In Table 2, the values of C_1 and C_2 are tabulated for the surfactants used in this study. As seen in Table 2, when the phase is in the hexagonal state (denoted by H_1) $C_1 \approx C_2$ indicating the absence of dispersion of the viscous phase ($L + H_1$). In Table 2, the correlation of C_g with the membrane chemistry is also apparent, especially for DODDMAC. As seen in this table C_g increases with increasing membrane hydrophilicity (i.e., increasing solubility parameter) as also shown previously (10).

Steady State Flux and Rejection Behaviour: Although all surfactants investigated here and previously by the present authors (7-14), yield very similar steady state flux J^* behaviour with increasing feed surfactant concentration, their

rejection behaviour can be substantially different as shown in Figs. 9, 10, 13 and 14. There are three aspects which makes the rejection behaviour of DODDMAC different from Aerosol OT and NaLAS . Firstly, even at low concentrations, DODDMAC rejection is very high. Secondly, the maximum rejection in DODDMAC can be in excess of 99.9 % while in Aerosol OT and NaLAS maximum rejections are ≈ 70 and 80 % respectively. Finally , although the rejection of DODDMAC increases continuously with increasing C_F while the flux decreases , for Aerosol OT and NaLAS, after $C_F \geq 20$ mM, rejection starts decreasing with increasing C_F while the steady state flux continues to decay. These results can be explained by considering the solubility of the surfactant, mechanical strength of the viscous (lamellar phase) and adhesion strength of the surfactant at the membrane surface and pores (15, 27, 32).

As seen in Table 2, both CMC and C_1 and C_2 values of DODDMAC are considerably smaller than that of the anionics, Aerosol OT and NaLAS indicating that the micelles are still present even at high feed concentrations and that the secondary membrane is unable to capture them. Since the permeate flux and rejection both decay when $C_F \geq 20$ mM for the anionics, the breakup of the viscous lamellar phase in these surfactants must require smaller stress power compared with DODDMAC (15,32).

Gel Concentration and Surfactant Phase Behaviour: Gel concentration, C_g , is important since it defines the practical limit of surfactant feed concentration which can be filtered. The value of C_g changes significantly with the type of membrane (10,27) as also shown in Table 2. For a given surfactant /membrane system, it can be seen from Table 2 that, C_g increases with increasing C_1 concentration (see Fig. 17 for definition of C_1). The results are plotted in Fig. 18 in which the scatter in the data is partly due to the differences in the membranes. Nevertheless, as seen in Fig. 18, a good correlation is obtained between C_g and C_1 for all the surfactants used in this study, as well as those obtained in the literature (34,35). It is interesting to note that for DODDMAC (7,8) C_g has been found to be independent of the physical characteristics of the membranes and operating conditions including temperature. This is due to the fact that the phase boundary concentrations C_1 and C_2 are insensitive to temperature(7,31). However, in the case of Aerosol-OT, one should expect C_g to increase with C_1 since C_1 increases with temperature as seen in Fig. 17.

Conclusions

The transient and steady state crossflow filtration behaviour of several types of well characterised surfactants are evaluated using membranes of similar pore size ratings but of varying hydrophobicity and surface charge. The transient permeate flux and rejection behaviour of the cationic surfactant, DODDMAC dispersion and

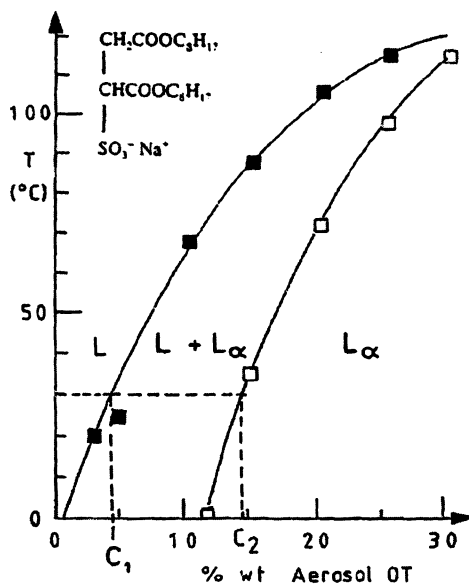


Figure 17. Phase diagram of sodium dioctylsulphosuccinate (Aerosol OT) / water binary system and the definitions of the concentrations C_1 and C_2 . Adopted with permission from reference (30).

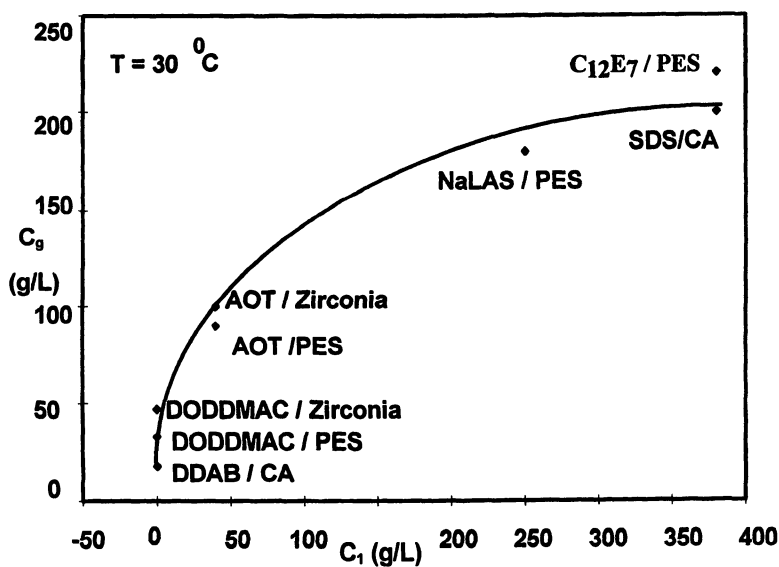


Figure 18. The variation of the gel concentration C_g , with C_1 concentration (see Fig.17 for definition) for several surfactants and membranes. Data plotted from Table 2.

membrane systems can be explained by the dynamics of surfactant deposition on the membrane.

The theoretical analysis indicate that, in the absence of any external electric field, the rate of surfactant capture by the membrane can be assumed to be proportional to the sum of van der Waals and electrostatic forces, as characterised by the Adhesion number, A_d , and Double layer asymmetry number D_a . It is found that for the cationic surfactant, DODDMAC, electrostatic interactions are not important but van der Waals interactions are, especially after the monolayer surfactant coverage of the membrane.

Although the steady state permeate flux behaviour of all the surfactants used in this study are very similar, the rejections show significant variations associated with the CMC values of the surfactants and the mechanical strength of the surfactant phase as well as the membrane /surfactant adhesion strength.

It is shown that the gel concentration, C_g correlates well with the phase boundary concentration, C_1 when the surfactant phase is transformed from the isotropic phase, L to $L + L_v$ phase. The secondary membrane formed by the surfactant is in the L_v phase. When L_v is the hexagonal phase (H_1), the $L + L_v$ phase is absent and hence $C_1=C_2$ where C_2 is the phase boundary concentration when L-phase or $L + L_v$ phase is transformed to L_v -phase

Acknowledgements

We are grateful to the Engineering and Physical Sciences Research Council, EPSRC, (UK) and Unilever for supporting this research. The support from the British Council for B. Keskinler and University of Botswana for P.T. Odirile are gratefully acknowledged.

References

1. Christian, S. D., and Scamehorn, J. F., in *Surfactant Based Separation Process*, Eds: J. F. Scamehorn and J.H. Harwell, Marcel Dekker, New York, 1989, Chapter 1, pp. 3-28.
2. Guo, W., Uchiyama, H., Turker, E. E., Christian, S. D., and Scamehorn, J. F., *Colloids and Surfaces A: Physico-chemical and Engineering Aspects*, 1997, 123, 695-703.
3. Klepark, J., Simmons, D.L., Taylor, R.W., Scamehorn, J. F., and Christian, S. D., *Sep. Sci. Technol.*, 1991, 26, 165-173.
4. Scamehorn, J. F., and Christian, S. D., and Ellington, R.T., in *Surfactant Based Separation Processes*, Eds: J. F. Scamehorn and J.H. Harwell, Marcel Dekker, New York, 1989, Chapter 2, pp. 29-51.
5. Markels, J.H., Lynn, S., and Radke, C. J., *AICHE Journal* 1995, 41, 2058-2066.
6. Charbit, F., Steinchen, A., Sadaoui, Z., and Charbit, G., *J. Membrane Sci.*, 1997, 133, 1-13.
7. Akay, G. and Wakeman, R.J., *Chem.Eng. Sci.*, 1994, 49, 271-283.

8. Akay, G. and Wakeman, R.J., *J. Membrane Sci.*, 1994, 88, 177-195.
9. Akay, G. Bhungara, Z., and Wakeman, R.J., *Chem.Eng.Res. Design* , 1995, 73, 783-796.
10. Wakeman, R.J., And Akay, G., *Filtration Separation*, 1997, 34, 511-519.
11. Akay, G., and Wakeman, R.J., *Chem. Eng. Res. Design*, 1996, 74, 517-525.
12. Yildiz, E., Pekdemir, T., Keskinler, B., Cakici, A., and Akay, G., *Chem. Eng. Res. Design*, 1996, 74, 546-553.
13. Keskinler, B., Danis, U., Cakici, A., and Akay, G., *Sep. Sci. Technol.*, 1997, 32, 1899-1920.
14. Akay, G., and Wakeman, R.J., *Chem. Eng. Res. Design*, 1993, 71, 411-420.
15. Akay, G., *Chem. Eng. Sci.*, (submitted) .
16. Kazeem, A., Akay, G., Derbyshire, W., and Morales, P.P., in *ICHEME Research Event*, University of Nottingham, Chameleon Press, London, 1997, pp.619-622.
17. Tirrell, M., and Malone, M.F., *J.Polymer Sci., Polymer Sci., Polymer Physics Edition*, 1977, 15, 1569-1583.
18. Akay, G., *Polymer Eng. Sci.*, 1982, 22, 798-804.
19. Akay, G., in *Encyclopedia of Fluid Mechanics*, Ed. N.P. Chermisinoff, Gulf Publishing, Houston, 1986 Vol. 1 Ch. 35 , pp 1155-1204.
20. Zydney, A.L., and Colton, C.K., *Chem. Eng. Commun.*, 1986,47, 1-21.
21. Lightfoot, E.N., Chiang, A.S., and Noble, P.T., *Ann. Rev. Fluid Mech.*, 1981, 13, 351- 378.
22. van de Ven, T.G.M., *Colloidal Hydrodynamics*, Academic Press, London, 1989.
23. Vaidyanathan, R., and Tien, C., *Chem. Eng.Sci.*, 1988, 42, 289-302.
24. van Oss, C.J., Chaudhury, M.K., and Good, R.J., *Chem. Rev.*, 1988, 88, 927-949.
25. Adamczyk, Z., Siwek, B., and Zembala, M., *J. Colloid Interface Sci.*, 1992, 151, 351- 369.
26. Bowen, W.R., and Cooke, R.J., *J. Colloid Interface Sci.*, 1991, 141,280-287.
27. Akay, G., and Wakeman, R.J., *Chem. Eng. Sci.*, submitted.
28. Barton, A.F.M., *CRC Handbook of Solubility Parameters and other Cohesion Parameters*, CRC Press, Boca Raton, Florida, 1983.
29. Visser, J., *Advances in Colloid Interface Sci.*, 1981, 15, 157-169.
30. Ekwall, P., in *Advances in Liquid Crystals*, Ed: G.H. Brown, Academic Press, New York, 1975, vol. 1, pp. 1-142.
31. Laughlin, R.G., and Munyon, R.L., *J. Physical Chem.*, 1990, 94, 2546-2552.
32. Akay, G., Danis, U., Keskinler, B., and Cakici, A., *J. Membrane Sci.*, submitted.
33. Akay, G., *Chem. Eng. Sci.*, 1998, 53,203-223.
34. Kekicheff, P., Grabielle-Madellmont, C., and Ollivon, M., *J. Colloid Interface Sci.*, 1989, 131, 112-132.
35. Scamehorn, J.F., Christian, S.D., El-Sayed, D.A., Uchiyama, H., and Younis, S.S., *Sep. Sci. Technol.*, 1994, 26, 809-830.
36. Degiorgio, V. In *Proceedings of International School of Physics*, North Holland Physics Publishing, Amsterdam, 1985, vol. 90, pp. 303-335.

Chapter 13

Organic Compounds Removal by Vesicle-Enhanced Ultrafiltration

Masahiko Abe ^{1,3} and Yukishige Kondo ^{2,3}

¹ Faculty of Science and Technology, Science University of Tokyo, 2641 Yamazaki, Noda, Chiba 278-8501, Japan

² Faculty of Engineering, Science University of Tokyo, 1-3 Kagurazaka, Shinjuku-ku, Tokyo 162-8601, Japan

³ Institute of Colloid and Interface Science, Science University of Tokyo, 1-3 Kagurazaka, Shinjuku-ku, Tokyo 162-8601, Japan

Solubilization of aromatic compounds has been investigated using didodecyldimethylammonium bromide (DDAB) vesicles with different diameters. It was found that solubilization of non-polar solutes changes abruptly at the phase transition temperature (T_c), while that of polar aromatic solutes exhibits a maximum at T_c . The aromatics with carboxyl groups were likely to be solubilized more strongly in larger vesicles (in diameter) than in small vesicles. Moreover, the incorporation of aromatic solutes by β -cyclodextrin dissolved in the inner water phase of the vesicles had little influence on the solubilization equilibrium constant. DDAB vesicles would be more efficient than conventional micelles in the solubilization of an alcohol (2-phenylethanol). Vesicular-enhanced ultrafiltration (VEUF) would thus be a useful ultrafiltration process for removal of organic solutes.

Surfactant vesicles consisting of curved bilayer membranes have recently attracted attention as biomembrane model systems, drug carriers in drug delivery systems (DDS) (1-4), new organic synthesis sites (5), inorganic synthesis sites, solubilizers in cosmetics, basic materials of sensors, etc. (6-8) However, there have been few studies related to the solubilization of organic compounds by vesicles and the removal of these solutes from water.

Micellar-enhanced ultrafiltration (MEUF) (9,10) is a novel and powerful separation process that can remove organic solutes from aqueous streams. In this method, a micellar solution containing organic solutes (retentate solution) is passed through a membrane with pore sizes smaller than the micellar diameter and the micelles and solubilized solutes are removed. The MEUF data indicate that the separations obtained are closely related to the solubilization equilibrium constants of organic solutes estimated from equilibrium dialysis data (9,11).

Vesicles are much larger in diameter and have lower monomer concentrations in their solutions than micelles. Therefore, the use of vesicles as the substitute for

micelles should lead to an improvement of MEUF, in that it brings about (1) an increase in the UF-membrane pore size, resulting in large fluxes, and (2) a reduction of the surfactant concentration in the permeate solution (the filtrate passed through the UF-membrane).

In the present work, solubilization of aromatic compounds by surfactant vesicles formed from didodecyldimethylammonium bromide (DDAB), a typical double-chained surfactant, has been investigated using the equilibrium dialysis (ED) method as a prerequisite step to apply vesicles to the removal of organic pollutants from water. We will discuss the value of solubilization equilibrium constant and the interaction between the bilayer vesicle membrane and aromatic solutes in terms of temperature, vesicle size, the fluidity of bilayer membrane, and vesicular-enhanced ultrafiltration (VEUF) as a novel ultrafiltration process.

Preparation and Stability of DDAB Vesicles

Needless to say, vesicles are thermodynamically unstable aggregates of surfactant molecules. Fusion and/or precipitation of these aggregates may occur in aqueous solutions. The stability of vesicles is a very important factor for their applications in many fields. We will discuss the stability of pure DDAB vesicles before discussing the solubilization of aromatic compounds by the vesicles (12).

Preparation of DDAB Vesicles. Figure 1 shows changes in the diameter of DDAB aggregates with ultrasonication time (13). Here, the preparation of 10.0 mM aqueous DDAB aggregate solution was performed by ultrasonication with a Bransonic 220 ultrasonic cleaner (output power: 125 W). The diameter of DDAB aggregates decreased with ultrasonication time, and then reached a constant value of approximately 17.5 nm at 90 min sonication, after which it remained unchanged for a long period of time.

Larger DDAB aggregates with different diameters (83 nm and 175 nm) were also prepared using polycarbonate membranes (pore sizes are 100 nm and 200 nm) by the extrusion method (14). The DDAB aggregates obtained were always smaller than the pore diameter in the membrane.

If the surfactant aggregates prepared here are surfactant vesicles, they should have an inner aqueous phase. To see if the aggregates have an inner aqueous phase, we measured the trapping efficiency of D-glucose, a water-soluble substance, as follows. First, a 10.0 mM DDAB vesicle solution was prepared in a 0.280 M aqueous glucose solution. The solutions were then placed in a regenerated cellulose tube for dialysis with the membrane having a molecular weight cut-off of approximately 13000 Da. The glucose in the outer phase of the vesicles was removed in 0.9 wt% aqueous sodium chloride solution at 0 °C. After the removal of the glucose in the outer phase, methanol was added to the vesicular solution to destroy the bilayer structure. A glucose CII-test Wako solution (Wako Pure Chemical Industries Co., Tokyo, Japan), a color-producing agent for the quantitative analysis of glucose, was utilized to determine the glucose concentration. Finally, the trapping efficiency was calculated as the ratio of the concentration of the glucose retained inside the vesicles to the total concentration of the glucose in the aqueous solution (0.280 M).

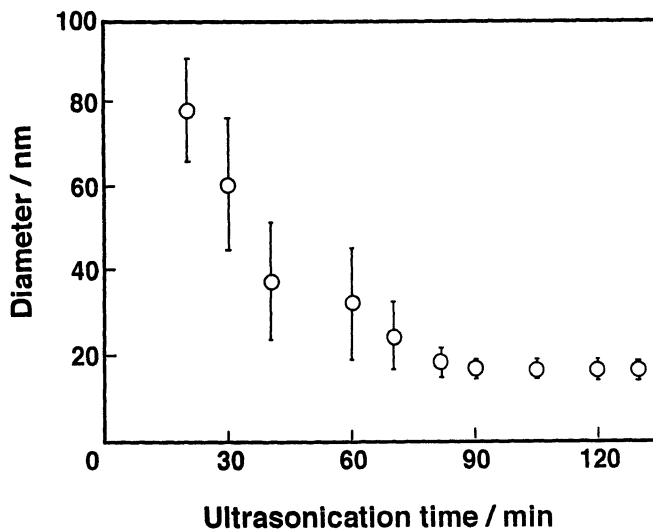


Figure 1. Change in the diameter of DDAB aggregates (vesicles) as a function of ultrasonication time ($[DDAB]=10.0$ mM). The ultrasonication was performed with a Bransonic 220 sonicator (power 125 W) at a temperature range of 25-35 °C. The diameter was determined by the dynamic light-scattering method at 30 °C.

As shown in Figure 2, the glucose trapping efficiency was 0.57 % for 17.5 nm size aggregate solution, and increased with the vesicular diameter up to 40 nm. The efficiency for the 83 nm and 175 nm size aggregates prepared by the extrusion method were 2.5 %. This demonstrates that the surfactant aggregates prepared in this study are really surfactant vesicles.

Stability of DDAB Vesicles. Figure 3 depicts the relationship between vesicular diameter and time at 30 °C. DDAB vesicles having a diameter of 50 nm (prepared by ultrasonication) were unstable and showed a phase separation near the air/water interface 3 or 4 days after preparation. On the other hand, DDAB vesicles with diameters in the range of 17.5 nm-40 nm, and those with diameters of 83 nm and 175 nm remained stable for at least 2 weeks. In particular, DDAB vesicles with an approximate diameter of 17.5 nm was very stable and no change in the diameter was observed even after 2 months storage. Meanwhile, the zeta-potential of DDAB vesicles was positive (about 90 mV) and independent of diameter up to 40 nm. The good stability of the vesicles prepared by ultrasonication may be attributed to their high zeta-potential.

Solubilization Equilibrium Constant

The solubilization equilibrium constants (K) of aromatic solutes between the surfactant vesicle phase and the bulk aqueous phase were measured by the equilibrium dialysis (ED) method (15). Commercial equilibrium dialysis cells with cellulose acetate membranes were used. The membranes had a 6000 Da MW cutoff, and they were washed thoroughly with water for 12 h before use. The solute solubilized solution, prepared by adding different amounts of the aromatic solute to 10.0 mM DDAB vesicle solution, was placed on one side of the membrane (retentate), and the other side (permeate) contained water. The ED cells were thermostated at a fixed temperature for 36 h (even though an equilibrium was attained in all cases within 26 h) and then the concentrations of aromatic solute and surfactant in the retentate and permeate solutions were determined by UV spectroscopy and the Orange II method (16) respectively, as reported previously (13). Finally, K values were calculated using the estimated DDAB and aromatic solute concentrations.

In this work, the solubilization equilibrium constant (K) of an aromatic solute in an aqueous vesicular solution is defined as

$$K = \frac{X_{\text{vesicle}}}{X_{\text{bulk}}} \quad (1)$$

where X_{vesicle} is the mole fraction of the aromatic solute in the vesicular phase, which is the ratio of the molar concentration of the solubilized solute to the total molar concentration of surfactant and aromatic solute in the vesicular phase, and X_{bulk} is the mole fraction of the monomeric aromatic solute in the bulk aqueous phase.

In this study, the DDAB concentration in the permeate solution after dialysis experiments was always lower than 7×10^{-2} mM. Since the micelle-forming concentration (cmc) of DDAB is 8×10^{-2} mM at 30 °C, determined by the conductivity method, no or few DDAB micelles would be present in the permeate solution of the ED

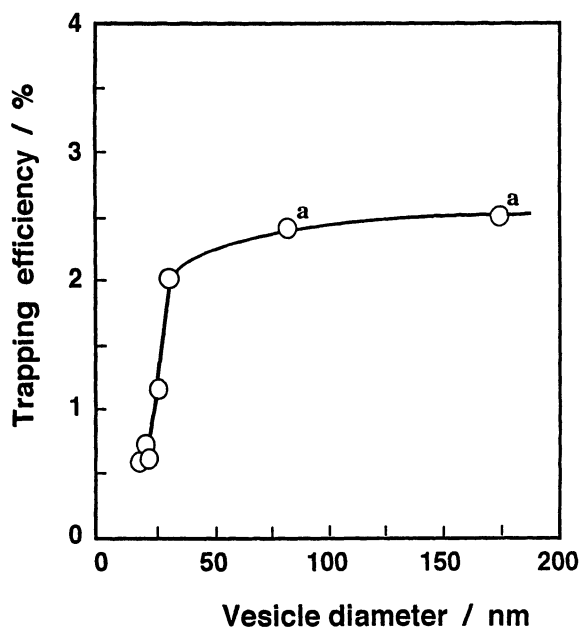


Figure 2. Relationship between the DDAB vesicle diameter and the D-glucose trapping efficiency of 10.0 mM DDAB vesicles. DDAB vesicles (a) of 83 nm and 175 nm diameter were prepared by the extrusion method. The other vesicles were prepared by the ultrasonication method. (Adapted from ref. 12.)

cell. Therefore, K values can be calculated from the equation

$$K = \frac{\frac{[O]_{ret} - [O]_{per}}{[O]_{ret} - [O]_{per} + [S]_{ret}^{ves}}}{\frac{[O]_{per}}{[O]_{per} + C_w + [S]_{per}}} \quad (2)$$

where [O] and [S] denote the concentrations of aromatic solute and DDAB, respectively, C_w is the molarity of water, and the subscripts *ret*, *per*, and *ves* represent the retentate side, permeate side, and the surfactant in vesicle form, respectively. Assuming that $C_w \gg \{[O]_{per} + [S]_{per}\}$, eq (2) can be transformed into

$$K = \frac{\frac{[O]_{ret} - [O]_{per}}{[O]_{ret} - [O]_{per} + [S]_{ret}^{ves}}}{\frac{[O]_{per}}{C_w}} \quad (3).$$

Temperature Dependence of Vesicular Solubilization

Surfactant vesicles abruptly change their bilayer membrane properties at a certain temperature, i.e., *gel-liquid crystal* transition temperature (T_c). At temperatures below T_c , the bilayer membranes are in the *gel* state, whereas the membranes are in the *liquid crystal* state above T_c . The vesicular solubilization behavior should change significantly around T_c , because the solubilization sites for hydrophobic solubilizates are in the bilayer membranes. In this section, small unilamellar vesicles of DDAB with a diameter of 17.5 nm were used, because these vesicles were stable as shown in Figure 3.

Solute Concentration Dependence of Solubilization Equilibrium Constants. Figure 4 shows the changes in the solubilization equilibrium constant K with $X_{vesicle}$ for benzene, ethylbenzene, phenol and benzoic acid in small DDAB vesicle solutions at 30 °C. The K values for phenol and benzoic acid decreased almost linearly with increasing $X_{vesicle}$, while those for benzene and ethylbenzene showed little solubilize concentration ($X_{vesicle}$) dependence. This tendency was observed at all other temperatures (5-30 °C). The K value at infinite dilution (the intercept on the ordinate of K- $X_{vesicle}$ line) decreased in the order benzoic acid > ethylbenzene > phenol > benzene. In contrast, the partition coefficients of the solutes between the *n*-dodecane phase and the water phase at infinite dilution were 1.8 (benzoic acid), 18000 (ethylbenzene), 0.9 (phenol), and 1340 (benzene), respectively. Namely, the K value at infinite dilution seems to be independent of the solute hydrophobicity. It was also found that phenol and benzoic acid are solubilized more strongly by DDAB vesicles in less concentrated solutions than in more concentrated solutions.

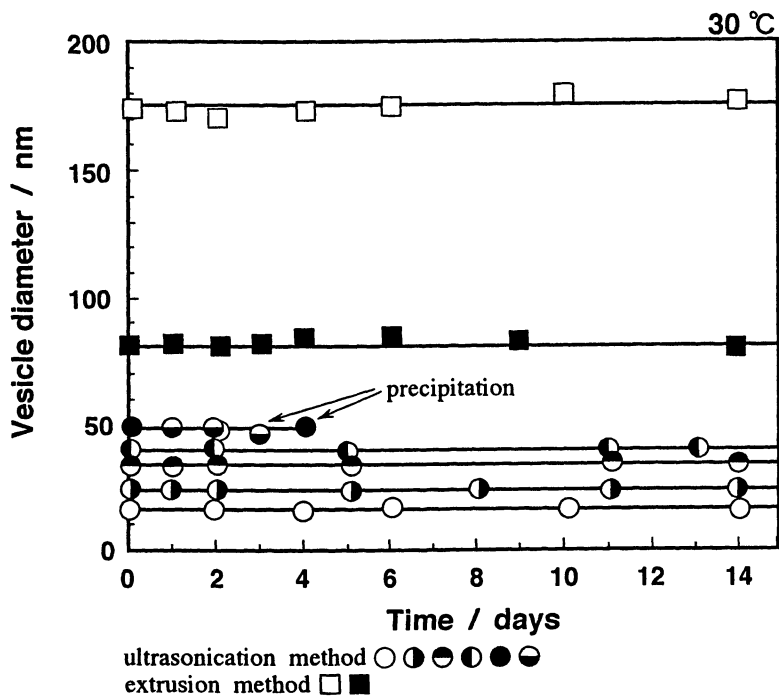


Figure 3. Relationship between DDAB vesicle diameter and time at 30 °C. (Reproduced with permission from ref. 12. Copyright 1993 Elsevier Science)

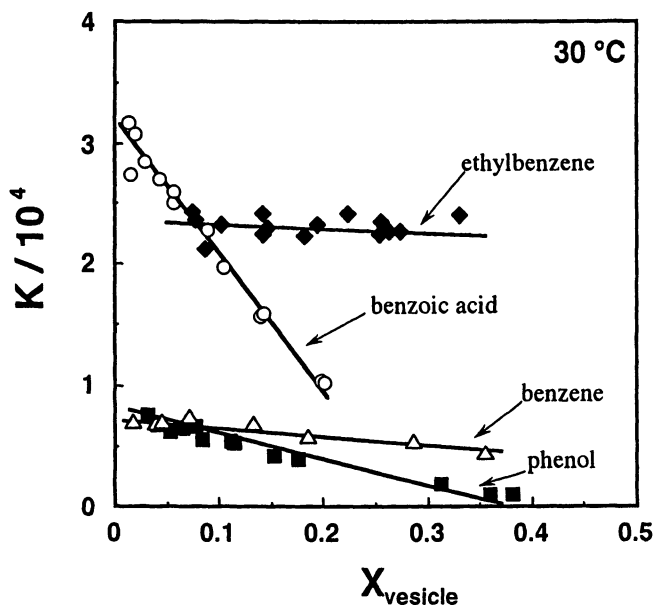


Figure 4. Dependence of solubilization equilibrium constant (K) on intravesicular mole fraction (X_{vesicle}) of aromatic solute in 10.0 mM DDAB vesicles having a diameter of 17.5 nm at 30 °C. (Reproduced with permission from ref. 15. Copyright 1997 JOCS)

Temperature Dependence of Solubilization Equilibrium Constants at Infinite Dilution. To determine the solubilization equilibrium constant at infinite dilution (K_0), the following equation was used to fit to the experimental data in Figure 4.

$$K = K_0 (1 - aX_{\text{vesicle}}) \quad (4)$$

where a is an empirical constant. Figure 5 shows the relationship between K_0 and temperature for the solutes in DDAB vesicles. The K_0 value should relate to the interaction of the solubilize with the vesicle bilayer membrane. For benzene and ethylbenzene, an abrupt change in K_0 was observed in the temperature range of 8-10 °C, and the K_0 value at temperatures below 8 °C was much lower than that at temperatures above 10 °C. In contrast the K_0 value was found to exhibit a maximum value at ca. 10 °C for phenol and benzoic acid. Interestingly, even at such low temperatures, these solutes were solubilized in DDAB vesicles, and the K_0 values at temperatures below 8 °C were rather larger than those in the temperature range 25-30 °C.

Solubilization equilibrium is affected more or less by the hydrophobicity of solute, which depends on temperature. We therefore employed the partition coefficient (K_{dodecane}) of the aromatic solute between the *n*-dodecane phase and the water phase to normalize the K_0 for the solubilize hydrophobicity. Thus, the K_0 values of the solutes were divided by their K_{dodecane} values at the same temperature. The relationships between the normalized solubilization equilibrium constant (K_0/K_{dodecane}) and temperature for the solutes are shown in Figure 6. K_0/K_{dodecane} -temperature curves were quite similar in shape to K_0 -temp. curves shown in Figure 5. In other words, the K_0/K_{dodecane} values for benzene and ethylbenzene also showed a sudden change, while those for phenol and benzoic acid had a maximum in the vicinity of 10 °C.

Effect of Fluidity of DDAB Vesicle Bilayer Membrane on Solubilization. The fluidity of DDAB vesicle bilayer was studied by the fluorescence polarization degree (P) of ANS (8-anilino-naphthalene-1-sulfonate ammonium salt) and I_E/I_M of pyrene as a function of temperature and the results are shown in Figure 7. ANS and pyrene are well-known typical fluorescence probes and bind to the hydrophilic region and the hydrophobic region of vesicle, respectively (17,18). The fluorescence polarization degree (P) of ANS is defined as

$$P = \frac{I_{//} - I_{\perp}}{I_{//} + I_{\perp}} \quad (5)$$

where $I_{//}$ and I_{\perp} are the emission intensity detected through polarizer oriented parallel and perpendicular to the polarization direction of excitation light, and serves as a measure of the fluidity of the bilayer membrane. Further, pyrene monomer forms an excimer by face-to-face collision. Thus, the excimer/monomer ratio of emission intensities (I_E/I_M) is indicative of the fluidity of the bilayer membrane.

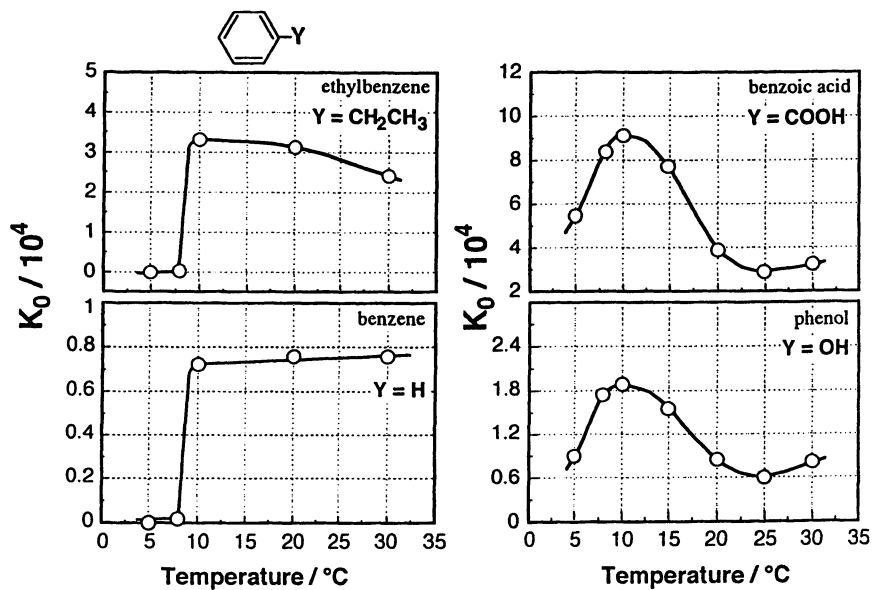


Figure 5. Relationship between the solubilization equilibrium constant at infinite dilution (K_0) and temperature. (Reproduced with permission from ref. 15. Copyright 1997 JOCS)

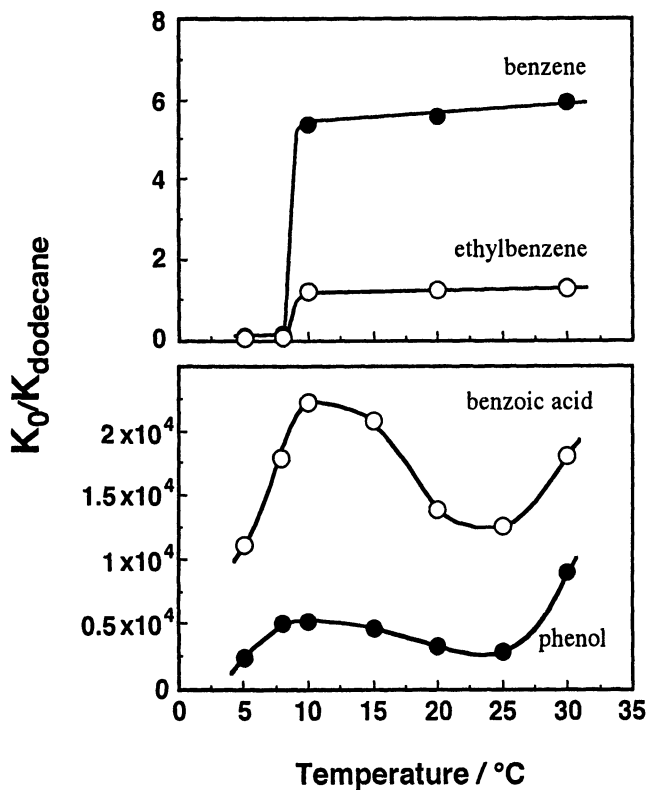


Figure 6. Dependence of the normalized solubilization equilibrium constant (K_0/K_{dodecane}) on temperature. (Reproduced with permission from ref. 15. Copyright 1997 JOCS)

As seen in Figure 7, a sudden change in the P value with an increase of temperature was observed in the range of 8-11 °C, indicating that the fluidity near the surface of DDAB vesicle decreases abruptly. On the other hand, the I_E/I_M value remained constant up to 9 °C, beyond which it increased linearly, suggesting that the fluidity of the DDAB vesicular interior also decreases with temperature. It has been reported that DDAB vesicles prepared by the ultrasonication method display a phase transition from the gel state to the liquid crystal state around 8 °C (19). This temperature is in fair agreement with the sudden change in the P and I_E/I_M values observed in Figure 7. For DDAB vesicles used in this work, the gel-liquid crystal phase transition clearly occurred between 8 and 11 °C. The phase transition temperature (T_c) determined from the midpoint of phase transition was about 9.5 °C.

In Figure 6, T_c of the DDAB bilayer membrane is found to agree well with the temperature, at which K_0/K_{dodecane} values of benzene and ethylbenzene showed a sharp change, and these solutes are shown to be solubilized in the *fluid state* of the vesicle bilayer membrane at temperatures above T_c . Thus, the solubilization of non-polar solutes such as ethylbenzene and benzene clearly depends on the fluidity of the bilayer membrane.

Note that the K_0/K_{dodecane} values of benzene above T_c are about 5.5. If the bilayer membrane interior is assumed to be hydrocarbon-like and the solubilize is located inside the membrane, the K_0/K_{dodecane} value must then be approximately 1. On the other hand, the previous papers (20,21) reported that the π electron cloud of the benzene ring interacts with the electric field induced by the cationic charge of surfactant head groups. This interaction should help the partition of the solute into the DDAB vesicle. The K_0/K_{dodecane} value of benzene which is larger than 1 would suggest that benzene molecules are located in the hydrophilic region of DDAB vesicles while interacting with the surfactant head groups. In contrast, the ethylbenzene molecule is thought to be solubilized inside the DDAB membrane without its own benzene ring attracted to the DDAB head groups, because the K_0/K_{dodecane} value is approximately 1. In general, the transfer of alkyl chain from water to the hydrocarbon medium is stabilized by the dehydration (20). The deeper solubilization site of ethylbenzene from the vesicular surface, when compared to benzene, seems to result from the hydrophobic property of the ethyl group.

From Figure 6, one should note that the K_0 values of phenol and benzoic acid are larger than their K_{dodecane} values by about three and four orders of magnitude, respectively. It seems that phenol and benzoic acid interact strongly with the particular region, present in DDAB vesicles but not in *n*-dodecane, that is, the hydrophilic region of the vesicles.

Effect of DDAB Head Group Charge on Solubilization. Figure 8 shows the relationship between the degree of dissociation (α) of the counter-ion Br^- from DDAB vesicles and temperature. The counter-ion dissociation degree exhibited a maximum value at 10 °C. The negatively charged polar groups such as phenolic hydroxyl and/or carboxyl groups seem to favor electrostatically the positive charge of the DDAB head group. Figure 9 shows the dependence of the normalized solubilization equilibrium

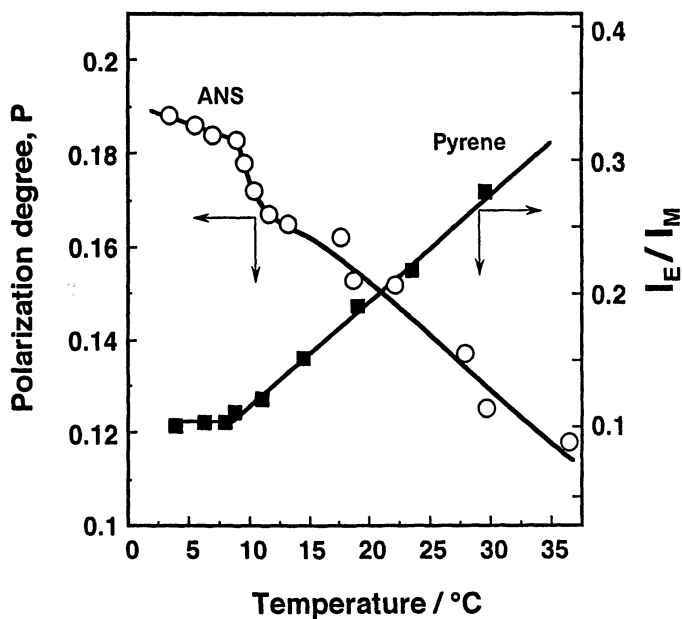


Figure 7. Changes with temperature in the fluorescence polarization degree (P) of 8-anilinoanthracene-1-sulfonate ammonium salt (ANS) and the excimer/monomer ratio (I_E/I_M) of emission intensities of pyrene in small unilamellar vesicles of DDAB having a diameter of 17.5 nm. (Adapted from ref. 15.)

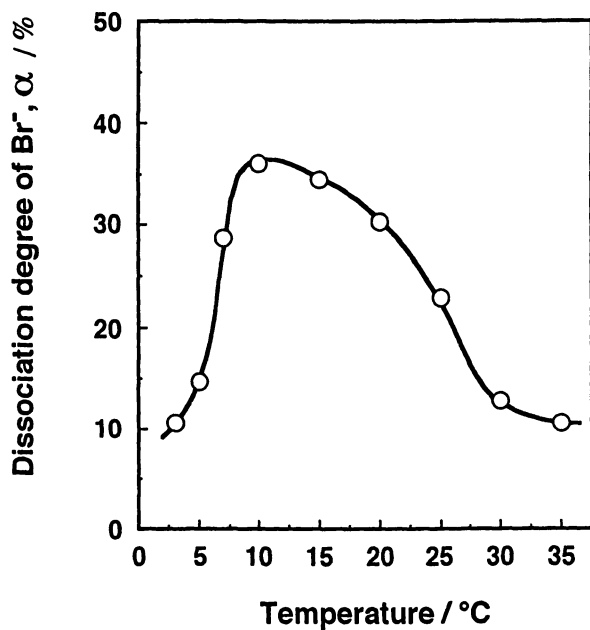


Figure 8. Relationship between the degree (α) of dissociation of the counter-ion Br⁻ from small unilamellar vesicles of DDAB having a diameter of 17.5 nm and temperature. (Reproduced with permission from ref. 15. Copyright 1997 JOCS)

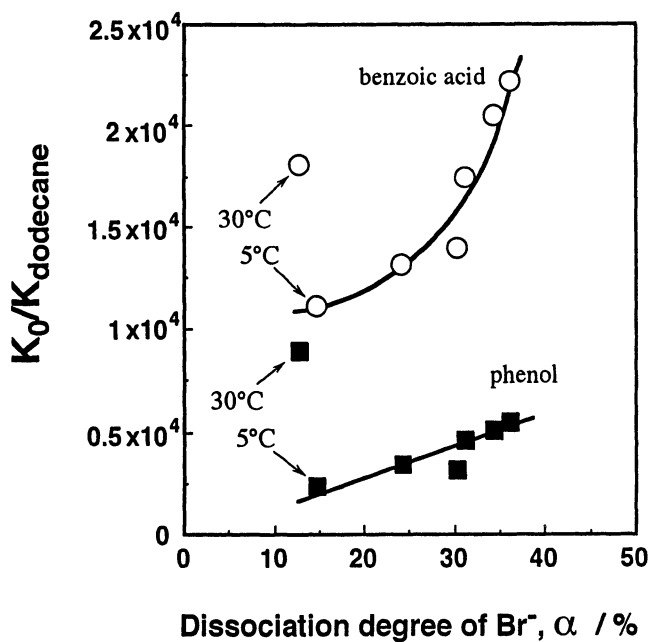


Figure 9. Dependence of the normalized solubilization equilibrium constants (K_0/K_{dodecane}) on the dissociation degree (α) of Br^- for benzoic acid and phenol. (Reproduced with permission from ref. 15. Copyright 1997 JOCS)

constant (K_0/K_{dodecane}) on α for phenol and benzoic acid. For both solubilizates, K_0/K_{dodecane} value increased with the dissociation degree, except for the data at 30 °C. It is clear that the solubilization of these polar solutes depends principally on the electric charge of DDAB vesicles. These solutes would be located in the hydrophilic region of DDAB vesicles with their polar groups being attracted to the charged head groups. Taking pKa into consideration, the large K_0/K_{dodecane} value for benzoic acid, compared to phenol, would result from the relatively strong electrostatic force between the DDAB head group and the solute polar group.

The K_0/K_{dodecane} values at 30 °C are larger than those at 5 °C, even though there is little difference in α value between 5 °C and 30 °C. One argument supporting this result is that the microviscosity of DDAB vesicle bilayer membrane at 30 °C affects the solubilization of the aromatic solute. It seems that solubilizate molecules can take a relatively favorable configuration to interact with surfactant molecules in the membrane in the *fluid* state as compared to the that in the *gel* state.

The following events would roughly explain the temperature dependence of the dissociation degree of DDAB vesicles. It is known that the area of surfactant head groups in vesicles increases during the phase transition from the gel state to the liquid crystal state (22,23). This enlargement of the head group area may be supported by the increase in the electrostatic repulsive forces between head groups, i.e., head group ionization. In contrast, the rise of temperature generally tends to cause decreased hydration of the surfactant head group, as pointed out for ionic micelle systems (24), which will lead to the depression of the ionization of head groups in vesicles. The relative magnitude of these two opposing effects on head group ionization seems to determine the α value of DDAB vesicles. Thus, it appears that the increase in α with temperature reflects the enlargement of the area of DDAB head groups by the phase transition, and the decrease of α beyond 10 °C is due to dehydration of DDAB head groups in vesicles.

Vesicle Diameter Dependence of Vesicular Solubilization

Three kinds of 10.0 mM DDAB vesicles with different diameters (diameters, 17.5 nm, 83 nm, and 175 nm) were used in this section. As mentioned above, the preparation of aqueous small DDAB vesicle solution (diameter 17.5 nm) was performed by the ultrasonication method, while the middle-size vesicles and the large vesicles were prepared by the extrusion method. We then examined the dependence of solubilization on vesicle size using benzoic acid, phenol, 3-phenylpropionic acid (HCA), and 2-phenylethanol (PEA) (25).

Vesicle Diameter Dependence of Solubilization Equilibrium Constants.

Figure 10 shows the solubilization equilibrium constants for benzoic acid and phenol in three kinds of DDAB vesicles with different diameters as a function of X_{vesicle} at 30 °C. The K values for phenol and benzoic acid decreased almost linearly with X_{vesicle} . Equation (4) was used to fit to the experimental data in the figure. Table I gives the optimized parameters in eq (4).

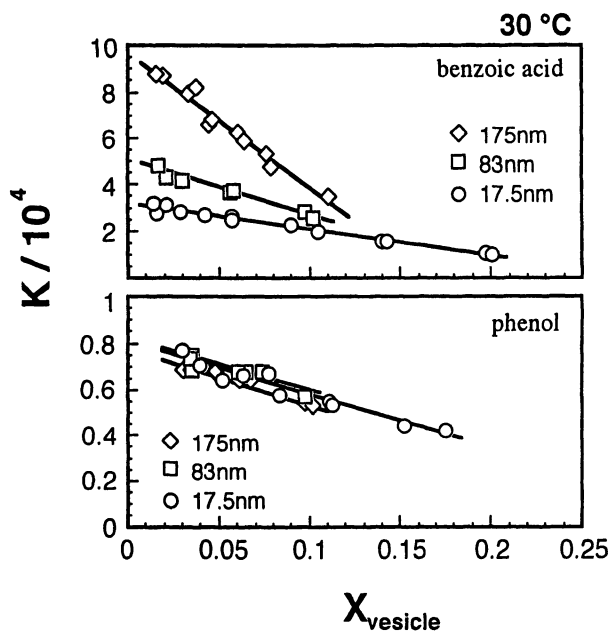


Figure 10. Dependence of solubilization equilibrium constants (K) for benzoic acid and phenol in 10.0 mM DDAB vesicles with different diameters on the intravesicular solute mole fraction (X_{vesicle}) at 30 °C. Symbols ◇, □ and ○ indicate DDAB vesicles having 175 nm, 83 nm and 17.5 nm, respectively. (Reproduced with permission from ref. 25. Copyright 1997 JOCS)

Table I. Parameters K_0 and a in Equation $K=K_0(1-aX_{\text{vesicle}})$

Solubilize	Vesicle Diameter / nm	K_0	a	r^a
benzoic acid	17.5	31650	3.5	0.990
	83	49800	4.6	0.986
	175	97650	6.1	0.984
phenol	17.5	8000	2.8	0.966
	83	8000	2.6	0.896
	175	7750	3.0	0.967
3-phenylpropionic acid (HCA)	17.5	15350	1.7	0.972
	83	27550	4.3	0.972
	175	71550	7.0	0.975
2-phenylethanol (PEA)	17.5	1950	1.6	0.959
	83	2000	1.6	0.956
	175	1950	1.4	0.956

^acorrelation coefficient

Reprinted with permission from ref. 25. Copyright 1997

As can be seen in Table I, eq (4) did provide each system with good correlation of data. For phenol, no dependence of the K_0 value on the vesicle diameter was observed, whereas K_0 for benzoic acid increased with an increase in the vesicle diameter. Figure 11 shows the K values as a function of X_{vesicle} for HCA and PEA in DDAB vesicles with different diameters at 30 °C. The K values for HCA and PEA also decreased linearly with an increase in X_{vesicle} . Summarized in Table I are the results obtained by fitting eq (4) to the experimental solubilization data in Figure 11. PEA yielded almost the same K_0 value at any vesicle diameters, although the K_0 value for HCA increased with vesicle size. The above results indicate that the aromatic solutes with carboxyl groups as the hydrophilic group are solubilized more strongly in large vesicles than in small vesicles.

In addition, a comparison of the K_0 values at the same vesicle size shows that the K_0 values for phenol and PEA are lower than those for the corresponding carboxylic acids, benzoic acid and HCA. Benzoic acid and HCA molecules dissolve as anions while phenol and PEA are almost electrostatically neutral. The larger K_0 values for benzoic acid and HCA would result from the relatively strong electrostatic attraction force between the cationic DDAB head group and the solute hydrophilic group.

As described in the previous section, benzoic acid molecules are likely to be solubilized in the hydrophilic region of DDAB vesicles. Therefore, the vesicle

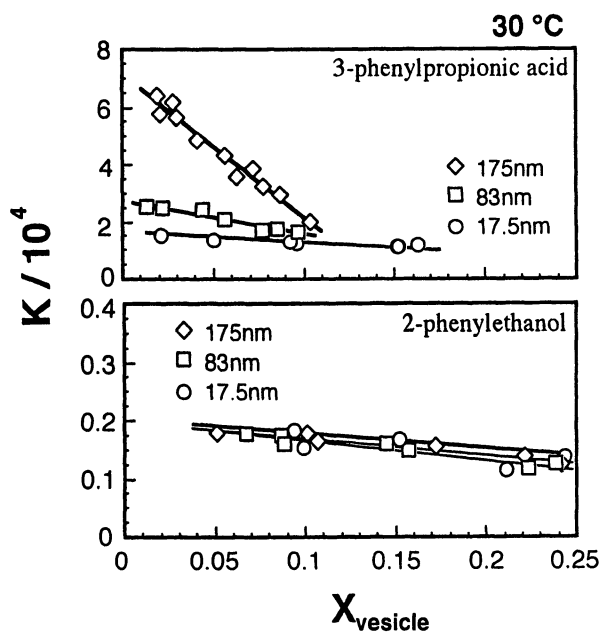


Figure 11. Dependence of solubilization equilibrium constants (K) for 3-phenylpropionic acid (HCA) and 2-phenylethanol (PEA) in DDAB vesicles with different diameters on the intravesicular solute mole fraction (X_{vesicle}) at 30 °C. Symbols \diamond , \square and \circ indicate DDAB vesicles having 175 nm, 83 nm and 17.5 nm, respectively. (Reproduced with permission from ref. 25. Copyright 1997 JOCS)

diameter dependence of K_0 observed for benzoic acid and HCA systems may reflect the circumstance of the hydrophilic region in DDAB vesicles. We then examined the vesicular hydrophilic region by measuring the polarization degree of ANS in DDAB vesicles.

Effect of Vesicular Hydration Layer on Solubilization. Figure 12 depicts the relationship between the polarization degree (P) of ANS solubilized in small and large DDAB vesicles (diameters 17.5 nm and 175.0 nm) and the total concentration of aromatic solute (benzoic acid or HCA) in the aqueous solution. For benzoic acid system, the P value in large DDAB vesicles increased with an increase in the benzoic acid concentration, while that in the small vesicles was independent of the benzoic acid concentration up to 0.12 mM. On the other hand, for HCA, the P value in the large vesicles increased with increasing HCA concentration, whereas that in the small vesicles remained constant in the concentration range below 0.25 mM. It is reported that the P value of ANS in vesicles increases as the surfactant head groups pack together closely (26). Further, Rupert *et al.* (19) have recently reported that the increase in packing density of the vesicular head groups may need the dehydration of the head groups and the reduction of the electrostatic repulsive force between the head groups in the presence of anionic species. Hence, the greater constancy of the P value observed at low aromatic solute concentrations for the small vesicles than that for the large vesicles would imply that the hydration layer of the small vesicles is bound more tightly on the surfactant head groups than that of the large vesicles. For the smaller vesicles, a higher aromatic solute concentration would be required to perturb the hydration layer. Thus, the increase in P at 0.12 mM for the 17.5 nm vesicle-benzoic acid system could be interpreted as dehydration of DDAB head groups, followed by the increase in head group packing density.

It is noted that the parameter a increased with increasing vesicle size for benzoic acid and HCA while the a values were almost independent of the vesicle diameter for phenol and PEA (Table I). Christian *et al.* have reported that the value $a/2$ is related to the number of sites occupied by one solubilizate molecule in the head group region, and the a value is equal to the ratio of the number of surfactant molecules to the number of solubilizate molecules per site, considering that the solubilization behavior is consistent with Langmuir's adsorption isotherm (27,28). The values of a for benzoic acid and HCA in small DDAB vesicles are 3.5 and 1.7 respectively. Thus, in the small vesicle solution, benzoic acid and HCA are solubilized with each of their molecule adsorbed to 3-4 and 1-2 DDAB molecules, respectively. Further, as the vesicle size increases, benzoic acid and HCA come to interact strongly with more DDAB molecules. On the other hand, the a value was almost constant in the vesicle diameter range used in this work for phenol and PEA, indicating that these compounds are respectively solubilized with each of their molecules adsorbed to 2-3 and 1-2 DDAB molecules in DDAB vesicles with any diameter.

From what have been mentioned so far, we can give the following explanations to the solubilization mechanism in this work. HCA and benzoic acid with a carboxyl group dissolve in aqueous solutions as anions, and hence, these molecules are likely to be solubilized in the hydrophilic region of cationic DDAB vesicles while interacting electrostatically with the latter's head groups. Since the attractive electrostatic interaction become stronger with decreasing distance between the aromatic

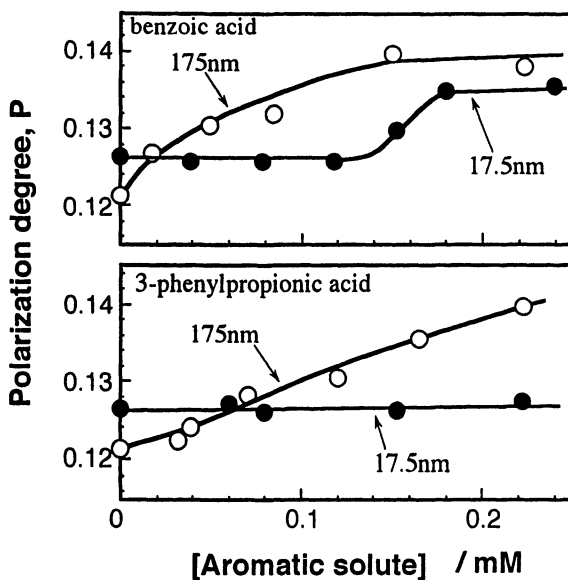


Figure 12. Relationship between the polarization degree (P) of the fluorescence from ANS in DDAB vesicles and the total solute concentration for benzoic acid and 3-phenylpropionic acid (HCA) at 30 °C. (Reproduced with permission from ref. 25. Copyright 1997 JOCS)

anion and the cationic head group, the aromatic anions should tend to disrupt the hydration layer of the vesicle to adsorb directly to the surfactant head groups. However, the tightly bound hydration layer of small vesicles, when compared to large vesicles, makes it difficult for the aromatic anions to adsorb directly to the surfactant head groups. This would be the reason why the α and K values for benzoic acid and HCA decrease with a decrease in the vesicle size.

On the other hand, phenol and PEA are slightly anionic and nonionic in aqueous solutions, respectively, and interact very weakly with the DDAB head group. The tendency for these solubilizates to disrupt the hydration layer bound on the surfactant head groups would be much poorer than that for benzoic acid and HCA. It seems that phenol and PEA are solubilized in the hydrophilic region of the vesicle with their phenolic- and alcoholic-OH groups bound weakly to water molecules constituting the hydration layer. This solubilization mechanism would be independent of the tightness of the hydration layer. As a result, the α and K values for phenol and PEA show little dependence on the vesicle diameter and are lower than those for the corresponding carboxylic acids. The difference in the tightness of hydration layer between small and large vesicles may be attributed to the difference in the dissociation degree of DDAB head groups (19). Thus, it is possible that hydration layer adsorbs less strongly to DDAB head groups in large vesicles, because large vesicles must have a lower dissociation degree of the head groups in order to arrange the surfactant molecules in a bilayer membrane with a relatively small curvature.

Comparison of Solubilizing Ability of DDAB Vesicles with That of Other Surfactant Micelles

It is very important to compare the solubilizing ability of DDAB vesicles with that of other surfactant micelles as a prerequisite step to develop the vesicular-enhanced ultrafiltration (VEUF) method. We have measured the solubilization equilibrium constants of 2-phenylethanol (PEA) using several kinds of typical micellar-forming surfactants. Table II shows the solubilization equilibrium constants at infinite dilution of PEA. The value of K_0 for DDAB vesicles was relatively large compared to those for other surfactant micelles (29), though it was smaller than K_0 for $C_{16}POE_{10}$ and $C_{16}POE_{20}$ (30). In addition, K_0 was found to be 940 for the solubilization by cationic dodecyltrimethylamine oxide (DDAO) (28). Thus, DDAB vesicles seem to have a rather great solubilizing ability compared to conventional surfactant micelles.

Effect of β -Cyclodextrin in the Internal Aqueous Phase on Vesicular Solubilization

One of the characteristics of vesicles is their ability to retain water-soluble substances in their internal aqueous phase (31,32). If intravesicular water-soluble substances could incorporate organic solutes, the amount of solutes solubilized in the entire vesicular systems would increase. In this section, we adopted β -cyclodextrin (CyD), which is capable of incorporating organic molecules of appropriate size in the inside, as the water-soluble substance, and HCA and benzoic acid as solubilizates, the former

Table II. Values (K_0) of Solubilization Equilibrium Constants at Infinite Dilution for 2-Phenylethanol in Different Vesicles and Micelles at 30 °C

Surfactant Aggregate		K_0
<i>vesicle</i>	DDAB (dia. 17.5 nm or 175 nm)	1950
	DDAB (dia. 83 nm)	2000
<i>micelle</i>	DTAB ^a	1000
	SDS ^b	1280
	C ₁₆ POE _n ^c $n=10$	2960
	$n=20$	2470
	$n=30$	1550
	$n=40$	1400

^adodecyltrimethylammonium bromide, ^bsodium dodecylsulfate, ^chexadecyl polyoxyethylene ether C₁₆H₃₃(C₂H₄O)_nH

being easily incorporated and the latter hardly incorporated by CyD (33). Then, the effect of CyD on the solubilization equilibrium constant K of the solutes was examined (34).

CyD-loaded DDAB vesicles were prepared by the ultrasonication method. After mixing DDAB with 1.0 mM aqueous CyD solution to make the surfactant concentration 10.0 mM, the mixture was subjected to ultrasonication (output power: 125 W) for more than 120 min. The resulting vesicular solution was then dialyzed using a cellulose membrane impermeable to substances of MW higher than 13000 Da to remove CyD remaining in the bulk aqueous phase at 0 °C. The procedure mentioned above resulted in CyD-loaded DDAB vesicles of 60 nm size.

It is well known that CyD easily incorporates straight-chain aromatic molecules. Therefore, K of HCA was determined for CyD-loaded DDAB vesicles at 30 °C (Figure 13). The data for CyD-free DDAB vesicles of 60 nm diameter are also shown for comparison. The preparation of CyD-free DDAB vesicles was performed by the extrusion method using a polycarbonate membrane (pore size 100 nm), followed by ultrasonication for 2 min. The K value for CyD-loaded vesicles was slightly larger than that for CyD-free DDAB vesicles of 60 nm diameter over the entire range of X_{vesicle} investigated. The K value appears to increase by incorporating straight-chain aromatic molecules such as HCA by CyD in the internal aqueous phase of vesicles.

Furthermore, the relationship between K and X_{vesicle} was examined using benzoic acid, which is an aromatic molecule hardly incorporated by CyD, as a solubilize (Figure 14). The K value for the CyD-loaded DDAB vesicles was found to be considerably larger than that for CyD-free DDAB vesicles over the wide range of

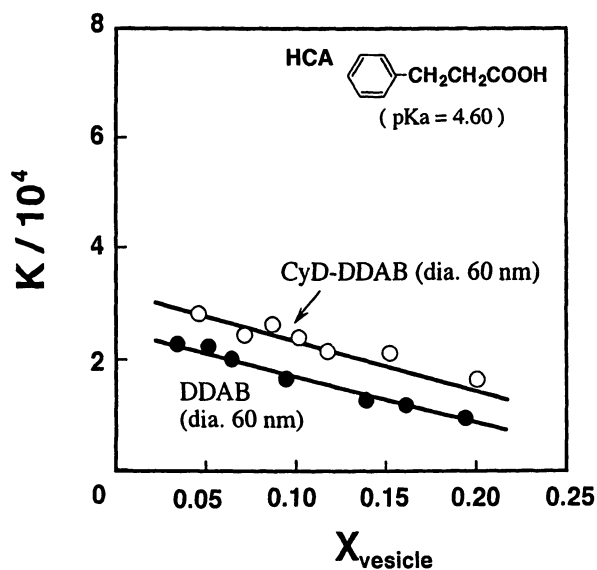


Figure 13. Solubilization equilibrium constant K as a function of X_{vesicle} of HCA in DDAB vesicles containing β -cyclodextrin (CyD-DDAB) at 30 °C. Open and filled circles show CyD-loaded DDAB vesicles having a diameter of 60 nm and CyD-free DDAB vesicles having a diameter of 60 nm, respectively. (Reproduced with permission from ref. 34. Copyright 1998 JSCM)

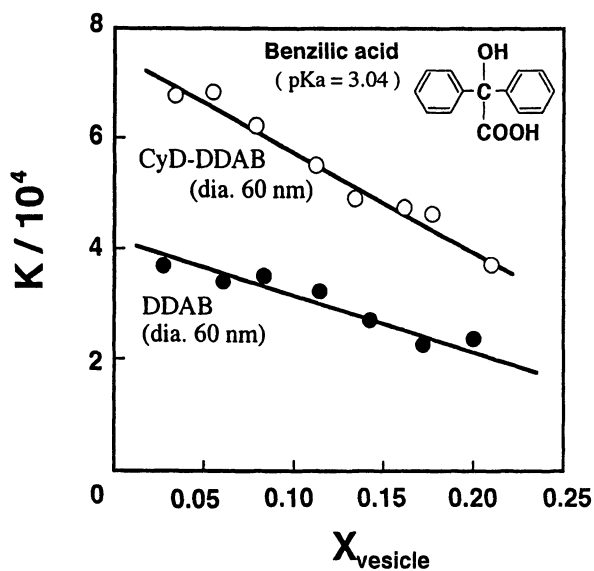


Figure 14. Solubilization equilibrium constant K as a function of X_{vesicle} of benzilic acid in DDAB vesicles containing β -cyclodextrin (CyD-DDAB) at 30 °C. Open and filled circles show CyD-loaded DDAB vesicles having a diameter of 60 nm and CyD-free DDAB vesicles having a diameter of 60 nm, respectively. (Reproduced with permission from ref. 34. Copyright 1998 JSCM)

X_{vesicle} investigated. Surprisingly, the effect of CyD was more remarkable in this case than the case involving the straight-chain aromatic compound.

The hydrogen bond between CyD and benzoic acid may be invoked to explain this result. The pKa value of benzoic acid is 3.04, which is lower than that of HCA (4.60). This indicates that benzoic acid is a stronger acid than HCA. In addition, benzoic acid has two polar groups, a hydroxyl group (OH) and a carboxyl group (COOH). It seems that benzoic acid molecules can easily form hydrogen bonds with hydroxyl groups of CyD compared to HCA. Therefore, it is thought that no appreciable increase is observed in the K value of HCA, a straight-chain aromatic compound easily incorporated by CyD, with addition of the CyD to the internal aqueous phase of the vesicle, while the K value of benzoic acid, an aromatic compound hardly incorporated by CyD, is considerably increased. The incorporation of aromatic solutes by CyD dissolved in the internal aqueous phase of the vesicles has little influence on the K value. β -Cyclodextrin would be efficient in enhancing the solubilization equilibrium constant via the formation of the hydrogen bonds with solubilizates.

Literature Cited

- (1) Singer, S. J.; Nicolson, G. R. *Science* **1972**, *175*, 720.
- (2) Ostro, M. J.; Cullis, P. R. *Am. J. Hosp. Pharm.* **1989**, *46*, 1576.
- (3) Komatsu, H.; Rowe, E. S. *Biochemistry* **1991**, *30*, 2463.
- (4) Hiff, T.; Kevan, L. *Colloids Surf.* **1990**, *45*, 185.
- (5) Shimomura, M.; Kunitake, T. *J. Am. Chem. Soc.* **1982**, *104*, 1757.
- (6) Mann, S.; Hannington, J. P.; Williams, R. J. P. *Nature* **1986**, *324*, 565.
- (7) Ingolia, T. D.; Koshland, D. E., Jr. *J. Biol. Chem.* **1978**, *253*, 3821.
- (8) Domazou, A. S.; Mantaka-Marketou, A. E. *Ber. Bunsenges. Phys. Chem.* **1990**, *94*, 428.
- (9) Christian, S. D.; Scamehorn, J. F. In *Surfactant-Based Separation Processes*; Scamehorn, J. F., Harwell, J. H., Eds.; Marcel Dekker, Inc.: NY, 1989; Chapter 1.
- (10) Abe, M.; Kondo, Y. *Material Technology* **1992**, *10*, 275.
- (11) Nguyen, C. M.; Christian, S. D.; Scamehorn, J. F. *Tenside Surfactants Deterg.* **1988**, *25*, 328.
- (12) Kondo, Y.; Abe, M.; Ogino, K.; Uchiyama, H.; Tucker, E. E.; Scamehorn, J. F.; Christian, S. D. *Colloids Surf. B. Biointerfaces* **1993**, *1*, 51.
- (13) Kondo, Y.; Abe, M.; Ogino, K.; Uchiyama, H.; Scamehorn, J. F.; Tucker, E. E.; Christian, S. D. *Langmuir* **1993**, *9*, 899.
- (14) Mayer, L. D.; Hope, M. J.; Cullis, P. R. *Biochim. Biophys. Acta* **1986**, *858*, 161.
- (15) Kondo, Y.; Yoshino, N.; Shinohara, T.; Sakai, H.; Abe, M. *J. Jpn. Oil Chem. Soc.* **1997**, *46*, 165.
- (16) Scott, G. V. *Anal. Chem.* **1968**, *40*, 768.
- (17) L'Heureux, G. P.; Fragata, M. *Biophys. J.* **1988**, *30*, 293.
- (18) Slavik, J. *Biochim. Biophys. Acta* **1982**, *694*, 1.

- (19) Rupert, L. A. M.; Engberts, J. B. F. N.; Hoekstra, D. *J. Am. Chem. Soc.* **1986**, *108*, 3920.
- (20) Bunton, C. A.; Minch, M. J.; Hidalgo, J.; Sepúlveda, L. *J. Am. Chem. Soc.* **1981**, *95*, 3262.
- (21) Hirose, C.; Sepúlveda, L. *J. Phys. Chem.* **1981**, *85*, 3689.
- (22) Hauser, H.; Pascher, I.; Pearson, R. H.; Sundell, S. *Biochim. Biophys. Acta* **1981**, *650*, 21.
- (23) Kreissler, M.; Lemaire, B.; Bothorel, P. *Biochim. Biophys. Acta* **1983**, *735*, 23.
- (24) *Surfactants and Interfacial Phenomena*; Rosen, M. J., Ed.; Second Ed.; Wiley Interscience: NY, 1989; Chapter 3.
- (25) Kondo, Y.; Yoshino, N.; Kaise, C.; Sakai, H.; Abe, M. *J. Jpn. Oil Chem. Soc.* **1997**, *46*, 323.
- (26) Inoue, T.; Muraoka, Y.; Fukushima, K.; Shimozawa, R. *Chem. Phys. Lipids* **1988**, *46*, 107.
- (27) Lee, B.-H.; Christian, S. D.; Tucker, E. E.; Scamehorn, J. F. *Langmuir* **1990**, *6*, 230.
- (28) Uchiyama, H.; Christian, S. D.; Scamehorn, J. F.; Abe, M.; Ogino, K. *Langmuir* **1991**, *7*, 95.
- (29) Abe, M.; Mizuguchi, K.; Kondo, Y.; Ogino, K.; Uchiyama, H.; Scamehorn, J. F.; Tucker, E. E.; Christian, S. D. *J. Colloid Interface Sci.* **1993**, *160*, 16.
- (30) Kondo, Y.; Mizuguchi, K.; Tokuoka, Y.; Uchiyama, H.; Kamogawa, K.; Abe, M. *J. Jpn. Soc. Colour Mater.* **1995**, *68*, 271.
- (31) Yamauchi, H.; Kikuchi, H. *Fragrance J.* **1987**, *87*, 68.
- (32) Abe, M.; Takao, Y.; Yamamoto, T.; Kwon, K. O.; Yamauchi, H.; Ogino, K. *J. Jpn. Oil Chem. Soc.* **1992**, *1*, 404.
- (33) Shiraishi, Y.; Hirai, H. *Surface* **1996**, *34*, 293.
- (34) Kaise, C.; Sakai, H.; Kondo, Y.; Yoshino, N.; Manosroi, J.; Manosroi, A.; Saito, Y.; Abe, M. *J. Jpn. Soc. Colour Mater.* **1998**, *71*, 16.

Chapter 14

Nonionic Surfactants as Collectors for the Flotation of Oxidized and/or Low-Rank Coal

Douglas W. Fuerstenau, Guy H. Harris, and Renhe Jia

**Department of Materials Science and Mineral Engineering,
University of California at Berkeley, Berkeley, CA 94720**

Ash minerals, including pyrite, can be separated from coal by flotation. Such separations are possible because of the natural hydrophobicity of the carbonaceous matter in coal, but an organic collector is required to overcome the deleterious effects of oxygen functional groups on the coal surface. This paper summarizes the flotation response of a high-sulfur coal, Illinois No.6 coal, using different nonionic oxygenated surfactants as the collector. The performance of these reagents is compared with that of two oily collectors, namely dodecane and nonylbenzene. One of the reagents gives comparable combustible matter recovery on an aged Illinois No.6 coal at around two percent of the amount of dodecane collector required. Mechanisms for the interaction of these compounds with coal are suggested.

Regarding the United States' energy situation, the increased use of coal and coal products is the most economical near-term solution to the problem of this country's excessive dependence on foreign oil imports (1). America has coal reserves of 440 billion tons, equivalent to about four times the proven oil reserves of the entire world (2). These coal deposits are estimated to last around 500 years at current consumption level (1). In 1997 U.S. coal production totaled a record high of 988 Mt [1.09 billion st], up by 2.3% from 1996, according to preliminary data from the Energy Information Administration, U.S. Department of Energy. The electric power industry, including utilities and independent power producers, used a record of 836.4 Mt [922 million st], up 2.8% from 1996, and provided 23% of the total domestic energy needs. The increase in coal use for electricity generation was attributable primarily to a substantial decline in nuclear-power generation and a moderate growth in electricity demand (3).

It has been estimated that approximately 23% of the world's economically recoverable coal reserves are low-rank coals. The vast world reserves of low-rank coals coupled with relatively easy access make them an attractive energy source (4). Flotation is becoming increasingly important as an effective method to upgrade coal fines, more of which are produced when more coal is mechanically mined.

Froth flotation is the process whereby small mineral particles in an aqueous suspension are captured by air bubbles and removed from the slurry as a froth. Individual mineral or solid particulates can be separated from a mixture of finely divided solids in a slurry, depending on the relative hydrophobicity/hydrophilicity of the various mineral species. Hydrophobic particles possess surfaces that are not wetted by water and therefore readily attach to gas bubbles and rise to the surface of the slurry as a froth, while the hydrophilic solids strongly interact with water and thus have no affinity for the gas phase. Ideally, all the hydrophilic solids are discharged from the flotation machine along with the slurry.

Coal is a solid combustible material that results from the alteration of vegetable matter, largely in the absence of air. Depending on the oxygen content of the coal surface, there is a progression in carbon content and hydrophobicity, and hence flotability of various coals. The mineral matter in raw coal is comprised of hydrophilic minerals, mainly clays (such as kaolinite and montmorillonite), quartz, carbonate minerals such as calcite and dolomite, gypsum, and pyrite.

The froth flotation of coal is a relatively small but important means of cleaning the fine fraction of mined raw coal, typically particles finer than 0.5 mm. In addition to recovering the fine coal, it also is an effective means for reducing the deleterious pyrite and ash-forming minerals from the coal. Coal flotation also plays an important role by removing coal fines from the plant water to be discharged and by removing fine coal particles from the discharged plant refuse. In summary, flotation recovers the valuable constituent in coal and separates it from the worthless ash-forming minerals.

Coal flotation is typically carried out with the natural fines (< 0.5 mm) as feed at very low solids concentration in the slurry (about 4%) at neutral pH. In the United States around 10% of the raw coal is processed with flotation, while on a worldwide basis, from 0 to 40% of the coal is treated by flotation. Coal flotation makes use of the natural hydrophobicity of the carbonaceous matter in coal. To enhance the hydrophobicity of the coal particles, oily materials, such as diesel oil and kerosene (5,6), are added industrially as collectors. In flotation, a reagent added to effect or enhance the hydrophobicity of a given mineral is called a collector. In mineral flotation most of the collectors are water-soluble surfactants. For higher-rank coals, the reagent consumption in flotation is low because of the natural hydrophobicity of the coal. However, for low-rank coals containing greater amounts of oxygen, flotation performance with these oily collectors is poor and large reagent dosages are required in order to obtain even moderate recovery of coal (7). Furthermore, most coals are susceptible to oxidation by weathering, which can occur at the mine site or during storage and transportation. Weathering processes result in the formation of oxygen functional groups, most commonly, carboxyl, phenolic and carbonyl functionalities on the coal surface, which reduce the hydrophobicity of the coal surface by increasing the number of sites that hydrogen bond with water molecules. This makes the coal more difficult to float with oily collectors (6,7,8). The objective of this paper is to present

the results of a study in which oxygenated polar groups are added to the collector molecule to provide a means for it to hydrogen bond with the oxygenated surface sites.

Previous work had shown that tetrahydrofurfuryl butyrate (designated here as THF-3) to be an effective collector for Illinois No.6 coal (9). Those results suggested that the THF series of reagents might be effective alternatives as collectors in the flotation of both low-rank and oxidized coal. The objective of this study was to investigate the collecting ability of THF compounds having various chain configurations as collectors for the flotation of unoxidized coals, laboratory-oxidized coals and naturally weathered coals. The results are compared with those of a few other collectors. It is expected that the oxygenated polar group of these nonionic surfactants will have stronger interactions with the surface oxygenated sites on the coal such that the surfactants can spread over the coal surface more readily than oily collectors and should not act as wetting agents.

Experimental Materials and Methods

Materials

A bituminous coal, Illinois No. 6 [from Peabody Coal Co., Marissa, IL] was used in this investigation. The proximate and sulfur analyses of the coal sample are given in Table 1. Illinois No.6 coal is much less hydrophobic than some high-rank coals, as indicated by its high moisture content [Table 1]. A variety of experimental measurements provide a measure of the wettability/flotability of Illinois No.6 bituminous coal. A standard flotation procedure had previously been developed in our laboratory for comparison between various flotation reagents (10). For this standard test with Illinois No.6 coal, the dosage of dodecane collector was 2.6 kg/tonne and that of the frother [methyl isobutyl carbinol, MIBC] was 0.53 kg/tonne. Using the sessile drop method, contact angles of samples that had been wet polished in air were found to be 51 degrees for Illinois No.6 coal (10). Induction times were measured on 100x150 mesh particles taken from coal samples that had been weathered for various time periods. Over the first few months of weathering, the induction time remained fairly constant and was determined to be 200 msec for Illinois No.6 coal, which is indicative of Illinois No.6 coal being quite hydrophilic. Film flotation tests conducted on particles that had been prepared from coal that had been weathered for 0.5 month showed that 56% of the Illinois No.6 coal particles were hydrophobic [that is, floated on water]. All of the results show that Illinois No.6 coal is considerably more hydrophilic than Pittsburgh No.8 and Upper Freeport coals previously used in our laboratory (10).

For the present work, all lump coal samples were first crushed to minus 6.4 mm, then split into 500-gram subsamples, and stored in plastic bags under inert environment to prevent further oxidation before being used for each set of flotation experiments.

Chemicals

The main chemicals used in this work were a series of tetrahydrofurfuryl esters [$C_4H_7O-CH_2OOC-R$]. Table 2 gives our designation, the chemical formula, and the source of these and other reagents used in this study. Some of these chemicals were

Table 1. The Proximate and sulfur analysis of the sample of Illinois No.6 coal in percentage (6).

<u>Coal</u>	<u>As Received Moisture</u>	<u>Fixed Carbon</u>	<u>Volatile Matter</u>	<u>Ash</u>	<u>Total Sulfur</u>	<u>Pyritic Sulfur</u>
Illinois No.6	9.5	49.2	36.2	14.6	4.61	2.36

Table 2. Chemical name and source of reagents used in this work

<u>DESIGNATION</u>	<u>CHEMICAL NAME</u>	<u>SOURCE</u>
THF-1	Tetrahydrofurfuryl acetate	Aldrich Chemicals
THF-3	Tetrahydrofurfuryl butyrate	CTC Organics
THF-7	Tetrahydrofurfuryl octonate	Made in our lab
THF-11	Tetrahydrofurfuryl laurate	Made in our lab
THF-17	Tetrahydrofurfuryl oleate	Pfaltz & Bauer, Inc.
THF-P	Tetrahydrofurfuryl benzoate	Pfaltz & Bauer, Inc.
THF-1-P	Tetrahydrofurfuryl phenyl acetate	Oxford Organics
THF-2-P	Tetrahydrofurfuryl 2-phenylpropionate	Made in our lab
THF-3-P	Tetrahydrofurfuryl 3-phenylbutyrate	Made in our lab
GH4	Polyethoxylated nonylphenol	Dow Chemical Co.
Dodecane	Dodecane	Fisher Chemical
Nonylphenol	Nonylphenol	Rohne-Poulenc
GHB	Nonylbenzene	Acros Organic
MIBC	4-methyl-2-pentanol	Kodak

purchased, while the rest were synthesized in our laboratory. The tetrahydrofurfuryl esters were prepared from equal molar amounts of tetrahydrofurfuryl alcohol and various carboxylic acids with a catalytic amount of toluenesulfonic acid in refluxing toluene. Refluxing was continued for a half hour after water had ceased being collected in the Dean Stark trap. The toluene was washed with aqueous solutions of sodium bicarbonate, water, and NaCl, which removed the catalyst and any possible remaining starting materials. The filtrate from the anhydrous magnesium sulfate drying agent gave the desired product after removal of the solvent in a rotary evaporator. The yields were almost quantitative.

Nonylphenol and polyethoxylated nonylphenol were obtained from Rhone-Poulenc and Dow Chemical Co., respectively.

Experimental Procedure

In this investigation, all flotation tests were conducted following a standard flotation procedure reported previously (10). Briefly, to start, a sample of the 500-gram minus 6.35mm coal was wet ground in a laboratory rod mill to prepare a product that was 95% passing 200 mesh (74 μ m) and then split into four parts. Flotation tests were conducted with a 2-liter Denver cell using 125 grams of coal at a pulp density of 6.25% solids at the natural pH of each coal. Distilled water was used in all experiments. The impeller speed of the flotation machine was 1200 rpm and the airflow rate was 4 liters per minute. In each flotation test, the pulp was first agitated in the flotation cell for 3 minutes, after which the collector was added and the pulp conditioned for an additional minute. MIBC frother [0.52 kg/t for Illinois No.6] was then added and the pulp was conditioned for an additional 3-minute period. After collecting the flotation concentrate for 5 minutes, the concentrate and tailing were filtered, dried, and weighed. The ash content of the sample was analyzed using a LECO MAC-400 Proximate Analyzer, the results of which were used to calculate combustible matter recovery.

Laboratory-oxidized coal was prepared by first wet grinding the coal to minus 200-mesh following our standard grinding procedures. The ground Illinois No. 6 coal was then oxidized in an oven for 90 hours at 105 °C and then stored for three days at room temperature. After undergoing the oxidation procedure, these coal samples were used for flotation tests with dodecane and some of THF surfactants. The effect of oxidizing the surface of a coal by heating is similar to using a coal of lower rank (11).

Dodecane and nonylbenzene were both used as the collector for comparative purposes.

Oil-water contact angles were measured on samples of coal that had been polished. For these measurements, the coal sample was immersed in water and oil droplets were placed on the coal surface for measurement with a goniometer. Contact angles were measured only for dodecane and THF-7.

Results and Discussion

Fine Coal Flotation

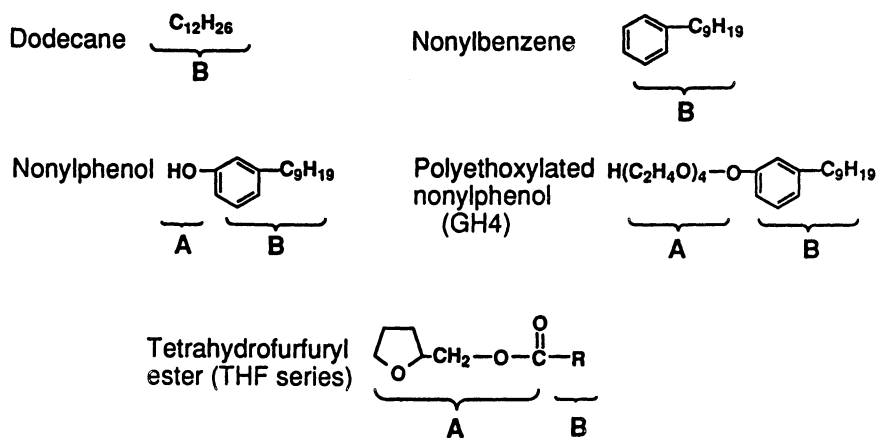
The flotation response of minus 200-mesh Illinois No.6 coal using dodecane, nonylbenzene and representative nonionic surfactants [THF-17en nonionic surfactant

as collector, together with that of nonylphenol, GH4 (polyethoxylated nonylphenol, $(C_9H_{19}-C_6H_4-O-(C_2H_4O)_4H)$) as the collector is presented in Figure 1. The upper part of Figure 1 gives the combustible matter recovery after 5 minutes of flotation as a function of reagent dosage in mol per tonne of coal and the lower plot presents the same data in terms of kg per tonne. Table 3 shows that the changes in the heteropolar nature of the collector molecules given in Figure 1 [A denotes the polar functional group and B the nonpolar hydrocarbon chain].

The results given in Figure 1 indicate that THF-17en is more effective than the other collectors for this coal. The plots also show that surfactants with an oxygenated group are generally more effective than those without one and that nonylbenzene is more effective than dodecane. This indicates that there might be two mechanisms for the interaction between the surfactants and coal surfaces. As we know, the surface of coal consists of inherently hydrophobic areas and also sites containing oxygenated moieties [such as carboxyl, carbonyl, phenolic and ester groups] (8,10,11,12). The first mechanism of interaction between the surfactants and the coal surface appears to be through the polar groups of the reagent interacting with the oxygenated functional groups on the coal surface by hydrogen bonding. The second mechanism involves the interaction of the nonpolar chain with the carbonaceous sites on the coal surface by dispersing water molecules from the coal surfaces. The interaction between an aliphatic chain and the coal surface is less pronounced than that of a benzene ring with the aromatic sites on the coal surface. This is due to strong Π -bonding interaction between the aromatic component of the coal matrix and the benzene ring of the reagent (8,9). Compared to dodecane, reagents containing a benzene ring, however, still have much better collecting ability. This indicates that although the benzene ring has stronger interaction with the aromatic coal surface than an aliphatic chain, the interaction is not as strong as that between the polar group of the reagents and the coal surface. This also suggests that hydrogen bonding of the oxygenated groups in the reagents is stronger than the van der Waals interaction of the aliphatic chains with the carbonaceous portions of the surface. It is for this reason that the THF series of reagents are much better collectors compared to dodecane for the flotation of Illinois No. 6 coal.

Figure 2 presents the results for the flotation of Illinois No.6 coal with the THF series of reagents as collector. These plots clearly show that at the same reagent dosage, all the nonionic surfactants are more effective than dodecane for the flotation of Illinois No.6 coal. For the surfactants containing an aliphatic chain, to obtain comparable combustible matter recovery, increasing the number of carbon atoms in the alkyl chain of the THF series of reagents lowers the required amount of reagent, and particularly so in comparison to dodecane. These plots also show that at the same reagent dosage, the combustible matter recovery obtained using aliphatic THF reagents is much higher than with those which contain a benzene ring. In surface chemistry, the benzene ring is equivalent to three methylene groups on an aliphatic chain (13). Since the reagents have the same polar functionality, the significant difference between these two subgroups of reagents is the benzene ring, which points to the benzene ring playing an important role in the interaction of the reagents with the coal surface.

Table 3. Molecular structure of the series of coal collectors, showing the polar group (A) and hydrocarbon chain (B) configuration.



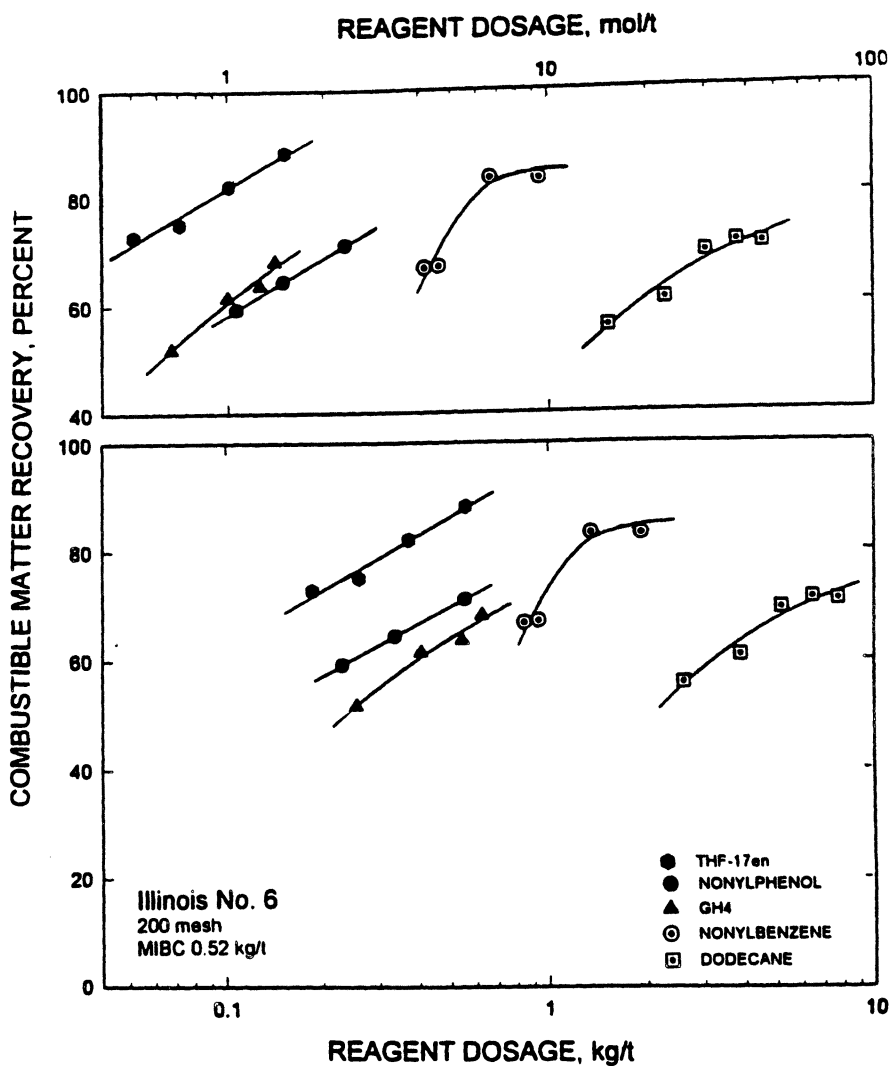


Figure 1. Comparison of the collecting ability of the nonionic THF-17en surfactant with that of dodecane, nonylphenol, nonylbenzene and GH4 for the flotation of 200-mesh Illinois No.6 coal. Reagent dosages in mol/t(upper figure) and kg/t(low figure).

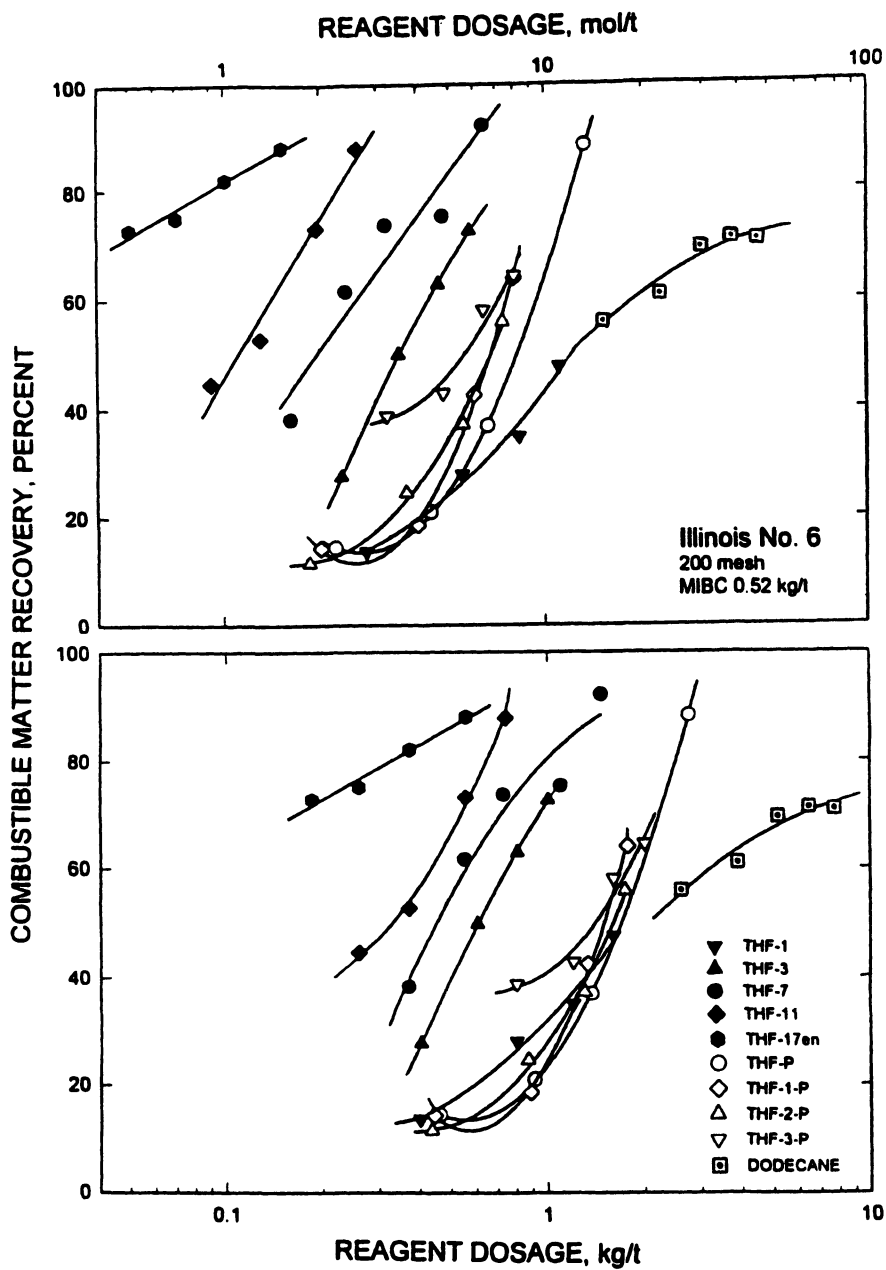


Figure 2. Comparison of the collecting ability of the nonionic THF surfactants with that of dodecane for the flotation of 200-mesh Illinois No.6 coal. Reagent dosages in mol/t(upper figure) and kg/t(lower figure).

Collection Mechanisms

In mineral flotation, most of the collectors are water-soluble, heteropolar organic compounds [soaps, sulfonates, amines, xanthates, etc.], and they impart hydrophobicity by adsorption at the mineral-water interface. The polar head group interacts with surface sites, thereby orienting the hydrocarbon chain of the adsorbed collector towards the water. [However, for the flotation of naturally hydrophobic molybdenite [MoS₂], a hydrocarbon oil is added to enhance its hydrophobicity--similar to coal flotation].

The insoluble oils used as collectors for the flotation of coal act by spreading over the hydrophobic coal surface. If the coal is somewhat oxidized, water molecules will tend to interact with the coal surface, reducing the oil/water contact angle, thereby reducing the tendency of the oil to spread over the coal surface. The spreading coefficient, $S_{o/w}$, for an oil phase displacing water on a solid surface is given by (14):

$$S_{o/w} = \gamma_{ow} (\cos \theta - 1)$$

Where γ_{ow} is the oil-water interfacial tension and θ is the contact angle measured through the oil phase. The spreading coefficient is determined by both the contact angle and the oil/water interfacial tension. A polar oil will tend to influence both parameters.

The oil/water contact angles, measured across the oil phase, were found to be 143° for dodecane and 81° for THF-7. The interfacial tension for the dodecane/water system is 51 mN/m and that for THF-7/water is assumed to be 10 mN/m. Thus, the spreading coefficient for dodecane in the dodecane/water/coal system is -91 and that for the THF-7/water/coal system is -10, indicating a much greater tendency for THF-7 than dodecane to spread on coal particles that are immersed in water.

In considering details of the action of the nonionic surfactants studied here, it should be noted that they are bifunctional: they possess **A**) oxygenated functional groups and **B**) a hydrocarbon chain. In the case of the THF series of reagents, the oxygenated functional groups themselves have two components: the tetrahydrofuran (a ring-structured saturated ether) and a methyl ester. Hydrogen bonding plays an important role in determining the physical properties of such compounds. Table 4 summarizes the aqueous solubility and the boiling point of various oxygenated four-carbon compounds. Considering the simple oxygenated compounds, all have significant solubility in the range of 8 parts per 100 parts water, which indicates strong hydrogen bonding with water. Except for diethyl ether [which cannot hydrogen bond with itself], the relatively high boiling points indicate internal hydrogen bonding of molecules with each other. Reducing the number of carbons by one in the case of butanol to propanol and ethyl methyl ketone to acetone leads to compounds that are completely miscible with water.

Furan, which is a ring-structured four-carbon unsaturated ether, is insoluble in water and has a boiling point similar to that of diethyl ether. The double bonds in the molecule strongly attract the electrons away from the oxygen, thereby eliminating its ability to hydrogen bond. On the other hand, tetrahydrofuran, which is simply comprised of a ring-structured saturated alkane, is miscible with water and boils at

66° C, both indicating strong hydrogen bonding capacity. Tetrahydrofurfuryl acetate, which is the basis of this series of reagents, is also miscible in water but boils at a high temperature, 194° C. The strong tendency of both the ether group in the tetrahydrofurfuryl molecule and the ester group to hydrogen bond must be responsible for hydrogen bonding action with polar sites on the coal surface. In order to reduce their solubility and to give the surfactants an oily character, hydrocarbon chains of various configurations were attached to the ester functional group on the THF series of reagents.

In Table 5, we can see that basicity of tetrahydrofurfuran is much greater than the other ethers (17). It is this basicity that contributes to hydrogen bonding of our reagents to the hydrophilic area of the lower rank/oxidized coal surfaces.

To see the effect of the chemical structure of the collectors on the flotation response of the coal, the reagents for 70% combustible matter recovery were taken from the results given in Figure 2. The reagent requirements expressed in terms of mol/tonne for Illinois No.6 coal are given in Figure 3. The effectiveness of dodecane and nonylbenzene are included for comparative purposes. In assessing collector interaction with Illinois No.6 coal, it should be noted that the surface of Illinois No.6 coal is comprised of aromatic carbonaceous sites plus oxygenated functional groups. This figure shows that the results exhibit distinctly different behavior, depending on whether they are aliphatic or aromatic.

In the case of the THF series of collectors, their interaction with the coal surface is strongly influenced by hydrogen bonding phenomena associated with the oxygen atoms in the tetrahydrofurfuryl ester part of the molecule. With Illinois No.6 coal, the most effective collectors are the aliphatic tetrahydrofurfuryl esters, with the aromatic collectors being less effective. Possibly, with the aromatic collectors, interaction of the benzene ring with the coal surface competes with hydrogen bonding at the other end of the collector molecule, and thereby affects the orientation of the molecules at the interface.

The attachment of the THF series of reagents to the coal surface can take place by three mechanisms:

- 1) Hydrogen bonding of oxygen atoms in the tetrahydrofurfuryl ester polar part of the molecule with oxygenated surface sites on the coal.
- 2) Hydrophobic bonding of the aliphatic hydrocarbon chain with the hydrophobic sites on the coal surface.
- 3) Pi-bonding of the benzene ring on the hydrocarbon chain of the collector to aromatic sites on the coal surface.

The interplay of these three mechanisms determines the effectiveness of the various THF reagents as a coal collector. For example, with low-rank coals that contain a large fraction of oxygen functional groups, such as Illinois No.6, attachment of the collector is through hydrogen bonding with the polar oxygen atoms of the collector. The collector chain will be oriented away from the coal surface, with the effectiveness of the collector increasing as the aliphatic hydrocarbon chain length is increased. Even though THF-1 has the shortest alkyl chain (only one CH₃ group) and is miscible

Table 4. Aqueous solubility and boiling points of some 4-carbon oxygenated compounds (15,16)

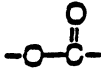

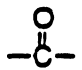
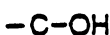
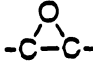


<u>FUNCTIONAL GROUP</u>	<u>REAGENT</u>	<u>SOLUBILITY, (parts per 100)</u>	<u>BOILING POINT °C</u>
	Ethyl acetate	8.5	77
	Diethyl ether	7.5	36
	Methyl ethyl ketone	24	80
	Butanol	7.4	118
	Butylene oxide	6	63
	Tetrahydrofuran	Miscible	66
	Furan	Insoluble	32
Tetrahydrofurfuryl acetate		Miscible	194

Table 5. Basicities of some saturated ethers in aqueous sulfuric acid

<u>Ether</u>	<u>pKa</u>
Dimethyl ether	-3.83±0.19
Diethyl ether	-3.59±0.10
Tetrahydrofuran	-2.08±0.18
Tetrahydropyran	-2.79±0.15
1,4-Dioxane	-2.92±0.12
Anisole	-6.54±0.02

SOURCE: Adapted from reference 17. Copyright 1960 American Chemical Society.

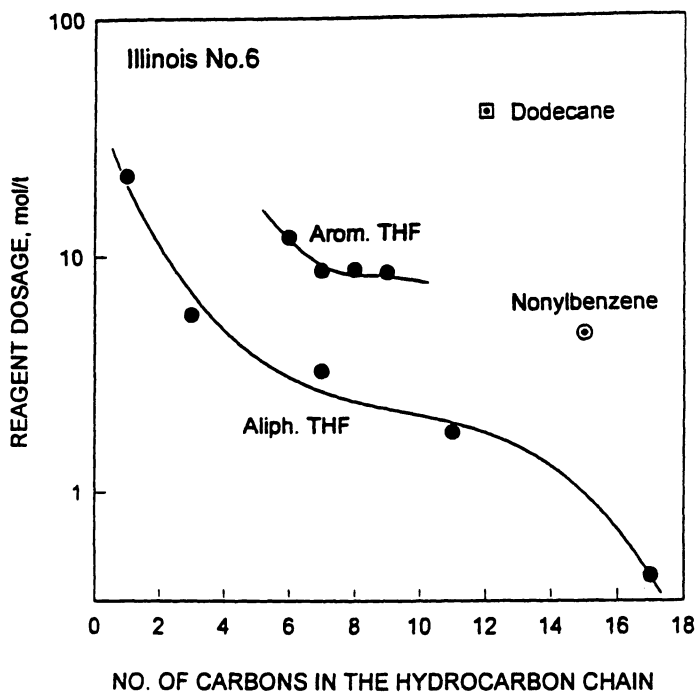


Figure 3. Comparison of the dosages required of the different reagents for the flotation of Illinois No.6 coal at 70% combustible matter recovery, showing the effect of chain structure of the tetrahydrofurfuryl esters on their effectiveness as collectors.

with water, it must adsorb through a hydrogen bonding mechanism that imparts some hydrophobicity to the coal surface. Figure 3 shows that it is about as effective as dodecane. The aromatic THF collectors as a group are less effective, probably because of competition of the benzene ring for the surface in relation to the oxygenated head group on the collector. This might lead to some orientation of the polar head of the collectors towards the water, possibly requiring a bilayer type of situation to achieve flotation response equivalent to that for aliphatic reagents. Without any oxygenated functional groups on the molecule, dodecane has limited affinity for a hydrophilic coal surface, thereby requiring a much larger dosage for equivalent flotation. On the other hand, the aromatic hydrocarbon nonylbenzene exhibits significantly greater collecting ability because of the interaction of the benzene ring with aromatic groups in the coal surface.

Figure 4 presents a plot of ash rejection as a function of the combustible matter recovery for the flotation of minus 200-mesh Illinois No.6 coal with the various collectors. The results show that similar selectivity in terms of ash rejection can be achieved with these nonionic surfactants as compared to dodecane.

Flotation of Oxidized Coals

Most coals are susceptible to oxidation through weathering, which results in the increased formation of oxygenated functional groups on the coal surface. This in turn results in a more hydrophilic surface and hence reduced flotability (10,18-23). As a result of the large number of hydrophilic oxygenated functional groups present in oxidized coal, it is expected that the THF series might be even more effective collectors as the coal is more heavily oxidized. To test this hypothesis, samples of Illinois No. 6 coal were oxidized under laboratory conditions described in the experimental procedure and then subjected to flotation tests using dodecane and some of THF surfactants as collectors. Figure 5 presents plots of the combustible matter recovery as a function of collector dosage for the flotation of lab-oxidized Illinois No.6 coal. The results show that the flotation recovery of combustible matter is very low when dodecane is used as the collector. However when THF reagents are used as the collector, for the same combustible matter recovery, a much lower dosage is required. These results indicate that the surfactants used have the ability to restore the flotability of oxidized coal. The decrease in flotation recovery at the higher dosages of THF-17en, for example, may be due to molecular orientation effects. The functional groups in the first layer being oriented to the surface sites and oriented towards the water as the collector coating thickens.

Summary and Conclusions

The flotation results of Illinois No. 6 show that the addition of oxygenated functional groups enhance the collecting ability of reagents. In particular, nonionic tetrahydrofurfuryl ester surfactants [THF series] are more effective collectors than the oily collector dodecane for both oxidized and unoxidized coals. For comparable combustible matter recovery, these non-ionic surfactants require substantially lower dosages than dodecane with similar flotation selectivity in terms of ash rejection and pyrite sulfur rejection. The reagents interact with coal surface through hydrogen bonding with oxygenated surface sites on the coal and through hydrophobic bonding

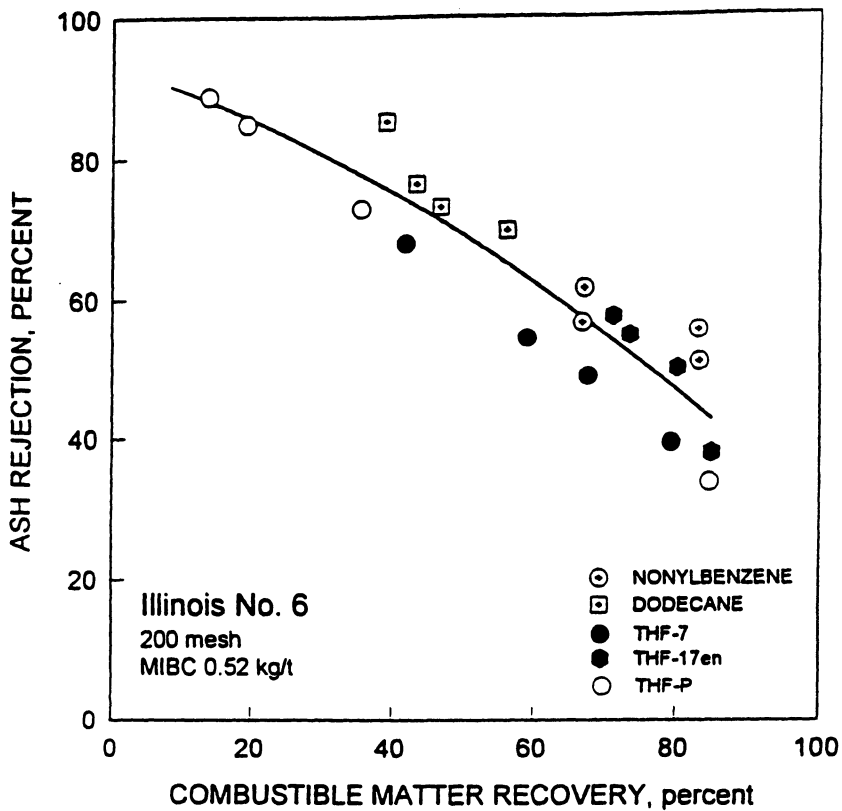


Figure 4. Ash rejection as a function of combustible matter recovery in the flotation of 200-mesh lab-oxidized Illinois No.6 coal with various collectors.

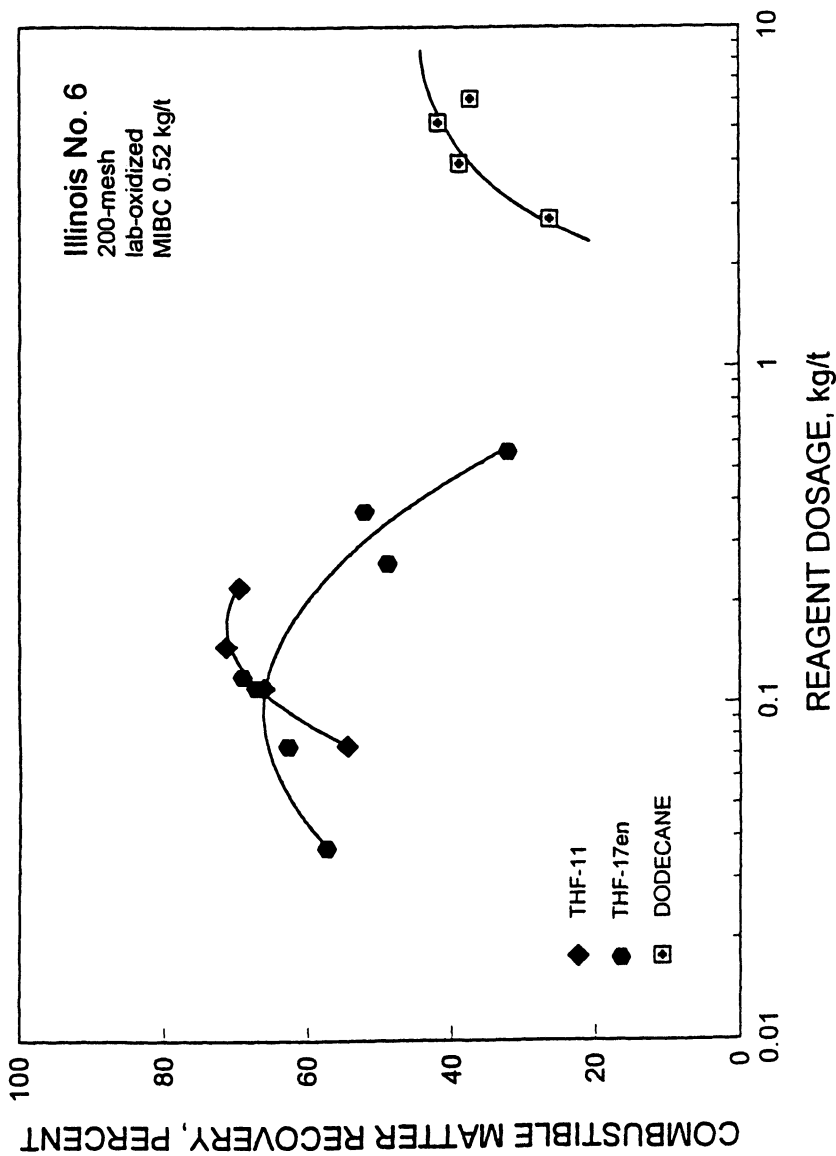


Figure 5. Comparison of the collecting ability of THF-17 and THF-11 with that of dodecane in the flotation of 200-mesh lab-oxidized Illinois No. 6 coal.

of the hydrocarbon chain of the collector with hydrophobic carbonaceous sites on the coal. The results suggest that the collector molecules containing a benzene ring are affected by the interaction of the benzene ring with aromatic rings in the coal surface. Experiments on the flotation of laboratory-oxidized coal show that, while it is difficult to float oxidized coal with dodecane, the THF series of reagents have the ability to restore the flotability of oxidized coal through their ability to hydrogen bond to oxygen functional groups on the coal surface.

References

1. Fuerstenau, D. W.; Diao, J.; *Surface Properties of Coal and Their Role in Coal Beneficiation*, Final Report, Project No. DE-FG22-86PC90507, March 1990.
2. Mataré, H. F.; *Energy: Facts and Future*, CRC Press, Inc.: 1989.
3. Hong, B. D.; *Mining Engineering*, **1988**, *50*, pp 49-120.
4. Mikula, R. J.; *Cleaning Low-Rank Coal*, Coal Preparation 5th Edition, Leonard III, J. W.; Hardinge, B. C., Eds.; SME: Littleton, CO, 1991; pp 957-965.
5. Aplan, F. F.; *Coal Flotation*, Flotation, A. M. Gaudin Memorial Volume, Fuerstenau, D. W. Ed.; AIME: New York, 1976, Vol. 2, pp 1235-1264.
6. Brown, D. J.; *Coal Flotation*, Froth Flotation, 50th Anniversary Volume, Fuerstenau, D. W., Ed.; AIME: New York, 1962, pp 518-538.
7. Laskowski, J. S.; Miller, J. D.; *Reagents in the Mineral Industry*, Jones, M. J.; Oblatt, R., Eds.; The Institute of Mining and Metallurgy, 1984, pp 145-154.
8. Fuerstenau, D. W.; Narayanan, K. S.; Diao, J. L.; Urbina, R. H.; *Assessing the Effect of Oxidation on the Wettability and Flotation Response*, 1987 International Conference on Coal Science, Mouligin, J. A., Ed.; Elsevier Science Publishers: Amsterdam, 1987, pp 475-478.
9. Harris, G. H.; Diao, J.; Fuerstenau, D. W.; *Coal Flotation with Nonionic Surfactant*, Preprint, SME Annual Meeting, Reno, Nevada, February, 1993.
10. Fuerstenau, D. W. et al.; *Coal Surface Control for Advanced Fine Coal Flotation*, Final Report, Project No. DE-AC22-88PC88878, March 1992.
11. Aplan, F. F.; *Industrial Practice of Fine Coal Processing*, Klimpel, R. R.; Luckie, P. T.; Eds.; SME: Littleton, CO, 1988, pp 99-111.
12. Harris, G. H.; Diao, J.; Fuerstenau, D. W.; *Coal Preparation*, **1995**, *16*, pp 135-147.
13. Shinoda, K.; Nakagawa, T.; Tamamushi, B.-I.; Isemura, T.; *Colloidal Surfactants*, Academic Press: New York, 1963.

14. Berg, J. C.; *Wettability*, Berg, J. C., Ed.; Marcel Dekker, Inc.: New York, 1993, pp148.
15. Lange, N. L.; *Handbook of Chemistry*, 10th Edition, McGraw-Hill Book Co.: New York, 1961.
16. Aldrich Catalog, *Handbook of Fine Chemicals*, 1994-1995.
17. Arnett, E. M.; Wu, C. Y.; *J. of the American Chemical Society*, **1960**, *82*, pp 4999-5000.
18. Fuerstenau, D. W.; Rosenbaum, J. M.; Laskowski, J. S.; *Colloids and Surfaces*, **1983**, *8*, pp 153-174.
19. Laskowski, J. S.; *High Efficiency Coal Preparation: An International Symposium*, Kawatra, S. K., Ed.; SME: Littleton, CO, 1995, pp 163-176.
20. Swann, P. D.; Allardice, D. J.; Evans, D. G.; *Fuel*, **1972**, *53*, pp 85-87.
21. Philips, K. M.; Glanville, J. D.; Wightman, J. P.; *Colloids and Surfaces*, **1987**, *21*, pp 1-8.
22. Gutierrez-Rodriguez, J. A.; Aplan, F. F.; *Colloids and Surfaces*, **1984**, *12*, pp 27-51.
23. Fuerstenau, D. W.; Yang, G. C. C.; Laskowski, J. S.; *Coal Preparation*, **1987**, *4*, pp 161-182.

Chapter 15

Flotation of PAH-Contaminated Dredged Sludge

Huib Mulleneers¹, Suzan Roubroeks¹, Harry Bruning¹, Wim Rulkens¹,
and Luuk Koopal²

¹ Sub-department of Environmental Technology, Bomenweg 2, 6703 HD,
Wageningen, Netherlands

² Laboratory for Physical Chemistry and Colloid Science, Dreijenplein 6, 6703 HB,
Wageningen Agricultural University, Wageningen, Netherlands

The applicability of dissolved air flotation to remediate contaminated sediments of "Overschie" (Rotterdam) and "Petrol Harbor" (Amsterdam) is studied. Several flotation reagents (Diesel Fuel, Montanol, Aerophine, Aerofroth) are applied to enhance the flotation efficiency. The physical chemical characteristics of the different particles in the presence of surfactants are investigated by contact angle measurements.

In the absence of reagents a one step batch flotation experiment removes around 85% of PAHs from both sludges. The remaining tailings contain 92% and 83% of the total mass for the Overschie and the Petrol Harbor sludge, respectively. When reagents are added the efficiency of the process decreases. The remaining tailings contain only 80 to 60% of the total mass, whereas the PAH removal is not substantially enhanced and in some experiments even dramatically reduced.

Surface water from rivers, lakes, ponds, canals, harbors etc., cover large areas of the Netherlands. Most of the water courses need regular dredging. Besides maintenance, environmental aspects can also be a reason for dredging. At certain sites the sediment is so polluted from discharge of harmful and toxic substances that it forms a threat to the aquatic ecosystem. It is estimated that between 1991 and 2010 around 590 million m³ will have to be dredged. From this amount 90 million m³ is dredged for environmental and 500 million m³ for nautical reasons. The total amount of slightly to heavily contaminated sediment from these dredge activities is 250 million m³ (1). Contaminated dredged sediments cannot be reused and have to be cleaned or stored. Deposition is the cheapest method, however, with the present quantities of dredge sludge only a temporarily solution. Therefore treatment, for example, in the form of sand reuse or microbial degradation of the harmful substances, is necessary. The goal

of the Dutch government for the year 2000 is treatment of 20% of contaminated dredged sediment. Remediation of sludge by classification is possible but the fraction below 63 μm , which is likely present in dredged sediments, may cause difficulties (2,3,4,5). Flotation techniques have proven to be a successful alternative remediation technique, also for the fine fractions (6-11).

Main pollutants in dredge sludge are Polycyclic Aromatic Hydrocarbons (PAHs), which arise from incomplete combustion of organic material (12). They are mostly present in the form of soot or coal-tar particles and their selective separation from sand by flotation resembles to some degree coal flotation (13,14).

Flotation techniques have been used in mineral processing for already almost 100 years (15,16). The success of the flotation process is described by the product of collision efficiency, the attachment efficiency of particles and bubbles and the stability of the bubble particle aggregate (17). In general, to enhance either or both the collision efficiency and the attachment efficiency and thereby the flotation efficiency, a "collector" is added. To enhance the stability efficiency "frothers" that produce a stable froth can be added (18-20). For inherently hydrophobic solids (coals, graphite, sulfur, molybdenite, talc), insoluble oil emulsified in water is often used as collector (21). The particle hydrophobicity is an important parameter for the attachment efficiency and therefore for the flotation efficiency itself (22-25). The hydrophobicity of the particles can be quantified by the contact angle.

In this paper we focus on the remediation of two different types of dredged sediments, both contaminated with PAHs. "Petrol Harbor" sludge is heavily contaminated, "Overschie" sludge is only slightly polluted. Earlier experiments have shown that soot particles can be selectively separated from sand by surfactant enhanced dissolved air flotation (10). Therefore the applicability of this technique, to remediate the contaminated sludges, is studied. The hydrophobicity of the different particles in the absence and presence of flotation reagents are investigated by contact angle measurements. The possibility of cleaning the two sludges with dissolved air flotation is tested in batch laboratory experiments.

Materials and Methods

Chemicals and water. The inorganic chemicals used were of analytical grade. The water used for the contact angle measurements was demineralized using a mixed bed ion exchanger. Ordinary (non chlorinated) tap water was used for the flotation experiments. The hardness of the tap water based on the total Mg^{2+} and Ca^{2+} concentration was 0.79 mmol/l.

Flotation Reagents. Aerophine 3418a, a commercial collector, is a 50% aqueous solution of sodium di-isobutylidithiophosphinate and Aerofroth 76a, a commercial frother, is a mixture of C4-C7 alcohols. Aerophine and Aerofroth were obtained from Cytec Industries B.V. Aerophine is suggested for the flotation of gold and silver and can be combined with Aerofroth, which is useful whenever a light yet lively frothing action is desired. Montanol 350, a fluid mixture of mainly higher alcohols and esters with additives was obtained from Hoechst A.G. (Germany). Montanol 350 is especially developed for the flotation of coal (<0,5 mm). Diesel Fuel" is a technical

grade oil composed mixture of C15-C25 alkane chains with additives. The use of an oil is also derived from coal flotation (21). In order to facilitate the dissolution of Diesel Fuel and Montanol, emulsions were prepared by blending 1 ml Diesel Fuel or 1 ml Montanol in 99 ml water with 1 ml of a 0.1 g/l Eumulgin ET 10 solution. Eumulgin ET 10 is a commercial ethoxylated fatty alcohol obtained from Henkel A.G. (Germany).

Sludges. Both sediments were obtained from "Oost baggerdepot" deposit in Den Helder, The Netherlands. Fractions with a particle size between 45-90 μm were studied. These fraction were obtained by sieving the wet sediments on Retsch sieves. "Overschie" sludge (Rotterdam), was slightly polluted with PAHs and oils. The "Petrol Harbor" sludge (Amsterdam) was heavily polluted. Both fractions contained mainly silica and organic matter. The organic matter was present as oil, coal-tar particles and natural organic matter (humus).

Contact Angles. The contact angles were determined on sessile drops using a contact angle microscope with goniometer (Erma Contact Angle Meter G-1). No special precautions were taken to control the humidity and vapor pressure. The contact angle on the organic fraction of the sludge was measured on pellets of this material, pressed at 14000 kg/m^2 . The sand fraction could not be pressed into stable pellets and therefore, like in a former study, clean oxidized silicon wafer strips from Wacker chemitronic (Germany) were used (10).

Pre-isolation of the organic matter from the two sludges, for the production of pellets for the contact angle measurements, was achieved by sieving and upflow separation. The effect of size and therefore weight on the upflow separation was minimized by sieving the 45-90 μm fractions of the sludges into two fractions of 45-63 μm and 63-90 μm . From the separated fractions the organic matter was isolated by upflow separation in tap water. The used upstream velocity to separate the organic particles of the 45-63 μm fraction was 0.105 cm/s and for the 63-90 μm fraction it was 0.115 cm/s . The obtained organic fractions (45-63 μm and 63-90 μm) were finally mixed together to obtain one fraction again (45-90 μm). The organic matter content of the obtained "organic fraction" of Overschie was 58.5%, and that of the "organic fraction" of Petrol Harbor 68.5%.

Before every experiment the silicon wafer strips were washed with acetone and water followed by a 30 minutes treatment with ozone/UV. After the experiments the strips were cleaned by thermal oxidation or chromic acid. The organic pellets were used as pressed and could not be cleaned by addition of chemicals neither by oxidation.

Flotation tests. For the flotation experiments a modified Hallimond tube (see Figure 1) was used. The tube has a narrow part near the bottom of the cell to decrease the turbulence in the middle part. The top part of the tube makes an angle of 60° with lower part to assure a better settling of entrained particles. Before entering the sludge sample in the Hallimond tube, it was conditioned in a beaker by stirring approximately 6 grams dry matter (6 g d.m.) in 40 ml of solution for 30 minutes. This conditioning step was done for all experiments, i.e. also when no flotation

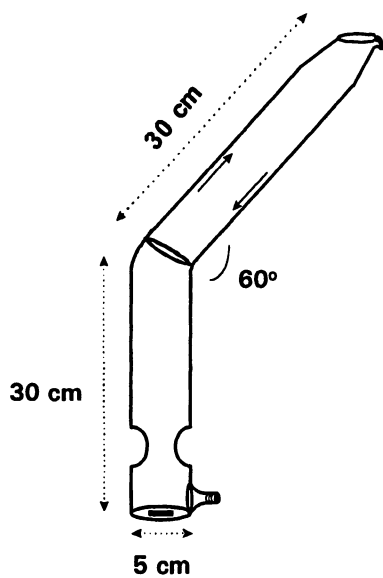


Figure 1. Hallimond type flotation tube

reagents were added. Diesel Fuel and Montanol additions were 50 μl per 6 g d.m.. The applied Aerophine dose was 43 μl per 6 g d.m. and the Aerofroth dose is 86 μl per 6 g d.m. After conditioning the slurry was transferred into the flotation tube and the tube was filled up with water. The flotation was carried out by feeding pressurized water with dissolved air (7 bar) into the cell (100 ml/min) for 9 minutes. The floated particles were collected in a buchner funnel and dried at 50° C. The tailing and the floated fraction were both analyzed for dry matter and organic matter, the tailings were also analyzed for PAH concentration.

Organic Matter analysis. Approximately 0.3 grams of dried material (50° C) were sampled and oxidized in a oven where the organic matter is oxidized at 550° C for 18 hours. The organic matter content was determined by the difference in weight between the dried and oxidized matter.

Oil analysis. Approximately 15 grams of dried (50° C) sludge was extracted with an acetone/hexane mixture. The hexane was separated from the acetone and purified with Florisil and sodium sulfate. The oil concentration in the purified hexane was analyzed on a Hewlett Packard 5890 gas chromatograph, with a simdist column of 10 m and a diameter of 32 mm. After injection of 5 μl hexane the temperature was kept constant (40° C) for the first 5 minutes. After this period it was linearly increased to 300° C in 25 minutes. Finally the temperature was stabilized at 300° C for the last 6 minutes. The oils were detected with a Flame Ionization Detector (FID). The total oil concentration was determined by a manual integration method.

PAHs analysis. The samples were dried (50° C) and extracted with a 99% 1-methyl 2-pyrrolidinone solution. The concentrations of 16 PAHs selected by the Environmental Protection Agency (USA) (16 EPA-PAHs) were determined in the sample extracts. The separation of the 16 EPA-PAHs was achieved by using a HPLC column with a length of 250 mm and a diameter of 4.6 mm, filled with Vydac 201TP54, a C18 reversed phase matrix, and eluted with a mixture of acetonitrile and degassed water (flow rate : 1.0 ml/min). The composition of the mobile phase was changed during elution: first a 50/50% (v/v) mixture of acetonitrile concentration and water for 5 minutes subsequently, the acetonitrile was linearly increased to 100% in 15 minutes, after which the acetonitrile concentration was kept at 100% for 19 minutes. The 16 EPA-PAHs were measured with a photodiode-array detector and identified in the chromatograms by manual comparison of the sample spectra with that of the 16 standard EPA-PAHs.

Results

Sludge composition. The PAH concentration, organic matter content and oil concentration of the two sludge samples are presented in table I.

Table I clearly shows that the Petrol Harbor sludge is highly contaminated with PAHs and oil, and Overschie relatively weakly. However, the organic content of both samples is comparable and much higher than the PAHs and oil content, indicating that also a lot of humus type substances are present.

Table I. PAH-, Oil concentration and Organic Matter content of Overschie and Petrol Harbor sludge.

	Overschie	Petrol harbor
PAH concentration (mg/kg d.m.)	24	1035
Organic Matter percentage (w/w)	6.0	6.6
Oil concentration (mg/kg d.m.)	46	> 1000

Contact Angles. The used droplets have a diameter of approximately 2.5 mm. The blank wetting solution contains 0.01 M NaCl and has a pH of 6. In the case of Diesel Fuel, Montanol and Aerofroth the blank solution is saturated with these fluids at 25° C. Aerophine concentrations range from 2 µl/l to 2 ml/l.

The results of the contact angle measurements are shown in table II.

Table II. Contact angles on silica pellets and organic pellets of Overschie and Petrol Harbor sludge

	silica	organic pellets Overschie	organic pellets Petrol Harbor
Blank	4	79	90
Diesel Fuel	18	80	90
Montanol	26	57	76
Aerophine	7	80	92
Aerofroth	9	57	69

The contact angles reported in table II are averages of 3 measurements. The standard error in the measurements is about 3°. However, it should be noted that the contact angle on the organic pellets are difficult to measure because the pellets are slightly porous and the droplets slowly absorb in the organic pellets absorb in the pellets. For Overschie pellets the absorption becomes noticeable after 30 seconds and for the Petrol Harbor after 60 seconds.

The contact angle of the blank solution on silica is 4°, showing that pure silica is wetted very well. The values of 79° and 90° for respectively the Overschie and Petrol Harbor samples indicate that the organic particles are fairly hydrophobic. When saturated solutions of Diesel Fuel are used the contact angle on the silica plates raises to 18° but those on the organic pellets remain the same within the experimental error. The effect of Aerophine over the studied concentration range is the same for all concentrations. The contact angle on silica is slightly enlarged to 7°. The contact angle on the organic pellets of Overschie and Petrol Harbor are hardly effected and the average values are 80 and 92° respectively. The saturated solution of Montanol decreases the contact angle on the organic pellets substantially, for the Overschie the angle is 57° and for Petrol Harbor it is 76°. To the contrary, Montanol increases the

contact angle on silica is considerably to 26°. These values indicate that Montanol is probably a very poor flotation reagent for the present system. Saturated solutions of Aerofroth show also a decrease of the contact angle on both the Overschie pellets (57°) as well as on the Petrol Harbor pellets (69°). However, the contact angle on the silica plates is only slightly increased to 9° by the Aerofroth solution.

Because of the porosity of the organic pellets, contact angles larger than 80° or 90°, like the blank solutions, are hardly possible. Besides that the contact angle of the blank solutions on the silicon wafers is extremely small. Therefore, only the negative influence of reagents, by which the contact angle on organic pellets decreases and those on silicon wafers increases, can be notified.

Flotation Tests. The efficiency of the flotation process is determined by the removal of PAHs from the sludges and the selectivity of this removal. This means that the PAH concentration in the tailings has to be very low and that the total mass of the tailing should be large. The final aim of the process is that the tailings can be reused as soil additive or building material and that the small but highly contaminated floated fraction can be treated by incineration.

To determine the flotation efficiency, the total dry matter (d.m.) and the organic matter of the floated fraction and tailings are measured. The PAH concentration in the tailings is measured too.

Overschie. The results of the flotation tests with the dredged sediment of Overschie are presented in Figures 2 and 3. The original sludge contains 24 mg/kg d.m. PAHs and of course 100% dry matter. When no flotation reagents are added the tailings contain 92% of the total mass and 3.6 mg/kg d.m. PAHs which is 15% of the total PAHs concentration. Addition of the reagents, Diesel Fuel, Montanol or the combination of Diesel Fuel and Montanol to the solution reduce the flotation efficiency. The removal of PAHs in the experiment with Diesel Fuel (residual PAHs are 3.4 mg/kg d.m.) is slightly better than with the blank but the dry matter content is only 70%. In the experiments with Montanol and Montanol combined with Diesel Fuel the residual PAHs concentrations in the tailings are 5.4 and 9.0 mg/kg d.m.. Both values are higher than in the experiment without reagents and also the percentage of dry mass of the tailings are smaller (60 and 70% respectively). Therefore, the efficiency is considerably decreased due to the addition of these reagents. The experiment with the combination of Aerophine and Aerofroth shows a tailing that contains 83% of the total dry mass and a PAHs concentration of 3.3 mg/kg d.m.. This means these experiments were more successful than the experiments with Diesel Fuel and/or Montanol. In comparison to the tests without reagent the PAH removal is slightly better but the dry mass in the tailings is lower.

The poor efficiency of the experiments with reagents is reflected in the low organic matter content of the floated material in relation to that of the experiment without reagents. The organic matter content of the floated material in absence of a reagent is 30% (Figure 3), whereas these values range from 12-14% for the experiments with Diesel Fuel and/or Montanol. The combination of Aerophine/Aerofroth gives, with 18% d.m., only a slightly better result and is still considerably lower than the 30% of the tests without reagent. The organic matter

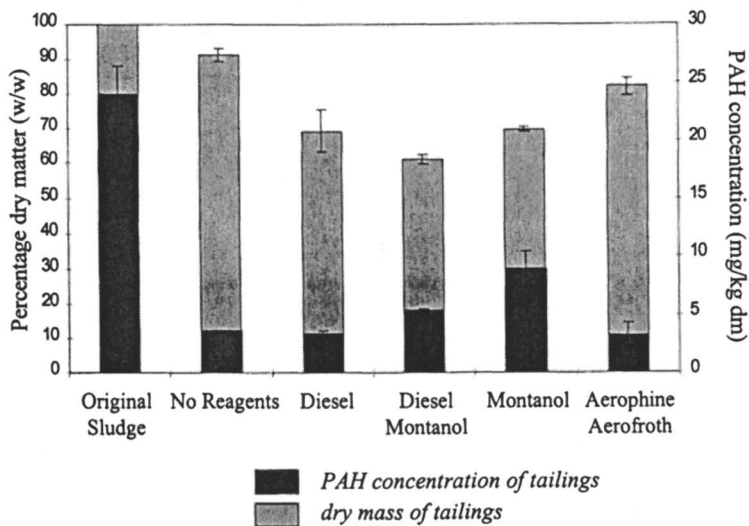


Figure 2. PAH concentration and dry matter content of the tailings and the original Overschie sludge

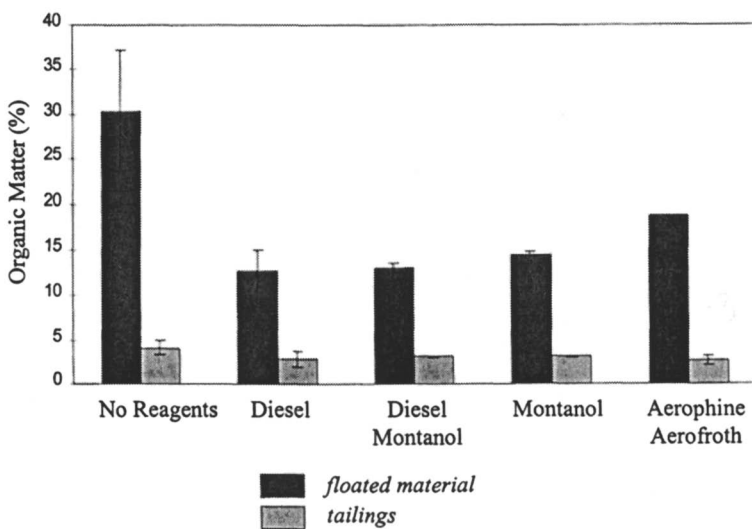


Figure 3. Organic matter content of both the tailings and floated material of Overschie sludge.

content of the tailing of the experiment without reagent is with 4% slightly higher than the organic matter contents (2 to 3%) of the experiments in which a reagent was added. However, as mentioned before the PAH concentration in the tailings are similar or higher. This suggests that there is no direct correlation between the PAH concentration of the tailings and the organic matter content. This is due to the fact that the organic matter is build up from coal-tar particles and natural organic matter. The coal-tar particles that contain the PAHs are probably floated more selectively than the natural organic matter.

Petrol Harbor. The results of the flotation experiments with this sludge are presented in Figure 4 and 5. The original sludge contained 1035 mg/kg d.m PAHs. Without flotation reagents the dry weight of the non-floated tailing is 83% of the total d.m. and it contains 148 mg/kg d.m. PAHs, which is a reduction of 86%. Adding Diesel Fuel decreases the efficiency. The percentage dry matter in the tailing is only 78% and the PAH concentration as much as 280 mg/kg d.m. This shows that only 73% of the PAHs is removed. Addition of Montanol and Diesel Fuel + Montanol leads to similar PAH removal as with the blank solution but also larger amounts of dry material (~ 40%) are removed, i.e. the process is less selective than in the absence of an reagent. The flotation in the presence of Aerophine and Aerofroth show a similar behavior, a good PAH removal (87%), but with a tailing of 70% d.m only a modest selectivity.

Similar as with the Overschie sludge the relatively poor selectivity in the presence of Montanol, Diesel Fuel + Montanol, or Aerophine + Aerofroth is reflected in the low organic matter content, ranging from 8 to 14% of the floated part as compared with to the 22% observed in the experiments without reagents.

Discussion and Conclusion

For both sediments the tests without chemicals were the most successful. With Aerophine and Aerofroth the PAHs removal could be increased but the selectivity is decreased. The effect of Diesel Fuel and Montanol on the flotation results was not the same for both sludges. In both sludges the efficiency of the flotation test was decreased but the poorest results in the experiments with the Overschie sludge was obtained when only Montanol was added and for the Petrol Harbor sludge when only Diesel Fuel was applied.

The fact that the applied chemicals do not enhance the flotation efficiency compares rather well with the results obtained for the contact angles. Without reagents the difference between the contact angle on the organic pellets and that on the silica plates was larger than with the reagents present. Especially the frother Montanol reduced the difference in contact angle substantially and this phenomenon is clearly reflected in the poor selectivity of the flotation experiments with Montanol. Also the other frother Aerofroth decreased the contact angle of the organic pellets. Therefore frothers should not be used in the conditioning step but should only be applied to the dissolved air stream to create a froth in the reactor.

That the PAH containing fraction of the sludges floats naturally is probably also due to the initial oil concentration in the sludges. Especially in the Petrol Harbor

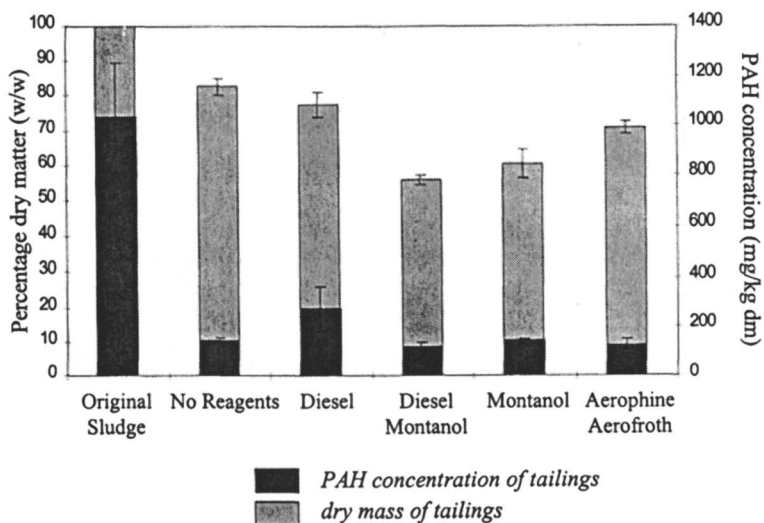


Figure 4. PAH concentration and dry matter content of the tailings and the original Petrol Harbor Sludge.

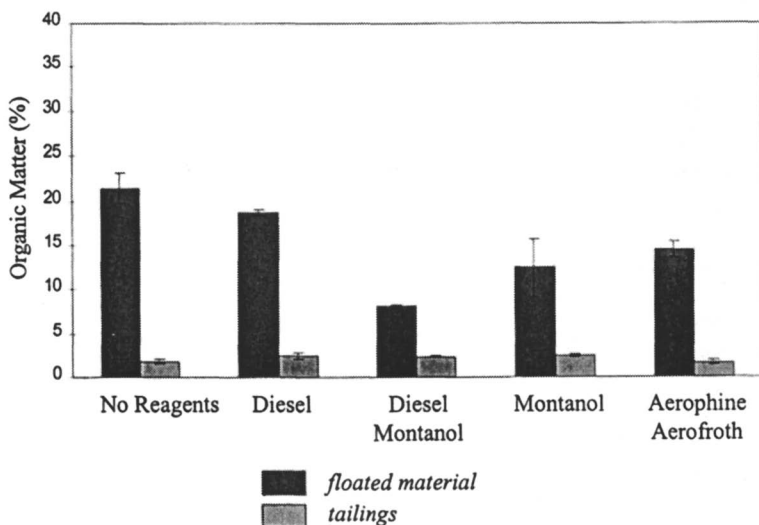


Figure 5. Organic matter content of both the tailing and floated material of Petrol Harbor sludge.

sludge the influence of the collector qualities of the oil makes it redundant to add an extra collector in the form of Diesel Fuel.

Acknowledgments

We like to thank Jowan Kelderman for the performance of the oil analyses.

References

1. Hofstra, M.A., in *POSW remediation of contaminated soil '95*; P.B. Roeters and G.N.M. Stokman (Eds.); Hageman Verpakkers: Zoetermeer (NL), 1995, pp.11-32.
2. Cuypers, M.P.; Grotenhuis, J.T.C. and Rulkens, W.H., *Wat. Sci. Tech.*, **1998**, *37*, 157-164.
3. Werther, J. and Wilichowski, M., in *Contaminated Soil '90*, F. Arendt, M. Hinsveld, W.J. van den Brink (Eds.); Kluwer Academic Publishers: Dordrecht (NL), Vol.II, 1990, pp. 907-921.
4. Feenstra, L.; Joziassse, J. and Pruijn, M., in *Contaminated Soil '95*; W.J. van den Brink, R. Bosman, F. Arendt (Eds.); Kluwer Academic Publishers: Dordrecht (NL), Vol II, 1995, pp.1123-1133.
5. Rulkens, W.H. and Bruning, H., in *Contaminated soil '95*, W.J. van den Brink, R. Bosman, F. Arendt (Eds.); Kluwer Academic Publishers: Dordrecht (NL), Vol II, 1995, pp. 761-773.
6. Wevers, H.H.A.G. and Lindenberg, J., in *POSW remediation of contaminated soil '95*; P.B. Roeters and G.N.M. Stokman (Eds.); Hageman Verpakkers: Zoetermeer (NL), 1995, pp.133-134.
7. Wilichowski, M. and Werther, J., *Chem-Ing-Tech.*, **1995**, *67*, 760-763.
8. Clifford, S.R., *Minerals and Metallurgic Processing*, **1993**, Nov. 195-199.
9. Bilz, E. and Weigel, H., *Umwelt*, **1994**, *24*, 445 - 447.
10. Mulleneers, H.A.E.; Koopal, L.K.; Swinkels, G.C.C.; Bruning, H.; and Rulkens W.H., *Colloid and Surfaces, A*; **1998**, in press
11. Venghaus, T. and Werther, J., *Advances in Environmental Research*, **1998**, *2*, 77-91.
12. Engbertsen, J.F.J. and de Groot, A.E., *Inleiding in de bio-organische chemie*; Pudoc: Wageningen (NL), 1988.
13. Peng, F.F., *Energy and Fuels*, **1996**, *10*, 6, 1202-1207
14. Osborn, D.G., *Coal Preperation Technology*; Graham @ Trotman Limited: London (UK), 1988, Vol.1.
15. Jameson, G.J., in *The Scientific Basis of Flotation*; K.J; Ives (Ed.), Martinus Nijhoff Publishers: The Hague (NL), 1984; pp.193-229.
16. Kitchener, J.A., in *The Scientific Basis of Flotation*; K.J. Ives (Ed.), Martinus Nijhoff Publishers: The Hague (NL), 1984; pp. 3-53.
17. Derjaguin, B.V. and Dukhin, S.S., *Bull. Inst. Min. Metall.*, **1961**, *70*, 221
18. Leja, J., *Surface Chemistry of Froth Flotation*; Plenum Press: New York (USA), 1982.
19. Jones, M.J. and Oblatt, R., *Reagents in the Mineral Industry*; Conference

- Proceedings from Reagents in the minerals industry: Rome, Italy, 18-21 Sept. 1984.
20. Crozier, R.D., *Flotation*; Pergamon Press: Oxford (UK), 1992
 21. Laskowski, J.S., in *Colloid Chemistry in Mineral Processing*; J.S. Laskowski and J. Ralston (Eds); Elsevier Science Publishers B.V: Amsterdam (NL), 1992; pp. 361-394
 22. Crawford, R. and Ralston J., *Int. J. Miner. Process.*, **1988**, *23*, 1-24.
 23. Subrahmanyam, C.A. Prestidge and J. Ralston, *Min. Eng.*, **1996**, *9*, 727-741.
 24. Fuerstenau, D.W., and Healy, T.W., in *Adsorptive bubble separation techniques*; R. Lemlich (Ed.); Academic Press: London (UK), 1972; pp. 91-131.
 25. Fuerstenau, D.W., *Soc. Min. Eng. AIME*, **1957**, *208*, 1365.

Chapter 16

Studies of Adsorption and Aggregation of Cationic Surfactants on Silica Surfaces Using EPR

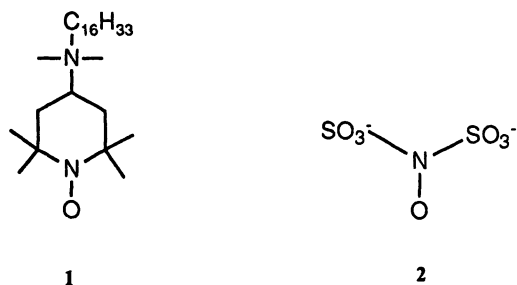
Martin G. Bakker, Gregory L. Turner, John Matthews, and Kunliang Zhang

Department of Chemistry, The University of Alabama,
Tuscaloosa, AL 35487-0336

The results of EPR experiments utilizing spin-labeled hexadecyl trimethyl ammonium bromide (HTAB*) to study adsorption of hexadecyltrimethylammonium bromide (HTAB) from aqueous solution onto silica, titanium dioxide and alumina surfaces are reported. The results are analyzed as evidence of a strong binding site that is present on silica surfaces. Preliminary results of the use of nitrosodisulfonate radical to study binding of counterions to HTAB surfactant aggregates is also reported.

Adsorption of surfactants onto the surface of mineral oxide particles has been used for many years in particles separation processes, primarily in the mining industry where flotation is commonly used to separate minerals from waste rock. Recently there has also been some interest in using shear flocculation for recovery and separation of fine mineral particles (1,2). In the last decade or so it has become clear that surfactants adsorbed onto particle surfaces can also bind hydrophobic molecules in a process called adsolubilization (3-5). This phenomenon has been used as the basis for admicellar chromatography (6) and as a medium in which chemical reactions such as polymerizations can be performed (7,8). There is also interest in the possible natural occurrence of such phenomena where adsorption of manmade and naturally occurring surfactants on colloidal mineral oxide surfaces might serve to enhance the solubility of pollutants (9) possibly giving rise to chromatographic effects, and cause pollutants to be sequestered during surfactant enhanced subsurface remediation. The behavior and properties of surfactants adsorbed on oxide surfaces depend upon how the surfactants are adsorbed on a surface. It is clear that above a certain critical concentration a two dimensional condensation occurs to give rise to surfactant aggregates which have properties similar to micelles. The structure of these aggregates is a matter of some controversy with a number of alternative structures being suggested. These include hemimicelles (10), admicelles (11), and small aggregates (12). At higher surfactant concentrations these aggregates merge into monolayers, bilayers and multilayers.

To study structure on the small length scale of the various aggregate forms suggested requires a spectroscopic technique or one of the newer microscopies such as Atomic Force Microscopy. The low solution concentration encountered in most surfactant/oxide particle systems places considerable demands on the sensitivity of spectroscopic techniques and so most studies have made use of the addition of a probe molecule to the system. This probe is then interrogated using luminescence (13-16) or Electron Paramagnetic Resonance (EPR) (2,17,18) spectroscopies. Our interest has been in using surfactants incorporating a stable free radical as a spin probe which can be monitored by EPR Spectroscopy and so report back on the molecular environment. This report summarizes some of our recent work using a spin-labeled analog of the quaternary ammonium surfactant hexadecyl trimethyl ammonium bromide (HTAB) in which one of the methyl groups has been replaced by the TEMPO radical group to give an EPR active probe molecule (1). Included also is an account of some preliminary work using the free radical nitrosodisulfonate (2) to study counterion binding around HTAB aggregates.



For brevity in the remainder of this contribution spin-labeled HTAB (1) will be abbreviated HTAB* and the regular form will be abbreviated HTAB. In previous reports (2,19) we have observed a number of different EPR signals due to HTAB* in different environments. The four types of EPR spectra observed are shown in a simulated form in Figure 1. Figure 1a shows HTAB* rotating very slowly. The peaks are broad and asymmetric. This is because the EPR spectrum for a single molecule depends upon the angle between the molecule and the external magnetic field. What is observed is an average of all the various orientations. As the molecule tumbles more rapidly spectral averaging begins to occur and the EPR spectrum begins to resemble Figure 1b which corresponds to the spectrum observed for HTAB* in a micellar aggregate of HTAB. As the tumbling becomes still more rapid the peaks narrow further until they are almost of equal height. This corresponds to the EPR spectrum of Figure 1c which is that of HTAB* in water below CMC. Note that the spectra in Figure 1 were generated for equal HTAB* concentration, then magnified as indicated on the figure. The sharper the line the more sensitive the EPR spectrometer becomes. The last case to be considered is for aggregates of HTAB*. As the number of HTAB* molecules in a surfactant aggregate increases the observed effect is to increase the linewidth of the experimental spectrum. This results primarily from Heisenberg spin exchange when two of the spin-labeled molecules collide with exchange of the spin of the electrons on the two molecules (if electrons could carry

name tags then this could be visualized as electrons hopping from one HTAB* to another). In the limit of an aggregate made up entirely of HTAB* a single extremely broad line is produced. This is shown in Figure 1d. The spectra in Figure 1b and 1d correspond to two limits of a continuum; at low ratios of HTAB* to HTAB in surfactant aggregates the spectra will be that of Figure 1b. As the ratio of HTAB* to HTAB rises the widths of the three lines will increase until the lines merge to form one line, which can broaden still further to give Figure 1d. It should be noted that because this line is so broad in comparison to the other components Figure 1d is plotted at a greatly enhanced vertical scale. As corollaries: when this type of spectrum is apparent to an observer the majority of the HTAB* is then in this form. Second, a substantial fraction of the spin label can be in this form but the intensity of the spectrum may be so low as to make observation very difficult.

Experimental

Materials. HTAB* was prepared according to the procedure of Kwan *et al.*(20). The nitrosodisulfonate was purchased from Aldrich as the dipotassium salt and used without further purification. The paramagnetic broadener used ($\text{Cr}(\text{maltolate})_3$) was prepared by the procedure of Burchfield *et al.*(21) Purity was checked by IR. HTAB was purchased from Aldrich. Surface tension studies did not show any minimum and so the surfactant was used without further purification. The Aerosil 200, Sipernat 50 and Sipernat 22 silicas were obtained from Degussa as was the P25 titanium dioxide. Aerosil 200 is reported to have a surface area of 200 m^2/g . We had previously determined that Aerosil 200 required 2 days in water to reach pH equilibrium and so all samples were allowed to equilibrate with stirring for this length of time with addition of acid or base to adjust the pH as required during this period. Unless stated otherwise all silica samples are Aerosil 200, and were adjusted to pH=7. **Equipment.** The EPR spectra were run on a Varian E-109 bridge with the magnetic field generated by an IBM 10" magnet controlled by a Bruker field controller. The spectrometer was controlled by a MacIntosh II computer which allowed repeated magnetic field scans to be averaged to improve the signal to noise ratio. All samples were run in 0.3 mm flat cells which were placed within a TE-102 microwave cavity. A number of spectra were run on a Bruker 200 EPR spectrometer using similar flat cells and cavity geometry.

Spectrum Analysis. Experimental spectra were simulated and fitted on MacIntosh PowerPC and IBM compatible computers. Two programs were used. To analyze the spectra produced by rapidly rotating spin labels an isotropic simulation program (FULL_ISO_FIT) was written in FORTRAN. This program allows isotropic spectra to be calculated, including calculation of the spin Hamiltonian using a second order perturbation (which is necessary for the nitrogen hyperfine coupling constant). The program will also allow different linewidths to be used for different M_I components, allowing for simulation of spectra in which the spin-label rotation is beginning to slow. The program includes a Simplex fitting algorithm using FORTRAN code directly from Press *et al.*(22) which allows all the parameters to be optimized. For the spin labeled HTAB used in this study there is unresolved hyperfine coupling, which can affect the shape of each line. These coupling constants are available for

HTAB* in methanol solution, but not for this molecule in a surfactant aggregate where changes in molecular geometry might be expected. After considerable data fitting we arrived on a set of parameters for the hydrogen hyperfine coupling which gave reasonable agreement with the observed lineshape. These were 0.452 G (6 hydrogens), 0.305 G (2 H) and 0.486 G (2 H). These parameters were used throughout the data fitting and were not allowed to vary in any of the optimization steps. The nitrogen hyperfine coupling (the "distance" between the three lines) was generally allowed to vary during optimization.

The slowly rotating spectral component was simulated using a version of a program written by Schneider and Freed (23) which was modified to run on Power Macintosh computers and to use a simplex algorithm to allow optimization of the parameters.

Spectra were analyzed by a process of iterative subtraction and fitting of each component separately. E.g. an initial estimate of the anisotropic (slowly rotating) component was made, and the spectrum simulated using the Schneider and Freed program. This simulated spectrum was then subtracted from the experimental spectrum. The resulting spectrum then gave an estimate of the isotropic (rapidly rotating) components of the spectrum. These were then simulated and fitted using FULL_ISO_FIT. This fitted spectrum was then subtracted from the experimental spectrum to give a better estimate of the anisotropic component, which was then simulated and fitted using the Schneider and Freed program etc. This cycle was continued until self-consistency was reached. At this point the experimental and the two simulated spectra were read into Excel and the contribution of the two components was determined by minimizing the sum of the square of the differences between the experimental and simulated spectra (i.e. "a least squares fit"). The relative amount of each spectral component was then determined by simulating just that component and then performing a double integration.

The EPR signal due to the quartz defect center in the sample cell was accounted for by subtracting the EPR spectrum from the empty cell. In cases where this did not give an appropriate correction, the section of the experimental spectrum masked by the quartz defect was not included in the fitting procedures.

Results for Hexadecyltrimethylammonium Binding on Silica

Figure 2a shows the EPR spectrum from a mixture of HTAB* and HTAB at a 1:50 ratio in an aqueous dispersion of Aerosil 200. The peak marked with a star is due to a paramagnetic quartz defect in the sample cell. The three peaks due to the HTAB* can be clearly seen. The unequal heights and linewidths are consistent with incorporation of HTAB* into surfactant aggregates formed on the silica surface. Because of the low concentration of HTAB* (*ca.* 5×10^{-6} M) the spectrum of HTAB* in solution is too weak to be observed. Figure 2b shows a simulation to the experimental spectrum generated using three lines of variable linewidth and height, but with a lineshape determined by the hydrogen hyperfine coupling constants given in the experimental section. The fit appears reasonable, however the integrated areas of the three peaks are very different which is not physically reasonable. A complete fit constraining the peaks to be of equal integrated area does not appear to be nearly in such good

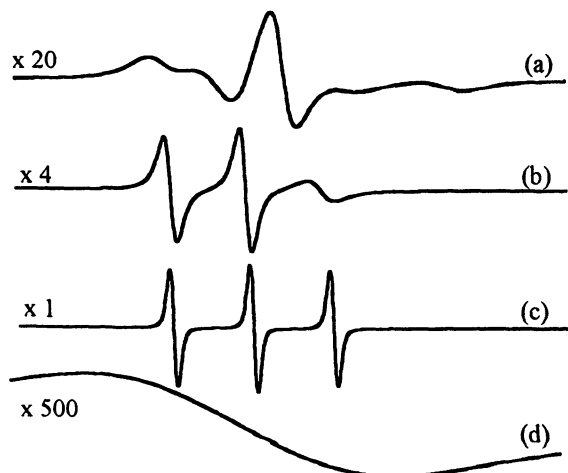


Figure 1. Simulated EPR Spectra of HTAB*. Multiplication factors as indicated. (a) slowly rotating HTAB* (b) in micellar aggregates of HTAB (c) in solution (d) in micellar aggregates of HTAB*

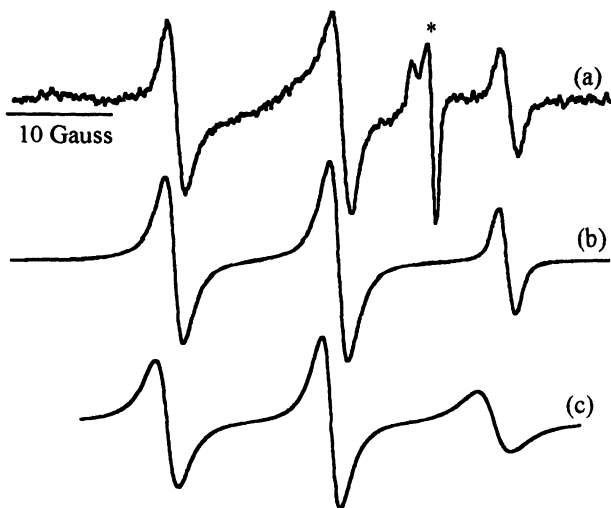


Figure 2. Experimental and Simulated EPR Spectra from HTAB and HTAB* adsorbed on Silica (a) experimental (b) simulation using three Lorentzian lines of variable height and linewidth (c) one species isotropic simulation

agreement as can be seen in Figure 2c. A check using the Schneider and Freed program gives the equivalent spectrum, and cross-validates the two programs (since it is extremely unlikely that errors in programming would give similar spectra in both cases). The inability of the two programs to provide acceptable simulations to the experimental spectrum is because there is a component to the spectrum which is not addressed by the model chosen.

The presence of this extra component can be demonstrated by adding a paramagnetic broadener. The same type of Heisenberg spin exchange that gives broad spectra for high local concentrations of the HTAB* also operates when a paramagnetic transition metal complex is present. The chromium maltolate complex used is a neutral complex with reasonable water solubility (*ca.* 50 mM) (21). Because this complex is neutral it is expected that the extent of adsorption on a silica surface will be much lower than for a charged complex. Figure 3 shows the effect of adding increasing amounts of the complex to a solution of 2 wt% silica and *ca.* 7.5×10^{-4} M total HTAB with 1:50 ratio of HTAB* to HTAB. In Figure 3a the spectrum from the aggregated species can be seen clearly (indicated by the arrows), but there are clear indications of the presence of another species (indicated by the # marks). Addition of *ca.* 4 mM broadener acts to completely broaden out the spectrum of the aggregated species, leaving only the spectrum of the second species. After addition of further broadener the spectrum of the second species also begins to broaden. The different behaviors confirm that there are two different species present. Given the reasonable water solubility of the broadener we would expect that individual HTAB* molecules on the surface would be broadened more slowly than those in solution. There is some evidence that the chromium maltolate complex is adsorbed (included in the surfactant aggregate) which is consistent with what is observed in Figure 3. From the separation of the peaks of the second species marked in Figure 3, the second species must be due to HTAB* rotating slowly. The HTAB* molecules that produce this spectrum must be adsorbed on the silica surface, since this spectrum is not that of HTAB* in solution or in micelles.

By increasing the ratio of surface area to HTAB* and by increasing the proportion of HTAB* to HTAB it is possible to obtain EPR spectra that show the slowly rotating component much more clearly. Figure 4a shows the EPR spectrum for *ca.* 1×10^{-4} M HTAB* adsorbed onto 2 wt% silica. Simulations with the Schneider and Freed program give a rotational correlation time of *ca.* 5×10^{-8} sec. This is notably slower than the *ca.* 10^{-10} sec observed in solution. By decreasing the temperature further the rate of rotation can be decreased until the molecule is virtually stationary on the EPR time scale. This can be seen in Figure 4c at a temperature of 100 K; at this point the z component of the tensor describing the anisotropic coupling constant can be read directly from the peak to peak width of the EPR spectra as indicated on Figure 4c. Interestingly the high field peak is somewhat wider than that observed for a solution of HTAB* at 100 K, suggesting that there may be a broader range of environments for HTAB on silica compared to ice. The coupling constant is also somewhat larger than that observed for water. This is consistent with the spin-label being in a somewhat more polar environment than that in water, but could also reflect changes in conformation due to adsorption on the silica surface.

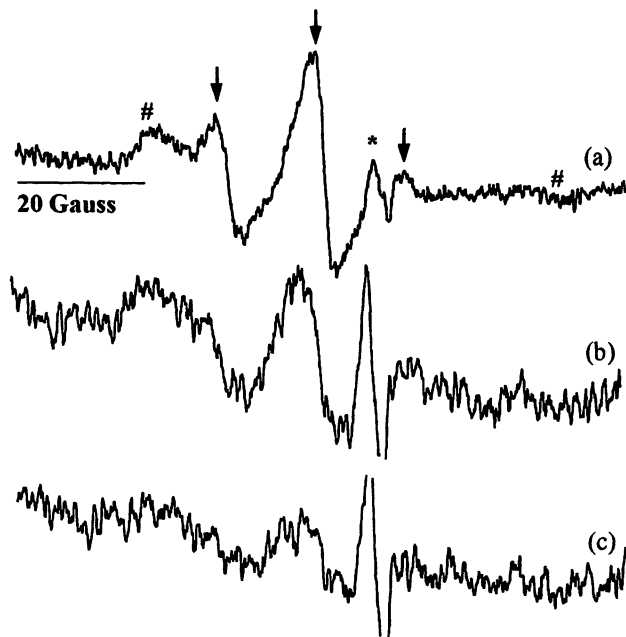


Figure 3. Effect of Addition of Paramagnetic Broadener to HTAB* adsorbed on Silica. (a) no broadener (b) 3.9 mM broadener (c) 5.99 mM broadener. Arrows indicate peaks from HTAB* in surfactant aggregates, # the peaks from the slowly rotating species, * from a quartz defect center in the sample cell.

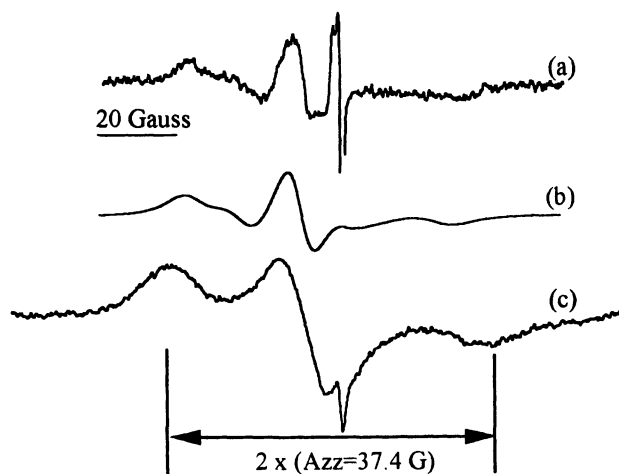


Figure 4. EPR Spectra of Slow Rotating HTAB* (a) 2 wt % silica, room temperature (b) simulated spectrum (c) spectrum at 100 K. * from a quartz defect center in the sample cell

Because of the relatively low solubility of HTAB* (*ca.* 2×10^{-4} M at 25 °C) it is difficult to obtain an adsorption isotherm over a significant range of concentrations. However the effect of changing the ratio of surface area to HTAB concentration can be explored by changing the amount of silica dispersed in solution. Figure 5 shows the EPR spectra for 1×10^{-4} M HTAB* with changing amount of silica between 0.1 wt% and 2.0 wt%, which represents a twenty fold change in effective surface area. Even without simulation the change from a spectrum dominated by the three peaks of HTAB* in solution to that of HTAB* adsorbed on the silica surface is apparent. However, even at 0.1 wt% careful examination of the spectrum shows that there is some of the surface HTAB species present. The experimental spectra are simulated (and fitted) using a model consisting of two species. One species is due to HTAB* in solution and gives the three narrow peaks. The other species is the slowly rotating species simulated using the Schneider and Freed program. The simulated spectra are shown on the right hand side of Figure 5 and show satisfactory agreement with the experimental spectra. The spectrum of the adsorbed species shows little change with silica concentration at the higher silica concentrations, which implies that the spectrum should be similar at the low silica concentrations. It is instructional to consider how much of the observed EPR spectral intensity is accounted for by the two different species. By doing double integrations of the observed EPR spectrum, and of the simulated spectra generated by the two species it is possible to obtain a ratio of simulated to experimental amount of HTAB*. Ideally this ratio would be 1, meaning that all the experimental intensity has been accounted for. A plot of this ratio is shown in Figure 6, and indeed at high silica concentrations the ratio is a satisfactory 0.92. However, as the weight % silica decreases the two species account for steadily less of the observed EPR spectrum. This implies that there is another spectral component which is not being simulated. This is most likely due to formation of surfactant aggregates on the surface. As discussed in the introduction, if the surfactant aggregates consist entirely or largely of HTAB* the resulting EPR spectrum is extremely broad. The extremely large linewidth of the spectrum from such aggregates makes it very difficult to detect. The data in Figure 6 would imply that at 0.1 wt% silica these aggregates would account for approximately 60% of the total HTAB*.

The other set of data in Figure 6 shows the ratio of the amount of HTAB* in solution to that adsorbed on the surface. Between 0.1 wt% and 0.5 wt% these ratios range from 0.05 to <0.001 (i.e. essentially all the HTAB* is adsorbed). The high degree of binding suggests that the HTAB* is strongly bound on the surface.

A further experiment that sheds some light on the situation is that in which HTAB* is added to silica suspensions (Figure 7 a) and then after the sample equilibrates for 2 days HTAB is added and allowed to equilibrate for a further day (Figure 7b). In Figure 7a the spectrum is dominated by individual HTAB* molecules adsorbed on the silica surface. After addition of HTAB a signal due to mixed HTAB/HTAB* surfactant aggregates adsorbed on the silica surface is observed. In this case because these aggregates are magnetically diluted (i.e. made up mainly of HTAB with a smaller amount of HTAB*) a three line spectrum results. Careful analysis allows the relative amounts of HTAB* in each of the three forms (solution, surface aggregates and slowly rotating) to be determined. We find that the amount of



Figure 5. Effect of Silica amount on EPR spectra of HTAB*. All samples are at pH=7 and 10^{-4} M HTAB*. Spectra simulated with HTAB* in solution (rapidly rotating) and HTAB* on the silica surface (slowly rotating).

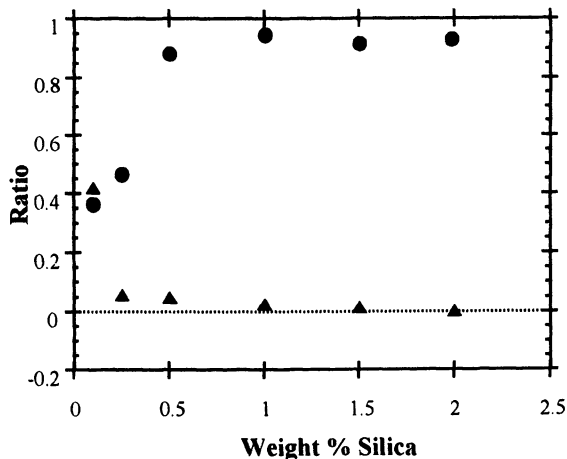


Figure 6. Effect of Silica concentration on EPR simulations. Ratio of simulated EPR intensity to experimental EPR intensity (●) and ratio of HTAB* in solution to that adsorbed (▲).

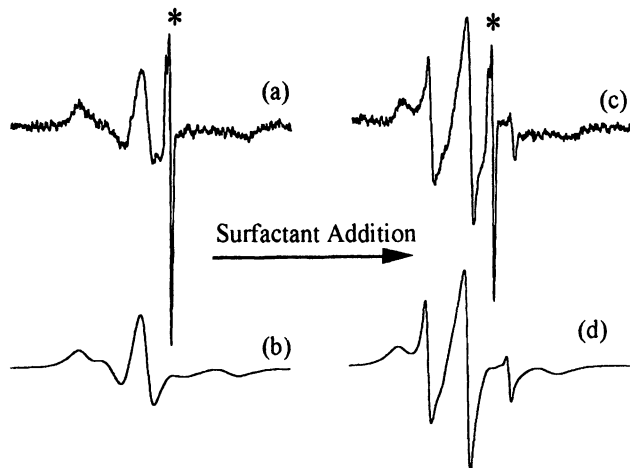


Figure 7. Effect of HTAB Addition to EPR Spectra from HTAB* previously adsorbed onto 1.5 wt% Silica. (a) experimental (b) spectra simulated with slowly rotating HTAB* (c) experimental after addition of 7.5×10^{-3} M HTAB (d) spectra simulated as 1.5% HTAB* in solution + 17% HTAB* in surface aggregates + 82% HTAB* slowly rotating (adsorbed on the surface)

HTAB* in solution increases, i.e. the HTAB* must be being displaced off the surface. However the amount of adsorbed label on the surface shows only a modest decrease.

The complimentary experiment in which HTAB is added first and allowed to equilibrate, and then the HTAB* is added shows that approximately 1 day is required for the sample to reach equilibrium, and that the final EPR spectrum appears to be independent of the order of addition of HTAB and HTAB*. The adsorption of HTAB* is rapid compared to the equilibration time; the majority of the addition appears to occur within 10 minutes.

Discussion: a Strong Binding Site on Silica

We believe that our results can best be explained on the basis of a finite number of surface sites on silica that bind HTAB* relatively strongly. The results of the HTAB addition experiments shown in Figure 7 can then be explained as due to competition between the labeled and unlabeled forms of HTAB for a limited number of binding sites, leading to displacement of some of the labeled form into solution when the unlabeled form is added. The comparatively modest decrease in the amount of HTAB* adsorbed on the silica is then an indication that the competition favors the labeled form. This would be consistent with the lower solubility of HTAB*. We do not believe that the increase in solution concentration results from displacement of HTAB* from aggregated forms of the surfactant: the lower water solubility of HTAB* favors incorporation of HTAB* into surfactant aggregates. That the binding is strong is supported by the observations that binding of HTAB* to silica is fast, but that the equilibration after addition of HTAB to silica with HTAB* adsorbed on it is slow. Fast adsorption and slow desorption imply an equilibrium constant strongly favoring adsorption. This model is summarized in Figure 8 which shows the various forms and equilibria being postulated. The weight of the arrows indicates where we believe the balance of each equilibrium lies. For the amounts of silica being used in this study, it is clear that binding of individual molecules to silica binding sites is competitive with aggregate formation. It is interesting to note that Wangnerud and Bengt (24) report evidence for an anomalous binding site on Spherosil X-015 Silica, based on extrapolation to zero concentration of their adsorption isotherm data. We have observed similar behavior in HTAB adsorbed on Aerosil 200 silica, and it seems possible that the EPR results at low HTAB* concentration and the adsorption isotherms are reporting on the same phenomenon.

This model also allows us to explain some of our pH dependence data. The balance between the aggregated and adsorbed surfactant is strongly sensitive to pH. For 1 wt % silica and 1×10^{-4} M HTAB*, at high pH (*ca.* 10 and above) the aggregated form becomes the dominant species. A trace of the adsorbed species remains even at pH 12, but better than 95% of the label appears as the aggregated form. This must be the result of greater surface charge density giving more efficient charge balance and so allowing surface bound aggregates to form at lower concentrations. The alternative assumption; that at the higher pH sufficient OH⁻ is present to provide charge compensation for the HTAB appears less likely given that [OH⁻] is still only 10^{-4} M, which is the same as the bromide ion already present. This

then argues that at lower pH there is not sufficient surface charge to allow formation of aggregates, so that HTAB* adsorbs as single molecules at discrete surface sites.

The presence of a strongly bound HTAB molecule at low HTAB concentrations could well serve as a nucleus for surfactant aggregation as suggested by Wangnerud and Bengt (24). This is in at least partial agreement with the model of Rupprecht and Gu (12) who have postulated the existence of strong binding sites on silica which individual molecules bind to, and then nucleate the formation of small surfactant aggregates on the silica surface. Full analysis of our data will hopefully allow us to give some estimate of the size of the surfactant aggregates formed. It is in theory possible to determine the number of spin-labels present in an aggregate from the width of the EPR lines. If the amount of adsorbed surfactant is also known (i.e. if the isotherm for the mixture of HTAB*/ HTAB is determined) then the average number of HTAB molecules per aggregate can be extracted.

The observation of a strong binding site on Aerosil 200 silica seems to be general for silica. In both Sipernat 22 and Sipernat 50 we also observe signals from HTAB* adsorbed onto the silica surface. For titanium dioxide and alumina at pH 11 we did not observe any such signal, instead at all concentrations of HTAB* we observed signals for HTAB* in solution. At sufficiently high concentrations we also observed the broad single line indicative of surfactant aggregate formation. Although the surface areas of the titanium dioxide and alumina are lower than those of Aerosil 200, they are comparable to those of the Sipernat 22, and at pH 11 the surface is negatively charged. Because the OH⁻ concentration is higher we cannot rule out enhancement of surfactant aggregation because of stronger counter-ion binding, but these results are certainly consistent with the absence of any strongly binding site on titanium dioxide and alumina.

Investigations of Counter-Ion Binding

From the above discussion of the possible impact of the binding of counterions on the extent of surfactant aggregation on surfaces it became clear that it was desirable to investigate this further. For cationic surfactants such as HTAB a suitable EPR probe needs to be negatively charged, relatively small and have an EPR spectrum which provides information on molecular environment. The number of probes that fit this description is relatively limited but one good candidate is nitrosodisulfonate (also known as peroxyamine disulfonate and Fremy's salt). This probe has good water solubility, but does suffer from limited stability in water (at low concentrations we observe *ca.* 15% decay over 8 hours). The absence of any of the hydrogen hyperfine seen for HTAB* results in much sharper lines in the EPR spectrum. This serves both to improve the signal to noise (and hence the sensitivity) and also increases the sensitivity to changes in linewidth resulting from decreases in rotation of the label. Figure 9a shows the EPR spectrum of nitrosodisulfonate in water and with HTAB above the CMC (Figure 9b). We confirmed that below the CMC of HTAB the spectrum was indistinguishable from that of Figure 9a (i.e. for the dilute nitrosodisulfonate). This proves that nitrosodisulfonate does not complex with individual HTAB molecules (which would result in decreased rotational motion and hence changes in the EPR linewidths). Likewise in the presence of 1 wt% silica the

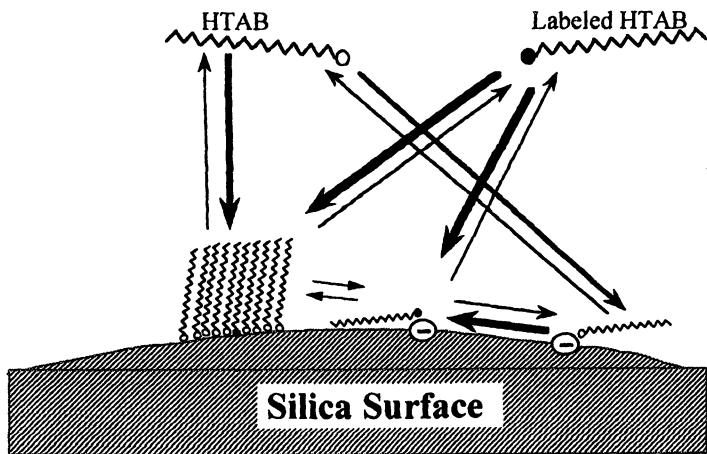


Figure 8. Schematic showing the various equilibria between the silica surface and HTAB and HTAB*.

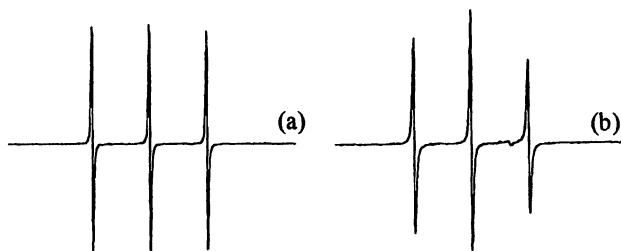


Figure 9. EPR spectra from nitrosodisulfonate (a) in dilute aqueous solution (b) with HTAB above CMC

spectrum was also indistinguishable from that in Figure 9a. Therefore the nitrosodisulfonate does not adsorb onto silica since there is no indication of either line broadening or of additional broader lines due to an immobilized label. Given that silica is strongly negatively charged this is not surprising. Above the CMC of HTAB there are clear changes in the line heights and linewidths, which must be caused by nitrosodisulfonate binding to the surface of a micelle where it is less free to rotate. There is no evidence that the spectrum of Figure 9b consists of the overlap of two spectral components, in which case there are two possibilities. One is that all the spin-probe is strongly bound to the surface of the HTAB micelle and so there is no signal from a spin-probe in solution. Alternatively, the spin-probe could be moving so rapidly on and off the surface of the micelle that what is observed is a weighted average. However it seems unlikely that such a motion could be faster than molecular rotation and so it would seem likely that the spin-probe is strongly bound to HTAB aggregates.

The nitrosodisulfonate spin-probe can be used to report on counter-ion binding to surfactant aggregates formed by addition of silica. Figure 10 shows EPR spectra from the nitrosodisulfonate spin probe added to suspensions of silica with different amounts of HTAB added. These are superimposed on the adsorption isotherm to simplify discussion. What is clear is that at points corresponding to considerable adsorption of HTAB effectively none of the spin-probe is associated with HTAB aggregates. It is only towards the plateau region that there is any indication of changes in the EPR spectrum. A broad component begins to appear, which must be due to a high local concentration of the spin-probe. This must be from binding of the spin-probe onto surfactant aggregates of some form. Since the solution

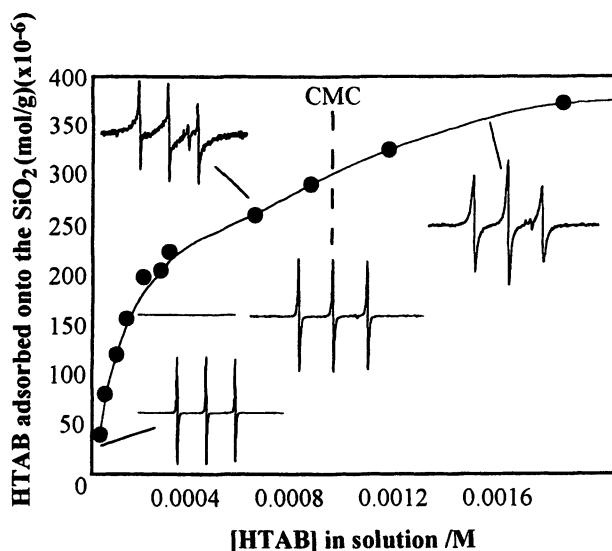


Figure 10. EPR spectra from nitrosodisulfonate and adsorption isotherm for HTAB adsorbed on silica.

concentration of HTAB is still below the CMC, it seems likely that the spin-probe is being bound to a surfactant aggregate formed on the surface. It is possible that the CMC of HTAB is depressed due to the presence of *ca.* 10^{-5} M spin-probe. This would result in formation of a limited number of micelles and give the high local concentration of spin-probes observed. However, considering the low spin-probe concentration this appears unlikely. Above the CMC micelle formation occurs and the EPR spectrum is clearly due to binding of the spin-probe to the surface of micelles.

Acknowledgments

The partial support of this work by the School of Mines and Energy Development at The University of Alabama (MGB) is gratefully acknowledged. Part of this work was carried out by MGB under a NATO travel grant, and the resulting stimulating discussions with Prof. Claude Treiner of the University Pierre et Marie Curie (Paris VI) are much appreciated.

References

1. Bilgen, S.; Wills, B. A. *Miner. Eng.* **1991**, *4*, 483.
2. Murphy, D. D.; Spears, D. R.; Bakker, M. G. *Colloid Surf.* **1995**, *96*, 143.
3. Lee, C.; Yeskie, M. A.; Harwell, J. H.; O'Rear, E. A. *Langmuir* **1990**, *6*, 1758.
4. Esumi, K.; Watanabe, N.; Meguro, K. *Langmuir* **1991**, *7*, 1775.
5. Park, J.-W.; Jaffe, P. R. *Environ. Sci. Technol.* **1993**, *27*, 2559.
6. Harwell, J. H.; O'Rear, E. A. In *Surfactant-Based Separation Processes*; J. F. Scamehorn and J. H. Harwell, Ed.; Surfactant Science Series; Marcel Dekker Inc.: New York, 1989; Vol. 33; pp 155.
7. Yu, C.-C.; Wong, D. W.; Lobban, L. L. *Langmuir* **1992**, *8*, 2582.
8. Yu, C.-C.; Lobban, L. L. In *Surfactant Adsorption and Surface Solubilization*; R. Sharma, Ed.; A.C.S. Symposium Series; American Chemical Society: Washington, D.C., 1995; Vol. 615; pp 67.
9. Kile, D. E.; Chiou, C. T. *Environ. Sci. Technol.* **1989**, *23*, 832.
10. Somasundaran, P.; Fuerstenau, D. W. *J. Phys. Chem.* **1966**, *70*, 90.
11. Yeskie, M. A.; Harwell, J. H. *J. Phys. Chem.* **1988**, *92*, 2346.
12. Rupprecht, H.; Gu, T. *Colloid Polym. Sci.* **1991**, *269*, 506.
13. Levitz, P.; Van Damme, H.; Keravis, D. *J. Phys. Chem.* **1984**, *88*, 2228.
14. Chandar, P.; Somasundaran, P.; Turro, N. J. *J. Colloid Interface Sci.* **1987**, *117*, 31.
15. Ottaviani, M. F.; Ghatlia, N. D.; Turro, N. J. *J. Phys. Chem.* **1992**, *96*, 6075.
16. Somasundaran, P.; Kunjappu, J. T. *Min. Metall. Proc.* **1988**, *5*, 68.
17. Chandar, P.; Somasundaran, P.; Waterman, K. C.; Turro, N. J. *J. Phys. Chem.* **1987**, *91*, 148.
18. Esumi, K.; Otsuka, H.; Meguro, K. *J. Colloid Interface Sci.* **1990**, *136*, 224.
19. Bakker, M. G.; Murphy, D. D.; Davis, B. M. In *Surfactant Adsorption and Surface Solubilization*; R. Sharma, Ed.; American Chemical Society: Washington, 1995; Vol. 615; pp 153.

20. Kwan, C. L.; Atik, S.; Singer, L. A. *J. Am. Chem. Soc.* **1978**, *100*, 4783.
21. Burchfield, J.; Telchowski, P.; Rosenberg, R. C.; Eaton, S. S.; Eaton, G. R. *J. Magn. Res. B* **1994**, *104*, 69.
22. Press, W. H.; Flannery, B. P.; Teukolsky, S. A.; Vetterling, W. T. *Numerical Recipes*; Cambridge University Press: New York, 1989.
23. Schneider, D. J.; Freed, J. H. In *Spin Labeling. Theory and Applications, Biological Magnetic Resonance*, 8; L. J. Berliner and J. Reuben, Ed.; Plenum: New York, 1989; Vol. 8; pp 1.
24. Wangnerud, P.; Bengt, J. *Langmuir* **1994**, *10*, 3542.

Chapter 17

Speciation of Metal-Containing Compounds Found in the Environment by Micellar Liquid Chromatography Interfaced to Inductively Coupled Plasma Mass Spectrometry

M. P. Dziewatkoski

Department of Chemistry, Western Reserve University, Kalamazoo, MI 49008

The speciation of metal and metalloid-containing compounds of environmental interest using micellar liquid chromatography with detection by inductively coupled plasma mass spectrometry is discussed. The charge on the compound dictates the type of surfactant used for the separation. For most analytes, retention times decrease with increasing concentrations of surfactant and 2-propanol. Separation involves interaction of the compounds with the stationary phase and partitioning into the micelle. This partitioning is dependent upon the hydrophilic and hydrophobic character of the compounds. A quantitative evaluation of this interaction for some metal containing compounds was made by calculating the equilibrium constant for partitioning between the bulk mobile phase and the micelle. Partitioning was found to increase with increasing aliphatic character of the compounds and decrease with increasing 2-propanol concentration.

Metal and metalloid containing compounds are prevalent in the environment. These compounds are of special interest since in some chemical forms they are harmless whereas ingestion of other chemical forms can result in both acute and chronic toxic effects (1-3). Evaluating the effects of these compounds on organisms in an ecosystem requires more than just a knowledge of total element concentrations. Determining the chemical form of the element present is therefore a necessity because of the link between toxicity and chemical form. For a metal or metalloid-containing compound, chemical form refers to the oxidation state of the metal or metalloid and the identity of attached inorganic or organic ligands. The process by which chemical form is determined is referred to as speciation. Typical speciation methods involve the use of a separation technique like liquid chromatography interfaced to either a non-

selective or selective detector (4,5). Comparison of retention times and/or signals obtained from the selective detector confirms the identity of the compound.

Liquid chromatography (LC) has been shown to be a useful technique for speciation studies (4,5). The versatility of this technique is a result of the many different stationary phases, mobile phases and mobile phase modifiers available for use. The majority of separations performed using LC are in the reverse phase mode (polar mobile phase and non-polar stationary phase). Traditional LC separations relied on the interaction of analytes between two distinct phases. During the past two decades, a useful modification to reverse-phase liquid chromatography (RPLC) was developed in which surfactants were added to the mobile phase (6,7). Surfactant concentrations above a specific concentration, referred to as the critical micelle concentration (cmc), results in the aggregation of surfactant molecules to form micelles. Adding additional surfactant results in the formation of more micelles while the free surfactant concentration remains constant. This type of liquid chromatography is referred to as micellar liquid chromatography (MLC). The formation of micelles effectively produces a third phase in addition to the bulk mobile phase and stationary phase. The three phases provide a unique environment in which both neutral and charged species can interact. Hence, MLC has found vast utility for the simultaneous separation of both charged and neutral organic compounds such as aromatic hydrocarbons and proteins (7).

There are many different surfactants available for use in MLC. This allows the researcher to manipulate surfactant type as an experimental variable. Each type of surfactant can be characterized by its charge and type of aliphatic tail. Surfactants are available in cationic, anionic and zwitterionic forms (6). Each surfactant has a unique cmc and aggregation number. When selecting a surfactant for MLC, all of these characteristics must be considered.

Properties of Metal and Metalloid Containing Compounds and Surfactants

Metal and metalloid containing compounds in solution phase are usually either cationic or anionic. For metal containing compounds, the charge is usually positive and is localized on the metal. Many metalloid compounds have a negative charge and the charge is usually delocalized among a group of electronegative atoms (such as O or S) attached as ligands to the metalloid. Compounds of these types can also possess aliphatic nature, in addition to charge, as a result of attached ligands such as methyl-, ethyl- or phenyl- groups. The ionic and aliphatic nature of these compounds determines the type and degree of interaction with the micelle.

Micelles can form in two ways depending upon the characteristics of the bulk mobile phase. If the bulk of the mobile phase is non-polar or slightly polar, the micelle will form with the polar headgroups on the inside and aliphatic tails on the outside. In a mostly aqueous mobile phase the charged headgroups will be on the outside of the micelle and the aliphatic tails will be on the inside. This property of surfactants warrants the consideration of two different interactions between the micelle and the charged analyte; namely hydrophobic and hydrophilic (electrostatic) interactions. In RPLC, the core of the micelle provides a region for hydrophobic interactions with the

analyte while the charged surface provides hydrophilic interactions. The separation of charged analytes can be accomplished if both interactions are taken into consideration. Hence, a surfactant having a charge that is opposite to that of the analyte is used in the separation. The degree of electrostatic interaction should depend on the charge density of the micelle and the analyte. For metal-containing compounds that have significant aliphatic character, hydrophobic interactions with the micelle will be of importance to the separation. A greater aliphatic character will result in greater hydrophobic interaction with the micelle.

Element Selective Detection with Inductively Coupled Plasma Mass Spectrometry

Commonly used detectors for RPLC such as absorption, fluorescence, refractive index, conductivity or electrochemical are of limited use for compounds containing metals or metalloids. These compounds will only exhibit UV or fluorescence activity if the attached ligands are highly conjugated systems. Refractive index, conductivity and electrochemical detection can be non-selective and can give erroneous results in complex samples (such as those obtained from the environment) as a result of interferences.

In the past decade, inductively coupled plasma mass spectrometry (ICPMS) has achieved widespread acceptance as a highly sensitive method for performing trace-level elemental analysis of liquid, solid and gas phase samples (8). Interfacing RPLC to ICPMS permits highly sensitive and element-selective detection (4). Compounds introduced to the plasma are completely dissociated to their constituent atoms. The atoms formed are efficiently ionized and then detected by the mass spectrometer. Structural information about the compounds cannot be directly obtained. However, chromatographic data can be obtained by monitoring one or more mass-to-charge (m/z) ratio values as a function of time and comparing retention times of unknowns with standards. The m/z values monitored will correspond to those for one or more of the metals or metalloids in the compounds of interest. This mode of detection greatly eliminates the possibility of erroneous results from interferences.

ICPMS will not tolerate large amounts of organic solvents introduced to the plasma such as the concentrations commonly used in RPLC with hydroorganic mobile phases (8). Once in the plasma, some of the carbon in the organic solvent will be reduced to elemental carbon which will plate-out on the plasma torch and sampling interface. Additionally, the presence of carbon in the form of soot particles will destabilize the plasma resulting in a noisy MS signal or possible extinguishing of the plasma. Reducing these adverse effects requires the addition of oxygen gas to the plasma flow (to convert free C to CO or CO₂) and the use of stringent desolvation. With the surfactant based mobile phases used in MLC, the total organic content in the mobile phase is small compared to hydroorganic mobile phases and so the addition of oxygen to the plasma flow is not needed and only mild desolvation is necessary.

Separation of Arsenic Containing Compounds in Bacterial Growth Medium

Arsenic compounds can be found in several inorganic and organic forms. Many of these compounds carry a negative charge in solution and can be separated by MLC using a positively charged surfactant (9). Additionally, the solubilizing characteristics of surfactants make them useful for the analysis of biological samples that may have a high protein content (7), such as a bacterial growth medium.

Speciation was performed on samples of bacterial growth medium containing arsenic compounds. The separation of a standard arsenic solution containing compounds likely to be in the growth medium was performed first. A sample chromatogram demonstrating the separation of these compounds is shown in figure 1. The mobile phase consisted of 0.05M cetyltrimethylammonium bromide (CTAB) and 0.02M boric acid buffer. Propanol (10%) was added as an organic modifier to the mobile phase to increase column efficiency. The separation was carried-out on a C-18 column having a length of 15 cm.

MLC was next applied to the speciation of arsenate and arsenite in a nutrient broth growth medium as shown in figure 2. The growth medium was used to grow the bacterial strain *alcaligenes faecalis* which has the ability to metabolize arsenite form of arsenic to the arsenate form. Sample preparation was as simple as filtering the samples through 0.45 μm filtering membranes and diluting with the micelle mobile phase used in the separation. The nutrient broth growth medium was diluted 1:100 with 0.05M CTAB surfactant solution, filtered and analyzed. Samples were injected directly on column without further preparation.

Separation of Inorganic and Organic Mercury Compounds

Inorganic and organic forms of mercury compounds can be found in the environment. These compounds were introduced to the environment as inorganic mercury salts or in some cases in alkylated forms (3). Some lower molecular weight alkylmercury compounds result from alkylation of inorganic mercury by bacteria found in the environment (3). Speciation of the different types of these compounds is a necessity since toxicity varies widely with compound type (1).

Both inorganic and organic forms of mercury will carry a positive charge on the metal in solution. Employing the electrostatic interaction between surfactant and analyte requires the use of a negatively charged surfactant. An example of the separation of mercury compounds using ammonium dodecyl sulfate (ADS) is shown in figure 3. The anionic surfactant moiety of ammonium dodecyl sulfate is identical to that found in the more common surfactant sodium dodecyl sulfate. The ammonium form was used (as opposed to the sodium form) to prevent signal suppression in the ICPMS and to prevent clogging of the skimmer cone of the mass spectrometer. The mobile phase used for the separation shown in figure 3 consisted of 0.08M ADS in 0.02M phosphate buffer with 10% added 2-propanol as a mobile phase modifier. The separation was carried-out on a C-8 column. The chromatogram shows that the most hydrophilic compounds elute first while the more hydrophobic ones elute later.

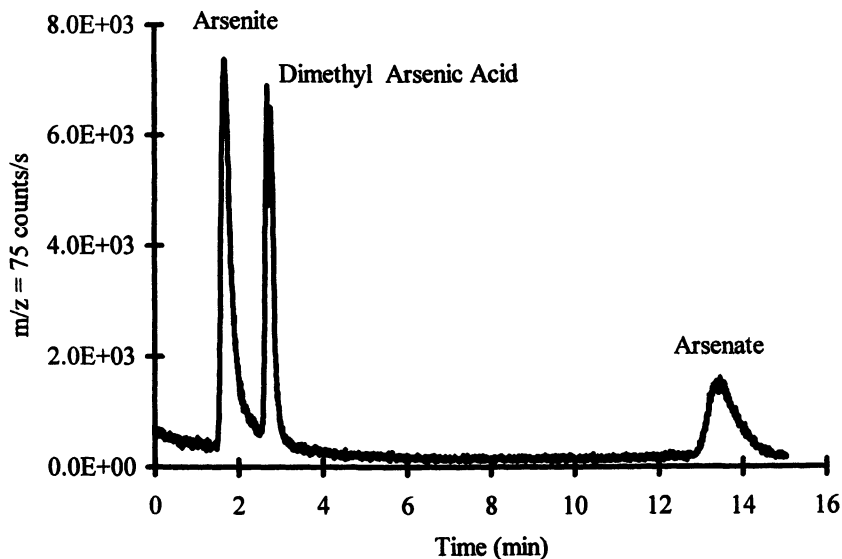


Figure 1: Sample separation of arsenic containing compounds using a mobile phase containing 0.05M CTAB, 10% propanol, 0.02M boric acid buffer and a 15cm long C-18 column.

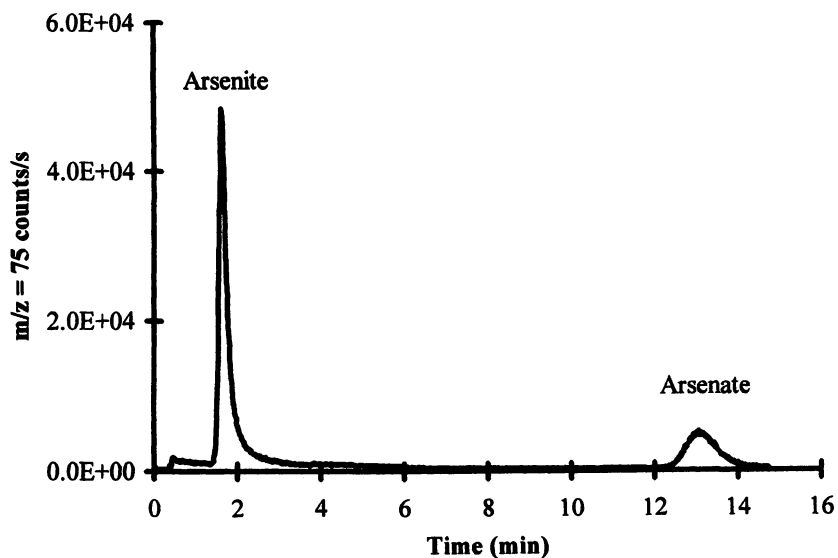


Figure 2. Separation of arsenic compounds in a nutrient broth matrix after growth of the bacterial strain *alcaligenes faecalis*. Same chromatographic conditions as figure 1.

Separation of Organo-Tin Compounds

Organo-tin compounds exist in a large variety of types having very different degrees of alkyl nature and different charges on the metal. The alkyl forms include mono-, di- and tri-alkyl of methyl, ethyl, propyl, butyl and phenyl. The mono-alkyl forms have a 3+ charge on the metal, the di-alkyl have a 2+ charge on the metal and the tri-alkyl have a 1+ charge. The combination of the varying degrees of charge and alkyl nature results in these compounds having a wide range of hydrophilic and hydrophobic character. Since all of these compounds are positively charged, a negatively charged surfactant can be used in the mobile phase as was done for mercury compounds. Because of the very different hydrophobic and hydrophilic character of the compounds, the type of column stationary phase used is crucial to the separation.

Separation of tri-methyl, tri-n-butyl and tri-phenyl tin compounds was performed using ADS surfactant and a CN column as shown in figure 4. The mobile phase consisted of 0.04M ADS, 3% 2-propanol and 0.02M phosphate buffer. A more polar column, like CN, is needed to effect the separation owing to the hydrophobic character of the compounds. These compounds are very strongly retained by C-18 and C-8 making the efficiency of the separation very poor. As shown in figure 4, tri-phenyl tin elutes last demonstrating the strong interaction of this more hydrophobic compound with the polar CN column.

Separation of mixtures of the most highly charged tin compounds, the mono-alkyl type, and the tri-alkyl compounds presents a unique problem. The mono-alkyl compounds are much more hydrophilic than the tri-alkyl compounds. A column must be chosen to allow an interplay between the hydrophobic/hydrophilic interactions between both the column and the micelles in the mobile phase. A compromise can be reached by using a hydrophobic column like C-18. Some of the surfactant will adsorb to the stationary phase as a result of interaction of the hydrophobic tail of the surfactant with the hydrophobic C-18 packing (10). This will provide a source of electrostatic interactions between ionic compounds and the column stationary phase which can aid in the separation.

The interplay of these effects is demonstrated by the separation of mono-methyl tin and tri-methyl tin shown in figure 5. The mobile phase consisted of 0.08M ADS, 0.02M phosphate buffer and was carried out on a C-18 column having a length of only 5 cm. The mono-methyl compound is only slightly retained by the chromatographic system with its retention time being about 40 seconds longer than that measured for unretained compounds. The tri-methyl compound has much more interaction with the chromatographic system and hence elutes at a longer time. This separation demonstrates that both charge and aliphatic character play a big role in the interaction of these compounds with the micelle/stationary phase/mobile phase system.

Interaction of Metal-Containing Compounds With Micelles

Developing MLC as an analysis technique for speciation requires the ability to predict how metal- and metalloid-containing compounds will interact with micelles in the

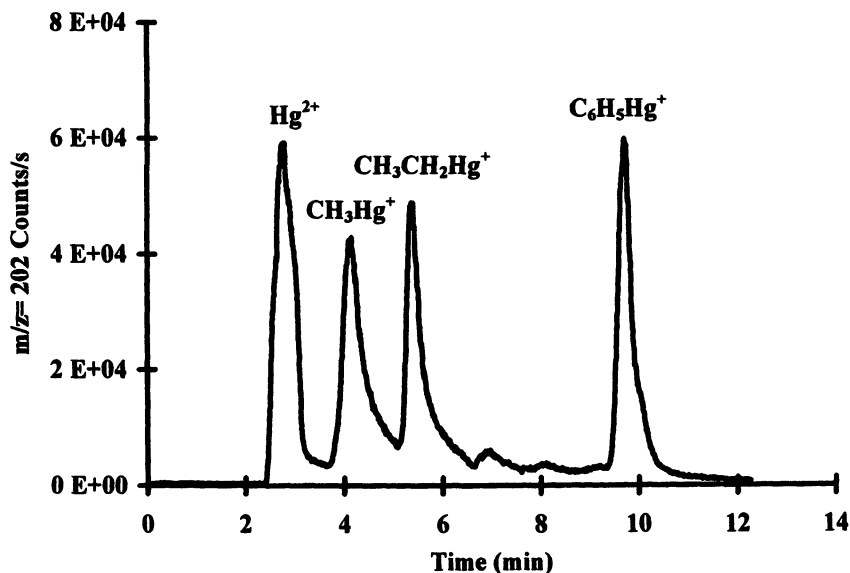


Figure 3. Separation of inorganic and alkyl mercury compounds using a mobile phase of 0.08M ammonium dodecyl sulfate, 0.02M phosphate buffer, 10% 2-propanol and a 25cm C-8 column.

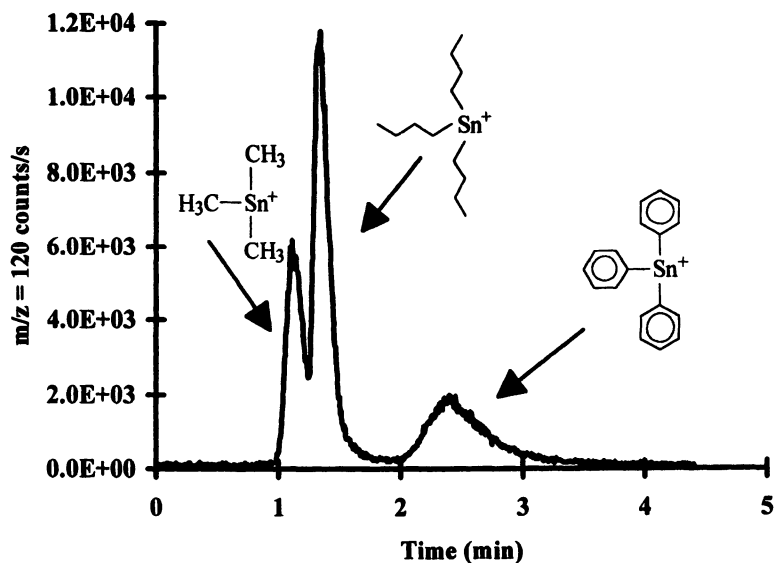


Figure 4. Separation of tri-alkyl tin compounds using a mobile phase of 0.04M ammonium dodecyl sulfate, 3% 2-propanol, 0.02M phosphate buffer and 15cm CN column.

mobile phase. Perhaps more importantly, understanding this interaction is useful in modeling the interaction of metals with biological membranes, studying the use of micelles for catalytic reactions and in studying how micelles can extract metal contaminants from soil or water matrices (7, 11-13). This understanding can be gained by studying the effects of manipulating experimental variables such as surfactant concentration and organic modifier concentration in the mobile phase and quantifying a change in the chromatographic system.

Effect of Surfactant Concentration. The degree to which several mercury-containing compounds interact with the micelle environment was assessed by determining the retention characteristics of the compounds as a function of surfactant concentration. All surfactant concentrations studied were above the cmc. The most appropriate way of quantifying retention characteristics is to use capacity factor, k' , defined as follows:

$$k' = \frac{t_R - t_m}{t_m}$$

where t_R is the retention time of the analyte and t_m is the retention time of an unretained substance. For the data presented here, Br^- was used as the unretained substance. A plot of k' as a function of surfactant concentration is shown in figure 6 for the following mercury compounds: Hg^{2+} , CH_3Hg^+ , $\text{CH}_3\text{CH}_2\text{Hg}^+$, $\text{C}_6\text{H}_5\text{Hg}^+$. Each compound has different hydrophobic and hydrophilic character. The mobile phase contained 3% 2-propanol and 0.02M phosphate buffer. A large change in k' with increasing surfactant concentration indicates strong interaction between the compound and the micelle. An increase in surfactant concentration results in an increase in the number of micelles in the mobile phase. For compounds that interact strongly with micelles, an increase in the number of micelles will result in increased interaction of these compounds with the mobile phase and thus the elution strength of the mobile phase will increase. The largest change in k' was observed for phenylmercury and the smallest change for Hg^{2+} . The trends indicate that alkyl-mercury compounds interact more with the micelles than does Hg^{2+} . In fact, the change observed for Hg^{2+} is almost negligible. All of the compounds studied will experience electrostatic interactions with the micelle, however, only hydrophobic compounds will engage in hydrophobic interactions with the hydrophobic core of the micelle. Therefore, Hg^{2+} will only be involved in hydrophilic interactions whereas the other compounds studied will take part in both types of interactions.

Effect of Added Organic Modifier. Adding organic modifiers, such as propanol, to aqueous micelle mobile phases has been shown to improve chromatographic efficiency by increasing the rate of mass transfer of the analyte from the mobile phase to the stationary phase (14,15). Additionally, adding 3-15% 2-propanol has been shown to increase the solvent strength of micelle mobile phases resulting in a decrease in analysis time (16,17). Increasing solvent strength means that the analyte has increased

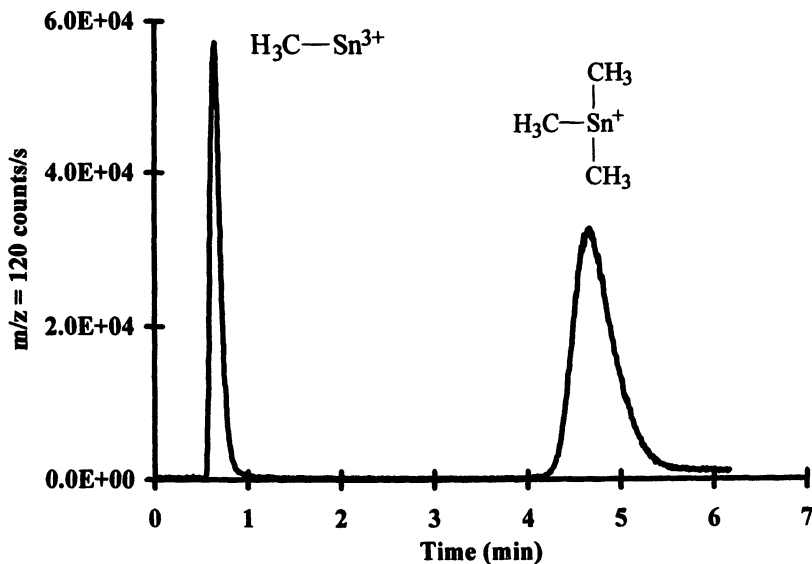


Figure 5. Separation of mono- and tri-methyl tin compounds using a mobile phase of 0.08M ammonium dodecyl sulfate, 0.02M phosphate buffer and a 5 cm C-18 column.

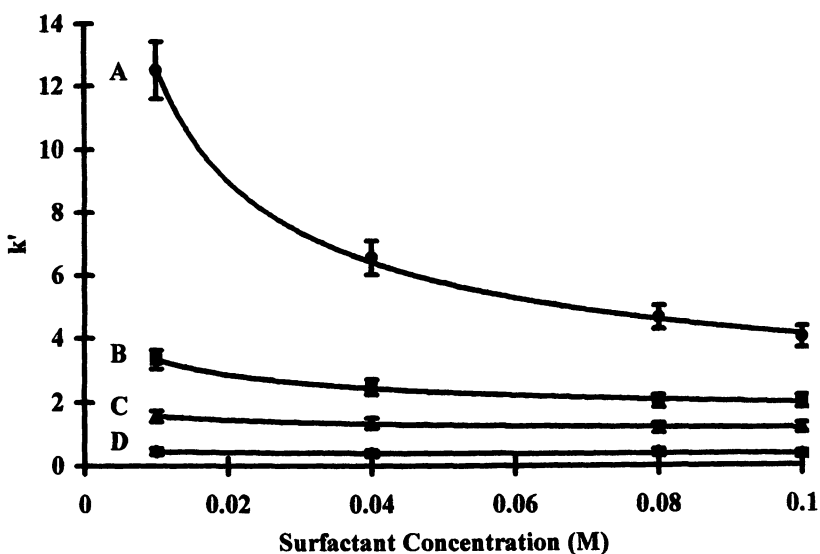


Figure 6. Variation of capacity factor (k') with ammonium dodecyl sulfate concentration for a mobile phase consisting of varying amounts of surfactant, 0.02M phosphate buffer and 3% 2-propanol. A: phenylmercury, B: ethylmercury, C: methylmercury, D: Hg^{2+}

affinity for the mobile phase in comparison to its affinity for the stationary phase. The increased solvent strength results from the ability of micelles to encapsulate organic solvent molecules within the hydrophobic core. This produces an environment favorable to compounds having both hydrophilic and hydrophobic character. This results in increased interaction of these compounds with the micelle phase having an effect similar to that of increasing surfactant concentration.

The effect of added 2-propanol was investigated by keeping the surfactant concentration constant at 0.08M and varying the percentage of 2-propanol in the mobile phase. Capacity factors were calculated for all compounds as a function of the concentration of 2-propanol in the mobile phase. The results are shown in figure 7. In general, k' decreases with increasing alcohol concentration for all of the alkyl-mercury compounds. The greatest effect on k' was observed for phenylmercury. There was practically no effect on the retention characteristics for Hg^{2+} .

The affect on retention observed for increasing 2-propanol concentrations is similar to that observed for increasing surfactant concentrations. The solubility of alkyl-mercury compounds is greater in polar organic solvents than for water. Therefore, decreasing k' values can be a result of more interaction of the analyte with the bulk mobile phase or more interaction with the micelle environment.

Partitioning Behavior of Metal-Containing Compounds Into Micelles

MLC can be modeled as a three phase system consisting of the bulk mobile phase, a micelle phase and the column stationary phase (18). The analyte can interact with all three phases and the interaction can be considered as a dynamic equilibrium between any two phases. Hence equilibrium constants exist for the partitioning of the analyte between the bulk mobile phase and micelle, between the bulk mobile phase and stationary phase and between the micelle and the stationary phase. The interaction of metal-containing compounds with the micelle environment can be quantitatively assessed through the calculation of the micelle-bulk mobile phase equilibrium constant.

The quantitative equilibrium interactions were first described mathematically by Armstrong and Nome and later modified by Arunyanart and Cline Love (18,19). This mathematical treatment yielded the following result:

$$\frac{1}{k'} = \frac{K_2}{\phi[L_S]K_1} C_m + \frac{1}{\phi[L_S]K_1}$$

The symbols are defined as follows:

k' : capacity factor

C_m : the concentration of the surfactant in the micelle (mol/L)

$[L_S]$: the concentration of available solute binding sites on the stationary phase.

K_2 : equilibrium constant for the solute between the micelle and bulk mobile phase.

K_1 : equilibrium constant for the solute between the stationary phase and bulk mobile phase.

ϕ : phase ratio

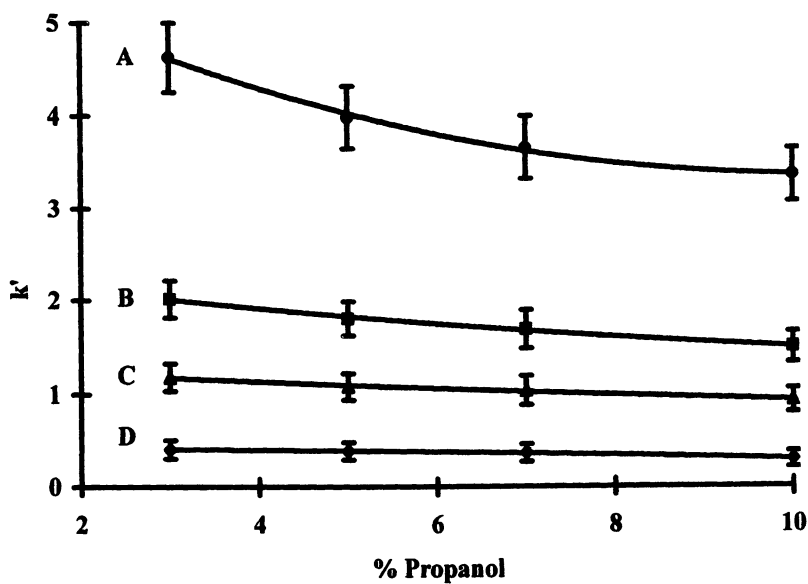


Figure 7. Variation of capacity factor (k') with 2-propanol concentration for a mobile phase consisting of varying amounts of 2-propanol, 0.02M phosphate buffer and 0.08M ammonium dodecyl sulfate. A: phenylmercury, B: ethylmercury, C: methylmercury, D: Hg^{2+}

In this treatment, k' is calculated using retention time data as the concentration of surfactant in the micelle is varied while keeping all other experimental parameters constant. If the interactions of the compounds of interest with the micelle environment can be modeled using this approach, then a plot of $1/k'$ versus C_m will yield a straight line with a positive intercept. The ratio of the slope to intercept permits the calculation of K_2 which is the equilibrium constant for the partitioning of the analyte between the micelle and bulk mobile phase, per monomer of surfactant in the micelle. To convert this to an equilibrium constant expressed as per micelle, K_{eq} , K_2 must be multiplied by the aggregation number of the micelle. The concentration of the surfactant in the micelle is calculated as the difference between the total surfactant concentration and the cmc.

The previous mathematical treatment was used to investigate the interaction of mercury containing compounds with the micelle environment. This was done using the surfactant ADS which has a cmc of 6.1×10^{-3} M and an aggregation number of 62 (20). The model was applied to chromatographic data collected using a mobile phase containing 3% and 10% 2-propanol and 0.02M phosphate buffer. For both cases with 3% and 10% 2-propanol, the largest scatter in the data and poorest linearity was observed for Hg^{2+} ($R^2 \leq 0.8$). The least error and best linearity was observed for phenylmercury ($R^2 \leq 1$). Positive intercepts were obtained in all cases.

The results for calculated values of micelle-solute equilibrium constants for these compounds are presented in table I. The relative standard deviations were calculated using the error in the slope and intercept obtained from linear regression analysis of the data.

Table I: Calculated Values for Micelle-Solute Equilibrium Constants

Compound	3% Propanol		10% Propanol	
	K_{eq} (L/mol)	%RSD	K_{eq} (L/mol)	%RSD
Hg^{2+}	166 +/- 83.3	50	315 +/- 116.0	37
Methyl-Hg	233 +/- 42.4	18	143 +/- 21.3	15
Ethyl-Hg	464 +/- 84.8	18	290 +/- 38.3	13
Phenyl-Hg	1442 +/- 177.4	12	921 +/- 56.9	6

For all compounds except Hg^{2+} , partitioning into the micelle was found to increase with increasing aliphatic character of the mercury compounds as made apparent by the increasing value of the equilibrium constant. Partitioning was found to decrease with increasing concentration of propanol.

In general, for metal-containing compounds of like charge, partitioning into the micelle increases with increasing aliphatic, and hence hydrophobic, character. The results for Hg^{2+} must be viewed with caution owing to the large errors associated with the equilibrium constant determination. The source of these errors can be traced back to the k' determination. The uncertainty associated with retention time determinations increases as k' decreases. Errors can be quite large for k' values less than 1. This

case is true for Hg^{2+} . For this particular species, being very hydrophilic, partitioning into the micelle could be expected to be minimal when compared to the other compounds studied. Being highly charged, Hg^{2+} could be expected to have strong electrostatic interactions with the charged headgroup of the surfactant.

The reasons for the effect of organic modifier on the partitioning of the analyte into the micelle warrants further study. The addition of organic solvents to a solution containing a surfactant has been shown to cause changes in aggregation number and cmc. The aggregation number and cmc can be either increased or decreased depending on the type of organic solvent (11,21). A change in these two physical parameters would lead to erroneous results from application of the partitioning model. Another reason for the change in analyte partitioning may result from the higher solubility of the alkyl-mercury compounds in polar organic solvents compared to pure water. In this case the organic modifier would create an environment in the bulk mobile phase in which partitioning into the micelle phase is less favorable. Our research continues to focus on the effects of organic solvents.

Effect of Analyte Charge Versus Hydrophobicity. Both analyte charge and hydrophobic character can play a role in the partitioning mechanism of the analyte into the micelle. Insight into the importance of each characteristic can be gained through studying a series of similar compounds having differing degrees of analyte charge and hydrophobic character. Our research thus far has indicated that both aliphatic character and charge have a large influence on partitioning. We have made preliminary measurements of equilibrium constants for two tin compounds having very different aliphatic and charge characteristics: monomethyl tin ($\text{CH}_3\text{Sn}^{3+}$) and trimethyl tin ($(\text{CH}_3)_3\text{Sn}^+$). These preliminary experiments have shown that monomethyl tin was so hydrophilic that an equilibrium constant was indeterminate with the particular experimental setup used. Trimethyl tin, on the other hand, was found to have an equilibrium constant of approximately 9000 L/mol. Future studies will involve further investigations into the effects of both analyte charge and aliphatic character.

Safety Considerations

Exposure to compounds discussed in this chapter can result in acute and/or chronic toxic effects. Alkylated metals are of special concern since absorption through the skin is possible. Risks can be minimized by wearing protective clothing and using fume hoods.

Acknowledgments

The author wishes to thank the Kalamazoo Foundation (Environment Now Fund) and Western Michigan University (Faculty Research and Creative Activities Support Fund) for providing funding for this research. The author also wishes to thank Dr. Gretchen Anderson (Indiana University-South Bend) for providing the bacterial growth samples for arsenic analysis.

Literature Cited

- (1) Friberg, L.; Nordberg, G. F.; Vouk, V. B. *Handbook on the Toxicology of Metals*; Elsevier: New York, NY, 1986; Vols. I&II.
- (2) *Lead, Mercury, Cadmium and Arsenic in the Environment*; Hutchinson, T. C., Meema, K. M., Eds.; John Wiley & Sons: New York, NY, 1987.
- (3) *Mercury Pollution Integration and Synthesis*, Watras, C. J., Huckabee, J. W., Eds., Lewis Publishers: Boca Raton, LA, 1994.
- (4) Vela, N. P.; Olson, L. K.; Caruso, J. A. *Anal. Chem.* **1993**, *65*, 585A-597A.
- (5) *Chemical Speciation in the Environment*, Ure, A. M., Davidson, C. M., Eds., Blackie Academic & Professional: London, 1995.
- (6) Cline Love, L. J.; Habarta, J. G.; Dorsey, J. G. *Anal. Chem.* **1984**, *56*, 1132A-1148A.
- (7) Khaledi, M. G. *J. Chromatogr. A* **1997**, *780*, 3-40.
- (8) Jarvis, K. E.; Gray, A. L.; Houk, R. S. *Handbook of Inductively Coupled Plasma Mass Spectrometry*; Chapman and Hall: New York, NY, 1992.
- (9) Hong, D., Wang, J., Dorsey, J. G., Caruso, J. A. *J. Chromatogr. A* **1995**, *694*, 425-431.
- (10) Berthod, A.; Girard, I.; Colette, G. *Anal. Chem.* **1986**, *58*, 1363.
- (11) Rosen, M. J. *Surfactants and Interfacial Phenomena*; John Wiley & Sons: New York, NY, 1978.
- (12) Woodrow, B. N.; Dorsey, J. G.; *Environ. Sci Technol.* **1997**, *31*, 2812-2820.
- (13) Tani, H.; Kamidate, T.; Watanabe, H. *J. Chromatogr. A* **1997**, *780*, 229-241.
- (14) Dorsey, J. G.; DeEchegaray, M. T.; Landy, J. S. *Anal. Chem.* **1983**, *55*, 924-928.
- (15) Armstrong, D. W.; Ward, T. J.; Berthod, A. *Anal. Chem.* **1986**, *58*, 579-582.
- (16) Khaledi, M. G.; Strasters, J. K.; Rodgers, A. H.; Breyer, E. D. *Anal. Chem.* **1990**, *62*, 130-136.
- (17) Kord, A. S.; Khaledi, M. G. *Anal. Chem.* **1992**, *64*, 1894-1900.
- (18) Armstrong, D. W.; Nome, F. *Anal. Chem.* **1981**, *53*, 1662-1666.
- (19) Arunyanart, M.; Cline Love, L. J. *Anal. Chem.* **1984**, *56*, 1557-1561.
- (20) Packer, A.; Donbrow, M. *J. Pharm. Pharmacol.* **1963**, *15*, 317-324.
- (21) Okada, T.; *Anal. Chem.* **1988**, *60*, 1511-1516.

Chapter 18

Selectivity in Micellar Liquid Chromatography

Surfactant-Bonded Phase Associations in Micellar Reversed Phase Liquid Chromatography

Barry K. Lavine ¹, Sumar Hendayan ¹, William T. Cooper ², and Yifang He ²

¹ Department of Chemistry, Clarkson University, Potsdam, NY 13699-5810

² Department of Chemistry, Florida State University, Tallahassee, FL 32306-3006

Abstract

Micellar reversed phase liquid chromatography (RPLC) and solid state NMR have been used to study the interactions of two ionic surfactants with alkyl and cyanopropyl bonded phase columns. The two surfactants, sodium dodecyl sulfate (SDS) and cetyltrimethylammonium bromide (CTAB) are commonly used in micellar RPLC. Differences in selectivity between CTAB and SDS micellar RPLC on alkyl bonded phases can be attributed to the differing nature of the SDS- and CTAB- bonded phase association. For SDS, the association leads to the formation of an anionic hydrophilic surface layer, which would explain the superior resolution achieved by SDS micellar mobile phases for hydrophilic compounds on C-18. For CTAB, the association leads to a more hydrophobic bulk stationary phase, where the nitrogen head group is partially incorporated into the C-18 phase because of strong hydrophobic interactions between the C-18 bonded chains and the methyl nitrogens. The unusual behavior exhibited by cyano bonded phase columns towards ionogenic compounds in SDS and CTAB micellar RPLC can be attributed to strong interactions between the polar head group of the ionic surfactant and the cyano functionality of the polar bonded phase. Models depicting the structure of the surfactant modified C-18 and cyanopropyl bonded stationary phase are proposed from solid state NMR data, and these models are in good agreement with the selectivity exhibited by these bonded phase columns toward polar and ionogenic compounds in micellar RPLC.

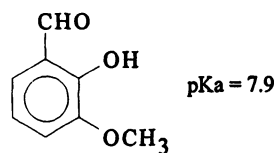
INTRODUCTION

The deliberate use of micelles and their unique properties for separations in reversed phase liquid chromatography (RPLC) has been the subject of numerous reports, since the pioneering work of Armstrong and Henry in 1980 [1]. They showed that traditional organic modifiers used in RPLC can be replaced with micelles, which are dynamic assemblies of surfactant molecules. Micelles provide a unique set of interactions for neutral and ionogenic compounds in the aqueous mobile phase. The solubilization of a compound by a micelle is akin to surface adsorption, where electrostatic and hydrophobic interactions are important.

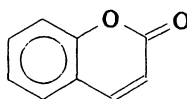
The unique capabilities of micellar mobile phases can be attributed to the ability of micelles to compartmentalize and organize solutes at the molecular level. For example, compartmentalization of organic molecules at the molecular level has been used to great advantage in the development of sensitive fluorescence detection schemes in MLC [2,3]. Fluorescence is enhanced via micelles because the viscosity of the micelle is higher, which retards the movement of the bound solute. Quenching becomes less of a problem, since collision induced radiationless decay is less likely to occur. Hence, the enhanced quantum yields and greater fluorescence intensities that occur with micellar mobile phases can be attributed to micelle solubilization, which protects the excited singlet state.

Although separational selectivity in MLC has received some attention [4], more work is needed to fully realize the potential of micellar mobile phases for enhancing chromatographic separations. The ability of micelles to selectively bind solute molecules is thought to be the basis for separations in micelle mediated liquid chromatography [5]. However, surfactant molecules are readily adsorbed on hydrocarbonaceous stationary phases. Since many stationary phase properties are affected by surfactant adsorption [6,7], the nature of the association between the surfactant monomer and the bonded phase can have profound implications with regard to retention and selectivity in MLC.

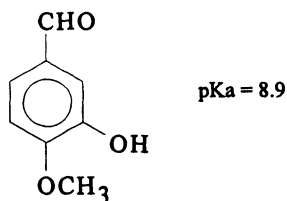
Employing a set of six vanillin compounds as retention probes (see Figure 1), the role of the surfactant coated stationary phase in the MLC separation process has been investigated. The effect of surfactant adsorption on selectivity in MLC was evaluated by examining the retention behavior of the vanillin compounds in sodium dodecyl sulfate (SDS) and cetyltrimethyl ammonium bromide (CTAB) micellar media. Differences in selectivity between CTAB and SDS micelle mediated liquid chromatography on C-18 can be attributed to the differing nature of the SDS- and CTAB-bonded phase association. For SDS, the association leads to the formation of an anionic hydrophilic surface layer, which would explain the superior resolution obtained by SDS for hydrophilic compounds on C-18. For CTAB, the association leads to a more hydrophobic bulk stationary phase, where the nitrogen head group is partially incorporated into the C-18 bonded phase because of strong hydrophobic interactions between the C-18 chains and the methyl nitrogens. The unusual behavior



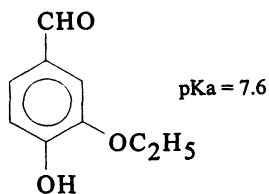
Orthovanillin



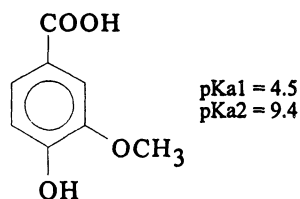
Coumarin



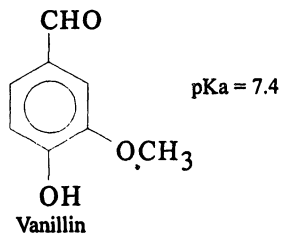
Isovanillin



Ethylvanillin



Vanillic acid



Vanillin

Figure 1. Vanillin test mixture. (Adapted from Figure 1 of reference 10 with the kind permission of the American Chemical Society.)

of cyanopropyl bonded phase columns towards ionogenic compounds in SDS and CTAB micellar RPLC can be attributed to the strong interactions between the polar head group of the ionic surfactant and the cyano functionality of the polar bonded phase. Models depicting the structure of the surfactant modified C-18 and cyanopropyl bonded phase are proposed from solid state NMR data, and these models are in good agreement with the selectivity exhibited by C-18 and cyanopropyl bonded phase columns toward ionogenic and polar compounds in MLC.

EXPERIMENTAL

Chemicals. Vanillin, isovanillin, orthovanillin, coumarin, ethylvanillin, and vanillic acid were obtained from Aldrich and were used as received. Stock solutions of the vanillin compounds were prepared in methanol and diluted to the appropriate working concentration using 50% methanol/water. The surfactants, SDS and CTAB, were purchased from BDH Chemicals Ltd. They were purified by first dissolving them in ethanol, followed by addition of activated charcoal to the solution. After the charcoal was separated from the mother liquor by filtration, the surfactant was recrystallized from the ethanol and dried in an oven at 65^o C.

SDS and CTAB micellar mobile phases were prepared from the recrystallized surfactants using HPLC grade distilled water. Methanol-water mobile phase solutions were also prepared from HPLC grade solvents (J.T.Baker). All mobile phase solutions were filtered twice with a 0.45 μm Nylon membrane filter (Rainin Instruments, Woburn, MA) to remove particulate matter. Prior to chromatographic use, the solutions were degassed and the pH was adjusted to 3 with hydrochloric acid to prevent ionization of the vanillin compounds in the mobile phase solutions.

Chromatographic Measurements. High performance liquid chromatographic (HPLC) measurements were made with a Rainin 81-20 M analytical HPLC system which incorporates two Rainin HP pumps (Rainin Instruments), an Apple Macintosh SE computer as the controller, a Model 7125 Rheodyne injection valve, a Rainin Dynamax mixer, and a Knauer variable wavelength UV-visible spectrometer (Berlin, Germany) as the detector. The analytical column was either an Apex I C-18 or Apex I cyanopropyl (10 cm x 4.6 mm id, 5- μm). The columns, which were purchased from Jones Chromatography (Golden, CO), were made from the same 5 μm silica support. Both the analytical column and mobile phase reservoir were water jacketed and temperature controlled. A silica precolumn (Rainin Instruments) was placed between the injector and the pump to saturate the mobile phase with silicates which minimized dissolution of the analytical column packing. Separate columns were used for CTAB and SDS, as well as the methanol/water mobile phase because of the strong adsorption of ionic surfactants on the stationary phase of C-18 and cyanopropyl bonded phase columns.

Solid State NMR Measurements. Adsorption of SDS and CTAB on C-18 and cyanopropyl chemically derivitized silica was investigated using cross polarization/magic angle spinning ¹³C NMR with high-power proton decoupling

(CP/MAS ^{13}C NMR). All NMR experiments were performed at 50 MHz on a Bruker/IBM WP-200 SY spectrometer equipped with an IBM solids control accessory and a Doty-type solid-state probe. The Doty-type probe, which was software controlled to permit automatic variation of all pulse parameters, was a double-tuned single-coil design with a bullet type rotor. Two different pulse sequences were utilized in the NMR experiments (see Figures 2 and 3), with each pulse sequence performed with a 3-s recycle time. The ^{13}C spectra were externally referenced to para-d-t-butyl benzene, and all chemical shift values were expressed as parts per million downfield from tetramethylsilane.

To prepare a sample for solid state NMR, 0.5 g of 5 μm C-18 or cyanopropyl reversed phase material was equilibrated with 10 ml of 0.05 M aqueous SDS or CTAB. The equilibration period was at least 24 hours. During equilibration, a wrist action shaker was used to agitate the sample. After equilibration, each sample was filtered onto a 0.45 μm Nylon 66 membrane filter and vacuum dried at 35 $^{\circ}\text{C}$ for 2 days prior to being packed into the rotor of the solid-state probe.

RESULTS AND DISCUSSION

Solid state NMR was used in this study to ascertain the mechanism through which SDS or CTAB is incorporated into and modifies the stationary phase of alkyl and polar bonded phase columns. An advantage of solid state NMR, which makes the technique well suited for this study, is its ability to differentiate surfactant molecules intercalated or in direct contact with the bonded phase from those not in contact with the bonded phase. Although solid state NMR can provide information about the nature of the association between the surfactant and the bonded phase, no direct information on how the surfactant modified stationary phase interacts with solutes in the mobile phase is provided by this NMR technique. One approach for the direct measurement of these interactions is the use of retention probes, which can be selected to emphasize specific physical or chemical interactions of the solute with the mobile or stationary phase. In this study, we chose a set of six vanillin compounds to serve as retention probes, because our objective was to study hydrophilic, not hydrophobic interactions in MLC. NMR and micellar RPLC retention data obtained for a C-18 and cyanopropyl bonded phase column are summarized and discussed below for SDS and CTAB.

C-18: Retention Data. A series of chromatograms were run to illustrate some of the unique advantages associated with micellar mobile phases. The test mixture consisted of vanillin, isomers of vanillin, and analogues of vanillin. Figure 4 shows the separation of the test mixture on an Apex I C-18 column with the following mobile phases: methanol/water, 0.02 M SDS, and 0.02 M CTAB. 20% methanol in water is recommended by Supelco for the separation of vanillin from the other compounds in extract of vanilla [8]. For SDS, the optimum separation is achieved using a 0.02 M SDS mobile phase, whereas 0.02 M CTAB does not give the optimum separation for the cationic surfactant. However, it is representative of the separation which can be obtained for the test mixture using CTAB micellar mobile phases and is shown for comparative purposes. For each of the mobile phases, the pH was adjusted to 3, which

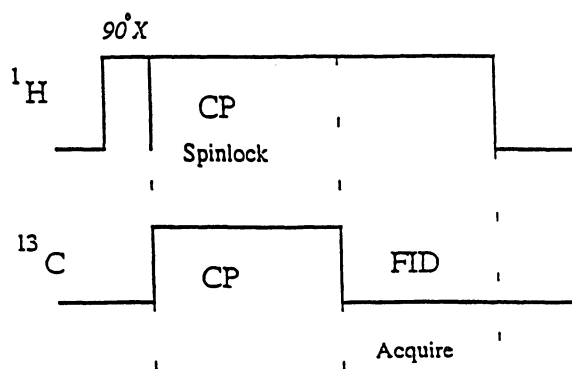


Figure 2. Pulse sequence used for the determination of T_{CH} . (Reprinted from Figure 2 of reference 6 with kind permission of Marcel Dekker.)

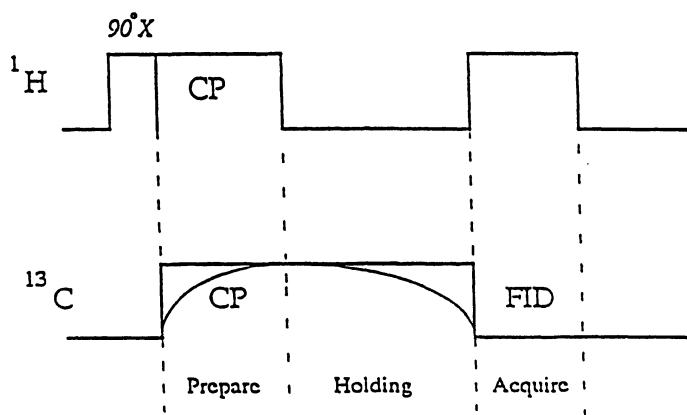


Figure 3. Pulse sequence used for the determination of $T_{1\rho C}$. (Reprinted from Figure 3 of reference 6 with kind permission of Marcel Dekker.)

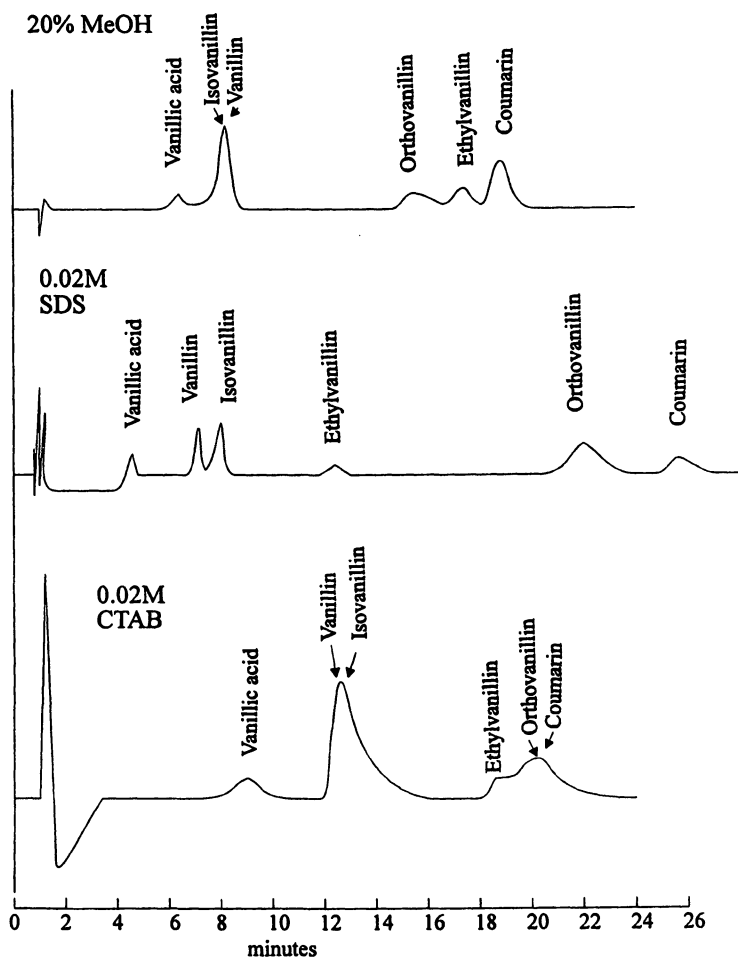


Figure 4. Chromatograms of the test mixture on Apex I C-18 with the following mobile phases: 20% methanol in water, 0.02 M SDS, and 0.02 M CTAB. Flow rate was 1.0 ml/min; pH of each mobile phase was 3.0. (Adapted from Figure 2 of reference 10 with kind permission of the American Chemical Society.)

ensured that protonic equilibria would not be a complicating factor in the interpretation of the retention data.

Several things are apparent from an examination of the data. First, the test mixture is separated by the SDS micellar mobile phase but not by the hydro-organic or CTAB mobile phase. Second, the variability in the resolution of the test mixture among the three mobile phases is due to differences in chromatographic selectivity, since the efficiency of the separation process for all three mobile phases appears comparable. Third, the retention time of four of the six vanillin compounds is greater with 0.02 M CTAB than with 0.02 M SDS, which is surprising because the CTAB mobile phase contains significantly more micelles. (The cmc of CTAB at ambient temperature is 0.9 mM, whereas the cmc of SDS is 8mM at ambient temperature.) This suggests that interactions between these compounds and the stationary phase are stronger with CTAB modified C-18 than with SDS modified C-18.

Figure 5 shows the separation of the test mixture at four different SDS concentrations: 0.02M, 0.03M, 0.04M, and 0.04M. Clearly, the separation of the vanillin test mixture is more favorable at low SDS concentrations. This suggests that solute-stationary phase interactions are primarily responsible for the successful separation of the test mixture. At higher SDS concentrations, there are more micelles in the mobile phase. The net result is a greater role for micelle-solute interactions in the separation of the vanillin compounds, which is not altogether beneficial. (Note that surfactant stationary phase interactions are independent of micelle concentration in the mobile phase, because the amount of surfactant adsorbed on the stationary phase remains constant once the concentration of surfactant in the mobile phase is above the cmc [9]).

For CTAB, the separation of the test mixture improves with higher surfactant concentration (see Figure 6), which implies that micelle solute interactions are beneficial for the separation of the test mixture on C-18 with CTAB. This result is not surprising, since the selectivity of CTAB micelles towards phenols is well known [10] and is probably the result of a secondary equilibrium process involving the transfer of a proton from the phenol to a water molecule in the Stern region of the CTAB micelle. Taken together, the longer retention time of the vanillin compounds with CTAB micellar mobile phases and the improvement in resolution of the test mixture with increasing CTAB concentration suggest possible differences in the nature of the SDS- and CTAB- bonded phase association.

C-18: Solid State NMR. Solid state NMR was used to study the interaction of the two ionic surfactants with the C-18 bonded phase. From an examination of the NMR spectra of C-18, pure SDS, pure CTAB, SDS adsorbed on C-18, and CTAB adsorbed on C-18, it was evident that the methylene carbon alpha to the polar head group of the surfactant could serve as a probe to study the sorptive behavior of SDS and CTAB on C-18. Resonances from the other surfactant nuclei were obscured by the bonded phase, preventing their use as probes. In other words, there was significant peak overlap in the 0 to 50 ppm region - one simply could not distinguish aliphatic surfactant

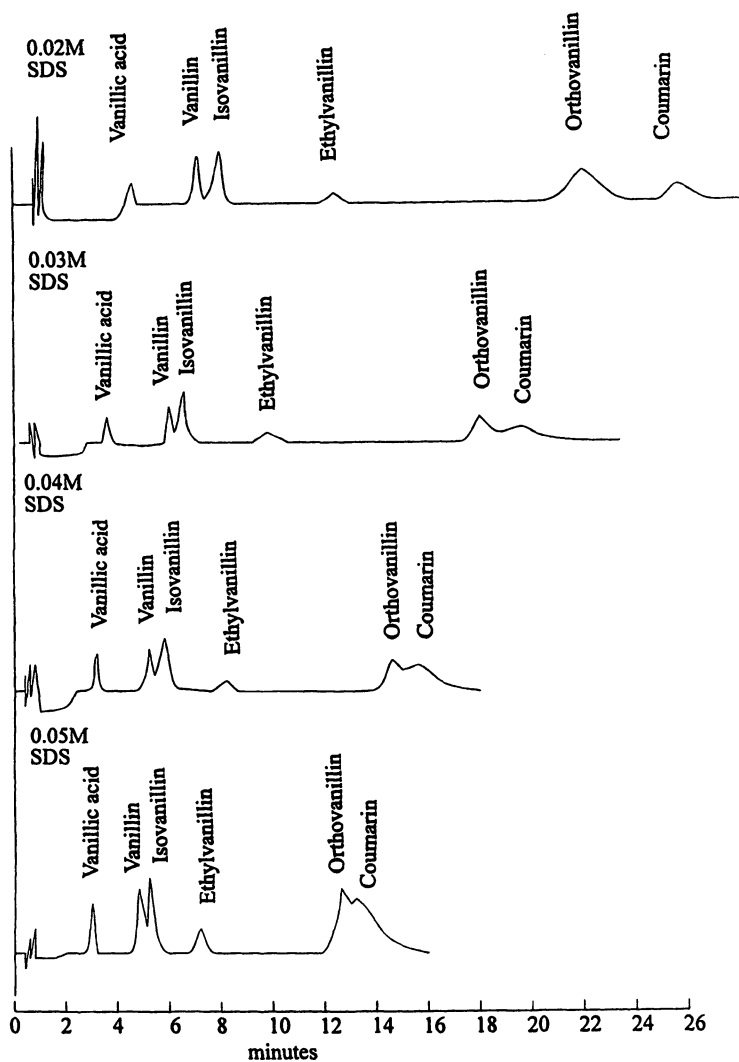


Figure 5. Chromatograms of the test mixture on Apex I C-18 with the following micellar mobile phases: 0.02 M SDS, 0.03 M SDS, 0.04 M SDS, and 0.05 M SDS. Flow rate was 1.0 ml/min, and the pH of each mobile phase solution was 3. (Adapted from Figure 3 of reference 10 with kind permission of the American Chemical Society.)

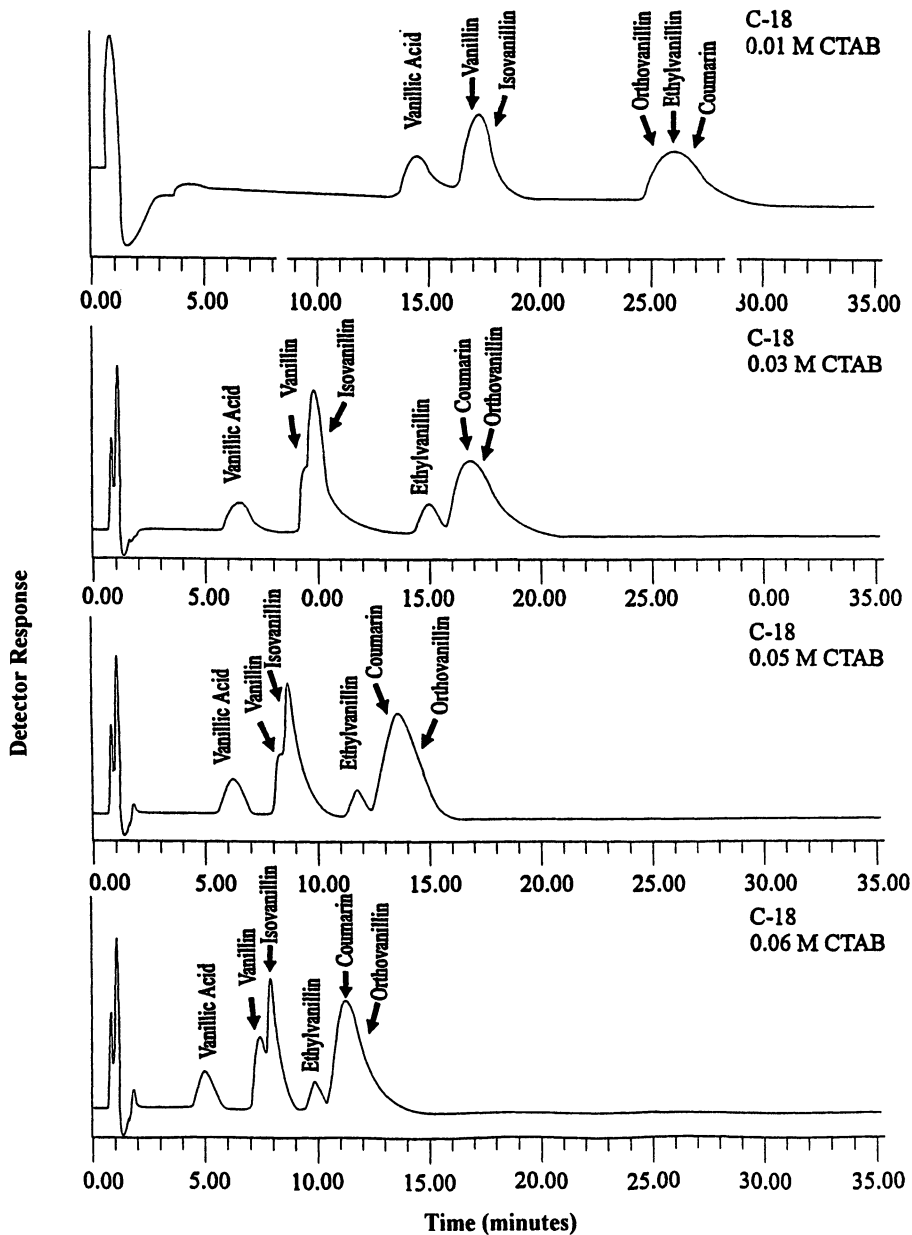


Figure 6. Chromatograms of the text mixture on Apex I C-18 with the following micellar mobile phases: 0.01 M CTAB, 0.03 M CTAB, 0.05 M CTAB, and 0.06 M CTAB. Flow rate was 1.0 ml/min, and the pH of each mobile phase solution was 3. (Adapted from Figure 14 of reference 6 with kind permission of Marcel Dekker.)

resonances from the other resonances due to the alkyl bonded phase. Although the ^{13}C nucleus of the N-methyl group of CTAB was not obscured by other resonances, we did not consider it a reliable probe for molecular motion because of the rapid rotation of the methyl group which can partially decouple the carbon and hydrogen nuclei.

Table 1 lists cross polarization time constants (T_{CH}) for the alpha carbon nuclei of SDS and CTAB before or after surfactant adsorption onto the bonded phase. Because T_{CH} is most efficient for static and near static C-H dipolar interactions, it can be related to the mobility of the nuclei under investigation. For SDS and CTAB, an increase in T_{CH} is observed after surfactant adsorption onto the C-18 bonded phase. This indicates that the alpha carbon of the surfactant is more mobile after surfactant adsorption. This observation, consistent with a model of the alpha carbon nuclei in direct contact with the fluid like bonded phase, is significant because it constitutes direct evidence for wetting of the bonded phase by the surfactant monomer.

Table 1. *Relaxation Parameters of the Alpha Carbon Nuclei in Pure and Adsorbed Surfactant

Nuclei	T_{CH}	$T_{1\rho\text{C}}$
alpha carbon of SDS	0.13 ± 0.03	203.4 ± 0.24
alpha carbon of SDS adsorbed on C-18	1.23 ± 0.01	Dispersion pattern
alpha carbon of CTAB	0.03 ± 0.003	14.50 ± 0.58
alpha carbon of CTAB adsorbed on C-18	0.54 ± 0.22	24.20 ± 1.58

*Uncertainties in T_{CH} and $T_{1\rho\text{C}}$ were computed from the statistical parameters of the least squares fitting of the data.

Figures 7 and 8 show the results of several variable holding time experiments for SDS and CTAB. The data were plotted in familiar semilog fashion. Information about the relaxation and motion behavior of the nuclei can be obtained from these plots. A linear decay plot suggests homogeneous relaxation behavior, whereas a nonlinear decay plot indicates a distribution of relaxation times for the nucleus. From the reciprocal of the slope of the semilog decay curve, $T_{1\rho\text{C}}$ can be obtained. The semilog decay curve for the alpha carbon of solid SDS is linear, which suggests homogeneous relaxation behavior. On the other hand, the decay curve for adsorbed SDS is not linear. The alpha carbon of adsorbed SDS does not exhibit homogeneous relaxation behavior. We attribute the so-called dispersion pattern in the decay plot to the sulfate head group of SDS, which is evidently quite mobile. The sulfate head group is not in direct contact with the bonded phase and has many different orientations available to it. Since the alpha carbon will possess a unique relaxation time for each orientation available to the sulfate head group, it is not surprising that a dispersion pattern is observed for the alpha carbon, when it is in direct contact with the fluid like C-18 alkyl bonded phase.

The semilog decay curves for CTAB and adsorbed CTAB are linear (see Figure 7), which indicates homogeneous relaxation behavior for the alpha methylene carbon atom of solid and adsorbed CTAB. The value of $T_{1\rho\text{C}}$ for the alpha methylene carbon atom of adsorbed CTAB is greater than $T_{1\rho\text{C}}$ for pure CTAB (see Table 1), suggesting that an

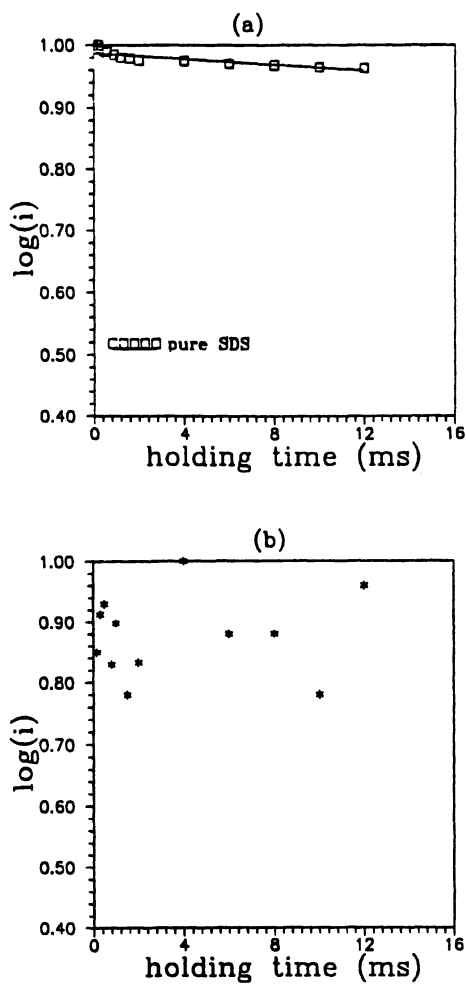


Figure 7. Semilog decay plots for the alpha carbon of solid and adsorbed SDS on C-18. (Adapted from Figure 8 of reference 6 with kind permission of Marcel Dekker.)

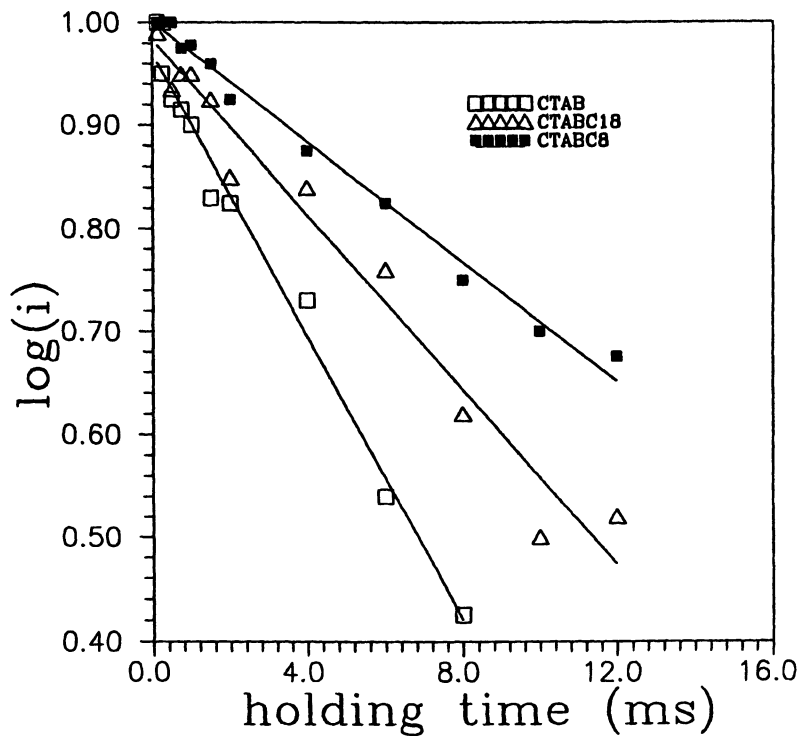


Figure 8. Semilog decay plots for the alpha carbon of solid and adsorbed CTAB on C-18. (Adapted from Figure 9 of reference 6 with kind permission of Marcel Dekker.)

increase in the mobility of the carbon nuclei has occurred after adsorption of CTAB onto the C-18 alkyl bonded phase. These conclusions are reinforced by the variable contact time data. Taken together, changes in T_{CH} and T_{IPC} indicate that the head group of CTAB is in intimate contact with the C-18 alkyl bonded phase.

We interpret the observed changes in alpha carbon mobility upon adsorption of surfactant on the bonded phase as resulting from two entirely different forms of surfactant monomer association with the bonded phase. For SDS, the hydrophobic tail is associated with the bonded alkyl phase; the sulfate head group is oriented away from the C-18 surface. Adsorption of SDS in the manner described would lead to the formation of a hydrophilic layer on C-18, which would explain the superior resolution achieved with SDS for the vanillin compounds, which probably undergo some type of selective hydrogen bonding interaction with the layer. The hydrophilic layer formed by adsorbed SDS would also affect the penetration depth of the vanillin compounds in the bonded phase because of strong hydrogen bonding interaction between these compounds and the layer. The expected result would be a decrease in hydrophobic interactions between the vanillin compounds and the C-18 stationary phase. Clearly, this is part of the answer as to why the retention time of the vanillin compounds is greater with 0.02 M CTAB than 0.02 M SDS.

For CTAB, the head group is oriented closer to the silica surface due to hydrophobic interactions between the N-methyl groups and the bonded phase. Evidently, CTAB is incorporated at least partly in the bonded phase giving rise to a modified bulk phase that is more hydrophobic than SDS modified C-18. Figure 9 depicts the proposed models for SDS and CTAB adsorption on C-18 from aqueous micellar solutions.

Berthod [11] has measured adsorption isotherms for SDS and CTAB on C-18 bonded phase columns. The presence of large amounts of sodium chloride (0.20 M) in the micellar mobile phase dramatically increases the amount of SDS adsorbed on C-18. This is consistent with the proposed model for SDS adsorption, since the presence of excess sodium chloride in the mobile phase diminishes electrostatic repulsion between the sulfate head groups of the adsorbed surfactant molecules. However, the presence of excess sodium chloride does not affect the total amount of CTAB adsorbed on the C-18 stationary phase. This is consistent with the proposed model for CTAB adsorption, since the N-alkyl head group of adsorbed CTAB is partly obstructed by the C-18 chains. Clearly, the addition of sodium chloride to the micellar mobile phase would not be expected to have a large effect on reducing electrostatic repulsion between the N-alkyl head group of adsorbed CTAB.

Cyanopropyl. Cyanopropyl bonded phase columns utilizing micellar mobile phases can exhibit selectivities very different from C-18 columns employing the same micellar mobile phase. For example, the retention time of some ionogenic compounds on cyanopropyl bonded phase columns actually increases with increasing micelle concentration, which is opposite of what is considered to be normal retention behavior in micellar RPLC [12]. This effect, known as antibinding behavior, occurs with

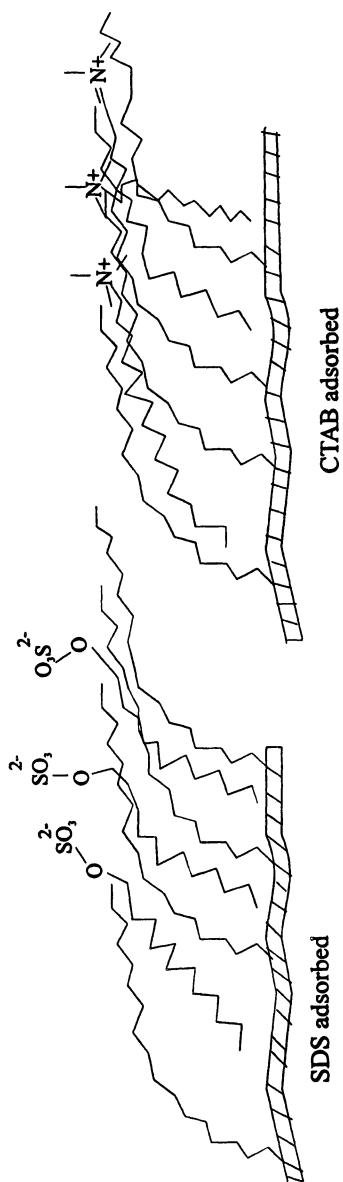


Figure 9. Proposed model for SDS and CTAB adsorption on C-18. (Adapted from Figure 6 of reference 10 with kind permission of the American Chemical Society.)

compounds that possess the same charge as the surfactant. It is an excluded volume effect, because the compound is excluded not only from the micelle, but from the double layer that surrounds the micelle. Clearly, antibinding behavior occurs as a result of a different form of surfactant monomer association with the cyanopropyl bonded phase, since it is not observed with C-18 alkyl bonded phases.

Solid state NMR was used to study the interactions of SDS and CTAB with the cyanopropyl bonded stationary phase. Figures 10 and 11 show the results from several variable holding time experiments for SDS and CTAB. The linear decay curves for the alpha methylene carbon atom indicate homogeneous relaxation behavior for both solid and adsorbed CTAB and SDS. (For SDS, only data at short holding times is shown due to low S/N at holding times greater than 1 ms.) Furthermore, $T_{1\rho C}$ for the alpha methylene carbon atom of solid SDS and CTAB is greater than $T_{1\rho C}$ for adsorbed SDS and CTAB (see Table 2). This result is surprising, because the bonded phase constitutes a more liquid like environment than crystalline surfactant. One would expect $T_{1\rho C}$ for the adsorbed surfactant to be larger than $T_{1\rho C}$ for the solid surfactant, which in fact is what we observed in our study on surfactant adsorption involving C-18 alkyl bonded phases (see Table 1). In all likelihood, this difference is due to a strong association between the head group of the surfactant and the cyano group of the polar bonded phase. The alpha carbon nuclei of the adsorbed surfactant is not experiencing random motion. It is not accessing all of the orientations available to it with respect to the magnetic field because of the strong association between the cyano group of the polar bonded phase and the polar head group of the surfactant. This would explain the ten-fold and two-fold decrease in the value of $T_{1\rho C}$ for the alpha carbon nuclei of adsorbed SDS and CTAB.

Table 2. *Relaxation Parameters of Alpha Carbon Nuclei in Pure and Adsorbed Surfactant

Surfactant	T_{CH} (ms)	$T_{1\rho C}$ (ms)
CTAB	0.03 ± 0.003	14.50 ± 0.58
CTAB adsorbed on cyanopropyl	0.25 ± 0.050	7.410 ± 1.09
SDS	0.13 ± 0.030	203.4 ± 0.42
SDS adsorbed on cyanopropyl	0.40 ± 0.030	2.19 ± 0.31

*Uncertainties in T_{CH} and $T_{1\rho C}$ were computed from the statistical parameters of the least squares fitting of the data.

Figure 12 shows semilog decay curves for the cyano group carbon atom before and after SDS and CTAB adsorption. (The cyano carbon resonance at 120 ppm is not obscured by resonances from surfactant or other bonded phase nuclei, so direct observation of the bonded phase was possible in this study.) The dispersion pattern of the cyano group for the pure stationary phase material can be rationalized on the basis of chemical considerations. Cyano groups are known to interact with residual silanols [13]. The fact that some residual silanols will and some will not interact with cyano groups and to the varying degrees they do would be expected to yield a dispersion pattern.

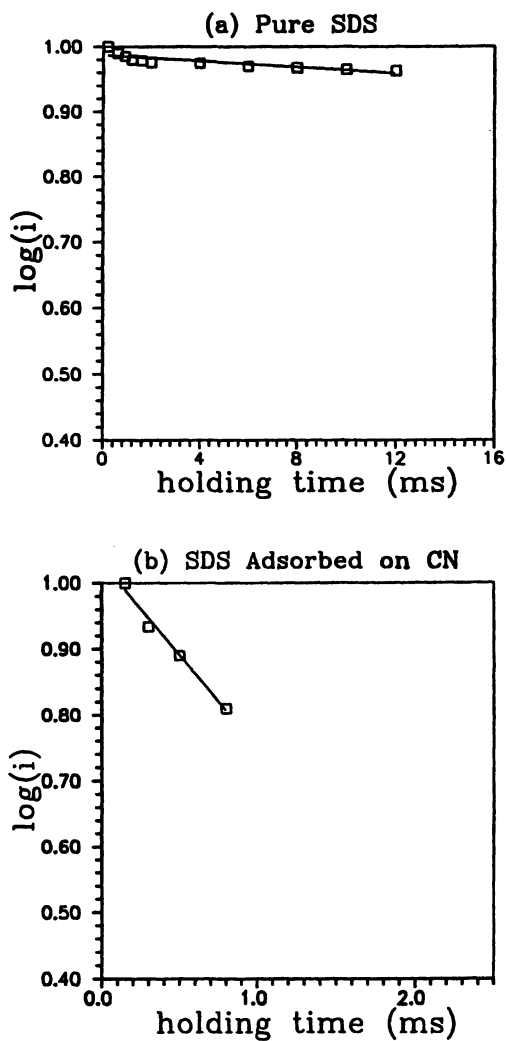


Figure 10. Semilog decay plots for the alpha carbon of solid and adsorbed SDS on cyanopropyl. (Adapted from Figure 11 of reference 6 with kind permission of Marcel Dekker.)

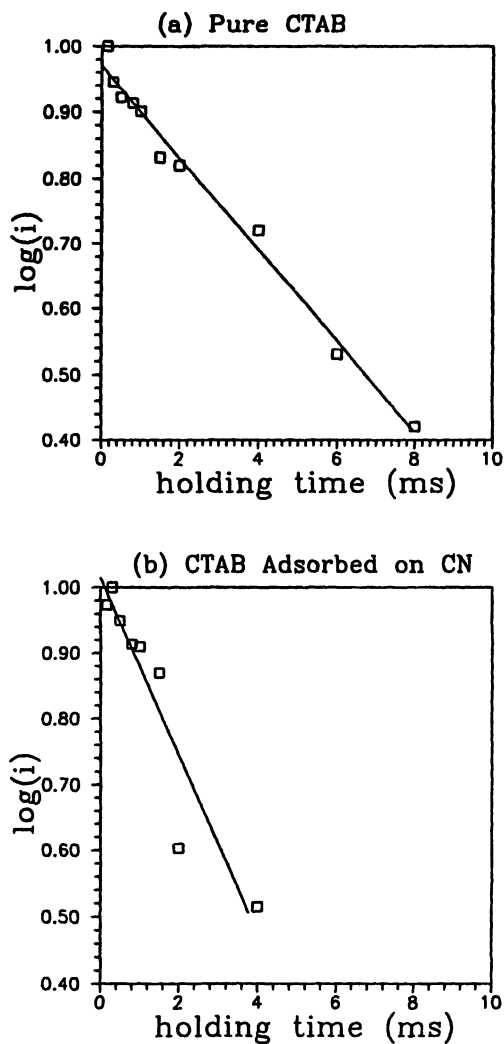


Figure 11. Semilog decay plots for the alpha carbon of solid and adsorbed CTAB on cyanopropyl. (Adapted from Figure 12 of reference 6 with kind permission of Marcel Dekker.)

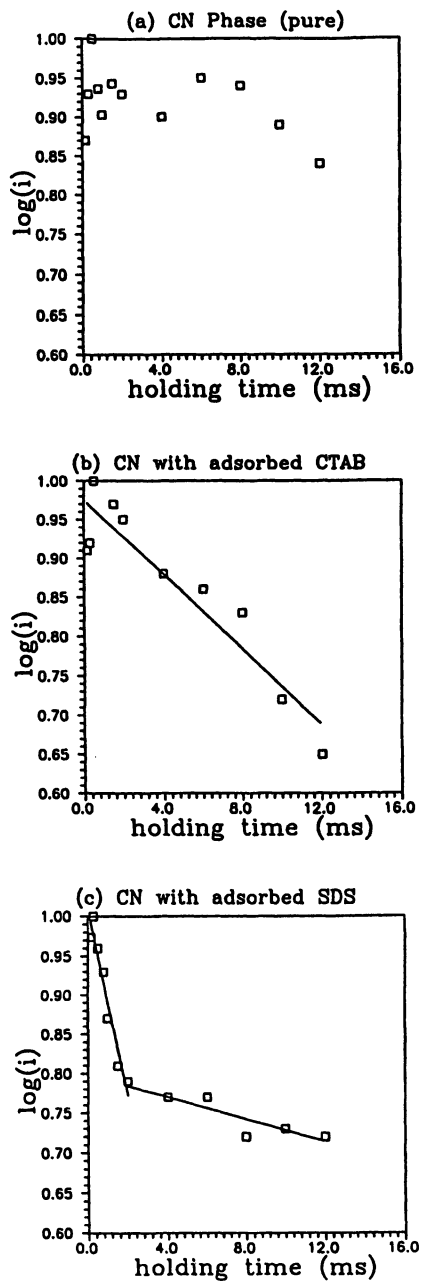


Figure 12. A plot of log intensity versus holding time for the cyano carbon of the (a) pure bonded phase, (b) cyano bonded phase with adsorbed CTAB, and (c) cyano bonded phase with adsorbed SDS. (Adapted from Figure 13 of reference 6 with kind permission of Marcel Dekker.)

The linear and bilinear decay curves obtained for the cyano group of the SDS and CTAB modified stationary phase suggest that a decrease in the number of relaxation states available to the cyano group has occurred as a result of surfactant adsorption. We attribute the decrease in the number of relaxation states to the strong association between the polar head group of the surfactant and the cyano group of the polar bonded phase. The sulfate head group of SDS and the N-alkyl head group of CTAB probably interact with the cyano group of the polar bonded phase through some form of electrostatic interaction.

It has been reported [5] that quaternary N-alkyl head groups interact with the OH groups on C-18 alkyl bonded phases. Because the OH groups are more accessible on cyano phases than on C-18 alkyl bonded phases, there is the possibility that some CTAB molecules will adsorb head down with their tails projected upward creating a pseudo alkyl bonded phase. Hence, a second group of CTAB molecules may associate hydrophobically forming a bilayer. Although there is no solid state NMR data to support this contention, the possibility of this bilayer being formed cannot be ruled out.

Our conclusions regarding the modification of the cyanopropyl bonded phase by SDS or CTAB can explain the unusual behavior exhibited by cyanopropyl bonded phase columns in micellar RPLC. For example, anti-binding behavior [14] occurs on a cyanopropyl column, because the charged head group of the adsorbed surfactant monomer is "tied up" by the cyano functionality of the polar bonded phase. Hence, there is little free electrostatic charge to prevent migration of the ionized solute into the polar bonded phase. By comparison, anti-binding behavior does not occur on C-18 alkyl bonded phases. This is because of the higher surface charge of SDS or CTAB modified C-18, which is a result of the sulfate or N-alkyl head group not being as strongly associated with the C-18 alkyl bonded phase.

Our conclusions regarding the modification of cyanopropyl bonded phase columns by SDS or CTAB adsorption can also explain differences in selectivity between C-18 and cyanopropyl bonded phase columns toward weak bases. When a C-18 column is used in SDS micelle mediated liquid chromatography, the retention time of the protonated form of the weak base is longer than that of the unprotonated form because of strong electrostatic interactions between it and the SDS modified alkyl bonded phase [15]. On the other hand, the protonated form of the weak base has a shorter retention time than that of the unprotonated form when a cyanopropyl bonded phase column is used because of strong interactions between the protonated form of the weak base and the SDS micelles. In all likelihood, the lower surface charge of the SDS modified cyanopropyl bonded phase is responsible for solute-micelle interactions playing a more important role in the retention of weak bases and other ionogenic compounds on cyanopropyl bonded phase columns in MLC.

The model for surfactant adsorption developed from the NMR data cannot explain the S-type adsorption isotherms obtained for either SDS or CTAB on cyanopropyl

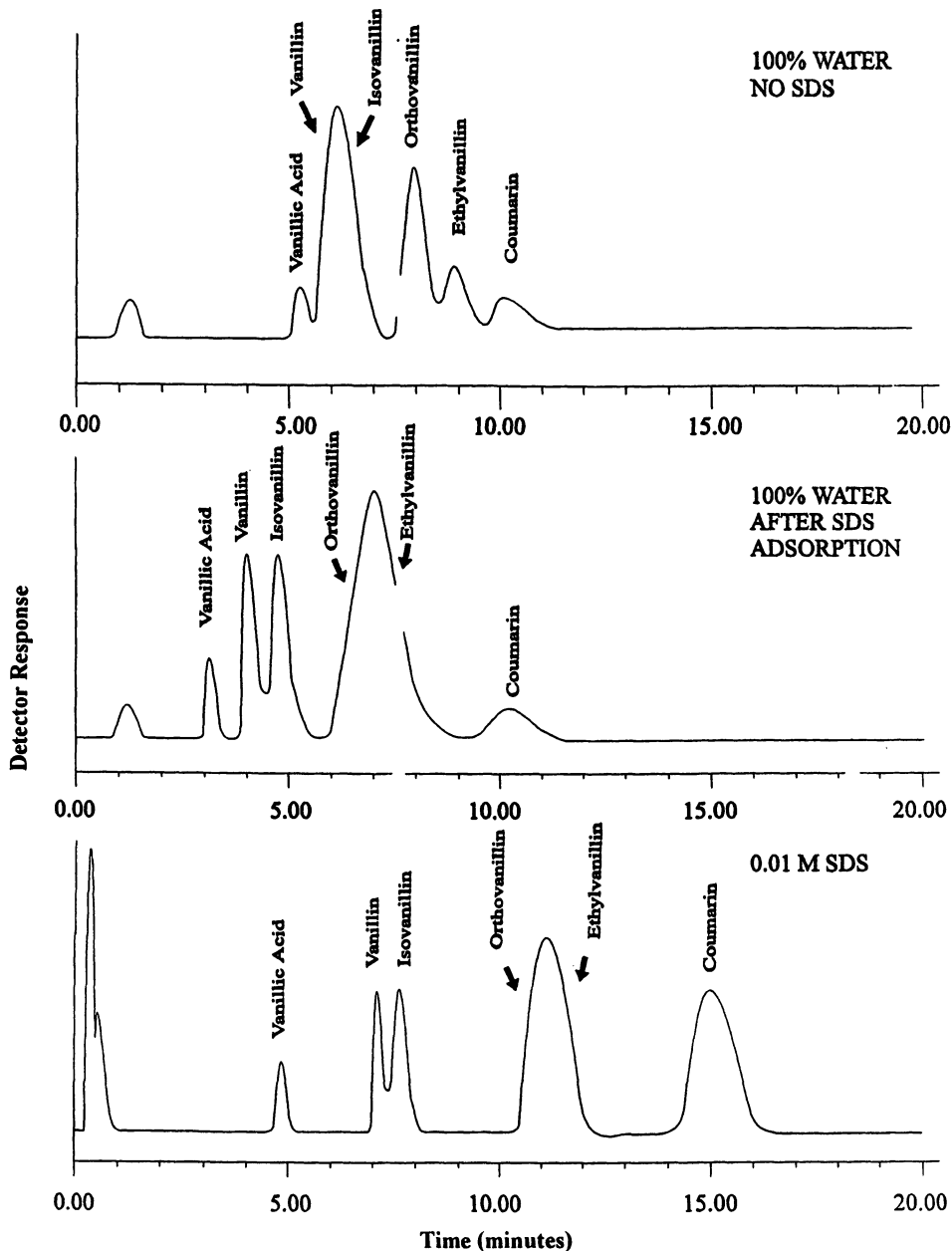


Figure 13. Chromatograms of the vanillin test mixture on a cyanopropyl column before, during, and after separations involving SDS micellar mobile phases. The pH of each mobile phase was 3, and the flow rate was 1.0 ml/min. (Adapted from Figure 14 of reference 6 with kind permission of Marcel Dekker.)

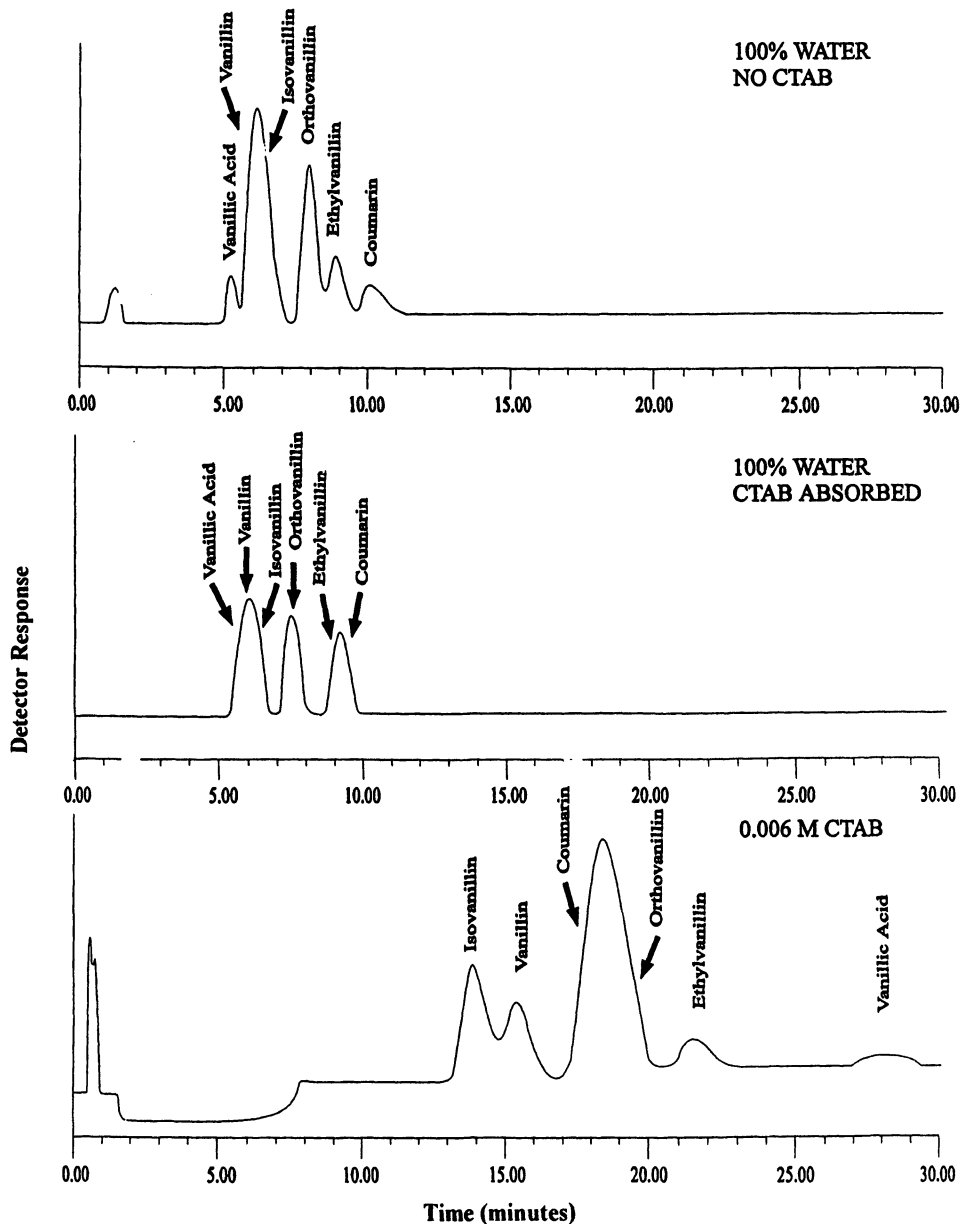


Figure 14. Chromatograms of the vanillin test mixture on a cyanopropyl column before, during, and after separations involving CTAB micellar mobile phases. The pH of each mobile phase was 3, and the flow rate was 1.0 ml/min. (Adapted from Figure 15 of reference 6 with kind permission of Marcel Dekker.)

columns [16], which can be interpreted as due to cooperative adsorption. Nor can the model explain the longer retention time of the vanillin compounds when either SDS or CTAB micellar solutions are used as mobile phases in lieu of water as the mobile phase (see Figures 13 and 14). This result is surprising in view of the greater solvent strength of a CTAB or SDS micellar mobile phase. Evidently, solute stationary phase interactions are greater when these micellar solutions are used as mobile phases instead of pure water as the mobile phase. In all likelihood, small surfactant aggregates form within the cyanopropyl bonded phase when SDS or CTAB micellar solutions are used as the mobile phase. This phenomena is probably analogous to surfactant decorated polymers [17], with the bonded cyano chain assuming the role of the polymer. This hypothesis is plausible because the surfactant monomer is adsorbing parallel to the cyanopropyl bonded phase surface. (Solid state NMR data suggests that the alpha carbon and the hydrocarbon tail of the surfactant are in intimate contact with the cyanopropyl bonded phase. This can only occur if SDS or CTAB adsorption is parallel to the surface, since each bonded cyano chain is only 4 carbons in length.) The formation of surfactant decorated cyano chains would explain the increase in retention time of the vanillin compounds, as well as the S-type adsorption isotherms obtained for CTAB and SDS on cyanopropyl.

CONCLUSION

The results of an in-depth study on the effect of the bonded phase and surfactant charge type on selectivity in MLC has been presented. A hydrophilic test mixture has been separated on a variety of chromatographic support materials using either SDS or CTAB micellar mobile phases. In order to explain the observed differences in selectivity of SDS and CTAB micelle mediated liquid chromatography, it was necessary to determine the nature of the SDS- and CTAB- bonded phase association. Our conclusions supported by solid state NMR data indicate that different surfactant molecular orientations on the stationary phase can lead to dramatic differences in selectivity in MLC.

REFERENCES

1. Armstrong, D.W.; Henry, S.J. *J. Liq. Chromatog.*, **1980**, *3*, 657.
2. W. L. Hinze, in "Solution Chemistry of Surfactants," K.L.Mittal, Ed., Plenum Press, New York, 1979, Vol. 1, p. 78.
3. D.W. Armstrong, W.L.Hinze, K.H. Bui, and H.N. Singh, *Anal. Lett.*, **1981**, *14*, 1659.
4. Armstrong, D.W.; Stine; Stine, G.Y. *Anal. Chem.*, **1983**, *55*, 2317.
5. Hinze, W.L., in W.L.Hinze and D.W.Armstrong (Eds.), *Ordered Media in Chemical Separations*, ACS Symposium Series 342, American Chemical Society, Washington, DC., **1987**, pp 2-82.
6. Lavine, B.K.; Hendayana, S.; Cooper, W.T.; He, Y. *J. Liq. Chromatog.*, **1997**, *20(3)*, 351-401.
7. Borgerding, M.F.; Hinze, W.L.; Stafford, L.D.; Fulp, G. W.; Hamlin, W.C. *Anal. Chem.*, **1989**, *61*, 1353-1358.

8. Supelco, Technical Report, 1992, 11(4), pp 15-16.
9. Hung, C.T.; Taylor, R.B. *J. Chromatogr.*, **1981**, 209, 175-190.
10. Lavine, B.K.; Hendayan, S.; Tetreault, J. *Anal. Chem.*, **1994**, 66, 3458.
11. Berthod, A.; Girard, C.; Gonet, C. *Anal. Chem.*, **1986**, 58, 1362.
12. Arunyanart, M.; Cline-Love, L.J. *Anal. Chem.*, **1984**, 56, 1551.
13. Boudreau, S.P.; Smith, P.L.; Cooper, W.T. *Chromatography*, **1987**, 2(5), 31.
14. Armstrong, D.W.; Stine, G.Y. *JACS*, **1983**, 105, 2962.
15. Arunyanart, M.; Cline-Love, L.J. *Anal. Chem.*, **1985**, 57, 2837.
16. Berthod, A.; Girard, C.; Gonet, C. *Anal. Chem.*, **1986**, 58, 1356.
17. Goddard, E.D. *Colloids Surf.*, **1986**, 19, 255.

Chapter 19

Determination of Distribution Ratios of Aromatic Compounds between Aqueous Solution and Surfactant-Covered Silica by a Chromatographic Method

Stefan Holzheu, Thilo Behrends, and Reimer Herrmann

Department of Hydrology, University of Bayreuth, 95440 Bayreuth, Germany

The knowledge of distribution constants between aqueous solution and surfactant covered solid phases is important for the understanding of the process of adsolubilization and for applications based on this process. In this work equilibrium constants of 26 aromatic compounds were determined by a chromatographic method as a function of pH and of the adsorption density of hexadecyltrimethylammonium-bromide (HDTMAB) on silica. The dependency of the retention times on surfactant adsorption changes with increasing HDTMA coverage and is modified by pH. The changes can be explained by the transition of electrostatically driven surfactant adsorption to hydrophobic aggregation. Formation of core regions in the surfactant aggregates due to hydrophobic aggregation favors adsolubilization of non-polar compounds. At the same time equilibrium constants of polar organic compounds decrease because of the reduced interfacial area per surfactant molecule. Facilitated deprotonation of carboxylic and phenolic groups at higher pH results in an increasing adsolubilization efficiency when hydrophobic aggregation is considered and superequivalent adsorption is enabled.

The adsorption of surfactants on solid surfaces can be used to increase the sorption of organic compounds. This process is termed adsolubilization (1) and is the fundamental principle for several surfactant-based separation techniques. Potential applications of surfactant coated materials include admicelle chromatography (2), water treatment (3) or they can also be used in "active walls" in groundwater remediation (4). The distribution ratios of organic compounds between solution and surfactant covered solid phase have to be known to assess the ability of such a material to retain organic compounds. O'Haver et al. (5) remark that surfactant aggregates at solid surfaces, called

admicelles, have a higher selectivity compared to micelles. This difference is explained by the greater packing densities which can be obtained in admicelles. Differences between solubilization and adsolubilization might also be caused by the influence of the solid surface on other structural characteristics of the surfactant aggregates like the orientation of the surfactant molecules. This means that partition ratios cannot be easily transferred from solubilization to adsolubilization, but must be experimentally determined. Chromatographic systems are an efficient method to evaluate distribution ratios of a large number of different compounds (6). Therefore we used a HPLC method to measure the partitioning of organic compounds between an aqueous solution and cationic surfactant covered silica.

Theory

The surfactant coverage on solid phases can be treated as a pseudophase and the equilibrium constant K can be used to describe the distribution of a substance between the aqueous phase and the surfactant coverage

$$K = \frac{X}{c_{\text{sol}}}$$

where X is the molar fraction of the substance in the surfactant pseudophase and c_{sol} the concentration in solution.

Figure 1 shows the model concept of adsolubilization in a chromatographic system. The equilibrium constant is related to the retention time Rt by:

$$K = \frac{X_{\text{ads}}}{c_{\text{sol}}} = \frac{Q}{A} \cdot \frac{Rt - Rt_0}{c_{\text{S-ads}}}$$

Q	mobile phase flow [l/min]
A	surface area of the column [m ²]
X_{ads}	molar ratio of the organic compound in the surfactant aggregate [Ø]
$c_{\text{S-ads}}$	surfactant coverage [mol/m ²]
Rt_0	retention time without surfactant addition

The equilibrium constant can thus be calculated from the difference between the retention times at different concentrations of adsorbed surfactant.

Experimental Section

Chemicals. Hexadecyltrimethylammonium (HDTMA)-bromide, the cationic surfactant, was purchased from Fluka (>98%). The investigated organic compounds used in the adsolubilization experiments are listed in Table I. NaNO₃, HCl, NaOH and HNO₃, applied to adjust ionic strength, pH and used to backflush the HPLC column, were of analytical grade. Methanol was of HPLC grade.

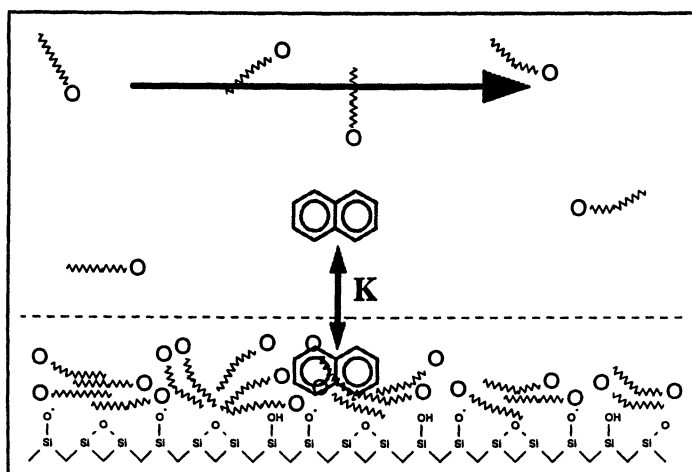


Figure 1. Schematic concept of partitioning of an organic compound between water and surfactant coated silica

Table I. Studied compounds

<i>Compound</i>	<i>purchased from</i>	<i>Purity</i>
Benzene	Merck	99.7 %
Toluene	Promochem	99.9 %
Ethylbenzene	Fluka	>99 %
o-Xylene	Fluka	>99.5 %
m-Xylene	Fluka	>99.5 %
p-Xylene	Fluka	>99.5 %
1,2-Dichlorobenzene	AccuStandard	n. n.
1,2,4-Dichlorobenzene	AccuStandard	n. n.
Naphthalene	Merck	>98 %
Nitrobenzene	Aldrich	>99 %
Quinoline	Aldrich	>96 %
Dimethylphthalate	AccuStandard	n. n.
Diethylphthalate	AccuStandard	n. n.
Diallylphthalate	AccuStandard	n. n.
9-Flourenone	Fluka	>99 %
Phenol	Fluka	p.A.
o-Cresol	Fluka	p.A.
m-Cresol	Fluka	>98 %
p-Cresol	Fluka	>98 %
2,3-Dimethylphenol	Fluka	>97 %
9-Fluorenol	Aldrich	>97 %
1-Naphthol	Aldrich	>99 %
Benzoic acid	Fluka	>99.5 %
2-Chlorophenol	Fluka	>97 %
4-Chlorophenol	Fluka	>97 %
3-Nitrophenol	Fluka	p.A.

Chromatography. The HPLC system contained two pumps and a UV-detector (Figure 2). The chromatographic column (10x4 mm) was thermostated at 30°C. All columns were filled with LiChrosphere 1000, which is a precipitated silica with wide pores (1000 Å), a particle size of 10 µm and with a manufacture reported surface area of about 30 m²/g. Each column contained approximately 72 mg LiChrosphere 1000 and the surface area was calculated to 2.2 m². Solutions containing HDTMAB (5 - 7.5·10⁻⁴ M) in 10⁻³ M NaNO₃ and a solution containing only 10⁻³ M NaNO₃ were prepared and purified by passing over packed silica columns (1 g). The pH of the solutions was adjusted by adding HCl or NaOH. Two columns (5x4 mm) were directly installed after the pumps before the mobile phase is mixed, to remove impurities which eventually remained after the first purification step. By changing the ratio of the pumping rates the surfactant concentration in the mobile phase could be varied. The system was allowed to equilibrate for at least 2 h (60 ml) after each alteration of the composition of the mobile phase until no further changes in retention time were ob-

served. Dead time of the system was determined by injecting $1.1 \cdot 10^{-3}$ M NaNO_3 solution.

The investigated organic compounds were dissolved in methanol and diluted with the mobile phase. Methanol content was always below 0.2 %. The injection volume was 100 μl . The standard deviation of retention time of benzene, toluene and ethylbenzene were less than 1.1 % at tenfold injection. Recorded peak shapes were almost symmetrical. In preliminary experiments it was ascertained that the calculated equilibrium constants were not influenced by the flow rates. The constants did not vary with the concentration of the injected compound within a concentration range of one half to ten times of the used concentrations.

To determine the amount of adsorbed surfactants the equilibrated column was removed and backflushed with 1) 1.5 ml $2 \cdot 10^{-2}$ M HNO_3 , 2) 6.5 ml $5 \cdot 10^{-4}$ M HCl and 3) 1.5 ml $2 \cdot 10^{-2}$ M HNO_3 . The effluent was collected quantitatively and filled up to 10 ml. The surfactant concentration was quantified by a TOC analyzer (Shimadzu TOC-5050). The desorption efficiency was tested previously by checking the balance in an adsorption/desorption experiment (Figure 3). The average balance lag was less than 0.05 μmol HDTMAB corresponding to 0.02 $\mu\text{mol}/\text{m}^2$ on the column.

Results:

Surfactant adsorption. In Figure 4a&b the adsorption of HDTMA on the silica gel in the column is presented in a linear and double logarithmic scale. The data were obtained by backflushing the column after equilibrating at pH 5 and pH 8. The amount of HDTMA adsorbed at pH 8 exceeds the adsorption at pH 5 at the same surfactant concentration. The course of the adsorption isotherms are in agreement with isotherms reported in literature determined by ellipsometry (7) or batch experiments (8,9).

According to Goloub and Koopal (10) the isotherms presented in a double logarithmic plot can be divided into four regions (Figure 5). At low surfactant densities (region I) surfactants are adsorbed through electrostatic attraction between the positively charged surfactant head-group and the negatively charged silica surface. The loss in electrostatic attraction due to the compensation of the surface charge leads to a decreased slope in region II. The transition between region I and II occurs at a surface excess of about 0.3 $\mu\text{mol}/\text{m}^2$ at pH 8 but cannot be observed for the measured isotherm at pH 5. In region III, at elevated surfactant concentration, the slope increases again caused by hydrophobic aggregation of the surfactant tails. Region II extends up to a surface coverage of about 0.6 $\mu\text{mol}/\text{m}^2$ at pH 8 whereas at pH 5 the transition between region II and III takes place at a coverage density of approximately 0.05 $\mu\text{mol}/\text{m}^2$. When the concentration in solution exceeds the critical micelle concentration (region IV) the chemical potential of the surfactant monomers remains nearly constant despite an increase of surfactant concentration. Thus the amount of adsorbed surfactant stays nearly constant.

Electrostatically driven adsorption of HDTMA on silica leads to a compensation of the surface charge in region II (10). Below the isoelectrical point (iep - region I and II) surfactants are expected to be adsorbed with their headgroups close to the surface. Koopal concludes from thermodynamic calculations that the alkyl chain is located close to the surface, too. This kind of orientation is referred to as head-on adsorption. Above the iep (region III) superequivalent surfactant adsorption occurs and

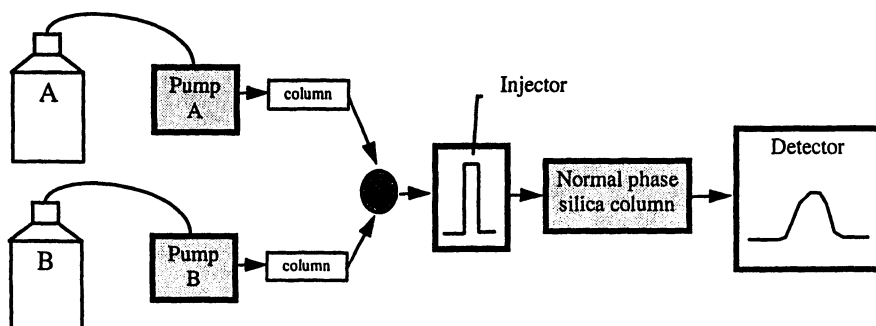


Figure 2. Experimental set-up for the determination of distribution constants by chromatography

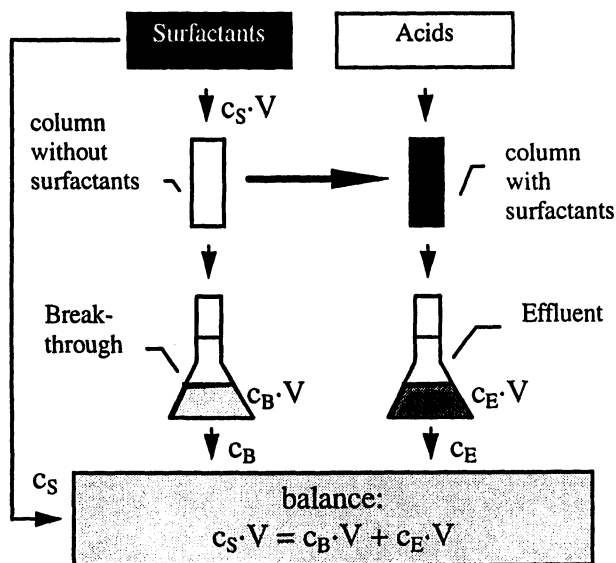


Figure 3. Experimental setup for the determination of the desorption efficiency ($V = \text{volume: } 10 \text{ ml}$, $c_X = \text{concentration}$)

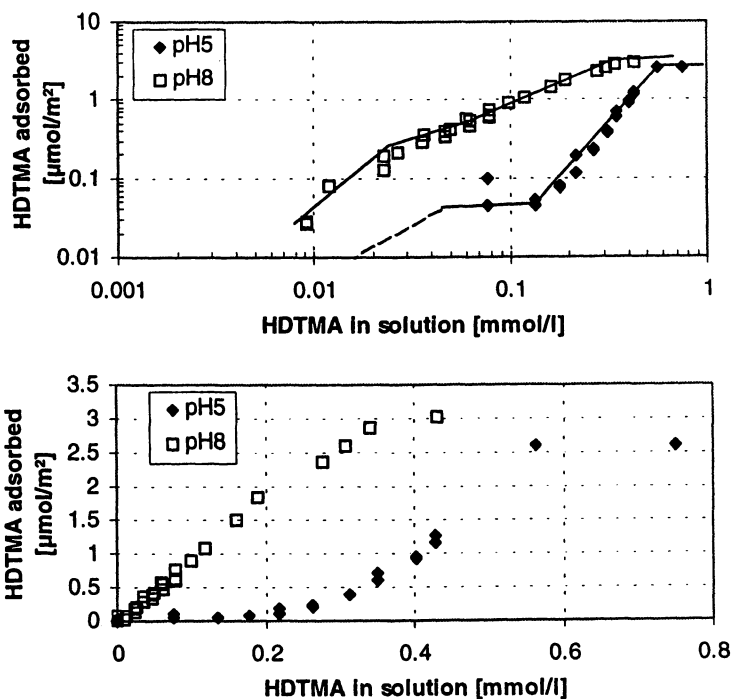


Figure 4. Measured surfactant adsorption isotherms of HDTMA on silica at pH 5 and pH 8 at a background electrolyte concentration of 10^{-3} M NaNO_3 .

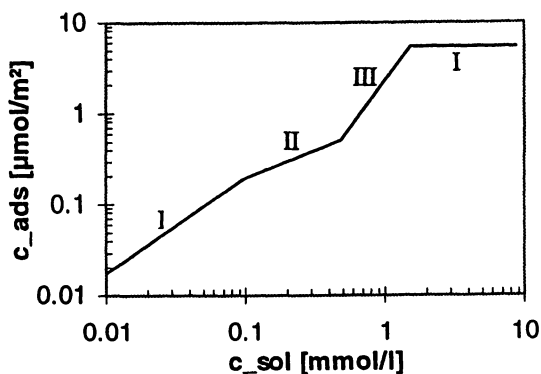


Figure 5. Characteristic four-region isotherm of a cationic surfactant on the silica surface at low ionic strength (Adapted from reference 10. Copyright 1997 American Chemical Society.)

new surfactant molecules predominately adsorb with their headgroups orientated to the solution (head-out). Possible structures of the adsorbed surfactants in the different regions are illustrated in figure 6.

We want to point out that the structure of the surfactant aggregates change with increasing surfactant concentration due to the transition from head-on to head-out adsorption. Increasing the pH leads to higher amounts of head-on adsorbed surfactant molecules. In the adsolubilization experiments we will focus on two questions: 1. Do the changes in the structure of adsorbed surfactant aggregates lead to changes in adsolubilization? 2. Are these changes related to the different HDTMA adsorption at pH 5 and pH 8?

Adsolubilization. Retention times of four selected substances are shown as a function of adsorbed HDTMA at pH 8 in Figure 7. Without any surfactant in the mobile phase the retention time is in the range of the dead time of the HPLC-system. The most striking points in Figure 7 are, (1) that none of the compounds shows a simple linear increase in retention time with increasing surfactant coverage and (2) that the compounds do not behave uniformly. It reveals that the dependency of the retention time on HDTMA adsorption changes at a surface excess of about $0.6 \mu\text{mol}/\text{m}^2$. This coincides with the transition from head-on to head-out adsorption. For this reason we calculated two equilibrium constants for each compound at pH 8: one in the range between 0 and $0.5 \mu\text{mol}/\text{m}^2$ adsorbed HDTMA and a second above $0.6 \mu\text{mol}/\text{m}^2$. If we compare the four different compounds, two principal behaviors can be distinguished. The initial slope of diallylphthalate is higher than its slope at elevated surfactant coverage. For 1,2-dichlorobenzene, 2,3-dimethylphenol and 4-chlorophenol it is the other way round, with the increase in slope being most pronounced for 4-chlorophenol.

The comparison of adsolubilization at pH 5 and pH 8 is presented in Figure 8. In general the retention times at pH 5 show (except for allylphthalate) a linear dependency on HDTMA coverage in the whole range examined. This agrees with the observation that the transition of region II to region III in the HDTMA adsorption isotherm occurs at much lower amounts of adsorbed surfactants at pH 5 than at pH 8. The surface excess of the transition point of $0.05 \mu\text{mol}/\text{m}^2$ is too low to become apparent in the adsolubilization experiments.

The retention time of 1,2-dichlorobenzene at the same coverage is higher at pH 5 than at pH 8. At elevated coverage ($>0.6 \mu\text{mol}/\text{m}^2$) they run virtually in parallel. The adsolubilization behavior of diallylphthalate is opposite to that of 1,2 dichlorobenzene. The retention times at pH 8 are higher at the same surface excess than at pH 5, but both curves run in parallel above the transition point when head-out adsorption is considered at pH 8. The adsolubilization of 2,3-dimethylphenol and 4-chlorophenol also is weaker at pH 5. In contrast to 1,2-dichlorobenzene and diallylphthalate the graphs are not parallel at elevated surfactant coverage.

The presented compounds are representatives of four groups we will distinguish in the further discussion:

1. Hydrophobic organic compounds (HOC): Benzene, toluene, ...
2. Non-ionic polar organic compounds (POC): Nitrobenzene, diallylphthalate...
3. Weak organic acids with pKa about 10 (WOA): Phenol, 2,3-dimethylphenol
4. Organic acids with pKa < 10 (OA): Benzoic acid, chlorophenols...

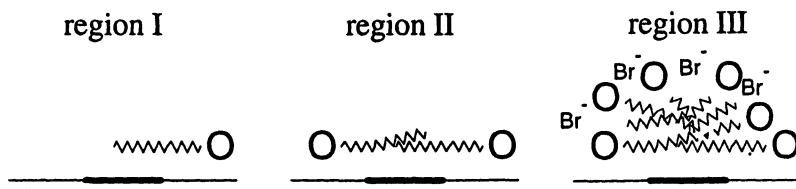


Figure 6. Proposed structure of the adsorbed surfactant aggregates in the different regions

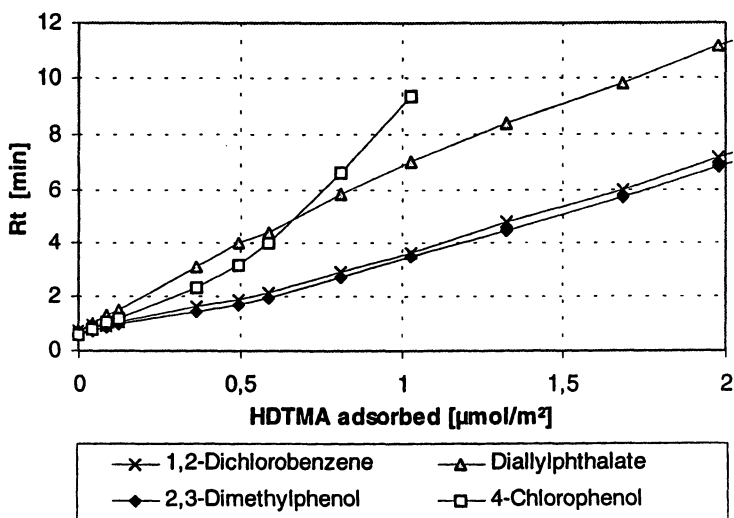


Figure 7. Retention times R_t of 1,2-dichlorobenzene, diallylphthalate, 2,3-dimethylphenol and 4-chlorophenol as a function of the surfactant coverage at pH 8, $I = 10^{-3}$ M and $Q = 0.5$ ml/min

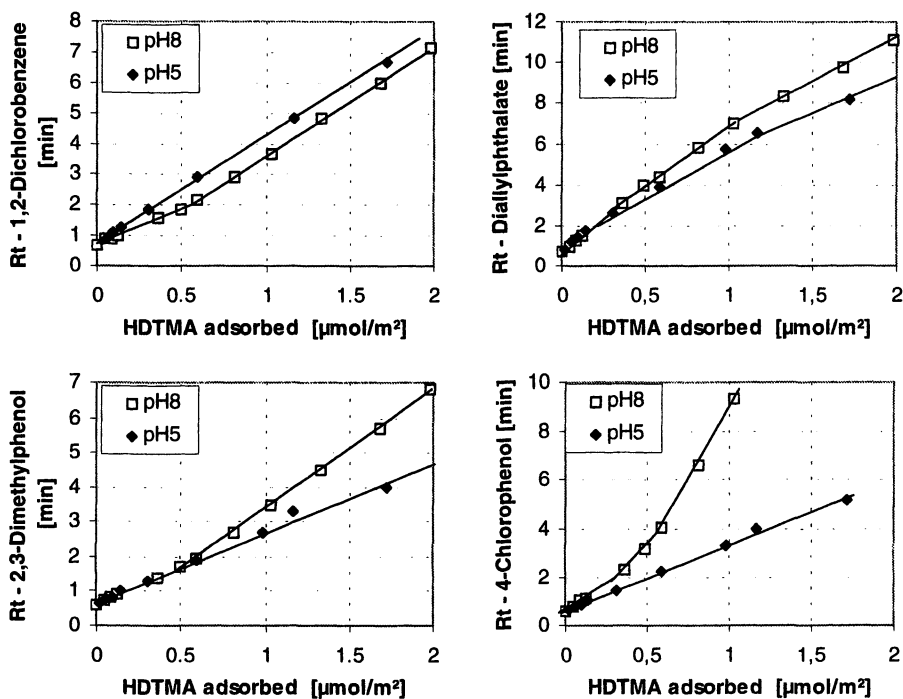


Figure 8. Comparison of adsolubilization behaviors of 1,2-dichlorobenzene, diallylphthalate, 2,3-dimethylphenol and 4-chlorophenol at pH 5 and pH 8 ($I = 10^{-3}$ M, $Q = 0.5$ ml/min)

In Table II the four groups and the assigned compounds are listed with the equilibrium constants below and above the transition point at pH 8 and above the transition point at pH 5. Because of the small amount of data below the transition point at pH 5 we were not able to calculate equilibrium constants in this range.

Table II. Slopes determined by linear regression in different regions expressed as K. Errors are standard errors of the linear regression.

<i>Ads. HDTMA</i> [$\mu\text{mol}/\text{m}^2$]	<i>pH5</i>		<i>pH8</i>				
	<i>Region III</i>		<i>Region I + II</i>		<i>Region III</i>		
	<i>K</i> [<i>1/M</i>]	<i>+/-</i>	<i>K</i> [<i>1/M</i>]	<i>+/-</i>	<i>K</i> [<i>1/M</i>]	<i>+/-</i>	
HOC	Benzene	45	3			45	5
	Toluene	154	2	129	12	149	1
	Ethylbenzene	402	2	274	15	380	4
	o-Xylene	370	11	276	51	370	15
	m-Xylene	405	10	304	24	417	2
	p-Xylene	414	3	306	6	428	8
	1,2-Dichlorobenzene	801	17	538	17	817	27
	1,2,4-Dichlorobenzene	2261	74	1166	61	2343	
	Naphthalene	1387		835	17	1385	
POC	Nitrobenzene	60	3	89	11	63	3
	Quinoline			115	8	83	2
	Dimethylphthalate	73	3	166	12	78	2
	Diethylphthalate	307	7	590	10	333	15
	Diallylphthalate	1074	14	1525	14	1232	68
	9-Flourenone	3144	122	2454	37	2979	29
WOA	Phenol	81	3	143	6	183	5
	o-Cresol	196	3	259	9	345	3
	m-Cresol	212	5	296	9	456	5
	p-Cresol	230	3	291	10	427	2
	2,3-Dimethylphenol	501	14	499	14	800	6
	9-Fluorenol	1490	67	1196	29	1665	30
	1-Naphthol	3684	57	5476	295		
OA	Benzoic acid			900	111	3617	174
	2-Chlorophenol	611	11	2044	176	6224	
	4-Chlorophenol	647	12	1181	50	2734	50
	3-Nitrophenol	369	7	2088	233	6927	

Figure 9 summarizes the changes of the distribution ratios at the transition of head-on to head-out adsorption at pH 8. While for the POC the constants decrease at the transition point (below the 1:1-line) the constants increase for DOC, OA and WOA (above the 1:1-line).

Figure 10 compares adsolubilization in region III, which is beyond the transition point, at pH 5 and pH 8. The K-values of the HOC and POC are similar for the two pH values. The WOA are located above the 1:1 line indicating a better adsolubilization at pH 8. The greatest increase of equilibrium constants due to increased pH was found for the OA.

Discussion

The coincidence of the transition from head-on to head-out surfactant adsorption and changes in the adsolubilization behavior indicates that the structure of the adsorbed surfactant aggregate determines the equilibrium constants. Behrends and Herrmann (11) have studied the adsolubilization behavior of anthracene on HDTMAB coated silica in batch experiments. At the same surfactant coverage they observed a smaller partitioning constant at pH 8 than at pH 5. They hypothesize that flat aggregates formed at pH 8 due to head-on adsorption are less effective to remove anthracene from the solution than aggregates formed at pH 5 due to head-out adsorption. The core region of surfactant aggregates is presumably the relevant location for adsolubilization of HOC. This hypothesis is supported by our results and agree with the adsolubilization characteristics of the HOC. The equilibrium constants assigned to adsolubilization in aggregates formed below the iep are smaller for the HOC than to those above the iep. It seems reasonable that aggregates formed by head-on adsorption provide no or a less favorable core region for adsolubilization compared to those formed due to head-out adsorption. The difference between pH 8 and pH 5 can be explained by the increased surface charge at pH 8 and therefore an enlarged head-on adsorption. When head-out adsorption is considered the equilibrium constants are of the same magnitude at both pH values. It is remarkable that the curves of the retention times of both pH values do not converge at high densities of adsorbed HDTMA. This suggests that the low adsolubilization efficiency of electrostatically adsorbed surfactant molecules remains unchanged although we assume that they are covered by head-out adsorbing surfactant molecules with increasing HDTMA concentration.

O'Haver and Harwell (12) point out that alkanes are preferentially absorbed in the core region of surfactant aggregates, whereas polar organic compounds stay in the palisade layer or at the interface between surfactant aggregate and aqueous solution. Lee et al. (13) propose a two-site model to describe the adsolubilization of alcohols. One site is the palisade layer of distinct double layer aggregates, the second one the edges of these aggregates. With increasing HDTMA adsorption the aggregates grow and therefore the surface area of the edges stays constant or decreases due to the merging of aggregates. This leads to an reduced increase of adsolubilization sites with increasing surfactant adsorption and in this way to an decrease of the partition constant. This model is based on the assumption, that "disk-shaped" admicelles exist at the solid surface. Although this assumption might not be valid for the HDTMA aggregates at the silica surface in principle this model explains the decline of the equilibrium constant at the transition from head-on to head-out adsorption. At this transition we expect that the increase of interfacial area between surfactant molecule and water is reduced caused by the coverage of head-on adsorbed molecules and by growing of primary aggregates. Nevertheless the model is not able to explain the differences of the adsolubilization of POC at different pH. We assume that the interface between head-on ad-

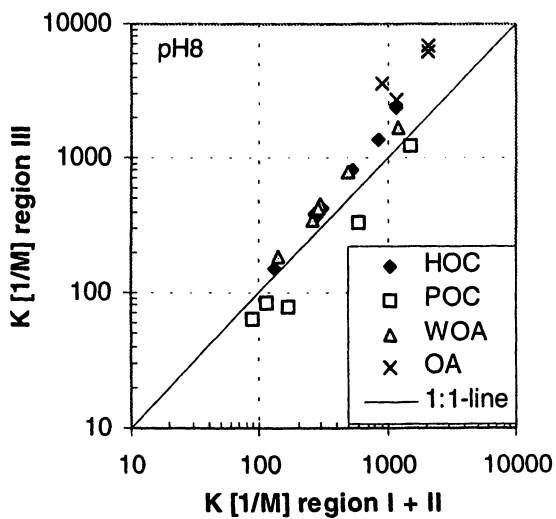


Figure 9. Comparison of slopes (expressed as K) of region I+II to region III at pH8

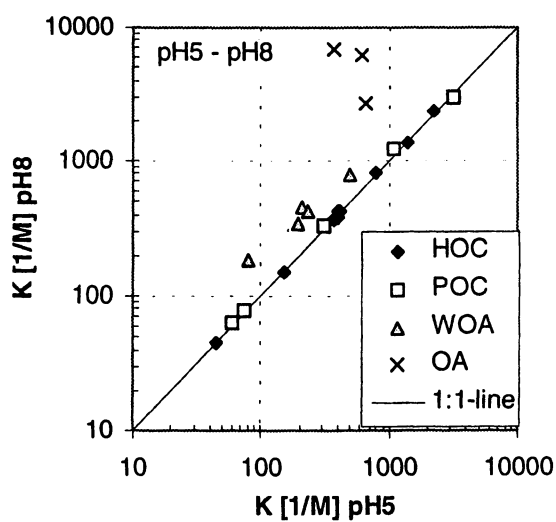


Figure 10. Comparison of slope (expressed as K) of region III at pH5 to pH8

sorbed HDTMA molecules and the silica surface is more favorable for adsolubilization of POC than the palisade region or the surfactant/water interface. This could be explained by additional energetic gain through hydrogen bonding of the POC, which all are Lewis-bases, and the silanol groups of the silica surface, which have Lewis-acid properties (14). Because of the higher quantity of head-on adsorbed surfactant molecules at pH 8 this interface is larger compared to pH 5 and therefore adsolubilization of POC is more emphasized.

The equilibrium constants of AO and WOA increase at the transition from head-out to head-on adsorption, this increase is more pronounced than that of HOC. Furthermore the increase is elevated at higher pH and the retention-time curves do not run in parallel but diverge with increasing HDTMA adsorption. Both classes of compounds are able to deprotonate. The uptake of the anion into the cationic surfactant aggregate is favored because the anion screens the head-group repulsion. The fraction of the anionic species is a function of pH and the dissociation constant. This fraction is about 1% or lower for the WOA even at pH 8, but due to the surface potential of the surfactant aggregates the pH at this surface must be corrected.

The surface pH_s can be calculated from:

$$\text{pH}_s = \text{pH}_b + \frac{F\Psi_s}{2.303 \cdot RT}$$

pH_s	surface pH
pH_b	bulk pH
F	Faraday constant [96485 Q mol ⁻¹]
Ψ_s	surface potential [V]
R	gas constant [8.314 J mol ⁻¹ K ⁻¹]
T	temperature [K]

The ξ -potential of a HDTMAB-bilayer at a ionic strength of 10⁻³ M was determined from Johnson et al. (15) to 100 mV. If we take this value as an approximation for Ψ_s the corresponding surface pH_s at pH 5 and pH 8 are 6.66 and 9.66, respectively. At a surface pH_s of 9.66 the OA are almost entirely dissociated and about 30% of the WAO are dissociated. This explains the increasing adsolubilization efficiency at higher pH. In the same way the increase of K at the head-out to head-on transition can be explained. In region I and II of the surfactant isotherms surface potential is negative. Only if superequivalent surfactant adsorption occurs will the surface potential become positive.

Conclusions

Our results indicate that adsolubilization is influenced by the properties of the solid surface which control the structure of surfactant aggregates at the solid surface. It is shown that partitioning is not a simple linear function of the surfactant coverage. Changes in the equilibrium constants can be attributed to the transition of head-on to head-out adsorption of surfactants. The effect of the transition is modified by the char-

acteristics of the adsolubilized compound. These differences can be explained by different adsolubilization-sites and mechanisms.

Acknowledgments

We thank the German Research Council (DFG) for support of this work (He 482/25).

References

1. Wu, J.; Harwell, J. H. and O'Rear, E. A. *Langmuir* **1987**, *3*, 531-537
2. Barton, J. W.; Fitzgerald, T. P.; Lee, C.; O'Rear, E. A. and Harwell, J. H. *Sep. Sci. Technol.* **1988**, *23*, 637-660
3. Holsen, T. M.; Taylor, E. R.; Seo, Y.-C. and Anderson, P. R. *Environ. Sci. Technol.* **1991**, *25*, 1585-1589
4. Bowman, R. S.; Haggerty, G. M.; Huddleston, R. G.; Neel, D. and Flynn, M. M., In *Surfactant-Enhanced Subsurface Remediation*; Sabatini, D. A.; Knox R. C.; Harwell, J. H., Eds.; *ACS Symposium Series 594*; American Chemical Society **1995**, 54-64
5. O'Haver, J. H.; Harwell, J. H.; Lobban, L. L. and O'Rear III, E. A. In *Solubilization in Surfactant Aggregates*; Christian S. D.; Scamehorn J. F., Eds.; *Surfactant Science Series 53*, Marcel Dekker; New York, **1995**, 277-296.
6. Goss, K.-U. *J. Colloid Interface Sci.* **1997**, *190*, 241-249
7. Wängnerud, P. and Olofsson, G. *J. Colloid Interface Sci.* **1992**, *153*, 392-398.
8. Goloub, T. P.; Koopal, L. K.; Bijsterbosch, B. H. and Sidorova, M. P. *Langmuir* **1996**, *12*, 3188-3194
9. Bijsterbosch, B. H. *J. Colloid Interface Sci.* **1974**, *47*, 186-198
10. Goloub, T. P. and Koopal, L. K. *Langmuir* **1997**, *13*, 673-681
11. Behrends, T.; Herrmann, R. *Phys. Chem. Earth* **1998**, *23*, 229-235
12. O'Haver, J. H.; Harwell, J. H., In *Surfactant Adsorption and Surface Solubilization*; Sharma, R., Ed.; *ACS Symposium Series 615*; American Chemical Society **1995**, 49-66
13. Lee, C.; Yeskie, M. A.; Harwell, J. H. and O'Rear, E. A. *Langmuir* **1990**, *6*, 1758-1762
14. Voumard, P.; Zhan, Q. and Zenobi, R. *Langmuir* **1995**, *11*, 842-848.
15. Johnson, S. B.; Drummond, C. J.; Scales, P. J. and Nishimura, S. *Langmuir* **1995**, *11*, 2367-2375.

Atmospheric Pressure Chemical Ionization–Mass Spectrometry and Capillary Electrophoresis for the Analysis of Chemical Warfare Agent Degradation Products

A-E. F. Nassar ^{1,4}, S. V. Lucas ¹, P. B. W. Smith ², and L. D. Hoffland ³

¹ Battelle Memorial Institute, 2012 Tollgate Road, Bel Air, MD 21015

² Geo-Centers Inc., P.O. Box 68 Gunpowder Branch, Aberdeen Proving Ground, MD 21010

³ U.S. Army Material Command Treaty Laboratory, Aberdeen Proving Ground, MD 21010

The use of the cationic surfactant, didodecyldimethylammonium hydroxide (DDAOH), to enable the reversal of electroosmotic flow (EOF) was the key strategy in the development of rapid and sensitive capillary electrophoresis (CE) analysis methods for the determination of nerve agent degradation products in aqueous matrixes. The target analytes, alkylphosphonic acids and their half-esters, are anionic degradation products of phosphonate ester-type nerve agents (e.g. Soman and Sarin) and are detected by indirect UV or conductivity. The CE separation uses coelectroosmotic conditions (the direction of the EOF and the electrophoretic mobility of the anionic analytes are both towards detection at the anode end), giving excellent separation in less than 3 minutes. The use of DDAOH for EOF reversal provided better performance than the more commonly used cetyltrimethylammonium hydroxide. The methods were evaluated on environmental samples. Recovery and linearity were evaluated and analyte identities for blind test samples were confirmed by mass spectrometry.

Chemical and biological warfare agents. Chemical and biological warfare agents have been around since the early part of the 20th century, having been used first by the Germans and eventually by both sides in World War I. By the end of the war, other countries were experimenting with chemical weapons, and continued researching and producing ever more deadly weapons. World War II and the Korean War era saw the beginnings of biological weapons development, involving anthrax, botulism, and other deadly disease agents. Both chemical and biological weapons are very dangerous and hard to protect against for several reasons: a very small amount can do great harm;

⁴ Current address: Bioanalytical R&D Department, Forest Laboratories, Inc., 220 Sea Lane, Farmingdale, NY 11735.

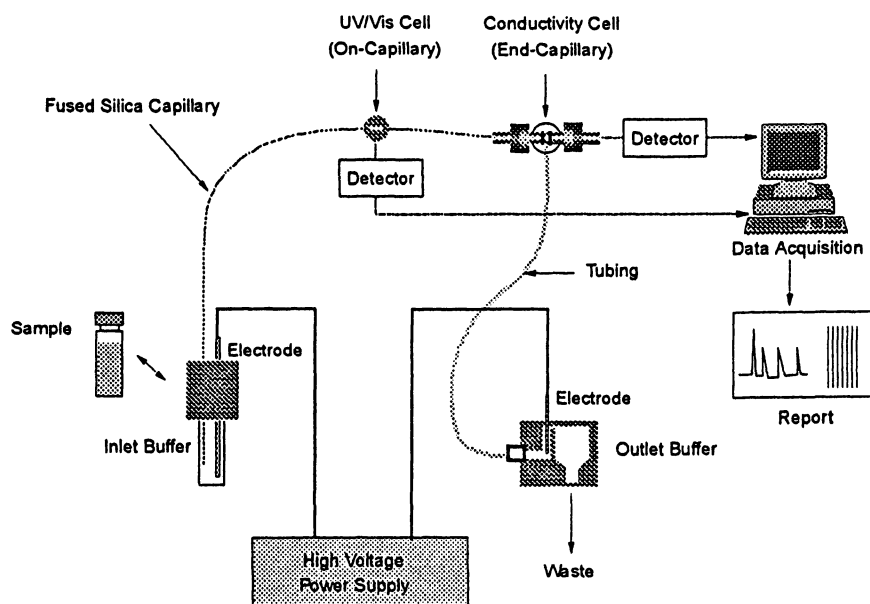
they are easily hidden and transported, and their effects may not become apparent for hours after their release. It is important to note, when dealing with chemical and biological weapons, that time is critical in effective detection, prevention and treatment for victims. Thus, it is essential that rapid, reliable, accurate and highly sensitive detection methods and equipment are available, both for the original agent(s) and for any later degradation products, and that these lead to the rapid deployment of correct treatments for victims.^{1,2} Such methods, especially if they were relatively easy to use and easily portable, would be invaluable in situations such as an accident or a chemical-warfare attack, where the first line of defense would likely be a rapid-response team using a mobile lab.

Almost since the inception of these weapons, governments and military leaders have been concerned with developing effective detection and counter-measures for protection against them. The recent approval of the Chemical Warfare Convention (CWC) has given rise to the Treaty Laboratory of the U.S. Army Materiel Command at Aberdeen Proving Grounds, Edgewood, MD. A primary responsibility of the Treaty Laboratory is to respond to the CWC's obvious need for reliable, verifiable, accurate, sensitive and portable methods of detection, as well as effective countermeasures against chemical warfare agents. Previous research has been done on the neutralization pathways of degradation for nerve agents such as Soman (GD) and Sarin (GB).³⁻⁵

Capillary Electrophoresis (CE). CE is a separation technique that has been commercially available for over 10 years.⁶ During those years CE has diversified into various separation modes, much as HPLC has. The separation modes are based upon the analytes' physicochemical properties. For the separation of small, highly mobile ions (such as chloride, sulfate, sodium and potassium) there is Capillary Ion Electrophoresis (CIE). Traditional Capillary Zone Electrophoresis (CZE) is optimized for small but somewhat larger charged molecules while Micellar Electrokinetic Chromatography (MECC) permits separation of both charged and uncharged species through addition of anionic surfactants into the electrolyte. For large polymeric type molecules that are substantially equivalent in mobility, the sieving action found in gel filled capillaries, Capillary Gel Electrophoresis (CGE), aids in their separation.

The key component to enabling these CE separation techniques is the availability of polyimide coated, narrow-bore fused silica tubing. Jorgenson and Lukacs were the first to show the advantages of this material.⁶ The capillary, which typically ranges from 50 to 100 μm ID, permits efficient transfer of Joule heating which if not removed would render the separations unusable due to extensive thermal dispersion.⁷ These small diameter capillaries have the benefit of significantly reducing the amount of electrolyte required for analysis and the amount of sample. Electrolyte consumption is measured in mL per day as compared to HPLC which consumes eluent measured in liters per day. Sample volumes injected are typically 10^{-4} smaller than HPLC, and are measured in low nanoliters (nL). All these attributes are beneficial for the demands required for Chemical Warfare Convention (CWC) analysis such as the transportability of instrumentation and minimal waste disposal.⁸

Figure 1, the CE system,^{9,10} consists of the following basic components:



1. Capillary Electrophoresis System Schematic With Two Detection Modes; On-capillary indirect UV and End-capillary Conductivity

- A high voltage power supply capable of delivering +/- 30kV;
- A polyimide-coated fused-silica capillary, where the separation takes place, which typically has an inner diameter ranging from 50 μm to 75 μm , an outside diameter of 375 μm , and a length ranging from 40 to 100 cm;
- An inlet electrolyte vial is where the sample entry side of the capillary and one high voltage (HV) power supply electrode are immersed;
- A means of pressurizing the inlet vial for flushing the capillary with buffer, conditioning solutions, or sample entry;
- An outlet electrolyte reservoir (or vial) where the outlet end of the capillary and the alternate polarity HV power supply electrode is immersed (or where tubing continuing the transport of analytes to an end-capillary detector or a post-capillary detector is connected);
- A detection device which, depending on the application, can be either on-capillary (for example, UV/Vis), end-capillary (for example, conductivity or fluorescence) or post-capillary (for example, mass spectrometry). For on-capillary detection, a small portion of the polyimide coating is removed just above the outlet vial to permit light transmission; and
- A data acquisition device for processing and storing the signals from the detector.

Mobility of Ions. In CE, the electrophoretic mobility (μ) of a charged molecular species is estimated with the Debye-Huckel-Henry equation

$$\mu = q/6 \pi \eta r,$$

where q is the charge on the particle, η is the viscosity of the electrolyte, and r is the Stokes' radius of the particle. Actual analyte mobilities will vary depending on the divergence of the molecule from spherical shape. Other factors affecting the analyte mobility include interaction with the wall of the capillary or with electrolyte additives used to change separation selectivity (mobility) such as ion-pair reagents or complexing agent.^{11,12} The second main force acting on the analyte is electroosmotic flow (EOF), first identified by Helmholtz.¹³ This is the bulk flow of liquid in the capillary induced by the inner wall charge or zeta potential (ζ). The EOF is an important feature in electrophoretic separations as it can augment or retard the mobility of analytes as it is a vector force that can be controlled through electrolyte chemistry or covalent modification of the inner capillary wall. In the "traditional" CE configuration where the inlet side of the capillary is positive and the inner wall of the capillary is bare silica, the natural direction of EOF is towards the cathode.

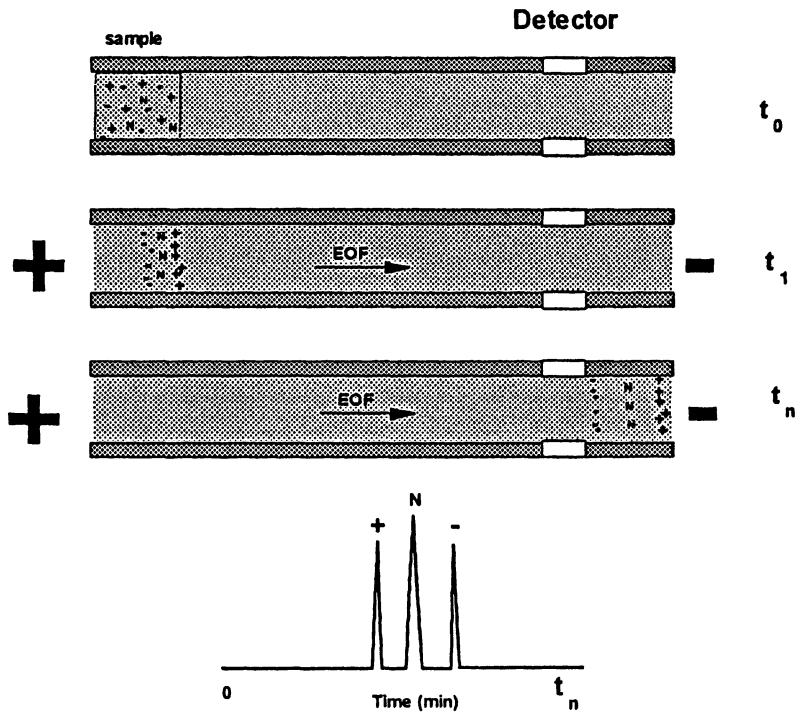
The sample is injected into the positive polarity end of the capillary by displacing small sample plug (a few nanoliters) into the opening of the capillary. In the sample plug the ions are represented by cations, anions and neutral species (designated "+", and "-" and "N", respectively, in Figure 3) which are homogeneously found in the plug. To start the CE separation, a voltage is applied and the cations migrate towards the cathode, the neutrals are dragged along by the EOF and the anions which are migrating towards the anode are also dragged to the cathodic side detector as the EOF, in this case, is greater than their electrophoretic mobilities. After all

analytes of interest have passed through the detection window of the capillary, the analysis is complete. Inside the capillary the analyte zones are resolved from each other due to differences in electrophoretic mobility. A representation of the separation is shown at the bottom of Figure 2. The cations are detected early in the separation as they are migrating toward the detector in the same direction as the EOF. The neutrals are the total sum of uncharged species including the water in the sample plug, and these are carried by the EOF to the detector without any differential separation between them (i.e., they have no electrophoretic component to their migration). The anions appear at the detector after the neutrals because their electrophoretic mobility is in the opposite direction to the EOF (see vector sum representation in Figure 3).

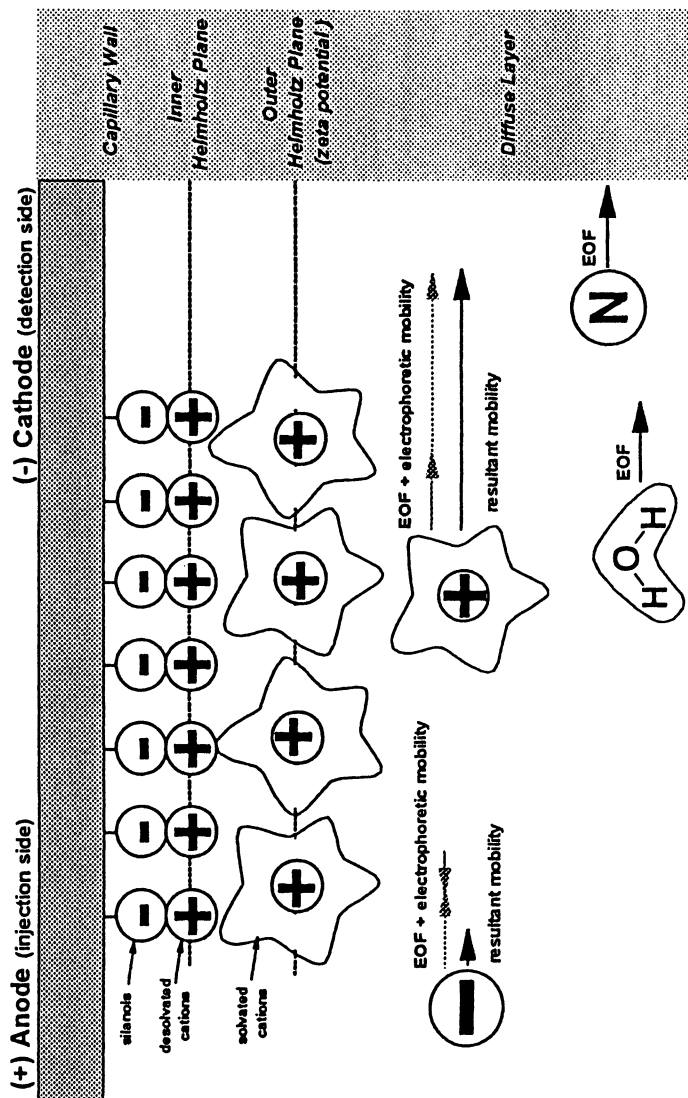
Figure 3 illustrates the physical phenomena which create the EOF. The tightly absorbed layer of immobilized cations are counterions to the stationary negative charge on the capillary wall created by dissociation of silanol groups. These immobilized cations are stripped of their hydration sphere and form the inner Helmholtz Plane (IHP) or Stern layer. The centers of the solvated cations contacting the adsorbed cations on the wall form the outer Helmholtz plane (OHP) where the zeta potential is considered to be formed. The remaining solvated cations outside the outer Helmholtz plane form the diffused layer. When an electric field parallel to the wall is applied, the solvated cations are driven to the cathode, carrying with them the bulk water phase through a network of hydrogen bonds, thereby creating the EOF.

Cations in the sample will migrate within the moving EOF according to their differences in electrophoretic mobility (thereby creating the CE separation) and will all arrive at the detector in advance of the neutral species which migrate with a speed identical to the EOF. Migration of anions is more complex. The small, highly mobile anion shown in the lower left of the figure has an electrophoretic mobility toward the injection (anode) end which is opposite in direction to and greater in magnitude than the EOF, hence it will not reach the detector. The larger anion above the fast anion has electrophoretic mobility which is lower in magnitude than the EOF so the vector sum is toward the detector, and these anions will be detected late in the electropherogram, separated from one another according to their differing electrophoretic mobilities.

Counter-electroosmotic and Co-electroosmotic flow. To analyze anionic species such as organophosphonates¹⁴ with normal electrophoretic polarity (i.e., cathode at the detector end, as in Figure 3), the EOF must be greater than the electrophoretic mobility of each of the phosphonates to ensure they reach the detector. This is called the counter-electroosmotic condition.¹⁵ Increased EOF is obtained by increasing the electrolyte pH which increases the degree of ionization of the weakly acidic silanol groups on the inner wall of the capillary. This, in turn, increases the charge density in the OHP which increases the EOF. Although this approach will work well with standards, real world matrixes contain interfering anions that can comigrate with some of the alkylphosphonates—two examples are carbonate and fluoride. Low pH electrolytes can be used to alter selectivity and eliminate these two interferences. However, at an electrolyte pH less than 2, the silanols can be assumed to be nearly



2. Migration Behavior of Anions, Cations and Neutral Species in a "Typical" Capillary Electrophoretic Run.

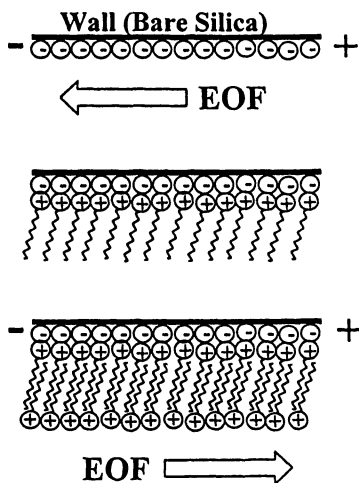


3. The Zeta Potential and Cathodically Directed EOF on an Unmodified Fused-Silica Capillary

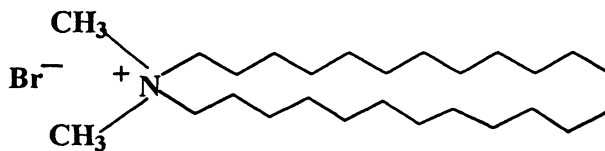
fully non-ionized, and a no-flow EOF condition is approached. In general, moving toward lower pH has several drawbacks: the run times will be increased due to the decreased EOF, electrophoretic mobilities will be diminished as the phosphonates become protonated, and the peaks will become broader as longitudinal diffusion increases as the analytes stay longer in the capillary.

The ideal situation is to reverse the polarity of the capillary (detector end anodic so that anion electrophoretic mobility is toward the detector). To create an anodic flow, the wall charge needs to be reversed (made positive). Tsuda¹⁶ and Zare¹⁷ were the first to use a cationic surfactant, cetyltrimethylammonium bromide (CTAB), as an electrolyte additive to reverse the EOF in CE. Here CTAB forms hemimicelles on the inner wall of the capillary as shown in **Figure 4**. The quaternary portion of the surfactant becomes the counter-ion to the stationary anions of the ionized silanol groups. Because the cation is permanently charged (quaternary amine), it is not sensitive to electrolyte pH and typically will provide a stable anodic EOF through a large alkaline pH range.¹² EOF reversal becomes problematic at acidic pH where the silanols lose their charge. Initially the hydroxide form of CTAB was used, CTAOH. Compared to separations using no EOF modifier added to the electrolyte, the separation was faster and eliminated a baseline perturbation observed in the separation omitting the CTAOH.⁸ Unfortunately resolution was poor. To improve resolution we sought to reduce the anodic EOF through usage of a "less efficient" EOF modifier. Reducing the EOF would permit more time for differential electrophoretic migration to produce analyte separation, improving resolution. The twin chain of diodecyltrimethylammonium cation (**Figure 5 DDAB**) was evaluated as an EOF reversal agent as it was rationalized that the steric interference from the second carbon chain would reduce the net number of quaternary groups exposed if hemimicelles are formed.⁸ Whether hemimicelles are formed or some variation thereof, the replacement of CTAOH with an equal mM concentration of DDAOH produced a slower anodic EOF and improved resolution of the analytes. The usage of DDAOH was found also to be beneficial for conductivity and indirect UV-based separations.

This chapter describes CE methods for the determination of CW agent degradation products in complex matrixes. All of the nerve agents produce a mono-acidic organophosphonate in the final step of hydrolysis, and these phosphonic acids have been the main focus of our analysis efforts. In October, 1996, and April, 1997, our recently-developed CE methods were applied in the analysis of two Round-Robin samples provided to all Treaty Laboratories by the Provisional Technical Secretariat/Preparatory Commission for the Organization for the Prohibition of Chemical Weapons (PTS/OPCW), and these CE methods proved to be highly successful. Compounds identified were ethylphosphonic acid, O-isopropyl ethylphosphonic acid, isopropylphosphonic acid, and O-(2-ethylhexyl) methylphosphonic acid. The CE electrolytes used in these methods were stable for at least one year, and no interferences from other anions were found.



4. Anodically Directed EOF From The Formation of Hemimicelles Of A Quaternary ammonium Surfactant



DDAB - didodecyldimethylammonium bromide

5. Structure of the cationic surfactant didodecyldimethylammonium hydroxide (DDAOH) used to control EOF

EXPERIMENTAL SECTION

Apparatus. All experiments were performed on either a Thermo CE (now Thermo Bioanalysis) Crystal 310 Capillary Electrophoresis System with a Crystal 1000 Conductivity Detector using a 60 cm X 50 μm (ID) ConCap fused-silica capillary (Santa Fe, NM) or a Hewlett-Packard Capillary Electrophoresis System with UV Detector using a 75 μm (ID) X 56 cm, (effective length) fused-silica capillary. Both instruments have the capability to control the temperature of the fused-silica capillary. The electropherogram signals were recorded using 4880 software for the conductivity detector and HP Chem-Station software for indirect UV.

Mass spectrometry (MS) on negative ions was done on a Finnigan TSQ 7000 tandem quadrupole mass spectrometer (Finnigan Corp., San Jose, CA.) using the Finnigan electrospray ion source. A solution of aqueous acetonitrile (50:50 v/v) containing 0.025 M ammonium acetate was infused into the Atmospheric Pressure Chemical Ionization (APCI) interface at a flow rate of 0.4 mL/min. The samples were introduced in the flow-injection mode (i.e, without the use of an HPLC column) using a Rheodyne 7125 injector (Cotati, CA) fitted with a 5 μL loop. Nitrogen (99.99%) was used as the nebulizing gas, and the vaporizer was maintained at a temperature of 400°C.

Reagents. Alkylphosphonic acids and their monoesters were synthesized in our laboratory (U.S. Army Material Command Treaty Laboratory, Aberdeen Proving Ground, Maryland). Isopropyl methylphosphonic acid (IMPA) 98% pure was custom synthesized by Radian International (Austin, TX). Commercial sources were: Pinacolyl methylphosphonic acid (PMPA) [pinacolyl=2-(3,3-dimethyl)butyl], Aldrich Chemical Co. (Milwaukee, WI); didodecyldimethylammonium bromide (DDAB) (>99%), Eastman Kodak (Rochester, NY); *i*-octylphenoxypolyethoxyethanol (Triton X-100), Union Carbide; and phenylphosphonic acid and boric acid, Sigma Chemical Company (St. Louis, MO). All reagent solutions and diluted samples were prepared using deionized water (Winokur Water System Corp., Barnstead, Dubuque, Iowa). Solutions were stored in Nalgene (polypropylene) plastic bottles. All buffers were degassed and filtered through a 0.45 μm cellulose nitrate membrane filter prior to use. All other chemicals were reagent grade. The didodecyldimethylammonium hydroxide (DDAOH) was obtained from their respective bromide salts by passing a 25 mM solution through a Dionex On-Guard A cartridge in the hydroxide form, (Dionex Corp., Sunnyvale, CA).

Procedures. New capillaries were pretreated with a ten minute rinse of deionized water, followed by ten minutes of 0.5 M sodium hydroxide, then ten minutes of deionized water, and finally a ten minute rinse of the analysis buffer. Rinses were performed at 2000 mbar (conductivity system) or 900 mbar (indirect UV system). Samples and standards were introduced by keeping the (pressure x time) product at 300 mbar-s for both detection methods. Constant voltage (negative polarity, detector side anodic) was used throughout to drive the separations, 25 kV and 30 kV for the conductivity system and indirect UV system, respectively. The wavelength used for indirect UV detection was 210 nm. The capillary temperature was ambient for the conductivity system and 40°C (optimized) for the indirect UV system. The electrolyte used for conductivity detection contained 30 mM His, 30 mM MES, 0.03 wt. % Triton X-100 and the electroosmotic flow (EOF) modifier was 0.35 mM DDAOH. For the indirect UV detection (indirect UV system), the buffer composition was: 200 mM

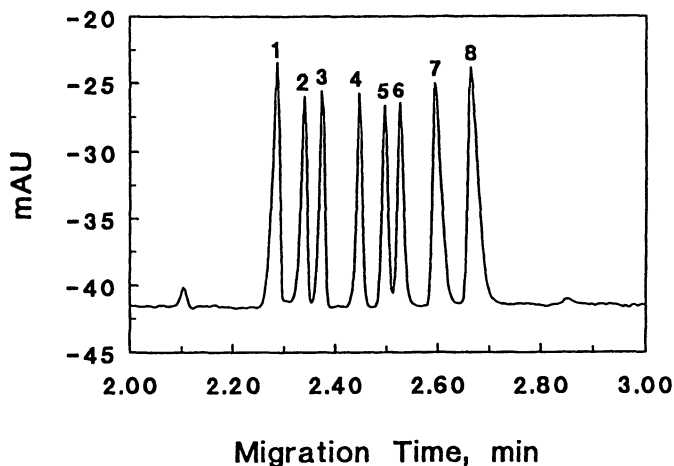
boric acid, 10 mM phenylphosphonic acid, 0.03 wt % Triton X-100, 0.35 mM DDAOH with final pH adjustment using aqueous NaOH. To obtain reproducible injections, an identical injection sequence was followed for each sample: the capillary was rinsed with deionized water for 3 min and then with run buffer for 5 min prior to each injection. For the HP System, the capillary inlet and outlet levels must be equal to ensure that there is no siphoning in either direction.

Conventional APCI mass spectra were acquired with Q1 over the mass range 50-500 m/z with a scan time of 1 s. Product ion tandem mass spectra were acquired over the mass range 20 m/z to a value just above the mass of the parent ion, with a scan time of 1 s. Both Q1 and Q3 were operated at unit resolution and argon (99.999%) was used as a collision gas at a pressure of 3.5 mTorr.

RESULTS AND DISCUSSION

The Role of Cationic Surfactants in CE Separations. Interactions between surfactants and the surface of the fused silica CE capillary are essential for control of electroosmotic flow (EOF). Surfactants can play important roles for separations at concentrations below the critical micelle concentration (CMC) by acting as solubilizing agents for hydrophobic solutes, by functioning as ion pairing reagents, or as capillary surface modifiers. The interaction of a surfactant with the solutes can occur by two mechanisms: ionic interactions with the charged end of the surfactant and/or through hydrophobic interactions between the alkyl chain and hydrophobic moieties of the solute. Cationic surfactants such as DDAOH or CTAOH can form a double-layer on the surface of the fused silica and reverse the capillary wall charge, thereby reversing the direction of the EOF. We reported that alkylphosphonic acids and their monoesters can be separated within three minutes by reversing the electroosmotic flow.⁸ Through the use of acidic electrolytes, this approach eliminates the potential of interference from fluoride, which reacts with the capillary wall at acidic pH, and carbonate/bicarbonate, which is not observed because of its weak acidity ($pK_a=6.3$). Furthermore, an acidic pH prevents buffer adsorption of atmospheric CO_2 , which is a principal cause of high-pH CE buffer spoilage. Our acidic, DDAOH EOF reversal buffers have a shelf life of one year for the buffers, and this level of storage stability is beneficial to other CE applications. **Figure 6** shows the separations of the alkylphosphonic acids shown in Table 1 with the cationic surfactant DDAOH. The electropherogram in Figure 6 shows that the analysis time using DDAOH was three minutes. Thus, this CE analysis system offers excellent sensitivity, freedom from interference, rapid analysis, and quantitative capability for these species.

Method Validation. We validated our CE/indirect UV method by quantitative determination of IMPA and PMPA in their respective reaction masses (the analysis of chemical warfare agent degradation products in agent neutralization matrixes). IMPA and PMPA are the major chemical neutralization products from the nerve agents GB (isopropyl methylphosphonofluoridate, Sarin) and GD (pinacolyl methylphosphonofluoridate, Soman), respectively, in the MEA/water destruction



6. Separation of the alkylphosphonic acids. Experimental conditions: buffer, 200 mM borate, 10 mM phenylphosphonic acid; 75 μm (ID) X 56 cm fused-silica capillary; peaks were detected by indirect UV detection at 210 nm; injection, 6 s at 50 mbar; and temperature, 40°C. With cationic surfactant (0.35 mM DDAOH) and 0.03 wt% Triton X-100^R, pH 4.0; voltage, 30 kV (negative polarity). Anions: 1=EHMPA, 2=MPA, 3=EMPA, 4=IMPA, 5=*i*-BuMPA, 6=*i*-PEPA, 7=CHMPA, and 8=PMPA. (Reproduced from reference 8. Copyright 1997 American Chemical Society.)

Table 1. The Hydrolysis Products of Nerve Agents and Related Compounds

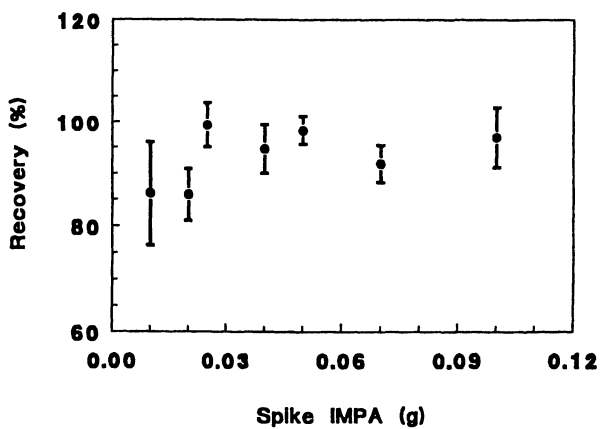
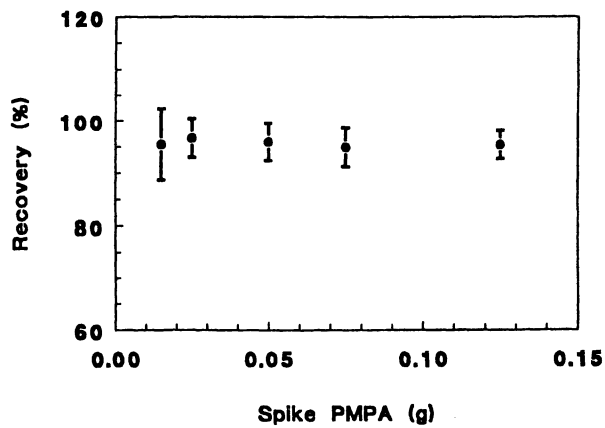
Compound	MW
<i>(a) Compounds from known nerve agents:</i>	
Methylphosphonic acid; MPA (2) ^a	96
Ethyl methylphosphonic acid; EMPA(3) ^a	124
Isopropyl methylphosphonic acid; IMPA(4) ^a	138
Pinacolyl methylphosphonic acid; PMPA(8) ^a	180
Isobutyl methylphosphonic acid; <i>i</i> -BuMPA(5) ^a	152
Cyclohexyl methylphosphonic acid; CHMPA(7) ^a	178
<i>(b) Related Compounds:</i>	
O -Isopropyl ethylphosphonic acid; <i>i</i> -PEPA(6) ^a	152
O -2-Ethylhexyl methylphosphonic acid; EHMPA(1) ^a	208
Ethylphosphonic acid; EPA	110
Isopropylphosphonic acid; <i>i</i> -PPA	124

^aThe number is corresponding to the peak in the electropherograms in Figure 6.

system. The accuracy of our method was assessed by spiking actual GB and GD reaction masses with known amounts of the respective destruction product (IMPA and PMPA). In each case, 0.2 gram of reaction mass was first spiked with IMPA or PMPA and then prepared for analysis by serial dilution. For IMPA, seven fortification levels were used, ranging from 0.01-0.10 g per 0.20 gram reaction mass, which corresponded to 20-220% of the IMPA background level in the reaction mass used. The five fortification levels used for PMPA ranged from 0.015 to 0.125 g per 0.20 g reaction mass, which corresponded to 10-150% of the PMPA background level. The data from these fortified samples were quantified against the full range calibration curve, and the known background IMPA or PMPA level was subtracted to generate found values resulting from the fortification. The accuracy of these found values is graphically shown in **Figure 7** where the recovery percentage is plotted against spiking amount (in grams) of the acids. The recovery percentages ranged from 86% to 99% for IMPA and 95% to 97% for PMPA, with %RSD ranging from 2.7 to 9.9 and from 2.7 to 6.8 for IMPA and PMPA, respectively.

The precision of the method was assessed using data from five analysis replications of three reference standards on each of five days, using the low, medium and upper standard levels of the calibration range. These three concentration levels were: 7.5 and 37.5 $\mu\text{g/mL}$ low and medium, respectively, for both IMPA and PMPA, with high level 75.0 $\mu\text{g/mL}$ for IMPA, and 87.5 $\mu\text{g/mL}$ for PMPA. The intra-assay (intraday) precision was determined at each level within each day by calculating the percent relative standard deviation (%RSD) of the found concentrations. The interassay (interday) precision was determined at each level by calculating the RSD of the found concentrations from all five days combined (%RSD from all 25 analyses). Table 2 shows that, for IMPA, the intra-assay precision ranged from 0.3 to 2.1 %RSD over the three levels while the interassay precision ranged from 0.7 to 1.9 %RSD. The corresponding values for PMPA were 0.3 to 4.0 %RSD intra-assay precision and 1.0 to 2.9 %RSD interassay precision. Clearly, there is no significant difference between the intra-/interassay precision for both IMPA and PMPA at least over the limited, 5-day period investigated here. Intra-assay precision for migration time was less than 4.0 %RSD for IMPA and 5.0 %RSD for PMPA. This work shows that the methods performed well in terms of sample solution stability, linear response over a wide range of concentrations, high precision and accuracy, and excellent recovery percentages. Other criteria applied to the validation of our method included demonstrating or establishing method specificity, limit of detection, limit of quantitation, linearity, robustness, and ruggedness; these are discussed at greater length in our previous work.¹⁸

Analysis of the Second (October, 1996) and Third (April, 1997) Official PTS/OPCW Proficiency Test Water Samples. **Figure 8** is an illustration of our results using CE for the Second (October, 1996) Official PTS/OPCW Proficiency Test water sample. The water sample gave two major peaks, the first of which had CE mobility similar to ethylphosphonic acid (EPA), while the second had mobility similar to O-isopropyl ethylphosphonic acid (*i*-PEPA). Using the same CE methods to analyze the Third (April, 1997) Official PTS/OPCW Proficiency Test water sample, we found two peaks. Standard addition experiments showed that the first peak had the



7. Recovery percentages from spiking PMPA and IMPA in the reaction masses

Table 2. Within- and Between-Day Precision for IMPA at Three Levels (RSD, among replicates, n= 5)

		level (ug/mL)		
		7.5	37.5	75.0
day 1	Mean	18.22	95.57	195.15
	SD	0.07	0.99	0.48
	% RSD	0.4	1.0	0.3
day 2	Mean	18.34	95.18	195.23
	SD	0.07	0.36	0.84
	% RSD	0.4	0.4	0.4
day 3	Mean	18.65	95.53	193.62
	SD	0.10	0.10	2.12
	% RSD	0.5	0.1	1.0
day 4	Mean	18.45	95.77	195.36
	SD	0.24	1.01	1.22
	% RSD	1.3	1.1	0.6
day 5	Mean	18.68	95.51	195.59
	SD	0.35	0.60	0.81
	% RSD	1.9	1.1	0.4
Interday*	Mean	18.54	95.88	195.13
	SD	0.36	0.95	1.43
	% RSD	1.9	1.0	0.7

* All 25 runs for each level

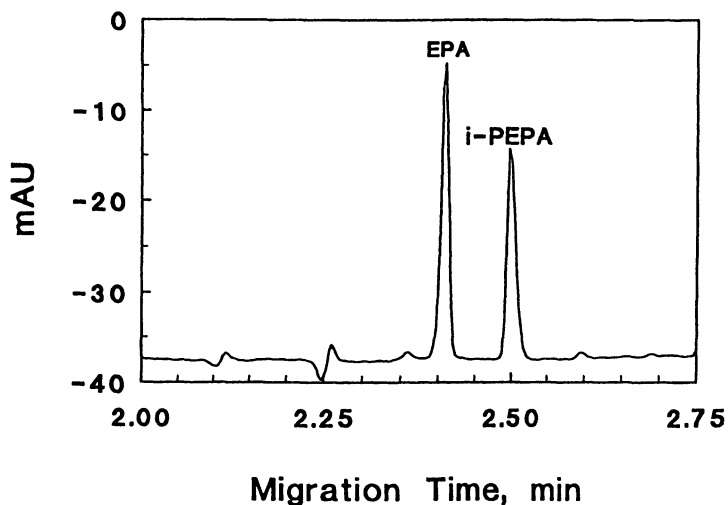
same mobility as isopropylphosphonic acid (*i*-PPA) and the second peak had the same mobility as O-(2-ethylhexyl) methylphosphonic acid (EHMPA). These CE analysis results were confirmed by derivatization followed by GC/MS/MS, as well as GC/AED.¹⁹ Table 3 summarizes the data from these two Official PTS/OPCW Proficiency Tests.

Besides the standard addition CE experiments, we also confirmed our peak identification for the free acid by using APCI/MS/MS. The positive ion APCI mass spectrum for the Third (April, 1997) Official PTS/OPCW Proficiency Test water sample indicated that it contained polyethylene glycol. No differences were readily apparent in a comparison of the positive ion APCI mass spectrum for this water sample and its corresponding blank water sample. However, the negative ion APCI mass spectrum for the water sample contained a prominent ion at m/z 151 indicating the presence of the one compound (M.W. 152) that was absent in the corresponding blank. The product ion mass spectra of this peak is reproduced in **Figure 9**, and shows that it contained a prominent ion at m/z 109, indicating that the compound contained an O-propyl group ($151-109 = 42$, mass of the lost neutral fragment, propene). Inspection of the product ion mass spectrum suggested that this peak was propyl ethylphosphonic acid. **Figure 10** shows that the negative ion APCI mass spectrum for the water sample contained a prominent ion at m/z 207, indicating the presence of the one compound (M.W. 208) that was absent in the corresponding blank. The product ion mass spectra of this m/z 207 parent ion contained a prominent m/z 95 daughter peak, corresponding to $\text{CH}_3\text{P}(\text{OH})(\text{O})\text{O}^-$ (the mono-anion of MPA), indicating that the compound contained a methylphosphonic group. Analogously to the parent/daughter transition for propyl ethylphosphonic acid (**Figure 9**), this mass 112 neutral loss, corresponding to C_8H_{16} , suggested an octyl methylphosphonic acid. Electron impact MS data suggested an isomeric octyl group, and high resolution GC clearly showed evidence of diastereomers with the asymmetric site near but not adjacent to the phosphorus center (i.e., an asymmetric carbon one carbon removed from the ester linkage). Synthesis of reference compounds proved these hypotheses with a positive identification of O-(2-ethylhexyl) methyl phosphonic acid. Thus, by combining the CE data with APCI/MS data, direct analysis of these acids for the Official PTS/OPCW Proficiency Test was definitive for the aqueous matrix sample. Additionally, given the availability of bona-fide reference standards for demonstration of co-chromatography in CE by standard addition, successful identification of these types of alkylphosphonic acids and their half-esters in unknown aqueous samples is clearly feasible using CE alone.

CONCLUSIONS

The described methods for the determination of CW agent degradation products in complex matrixes offer several advantages over traditional IC, GC/MS and LC methods. The method is simple, easy, fast, and effective, and does not require expensive instrumentation. The key aspects are:

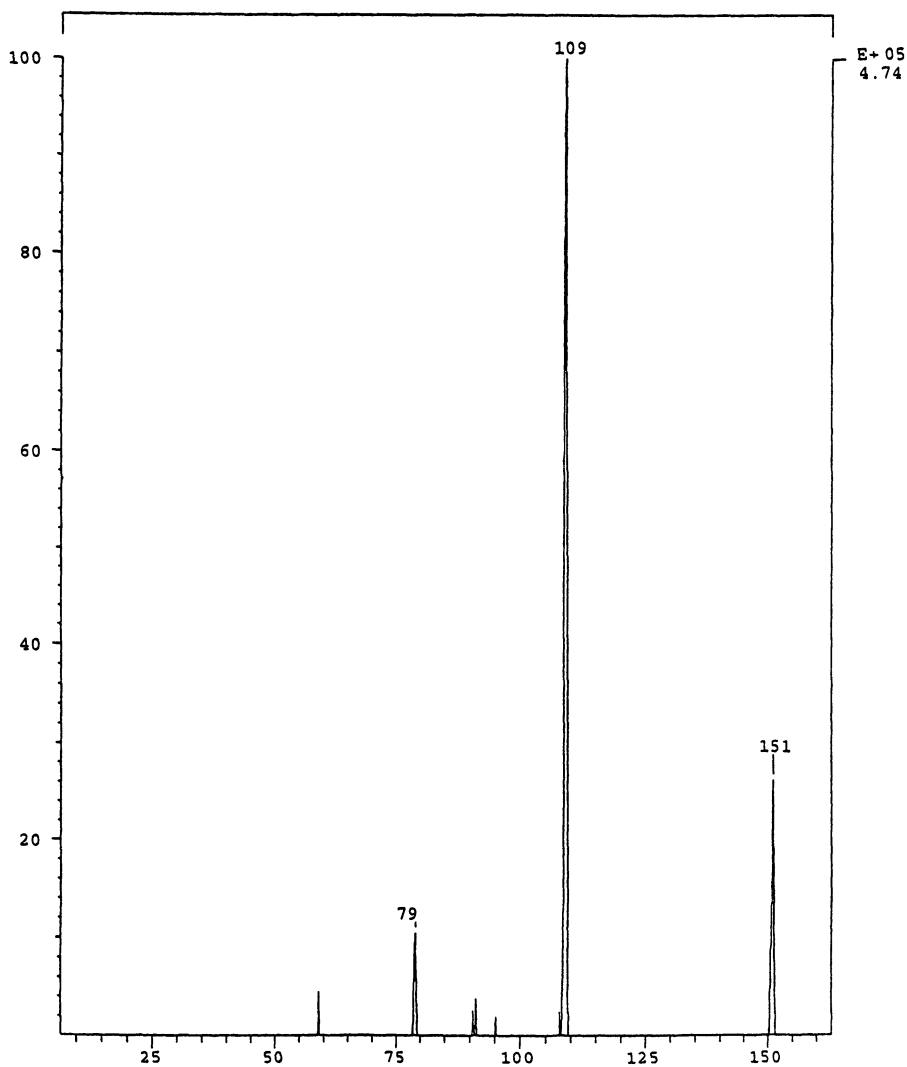
- Minimal preparation steps for analysis of samples



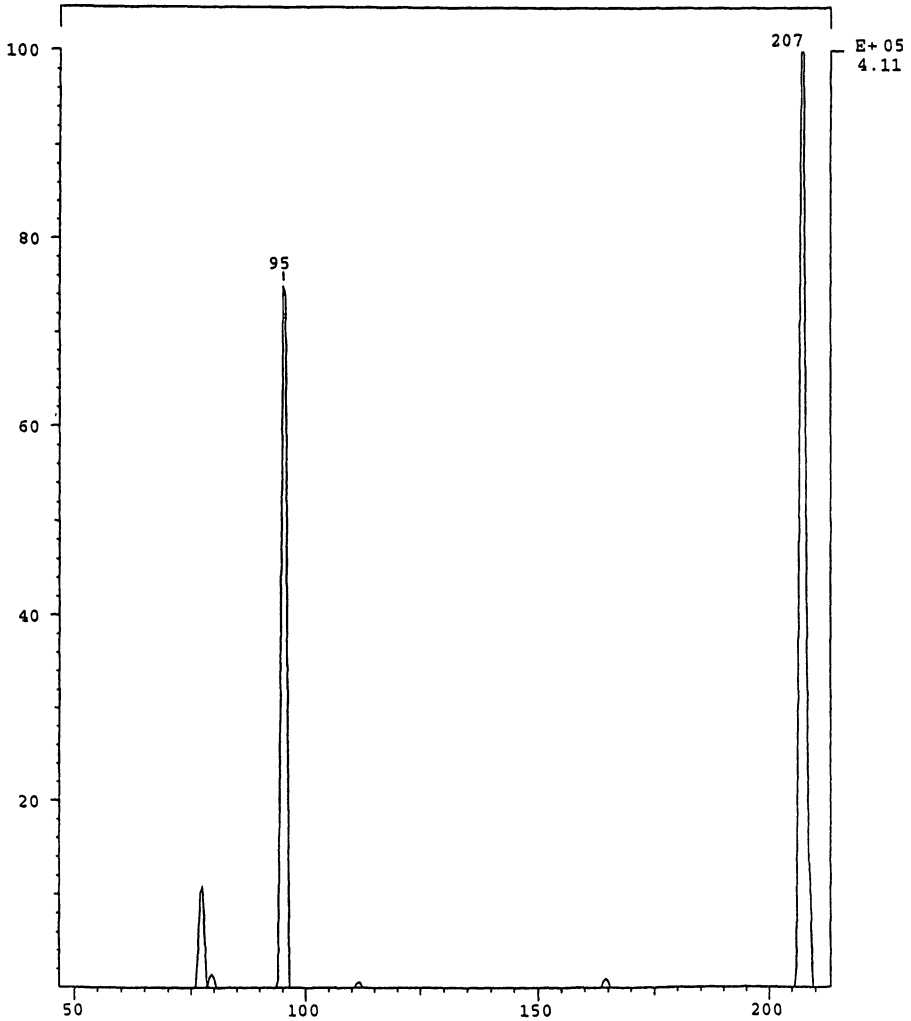
8. Analysis of aqueous sample from the Second (April 1997) Official PTS/OPCW Proficiency Test water sample. Experimental conditions are same as in Figure 6.

Table 3. The Results from the Second and Third Official PTS/OPCW Proficiency Tests (Water Samples)

	Compound	
Second (October, 1996)	<i>i</i> -PEPA	EPA
Third (April, 1997)	EHMPA	<i>i</i> -PPA



9. Analysis of the aqueous sample from third official PTS/OPCW proficiency test. Experimental conditions: Mass spectrometry (MS) on negative ions was done on a Finnigan TSQ 7000 tandem quadrupole mass spectrometer using the Finnigan electrospray ion source. A solution of aqueous acetonitrile (50:50 v/v) containing 0.025 M ammonium acetate was infused into the Atmospheric Pressure Chemical Ionization (APCI) interface at a flow rate of 0.4 mL/min. Nitrogen (99.99%) was used as the nebulizing gas, and the vaporizer was maintained at a temperature of 400°C.



10. Analysis of the aqueous sample from third official PTS/OPCW proficiency. Experimental conditions are same as in Figure 9.

- Excellent separation efficiency and no interfering background substances observed for environmental matrixes
- The co-electroosmotic conditions reduced the analysis time and eliminated the observed baseline anomalies observed when the EOF modifier was absent with complete separations achieved in a 3-minute electropherogram
- Analyte detection limits are in the ng/mL range using pressure injections and separations are robust with migration time variations less than 5.0 %RSD on a day-to-day basis.
- The interday and intraday reproducibility for the anions were in the range of about 1 to 3 %RSD with accuracy reflected by spike recoveries in actual reaction masses of not less than 86%.
- The use of acidic pH electrolytes eliminated several interferences such as fluoride, carbonate anion and humic acids found in soil sample.
- Acidic electrolytes also increase the shelf life of the buffer as it does not absorb atmospheric CO₂ (which drops the pH) as readily as alkaline pH electrolytes. The shelf life of the buffers for both detection methods is one year, and this level of storage stability would be a great benefit in many other CE applications.
- The derivatization steps required for direct UV visualization of the nonchromophoric analytes are eliminated for both indirect UV and conductivity detection as the analytes are detected as differences between the measured properties of the electrolyte co-ion and the analyte itself.
- Finally, our CE methods are versatile and flexible and may therefore be adapted to many different applications.

ACKNOWLEDGMENTS

We thank the U. S. Army Materiel Command's Treaty Laboratory, Aberdeen Proving Ground, Maryland for its support. The authors express sincere appreciation to W. Jones of Thermo Bioanalysis for his helpful suggestions.

References

1. Conference on Disarmament Special Committee on Chemical Weapons. CD/CW/WP. 367 Geneva, October 7, 1991.
2. Kingery, A. F.; Allen, H. E. *Toxicological and Environmental Chemistry*, **1995**, *47*, 155-184
3. Epstein, J.; Bauer, V. E.; Saxe, M.; Demek, M. M. *J. Am. Chem. Soc.*, **1956**, *78*, 4068-4071.
4. Davis, G. T.; Demek, M. M.; Sowa, J. R.; Epstein, J. *J. Am. Chem. Soc.*, **1971**, *93*, 4093-4103.
5. Vasil'ev, I. A.; Shvyryaev, B. V.; Liberman, B. M.; Sheluchenko, V. V.; Petrunin, V. A.; Gorskii, V. G. *Mendeleev Chemistry Journal*, **1996**, *39*, 4, 3-10.

6. For example see: (a) Jorgenson, J. W.; Lukacs, K. D. *Anal. Chem.*, **1981**, *53*, 1298-1302. (b) Jorgenson, J. W.; Lukacs, K. D. *Science*, **1983**, *222*, 181-189. (c) Jorgenson, J. W. *ACS Symp. Ser.* **1987**, *335*, 182-198. (d) Walbroehl, Y.; Jorgenson, J. W. *J. Microcolumn Sep.* **1989**, *1*, 41. (e) Kennedy, R. T.; Oates, M. D.; Cooper, B. R.; Nickerson, B.; Jorgenson, J. W. *Science* **1989**, *246*, 57-63.
7. Hjerten, S. *Electrophoresis* **1990**, *11*, 665.
8. Nassar, A-E. F.; Lucas, S. V.; Jones, W. R.; Hoffland, L. D.; *Anal. Chem.*, **1998**, *70*, 1085-1091.
9. Landers, J. P. (Editor) in *Handbook of Capillary Electrophoresis*, CRC Press, Boca Raton, New York, 2nd ed., Chapter 6, 1996.
10. P. G. Righetti, (Editor) in *Capillary Electrophoresis in Analytical Biotechnology*, CRC Press, Boca Raton, New York, 1996, 1st ed.
11. Jandik, P., Jones, W.R., Weston, A., and Brown, P.R., *LC GC*, **1991**, *9*, 634.
12. Jones, W.R., and Jandik, P., *J. Chromatogr.* **1991**, *546*, 445.
13. Helmholtz, H. Z. *Annal. Phys. Chem.*, **1879**, *7*, 337.
14. (a) Nassar, A-E. F.; Emery, A.; Hoffland, L. D.; *Proceeding of ACS Div. Env. Chem.*, 1997, *37* (1), 39-42. (b) Hoffland, L. D.; Calloway, R.; Emery, A.; Nassar, A-E. F; *Proceeding of ACS Div. Env. Chem.*, 1997, *37* (2), 41-43.
15. Jandik, P., and Bonn, G., *Capillary Electrophoresis of Small Molecules and Ions*, VCH Publishers, NY, NY, **1993**, p 42.
16. Tsuda, T.; Nomura, K.; G. Nakagawa, *J. Chromatogr.*, **1983**, *264*, 385.
17. Huang, X.; Luckey, J. A.; Gordon, M. J.; Zare, R. N. *Anal. Chem.*, **1989**, *61*, 766.
18. Nassar, A-E. F.; Lucas, S. V.; Myler, C. A.; Jones, W. R.; Campisano, M.; Hoffland, L. D., *Anal. Chem.*, **1998**, in press.

Chapter 21

Particulate Removal from Oxygen Systems Using Surfactant-Enhanced Fluorinated Solvents

Gerard K. Newman¹, Jeffrey H. Harwell¹, Bijo Mathew², Greg Caudill²,
Christy Crowe², Marc Powers², and Bhanu Gunturi²

¹School of Chemical Engineering and Material Science, University of Oklahoma,
Norman, OK 73019

²Surfactant Associates, Inc., P.O. Box 2705, Norman, OK 73070-2705

Recent presidential directive has banned the regular use within the military of all chlorofluorocarbons (CFCs) and other volatile ozone depleting compounds. Consequentially, work has been focused on finding alternative solvents. Due to their non-reactive or non-toxic nature, fluorocarbons (FCs), some hydrofluorocarbons (HFCs), and hydrofluoroethers (HFEs) are all possible candidates. Surfactant Associates Inc.'s (S.A.) examines the use and effectiveness of several such replacement solvents in the presence of surfactants for the removal of particulate from aircraft oxygen reservoirs and lines. Scanning Electron Microscopy (SEM), digital image analysis and particle dispersion studies are used to evaluate the ability of various surfactants to affect an increase in cleaning performance for these solvents. Novel pseudo-*in-situ* SEM studies were also performed on the most promising solvent-surfactant systems in order to evaluate their performance under actual flow conditions found in aircraft line cleaning at various fluid velocities.

The specific problem motivating replacement of many chlorofluorocarbon (CFC) solvents is their effect on ozone. Depletion of ozone in the upper atmosphere increases the intensity and range of harmful radiation transmitted to the earth surface. Due to this effect, use of chemicals with a known ozone depleting potential (ODP) are being phased out of industrial and commercial use. In particular, chlorofluorocarbon chemicals (CFCs) have high ODP ratings. Previous, pervasive use of CFCs as refrigerants and industrial solvents have had a significant effect on ozone concentrations in the upper atmosphere. Although CFCs are still in limited commercial use until officially completely phased out by year 2000, recent Presidential Directives concerning the military's release of CFCs

into the atmosphere, have mandated that Freon R-113, methyl chloroform (TRIC) or other ODPs no longer be used legally for cleaning purposes (1,2,3,4).

Of the many manufacturing and processing activities adversely affected by this decision, one has been the cleaning of oxygen distribution lines and storage systems in several military aircraft. The contaminants and particulates within these oxygen systems can pose significant hazards to both aircraft and personnel. Particulates, impinging on surfaces from gas streams of pure or highly concentrated oxygen, can be sources of ignition and have been identified as a possible source of fires on military vessels and aircraft (3,5). Such particulates also pose significant threat to the health of personnel as emphasized in EPA's revised guidelines for particulate matter (6). Use of ODP solvents, such as Freon R-113; have been integral within the military for removing particulates and other contaminants from oxygen lines and other systems. In today's environment of pollution minimization, regular maintenance on these aircraft life support systems must incorporate environmentally acceptable solvents to maintain the effective functioning and health of the aircraft crewmembers. The specific problem facing military maintenance personnel is that, as yet, few alternative cleaning solvents, formulations, or alternative methods have been identified as candidates for use in military oxygen systems.

CFCs

The proposed ban of CFC-113, in accordance with Presidential Directives and the Clean Air Act, creates one of the most difficult challenges for the military. Trichlorotrifluoroethane (CFC-113) has been the solvent of choice for over 25 years to clean oxygen systems and other vital components in military aircraft. It displays performance and safety characteristics that are uniquely suited for the cleaning of oxygen systems. It is non-flammable, chemically inert, essentially nontoxic, and compatible with many metallic and non-metallic materials. It demonstrates excellent cleaning characteristics for contaminants such as hydrocarbons, silicone, and fluorinated oils and greases. Specific military uses for FreonR-113 and 1,1,1-trichloroethane range from applications in cleaning gauges and instruments, degreasing equipment and parts, cleaning oxygen piping, and components to spray cleaning field equipment (3).

The CFC solvents are easily analyzed for residual contamination by infrared (IR) spectroscopy or evaporative non-volatile residue (NVR). These techniques permit quick quantitative verification of cleanliness (3). The versatility of these solvents is indicative of the need to develop alternative solutions to address the potential vacuum created by their discontinued use.

OXYGEN LINE CLEANING

Contaminants accumulate within oxygen systems on military aircraft from various sources, resulting in the need for maintenance and overhaul of these life support systems. This may include stripping the oxygen lines from the aircraft and replacing them (5). Considerable down time for the aircraft can be involved in this procedure. Cost benefit analysis favors an *in situ* cleaning process over disassembly and replacement.

Military personnel have suggested that the possible contaminants within the lines are zeolite dust from onboard oxygen generation units, glycol, jet fuel residues, and dust (20). Several possible health hazards have been attributed to the presence of these contaminants in the aircraft oxygen distribution system. An EPA review, of a fourteen year long air pollution study in London, showed that the presence of particulate in air leads to deposition of particulate in lungs that correlates with early death and illness. Though the data from this study did not indicate a definitive safe particulate size, there is reason to believe small particulate in the range of ~ 2.5 microns represent a serious health threat, as they are uniquely difficult for the lungs to handle (6). From a mechanical aspect, Air Force personnel have also indicated that there is potential for explosions from clogged valves in some systems using liquid oxygen reservoirs as well as possibility of oxidation ignition initiated from particle impingement on surfaces (3,5).

PARTICLE ADHESION AND DISPERSION

The major difficulty in cleaning particulate from surfaces is the tenacity of their adherence. Research conducted on particle adhesion in the microelectronic industry have shown that for a 1-micron diameter particle, the force of adhesion exceeds the force due to gravity by more than a factor of 10^6 . The total adhesion forces holding small particles to surfaces can range from 10^5 to 10^2 dynes. This range represents a force per unit area for micron size particles of $>10^9$ dynes/cm² (7). With such large adhesion forces adhering the particulate to the surface, it would seem that only the removal of larger particles (>5 microns) needs be addressed. Particulate smaller than 5 microns would seem to experience such large adhesion forces that they would not be capable of being dislodged and becoming airborne under normal oxygen flow rates. Published literature indicates this is not necessarily true. Even quite small particulate are easily dislodged, if the lines are flexed or moved. Flexing of the lines exerts significant physical force on the particle; these physical forces can potentially cause the particulate to overcome their adhesion forces to the surface (7). The flexing of lines on aircraft is very possible as they may undergo thermal expansion and compression during flight, in addition to the movement and vibration that occurs during normal flight operation and maintenance.

PREVIOUS CLEANING ALTERNATIVES

Current oxygen line cleaning procedures require that the oxygen lines be removed from the aircraft, be cleaned, and be certified prior to reinstallation. A similar procedure is followed for aircraft with oxygen reservoirs. In spite of extensive effort by a number of material suppliers, no environmentally suitable replacements have been found that produces the levels of cleanliness achievable with CFC-113 and TRIC (1,1,1-trichloroethane). The various candidates that have been proposed—water, terpenes, alcohols, and hydrogenated chlorofluorocarbons (HCFCs)—introduce manufacturing, health, and safety problems of one sort or another which further detract from their use (8).

The alternative cleaning methods in use, proposed, or that have been used include but are not limited to the following (20):

A. Navy Oxygen Cleaner (NOC) Flush

An aqueous wash using Navy Oxygen Cleaner (NOC) or a similar surfactant-enhanced water solution to remove contaminants is used, followed by a deionized water rinse and a hot (200°F), dry nitrogen gas purge (9). This method is good for short tubing runs with limited bend radii. The potential risk associated with this process is that water left in the lines from system low points tends to freeze, which cause line blockages and component failures. The NOC cleaner, which is highly alkaline (pH ~11), can cause pitting on the tubing walls if not used properly. Water-based cleaners even with surfactants to improve wettability do not penetrate crevices and blind holes as readily as solvents and often have even greater difficulty evaporating out of them due to capillary action. While most metals are insoluble in alkaline solutions, some react chemically with some cleaner's active ingredients. For example, sodium hydroxide (NaOH) and any other compound containing a hydroxyl group (-OH) attack aluminum and stain brass and other copper alloys (2).

B. Trichloroethylene (TRIC) Flush

Flush with trichloroethylene (TCE) followed by a purge with hot (200°F), dry nitrogen gas. The problem associated with this process is that TCE is an EPS-17 toxic chemical with costly disposal requirements.

C. Alcohol Flush

An alcohol (TT-E-735) flush followed by a hot (200°F), dry nitrogen purge. The danger associated with this process is that alcohol vapor can ignite causing fire; the vapors can explode with an initiation spark in an enriched oxygen environment causing equipment failure and injury to personnel (10).

ALTERNATIVE SOLVENTS AND CLEANING TECHNIQUES

The search for viable solvents has been an on-going process for industry. In the first part of this century, chemists found that replacing the hydrogen on a small hydrocarbon molecule with chlorine often enhanced its solvent ability as well as its inflammability. Chlorinated hydrocarbons soon became popular for a variety of cleaning processes such as degreasing and dry cleaning. This replacement of hydrogen with chlorine soon led to investigation of another halogen, fluorine. Fluorinated carbons were quickly recognized to have attractive properties. Their inertness to oxidation with oxygen occurs because fluorine is the most electronegative element in the periodic table; oxygen is the second. In essence, these compounds' carbon backbone has already been oxidized by an element more oxidative than oxygen and will not be effected by flames. Today, perfluorocarbons (PFCs) and the newly emerging hydrofluorocarbons (HFCs) are generally recognized as

biologically inert and nonflammable and are excellent candidates as replacement solvents. Excepting the case of a fluid at its critical point, fluorocarbons are unique in having the lowest surface tensions of any fluids. This allows the fluorocarbon molecules to quickly wet surfaces and penetrate pores and cracks that exist between particles and their supporting substrate. Low surface tension lowers the energy required in lifting a particle from a surface. Table 1 below displays the very low surface tension of a fluorocarbon relative to other liquids (11).

TABLE 1 Surface tension values of various liquids

Liquid	Surface tension mN/m
Mercury, Hg	486.5
H ₂ O	73.0
Benzene	28.9
Heptane	20.1
Perfluoroheptane	13.2

Potentially, surfactants, in low concentrations, can be used to tailor the properties of PFCs and HFCs, creating an overall solvent formulation with the desired characteristics for a specific application.

A. Cleaning Techniques

The problem of particulate contamination in the microelectronic industry has been a driving force in understanding particle adhesion forces and in development of precision cleaning methods. There are over 25 methods purported to remove particles smaller than 25 microns in diameter. Included in the 25 methods are: ultrasonic, megasonics, wiping, brush scrubbing low pressure surfactant spraying, high pressure jet spraying, etching, centrifugal mechanical abrasion, chemical displacement and emulsion, electrostatic elimination, rinsing, UV/ozone treatment, plasma etching, ion milling, polishing and buffing, laser cleaning, heat treatment, ion bombardment, immersion, aqueous vapor degreasing, strippable adhesive coatings, combustion, and leaching (12). Most of the cleaning methodologies listed above are difficult to apply to the inside of oxygen lines. A few of these methods are purported to remove very small particulate. There are a few publications that support this data (13-18). The following, Table 2, is a summary of the lowest particle size that the most viable methods can remove.

TABLE 2 Lowest particle size that can be removed by these methods (12).

PARTICLE SIZE (μm)	CLEANING METHODS
0.2	Megasonic cleaning
0.2	Low-Pressure Surfactant Spraying
0.2	High-pressure Jet Spaying(15,000psi)
0.3	High-Pressure Jet Spaying (10,000psi)
0.5	Brush Scrubbing
0.5	Centrifugal Spray Cleaning
0.5	High-Pressure Jet spraying (4,000psi)
0.5	Etching
5.0	Wiping
25.0	Ultrasonic cleaning

Of the cleaning methods listed above, surfactant spray cleaning has been reported as effective in removing small particles down to 0.2 μm . For aqueous solutions without a surfactant present, pressures up to 15000 psi are required for equivalent cleaning. Surfactant spray cleaning simply passes a surfactant solution across a surface with a low but sufficient velocity to lift particulate from the surface. The aqueous solution with the surfactant present requires much lower velocity to overcome particulate adhesion forces than does the solely aqueous high-pressure jet spaying. This difference between using a solely aqueous stream or a surfactant based solution is quite significant in light of the very strong forces holding particles to a surface. As noted earlier, we know that adhered colloidal particles below about 0.2 microns in diameter are extremely difficult to remove and that removal is difficult even for particles as large as 10 microns. Yet, the surfactant spray cleaning method seems to have some success in removing such particles. One paper has reported that significant detachment of small particles can occur in a non-aqueous surfactant solution by polymeric detergency (18). The exact mechanism, although not fully understood, is thought to involve a facilitated repulsion of the particle with the surface where, the detergent molecule acts as a molecular wedge or lever. To be successful, the detergent molecules must be small enough to penetrate the cracks between the particle surface and the substrate surface. Size of the surfactant molecule is very critical. The structure of a particular surfactant may also determine if it more easily penetrates and adsorbs on the particle and or substrate. Different types of surfactants may adsorb more strongly than other surfactants. Factors affecting detachment of the particles are bulk phase viscosity, drop radius, contact angle--whether advancing or receding contact angles. If the adhering particle is a mixture of organic film and particulate, the surfactant causes the contact angle to increase so that the mixture elongates and may be carried away from the surface.

CURRENT RESEARCH BACKGROUND

There is some evidence that PFC and or HPCs with surfactants may be viable candidates for cleaning particulate from surfaces. Entropic Systems, Inc. (ESI) has published research establishing that small particles are more effectively removed from a variety of surfaces, when exposed to ultrasonic agitation in the presence of dilute solutions of high molecular weight fluorocarbon surfactant solutions. The fluorocarbon surfactant solutions performed better than either pure CFC-113, or a perfluorinated liquid that does not contain any dispersing agent (δ). Such formulations could be optimized for a variety of cleaning processes including oxygen systems. These fluorocarbon surfactant solutions have many of the properties that make CFC a choice solvent. However, it is not likely that megasonic or ultrasonic cleaning could be successfully implemented for cleaning oxygen line or reservoirs due to several physical constraints. The small diameter of the lines and the presence of control valves and other equipment would quickly dissipate the energy. However, the method might be used successfully in oxygen reservoirs, if military regulations did not prevent the introduction of any foreign components like an ultrasonic probe into the reservoir. Constraints, such as these, also eliminate the effectiveness of many other cleaning methodologies. In essence, it may be concluded that no checklist exists to match applications with cleaning method and chemical. Just about every solvent replacement problem will need to be considered individually [1].

A. Non-aqueous Surfactant Based Cleaning Formulations

The solution to this dilemma according to Surfactant Associates Inc. (S.A.), may lie not in the development of an alternative drop-in replacement for CFC-113 and TRIC, but in a novel replacement formulation that uses the synergy of adding a specific surfactant to an already developed and acceptable environmentally friendly solvent. The addition of a surfactant can potentially alter the cleaning characteristic of the solvent in a uniquely desirable way. By tailoring the surfactant-solvent formulation to suit the cleaning need, specific engineering needs may be uniquely addressed. Most importantly, the tailoring of surfactant and solvent may be achieved without altering the environmentally desirable characteristics of the solvent. Choosing already commercially available surfactants and solvents would allow the quick approval of formulations that could potentially equal or surpass the previous oxygen cleaning solvents.

EXPERIMENTAL SECTION

A. Cleaning of Oxygen Line and Reservoirs

Three fluorosurfactants are evaluated at different concentrations in five fluorinated solvents for their ability to enhance particle removal from three types of surfaces. One surface is a metal alloy coupon cut from the interior of a liquid oxygen storage vessel commonly used in military aircraft. The second surface is that of standard glass microscope slides. . The third test surface is from the inner tube wall of aluminum lines

commonly used to transmit enriched oxygen. All test surfaces are physically cleaned before adding a contaminant particulate. The particulate used to contaminate these surfaces is commercially available under the trade name of Arizona Road Dust. This contaminant is an A. C. Fine Test Dust from the Duke Scientific Company. The contaminant has a stated size distribution of 2 to 80 μm . The contamination procedure uses a solution of a two grams of Arizona Road Dust dispersed in thirty milliliters of acetone. An eyedropper is used to transfer the contaminant solution on to the test slides and surfaces. The doped sample surfaces are allowed to dry at room temperature. The contaminated metal sample surfaces are characterized with scanning electron microscopy (SEMs). These surfaces were previously marked to allow re-examination of the same area for direct comparison both before and after cleaning. The glass sample slides are fitted into a manufactured jig. An optical imaging system (Nikon Digital Microscope using Optimas® imaging software), is used to count the total area of the surface covered by particles before and after cleaning. Image analysis allowed quantification of the area cleaned including determination of the size and number of particulate removed. The ability of various surfactant-enhanced solvents to remove particulate from the test surfaces was characterized using three types of cleaning procedures: the standard ASTM procedure G93-88, Standard Practice for Cleaning Methods for Material and Equipment Used in Oxygen-Enriched Environments, ultrasonic cleaning to test the particulate removal ability of various formulations at different sonication times under a constant ultrasound intensity, and a flush of surfactant-enhanced solvent to remove particulate from the surfaces of standard oxygen lines at different flush velocities. Each cleaning procedure was performed with each solvent at increasing concentrations of surfactant

B. Materials

The particulate removal properties of five perfluorocarbon and hydrofluorocarbon formulations using three Fluorosurfactants, (Krytox® Alcohol, Zonyl® UR, and Krytox® 157FSM) are examined. The first candidate is Krytox® Alcohol, a nonionic fluorosurfactant, hexafluoropropylene oxide homopolymer alcohol, purchased from 3M. The second candidate is Zonyl UR®, an anionic fluorosurfactant, Telomer B phosphate, CAS# 65530-61-2, also purchased from Dupont. The third fluorosurfactant, Krytox® 157FSM, is a perfluoropolyether carboxylic acid, CAS# 51798-33-5 100. Of the solvents used in this study, FC-72, FC-77, FC-43 are perfluorocarbons. The hydrofluorocarbon solvents used are HFE-7100 and HFC-236fa. All of these solvents were purchased or made available by 3M or Dupont. The trade name of FC-72 is FC-72 Fluorinert Electronic Liquid (CAS# 86508-42-1), and it is a mixture of primarily fluorinated compounds with 6 carbons. FC 77 is composed of perfluorocarbon compounds of primarily 8 carbons; it's CAS# is 86508-42-1. HFE-7100 is a mixture of methyl nonafluorobutylether and methyl nonafluoroisobutylether, CAS# 163702-07-6 and CAS# 163702-08-7. HFC-236fa (1,1,1,3,3,3-hexafluoropropane) is an experimental product under development by 3M that has not yet reached full commercial status.

C. Experimental Setup for Cleaning Oxygen Reservoirs

Spherical double walled vacuum-sealed reservoirs are used as liquid oxygen storage systems on military aircraft. These metal storage tanks store oxygen used by the pilots during flight. During scheduled cleanings, the reservoirs are cleaned to a level B cleanliness in accordance with the specifications listed in ASTM G93-88. Level B cleanliness is considered satisfactory when 3 mg per square meter of particulate or less is measured in a filtered and dried sample of solvent effluent (5).

For our experimental studies, several small pieces (approximately 1 in x 1 in) are cut from a oxygen reservoir. The samples are measured to calculate their area and wiped with an acetone-loaded Kimwipe® to remove any foreign particulates. These pieces are contaminated by placing one drop of a solution made from 2 gms of Arizona Road Dust dispersed in 30 ml of acetone. The contaminated reservoir pieces are appropriately numbered and then photographed using a scanning electron microscope (SEM). The numbered sample pieces are placed in petri dishes and cleaned in accordance with ASTM G93-88. ASTM G93-88 cleaning guidelines are simulated in the laboratory by placing a reservoir piece in a 50 ml covered petri dish with the contaminated side facing up, adding 10 ml of solvent with or without surfactant, and swirling the liquid over the reservoir piece to perform a wash. After one wash, the solvent in the dish is poured through a pre-weighed filter paper. The solvent is allowed to evaporate the, and the paper is weighed to see if it meets the criterion for Level B cleaning. If the criterion is not met, the tests are repeated.

D. Results of ASTM G93-88 Procedure

Figure 1 shows the SEM photograph of a sample surface cleaned following the ASTM G93-88 procedure with pure Freon R-113. Figure 1 shows that after cleaning with Freon R-113, a mass of particulate covering approximately 15% of the surface is still present. Figure 2(a) to 2(f) shows the SEM photographs of sample surfaces from the interior of an oxygen reservoir before and after cleaning with various solvent-surfactant combinations using the swirling test. These surfaces were cleaned using solvents containing a concentration of 0.1 wt% fluorosurfactant. The effect of each fluorosurfactant, Krytox^c 157 FSM, Zonyl-UR, and Krytox[®] Alcohol, in HFE-7100 and FC-72, can be determined from the photographs. Figure 2(a) through Figure 2(c) show the coupons cleaned using HFE-7100 solvent while Figure 2(d) through Figure 2(f) show the coupons cleaned using FC-72 solvent. As shown, all of the surfactant-enhanced solvent combinations are effective in removing particulate from the coupon surfaces. Even the heavily coated particulate layer shown in Figure 2(f), became cleaner. Although, not shown, these photographs for HFE-7100 and Fc-72 are representative of the effect achieved when using FC-77, Fc-43, and HFC-236fa.

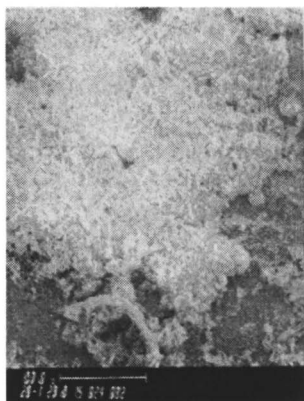
Figure 1**Pure FREON****BEFORE****AFTER**

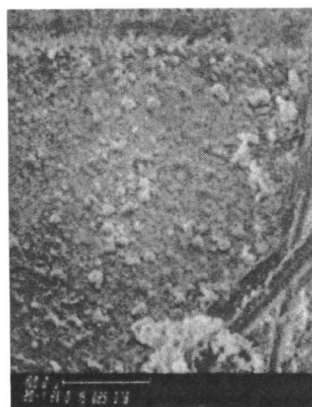
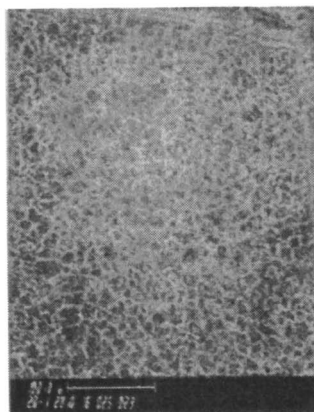
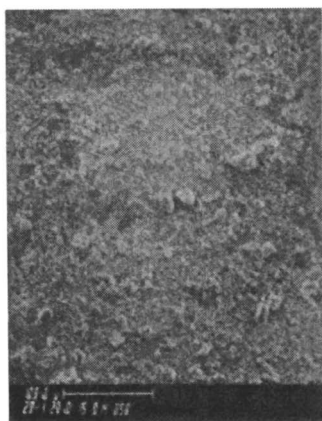
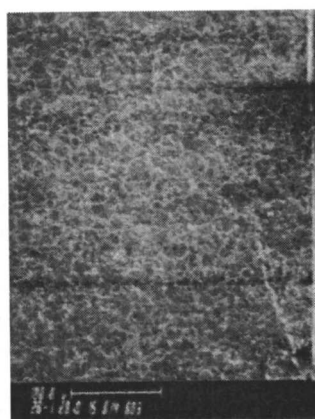
Figure 2(a) 0.1 % 157 FSM in HFE 7100**BEFORE****AFTER****Figure 2(b) 0.1% Zonyl-UR in HFE 7100****BEFORE****AFTER**

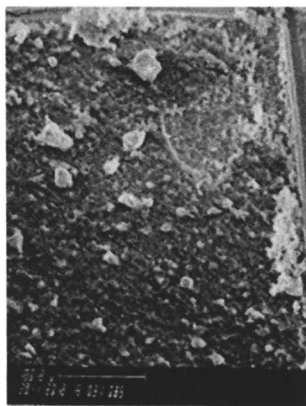
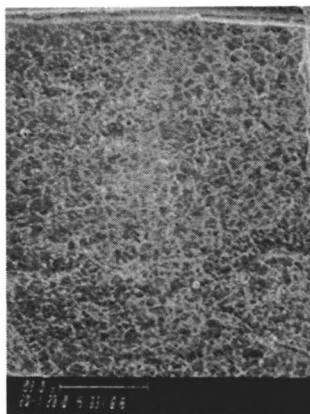
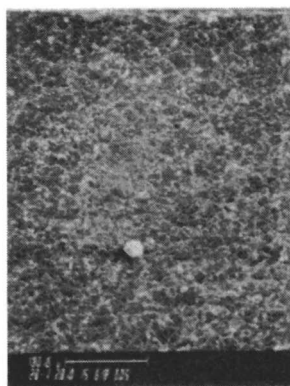
Figure 2(c) 0.1% Krytox Alcohol in HFE-7100**BEFORE****AFTER****Figure 2(d) 0.1 %157 FSM in FC-72****BEFORE****AFTER**

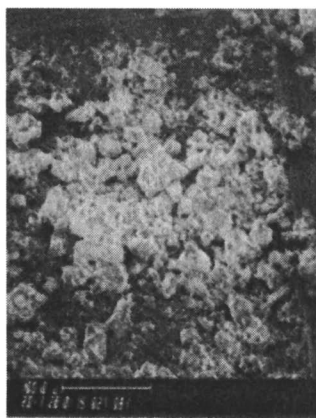
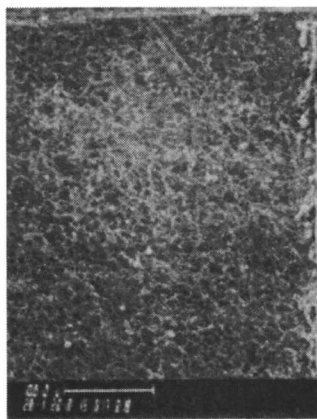
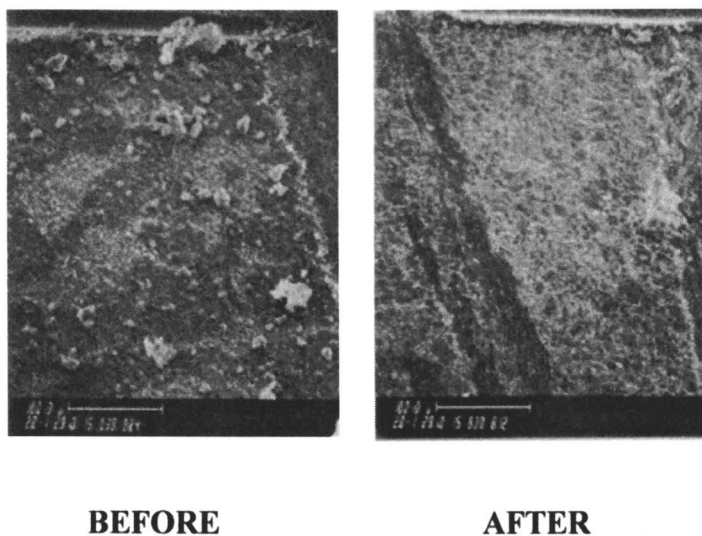
Figure 2(e)**0.1 % Zonyl-UR in FC-72****BEFORE****AFTER**

Figure 2(f) 0.1% Krytox Alcohol in FC-72

ASTM CLEANING OF METAL COUPOUNS

The SEM photograph results indicate that the smaller particulate below 10 microns are easily removed with the fluorosurfactant-solvent combinations at the reported concentration. The number of washes required to obtain a level B cleaning was minimal using the surfactant-enhanced solvents. The SEM photographs of the metal coupons indicate the presence of considerable levels of Arizona Road Dust particulate left on the metal surface. The ASTM G93-88 method appears to be a poor indicator of the level of particulate cleanliness in the interior of the oxygen reservoirs. Even though the level B cleaning criterion was met, SEM photographs indicate the surfaces are still supporting large numbers of particles. This result may or may not be indicative of the true situation in the oxygen reservoirs since the contaminants used in this study may not be a true representation of the actual contaminants present inside the oxygen reservoir. However, the test result indicates that the cleanliness standard applied to oxygen reservoirs warrants a re-evaluation based on the current findings.

The tests of the perfluorocarbon and hydrofluorocarbon solvents with the three different fluorosurfactants, Krytox[®] Alcohol, Zonyl[®] UR, and Krytox[®] 157-FSM, indicate different levels of cleaning for the same solvent. Testing indicates that the cleaning potential of the fluorosurfactant-solvent formulation needs to be evaluated with other pertinent engineering constraints.

GLASS SLIDE STUDY USING ULTRASOUND

To minimize surfactant and solvent waste and to sample a high number of surfactant solvent combinations over different time periods, ultrasonic studies on glass are performed. The glass slide studies are based on similar studies performed by Kaiser and Ambati (19). A Fisher Scientific Sonic Dismembrator[®] is used to pulse a sonic wave against a glass slide suspended in a surfactant-enhanced solvent solution. The glass slide is positioned in the apparatus to allow the sonic wave to impinge directly on the doped area. A glass chamber sealed with Teflon plugs held both the sonic probe and the particulate doped glass slide.

Approximately 180 mL of pure solvent or surfactant-enhanced solvent is added to the test chamber containing the probe and the slide. The chamber is sealed to prevent solvent loss. Six runs, two each at 30 seconds, 1 minute, and 2 minutes are performed with the solvent using surfactant at 0.05 wt%, 0.1, or 0.5 wt%. Upon completion of a run, each slide is immersed in a beaker of pure solvent to rinse off residual surfactant.

The untreated, glass slides are contaminated with 2 gm of A. C. Fine Dust (Arizona Road Dust) from Duke Scientific Company suspended in approximately 30 mL of acetone. The vial containing the contaminant solution is shaken and allowed to settle for four to five minutes. An eyedropper is used to drop the solution on the numbered slide. One drop of solution is placed on the numbered slide and allowed to dry at room temperature.

The slides are imaged prior to sonication using a Nikon Digital Microscope at 10X magnification and using Optimas[®], computer software that allows the images of the slides to be recorded digitally. Optimas[®] also calculates the area covered by the particulate by measuring the area and major axis length of the particles. The images are saved for comparison with the images taken after completion of an experimental run. The particulate areas are tabulated and the results saved to a Microsoft[®] Excel spreadsheet for analysis.

Ultrasonication of Glass Slides

The test results indicate that in every case of comparison the cleaning efficiency of the solvents, HFE-7100, R-236, FC-77 and FC-72, did much better than pure Freon R-113. The cleaning efficiency of HFE-7100 in removing particulate, Figure 3(b), improved by a factor of approximately two with the addition of the fluorosurfactants at their respective weight percents. A significant improvement in cleaning was observed at a very low concentration of surfactant (0.05 wt%) that was far superior to that done by Freons.

As seen in Figure 3(c) through Figure 3(e), R-236, FC-77, and FC-72 do not indicate for just particulate removal a statistically significant increase in cleaning efficiency with the addition of the surfactants. These results are contra-indicated by the ASTM tests. The results seem to indicate that the cleaning may be dominated by the cavitation produced from the impinging microscopic bubbles and not by the surfactant present in the solvent. This causes a mechanical scouring of the surface, thereby loosening the particulate from the surface (7). However, the two studies are also performed at differing levels of energy input and for differing time spans. Possible

suggestions for the differences in cleaning may also be from the differences in the surface tension of the fluids in conjunction with the density of the fluids. Dense fluids theoretically enhance the transfer of ultrasonic energy and low surface tension fluids allow better penetration of fluid between the particulate and the surface.

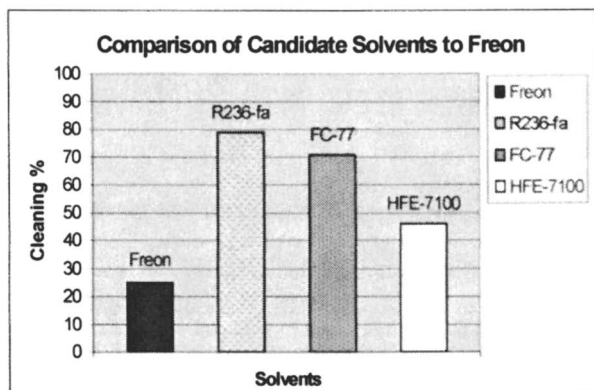


Figure 3(a) Comparison of Pure Solvents and R-113

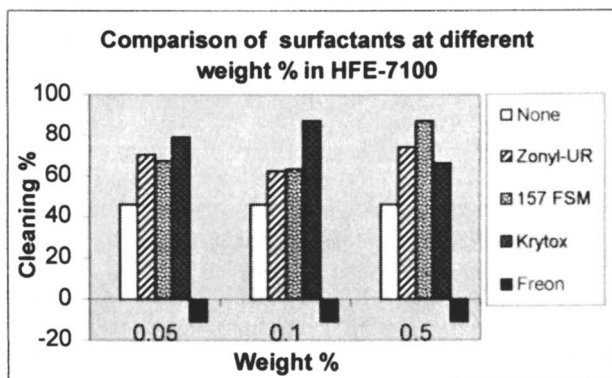


Figure 3(b) Comparison of Surfactant Performance in HFE-7100

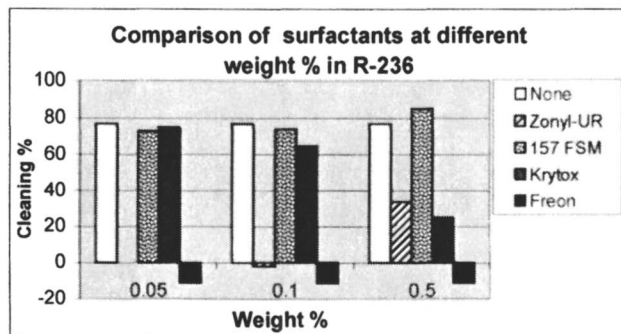


Figure 3(c) Comparison of Surfactant Performance in R-236fa

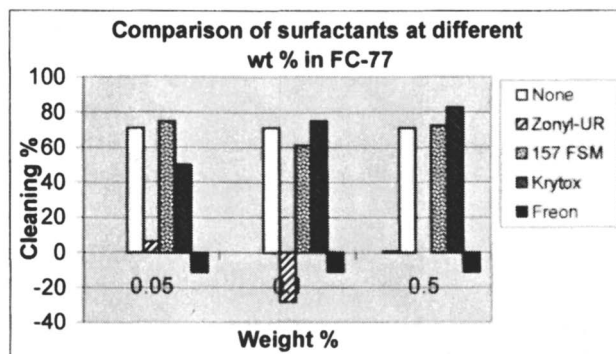


Figure 3(d) Comparison of Surfactant Performance in FC-77

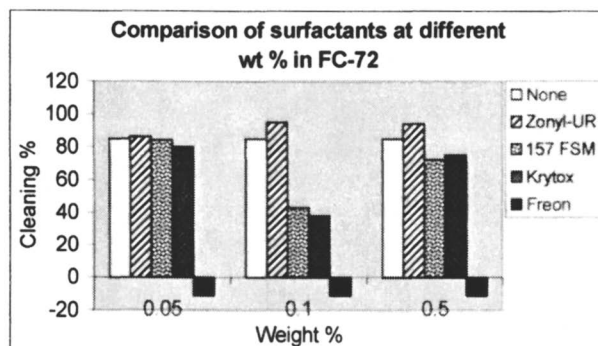


Figure 3(e) Comparison of Surfactant Performance in FC-72

Cleaning of Oxygen Lines

In order to simulate possible field cleaning conditions and possible construction of field service equipment, S.A. has constructed a bench scale mockup of a military aircraft oxygen line system, using aircraft aluminum tubing and fittings (See Figure 4(a)).

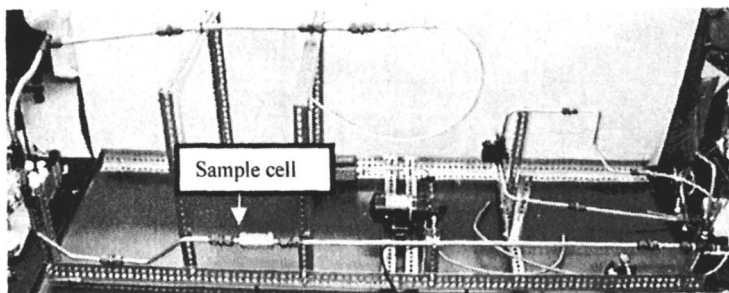


Figure 4(a) Oxygen line Bench scale unit

To provide representative experimental sample surfaces, a section of the aluminum tubing has been cut with an electron beam cutter to provide a sample point with precise cuts, Figure 4(b). The sample points are contaminated with a solution composed of ground zeolite dust and JP-8 jet fuel. The zeolite was removed from a Molecular Sieve Oxygen Generator System (MSOGS) unit used on military aircraft. The zeolite particles are hand-ground to create fines and suspended in a 20-ml sample of JP-8. The sample points are doped using an eyedropper filled with the solution. The doped sample piece is warmed to vaporize the jet fuel depositing the contaminants on the surface. The sample piece is SEM photographed to record the deposition of contaminants. A gasket matching the precise 0.010 inch cuts seals the sample when clamped into place during actual flow conditions.

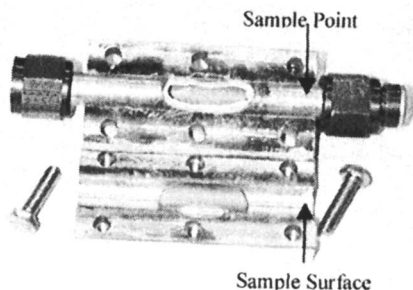
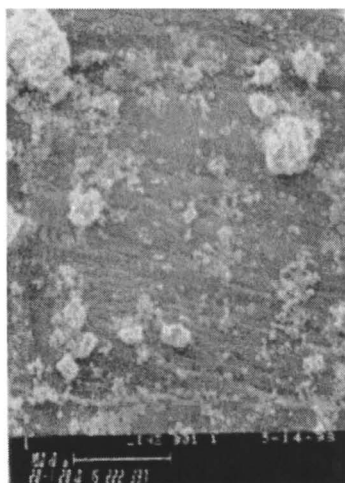
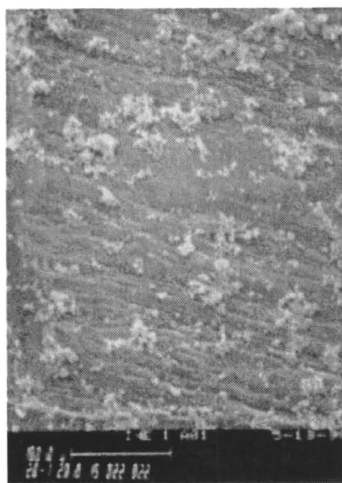


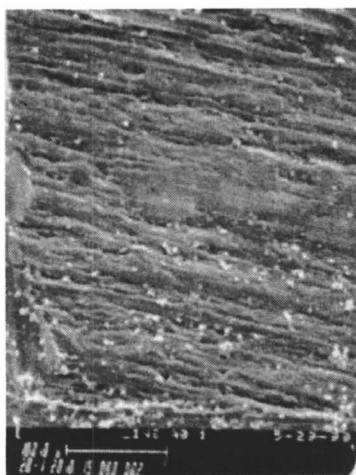
Figure 4(b): Mockup Sample Point



Contaminated surface



After flush with pure R236fa



After Flush with 0.1 wt% Krytox 157 FSM in R236fa

Figure 4(c): SEM photographs of the samples used in the line system.

After the sample surface is sealed into the line, the system is flushed with a surfactant-enhanced solvent containing 0.1 weight percent of the surfactant. Upon completion of a run, the sample is removed and re-photographed with a SEM. A mark etched into the sample inner wall forms a reference mark to allow imaging the same position each time. SEM analysis of this minimally invasive sample point helps us determine the effectiveness of the surfactant-enhanced solvent.

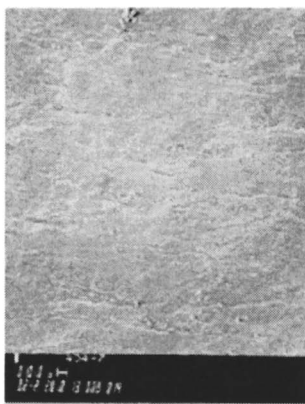
A visual analysis of the first two photographs of Figure 4(c), indicates flushing pure R236fa in a single 1.5 minute pass through the lines does breakup some of the larger aggregates, but the flow is inadequate and results in rearranged particulate on the surface. However, as indicated in the third SEM photograph, a single 1.5 minute run of R236fa with 0.1wt% of Krytox[®] 157 FSM at a flowrate of 2.1 liters per minute produces a higher level of particulate removal.

Runs are conducted using other surfactant enhanced solvents and two significant trends emerge. Particulate removal is enhanced by increasing the flowrate across a contaminated surface; there appears to be a critical flowrate below which particulate removal becomes reduced. This flowrate effect may be seen in Figure 4(d), which shows significant surfactant enhanced solvent cleaning at a higher flowrate, 3.8 liter per minute for 30 minutes, but does not appear to clean, as seen in Figure 4(e), at a lower flowrate of 1.55 liters per minute for 30 minutes.

Figure 4(d) After 30 minutes Flushing with 0.1 wt% Krytox Alcohol in R236fa, (flow rate 3.8 liter per minute)



BEFORE



AFTER

Figure 4 (e) After 30 minutes Flushing with 0.1 wt% Krytox Alcohol in R236fa, (flow rate 1.55 liter per minute)

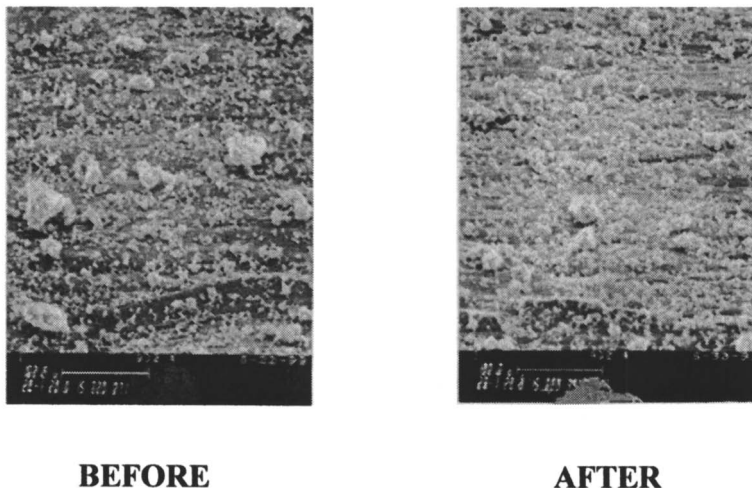


Figure 4(e) results may be contrasted to Figure 4(c) above, where a 1.5 minute flush at 2.1 liter per minute cleans the surface.

Conclusions

Fluorosurfactant-solvents work in conjunction with a critical value of shear to remove particulate from metal surfaces and are superior to FreonR-113 in their cleaning ability. The critical value of shear required to remove the particulate is significantly lowered for the perfluorocarbon, hydrofluorocarbon solvents with the added fluorosurfactants than with the pure solvents or Freon R-113. A low concentration (0.05 wt%) of fluorosurfactant in conjunction with the critical value of shear allows the easy removal of small particulate (below 10 μ m) in addition to the large particulate. The critical value of shear provided from flow of the fluorosurfactant-solvent formulation through the tubing is sufficient for removing the particulate, thereby negating the requirement for an external source of agitation.

Acknowledgement

We would like to thank Oklahoma Air Logistic Center for funding this work.

REFERENCES

1. Robert B. Aronson; *Manufacturing Engineering*, September 1993. pp.79-89.
2. James R. Koelsch; *Manufacturing Engineering*, February 1993. pp. 49-54.
3. Neil Antin; *NAVSEA Elimination of Ozone Depleting Solvents from the Manufacture and Maintenance of Oxygen Systems*
4. Akira Sekiya; Susumu Misaki; *ChemTech*, December 1996. pp.44-48.
5. ASTM G 93 - 88 Standard Practice for Cleaning Methods for Material and Equipment Used in Oxygen-Enriched Environments
6. *Where the Bodies Lie*, Scientific American, June 1998, pp. 30-32.
7. R.Allen Bowling; *A Theoretical Review of Particle Adhesion*, "Particles on Surfaces 1"; Edited by K.L. Mittal, Plenum Press, New York, 1988. pp. 129-142.
8. Robert Kaiser; *Enhance Particle Removal from Inertial Guidance Instrument Parts by Fluorocarbon Surfactant Solution*, "Particles on Surfaces"; Edited by K.L. Mittal, Marcel Dekker, Inc., New York, 1995. pp. 395-404.
9. MIL-STD-1330D, Section 4.3.1.6
10. Jan Goldberg; Aircraft Oxygen Lines Cleaning Project report EM-951036, Tinker Air Force Base Pollution Prevent Division.
11. J. H. Harwell; J. Scamehorn; S. Christian; "Short Course in Applied Surfactant Science and Technology", November 7, 1997
12. Juan Bardina; *Methods for Surface Particle Removal: A comparative Study*, "Particles on Surfaces 1 "; Edited by K.L. Mittal, Plenum Press, New York, 1988. 329-338.
13. I. F. Stowers and H. G. Patton, in "Surface Contamination: Genesis, Detection and Control", K. L. edited by Mittal, Plenum Press, New York, 1984, Vol.1, pp. 341-349.
14. A. Mayer and S. Shwartzman, Megasonic Cleaning: A new cleaning and drying system for use in semiconductor processing. *J. Electronic Mater.*, 8 (6), 1979, p. 855.
15. R.P. Musselman and T. W. Yarbrough, Shear stress removal of submicron particles from surfaces, *J. Environmental Sci.*, 51 (January/February), 1987.
16. P. S. Burggraaf, Wafer Cleaning: Sonic Scrubbing, *Semiconductor Intl.*, 103, July 1981.
17. G. Fong and M. Daszko, Wafer cleaning technology for the eighties, *Microelectronic Manufacturing & Testing*, 1, May 1978.
18. E. J. Clayfield and E. C. Lamb, *Disc. Faraday Soc.*, 42, 1966 pp. 285.
19. R. Kaiser, R.R. Ambati, *Effects of Process on Surface Cleaning in Perfluorinated Liquid Solutions*, Proc. Internl. Rolling Element Bearing Symposium, 1994.
20. Scientific and Technical Report prepared by BATTELLE; Analysis of Carrier Gas and Additives CDRL A002,DI-MISC-8-711 for R&M Assessment of Oxygen Line Cleaning, Contract No, F09603-95-D-0180-SD03

Reversed Micelles as Novel Protein Refolding Media

Masahiro Goto, Tsutomu Ono, and Shintaro Furusaki

Department of Chemical Systems and Engineering, Graduate School of Engineering, Kyushu University, Hakozaki, Fukuoka 812-8581, Japan

Refolding of denatured RNase A was conducted by a nanostructural surfactant-based molecular assembly formulated with sodium di-2-ethylhexyl sulfosuccinate (AOT) in isooctane. In the novel refolding technique, a solid-liquid extraction was utilized as an alternative to the ordinary protein extraction by reversed micelles based on a liquid-liquid extraction. The effects of operational parameters such as concentration of AOT, W_o ($=[\text{H}_2\text{O}]/[\text{AOT}]$), and pH were examined on the solubilization of denatured proteins into a reversed micellar solution. The typically denatured form of the protein being isolated is reactivated due to its refolding ability within the confines of the reversed micelle medium. A complete renaturation of RNase A was accomplished by adjusting the composition of the redox reagent even at a high protein concentration in which protein aggregation would usually occur in aqueous media. In the final step, the renatured RNase A was effectively recovered from the reversed micellar solution without the loss of the enzymatic activity.

A large number of proteins from eukaryotic genes cultivated in a bacterial system by recombinant DNA technology are often produced inactive misfolded or aggregated proteins, which actually consist only a small portion of native and active conformation (1). These insoluble aggregates in an aqueous solution are misfolded protein molecules. In order to obtain biologically active proteins, these insoluble proteins must first be extracted from the inclusion bodies and solubilized using strong denaturants such as guanidine hydrochloride or urea under reducing conditions (in case of proteins which possess disulfide bonds). On the removal of the denaturant by dialysis or dilution with an appropriate buffer, the proteins are allowed to refold up to the native and active conformation. However, a high refolding yield may not be obtained at high protein concentration due to the formation of irreversible aggregates by the excess inactive protein molecules.

Recently, a novel preparation method aimed at improving the efficiency of refolding at higher protein concentration has been reported (2,3). Hagen et al. has suggested that isolating protein molecules in a reversed micellar matrix reduces intramolecular interaction which causes formation of irreversible aggregates. Reversed micelles provide nano-structural aqueous droplets constituting water pools in an organic solvent, so that proteins solubilized in the water pool can maintain their high-structural conformation and activity. These features are favorable for protein refolding, because protein molecules can be isolated from each other during the refolding process. However, during the solubilization of denatured RNase A into a reversed micellar solution by a liquid-liquid phase transfer method, the mass transfer was considerably inhibited by the denaturants contained in the aqueous solution (20% transfer yield at 1M GuHCl and 60% transfer yield at 0.5M) (2). We considered that in this process the protein refolding efficiency is remarkably reduced. The overall process being : extraction of denatured proteins, renaturation in reversed micelles and back extraction of active proteins to a fresh Tris-HCl buffer aqueous solution.

In the present study, we demonstrate that the reversed micellar system utilizing solid-liquid extraction is a new promising and attractive technique for refolding proteins. Some key operational parameters were investigated on the efficiency of refolding denatured RNase A which was chosen as a model protein of inclusion bodies. This novel refolding process is schematically shown in Figure 1. Furthermore the optimal conditions are also discussed in this paper.

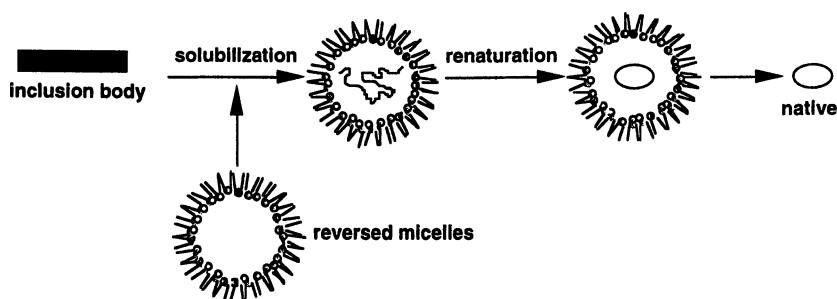


Figure 1. Schematic illustration of protein refolding by reversed micellar solution utilizing solid-liquid extraction technique.

Experimental

Materials. Bovine pancreatic RNase A (EC 3.1.27.5) and cytidine 2':3'-cyclic monophosphate were obtained from Sigma Chemicals Co. (USA). AOT (Sodium bis-2-ethylhexyl sulfosuccinate), urea and b-mercaptoethanol were purchased from Kishida Chemicals Co. (Japan). Reduced and oxidized glutathione (GSH, GSSG) were purchased from Wako Pure Chemical Industries, Ltd. (Japan). Other chemicals were of the highest grade commercially available.

Preparation of Solid Denatured RNase A as a Model of Inclusion Bodies. Native RNase A (10 mg/ml) was denatured with 8 M urea and 0.3 M β -mercaptoethanol. Proteins were then precipitated using a cold mixture solution of acetone and 1 N-HCl (39/1 by vol.). Subsequently, the precipitate was washed with acetone and further by ethyl ether. The precipitates were collected by centrifugation and were then lyophilized for 24 hours. It was confirmed that the precipitates did not show any enzymatic activity and were not soluble in both aqueous and organic solutions. Detailed experimental procedures were the same as what have been reported by White (4).

Solubilization of Solid Denatured RNase A into Reversed Micelles by the Solid-Liquid Extraction Technique. A reversed micellar solution was prepared by injecting a 0.1 M Tris-HCl buffer, (pH 6.0-10.4, 1 mM EDTA (ethylenediamine tetraacetic acid)) into a 50-400 mM AOT-isooctane solution. The solid denatured RNase A was dissolved into the reversed micellar solution under ultrasonic irradiation for approximately 1 hour. The concentration of RNase A solubilized in the reversed micellar solution was determined by measuring its absorbance at 278 nm with a UV-VIS spectrophotometer (U-best 570 JASCO). The average diameter of reversed micelles containing proteins was analyzed by a DLS-7000 system (75mW Ar-laser, Otsuka Electric Co. Ltd., Japan).

Renaturation of RNase A in Reversed Micelles. Various amount of reduced glutathione (GSH) and oxidized glutathione (GSSG) were dissolved in 0.1 M Tris-HCl buffer (pH 8.7, 1 mM EDTA). 1 ml of this solution was injected into 10 ml of 400 mM AOT-isooctane solution. Renaturation was initiated by adding 1 ml of reversed micellar solution containing glutathione into the 2 ml reversed micellar solution containing solubilized RNase A. The specific activity of RNase A in the reversed micelles was measured against time progress, considering the time when glutathione solution was added as the initial time. The renaturation yields of denatured RNase A was evaluated by comparing the enzymatic activity of denatured RNase A to that of native RNase A which was solubilized in the reversed micelles as a control experiment.

RNase A Activity Assay.

a) In aqueous solution

A substrate solution for the RNase A assay was 0.1 mg/ml cytidine 2':3'-cyclic monophosphate dissolved in a 0.025 M phosphate buffer (pH 7.5). 0.06 ml of sample was then added to 0.84 ml of the substrate solution. The change in absorbance at 286 nm was recorded against time. RNase A activity was determined by calculating the initial slope of the absorbance curve.

b) In reversed micelles

A reversed micellar solution containing a substrate was prepared by injecting 0.6 ml of 10 mg/ml cytidine 2':3'-cyclic monophosphate in a 0.05 M borate buffer (pH 9.5) into a 36 ml of 50 mM AOT-isooctane solution. A 200 μ l sample was added to 1 ml of substrate solution. RNase A activity was estimated by observing the increase in absorbance at 286 nm (5).

Recovery of Renatured RNase A from Reversed Micelles. One volume of reversed micellar solution containing the renatured RNase A was added into 5-40 volumes of cold acetone and stirred in a magnetic stirrer for 20 minutes. The reprecipitated RNase A was collected by centrifugation and washed several times with cold acetone to remove AOT molecules that may be adsorbed to the collected RNase A. Furthermore, the precipitates were dried under vacuum condition. It was confirmed that AOT molecules were completely removed by the results of elementary analysis. The obtained precipitates were solubilized in a 0.025 M phosphate buffer (pH 7.5). The amounts of recovered RNase A were determined by measuring the absorbance in the buffer solution at 278 nm with the UV-VIS spectrophotometer. The activity of the recovered RNase A in a buffer solution was also measured by the previously described method and the enzymatic activity was determined by comparing them to the specific activity of native RNase A that was solubilized in the same buffer solution as a control experiment.

Results and Discussion

Solubilization of Solid Denatured RNase A into Reversed Micellar Solution by Solid-Liquid Extraction Technique. In the previous study (2) protein refolding utilizing reversed micelles showed that solubilization of denatured RNase A into reversed micelles was difficult owing to a huge amount of denaturant (6M GuHCl or 8M urea) in aqueous solution, which interrupts the mass transfer of proteins. The denaturant reduces the electric interaction between surfactants and the surface of proteins, which is considered to be one of the main driving forces in protein extraction by reversed micelles. Therefore, the denaturant concentration ought to have been reduced to an appropriate concentration which would have facilitated denatured RNase A to be transferred efficiently into reversed micelles in the unfolded state. The denatured RNase A is extracted into reversed micelles along with the denaturant into the water pools of reversed micelles. In this case, the denaturant must be removed from the reversed micellar phase to refold the protein by repeated washing with a fresh aqueous solution.

In order to improve the overall yield in the protein refolding process, we have introduced solid-liquid extraction technique to enhance the solubilization of unfolded proteins directly into reversed micelles (6). In the present study, the effects of some important parameters in preparing the reversed micellar solution (concentration of AOT, W_o ($=[\text{H}_2\text{O}]/[\text{AOT}]$), pH of water pools) were examined on the solubilization of solid denatured RNase A. The degree of solubilization of the solid denatured protein was significantly influenced by these operational parameters. Figure 2 shows the effect of AOT concentration in iso-octane on the solubilization of the solid denatured RNase A into the reversed micellar solution along with the average diameter of reversed micelles formed after the solubilization of protein. A high concentration of AOT in iso-octane facilitates the solubilization of the denatured proteins. Furthermore, the size of reversed micelles significantly was decreased by increasing AOT concentration. These phenomena are based on specific interaction between AOT molecules and protein, and somehow are favorable for solubilization of a solid protein aggregate. When the surfactant-protein interaction is stronger than the protein-protein

interaction in the denatured proteins, the protein solubilization into the reversed micelles proceed well.

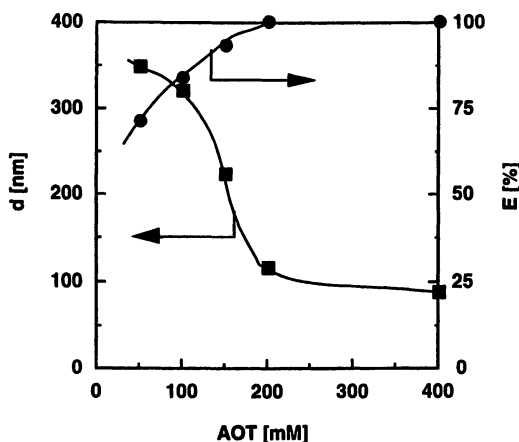


Figure 2. Effect of AOT concentration in isoctane on both solubilization and average diameter of reversed micelles after solubilization: 2.3 mg/ml RNase A, $W_o=20$, pH 8.7.

From the result of DLS measurement, it was found that the average diameter of the stable reversed micelles containing denatured RNase A in the organic solvent was approximately 100 nm. On the other hand, under the same experimental condition the average diameter of reversed micelles which contain native RNase A was only about 10nm. This result means that the solubilization state of the denatured proteins is different from that of native proteins. The denatured proteins are considered to form a small cluster in reversed micelles.

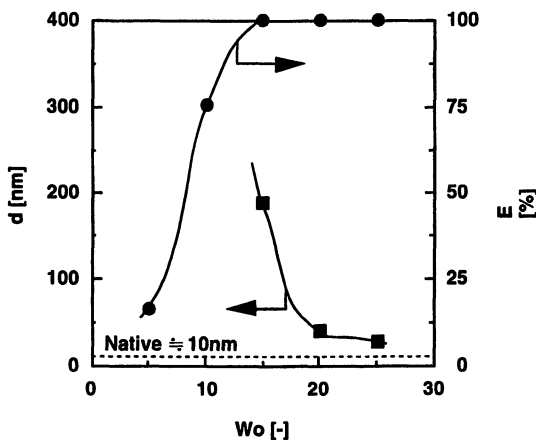


Figure 3. Effect of W_o ($=[H_2O]/[AOT]$) on solubilization and average diameter of reversed micelles after solubilization of denatured protein: 2.3 mg/ml RNase A, 400 mM AOT, pH 8.7.

The effect of water content of the reversed micelles on the solubilization of solid denatured RNase A is shown in Figure 3. The degree of solubilization of denatured RNase A into reversed micelles increases along with the increase of water content. These results suggest that water molecules in organic media play an important role for solubilization and dispersion of denatured protein aggregates. Moreover, it is considered that hydration of proteins is essential for dissociation of nonspecific interactions among aggregated protein molecules. Later it became clear that the dependence of W_o on the diameter of reversed micelles supports this idea since the size of reversed micelles containing denatured proteins decreases with increasing W_o in the reversed micellar system.

It is known that one of the main driving forces for the protein solubilization by reversed micelles is an electrostatic attraction between surfactant molecules and the surface of proteins. Thus, in protein solubilization into a reversed micellar solution by liquid-liquid extraction a favorable result is generally obtained in a lower pH range than pI, when using an anionic surfactant like AOT. Recently, Hayes (7) has reported the solubilization mechanism of a solid protein by AOT reversed micelles. The mechanism involves three steps: 1) adsorption of reversed micelles to the solid proteins, 2) transfer of the resulting AOT-protein complex from the solid phase to the reversed micellar phase, and 3) formation of protein-containing reversed micelles accompanied with the exchange reaction between the protein-containing and the empty reversed micelles. In this case the driving force of the solid protein solubilization is also considered to be the electrostatic interaction between the surfactant AOT and the positively charged protein. It is also mentioned that in the case of solubilization of native proteins by solid-liquid extraction each protein molecule was solubilized in encapsulating reversed micelles. This fact is supported by the result of the diameter measurement of reversed micelles after solubilization of native proteins (Figure 2, Figure 3).

Although the denatured solid protein was solubilized, we found that the solubilization rate of denatured proteins is much lower compared to that of native solid proteins. Native proteins can dissolve into the AOT reversed micelles immediately, but it takes a few minutes for the case of denatured proteins. According to the basically difference mentioned above, it is reasonable enough to assume that the solubilization mechanism of the denatured proteins is different from that of native proteins. This assumption was then supported by the results of aqueous pH effect in the reversed micellar solution on the solubilization of denatured proteins (data not shown). A high pH (alkali pH) of water pools in reversed micelles facilitates the protein solubilization to occur more efficiently, and the effect become more significant around the isoelectric point of RNase A (pI 7.8). This tendency was quite opposite to the reported result concerning protein solubilization into reversed micelles based on the ordinary liquid-liquid extraction or any other reports ever published. The favorable solubilization at a higher pH is considered to be the enhancement effect for the dissociation of protein aggregates. Due to the electric repulsion, negatively charged proteins facilitate the dissociation to take place a lot more easier.

Renaturation of Denatured RNase A in Reversed Micelles by Redox Reagents. According to circular dichroism (CD) spectra, it is obvious that the conformation of denatured RNase A solubilized in reversed micelles remained in denatured states (data

not shown) and the activity was almost zero. This implies that reoxidation of reduced thiols is essential to obtain native conformation and to recover the enzymatic activity. It is known that both the formation and the reshuffling of disulfide bonds are useful for protein refolding (8). Hence we used reduced and oxidized glutathione (GSH and GSSG, respectively) which are the most widely used compound as thiol/disulfide reagents. It was reported that the optimum composition is $[GSH]=2$ mM and $[GSSG]=0.2$ mM for reoxidation of RNase A in an aqueous solution (9). Hagen et al. (1990) indicated that the optimum ratio GSH/GSSG for the reoxidation of solubilized RNase A in reversed micelles was three in liquid-liquid extraction. In the present study, the optimum condition for the reoxidation by GSH/GSSG was investigated in the solid-liquid extraction system. The GSSG forms the mixed disulfide intermediate which is required for the formation of disulfide bonds in proteins. The GSH re-shuffle the incorrectly formed disulfides.

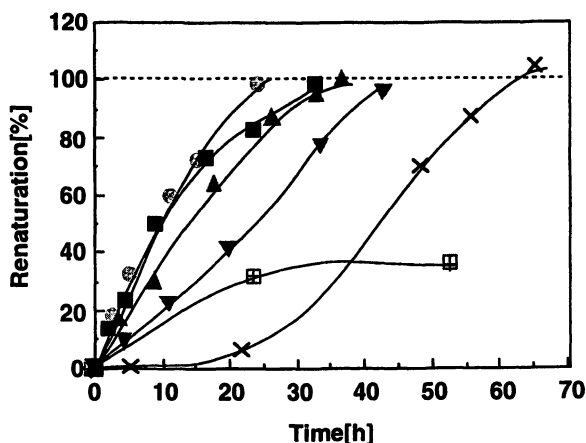


Figure 4. Effect of the ratio of reduced and oxidized glutathione on both renaturation yield and renaturation rate: 2.3 mg/ml RNase A, 400mM AOT, $W_o=20$, pH 8.7.

Total glutathione concentration is 0.61mM based on the organic phase.

(●) GSSG alone, (■) GSSG/GSH=3/1, (▲) GSSG/GSH=1/1, (▼) GSSG/GSH=1/3, (×) GSH alone, (◻) glutathione free.

Figure 4 shows the effect of GSH/GSSG ratio on the renaturation of RNase A in reversed micelles. The total glutathione concentration in the reversed micellar system was kept constant at 0.61 mM based on the organic phase. This concentration offered a maximum reactivation rate. Result shows that the reactivation rate was influenced by the ratio of GSH/GSSG, however, the renaturation yields were almost 100 % in all cases expect for the glutathione free system. For protein refolding in aqueous media, it was reported that the ratio of reduced and oxidized glutathione affects the competition between aggregation and folding, so that the reactivation yields is also influenced by the ratio (10). It was also found that RNase A in reversed micelles recovered its enzymatic activity up to about 36 % even without the addition of glutathione. This process might be due to the air reoxidation. We also examined the effect of GSSG concentration on reoxidation of RNase A in reversed micelles under a high protein

concentration (4.8 mg/ml). Both the reactivation yields and rates attained a maximum at 0.61-1.21 mM of GSSG based on the organic phase and decreased in either lower or higher concentrations. These results can be explained by the equilibrium of the GSH/GSSG redox system during the reoxidation process.

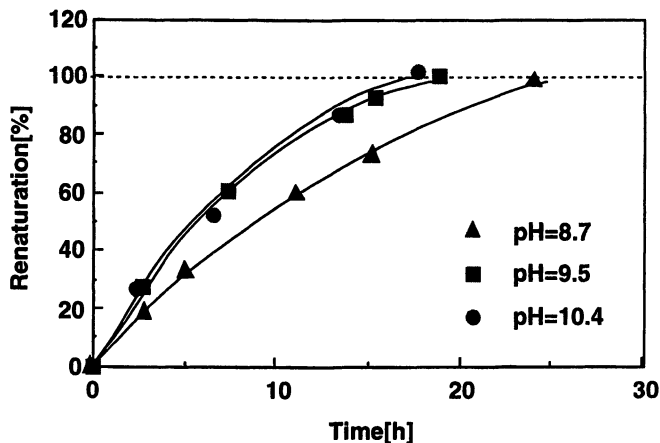


Figure 5. Effect of pH of water pools in reversed micelles on both renaturation yield and renaturation rate: 2.3 mg/ml RNase A, 20 mM GSSG, 400 mM AOT, $W_o=20$.

Figure 5 shows the effect of pH in the water pools of reversed micelles on renaturation of RNase A. We improved the renaturation rates by operating at a high pH which is favorable for the cysteine groups to carry on a nucleophilic attack against GSSG. As expected, the rates were enhanced under a high pH conditions (9.5-10.4). However, we concluded that the optimum pH for the reoxidation of protein refolding is around 9, because higher pH than this value may affect the stability of native proteins and cause irreversible dissociation of disulfide bonds.

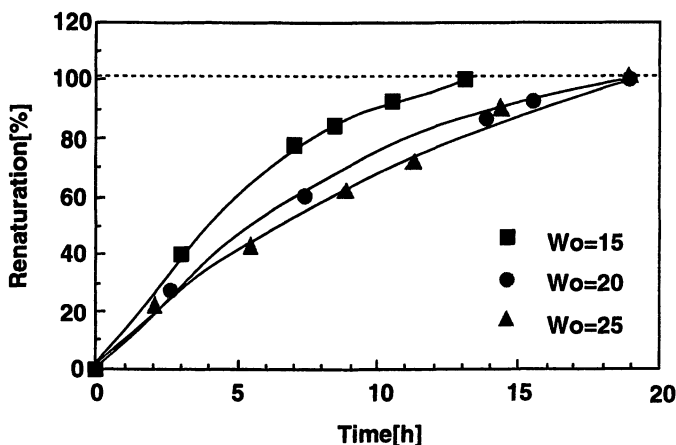


Figure 6. Effect of W_o on both renaturation yield and renaturation rate: 2.3 mg/ml RNase A, 20 mM GSSG, 400 mM AOT, pH 9.5.

Figure 6 represents the effect of water content in reversed micelles on the renaturation rates. The renaturation will be more favorable as the W_o value decrease. This is because along with the decrease of W_o value the added redox reagents in the water pool of reversed micelles will be more concentrated and be more effectively functioned. However, we should note that low W_o values are unfavorable for the solubilization of denatured proteins into the reversed micellar solution as shown in Figure 3.

Recovery of Renatured RNase A from Reversed Micelles. Denatured RNase A has now been successfully reactivated in reversed micellar media. The final step in our novel refolding process is to recover the active proteins from the reversed micellar solution. The recovery of proteins solubilized in reversed micelles has been performed by "back extraction" operation, in which the reversed micellar solution contacts with a fresh aqueous solution with a high ionic strength and a pH value that facilitates electrostatic repulsion between the encapsulated protein and the head group of surfactant molecules. However this method often provides a low extraction yield due to the formation of irreversible precipitates which involve surfactant molecules at the organic-aqueous interface. Furthermore, the activity of recovered proteins are often reduced during the back-extraction operation.

We first attempted the recovery of the activated RNase A from reversed micelles with the conventional back-extraction method. The favorable recovery yields was achieved at a low protein concentration (below 1 mg/ml), however, the yields drastically decreased due to formation of aggregates at the organic-aqueous interface (data not shown) as the protein concentration in reversed micelles increased. The size of the complexes between the RNase A and AOT molecules increased along with the increase in the concentration of solubilized proteins. The large complex formed further induced the formation of aggregates at the interface.

Table I. Effect of amounts of added acetone on both recovery and activity yields of renatured RNase A from reversed micellar solution.

Vacetone / V _{rm}	Recovery [%]	Activity ^a [%]
5	88.4	>100 ^b
10	84.4	>100 ^b
20	92.0	>100 ^b
40	94.2	>100 ^b

^a Renaturation conditions: 2.3 mg/ml RNase A, 20 mM GSSG, 400 mM AOT, $W_o=20$, pH 9.5. Vacetone: volume of added acetone, V_{rm}: volume of reversed micellar solution. ^b The activity of RNase A recovered from reversed micellar solution was over 100%. This is due to the refinement of commercial native RNase A (85% purity).

In order to overcome this problem, we introduced a different approach to recover the proteins from the reversed micellar solution more effectively. This approach is the precipitation method in which a solid protein was recovered by the addition of a polar organic solvent. In the present study, acetone was used as the polar organic solvent. The effect of the amount of the added acetone on the recovery and activity yields of renatured RNase A from the reversed micellar solution is summarized in Table 1.

The addition of 5-40 times volume of acetone to the reversed micellar solution provided 84-94 % recovery yields. Furthermore, the recovered RNase A retained a high enzymatic activity. The addition of acetone induces destabilization of reversed micelles. The resulting proteins can be released from the reversed micellar solution as a solid. A similar method is reported by Gupta et al. (11) using molecular sieves and Marchino and Hayes (7) using 1-butanol as a polar co-solvent. The overall yield of the novel process was found more favorable in comparison with the conventional dilution method. Thus, this reversed micellar system utilizing the solid-liquid extraction technique was demonstrated to be effective for protein refolding even at high dosage of proteins. Our next objective is to extend the scope of this study to the direct refolding of inclusion bodies by utilizing the solid-liquid extraction technique.

The benefits of the novel process are that a high concentration of proteins can be dealt with and that the amount of an expensive redox reagent can be reduced due to the small water content in reversed micelles. However, the most advantage of this novel reversed micellar refolding process compared to the conventional dilution method is that the novel process does not require denaturants such as guanidine chloride or urea. It is hoped that this solid-liquid extraction technique will be found useful for application in the biochemical industry.

Acknowledgments

This work was partially supported by a Grant-in-Aid for Scientific Research (No. 10555284) from the Ministry of Education, Science, Sports and Culture of Japan, and Chemical Materials Research & Development Foundation.

Literature Cited.

1. Marston, F. A. O. *Biochem. J.* **1986**, *240*, 1.
2. Hagen, A.J.; Hatton, T. A.; Wang, D. I. C. *Biotechnol. Bioeng.* **1990**, *35*, 955.
3. Batas, B.; Chaundhuri, J. B. *Biotechnol. Bioeng.* **1996**, *50*, 16.
4. White, F. H. JR. *J. Biol. Chem.* **1961**, *236*, 1353.
5. Wolf, R., Luisi, P. L. *Biochem. Biophys. Res. Commun.* **1979**, *89(1)*, 209.
6. Hashimoto, Y.; Ono, T.; Goto, M.; Hatton, T. A. *Biotechnol. Bioeng.* **1998**, *57*, 620.
7. Hayes, D. G. *Biotechnol. Bioeng.* **1997**, *53*, 583.
8. Gilbert, H. F. *Adv. Enzymol.* **1990**, *63*, 69.
9. Lyles, M. M.; Gilbert, H. F. *Biochemistry* . **1991**, *30*, 613.
10. De Bernardez Clark, E.; Havehan, D.; Szela, S.; Maachupalli-Reddy, J. *Biotechnol. prog.* **1998**, *14*, 47.
11. Gupta, R. B.; Han, D. J.; Johnston, K. P. *Biotechnol. Bioeng.* **1994**, *44*, 830.

Chapter 23

Deinking of Papers Printed with Water-Based Inks: An Overview

John K. Borchardt

Shell Chemical Company, P.O. Box 1380, Houston, TX 77251-1380

Deinking paper printed with water-based inks results in several operational problems for deinking mills:

- low pulp brightness due to the very small size of dispersed ink particles.
- redeposition of ink onto cellulose fibers being greater than for offset ink particles that are larger. Redeposition can occur in all the mill unit operations but is probably greatest in the pulper when the concentration of dispersed ink particles and cellulose fibers is greatest.
- dispersed flexographic ink particles are poorly sized for good flotation deinking efficiency. The optimum size range for best flotation efficiency may vary somewhat from one type of flotation cell to another. However, the optimum ink particle range for flotation deinking is considered to be about 10 microns up to about 100 microns. The absence of an oil vehicle makes agglomeration of the carbon black particles by fatty acid flotation agents more difficult than offset and letterpress ink agglomeration.
- many dispersed flexographic ink particles are too small to be optimally sized for wash deinking. Washing is effective for particles in the 3-25 micron size range with the highest efficiency obtained for 5-15 micron particles.
- dispersed flexographic ink particles are more difficult to remove from process water by dissolved air flotation and other conventional water clarification methods than are larger ink particles. As a result, more suspended small ink particles are present in recycled process water and are well sized for redeposition onto cellulose fibers.

There are three critical steps required for efficient deinking:

1. detachment of ink from cellulose fibers and ink dispersal in the process water
2. separation of dispersed ink particles from cellulose fibers
3. removal of dispersed ink from process water for water reuse

The objective of this paper is to review results obtained when deinking paper printed with water-based inks, understand the factors limiting effectiveness of each of the above three processes, review methods proposed to overcome these limitations, and suggest directions for future research. Many articles have been published on flexographic newsprint deinking. In addition, reports in the detergency literature describe surface chemistry results that are relevant to the problem of flexographic newsprint deinking. A critical review and summary of this literature will aid in defining the causes of the difficulty in deinking flexographic newsprint. This improved understanding will aid in the development of improved chemicals, process equipment, and process designs for deinking flexographic newsprint.

The major driving force in the use of water-based inks is the reduction in the emission of volatile organic carbon compounds associated with many conventional solvent-based inks. Printing is crisp and pleasing to the eye. The print does not rub off on readers' fingers. Both flexographic inks used for printing newspapers and water-based gravure inks are commercially available and their deinking behavior appears similar (1).

Deinking mill personnel are less pleased with this furnish. The difficulty in deinking flexographic inks from newsprint compared to removal of letterpress and offset inks is a major concern in many mills deinking newsprint (2-11). The presence of as little as 10% flexographic newsprint in an old newsprint/old magazine furnish can substantially reduce the flotation deinking step brightness gain (Figure 1) (12). The difficulties in deinking paper printed with water-based inks are related to the ink surface chemistry that is very hydrophilic. As a result of this hydrophilicity, water-based inks disperse into very small particles on pulping. This concern over flexographic ink is coming even more serious as mills close their water loops. Without efficient water clarification that removes suspended ink, the ink load on the system increases reducing pulp brightness (13-15). This is a particularly serious problem with flexographic newsprint due to the very small ink particles formed on pulping. These suspended ink particles are particularly difficult to remove during clarification of mill process water.

Being able to economically process furnishes containing flexographic inks would provide mill with a competitive advantage because being able to process furnishes containing flexographic newsprint can significantly reduce furnish costs. Old newspapers collected from the U.S. Pacific Coast and New

**EFFECT OF % FLEXO ON DEINKED SHEET
BRIGHTNESS OF FLEXO/OFFSET FURNISH**

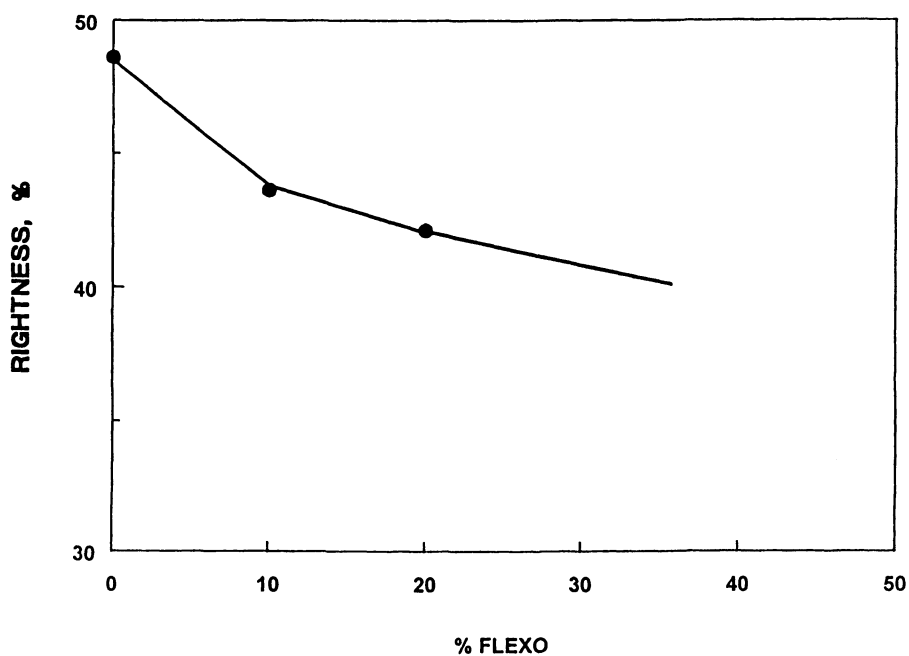


Figure 1. Effect of Flexographic Ink Content of Furnish on Deinked Sheet Brightness

England areas in particular can contain substantial levels of flexographic newsprint. Much newsprint from these areas is exported to Canada for deinking.

Reasons for the greater difficulty in separating dispersed flexographic inks (compared to letterpress and offset inks) from fiber differ in part for wash and flotation deinking. Understanding these reasons is critical to developing effective deinking processes and chemicals for flexographic newsprint furnishes. Separation of the dispersed ink particles from process water for water recycling is also important to efficient deinking mill operation.

Flexographic Ink Chemistry

Morphology of offset and flexographic ink printing appears very similar in environmental scanning microscope studies (16). Representative micrographs of paper printed with these two types of inks are shown in Figures 2 and 3. So it is most unlikely that ink morphology differences between offset and flexographic inks can account for the greater difficulty in deinking flexographic furnishes.

In contrast, the surface chemistry of flexographic inks differs greatly from that of other newsprint inks. Letterpress and offset inks are oil-based. Flexographic inks are water-based. Simplified black newsprint ink compositions are summarized in Table 1.

Table 1. Newsprint Ink Compositions^a (17)

<u>Ink Type</u>	<u>Pigment</u>	<u>Binder</u>	<u>Carrier (Vehicle)</u>	<u>Additives</u>
Flexographic	Carbon Black (12-16%)	Acrylic Resin (9-12%)	Water (65-77%)	Defoamers Waxes Dispersants
Offset	Carbon Black (16-20%)	Alkyd Resin (0-15%)	Mineral Oil (55-80%)	Waxes
Letterpress	Carbon Black (10-15%)	Various Resins (0-15%)	Mineral Oil (70-90%)	Waxes

a. All percentages are by weight

Recent reports describe the composition of water-based inks in some detail (18,19). The carbon black pigment in flexographic inks are grades having a specific surface area of about 100 m²/g and an average particle size of 25 nm (20). (1 nanometer = 1000 micrometers (microns).) Oxidation is often used to increase the polarity of flexographic ink carbon black. This increases its hydrophilic character.

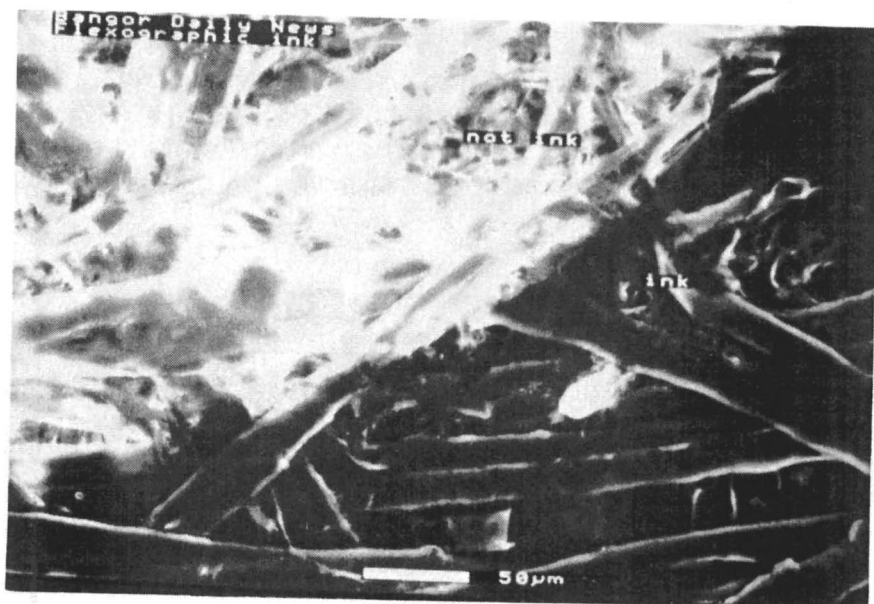


Figure 2. Environmental Scanning Electron Microscope Image of Flexographic Ink Character on Newsprint

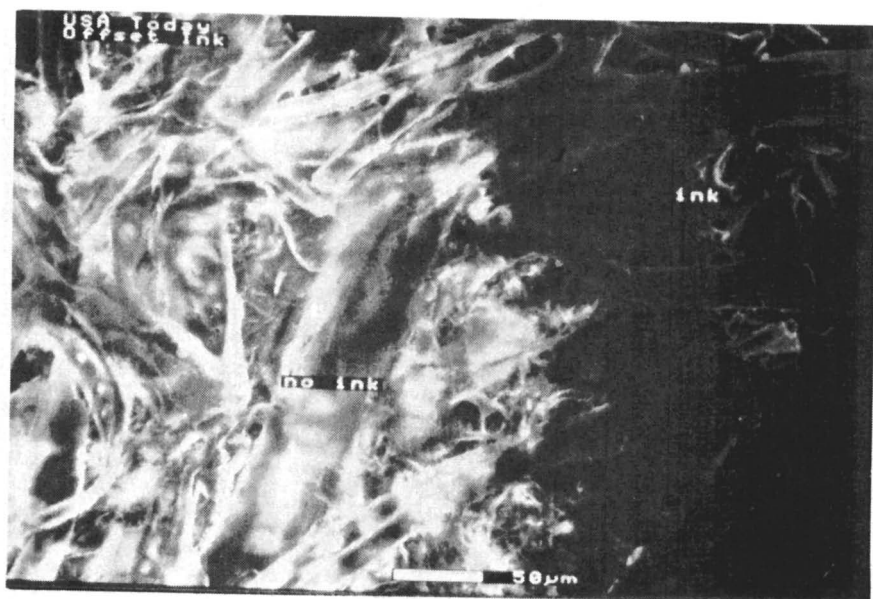


Figure 3. Environmental Scanning Electron Microscope Image of Offset Character on Newsprint

The water vehicle of flexographic inks is readily dispersible in aqueous pulping media. The basic pH used in newsprint pulping can convert the acrylate groups in the acrylic binder resins to anionic carboxylic acid groups. Charge repulsion and polarity effects make the binder resin readily dispersible and/or soluble in alkaline pulping media. As a result of these factors, detachment of flexographic inks from cellulose fibers is not particularly difficult. So difficulty in detaching flexographic ink from cellulose fibers is not responsible for the difficulty in deinking flexographic newsprint. Water-based inks are most strongly dispersed at a pH of approximately 8 (21), a value commonly encountered in deinking and water clarification. This dispersion plus steric hindrance to the approach of collectors makes ink agglomeration difficult (4). This steric hindrance is due to binder resin adsorbed onto carbon black particles.

Ink Particle Size After Pulping

Factors contributing to the formation of very small ink particles when pulping flexographic newsprint include:

- electrostatic repulsion of ionized acrylic acid binder resin carboxylate groups during alkaline pulping promotes formation of small dispersed ink particles (4).
- efficient contact between the carbon black surface and the alkaline medium promotes ionization of carbon black carboxylate groups. This ionization creates electrostatic repulsion between carbon black particles thus promoting carbon black dispersion (22).

Pulping flexographic newsprint results in the formation of many more small ink particles than obtained when pulping offset newsprint (Figure 4). The number of flexographic newsprint ink particles after pulping was increasing rapidly as the lower detection limit of the image analysis system (about 1 micron in the longest ink particle dimension) was approached (23, 24). One report indicates that, after pulping, 90% of the flexographic ink particles are smaller than 5 microns in diameter (25).

Using a different type of particle size analyzer than used in deinked handsheet analysis indicated the average particle size of dispersed flexographic inks is about 200 nanometers (nm). This is about three times greater than the size of individual carbon black particles (21). (1 micron = 1,000 nanometers.) Scanning probe microscopy (SPM) indicated ink particles as small as individual carbon black particles are formed upon pulping newspapers printed with flexographic ink (16). Thus oil-based ink droplets dwarf the particles of a flexographic ink dispersion. The specific area of a 10 micron oil-based ink droplet can be as much as 300-times greater than that of the smallest - flexographic ink particle, a single carbon black particle (20).

Figure 5 shows an SPM image of a small portion (0.3 microns in width) of a character on newsprint printed with flexographic ink (16). The individual carbon black particles contained in the ink are clearly seen as being less than 100 nm in size. Samples of a 75:25 offset:flexographic newsprint after

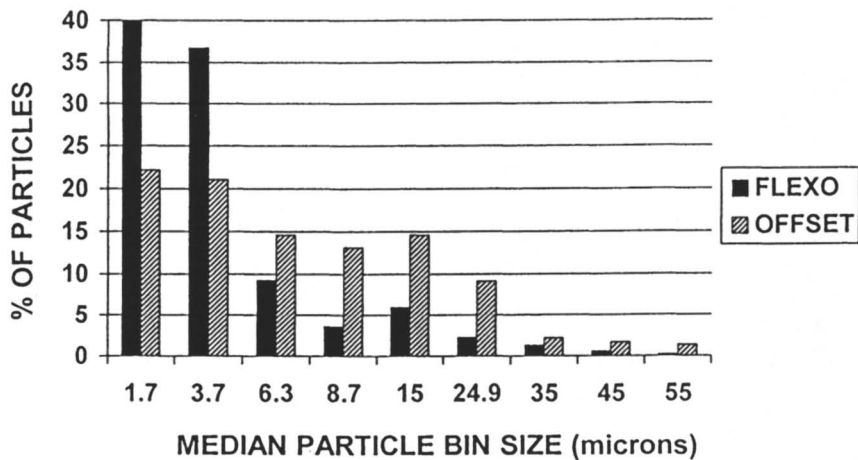


Figure 4. Ink Particle Size Distributions for Offset and Flexographic Newsprint Ink After Pulping (based on data taken from reference 23).

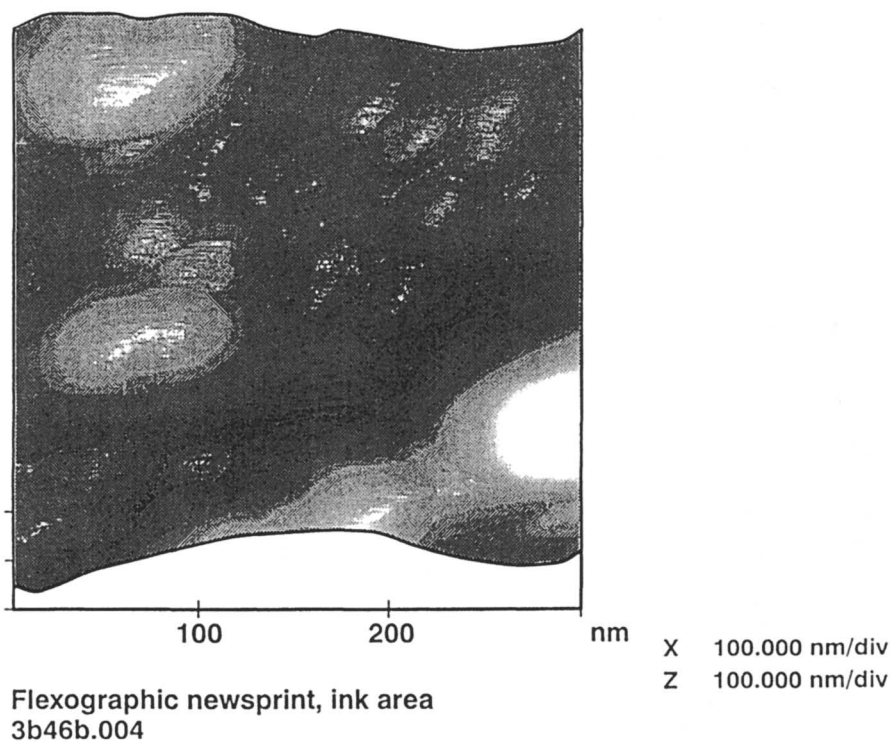


Figure 5. Scanning Probe Microscopy of Flexographic Ink Printing on Newsprint

pilot mill pulping and flotation - wash deinking were also analyzed by SPM. Figure 6 depicts residual ink particles less than 50 nanometers in diameter. Some of the particles are approximately 20 nanometers in diameter. Schematic representations of the data may be more indicative. The ink particles appear as small hemispherical objects on the sample surface depicted in Figure 7. The size of these discrete particles indicates that they are probably individual carbon black particles that adsorbed on paper fibers after being dispersed during pulping.

The deinking agent can have an effect on ink particle size obtained in pulping. In laboratory pulping of a flexographic ink printed furnish, a lower hydrophilic:lipophilic balance (HLB) alcohol ethoxylate (HLB 11.8) provided a brightness of 44.5 while a more dispersing alcohol ethoxylate with a higher HLB (HLB 14.3) provided a lower brightness, 39 (26). When higher shear pulping conditions were used, the brightness provided by the lower HLB surfactant decreased to 39.5 while that provided by the higher HLB surfactant was essentially unchanged. Thus the brightness difference between surfactants was substantially less under conditions promoting greater ink particle dispersion. Unsurprisingly, pulping conditions, either chemical or mechanical, promoting greater ink particle higher dispersion resulted in lower pulp brightness.

Extended pulping time can both reduce ink particle size (promoting increased particle redeposition (see below) and allow more time for redeposition processes to occur (26). Detergency studies have indicated that carbon black deposition onto cotton fabric increases linearly with time (27). Pulping at an acidic pH of 5 provided a brightness value 5 points higher than pulping under the same conditions at pH 9. After flotation, the brightness differential decreased to 1.6 points but increased to 4.6 points after subsequent washing.

Redeposition of Ink Particles on Fiber

Carbon black particle redeposition increases with decreasing particle size (27). The very small size of flexographic ink particles (20-to-50 nm as confirmed by the scanning probe microscopy studies) make them quite susceptible to redeposition onto fibers. By interacting with the binder resins, water hardness ions reduce the electrostatic repulsion between the suspended particles and the cellulose fibers thus increasing ink particle redeposition (28).

A study has been performed to directly study deposition of dispersed flexographic ink particles onto cellulose fibers (26). The flexographic ink was printed on Mylar® plastic film using a Dow Lab Coater with a rod. The thickness of the ink on the Mylar film was about one micron, the approximate thickness of flexographic ink on paper. After printing and aging, the ink was detached from the plastic and pulverized to form fine particles. Two flexographic inks were used but only the chemical composition of only one was available (Table 2).

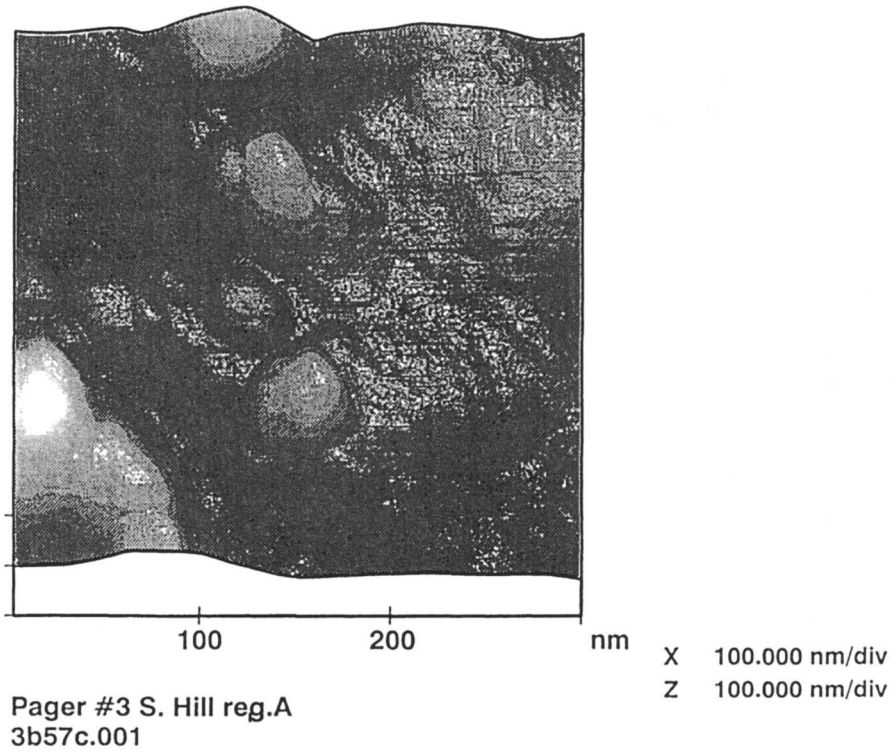


Figure 6. Scanning Probe Microscopy Image of Residual Flexographic Ink Particles After Deinking

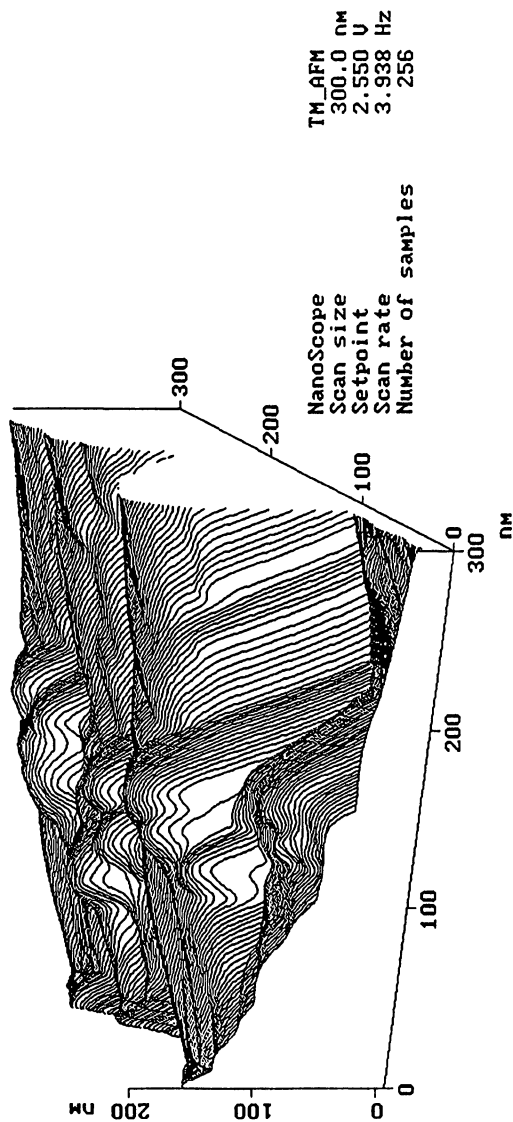


Figure 7. Line Drawing of Figure 6

Table 2. Composition Flexographic Ink 1 (26).

<u>Ingredient</u>	<u>Percent by Weight</u>	
carbon black	18.0	
styrene-acrylic acid resin ^a		5.65
alcohol	1.0	
defoamer	0.01	
sodium hydroxide	<1.0	
water	65.4	

Unprinted paper was pulped for twenty minutes at pH 5 and 25°C in the presence of 0.1% alcohol ethoxylate using the pulping apparatus described in reference 26. The ink was then added. Pulp samples were collected 5, 10, 15, and 30 minutes later. Fifteen pulp washings of these pulp samples with deionized water using a Dynamic Britt Jar were required to obtain constant pulp brightness. The difference between the original paper brightness of 67 and the brightness after fifteen washings is defined as the brightness loss due to flexographic ink redeposition onto cellulose fibers.

The pulp samples taken after each pulping time were then washed (fifteen times) in a Dynamic Britt Jar to constant brightness (26). These washed pulp brightness values are reported in Figure 8 as a function of the original pulping time. Increased pulping time led to lower washed pulp brightness. This can be seen more clearly in Figure 9, a plot of washed pulp brightness loss as a function of pulping time. The brightness loss increased with increasing pulping time. This was true for both Ink 1 and Ink 2. However, these inks did differ in properties as Ink 2 provided a higher brightness pulp at all pulping times.

Since the paper being pulped was unprinted and the brightness after fifteen pulp washings was no longer changing, observed brightness losses could be attributed to irreversible deposition of flexographic ink particles onto cellulose fibers. As Figure 9 indicates, brightness decreased (and thus ink deposition occurred) most rapidly at short pulping times. This is consistent with results obtained in a study of the redeposition of a carbon black onto cotton fiber (27).

The brightness differences between Ink 1 and Ink 2 may be due to differences in particle size and particle size distribution of the carbon black pigment, different ink particle surface chemistry, differences in the binder resins, and different pigment:resin ratios. It would be interesting to study these variables systematically to determine their effects on pulp brightness. The results could help guide the development of improved flexographic inks.

The very small ink particle size of water-based inks after pulping leads to ink redeposition on cellulose fibers and reduced deinked sheet brightness. Studies of the redeposition of carbon black on cotton fabric indicate redeposition increases as carbon black particle size decreases (27, 28). Microscopy studies

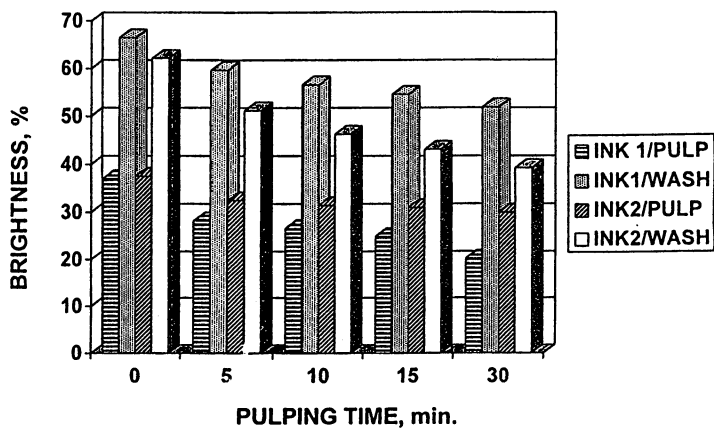


Figure 8. Effect of Pulping Time on Pulp Brightness After Pulping and After Washing for Two Different Black Flexographic Inks in the Presence of Unprinted Paper

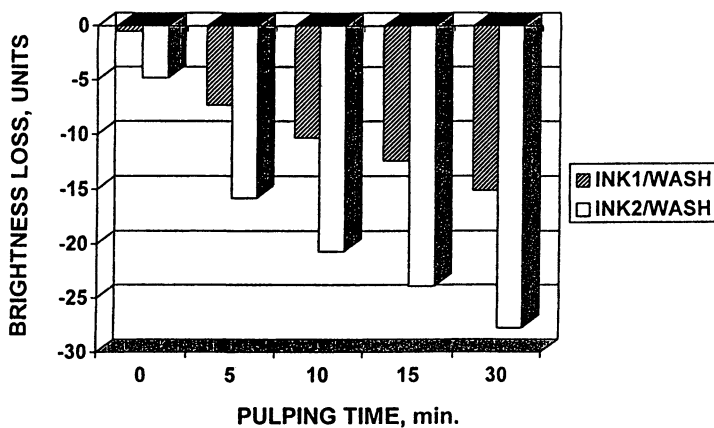


Figure 9. Effect of Pulping Time on Pulp Brightness Loss Relative to Unprinted Paper in the Absence of Ink

suggest that flexographic ink particles can redeposit in the pores of softwood fibers (29). The particles appear to enter the lumens through the fiber ends. These redeposited ink particles would be very difficult to remove by chemical or mechanical processes.

As noted, the above experiments above experiments were performed at pH 5. An experiment performed at pH 8.5 was performed in which flexographic ink was added to a long fiber fraction of a Kraft pulp after pulping (30). The pulp was then thickened from 0.5% to 10% consistency. Little ink adsorption occurred during this thickening process. The apparent discrepancy between this and the reference 26 results may be due to differences in experiment design.

Water-based Gravure Inks

Water-based gravure and flexographic inks appear to behave similarly in deinking processes (1). Water-based gravure inks also form very small ink particles during pulping resulting in low pulp brightness. Wash deinking efficiency of water-based gravure inks (without process water recycle) is good, particularly at low water hardness. Flotation deinking efficiency using fatty acid soaps is limited. Flotation ink removal efficiency as indicated by pulp brightness is greater in the absence of fibers suggesting that redeposition of the very small ink particles onto cellulose fibers is occurring.

Flotation Efficiency

Flotation deinking is effective in removing ink particles in the 20 - 200 micron size range. Using fatty acids or conventional nonionic flotation deinking surfactants, the very small flexographic newsprint particles are poorly sized for removal by flotation deinking (12, 31-35) using conventional deinking surfactants (Figure 1). For example, using a high alcohol ethoxypropoxylate proven quite effective on offset-printed newspapers, addition of as little as 10% flexographic-printed newspapers to an offset newsprint furnish reduced deinked sheet brightness after flotation (Table 3 and Figure 1).

TABLE 3. Effect of Flexographic Newsprint on Deinked Sheet Brightness of an Offset Newsprint Furnish (15).

% Flexographic ONP in Furnish	ISO Brightness (%) After Flotation	Brightness (%) After Washing	Brightness Difference Washing - Flotation
0	56.0	58.4	2.4
10	54.2	57.5	3.2
20	50.0	56.5	6.5
30	45.5	53.8	8.2

The concentration of deinking agent was constant in these tests. As the number of very small ink particles increased with increasing flexographic ONP content

of a furnish, the ink specific surface area greatly increases. The ratio of deinking agent concentration to ink surface area decreases. Thus, the amount of surfactant available to agglomerate the ink into more easily removed particles becomes insufficient (16).

The collision frequency of ink particles and air bubbles during flotation plays an important role in determining flotation efficiency. The low collision probability of the very small flexographic ink particles with air bubbles during flotation results in low flotation efficiency (25, 35, 36). However, at a given air:liquid ratio, small air particles were more efficient than large bubbles due to their higher specific surface area (37). The role of surface chemistry must be considered in resolving the apparent dichotomy between the effect of ink particle size and air bubble size.

At alkaline pH in the presence of divalent metal ions such as calcium ions, unstable flexographic ink particle aggregates are formed (38). However, flotation ink removal efficiency is not increased unless a fatty acid is also present. Flexographic ink particles spontaneously adsorb onto calcium soap particles at calcium ion concentrations greater than 1.0 mmol/liter (equivalent to 4.45% by weight calcium chloride) (39).

The hydrophilic nature of flexographic ink particle surfaces reduces the stability of the ink particle - air bubble aggregate. This decreases flotation efficiency. In flotation, surfactants should promote formation of hydrophobic ink particles. These adhere to bubble surfaces and are removed when froth is skimmed from the pulp slurry. When the ink vehicle is water rather than oil, as in flexographic inks, it is difficult to do this (40).

The behavior of the small flexographic ink particles in flotation appears consistent with recently proposed process models (41-43). The capture radius is the minimum bubble-ink particle distance at which a bubble can capture an ink particle. A disjoining film model (43) is used to study the physical chemistry factors affecting the capture radius. This model predicts, for a given bubble rupture time, that intermediate sized ink particles are preferentially floated compared to very small (such as flexographic ink) and very large (such as toner) ink particles. Repulsive electrostatic forces between bubbles and ink particles are greater for flexographic ink particles than for offset and letterpress ink particles. This makes it more difficult for attractive London - van der Waals dispersion forces to promote ink particle - bubble attachment (43).

Alcohol ethoxylate deinking surfactant HLB value was systematically varied from 10 to 14.5 in a laboratory flotation deinking study (26). Results indicated that the highest deinked flexographic pulp brightness was obtained at an HLB of 11.8. Yield losses were lower at HLB 11.8 than for higher HLB alcohol ethoxylates.

Wash Deinking

Wash deinking can be effective in deinking flexographic newsprint (44). Washing is more effective than flotation in removing the very small dispersed flexographic ink particles. This can be seen in three different pieces of evidence:

- At a given percentage of flexographic ink, washing provided a higher brightness value than did flotation deinking (Table 3).
- Compared to flotation deinking, wash deinking is less adversely affected by the presence of flexographic ink in the furnish. The brightness decrease with increasing content of flexographic ink in the furnish was less for washing than for flotation deinking (Table 3). This can be seen clearly in Figure 10. The negative slope of the brightness vs. % flexographic ONP line was less for washing than for flotation deinking.
- The brightness difference between washing and flotation deinking increased with increasing percentage of flexographic ONP in the furnish (Table 3).
- Wash deinking was less adversely affected by increased pulping time than was flotation (Figure 11).

For wash deinking flexographic ink printed paper with alcohol ethoxylates, the optimum HLB was approximately 14.5 (26), similar to the value found for wash deinking letterpress newsprint (45). The deinked pulp brightness increased approximately linearly (correlation coefficient 0.97) with HLB value over the HLB range tested, 10.8 - 14.5 (26).

Results in a commercial flotation - wash deinking mill trial provided additional evidence of the effectiveness of wash deinking in removing dispersed flexographic ink particles from pulp (15). These results are summarized in Table 4.

Table 4. Deinking Results for a 90:10 Offset:Flexographic Newsprint Furnish (15)

Process Step	ISO Brightness (%)	Brightness Change (vs. Previous Process step)
flotation feed	45	---
2 stages of flotation	49.7	4.7
2 more stages of flotation (for a total of 4 stages)	52	2.3
2 more stages of flotation (for a total of 6 stages)	53	1
overall flotation brightness gain		8
subsequent washing	59	6

The overall eight-point flotation brightness gain indicated that a substantial number of very small ink particles were removed. The final two stages of flotation resulted in an additional brightness gain of only one point suggesting that

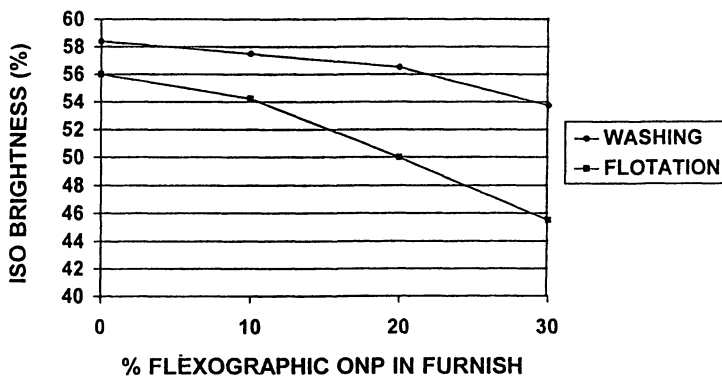


Figure 10. Effect of Increasing Flexographic Ink Content of Furnish on Pulp Brightness After Flotation and Washing

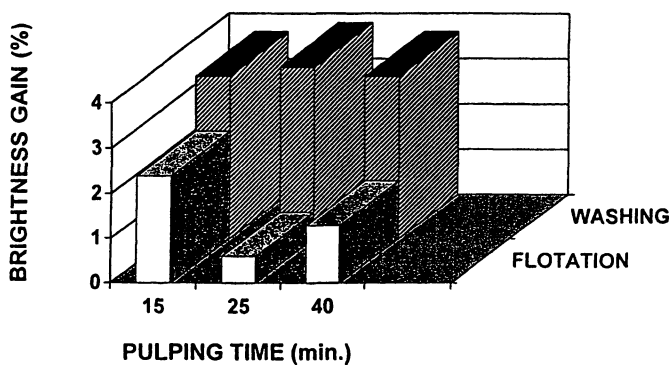


Figure 11. Effect of Pulping Time on Brightness Gain in Flotation and Post-Flotation Step

flotation had removed very nearly all the very small ink particles it could. Yet the subsequent washing step resulted in an additional brightness gain of six points indicated a substantial additional number of very small ink particles were removed. Thus a substantial number of small ink particles remained after subsequent flotation.

As Table 4 indicates, combining a washing step with flotation can increase deinked pulp brightness (5,8,23). This can be seen in the laboratory flexographic paper deinking experiments discussed above (26) and summarized in Figure 11. A post-flotation washing step resulted in substantial pulp brightness gains compared to the brightness provided by flotation. Wash deinking is more efficient than flotation in removing the small flexographic ink particles from the pulp slurry (23,25,46). Decreasing the consistency in a post-flotation washing step increases the brightness gains (47). This decrease in consistency would be predicted to reduce ink particle redeposition onto cellulose fibers.

Dispersed flexographic inks have been shown to deposit in fiber mats of the sort formed in many wash deinking units (48). (However, the reference 30 laboratory results discussed above exhibited only modest adsorption of flexographic inks onto cellulose fiber mats.) Once deposited, these ink particles are difficult to remove. This suggests that turbulent washers that minimize fiber mat formation would be most effective in wash deinking flexographic newsprint. This was in fact found in pilot plant deinking tests. Table 5 indicates that the type of washer that minimized mat formation provided the highest deinked flexographic newsprint pulp brightness.

Table 5. Brightness of Deinked Flexographic Newsprint Using Different Types of Washers (23).

Washer Type)	Fiber Mat Formation ^a	Deinked Pulp Brightness	
		Brightness (%)	Gain
centrifuge	4	48.4	0.9
decker	3	49.4	1.9
sidehill screen	2	53.0	5.5
high turbulence	1	54.7	7.2

a. Rank Order, 1 = least, 4 = most

Ink deposition onto fiber mats was greatest at low pH and also under alkaline conditions in the presence of sodium oleate and calcium ions (48). Increased pulp brightness indicated that chelation of the calcium ions with ethylenediaminetetraacetic acid (EDTA) decreased flexographic ink particle deposition onto the cellulose fiber mat (48).

Improved Deinking of Flexographic Furnishes

Improving Flotation Ink Removal Efficiency. Flotation at acidic or neutral pH is among the techniques advocated for improving flotation deinking of flexographic ink-containing newsprint (49). For at least some surfactants, brightness of deinked flexographic furnish reaches a maximum at a flotation pH of 5-7 (50,51). (However, one group (4) reported only a minor increase in pulp brightness upon decreasing the flotation pH from alkaline to acidic.) While most deinking surfactants are less efficient in detaching offset ink from fibers at acidic pH than basic pH (50), exceptions to this generalization are described below. Cationic surfactants have also been suggested for use in pH 5 flotation deinking (51).

One way to achieve an acidic flotation pH is to use CO₂ as the gas phase (52). This has been reported to reduce the slurry pH to about 4.8. However, no reports of the use of CO₂ as the gas phase in deinking flexographic newsprint were found in the literature.

The reason acidic conditions improve flexographic ink removal efficiency is probably related to ink chemistry. At acidic pH values, acrylic resin binders in many flexographic inks are not ionized and the inks are less hydrophilic. The removal efficiency of dispersed flexographic ink particles by flotation was greater at pH 3 than at pH 6 (22).

How relevant is this data to deinking of paper printed with flexographic ink? In the absence of cellulose fibers, the zeta-potential of a flexographic ink dispersion dropped from -45 at pH 8 to -15 at pH 4 (22). This is consistent with the pK_a of acrylic acid being 4.3. It is also consistent with the effect of pH on ink particle zeta-potential reported by two other research groups (21,53). The lower zeta-potential under acidic conditions increases the probability of attachment of ink to air bubbles and thus promotes a greater flotation step ink removal rate. Indeed, as noted above, the flotation rate at pH 3 in the same study was greater than the rate under neutral pH conditions (22).

Being negatively charged, cellulose fibers also would be expected to have a less negative zeta-potential under acidic conditions. This similarity to the ink zeta-potential would promote ink particle redeposition on fibers. This increased ink redeposition would reduce any improvement of flexographic ink removal at acidic pH. Some experimental results indicate that conditions favorable for flexographic ink flotation also promote redeposition on the fibers (22).

Among the factors determining the behavior of water-dispersed carbon black particles are the particle diameter, specific surface area, and surface chemistry. Various methods of oxidation can increase the number of acidic groups (-CO₂H and -OH) on the surface of carbon black particles (54).

Oxidation left the mean particle diameter unchanged but decreased the specific surface area. The build-up of negative charges on the carbon black surface by hydroxide ion adsorption contributes to a high zeta-potential and increased hydrophilic character. So does the reaction of the acidic sites with water.

One way to measure the ionic character of a surface is the cationic demand. This is the milliequivalents of a cation that will react with a kilogram of substrate. The cationic demand of flexographic and of offset inks are similar under neutral conditions. However, the cationic demand of flexographic ink is much greater under alkaline conditions. This is presumably due to the ionization of carboxylic acid groups on the carbon black surface. The cationic demand reflects the greater hydrophilic character of flexographic ink and its greater tendency to disperse under alkaline conditions compared to offset ink.

Particulate soil removal from fibers in laundering has been interpreted in terms of DLVO theory (55). Redeposition results from the interaction of two dissimilar electrical double layers. However, DLVO theory does not take into account hydration and steric repulsion forces associated with the ink binder resin adsorbed onto carbon black particles (56,57). Published reports (22,48) indicate binder resins of black flexographic newsprint inks contain 20-35% by weight carboxylate groups. Sterically stabilized aggregates existing at pH 5 may be readily redispersed at pH 9 upon ionization of binder resin carboxylate groups - the reverse reaction of the first chemical equation shown above.

Reducing Ink Redeposition onto Cellulose Fiber. To minimize ink redeposition, paper printed with water-based inks should be pulped for the shortest possible period required and with the least amount of agitation necessary to disaggregate the paper (26). Drum pulping is a low agitation means of pulping and should be considered for use in deinking paper printed with water-based inks.

Water hardness has been shown to have a much greater adverse effect on flotation - wash deinking performance when the furnish contains substantial amounts of flexographic ink (15). This can be seen in Figure 12. Pulp brightness after flotation decreased with both increasing water hardness and increasing flexographic ONP content of the furnish. The decreased brightness is probably due to increased ink redeposition onto cellulose fibers at higher water hardness. The effect of calcium soaps and high concentrations of calcium ions have been shown to increase deposition of flexographic ink particles on fiber mats in washing (30). Extensive washing with water did not desorb these ink particles. The adverse effect of water hardness on cloth brightness due to increased soil redeposition is widely known in laundering (5).

Anti-redeposition agents are widely used in laundry detergent formulations to reduce redeposition of dispersed soils. These work by increasing steric hindrance and electrostatic repulsion between the substrate fibers and the

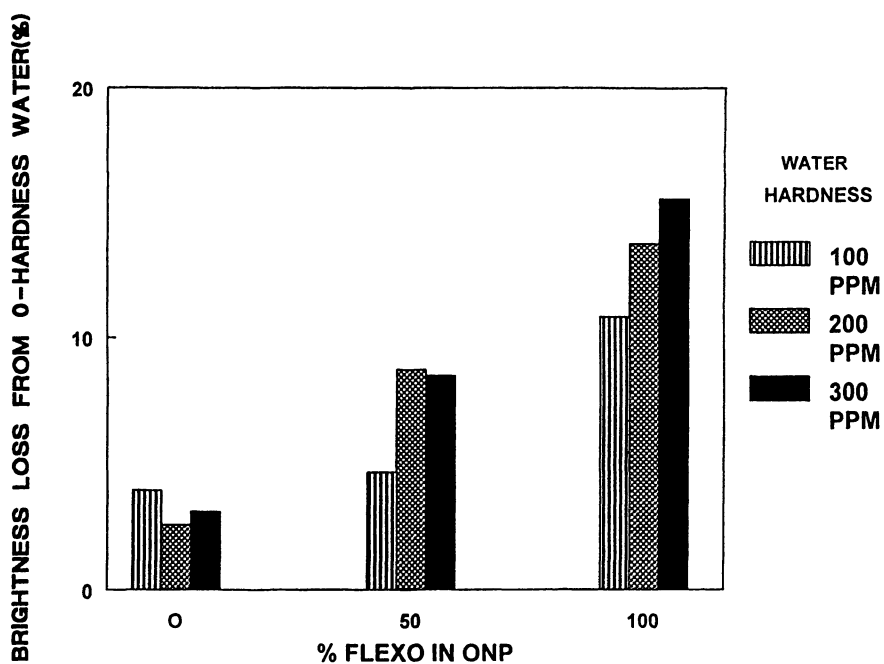


Figure 12. Effect of Water Hardness on Deinked Sheet Brightness After Flotation and Washing

soil. These repulsive forces prevent the close approach of the soil to the fibers preventing the onset of van der Waals attractive forces.

The use of anti-redeposition agents to reduce ink particle redeposition on cellulose fibers during pulping of offset newsprint has been reported (58-60). These include copolymers of ethylene oxide and propylene oxide that are more commonly considered dispersants (60). The use of anti-redeposition agents in deinking furnishes containing flexographic ONP has also been reported (16). At the concentration used, 150-450 ppm in the aqueous phase, these agents varied in their effectiveness (Figure 13). Of the seven chemical agents studied, addition of polyacrylate and carboxymethyl cellulose (CMC) to the pulper produced the highest brightness gains relative to the same experiment performed without anti-redeposition agent. At a loading of 450 ppm in the pulping water, TAPPI brightness gains of 7-8 points were obtained (without bleaching). A polyacrylate anti-redeposition agent was used in pilot plant flotation - wash deinking of a 1:1 mixture of over-issue flexographic newspaper and offset newspaper (combined with 30% old magazines). Using this anti-redeposition agent resulted in a deinked sheet brightness only one point lower than obtained when only offset newsprint was used in the furnish (Figure 14).

The use of an anti-redeposition agent in acidic pulping provided a small, but significant increase in deinked newsprint brightness in a short sequence deinking process (34). However, when a washing stage was added to the process, the brightness increase due to anti-redeposition agent was reduced to perhaps one point.

A cationic polymer of unspecified structure has been used as a flotation additive in flotation deinking of flexographic newsprint furnishes (59). An unspecified polymer that may or may not be an anti-redeposition agent was used as a flotation additive in a more recent report (61). A patent application (62) suggests this polymer is poly(dimethylamine - co- epichlorohydrin) with a molecular weight of 450,000 daltons and a cationicity of 95%. The deinking surfactant used with it is a polyoxyalkylene having a fatty acid or fatty alcohol hydrophobe (62). In both cases, significant brightness gains were achieved using the polymer additive.

Mills receive flexographic furnish mixed with offset and letterpress printed newsprint. Acidic deinking conditions are less efficient than basic conditions in deinking offset printed newsprint. Therefore, simply reducing the pH to improve flexographic newsprint deinking is not a feasible solution in many mills. Separate neutral or acidic flotation loops to remove flexographic ink followed by a basic loop to remove offset ink have been proposed (5-7). Optical properties of flexographic newsprint after pulping at neutral and acidic pH are summarized in Table 6.

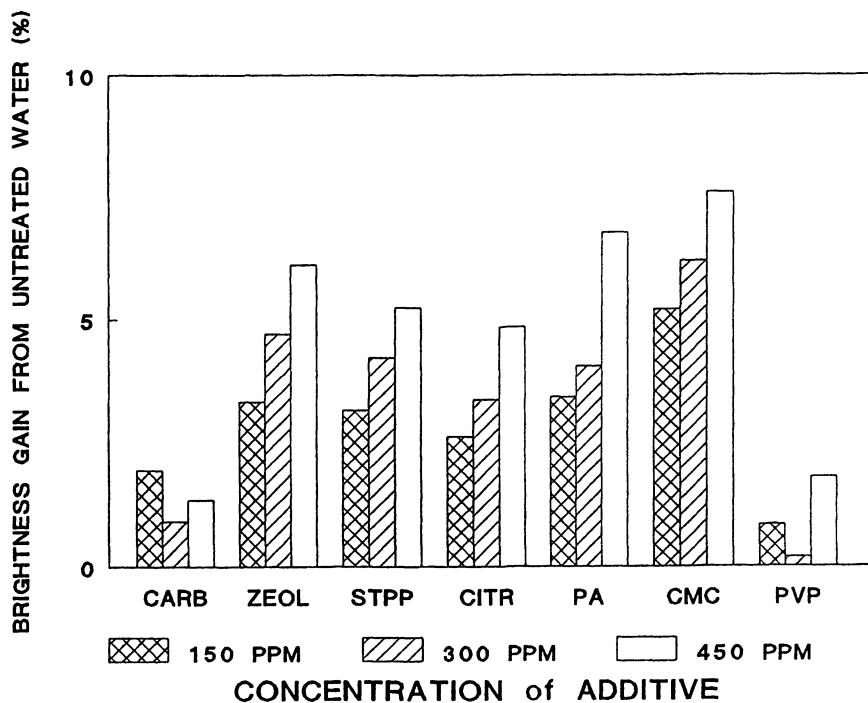


Figure 13. Effect of Anti-redeposition Agents on Brightness.

CARB = sodium carbonate,

ZEOL = zeolite 4A, STPP = sodium tripolyphosphate,

CITR = sodium citrate, CMC = sodium

carboxymethylcellulose,

PA = sodium polyacrylate, PVP = polyvinyl pyrrolidone.

The deinking surfactant was 0.20% (by weight relative to furnish) SDA-34. Water hardness was 200 ppm calcium.

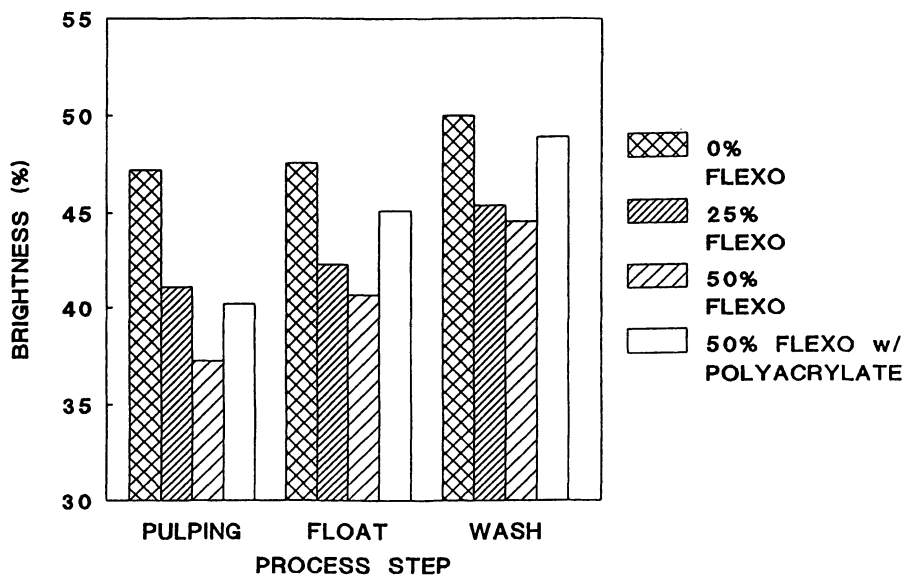


Figure 14. Pilot Plant Test. Effect of Sodium Polyacrylate on Pulp Brightness. 0.25% SDA-34 deinking surfactant and 0.25% by weight sodium polyacrylate (both percent by weight relative to furnish. Western Michigan University Pilot Plant.

Table 6. Flexographic Newsprint. Optical Properties After Pulping (8).

Analysis	After Pulping pH		After Hyperwashing ^a	
	Neutral	Alkaline	Neutral	Alkaline
Brightness, %	33	26	41	38.5
ERIC, ppm	2800	4760	1006	1272

a. Hyperwashing is the process of pulp washing until the brightness and ERIC measurements reach stable values.

Image analysis indicated the presence of more ink particles greater than 1.3 microns in diameter under alkaline pulping conditions.

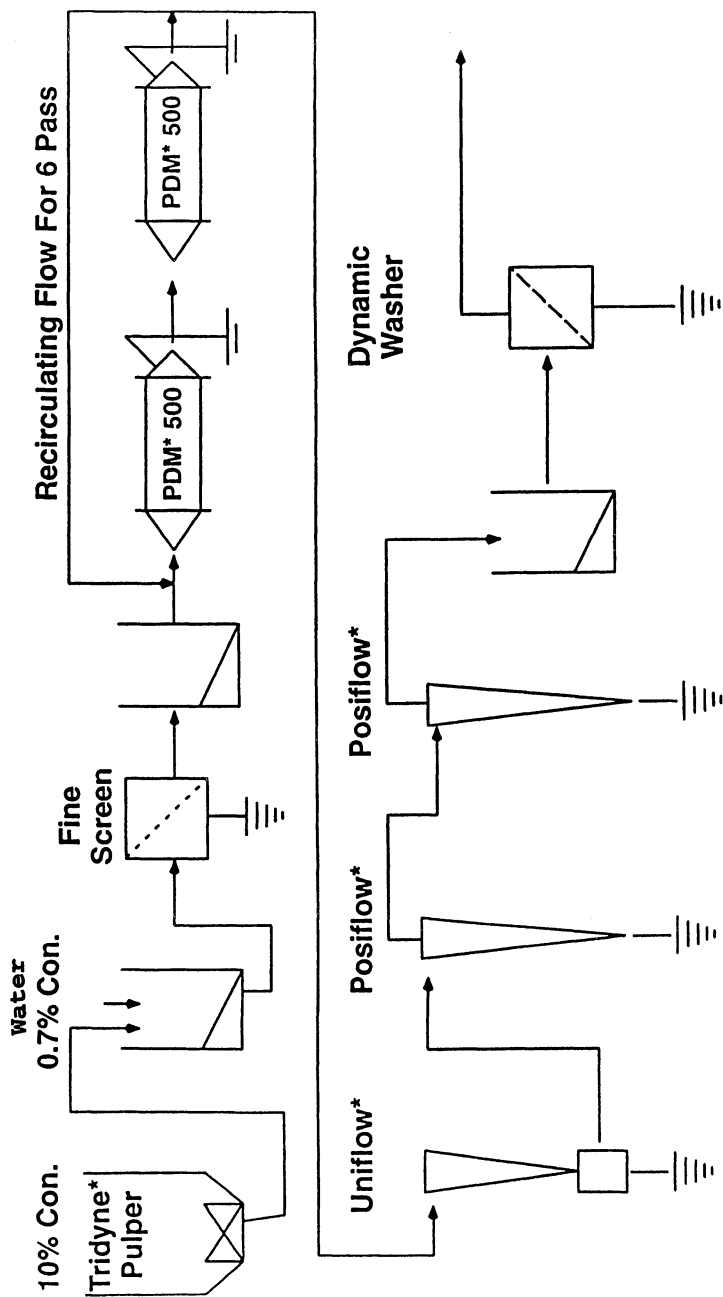
The low brightness and high ERIC values observed after hyperwashing are not due to dispersed small ink particles since these would have been removed in the hyperwashing process. The poor pulp optical properties appear to be due to redeposition of very small ink particles onto fibers. Once deposited, these particles are difficult to remove. This is consistent with results of studies of the deposition of dispersed flexographic ink particles onto cellulose fiber mats (23,26,30). It is also consistent with results indicating very small ink particles adsorbed onto fiber surfaces and even into the openings of cellulose lumen (9).

The lower brightness and higher ERIC values after hyperwashing indicate that ink particle redeposition onto cellulose fibers was greater at alkaline conditions than at neutral pH. The hyperwashing results (and the reference 26 results discussed above) indicate that this redeposition is essentially permanent. Considering these and other results, a two-loop deinking process, first a neutral pH loop and then an alkaline loop, was proposed (8). (A similar process design with the additional characteristic of low temperature has been suggested to facilitate stickies removal in centrifugal cleaners has been proposed (63).)

Small Ink Particles in Offset Newsprint Deinking. Analysis of results from pilot mill flotation - wash deinking studies (64) provides additional information on the role of small ink particles in deinking. The deinking process is depicted in Figure 15. Most of the newspapers used in this study were offset printed. Furnish variations probably account for the relatively minor differences in the number of small (1.2-5 microns) ink particles formed after pulping using three different surfactants (Table 7).

Flotation step ink removal efficiency for particles less than 5 microns in diameter was low (Table 8).

The most effective surfactant removed only 9% of the small ink particles. Only for particles above 20-30 microns in diameter did flotation remove substantial amounts of ink. Forward cleaning had little effect on the number of small (<50 micron in diameter) ink particles. The subsequent washing



*Trademark of Beloit Corporation

Figure 15. Pilot Plant Process Flow Diagram for Figure 17 Results

step removed 44-78% of the small ink particles. (These statements are based on the assumption that larger ink particles are not dispersed into smaller ones during the deinking process.)

Table 7. Ink Particle Size Distribution of 70:30 ONP:OMG Furnish After Pilot Plant Pulping in the Presence of Three Different Proprietary Deinking Surfactants (64).

Particle Size (microns)	Particles After Pulping in the Presence of		
	SDA-30	SDA-31	SDA-52
1.2 - 3	1760	1854	1936
3 - 5	1692	1705	1937
4 - 7.5	2048	1950	2120
7.5 - 10	1550	1408	1500
10 - 15	1995	1700	1949
15 - 20	1064	944	1034
20 - 30	847	716	816
30 - 40	247	231	248
40 - 50	94	69	69
Total Particles			
< 50 microns	11,297	10,577	11,604
Mean Diameter (microns)	10.1	9.6	9.7
Median Diameter (microns)	7.7	7.2	7.3

The median small particle diameter declined modestly in the flotation step while decreasing significantly in the washing step (Figure 16) despite the high overall efficiency of washing in removing small ink particles (64). Similar results were observed in office paper deinking (65). There was little change in the median small particle diameter after screening and after forward cleaning.

In studying the effective of the order of unit operations in deinking processes employing both wash and flotation deinking steps, overall deinking efficiency was greatest for the flotation - wash sequence (66). This was true for both newsprint and office paper inks. However, the wash - flotation deinking sequence was the more effective in removing ink particles 2.5 - 160 microns in size. This suggests that the preferable sequence of unit operations for papers with a high content of water-based inks would be first wash deinking and then flotation.

Table 8. Pilot Plant Deinking. Ink Removal Efficiency in Flotation and Wash Deinking Unit Operations (64).

Particle Size (microns)	<u>Flotation Ink Removal (%)</u>			<u>Washing Ink Removal (%)</u>		
	<u>Deinking Surfactant</u>			<u>Deinking Surfactant</u>		
	<u>SDA-30</u>	<u>SDA-31</u>	<u>SDA-52</u>	<u>SDA-30</u>	<u>SDA-31</u>	<u>SDA-52</u>
1.2 - 3	1.3	0	1.4	15.4	30.8	38.6
3 - 5	8.8	11.9	16.0	73.9	78.6	79.0
5 - 7.5	18.6	9.1	20.6	81.6	83.6	85.0
7.5 - 10	25.1	6.1	29.6	86.8	88.2	85.7
10 - 15	29.6	12.0	27.8	88.0	87.6	86.2
15 - 20	29.5	18.7	31.7	84.4	87.7	88.1
20 - 30	41.9	31.0	39.9	83.4	84.7	87.6
30 - 40	47.0	48.2	49.6	66.1	82.3	84.5
40 - 50	64.3	54.1	34.7	51.6	68.4	86.6
<u>Particle Removal</u>						
< 5 microns	5.1	4.3	9.2	44.4	56.4	59.6
< 50 microns	21.5	12.0	23.0	70.8	76.0	77.0

Process Water Clarification. The concentration of small, sub-visible ink particles that have a negative effect on brightness can build-up in recycled mill process water if these ink particles are not removed efficiently in the water clarification process. This was the reason the brightness of deinked newsprint steadily decreased during the course of a flotation - wash mill trial testing a deinking agent known to be effective on offset printed ONP (15). The mill was processing furnish containing flexographic inks. The brightness decrease occurred despite a decrease in the TAPPI dirt count compared to results obtained using the mill's standard deinking agent.

The small flexographic ink particle size and the hydrophilic nature of ink particle surfaces make process water clarification difficult (13). The acrylic binder resin of flexographic inks creates an electrostatic barrier to ink particle flocculation and may offer steric inhibition to interaction of the flocculant and the ink particle (21). An increasing ink load in recycled process water can reduce deinked sheet brightness in wash deinking mills with some closure of their water loops. However, at least one mill using a flotation - wash deinking process has reported success in deinking furnish containing flexographic printed newsprint (37). The flexographic newsprint is added to the pulper in metered amounts.

Process water clarification at neutral pH has been reported to require lower levels of water clarification chemicals than clarification at alkaline pH

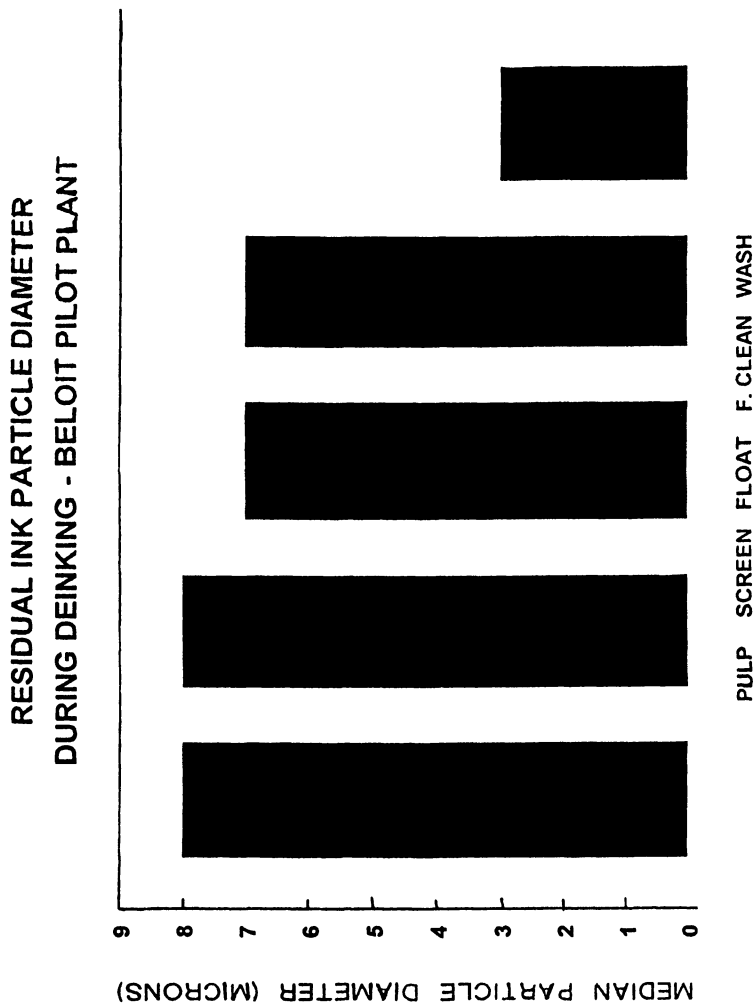


Figure 16. Effect of Pilot Plant Unit Operation on Residual Ink Particle Diameter

(11). This technology may have application for flexographic newsprint deinking at neutral or acidic pH.

Possible Future Developments

Improved Flotation Deinking Agents. Pilot plant flotation deinking brightness results using a proprietary deinking surfactant (Figure 17) indicate deinked sheet brightness did not decline significantly until the flexographic content of the furnish increased to above 50% (16). There are two possible explanations for this behavior. The deinking surfactant could have reduced ink particle dispersion. However, the initial brightness after pulping militated against this explanation. The second possibility is that the proprietary deinking surfactant altered flexographic ink surface chemistry (increased hydrophobicity) to increase the ink removal efficiency of flotation. This explanation seems more likely. Microscopy studies have indicated that ink particles as small as ca. 5 microns (the detection limit of the technique) can adhere to relatively large air bubbles (68).

Reducing the pH can increase the efficiency of flotation deinking of flexographic furnish. However, the same pH reduction typically reduces the efficiency of flotation deinking of offset printed newspapers (67). Improved deinking surfactants could solve this problem and allow low acidic flotation deinking of mixed flexographic ONP/offset ONP furnishes. For example, results for four different proprietary surfactants indicate that surfactants can be designed to deink offset newsprint efficiently at basic or acidic pH with no decline in flotation efficiency at acidic pH (16).

Use of a deinking agent consisting of a synergistic combination of a surfactant, a fatty acid, and a water-soluble polymer for deinking of furnishes with substantial flexographic ink content has been reported (61,62). Laboratory and pilot plant tests were performed using 5% and 15% flexographic newsprint in ONP/OMG furnishes. Process water could be reused without clarification in these tests. When the pulper pH was reduced from 10 to 8.6, brightness was reduced from 54% to 44%. Some water hardness was required for optimum flotation. This was not too surprising since fatty acid is one of the deinking agent ingredients and the OMG content was the furnish was 20%.

The presence of wood resin acids in a tall oil fatty acid has been reported to enhance flotation removal of flexographic ink (69). Condensation products of fatty acids and alkoxyated amines have also been claimed to provide improved flexographic ink removal in flotation (70).

Fatty oil alkylene oxides have been reported to agglomerate flexographic ink particles less than 5 microns in size (37). A solvent encapsulated surfactant was studied using a furnish containing a substantial amount of flexographic newsprint (71). The deinking agent promoted the agglomeration of ink particles less than 5 microns in diameter. The larger ink

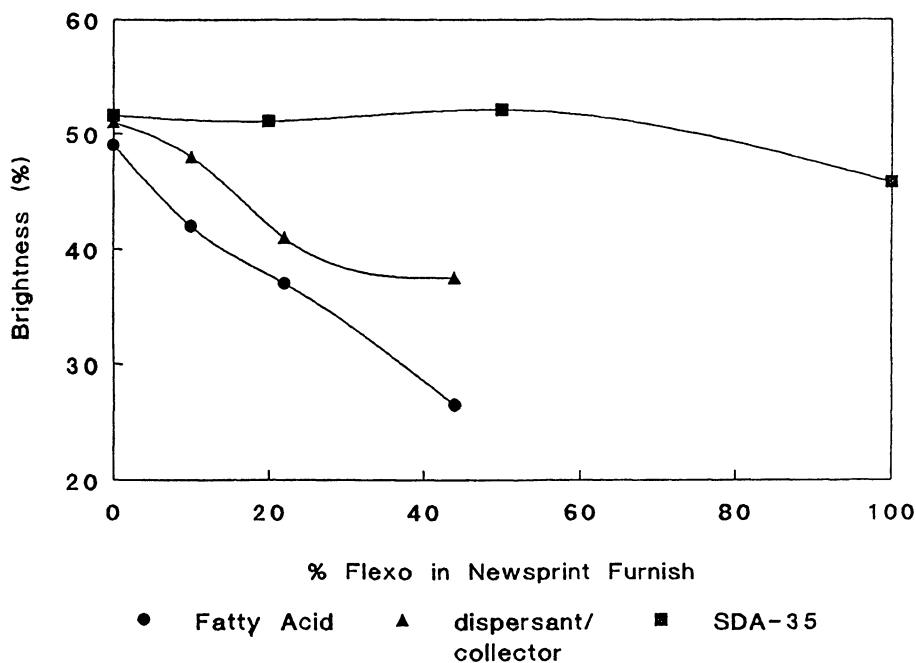


Figure 17. Flotation Deinking of Newsprint:Magazine Furnishes Using Three Different Deinking Surfactants. Data for the fatty Acid and dispersion/collector obtained from reference 46. Data for SDA-35 obtained from reference 16. The brightness values cannot be compared directly. What is important is the trend of brightness with increasing flexographic ink content of the furnish.

particles were more amenable to removal by flotation and flotation ink removal efficiency was improved. A different encapsulated deinking agent was shown to agglomerate carbon black particles with an average size less than 3.8 microns to a size suitable for flotation deinking (72). Improved deinked pulp brightness resulted.

At neutral pH, addition of a cationic "promoter" to a flotation cell promoted aggregation of small ink particles to a size more amenable to removal by flotation (53). This resulted in higher deinked pulp brightness. Even at neutral pH, zeta-potential measurements indicate the ink particles remain negatively charged. This promotes adsorption of the cationic promoter onto the ink particles. The use of cationic surfactants has been suggested for flotation deinking of furnishes containing high levels of flexographic inks (73).

Improved Water Clarification. Improved water clarification polymers could more effectively clarify process water containing flexographic ink particles. An effective dissolved air flotation process for clarifying process water containing dispersed flexographic ink particles involved addition of a vinylamine - containing coagulant followed by a high molecular weight polyacrylamide (74).

Due to the difficulty in flocculating very small ink particles, membrane techniques are being investigated as a means of removing dispersed ink and other small particles from pulp slurries and process water (75-77). These processes include reverse osmosis, ultrafiltration, and nanofiltration. In particular, ultrafiltration has been reported to be effective in clarifying washer effluent from flexographic ink-containing pulp at high membrane permeation rates (76,77). The addition of a proper level of surfactant in dilute ink dispersions increased the permeation rate and enhanced flux stability. This suggested that some deinking surfactants could reduce the degree of membrane fouling (77).

Improved Water-based Inks. Flexographic ink composition is known to affect deinking effectiveness. While unprinted paper brightness was similar, deinking a flexographic ONP from the U.S. East Coast ("Bangor Daily News") and U.S. West Coast ("San Francisco Chronicle & Examiner") provided brightness values that differed by a very significant 4 points (16). Flexographic inks 1 and 2 in the reference 26 study provided different deinked sheet brightness. Another study indicated that different flexographic ink - printed European newspapers differed in brightness after pulping and deinking, probably due to difference in ink composition (6). A third study comparing the flotation deinking of seven U.S. and four Italian flexographic newspapers also indicated significant differences in deinkability among the various newspapers (58). The Italian newspapers were generally more deinkable than the U.S. newspapers. However, there were also significant differences in deinkability among the Italian as well as among the U.S. newspapers.

These observations suggest that it could be possible to develop improved water-based inks that deink more easily. From the mills' perspective,

ink reformulation is the easiest solution to the difficulty of deinking paper printed with water-based inks. Two approaches are conceivable. The first is to coat the carbon black or other pigments with a hydrophobic film so they tend to disperse less readily (78). Another is to alter the flexographic ink binder resin. Using different binder resins such as water-soluble cationic resins can improve flotation deinking results (47).

Some progress is being made in developing improved flexographic inks (9). A recent study (79) compared the flotation results on deinking eight different North American flexographic newspapers (35% in combination with 35% of a letterpress printed newspaper and 30% old magazines). Deinked pulp brightness ranged from less than 45 to almost 55. Using an offset printed newsprint instead of a flexographic newspaper resulted in a brightness greater than 60. Other flexographic inks also provided higher brightness results compared to a currently commercial flexographic ink. These improved flexographic inks appeared to be experimental samples (79).

Improved Deinking Process Equipment. As noted above, the reduced shear forces imparted by drum pulpers could lead to lower ink dispersion, reduced ink redeposition, and consequent improved flexographic ink removal efficiency. An improved flotation cell design said to be more effective in removing ink particles less than 5 microns in diameter has been demonstrated on a laboratory scale (31). High turbulence washers proved improved flexographic ink removal efficiency through reduced deposition on fiber mats (23).

Acknowledgments

It is a pleasure to acknowledge the contributions of my coworkers to some of the laboratory work described herein and cited below. The hard work of Kirk Raney, Drew Matalamaki, Vevolyn Lott and Gregory Shpakoff in both the laboratory and the pilot plant is greatly appreciated. The helpful discussions and pilot plant work of David Grimes and Kirk Raney must be acknowledged. Discussions with Gordon Leighton, Mahendra Doshi and Gerald Wouch were most helpful. David Denley performed the microscopy work that was helpful in the course of this research.

Literature Cited

1. Hooper, C.; Daneault, C.; Dorris, G.M. *Pulp & Paper Canada*, **August 1996**, 97 (8), T269 - T231.
2. Jarrehuit, B., Lindqvist, M., Hanecker, E., and Tri Phan, D.: *Wochenbl. Papierfabr.*, **1991**, 119 (20), 811-818.
3. Bast, I. *Eucepa Conference Preprints*, **Oct. 1990**, Barcelona, Spain, pp. 95-104.
4. Liphard, M.; Schreck, B.; Hornfeck, K. *Proc. TAPPI Pulping Conference*, TAPPI Press, Atlanta, GA, **1990**, 965-975.

5. Suss, H.U., Schumacher, W., Nimmerfroh, N., and Hopt, B.: *Das Papier*, **1991**, 45 (3), 89-96 (1991).
6. Galland, G.; Vernac, Y. *Pulp & Paper Canada*, **1993**, 94 (6), T181-T185.
7. Galland, G.; Vernac, Y. Carré, B. *Pulp & Paper Canada*, **June 1997**, 98 (6), T182-T185.
8. Galland, G.; Vernac, Y.; Carré, B. *Pulp & Paper Canada*, **July 1997**, 98 (7), T254-257.
9. Ackermann, C.; Putz, H.J.; Göttching, L. *Pulp & Paper Canada*, **August 1994**, 95(8), 28-33.
10. Kubler, R. *Wochenbl. Paperfabr.*, May 1988, 116 (10), 386, 388-390.
11. Tremont, S.R. *Proceedings of the TAPPI Pulping Conference*, TAPPI Press, Atlanta, GA, 1993, 749-756.
12. Phillippe, I.J. *Proc. TAPPI Pulping Conference*, TAPPI Press, Atlanta, 1996, 805-810.
13. Schriver, K.E.; Friel, T.C. *Proc. TAPPI Pulping Conference*, TAPPI Press, Atlanta, GA, 1992, 439-443.
14. Hodgson, K.T. *Prog. Paper Recycling*, **May 1996**, 4 (3), 71-74.
15. Masamizu, K.; Egawa, J.; Hagiwara, M.; Kawai, K. *Proc. TAPPI Recycling Symposium*, TAPPI Press, Atlanta, GA, 1997, 435-451.
16. Borchardt, J.K.; Raney, K.H.; Shpakoff, P.G.; Matalamaki, D.W.; Denley, D.R. *Proc. TAPPI Pulping Conference*, TAPPI Press, Atlanta, GA, 1994, 1067-1103.
17. Chabot, R.; Daneault, C.; Lapointe, M.; Marchildon, L. *Prog. Paper Recycling*, **August 1993**, 2 (4), 21-29.
18. Wasilewski, O. *Proc. TAPPI Pulping Conference*, TAPPI Press, Atlanta, GA, 1987, 25-28.
19. Fishman, D.H.; Shah, S. *American Ink Maker*, 18-22 (January 1990).
20. Borchardt, J.K. "Recycling - Paper," in eds. Kroschwitz, J.I.; Howe-Grant, M. *Kirk - Othmer Encyclopedia of Chemical Technology*, John Wiley & Sons, Inc., New York, NY, 1997, Vol. 21, pp. 11 - 22.
21. Fernandez, E.O.; Hodgson, K.T. *J. Pulp Pap. Sci.*, **Nov. 1996**, 22 (11), J452-J456.
22. Dorris, G.M.; Nguyen, N. *J. Pulp Pap. Sci.*, **1995**, 21 (2), J55.
23. Rangamannar, G.; Grube, G.; Karneth, A.M. *Proc. TAPPI Pulping Conference*, TAPPI Press, Atlanta, GA, 1992, 933-939.
24. Togashi, T.; Okada, E. *Proc. TAPPI Pulping Conference*, 1989, TAPPI Press, Atlanta, GA, 343.
25. Putz, H.J. *New Developments in Wastepaper Processing and Uses: The PIRA Secondary Fibre Programme* March 1989, Vol. 1, Session 2, Paper No. 10.
26. Ciampa, S.L. *The effect of pulping variables in the deinking of flexographic inks*, 1995, M.S. Thesis, Western Michigan University.
27. Vaeck, S.V.; de Pauw, L. *Tenside*, (1973) 10, 290.
28. E. Kissa, "Kinetics of Soiling and Detergency," in eds. Cutler, W.G.; Kissa, E.; *Detergency: Theory and Technology*, Surfactant Science Series, Volume 20, Marcel Dekker, New York, NY, 1987, 193-331.

29. Gottsching, L.; Putz, H-J. *Proc. TAPPI Recycling Symposium*, TAPPI Press, Atlanta, GA, 1994, 207-210.
30. Ben, Y.; Pelton, R.; Dorris, G.M. *J. Pulp Pap. Sci.*, **November 1996**, 22 (11), J411-J419.
31. Naujock, H.J.; Strunz, A.M.; Wolf, W) *Papier (Darmstadt)*, 1992, 46 (10A), 121-130.
32. Cartwright, T.B.; Forsberg, P.; Johnson, D.A.; Genco, J.M. *Progress in Paper Recycling*, **May 1994**, 3 (3), 15-19.
33. McCool, M.A.: "Flotation Deinking" in ed. Spangdenberg, R.J. *Secondary Fiber Recycling*, TAPPI Press, Atlanta, GA, 1993, 159.
34. Ferguson, L.D. *Proceedings of the TAPPI Pulping Conference*, TAPPI Press, Atlanta, GA, 1993, 793-799.
35. Larsson, A.; Stenius, P.; Oldberg, L. *Svensk Papperstidning*, **1984**, 8 (18), R158-R164.
36. Furstenu, D.W.; Healy, T.W. "Principles of Mineral Flotation" in ed. Lemlich, R. *Adsorptive Bubble Separation Techniques*, Academic Press, New York, 1972, 91-131.
37. Saint Armand, F.J.; Perrin, R. *Pulp & Paper Canada*, October 1993, 94 (10), 25-28.
38. Milanova, E.; Dorris, G.M. *J. Pulp Pap. Sci.*, **1993**, 19 (5), J194.
39. McLennan, I.J.; Pelton, R. *J. Pulp Pap. Sci.*, **1997**, 23 (6), J263-J269.
40. Hruzewicz, J.N. *Flexo*, **June 1992**, 28-33.
41. Pan; R. Bousfield, D.W.; Thompson, E.V.: "Modeling Particle - Bubble Dynamics and Adhesion in Air Bubble/Solid Particle/Liquid Systems," "Proc. TAPPI Pulping Conf.," TAPPI Press, Atlanta, GA (1992), pp. 941-956.
42. Pan, R.; Paulsen, F.G.; Johnson, D.A.; Bousfield, D.W.; and Thompson, E.V.: "A Global Model for Predicting Flotation Efficiencies: Model Results and Experimental Studies," Proc. TAPPI Pulping Conference, Atlanta, TAPPI Press, Atlanta, GA (1993) pp. 1155-1164.
43. Paulsen, F.G.; Pan, R.; Bousfield, D.W.; Thompson, E.V. *Proceedings of the CPPA 2nd Research Forum on Recycling*" Ste-Adele, Quebec, Canada, October 1993, 1-12.
44. Fuchs, B. *Newspaper Techniques*, **Feb. 1988**, 60-63.
45. Turai, L.L.; Williams, L.D. *Tappi J.*, **Nov. 1977**, 60 (11), 167.
46. Jarrehuit, B.; Horacek, R.G.; Lindqvist, M.L. *Proceedings TAPPI Pulping Conference*, TAPPI Press, Atlanta, GA, 1991, 85.
47. Ackerman, C.; Putz, H-J.; Gottsching, L. *Proceedings of the CPPA 2nd Research Forum on Recycling*," Ste-Adele, Quebec, Canada, October 1993, 201-206.
48. Chabot, B.; Daneault, C.; Dorris, G.M. *J. Pulp Pap. Sci.*, **Sept. 1995**, 21 (9), 296-301.
49. Mattingley, J.T. *Proc. 1983 TAPPI Pulping Conference*, TAPPI Press, Atlanta GA, 1983, 515.
50. Shrinath, A.; Szweczek, J.T.; Bowen, I.J. *TAPPI J.*, **July 1991**, 74 (7), 85.
51. Putz, H.J.; Schaffrath, J.J.; Gottsching, L. *Pulp & Paper Canada*, **July 1993**, 94 (7), 16-20.

52. Marchildon, L.; Castro, C.C.; Lapointe, M.W.; Daneault, C. *Tappi J.*, 1993, 76 (3) 155-9.
53. Takahashi, H.; Irinatsu, Y.; Shiroishi, T.; Edo, T.; Ueda, Y. *Proc. TAPPI Pulping Conference*, TAPPI Press, Atlanta, GA, 1996, 811-812.
54. Murata, T.; Imgawa, H. *Denki Kagaku*, 1973, 41, 708.
55. Schott, H. "Removal of particulate soil," in *Detergency: Theory and Test Methods*, Surfactant Science Series, Vol. 5, Part 1, Marcel Dekker, New York, NY, 1973, 154-235.
56. Neuman, R.D.; Berg, J.M.; Claesson, P.M. *Nord. Pulp Paper Res. J.*, 1993, 8 (1), 96-104.
57. Pelton, R. *Nord. Pulp Paper Res. J.*, 1993, 8 (1), 113-119.
58. Baumgarten, H.L.; Grossmann, H. *Proceedings of the TAPPI Recycling Symposium*, TAPPI Press, Atlanta, GA, 1994, 181-186.
59. Liphard, M.; Schreck, B.; Hornfeck, K. *Proc. TAPPI Pulping Conference*, TAPPI Press, Atlanta, GA, 1991, 1031-1038.
60. Ferguson, L.D. *Tappi J.*, August 1992, 75 (8), 49-58.
61. Skaar, T.F. *Proc. TAPPI Pulping Conference*, TAPPI Press, Atlanta, GA, 1994, pp. 885-904.
62. Robinson, P.; Skaar, T.; Urushibata, H.; Williams, S. "Flotation deinking of printed media," PCT Intl. Appl. WO 94 28,237 (Dec. 8, 1994).
63. Clement, J.M. *Proc. TAPPI Pulping Conference*, TAPPI Press, Atlanta, GA, 1993, 1025.
64. Borchardt, J.K.; Matalamaki, D.W. *Proc. 2nd Research Forum on Recycling*, Canadian Pulp and Paper Association, Montreal, QC, Canada, 1993, 79-92.
65. Borchardt, J.K.; Matalamaki, D.W.; Lott, V.G.; Grimes, D.B. *Proc. TAPPI Recycling Symposium*, TAPPI Press, Atlanta, GA, 1997, 507-526.
66. Davila, A.; Scott, G.M.; Klungness, J.H.; Doshi, M. *Prog. Paper Recycling*, Feb. 1996, 4 (2), 23-34.
67. Galland, G.; Vernac, Y. *Pulp & Paper Canada*, June 1993, 94 (6), 71-75.
68. K.H. Raney, unpublished results.
69. Fossas, F.F.; Ferre, P.F.; Castano, N.R.; Williams, S.P.; Salem, W.; Urushibata, H. "Deinking formulation for flexographic inks," U.S. Patent 5,417,807 (May 1995).
70. Hou, M.-J.; Seenivasan, N. "Deinking wastepaper printed with water-based ink," U.S. Patent 5,384,010 (Jan. 24, 1995).
71. Sain, M.M.; Marchildon, L. Daneault, C. *Progress in Paper Recycling*, Nov. 1995, 4 (1), 54 - 64.
72. Sheridan, G.P.; Rohlf, E.A.; Aston, D. *Proc. TAPPI Pulping Conference*, TAPPI Press, Atlanta, GA, 1992, 487-492.
73. Putz, H.-J. *Proc. 1st Research Forum on Recycling*, Canadian Pulp and Paper Association, Montreal, QC, Canada, 1991, 183-190.
74. Chung, D.; Sommese, A.; Tubergen, K. "Clarification of deinking process water using polymers containing vinylamine," U.S. Patent 5,573,675, assigned to Nalco Chemical Co. (Nov. 12, 1996).
75. Bredael, J.; Sell, N.J.; Norman, J.C. *Prog. Paper Recycling*, Nov. 1996, 6 (1), 24-31.

76. Upton, B.H.; Krishnagopalan, G.A.; Abubakr, S. *Tappi J.*, Feb. 1997, 80 (2), 155-164.
77. Upton, B.H., Krishnagopalan, G.A., and Abubakr, S. *Proc. TAPPI Recycling Symposium*, TAPPI Press, Atlanta, GA, 1997, 175-197.
78. Borchardt, J.K.; Wouch, G. unpublished results.
79. Mah, T.; Reid, F.; Yau, T. "Deinking of Flexographic Ink by Flotation Process" in *The News in ONP*, 105, Miller Freeman Inc., San Francisco (1994).

Author Index

- Abe, Masahiko, 201
Akay, G., 175
Alvarez, F. R., 57
Armentrout, R. Scott, 113
Bakker, Martin G., 260
Behrends, Thilo, 314
Borchardt, John K., 384
Bruning, Harry, 248
Caudill, Greg, 351
Christian, Sherril D., 158
Cooper, William T., 290
Crowe, Christy, 351
Dierkes, F., 35
Dziewatkoski, M. P., 276
Fuerstenau, Douglas W., 230
Furusaki, Shintaro, 374
Giroux, E. L., 57
Goto, Masahiro, 374
Gunturi, Bhanu, 351
Haegel, F.-H., 35
Harris, Guy H., 230
Harwell, Jeffrey H., 1, 76, 351
He, Yifang, 290
Hendayan, Sumar, 290
Hermann, Reimer, 314
Hitchens, L., 57
Hoffland, L.D., 329
Holzheu, Stefan, 314
Jia, Renhe, 230
Keskinler, B., 175
Keurentjes, Jos T.F., 92, 123
Kitiyanan, B., 76
Kondo, Yukishige, 201
Koopal, Luuk, 248
Kowalski, S., 35
Lavine, Barry K., 290
Lucas, S. V., 329
Mathew, Bijo, 351
Matthews, John, 260
McCormick, Charles H., 113
Mönig, K., 35
Mulleneers, Huib, 248
Nassar, A.-E. F., 329
Newman, Gerard K., 351
O'Haver, J. H., 76
Odirile, P. T., 175
Ono, Tsutomu, 374
Overdevest, P. E. M., 123
Pope, G. A., 16, 23
Powers, Marc, 351
Richardson, Michael F., 113
Roberts, Bruce L., 158
Roubroeks, Suzan, 248
Rulkens, Wim, 248
Sabatini, D. A., 76
Scamehorn, John F., 1, 158
Schwuger, M. J., 35
Smith, P. B. W., 329
Subklew, G., 35
Thiele, P., 35
Tonçre, Christian, 139
Turner, Gregory L., 260
van 't Riet, K., 123
van der Padt, A., 123
Vane, L. M., 57
Wade, W. H., 16, 23
Wakeman, R. J., 175
Weerasooriya, V., 16, 23
Yeh, S.L., 23
Zhang, Kunliang, 260

Subject Index

A

Admicellar chromatography

- application of adsolubilization, 314
- basis in adsolubilization, 260

Admicelles

- selectivity compared to micelles, 314–315
- surfactant aggregates, 9, 260

Adsolubilization

- adsorbed surfactants on particles
 - binding hydrophobic molecules, 260
- alternative to adsorption, 11
- chemicals in experiments, 315, 317*t*
- comparison at pH 5 and pH 8, 321, 323*f*
- differences from solubilization, 315
- equilibrium constants for compounds in study, 324*t*
- fundamental principle for surfactant-based separations, 314
- model concept in chromatographic system, 316*f*
- potential applications, 314
- retention times of selected compounds as function of adsorped surfactant at pH 8, 321, 322*f*

See also Distribution ratios of aromatic compounds between aqueous solution and surfactant covered silica

Adsorption, separation process, 9

Adsorption, head-out to head-on transition. *See* Distribution ratios of aromatic compounds between aqueous solution and surfactant covered silica

Adsorption and aggregation of cationic surfactants on silica surfaces

- effect of addition of paramagnetic broadener to spin-labeled hexadecyl trimethyl ammonium bromide

(HTAB*) adsorbed on silica, 265, 266*f*

- effect of HTAB addition to electron paramagnetic resonance (EPR) spectra from HTAB* previously adsorbed onto 1.5 wt% silica, 267, 269*f*, 270
- effect of silica amount on EPR spectra of HTAB*, 267, 268*f*
- effect of silica concentration on EPR simulations, 267, 269*f*
- EPR equipment, 262
- EPR spectra from nitrosodisulfonate, 271, 272*f*, 273
- EPR spectra from nitrosodisulfonate and adsorption isotherm for HTAB on silica, 273–274
- EPR spectra of slow rotating HTAB*, 265, 266*f*
- experimental and simulated EPR spectra from HTAB and HTAB* adsorbed on silica, 263, 264*f*, 265
- experimental materials, 262
- HTAB surfactant, 261
- investigations of counter-ion binding, 271, 273–274
- results for HTAB binding on silica, 263, 265–270
- schematic showing various equilibria between silica surface and HTAB and HTAB*, 270, 272*f*
- simulated EPR spectra of HTAB*, 261–262, 264*f*
- spectrum analysis methods, 262–263
- spin-labeled HTAB (HTAB*), 261
- strong binding site on silica, 270–271
- strongly bound HTAB at low HTAB as nucleus for surfactant aggregation, 271
- studying structure on small length scale by EPR, 261

Aggregates

- surfactant, 260

use in ultrafiltration, 4

Air stripping, water remediation, 92

Alkylphosphonic acids

reagents for chemical warfare

degradation testing, 338

role of cationic surfactants in capillary

electrophoresis (CE) separations,

339, 340*f*

See also Capillary electrophoresis

(CE)

Alkyl polyethoxylates

experimental, 41

See also Soil remediation with

microemulsions

Alkyl polyglycoside (Glucopon

625FE). *See* Surfactant-enhanced

aquifer remediation (SEAR)

Analytical separations, micellar

liquid chromatography, 11

Anionic/nonionic bicontinuous

microemulsions

extraction experiments, 44

pollutant separation, 53–54

soil extraction, 50

Anionic surfactants

dodecyl sodium sulfate (SDS), 160

microemulsions with mixed nonionic

and, 47

See also Micellar-enhanced

ultrafiltration (MEUF)

Anti-redeposition agents

effect of sodium polyacrylate on pulp

brightness, 406*f*

effect on brightness, 405*f*

reducing redeposition onto cellulose

fibers, 402–407

use in acidic pulping, 404, 407*t*

See also Deinking papers with water-

based inks

Aqueous surfactant streams. *See*

Liquid-liquid extraction in hollow

fiber membrane

Aquifer remediation

demonstration of components, 8

promising process in scale-up, 8

surfactant-enhanced, 5–9

See also Surfactant-enhanced aquifer

remediation (SEAR)

Aromatic compounds. *See*

Distribution ratios of aromatic compounds between aqueous solution and surfactant covered silica

Arsenic containing compounds

sample separation, 280*f*

separation in bacterial growth

medium, 279

separation in nutrient broth matrix

after growth of bacterial strain

alcaligenes faecalis, 280*f*

See also Speciation of metal-

containing compounds

B

Benzoic acid

dependence of solubilization

equilibrium constant (K) for benzoic

acid in didodecyl dimethyl

ammonium bromide (DDAB)

vesicles on intravesicular solute

mole fraction, 217*f*

dependence of normalized K on

dissociation degree of Br⁻ for

benzoic acid, 215*f*

parameters for K equation, 218*t*

vesicle diameter dependence of K,

216–220

See also Vesicle-enhanced

ultrafiltration (VEUF)

Bicontinuous microemulsions,

nonionic surfactants, 45–47

Biotreatment, water remediation, 92

Block copolymer micelles for water

remediation

amphiphilic poly(ethylene oxide)–

poly(propylene oxide)–

poly(ethylene oxide) (PEO–PPO–

PEO) type, 93

basic physical properties of L64,

P103, P104 block copolymers, 98*t*

- calculated and experimental
 normalized partition coefficients at
 different temperatures, 108*f*
- concept process design, 107, 109
- differential scanning calorimetry
 (DSC) experiments, 107
- DSC diagram of pure polypropylene
 glycol (PPG) and P104, 108*f*
- enthalpy and entropy of mixing, 95–
 97
- experimental, 97
- experimental setup for determination
 of naphthalene solubility, 98*f*
- Flory–Huggins model, 95–96
- Flory–Huggins model versus
 experimental, 99
- fraction polar polymer at demixing at
 different temperatures, 101*f*
- generalized phase diagram for
 aqueous solutions of PEO–PPO–
 PEO, 94*f*
- Gibbs–Thomson equation, 103, 107
- modeling hydrocarbon solubilization,
 103, 107
- modeling PEO–PPO systems, 99–103
- modeling solubilization properties,
 95–97
- modified Flory–Huggins model, 96–
 97
- modified Flory–Huggins model
 corresponding with experimental,
 99, 103
- nomenclature, 109, 111
- normalized partition coefficients for
 L64, P103, and P104, 106*f*
- normalized saturation ratios, 103
- phase diagram for PEO–water system,
 100*f*
- phase diagram for PPO–water system,
 102*f*
- process options for organic pollutant
 removal from aqueous streams, 110*f*
- saturation experiment parameters
 using modified Flory–Huggins
 model, 106*f*
- solubility of naphthalene in 10 wt%
 polymer solutions, 105*f*
- solubility of naphthalene in P104
 solutions as function of temperature,
 104*f*
- solubility of naphthalene in polymer
 solution relative to solubility in pure
 water, 104*f*
- solubilization of hydrocarbons, 103
- solubilization transition and DSC
 experiments for 10 wt% P104 and
 L64 solutions, 110*f*
- theory, 93–97
- UNIFAC (Uniquac Functional Group
 Activity Coefficients) model, 95
- UNIFAC prediction versus
 experimental, 99
- Brightness**
- brightness after flotation, 396–397
- commercial flotation-wash deinking
 mill trial, 398
- effect of anti-redeposition agents, 404,
 405*f*
- effect of different type of washers, 400
- effect of flexographic ink content of
 furnish on deinked sheet brightness,
 385, 386*f*
- effect of increasing flexographic ink
 content of furnish on pulp brightness
 after flotation and washing, 398,
 399*f*
- effect of pulping time on brightness
 gain in flotation and post-flotation
 step, 398, 399*f*
- effect of pulping time on pulp
 brightness after pulping and
 washing, 394, 395*f*
- effect of pulping time on pulp
 brightness loss relative to unprinted
 paper, 394, 395*f*
- effect of sodium polyacrylate on pulp
 brightness, 404, 406*f*
- effect of water hardness on deinked
 sheet brightness after flotation and
 washing, 402, 403*f*

optical properties of flexographic newsprint after pulping, 404, 407f
 redeposition of carbon black on cellulose fibers and reduced deinked brightness, 394, 396

See also Deinking papers with water-based inks

iso-Butylbenzene (IBB), contaminant in liquid-liquid extraction study, 81, 82f

4-*t*-Butylphenol (TBP)

comparison of TBP concentrations for different spiral wound membranes, 165, 168, 169f

permeate concentrations of TBP for different spiral wound membranes, 165, 168, 170f

permeate TBP concentration for stirred cell and spiral wound membranes, 165, 167f

permeate TBP concentration using spiral wound membrane, 162, 164f
 target organic, 160

See also Micellar-enhanced ultrafiltration (MEUF)

C

C-18 bonded phase columns

chromatograms of vanillin test mixture, 296f

proposed model for surfactant adsorption, 304f

relaxation parameters of alpha carbon nuclei in pure and adsorbed surfactant, 300f

retention data for mobile phases methanol/water and ionic surfactants, 294, 297

solid state nuclear magnetic resonance (NMR) studying interaction of ionic surfactants with C-18, 297, 300–303

See also Selectivity in micellar liquid chromatography (MLC)

Capillary electrophoresis (CE)

advantages over traditional methods for determination of chemical warfare degradation products, 345, 349

analysis of aqueous sample from second official Provisional Technical Secretariat/Preparatory Commission for Organization for Prohibition of Chemical Weapons (PTS/OPCW) proficiency test water sample, 346f

analysis of aqueous sample from third official PTS/OPCW proficiency test water sample, 345, 347f, 348f

analysis of second and third official PTS/OPCW proficiency test water samples, 342, 345

anodically directed EOF from formation of hemimicelles of quaternary ammonium surfactant, 336, 337f

basic components, 330, 332

CE/indirect UV method validation, 339, 342

CE methods for determining chemical warfare agent degradation products, 336

CE system schematic with two detection modes, 331f

conventional atmospheric pressure chemical ionization (APCI) mass spectra procedure, 339

counter-electroosmotic and co-electroosmotic flow, 333, 336

Debye–Huckel–Henry equation, 332

electroosmotic flow (EOF), 332

electrophoretic mobility of charged molecular species, 332

end-capillary detector, 331f, 332

experimental apparatus, 338

experimental procedures, 338–339

hydrolysis products of nerve agents and related compounds, 341f

migration behavior of anions, cations, and neutral species in typical CE run, 334f

mobility of ions, 332–333
 obtaining increased EOF, 333, 336
 on-capillary detector, 331*f*, 332
 physical phenomena creating EOF, 333
 reagents, 338
 recovery percentages from spiking pinacolyl methylphosphonic acid (PMPA) and isopropyl methylphosphonic acid (IMPA) in reaction masses, 343*f*
 results from second and third official PTS/OPCW proficiency tests, 346*f*
 role of cationic surfactants in CE separations, 339
 separation of alkylphosphonic acids, 340*f*
 separation technique, 330–332
 structure of cationic surfactant didodecyldimethylammonium hydroxide (DDAOH) to control EOF, 336, 337*f*
 within- and between-day precision for IMPA at three levels, 344*f*
 zeta potential and cathodically directed EOF on unmodified fused-silica capillary, 333, 335*f*
See also Chemical and biological warfare agents

Cationic surfactants
 cetyl pyridinium chloride (CPC), 160
See also Adsorption and aggregation of cationic surfactants on silica surfaces; Micellar-enhanced ultrafiltration (MEUF)

Cellulose nitrate (CN) membranes.
See Crossflow microfiltration behavior of surfactants

Cetyl pyridinium chloride (CPC)
 comparison of CPC concentrations for different spiral wound membranes, 165, 167*f*, 168
 permeate CPC concentration for stirred cell and spiral wound membranes, 165, 166*f*
 permeate CPC concentrations using

spiral wound membrane, 162, 164*f*
 relative permeate flux using CPC and spiral wound membrane, 162, 163*f*
See also Micellar-enhanced ultrafiltration (MEUF)

Cetyl trimethyl ammonium bromide (CTAB)
 chromatograms of vanillin test mixture at different CTAB concentrations, 297, 299*f*
 chromatograms of vanillin test mixture on cyanopropyl column, 311*f*
 electrolyte additive reversing electroosmotic flow (EOF) in capillary electrophoresis, 336, 337*f*
 micellar media for micellar liquid chromatography (MLC), 291, 293
 mobile phase preparation, 293
 proposed mechanism for adsorption on C-18, 304*f*
 relaxation parameters of alpha carbon nuclei in pure and adsorbed surfactant on C-18, 300*f*
 relaxation parameters of alpha carbon nuclei in pure and adsorbed surfactant on cyanopropyl bonded phase, 305*f*
 solid state NMR studying interactions with cyanopropyl bonded phase, 305, 306*f*, 307*f*
 solid state nuclear magnetic resonance (NMR) studying interaction with C-18 bonded phase column, 297, 300–303
See also Capillary electrophoresis (CE); Selectivity in micellar liquid chromatography (MLC)

Chemical and biological warfare agents
 history, 329–330
 hydrolysis products of nerve agents and related compounds, 341*f*
See also Capillary electrophoresis (CE)

Chemical potential difference,

- separation methods, 76–77
- Chirotechnology, applied science of enantiomer separation, 123–124**
- Chlorinated hydrocarbons, contaminating water supply, 16**
- Chlorofluorocarbon (CFC) solvents**
 ozone problem motivating replacement, 351–352
 proposed ban of trichlorotrifluoroethane (CFC-113), 352
See also Particulate removal from oxygen systems
- Cholesterol-L-glutamate**
 chiral selector molecule, 124, 128
 ultrafiltration of nonionic enantioselective micelles with, 135, 137
See also Enantioselective micelles in ultrafiltration systems
- Chromate ions, comparison of CrO₄²⁻ concentration for semi-equilibrium dialysis cell membrane and spiral wound membranes, 168, 172**
- Cloud point extraction, extraction process, 11–12**
- Coacervate extraction, extraction process, 11–12**
- Coal**
 aqueous solubility and boiling points of some 4-carbon oxygenated compounds, 241*t*
 ash rejection as function of combustible matter recovery with various collectors, 244*f*
 basicities of saturated ethers in aqueous sulfuric acid, 241*t*
 collection mechanisms, 239–243
 comparison of collecting ability of nonionic THF-17en surfactant with dodecane, nonylphenol, nonylbenzene, and GH4 (polyethoxylated nonylphenol), 237*f*
 comparison of collecting ability of THF-17 and THF-11 with dodecane, 245*f*
 comparison of required dosages of different reagents for Illinois No. 6, 242*f*
 deposits and production, 230
 experimental material, 232
 fine coal flotation, 234–235
 flotability, 231
 flotation, 231–232
 flotation method, 231
 flotation of Illinois No. 6 coal with THF series of reagents as collectors, 235, 238*f*
 flotation of oxidized, 243
 flotation results of Illinois No. 6, 243, 246
 flotation tests, 234
 low-rank reserves, 231
 mechanisms for attachment of THF series, 240, 243
 molecular structure of series of collectors, 236*t*
 series of tetrahydrofurfuryl esters as collectors, 232–234
 tetrahydrofurfuryl butyrate effective collector, 232
- Cobalt ions**
 increasing partition coefficient of complexing agent, 149, 150*f*
 kinetic separations, 146, 148*f*
See also Metal ion removal from aqueous environments
- Colloidal particles as extracting phase. *See* Metal ion removal from aqueous environments**
- Complexation isotherms. *See* Enantioselective micelles in ultrafiltration systems**
- Confidence intervals**
 equation, 131
 single-component isotherms, 132
 single-component Langmuir parameters and, 131–132
- Contact angles**
 determination method, 250
 silica and organic pellets of Overschie and Petrol Harbor sludge, 253–254

See also Flotation of polycyclic aromatic hydrocarbon (PAH) contaminated dredged sludge

Contaminated soils, existing approaches, 8–9

Copper ions

chemical factors affecting reaction rate, 143, 146

comparison of Cu^{+2} concentration for stirred cell and spiral wound membranes, 168, 171*f*

ionization state of extractant, 143, 145*f*

lipophilicity of extractant, 143, 144*f*

micellar surface charge, 143, 146

rate of extractant/metal complex formation in microheterogeneous systems, 147*i*

rejection for spiral wound membrane, 168, 171*f*

yields of extraction versus pH, 154, 155*f*

See also Metal ion removal from aqueous environments

***p*-Cresol**

model foulant, 115, 121

See also Wastewater remediation

Crossflow filtration

establishment of steady state conditions, 176–177

secondary membrane formation, 176

Crossflow microfiltration behavior of surfactants

components of interaction force fields, 181–182

components of particle flux vector, 181

crossflow filtration equipment, 185*f*

crossflow membrane separation of surfactant dispersions, 180*f*

decay of transient permeate flux with time for cellulose nitrate (CN) membrane at different pH, 187*f*

development/decay of transient permeate flux with time for various membranes, 187*f*

development of secondary membrane, 179–183

development of transient rejection with time for various membranes, 188*f*

dimensionless parameters, 183

dioctadecyldimethylammonium chloride (DODDMAC) surfactant results, 184, 186, 190

effect of electrostatic forces on flux decay and rejection, 194

effect of membrane physical chemistry on capture of surfactant particles, 183

effects of organics and electrolytes, 179

effects of van der Waals forces on flux decay and rejection, 194

estimation of surfactant concentration in secondary membrane, 178

experimental equipment, 183–184

experimental membranes, 184

experimental surfactants, 184

variation of steady state rejection (R) for DODDMAC as function of dimensionless time for several membranes, 193*f*

gel concentration, 196*t*, 197

gel or pseudo-gel concentration, 178

growth rate of gel layer, 182–183

inclusion of reaction term Q in mass balance equation, 182–183

phase behavior of surfactant/water system, 196, 198*f*

physico-chemical and physical characteristics of membranes, 186*t*

primary membrane nature under steady state conditions, 177–178

results for anionic and non-ionic surfactant, 186, 190

secondary membrane formation and transient permeate flux, 177

steady state filtration characteristics of surfactants, 196–197

steady state flux and rejection behavior, 196–197

steady state permeate flux and surfactant rejection, 186

summary, 197, 199

surfactant deposition, formation and structure of secondary membrane, 190, 194

surfactant phase behavior, 196*t*, 197

surfactant phase diagrams, 178–179

surfactant-water-membrane interactions, 190, 194

theory, 179–183

transient flux and surfactant rejection, 184, 186

transient rejection, 177

variation of gel concentration with C1 concentration for several surfactants and membranes, 198*f*

variation of steady state permeate flux with feed concentration for DODDMAC using polyethersulphone (PES) membranes, 188*f*

variation of steady state permeate flux with feed concentration for DODDMAC using zirconia membranes, 189*f*

variation of steady state permeate flux with surfactant feed concentration for sodium diocylsulphosuccinate (Aerosol OT) using PES membranes, 191*f*

variation of steady state permeate flux with surfactant feed concentration for sodium linear alkyl (C₁₀–C₁₃) benzene sulphonate (Marion A390) using PES membranes, 192*f*

variation of steady state surfactant rejection with feed concentration for DODDMAC using PES membranes, 189*f*

variation of steady state surfactant rejection with feed concentration for DODDMAC using zirconia membranes, 191*f*

variation of steady state surfactant

rejection with feed surfactant concentration for Aerosol OT using PES and zirconia membranes, 192*f*

variation of steady state surfactant rejection with feed surfactant concentration for Marion A390 using PES membranes, 193*f*

variation of time shift parameter with Hamaker constant for membrane-water-surfactant system for several membranes and DODDMAC, 195*f*

zeta-potential of cationic surfactant DODDMAC and zirconia and cellulose nitrate (CN) membranes, 184, 185*f*

Cyanopropyl bonded phase columns

antibinding behavior, 303, 305

chromatograms of vanillin test mixture, 309, 310*f*, 311*f*, 312

relaxation parameters of alpha carbon nuclei in pure and adsorbed surfactant, 305*t*

semilog decay curves for cyano group carbon atom before and after surfactant adsorption, 305, 308*f*, 309

semilog decay plots for alpha carbon of solid and adsorbed ionic surfactants, 305, 306*f*, 307*f*

variable holding time experiments for ionic surfactants, 305

See also Selectivity in micellar liquid chromatography (MLC)

β-Cyclodextrin

effect in internal aqueous phase on vesicular solubilization, 222–226

See also Vesicle-enhanced ultrafiltration (VEUF)

D

Debye–Huckel–Henry equation, electrophoretic mobility, 332

Deinking papers with water-based inks

- carbon black particle redeposition, 391
- critical steps for efficient deinking, 385
- difficulty in deinking flexographic inks, 385
- driving force for use of water-based inks, 385
- effect of flexographic ink content on furnish on deinked sheet brightness, 386*f*
- effect of pilot plant unit operation on residual ink particle diameter, 411*f*
- flexographic ink chemistry, 387–389
- flotation deinking of
newsprint: magazine furnishes using different deinking surfactants, 413*f*
- flotation efficiency, 396–397
- improved deinking of flexographic furnishes, 401–412
- improved deinking process equipment, 415
- improved flotation deinking agents, 412–414
- improved water-based inks, 414–415
- improved water clarification, 414
- ink particle size after pulping, 389–391
- ink particle size distribution after pilot plant pulping with three different proprietary surfactants, 409*t*
- ink removal efficiency in flotation and wash deinking unit operations in pilot plant deinking, 410*t*
- operational problems for deinking mills, 384
- pilot mill flotation-wash deinking process flow diagram, 408*f*
- possible future developments, 412–415
- process water clarification, 410, 412
- redeposition of ink particles on fiber, 391, 394–396
- reusing paper fibers or printed plastic, 12
- small ink particles in offset newsprint deinking, 407–410
- wash deinking, 398–400
- water-based gravure inks, 396
See also Flexographic inks
- Denatured proteins. *See* Reversed micelles as novel protein refolding media**
- Dense non-aqueous phase liquids (DNAPL)**
increasing effective aqueous solubilities, 24
long-term source of contamination, 23
release of, 6
See also Sulfosuccinate surfactant mixtures; Surfactant-enhanced aquifer remediation (SEAR)
- Detergency studies, 391**
- Detergent manufacturing, recovery of surfactants for recycling, 176**
- Device design, ultrafiltration considerations, 4–5**
- Didodecyldimethylammonium bromide (DDAB)**
preparation, 202–204
stability, 204
See also Vesicle-enhanced ultrafiltration (VEUF)
- Didodecyldimethylammonium hydroxide (DDAOH)**
cationic surfactant, 338
counter-electroosmotic and co-electroosmotic flow, 333, 336
structure of DDAOH controlling electroosmotic flow (EOF), 337*f*
See also Capillary electrophoresis (CE)
- Dinonyl phenol polyoxyethylene (18) (DNP-18). *See* Surfactant-enhanced aquifer remediation (SEAR)**
- Diocetyltrimethylammonium chloride (DODDMAC). *See* Crossflow microfiltration behavior of surfactants**
- Diphenyl oxide disulfonates (DPDS), surfactant in liquid-liquid extraction study, 82**
- Disposal in secure landfill, dealing with contaminated soils, 8**

Distribution ratios of aromatic compounds between aqueous solution and surfactant covered silica

adsolubilization, 321, 324–325
 changes of distribution ratios at transition of head-on to head-out adsorption at pH 8, 326*f*
 characteristic four-region isotherm of cationic surfactant on silica surface at low ionic strength, 320*f*
 chemicals in study, 315, 317*t*
 chromatography, 317–318
 comparison of adsolubilization behaviors of 1,2-dichlorobenzene, diallylphthalate, 2,3-dimethylphenol, and 4-chlorophenol at pH 5 and pH 8, 321, 323*f*
 comparison of slope of region III at pH 5 to pH 8, 326*f*
 comparison of slopes of region I+II to region III at pH 8, 326*f*
 compounds representative of four groups, 321, 324*t*
 equilibrium constant equation, 315
 equilibrium constants for compounds in study, 324*t*
 equilibrium constants of organic acids (OA) and weak organic acids (WOA) at transition from head-out to head-on adsorption, 327
 experimental, 315, 317–318
 experimental set-up for determination of desorption efficiency, 319*f*
 experimental set-up for determination of distribution constants by chromatography, 319*f*
 hexadecyltrimethylammonium (HDTMA) bromide surfactant, 315
 hydrophobic organic compounds (HOC), 321, 324*t*
 measured surfactant adsorption isotherms of HDTMA on silica at pH 5 and pH 8, 320*f*
 model concept of adsolubilization in

chromatographic system, 316*f*
 non-ionic polar organic compounds (POC), 321, 324*t*
 OA with $pK_a < 10$, 321, 324*t*
 preferential adsorption of alkanes over polar organic compounds, 325
 proposed structure of adsorbed surfactant aggregates in different regions, 322*f*
 proposed two-site model describing adsolubilization, 325, 327
 retention times of 1,2-dichlorobenzene, diallylphthalate, 2,3-dimethylphenol, and 4-chlorophenol as function of surfactant coverage at pH 8, 322*f*
 structure of adsorbed surfactant aggregate determining equilibrium constants, 325
 surface pH calculation, 327
 surfactant adsorption, 318, 321
 theory, 315
 WOA with pK_a about 10, 321, 324*t*

Dodecane

collector for comparative purposes, 234

See also Coal

Dredged sludge

pollutants, 249
 remediation, 248–249
 water courses requiring dredging, 248
 See also Flotation of polycyclic aromatic hydrocarbon (PAH) contaminated dredged sludge

E

Economics, mobilization and solubilization process, 7–8

Electron paramagnetic resonance (EPR)

addition of paramagnetic broadener, 265, 266*f*
 equipment, 262

spectrum analysis methods, 262–263
See also Adsorption and aggregation
 of cationic surfactants on silica
 surfaces

Electroosmotic flow (EOF)

anodically directed EOF from
 formation of hemimicelles of
 quaternary ammonium surfactant,
 337*f*
 cationic surfactant didodecyl dimethyl
 ammonium hydroxide (DDAOH)
 controlling EOF, 336, 337*f*
 counter-electroosmotic and co-
 electroosmotic flow, 333, 336
 force affecting mobility of ions, 332–
 333
 physical phenomena creating EOF,
 335*f*
 zeta potential and cathodically
 directed EOF on unmodified fused-
 silica capillary, 335*f*
See also Capillary electrophoresis
 (CE)

Electrophoretic mobility

Debye–Hückel–Henry equation, 332
 mobility of ions, 332–333
See also Capillary electrophoresis
 (CE)

Enantiomer separation

chirotechnology, 123–124
 use of membranes for resolution of
 racemates, 124

Enantioselective micelles in

ultrafiltration systems
 analytical methods, 129
 apparent enantioselectivity, 135, 136*f*
 enantioselectivity, 127
 equation for confidence intervals, 131
 equations for single- and
 multicomponent isotherms, 126
 experimental materials D-, L-, and DL-
 phenylalanine (Phe), 127–128
 experimental set-up of Amicon cell
 and impression of enantiomer
 separation at membrane, 124, 125*f*
 fitting multicomponent complexation

isotherms, 132–135
 fitting single-component complexation
 isotherms, 129, 131–134
 intrinsic enantioselectivity and 95%
 confidence intervals from single-
 component isotherms, 132
 intrinsic enantioselectivity from
 multicomponent isotherms, 135
 Langmuir constants, intrinsic
 selectivity, and 95% confidence
 intervals by fitting single- and
 multicomponent isotherms, 131*f*
 measured permeate concentrations,
 129
 membranes for resolution of
 racemates, 124
 multicomponent Langmuir
 parameters, 133
 parity plots of measurements and
 predictions for D-Phe and L-Phe,
 134*f*
 residual sum of squares calculation,
 129, 131
 single- and multicomponent
 complexation isotherms of D-Phe
 and L-Phe, 134*f*
 single- and multicomponent Langmuir
 complexation isotherms, 126–127
 single-component complexation
 isotherms of D-Phe and L-Phe, 130*f*
 single-component Langmuir
 parameters and 95% confidence
 intervals, 131–132
 standard error of D-Phe and L-Phe
 permeate concentrations as function
 of permeate concentration, 130*f*
 standard error of intrinsic
 enantioselectivity, 132
 theory, 126–127
 total solute concentrations and
 conditions in ultrafiltration
 experiments, 128*f*
 ultrafiltration experiments, 128
 variance-covariance matrix, 131
Enantioselectivity, theory, 127
Enthalpy and entropy of mixing

Flory–Huggins model, 95–96
 modified Flory–Huggins model, 96–97

Environmentally responsive polymeric surfactants. *See* Wastewater remediation

Environmental Protection Agency's National Risk Management Research Laboratory (EPA–NRMRL)

application of pervaporation to surfactant solutions, 60–61
 performance of EPA–NRMRL pervaporation pilot unit, 62*f*
 pilot and bench-scale tests of pervaporation, 61
See also Pervaporation; Volatile organic compound separation from surfactants by pervaporation

Environmental remediation

conventional "pump-and-treat" for remediating NAPL contaminated aquifers, 6
 difficulty of removing light non-aqueous phase liquid (LNAPL), 5
 proposed mechanisms for remediating NAPL contaminated aquifers, 6–8
 recovery of surfactants for recycling, 176
 solubilization and mobilization
 , mechanisms, 6–8
 use of surfactants, 5

Equilibrium dialysis

analysis of experiments, 115–116
 experiments, 115
 modeling micellar-enhanced ultrafiltration (MEUF), 114

See also Wastewater remediation

Equilibrium partitioning in closed systems (EPICS) headspace method, determining Henry's law constants, 64, 68

Excavation and disposal, contaminated soils, 8–9

Ex situ soil treatment

representation of multi-step ex situ extraction with microemulsion, 52*f*

soil remediation, 36
 solid/liquid separation, 51

Ex situ surfactant soil washing, decontaminating excavated soils, 8

Extraction

cloud point or coacervate, 11–12
 use of reverse micelles, 11

F

Flexographic inks

acidic conditions improving removal efficiency, 401
 adverse effect of water hardness on flotation-wash deinking, 402, 403*f*
 anti-deposition agents in laundry detergent formulations, 402, 404
 behavior of small particles in flotation, 397
 brightness differences, 394
 brightness of deinked flexographic newsprint using different washer types, 400*t*
 cationic polymer as flotation additive in flotation deinking, 404
 chemistry, 387–389
 composition of ink 1, 394*t*
 deinking results for 90:10
 offset:flexographic newsprint furnish, 398*t*
 difficulty in deinking from newsprint, 385
 direct study of deposition of dispersed particles onto cellulose fibers, 391
 dispersed inks depositing in fiber mats, 400
 economical process for competitive advantage, 385, 387
 effect of anti-deposition agents on brightness, 405*f*
 effect of flexographic ink content on furnish on deinked sheet brightness, 386*f*
 effect of flexographic newsprint on deinked sheet brightness of offset newsprint furnish, 396*t*

- effect of increasing flexographic ink content of furnish on pulp brightness after flotation and washing, 399*f*
- effect of pilot plant unit operation on residual ink particle diameter, 411*f*
- effect of pulping time on brightness gain in flotation and post-flotation step, 399*f*
- effect of pulping time on pulp brightness, 394, 395*f*
- effect of pulping time on pulp brightness loss relative to imprinted paper in absence of ink, 394, 395*f*
- environmental scanning electron microscope (SEM) image of flexographic ink character on newsprint, 388*f*
- factors contributing to formation of very small ink particles in pulping, 389
- flotation efficiency, 396–397
- hyperwashing, 407
- improved deinking of flexographic furnishes, 401–412
- improved deinking process equipment, 415
- improved flotation deinking agents, 412–414
- improved water-based inks, 414–415
- improved water clarification, 414
- improving flotation ink removal efficiency, 401–402
- ink particle distribution after pilot plant pulping, 409*f*
- ink particle size after pulping, 389–391
- ink particle size distributions for offset and flexographic newsprint ink after pulping, 390*f*
- ink removal efficiency in flotation and wash deinking unit operations, 410*f*
- line drawing of residual flexographic ink particles after deinking, 393*f*
- newsprint ink compositions, 387*f*
- optical properties of flexographic newsprint after pulping, 407*f*
- pilot plant process flow diagram, 408*f*
- pilot plant test for effect of sodium polyacrylate on pulp brightness, 406*f*
- possible future developments, 412–415
- process water clarification, 410, 412
- readily dispersible in aqueous pulping media, 389
- redeposition of ink particles on fiber, 391, 394–396
- redeposition onto cellulose and reduced brightness, 394, 396
- reducing ink redeposition onto cellulose fiber, 402–407
- role of collision frequency in determining flotation efficiency, 397
- scanning probe microscopy (SPM) of flexographic ink printing on newsprint, 390*f*
- small ink particles in offset newsprint deinking, 407–410
- SPM image of residual flexographic ink particles after deinking, 392*f*
- use of anti-deposition agents, 404
- varying alcohol ethoxylate deinking surfactant HLB (hydrophilic:lipophilic balance) value in flotation study, 397
- wash deinking, 398–400
- water-based gravure inks, 396
- Flory–Huggins**
- model for solubilization properties of PEO–PPO block copolymer, 95–96
- prediction versus model, 99
- Flory–Huggins, modified**
- model for solubilization properties of PEO–PPO block copolymer, 96–97
- modeling hydrocarbon solubilization, 103, 107
- See also* Block copolymer micelles for water remediation
- Flotation based processes**
- coal flotation, 231–232
- deinking, 12
- fine coal flotation, 234–235

froth flotation, 9–10
 most commercially important
 application of surfactants in
 separations, 10
 oxidized coals, 243
 separation, 9–11
 Winsor Type III microemulsion result,
 9–10

See also Coal

Flotation deinking

controversial mechanism, 12
 flotation efficiency, 396–397
 improved agents, 412–414
 improving efficiency, 401–402
See also Deinking papers with water-
 based inks; Flexographic inks

Flotation of polycyclic aromatic hydrocarbon (PAH) contaminated dredged sludge

chemicals and water, 249
 contact angles, 253–254
 determination of contact angles, 250
 efficiency of test for sludges, 256, 258
 experimental materials and methods,
 249–252
 flotation reagents, 249–250
 flotation test methods, 250–252
 flotation tests, 254–256
 Hallimond type flotation tube, 251*f*
 oil analysis, 252
 organic matter analysis, 252
 organic matter content of both tailings
 and floated material of Overschie
 sludge, 255*f*
 organic matter content of both tailings
 and floated material of Petrol
 Harbor sludge, 257*f*
 Overschie and Petrol Harbor sludges,
 250
 Overschie sludge, 254, 256
 PAH concentration and dry matter
 content of tailings and original
 Overschie sludge, 255*f*
 PAH concentration and dry matter
 content of tailings and original
 Petrol Harbor sludge, 257*f*

PAHs analysis, 252
 Petrol Harbor sludge, 256
 sludge composition, 252, 253*t*

Fluorinated solvents. *See* Particulate removal from oxygen systems

Flux decay, effect of electrostatic and van der Waals forces, 194

Fluxes. *See* Spiral wound ultrafiltration

Fractionation

foam, 10
 phenomenon as basis for foam, 9
 separation process, 9–10

Froth flotation, mineral particles in aqueous suspension, 231

Fuel leaks, environmental remediation, 5

G

Gel concentration

estimation of surfactant concentration
 in secondary membrane, 178
See also Crossflow microfiltration
 behavior of surfactants

Gel polarization and rejection. *See* Crossflow microfiltration behavior of surfactants

Gibbs–Thomas equation

modeling hydrocarbon solubilization,
 103, 107

D-Glucose, trapping efficiency in vesicles, 202, 204, 205*f*

H

Hamaker constant

surfactant/water/membrane system,
 182
 values for membranes, 186*t*

Head-out to head-on adsorption. *See* Distribution ratios of aromatic

compounds between aqueous solution and surfactant covered silica

Headspace method, determining Henry's law constants, 64, 68

Hemimicelles, surfactant aggregates, 9, 260

Henry's law constants

headspace method for determining, 64, 68

magnitude of impact of surfactant with type of volatile organic compound (VOC), 67*f*, 68

Hexadecyl trimethyl ammonium bromide (HTAB)

adsorption on silica gel at pH 5 and pH 8, 318, 320*f*

binding on silica, 263, 265–270

cationic surfactant, 315

effect of HTAB addition to electron paramagnetic resonance (EPR)

spectra from spin-labeled HTAB (HTAB*) adsorbed onto 1.5 wt% silica, 267, 269*f*, 270

effect of silica amount on EPR spectra of HTAB*, 267, 268*f*

electrostatically driven adsorption on silica, 318, 321

EPR spectra of slow rotating HTAB*, 265, 266*f*

experimental, 262–263

experimental and simulated EPR from HTAB and HTAB* adsorbed on silica, 264*f*

HTAB*, 261

investigations of counter-ion binding, 271, 273–274

nitrosodisulfonate spin-probe, 273–274

presence of paramagnetic broadener, 265, 266*f*

quaternary ammonium surfactant, 261

schematic showing various equilibria between silica surface and HTAB and HTAB*, 272*f*

strong binding site on silica, 270–271

See also Adsorption and aggregation of cationic surfactants on silica surfaces; Distribution ratios of aromatic compounds between aqueous solution and surfactant covered silica

Hollow fiber, ultrafiltration unit, 4

Hollow fiber membrane

contactor, 79–80

See also Liquid-liquid extraction in hollow fiber membrane

Hydrocarbons

difficulty in removing, 5–6

modeling solubilization, 103, 107

solubilization, 103

Hydrofluorocarbons (HFCs)

current research background, 357

experimental materials, 358

See also Particulate removal from oxygen systems

Hydrophobic nonvolatile

contaminants, liquid-liquid extraction, 77–78

Hyperwashing pulp washing, 407

I

Inductively coupled plasma mass spectrometry (ICPMS)

element selective detection, 278

See also Speciation of metal-containing compounds

Inks. *See* Deinking papers with water-based inks; Flexographic inks; Offset inks

In situ soil treatment soil remediation, 36

Intrinsic enantioselectivity

multicomponent isotherms, 135

single-component isotherms, 132

See also Enantioselective micelles in ultrafiltration systems

Ionic surfactants, microemulsions, 39

Isotherms, complexation. *See* Enantioselective micelles in ultrafiltration systems

J

Jacobian matrix, variance-covariance matrix equation, 131

K**Kinetics**

complex formation, 146–152
 kinetic separations, 146
 ways of affecting complex formation, 149, 152
See also Metal ion removal from aqueous environments

L

Landfilling, alternatives to, 8–9

Langmuir complexation isotherms

fitting multicomponent, 132–135
 fitting single-component, 129, 131–132
 multicomponent parameters, 133
 single-component parameters, 131–132
 theory of single- and multicomponent, 126–127
See also Enantioselective micelles in ultrafiltration systems

Leakage of monomer, ultrafiltration technology, 2–3

Letterpress inks

newsprint ink compositions, 387*f*
See also Deinking papers with water-based inks

Ligand-modified micellar-enhanced ultrafiltration, metal ion removal, 3–4

Light non-aqueous phase liquid (LNAPL)

addressing residual contamination, 6
 difficulty of removing, 5

Liquid chromatography, versatility of technique, 277

Liquid-liquid extraction, water remediation, 92–93

Liquid-liquid extraction in hollow fiber membrane

background, 77–81
 contaminant removal at different aqueous and squalane flowrates, 86–87
 contaminants tetrachloroethylene (PCE) and *iso*-butylbenzene (IBB), 81–82
 diphenyl oxide disulfonates (DPDS) and polyethoxylated nonylphenol (ENP) surfactants, 82
 effect of micellar surfactant in liquid-liquid extraction, 79
 effect of presence of micellar pseudophase on contaminant removal, 84–85
 establishing counter-current flow of oil and aqueous phase, 83
 experimental methods, 83–84
 high performance liquid chromatograph (HPLC), 84
 hollow fiber membrane contactor, 79–80
 interface in pores of hydrophobic membrane, 80*f*
 liquid-liquid extraction, 77–78
 materials, 81–83
 membrane column for liquid-liquid extraction experiments, 83
 micellar partition coefficient, 78
 model, 80–81
 overall mass transfer coefficient, 87–88
 partition coefficients for PCE and IBB, 84
 percent contaminant removal from DPDS and ENP solutions, 85, 86*f*
 properties of squalane, 83*f*
 pseudophase separation model of liquid-liquid extraction, 81*f*
 solvent-water partition coefficient, 77
 squalane as solvent, 82
 squalane-water-contaminant equilibrium experiments, 83

surfactant properties, 78–79

M

Mass transfer coefficient

calculation, 87
 comparing to values from empirical equations, 88
 overall coefficient with varied aqueous and constant oil flowrate, 88*f*
See also Liquid-liquid extraction in hollow fiber membrane

Membranes

experimental for crossflow microfiltration, 184
 physico-chemical and physical characteristics, 186*t*
See also Crossflow microfiltration behavior of surfactants

Mercury compounds

capacity factor (k') definition, 283
 effect of added organic modifier, 283, 285
 effect of surfactant concentration, 283
 interaction with micelles, 281, 283, 285
 separation of inorganic and alkyl mercury compounds, 282*f*
 separation of inorganic and organic, 279
 variation of k' with 2-propanol concentration in mobile phase, 286*f*
 variation of k' with ammonium dodecyl sulfate concentration, 284*f*
See also Speciation of metal-containing compounds

Metal and metalloid containing compounds

determining chemical form, 276
 effect of analyte charge versus hydrophobicity, 288
 interaction with micelles, 281, 283, 285
 partitioning behavior into micelles, 285, 287–288

partitioning into micelle, 287–288
 properties, 277–278
 typical speciation methods, 276–277
See also Speciation of metal-containing compounds

Metal ion removal, ligand-modified micellar-enhanced ultrafiltration, 3–4

Metal ion removal from aqueous environments

advantages and drawbacks of micellar extraction compared to solvent extraction, 152, 154
 chemical factors affecting rejection rate of metal ions, 143, 146
 copper complexation rate constants versus temperature by diC₁₂NMePyr in vesicles, 152, 153*f*
 copper extraction versus pH for C₁₁-HQ (7-(4-ethyl-1-methyloctyl)-8-hydroxyquinoline) in C₁₂EO₆ micelles and in biphasic water/isooctane systems, 154, 155*f*
 extractants solubilized in micelles, 140, 141*t*
 extraction of copper(II) in CTAB micelles, 143, 144*f*
 increasing partition coefficient of complexing agent by adding oil to micellar core, 149, 150*f*
 increasing separation between complexing agent and metal ion, 149
 ionization state of extractant, 143
 kinetic separation and factors influencing kinetics of complex formation, 146–152
 kinetic separation of mixture of Ni²⁺ and Co²⁺ ions, 146, 148*f*
 kinetic separations, 146
 lipophilicity of extractant, 143
 micellar surface charge, 143, 146
 rate of extractant/metal complex formation in microheterogeneous systems at 25°C, 146, 147*t*
 stabilizing complexing agent inside micelles by ion-pairing interactions

- between surfactant and complexing agent, 149, 151*f*
- surfactant-based colloidal particles and investigated parameter, 142*f*
- using polymerized micelles or vesicles, 149, 152
- variation of copper complexation rate constants as function of n in extractant $C_nNHMePyr$ (6-(alkylamino)methyl-2-(hydroxymethyl)pyridines), 152, 153*f*
- ways of affecting kinetics of complex formation, 149, 152
- yield of copper extraction versus extractant to metal ratio, 143, 145*f*
- Metallic ions, separation in mixture, 140**
- Micellar-enhanced ultrafiltration (MEUF)**
- addition of micelle solution to polluted stream, 93, 113–114, 158–159, 201
- basis for, 176
- comparison of cetyl pyridinium chloride (CPC) and 4-*t*-butylphenol (TBP) concentrations for different molecular weight cutoff (MWCO) spiral wound membranes, 167*f*, 169*f*
- comparison of CPC, sodium dodecyl sulfate (SDS), and TBP permeate concentrations for different spiral wound MWCO membranes, 165, 168
- comparison of flux for stirred cell and spiral wound 5,000 MWCO membranes, 165, 166*f*
- comparison of permeate CrO_4^{2-} concentration for semi-equilibrium dialysis cell membrane and spiral wound membrane, 172*f*
- comparison of permeate Cu^{2+} concentration for stirred cell and spiral wound membranes (20,000 MWCO), 168, 171*f*
- comparison of SDS and TBP permeate concentrations for different MWCO spiral wound membranes, 169*f*, 170*f*
- comparison of stirred cell and spiral wound permeate concentrations for organic solute with 5,000 MWCO membrane, 165
- concentrating surfactant prior to reinjection, 8
- concentration step, 25
- device design considerations, 4–5
- economic advantages, 158
- effect of added electrolyte on surfactant permeate concentration, 168, 170*f*
- enantiomer separation, 124, 125*f*
- equilibrium dialysis experiments with Pluronic F127 as solubilization agent, 114
- experimental materials, 160
- experimental methods, 160
- first surfactant-enhanced process, 2–5
- flow diagram of ultrafiltration apparatus, 161*f*
- fluxes and permeate concentrations for SDS, 162
- fluxes using CPC surfactant and target organic TBP, 162, 165
- illustration of components of ultrafiltration spiral wound membrane, 163*f*
- illustration of MEUF applied to removal of target organic and multivalent cationic metal in aqueous solution, 161*f*
- monomer leakage, 2–3
- permeate concentrations of TBP and CPC with outlet retentate flowrate, 162, 165
- permeate CPC and TBP concentration for stirred cell and spiral wound membranes, 166*f*, 167*f*
- permeate CPC and TBP concentrations using CPC and 5,000 MWCO spiral wound membrane, 164*f*
- pilot plant with spiral wound membrane, 161*f*

- predicting efficiency, 159
 rejection of Cu^{2+} for spiral wound
 10,000 MWCO membrane, 171*f*
 relative permeate flux using CPC and
 5,000 MWCO spiral wound
 membrane, 163*f*
 removal of organic pollutants from
 aqueous streams, 109, 110*f*
 removing anionic or cationic
 multivalent species, 159
 selectivity in solute removal, 3–4
 spiral wound/semi-equilibrium
 dialysis systems with metal
 ions/metal complexes, 168, 172
 spiral wound unit separating nonionic
 organic solute using anionic or
 cationic surfactant, 162
 surfactant regeneration, 3
 use of surfactant aggregates other than
 micelles, 4
See also Enantioselective micelles in
 ultrafiltration systems; Surfactant-
 enhanced aquifer remediation
 (SEAR); Ultrafiltration; Wastewater
 remediation
- Micellar extraction, evaluating
 advantages and drawbacks, 152,
 154**
- Micellar liquid chromatography
 (MLC)**
 enhancing analytical separations, 11
 surfactants for use, 277
See also Selectivity in micellar liquid
 chromatography (MLC); Speciation
 of metal-containing compounds
- Micellar partition coefficient,
 definition, 78**
- Micellar reversed phase liquid
 chromatography (RPLC). *See*
 Selectivity in micellar liquid
 chromatography (MLC)**
- Micellar surfactant, effect in liquid-
 liquid extraction, 79**
- Micelles**
 admicelles, 9
 effect of added organic modifier on
 interaction with metal-containing
 compounds, 283, 285
 effect of surfactant concentration on
 interaction with metal-containing
 compounds, 283
 formation dependence upon bulk
 mobile phase characteristics, 277–
 278
 hemimicelles, 9
 interaction with metal-containing
 compounds, 281, 283, 285
 interior solubilizing organic solutes,
 159
 polymeric surfactants forming, 2
 role in separation processes, 139–140
 surfactant aggregates, 9
 surfactant aggregates other than, 4
 surfactant-based colloidal particles
 and investigated parameter, 140,
 142*t*
- Microelectronic industry, particulate
 contamination problem, 355**
- Microemulsions**
 bicontinuous, with nonionic
 surfactants, 45–47
 formulation, 45–47
 ionic surfactants, 39
 mixtures of nonionic and ionic
 surfactants, 39, 47
 nonionic surfactants, 37, 47
 phase behavior of systems, 37–39
 pollutant separation, 51–54
 properties, 36
 remediation processes, 41
 soil extraction with oil/water (O/W),
 48
 surfactant aggregates, 4
See also Nonionic bicontinuous
 microemulsions; Soil remediation
 with microemulsions
- Mineral flotation, collectors, 239**
- Mobilization, mechanism for
 remediating non-aqueous phase
 liquid (NAPL) contaminated**

aquifers, 6–8

Modified Flory–Huggins

corresponding with experimental, 99, 103

model for solubilization properties of PEO–PPO block copolymer, 96–97

modeling hydrocarbon solubilization, 103, 107

See also Block copolymer micelles for water remediation

Monomer leakage, limitation of ultrafiltration technology, 2–3

N

Newsprint deinking. *See* Deinking papers with water-based inks; Flexographic inks

Nickel ions

kinetic separations, 146, 148*f*

rate of extractant/metal complex formation in microheterogeneous systems, 147*t*

stabilizing complexing agent inside micelles, 149, 151*f*

See also Metal ion removal from aqueous environments

Nitrosodisulfonate radical

electron paramagnetic resonance (EPR) spectra, 271, 272*f*, 273

EPR spectra from nitrosodisulfonate spin probe added to suspensions of silica with different amounts of surfactant, 273–274

structure, 261

See also Adsorption and aggregation of cationic surfactants on silica surfaces

Non-aqueous phase liquid (NAPL)

conventional approach to remediating NAPL contaminated aquifers, 6
solubilization and mobilization mechanisms, 6–8

Nonionic bicontinuous

microemulsions

extraction experiments, 43

pollutant separation, 51

soil extraction, 47–48, 50

Nonionic surfactants

microemulsions, 37

microemulsions with mixed anionic and, 47

Nonionic surfactants as collectors

aqueous solubility and boiling points of some 4-carbon oxygenated compounds, 241*t*

ash rejection as function of

combustible matter recovery with various collectors, 244*f*

basicities of saturated ethers in aqueous sulfuric acid, 241*t*

chemical name and source of reagents in study, 233*t*

collection mechanisms, 239–243

comparison of collecting ability of nonionic THF-17en surfactant with dodecane, nonylphenol, nonylbenzene, and GH4 (polyethoxylated nonylphenol), 237*f*

comparison of collecting ability of nonionic THF-17 surfactants with dodecane for coal flotation, 238*f*

comparison of collecting ability of THF-17 and THF-11 with dodecane, 245*f*

comparison of required dosages of different reagents, 242*f*

experimental materials, 232

experimental procedure, 234

fine coal flotation, 234–235

flotation of oxidized coals, 243

flotation results of Illinois No. 6 coal, 243, 246

mechanisms for attachment of THF series to coal surface, 240, 243

molecular structure of series of coal collectors, 236*t*

series of tetrahydrofurfuryl esters, 232, 234

tetrahydrofurfuryl butyrate effective collector for Illinois No. 6 coal, 232

O

Offset inks

effect of flexographic newsprint on deinked sheet brightness of offset newsprint furnish, 396*t*
 environmental scanning electron microscope (SEM) image of offset character on newsprint, 387, 388*f*
 ink particle size distributions for offset and flexographic newsprint ink after pulping, 390*f*
 newsprint ink compositions, 387*t*
 small ink particles in offset newsprint deinking, 407–410
See also Deinking papers with water-based inks; Flexographic inks

Oils

choice for treatment of contaminated soils, 41
 determination, 45

Organic compound removal. *See* Vesicle-enhanced ultrafiltration

Organo-tin compounds

separation, 281
 separation of mono- and tri-methyl tin compounds, 284*f*
 separation of tri-alkyl tin compounds, 282*f*
See also Speciation of metal-containing compounds

Oxygen systems

alcohol flush, 354
 alternative solvents and cleaning techniques, 354–356
 ASTM cleaning of metal coupons, 364
 cleaning techniques, 355–356
 experimental perfluorocarbons (PFCs) and hydrofluorocarbons (HFCs), 358
 experimental setup for cleaning oxygen reservoirs, 359

glass slide study using ultrasound, 365–371
 importance of cleaning, 352
 lowest particle size removable by various methods, 356*t*
 Navy oxygen cleaner (NOC) flush, 354
 oxygen line cleaning, 352–353
 particle adhesion and dispersion, 353
 previous cleaning alternatives, 353–354
 results of ASTM G93-88 procedure, 359–364
 surface tension values of various liquids, 355*t*
 trichloroethylene (TRIC) flush, 354
See also Particulate removal from oxygen systems

Ozone depletion

motivating search for chlorofluorocarbon (CFC) replacements, 351–352
See also Chlorofluorocarbon (CFC) solvents

P

Paper recycling

deinking processes, 12
 surfactant-induced deinking, 1

Particulate removal from oxygen systems

alcohol flush, 354
 alternative solvents and cleaning techniques, 354–356
 ASTM cleaning of metal coupons, 364
 cleaning of oxygen lines, 368–371
 cleaning procedures by ASTM G93-88 procedure, 358
 cleaning techniques, 355–356
 comparison of pure solvents and Freon R-113, 366*f*
 comparison of surfactant performance in hydrofluorocarbon (HFC) and perfluorocarbon (PFC) solvents, 366*f*, 367*f*

current research background, 357
 enhancement by increasing flowrate
 across contaminated surface, 370,
 371*f*
 experimental cleaning oxygen line and
 reservoirs, 357–358
 experimental PFCs and HFCs, 358
 experimental setup for cleaning
 oxygen reservoirs, 359
 factors affecting detachment of
 particles, 356
 glass slide study using ultrasound,
 365–371
 lowest particle size removable by
 various methods, 356*t*
 mockup sample point, 368*f*
 Navy oxygen cleaner (NOC) flush,
 354
 non-aqueous surfactant based cleaning
 formulations, 357
 oxygen line bench scale unit, 368*f*
 oxygen line cleaning, 352–353
 particle adhesion and dispersion, 353
 PFCs and HFCs as replacement
 candidates, 354–355
 previous cleaning alternatives, 353–
 354
 results of ASTM G93-88 procedure,
 359
 scanning electron microscopy (SEM)
 photograph of sample surface
 following ASTM G93-88 procedure
 with pure Freon R-113, 360*f*
 SEM photographs of samples used in
 line system, 369*f*
 SEM photographs of surfaces from
 interior of oxygen reservoir before
 and after cleaning with various
 solvent-surfactant combinations
 using swirling test, 361*f*, 362*f*, 363*f*,
 364*f*
 surface tension values of various
 liquids, 355*t*
 surfactant spray cleaning, 356
 trichloroethylene (TRIC) flush, 354

ultrasonication of glass slides, 365–
 367

**Partition coefficient, contaminants
 tetrachloroethylene (PCE) and iso-
 butylbenzene (IBB), 84**

Partitioning

behavior of metal-containing
 compounds into micelles, 285, 287–
 288

calculated values of micelle-solute
 equilibrium constants, 287*t*

concept of organic compound between
 water and surfactant coated silica,
 316*f*

effect of analyte charge versus
 hydrophobicity, 288

effect of temperature and surfactant
 concentration on vapor-liquid, 64,
 66*f*, 68

pictorial representation between
 surfactant micelles and extramolecular
 region, 63–64, 65*f*

See also Volatile organic compound
 separation from surfactants by
 pervaporation

Perchloroethylene (PCE)

aquifer contamination for testing, 24–
 25

PCE solubilization versus salinity for
 80/20 system, 30, 31*f*

See also Sulfosuccinate surfactant
 mixtures

Perfluorocarbons (PFCs)

current research background, 357

experimental materials, 358

See also Particulate removal from
 oxygen systems

**Perraction-based process, removal
 of organic pollutants from aqueous
 streams, 109, 110*f***

Pervaporation

application to surfactant solutions, 60–
 61

background, 58–61

comparison of predicted to observed

pervaporation performance, 71–72
current uses, 60

demonstrations for volatile organic compounds (VOC) recovery from groundwater, 60

Henry's law constant, 64

impact of surfactants on removal of VOCs, 63–72

Lévêque's correlation, 63

Reynolds (Re) and Schmidt (Sc) numbers, 61

schematic diagram of cell, 59f

schematic diagram of proposed integrated field demonstration of surfactant remediation and recovery/reuse, 62f

schematic diagram of system, 59f
theory, 61, 63

See also Surfactant-enhanced aquifer remediation (SEAR); Volatile organic compound separation from surfactants by pervaporation

Phenol

dependence of K for phenol in didodecyl dimethyl ammonium bromide (DDAB) vesicles on intravesicular solute mole fraction, 217f

dependence of normalized solubilization equilibrium constant (K) on dissociation degree of Br⁻ for phenol, 215f

parameters for K equation, 218t

vesicle diameter dependence of K, 216–220

See also Vesicle-enhanced ultrafiltration (VEUF)

2-Phenylethanol (PEA)

dependence of K for PEA in didodecyl dimethyl ammonium bromide (DDAB) vesicles on intravesicular solute mole fraction, 219f

parameters for solubilization equilibrium constant (K) equation, 218t

solubilizing ability of DDAB vesicles, 222

values of K at infinite dilution for PEA in different vesicles and micelles, 223t

vesicle diameter dependence of K, 216–220

See also Vesicle-enhanced ultrafiltration (VEUF)

3-Phenylpropionic acid (HCA)

dependence of K for HCA in didodecyl dimethyl ammonium bromide (DDAB) vesicles on intravesicular solute mole fraction, 219f

parameters for solubilization equilibrium constant (K) equation, 218t

vesicle diameter dependence of K, 216–220

See also Vesicle-enhanced ultrafiltration (VEUF)

Phenylalanine (Phe)

apparent enantioselectivity, 135, 136f
D- and L- enantiomers, 127

fitting multicomponent complexation isotherms, 132–135

fitting single-component complexation isotherms, 129, 131–132

ultrafiltration experiments, 128

See also Enantioselective micelles in ultrafiltration systems

Plastic recycling, deinking processes, 12

Plate and frame, ultrafiltration unit, 4

Pluronics

amphiliphilic poly(ethylene oxide)–poly(propylene oxide)–poly(ethylene oxide) (PEO–PPO–PEO) type, 93

See also Block copolymer micelles for water remediation; Wastewater remediation

Pollutants

separation, 51–54

separation form nonionic bicontinuous microemulsion, 51

separation from anionic/nonionic
bicontinuous microemulsion, 53–54
separation from O/W microemulsion,
51, 53

Polychlorinated biphenyls (PCB)

determination, 44–45
separation from anionic/nonionic
bicontinuous microemulsion, 53–54
soil doping, 43
See also Soil remediation with
microemulsions

**Polycyclic aromatic hydrocarbons
(PAH)**

contaminant for soil extraction, 47–48,
50
pollutants in dredge sludge, 249
See also Flotation of polycyclic
aromatic hydrocarbon (PAH)
contaminated dredged sludge; Soil
remediation with microemulsions

Polyethersulphone (PES)

membranes. *See* Crossflow
microfiltration behavior of
surfactants

**Polyethoxylated nonylphenol (ENP),
surfactant in liquid-liquid
extraction study, 82**

**Poly(ethylene oxide)–poly(propylene
oxide)–poly(ethylene oxide) (PEO–
PPO–PEO)**

equilibrium dialysis experiment using
F127 triblock copolymer as
solubilization agent, 114
generalized phase diagram, 94f
See also Block copolymer micelles for
water remediation; Wastewater
remediation

**Polymeric surfactants, micelles and
complexes solubilizing organic
solutes, 2**

Polymerized micelles

affecting kinetics of complex
formation, 149, 152
kinetics of copper complexation, 152,
153f

surfactant aggregates, 4
surfactant-based colloidal particles
and investigated parameter, 140,
142f

**Polymer/surfactant complexes,
solubilizing organic solutes, 2**

**Polyoxyethylene (20) sorbitan
monooleate (Tween 80). *See*
Surfactant-enhanced aquifer
remediation (SEAR)**

**Polyoxyethylene (4) sorbitan
monolaurate (Tween 21). *See*
Surfactant-enhanced aquifer
remediation (SEAR)**

**Propylene oxide (3.8) sulfate
(Isalchem 145). *See* Surfactant-
enhanced aquifer remediation
(SEAR)**

**Protein refolding. *See* Reversed
micelles as novel protein refolding
media**

Provisional Technical

**Secretariat/Preparatory
Commission for Organization for
Prohibition of Chemical Weapons
(PTS/OPCW), 0laboratories for
Round-Robin testing**

analysis of aqueous sample from
second official PTS/OPCW
proficiency test water sample, 346f
analysis of aqueous sample from third
official PTS/OPCW proficiency test
water sample, 345, 347f, 348f
analysis of second and third official
PTS/OPCW proficiency test water
samples, 342, 345
laboratories for Round-Robin testing,
336
results from second and third official
PTS/OPCW proficiency tests, 346f
See also Capillary electrophoresis
(CE)

**Pseudo-phase equilibrium model,
study of air stripping and liquid-
liquid extraction processes, 80–81**

Pump-and-treat

- conventional approach to remediating non-aqueous phase liquid (NAPL) contaminated aquifers, 6
- expediting process in groundwater remediation, 76
- mass transfer limitations of dense non-aqueous phase liquids (DNAPL), 23–24

Pyrene

- contaminant for soil extraction, 47–48, 50
- determination, 44
- distribution after splitting, 44
- experimental, 41
- separation from O/W microemulsion, 51, 53
- See also* Soil remediation with microemulsions

R**Racemates**

- resolution, 124
- See also* Enantioselective micelles in ultrafiltration systems

Rape oil methyl ester (RME)

- determination, 45
- experimental, 43
- extraction of pyrene from O/W microemulsion, 51, 53
- ideal oil for bicontinuous emulsions, 41
- microemulsion formulation, 45–47
- temperature-induced separation of RME and pyrene from doped microemulsion, 52*f*

Refolding of protein. *See* Reversed micelles as novel protein refolding media

Regeneration of surfactant, ultrafiltration technology, 3**Rejection**

- effect of electrostatic forces, 194

- effects of van der Waals forces, 194
- surfactant, 186
- transient, 177

See also Crossflow microfiltration behavior of surfactants

Remediation. *See* Environmental remediation; Wastewater remediation**Removal of solvent, selectivity in ultrafiltration technology, 3–4**

- Residual sum of squares (RSS)** multicomponent equation, 133
- single component equation, 129

Resolution of enantiomers. *See* Enantioselective micelles in ultrafiltration systems**Reversed micelles as novel protein refolding media**

- effect of added acetone on recovery and activity yields of renatured RNase A from reversed micellar solution, 382*t*, 383
- effect of pH in water pools of reversed micelles on renaturation of RNase A, 381*f*
- effect of ratio of reduced and oxidized glutathione on renaturation yield and renaturation rate, 380*f*
- effect of sodium di-2-ethylhexyl sulfosuccinate (AOT) concentration in isooctane on both solubilization and average diameter of reversed micelles after solubilization, 378*f*
- effect of water content in reversed micelles on renaturation rates, 381*f*
- effect of water content on solubilization of solid denatured RNase A, 378*f*
- electrostatic attraction between surfactants and protein surface, 379
- experimental materials, 375
- improving efficiency of refolding at higher protein concentration, 375
- preparation of solid denatured RNase A as model of inclusion bodies, 376

recovery of renatured RNase A from reversed micelles, 377, 382–383
 renaturation of denatured RNase A in reversed micelles by redox reagents, 379–382

renaturation of RNase A in reversed micelles, 376

RNase A activity assay in aqueous solution and in reversed micelles, 376

schematic of protein refolding by reversed micellar solution utilizing solid-liquid extraction technique, 375*f*

solubilization of solid denatured RNase A into reversed micelles by solid-liquid extraction, 377–379

solubilization of solid denatured RNase A into reversed micelles by solid-liquid extraction technique, 376

Reversed phase liquid

chromatography (RPLC). See

Selectivity in micellar liquid

chromatography (MLC)

Reynolds (Re) number, definition, 61

S

Scatchard plots, Pluronic F127 and *p*-cresol foulant system, 118

Schmidt (Sc) numbers, definition, 61

Secondary membrane

crossflow membrane filtration of surfactant, 177

estimation of surfactant concentration, 178

theory of development, 177–183

See also Crossflow microfiltration behavior of surfactants

Selectivity in micellar liquid

chromatography (MLC)

C-18 bonded phase column retention data, 294, 297

changes in alpha carbon mobility resulting from surfactant monomer association with bonded phase, 303

chromatograms of test mixture on Apex I C-18 with mobile phases: methanol/water, 0.02 M sodium dodecyl sulfate (SDS), and 0.02 M cetyl trimethyl ammonium bromide (CTAB), 294, 296*f*

chromatograms of vanillin test mixture on cyanopropyl column before, during, and after separation involving CTAB micellar mobile phases, 311*f*

chromatograms of vanillin test mixture on cyanopropyl column before, during, and after separation involving SDS micellar mobile phases, 310*f*

chromatographic measurements, 293
 cyanopropyl bonded phase columns, 303, 305–312

differences in selectivity between C-18 and cyanopropyl bonded phase columns towards weak bases, 309

differences in selectivity between CTAB and SDS MLC on C-18, 291, 293

experimental chemicals, 293

preparation of sample for solid state nuclear magnetic resonance (NMR), 294

proposed model for SDS and CTAB adsorption on C-18, 304*f*

pulse sequences for NMR experiments, 295*f*

relaxation parameters of alpha carbon nuclei in pure and adsorbed surfactant on C-18, 300*t*

relaxation parameters of alpha carbon nuclei in pure and adsorbed surfactant on cyanopropyl, 305*t*

retention times of vanillin compounds with SDS or CTAB as mobile phases, 309, 312

role of surfactant coated stationary phase in MLC, 291, 293
 semilog decay curves for cyano group carbon before and after SDS and CTAB adsorption, 305, 308*f*, 309
 semilog decay plots for alpha carbon on solid and adsorbed CTAB on C-18, 302*f*
 semilog decay plots for alpha carbon on solid and adsorbed CTAB on cyanopropyl, 307*f*
 semilog decay plots for alpha carbon on solid and adsorbed SDS on C-18, 301*f*
 semilog decay plots for alpha carbon on solid and adsorbed SDS on cyanopropyl, 306*f*
 separation of test mixture at four different CTAB concentrations, 297, 299*f*
 separation of test mixture at four different SDS concentrations, 297, 298*f*
 separations in reversed phase liquid chromatography (RPLC), 291
 solid state NMR measurements, 293–294
 solid state NMR studying interaction of ionic surfactants with C-18 bonded phase, 297, 300–303
 unique capabilities of micellar mobile phases, 291
 unusual behavior by cyanopropyl bonded phase columns in micellar RPLC, 309
 vanillin compounds as retention probes, 291
 vanillin test mixture, 292*f*
 variable holding time experiments for SDS and CTAB on C-18, 300, 303
 variable holding time experiments for SDS and CTAB on cyanopropyl, 305
Selectivity in solute removal, ultrafiltration technology, 3–4
Semi-equilibrium dialysis

comparison to spiral wound micellar-enhanced ultrafiltration (MEUF) for chromate concentration, 172
 systems with metal ions/metal complexes, 168, 172

Separating agent, advantages of using, 1

Separations

adsorption of surfactants onto surface of mineral oxide particles, 260
See also Adsorption and aggregation of cationic surfactants on silica surfaces; Surfactant-based separations

Silica. *See* Distribution ratios of aromatic compounds between aqueous solution and surfactant covered silica

Silica surfaces

hexadecyl trimethyl ammonium bromide (HTAB) binding from aqueous dispersion, 263, 265–270
 HTAB addition to silica suspensions, 267, 269*f*, 270
 strong binding site, 270–271
See also Adsorption and aggregation of cationic surfactants on silica surfaces

Sludge

flotation tests, 254–256
 Overschie and Petrol Harbor, 250
See also Flotation of polycyclic aromatic hydrocarbon (PAH) contaminated dredged sludge

Sodium di-2-ethylhexyl

sulfosuccinate (AOT). *See* Reversed micelles as novel protein refolding media

Sodium dihexylsulfosuccinate

(Aerosol MA-80I). *See* Surfactant-enhanced aquifer remediation (SEAR)

Sodium dioctylsulfosuccinate

(Aerosol OT). *See* Crossflow microfiltration behavior of surfactants; Surfactant-enhanced

aquifer remediation (SEAR)**Sodium dodecyl sulfate (SDS)**

- chromatograms of vanillin test mixture at different SDS concentrations on C-18, 297, 298*f*
- chromatograms of vanillin test mixture on cyanopropyl column, 310*f*
- comparison of SDS concentration at different copper feed concentrations for spiral wound membrane, 168, 170*f*
- media for micellar liquid chromatography (MLC), 291, 293
- mobile phase preparation, 293
- permeate concentrations of SDS for different spiral wound membranes, 165, 168, 169*f*
- proposed mechanism for adsorption on C-18, 304*f*
- relaxation parameters of alpha carbon nuclei in pure and adsorbed surfactant on C-18, 300*t*
- relaxation parameters of alpha carbon nuclei in pure and adsorbed surfactant on cyanopropyl bonded phase, 305*t*
- solid state NMR studying interactions with cyanopropyl bonded phase, 305, 306*f*, 307*f*
- solid state nuclear magnetic resonance (NMR) studying interaction with C-18 bonded phase column, 297, 300–303
- See also* Micellar-enhanced ultrafiltration (MEUF); Selectivity in micellar liquid chromatography (MLC)
- Sodium linear alkyl (C₁₀-C₁₃) benzene sulphonate (Marlon A390). *See* Crossflow microfiltration behavior of surfactants**
- Sodium *n*-hexadecyl diphenyloxide disulfonate (Dowfax 8390). *See* Surfactant-enhanced aquifer**

remediation (SEAR)**Soil extraction, nonionic****bicontinuous microemulsion, 47–48, 50****Soil remediation**

- achieving separation, 35
- combination of techniques, 36
- existing approaches, 8–9
- surfactant-enhanced, 5–9
- thermal and biological techniques, 35–36

Soil remediation with**microemulsions**

- bicontinuous microemulsions with nonionic surfactants, 45–47
- choice of components, 39, 41
- choice of oils, 41
- choice of surfactants, 39
- determination of polychlorinated biphenyls (PCB), 44–45
- determination of phase diagrams, 43
- determination of pyrene, 44
- determination of surfactants and oils, 45
- distribution of pyrene after splitting, 44
- doping of soil with PCB, 43
- experimental materials, 41, 43
- experimental methods, 43–45
- extraction experiments with nonionic bicontinuous microemulsions, 43
- extraction result for polycyclic aromatic hydrocarbons (PAH)-contaminated fine fraction from outlet of soil washing plant, 49*f*
- extraction with anionic/nonionic bicontinuous microemulsion, 44
- extraction with oil/water (O/W) microemulsion, 44
- fundamentals, 36–41
- legend of symbols and abbreviations, 54–55
- microemulsion formulation, 45–47
- microemulsions with ionic surfactants, 39
- microemulsions with mixed nonionic

and anionic surfactants, 47, 49f
 microemulsions with mixtures of
 nonionic and ionic surfactants, 39,
 40f
 microemulsions with nonionic
 surfactants, 37
 O/W microemulsions with nonionic
 surfactants, 47
 parameters and results for liquid/liquid
 extraction of O/W microemulsion,
 53f
 phase behavior of microemulsion
 systems, 37–39
 phase prism of microemulsion system,
 38f
 pollutant separation from
 anionic/nonionic bicontinuous
 microemulsion, 53–54
 pollutant separation from nonionic
 bicontinuous microemulsion, 51
 pollutant separation from O/W
 microemulsion, 51, 53
 properties of microemulsions, 36
 pseudobinary phase diagram for
 microemulsions with C_{9/11}E₃, 46f
 pseudobinary phase diagram for two
 microemulsions with two alkyl
 polyethoxylates, 46f
 pseudobinary phase diagram of
 microemulsion with nonionic
 surfactant, 38f, 40f
 remediation processes with
 microemulsions, 41
 schematic of ex situ treatment of
 contaminated soil with bicontinuous
 microemulsion, 42f
 schematic of in situ remediation of
 contaminated soil with O/W
 microemulsion, 42f
 schematic of multi-step ex situ
 extraction with microemulsion, 52f
 separation of oil phase by
 temperature-induced splitting of
 anionic/nonionic microemulsion, 54f
 separation of pollutant, 51–54
 soil extraction, 47–48, 50

soil extraction with anionic/nonionic
 bicontinuous microemulsions, 50
 soil extraction with nonionic
 bicontinuous microemulsion, 48
 soil extraction with O/W
 microemulsion, 48
 solid/liquid separation, 51
 temperature-induced separation of
 RME and pyrene from doped
 microemulsion, 52f

Soil washing, soils with fine particle content, 36

Solid-liquid extraction

enhancing solubilization of unfolded
 proteins, 377
 promising technique for refolding
 proteins, 375

See also Reversed micelles as novel
 protein refolding media

Solid/liquid separation, soil treatment, 51

Solid state nuclear magnetic resonance (NMR)

ascertaining mechanism for surfactant
 incorporation into alkyl or polar
 bonded phase columns, 294
 measurements, 293–294
 pulse sequences for NMR
 experiments, 295f

See also Selectivity in micellar liquid
 chromatography (MLC)

Solubilization

differences from adsolubilization, 315
 mechanism for remediating non-
 aqueous phase liquid (NAPL)
 contaminated aquifers, 6–8
See also Vesicular solubilization

Solubilization equilibrium constant (K)

definition, 204
 dependence of K on intravesicular
 mole fraction of aromatic solute in
 didodecyl dimethyl ammonium
 bromide (DDAB) vesicles, 208f
 dependence of normalized K on
 temperature, 211f

equation for calculation, 206
 parameters in equation for K, 218*t*
 relationship between K at infinite dilution and temperature, 210*f*
 solute concentration dependence of K's, 206
 temperature dependence of K's at infinite dilution, 209
 vesicle diameter dependence of K's, 216–220

See also Vesicle-enhanced ultrafiltration (VEUF)

Solvent extraction, advantages and drawbacks of micellar extraction in comparison, 152, 154

Solvent leaks, environmental remediation, 5

Solvent removal, selectivity, ultrafiltration technology, 3–4

Solvent-water partition coefficient, definition, 77

Speciation of metal-containing compounds

calculated values for micelle-solute equilibrium constants, 287*t*
 capacity factor (*k'*) definition, 283
 effect of added organic modifier on metal-containing compound interaction with micelles, 283, 285
 effect of analyte charge versus hydrophobicity on partitioning behavior, 288
 effect of surfactant concentration on metal-containing compounds interaction with micelles, 283
 element selective detection with inductively coupled plasma mass spectrometry (ICPMS), 278
 interaction of metal-containing compounds with micelles, 281, 283, 285
 partitioning behavior of metal-containing compounds with micelles, 285, 287–288
 properties of metal and metalloid containing compounds and

surfactants, 277–278
 quantitative equilibrium interactions, 285
 safety considerations, 288
 sample preparation of arsenic containing compounds, 280*f*
 separation of
 arsenic compounds in nutrient broth matrix after growth of bacterial strain *alcaligenes faecalis*, 280*f*
 arsenic containing compounds in bacterial growth medium, 279
 inorganic and alkyl mercury compounds, 282*f*
 inorganic and organic mercury compounds, 279
 mono- and tri-methyl tin compounds, 284*f*
 organo-tin compounds, 281
 tri-alkyl tin compounds, 282*f*
 variation of capacity factor with ammonium dodecyl sulfate concentration, 284*f*
 variation of *k'* with 2-propanol concentration in mobile phase, 285, 286*f*

Spiral wound ultrafiltration
 comparison between stirred cell and spiral wound membrane flux results, 162, 165, 166*f*, 167*f*
 comparison of permeate concentrations for different molecular weight cutoff (MWCO) membranes, 165, 167*f*, 168, 169*f*
 comparison of stirred cell and spiral wound permeate concentrations for organic solute, 165
 comparison to semi-equilibrium dialysis chromate concentration, 172
 comparison to stirred cell copper concentration, 168, 171*f*
 experimental materials, 160
 experimental methods, 160
 fluxes and permeate concentrations for spiral wound membranes, 162, 163*f*, 164*f*

illustration of major components of spiral wound membrane, 163*f*
 pilot plant with spiral wound membrane, 161*f*
 separating nonionic organic solute using anionic or cationic surfactants, 162
 spiral wound/semi-equilibrium dialysis systems with metal ions/metal complexes, 168, 172
 unit, 4

See also Micellar-enhanced ultrafiltration (MEUF)

Squalane

properties, 83*f*
 solvent in liquid-liquid extraction study, 82

Steam stripping, water remediation, 92

Stirred cell

comparison of flux for spiral wound and, 165, 166*f*
 comparison of spiral wound and stirred cell permeate copper concentration, 168, 171*f*
 comparison with spiral wound permeate concentrations for organic solutes, 165, 166*f*, 167*f*

See also Spiral wound ultrafiltration

Sulfosuccinate surfactant mixtures

Aerosol MA (sodium dihexyl sulfosuccinate) and Aerosol OT (sodium dioctyl sulfosuccinate), 17
 dense non-aqueous phase liquid, perchloroethylene (PCE), 16–17
 effect of Ca^{2+} and isopropyl alcohol cosolvent on optimum salinity and solubilization ratio, 18, 21
 experimental parameters for 8 wt% MA/OT with PCE at 25°C, 21*f*
 research description, 17
 solubilization parameter as function of mass fraction of Aerosol OT, 18, 19*f*
 surfactant structures, 18*f*
 volume fraction diagram for Aerosol MA/OT mixture with PCE at 25°C, 18, 20*f*

See also Surfactant-enhanced aquifer remediation (SEAR)

Surfactant aggregates, use in ultrafiltration, 4

Surfactant-based separations

adsorption, fractionation, and flotation based processes, 9–11
 advantages of using separating agent, 1
 extraction and deinking processes, 11–12
 soil and aquifer remediation, 5–9
 status of progress, 1–12
 ultrafiltration, 2–5

Surfactant-enhanced aquifer remediation (SEAR)

Aerosol MA-80I (sodium dihexyl sulfosuccinate) studies, 30, 32
 comparison of viscosity measurements for selected surfactant systems, 31*f*
 concept of integrated SEAR, 24
 criteria and factors influencing surfactant selection, 25–26
 effect of Aerosol OT-100 (sodium dioctyl sulfosuccinate) on perchloroethylene (PCE) solubilization by Aerosol MA-80I, 29*f*
 efficient surfactant recovery and reuse, 58
 experimental procedure, 28
 incorporating subsurface remediation and surfactant recycle processes, 24
 increasing aqueous solubilities of dense non-aqueous phase liquids (DNAPL), 24
 necessity of robust surfactant system, 32
 new propoxylated sulfate surfactant results, 32
 PCE solubilization versus salinity for 80/20 system, 30, 31*f*
 pervaporation and micellar-enhanced ultrafiltration (MEUF), 24–25
 preparation of surfactant solutions, 28
 removing chlorinated hydrocarbons, 17

summary of phase behavior studies, 29*t*

surfactant descriptions, 26, 27*t*

surfactant screening, phase behavior studies, 26–30

technology moving towards commercialization, 33

Surfactant enhanced subsurface remediation, expediting pump-and-treat process in groundwater remediation, 76

Surfactant regeneration, ultrafiltration technology, 3

Surfactant spray cleaning
proposed mechanism, 356

See also Oxygen systems; Particulate removal from oxygen systems

Surfactants

ability to form well-ordered molecular aggregates and structures, 176

choice for treatment of contaminated soils, 39

determination, 45

ink particle size distribution after pulping in presence of deinking surfactants, 409*t*

phase behavior of surfactant/water system, 196

phase diagrams, 178–179

promising in ex situ decontamination of soils, 8

properties, 78–79

removal for recycling, 176

role of cationic, in capillary electrophoresis separations, 339

steady state filtration characteristics, 196–197

See also Crossflow microfiltration behavior of surfactants; Deinking papers with water-based inks

Synperonics

amphiphilic poly(ethylene oxide)–poly(propylene oxide)–poly(ethylene oxide) (PEO–PPO–PEO) type, 93

See also Block copolymer micelles for water remediation

T

Tetrachloroethylene (PCE), contaminant in liquid-liquid extraction study, 81, 82*t*

Tin compound separation

mono- and tri-methyl tin compounds, 284*f*

organo-tin compounds, 281

tri-alkyl tin compounds, 282*f*

See also Speciation of metal-containing compounds

Transient permeate flux. *See* Crossflow microfiltration behavior of surfactants

Transient rejection. *See* Crossflow microfiltration behavior of surfactants

U

Ultrafiltration

concentrating surfactant prior to reinjection, 8

device design considerations, 4–5

monomer leakage, 2–3

options for downstream treatment, 3

removing and recovering solute species, 158

selectivity in solute removal, 3–4

surfactant regeneration, 3

use of surfactant aggregates other than micelles, 4

See also Enantioselective micelles in ultrafiltration systems; Micellar-enhanced ultrafiltration (MEUF); Vesicle-enhanced ultrafiltration

Ultrasound

cleaning oxygen lines, 368–371

glass slide study, 365–371

ultrasonication of glass slides, 365–367

See also Particulate removal from oxygen systems

Uniquac Functional Group Activity Coefficients (UNIFAC)

model for solubilization properties of
PEO-PPO block copolymer, 95
prediction versus experimental, 99

V

Vanillin compounds

retention probes for micellar liquid
chromatography study, 291, 293
structures and names, 292*f*
See also Selectivity in micellar liquid
chromatography (MLC)

Vapor-liquid partitioning, effect of temperature and surfactant concentration, 64, 66*f*, 68

Variance-covariance matrix, estimated parameters, 131

Vesicle-enhanced ultrafiltration (VEUF)

changes in diameter of didodecyl
dimethyl ammonium bromide
(DDAB) aggregates with
ultrasonication time, 203*f*
changes with temperature in
excimer/monomer ratio of emission
intensities of pyrene in DDAB
vesicles, 213*f*

changes with temperature in
fluorescence polarization degree (P)
of 8-anilino-1-naphthalene-sulfonate
ammonium salt (ANS), 213*f*

comparison of solubilizing ability of
DDAB vesicles with other
surfactant micelles, 222

dependence of K (solubilization
equilibrium constant) on
intravesicular mole fraction of
aromatic solute in DDAB vesicles,
208*f*

dependence of K's for benzoic acid
and phenol in DDAB vesicles on
intravesicular solute mole fraction,
217*f*

dependence of K's for 3-
phenylpropionic acid (HCA) and 2-
phenylethanol (PEA) in DDAB

vesicles on intravesicular solute
mole fraction, 219*f*

dependence of normalized K on
temperature, 211*f*

dependence of normalized K's on
dissociation degree of Br⁻ for
benzoic acid and phenol, 215*f*

effect of β -cyclodextrin in internal
aqueous phase on vesicular
solubilization, 222–226

effect of DDAB head group charge on
solubilization, 212, 216

effect of fluidity of DDAB vesicle
bilayer membrane on solubilization,
209, 212

effect of vesicular hydration layer on
solubilization, 220–222

glucose trapping efficiency of 10.0
mM DDAB vesicles, 205*f*

K as function of solute mole fraction
of benzoic acid in DDAB vesicles
containing β -cyclodextrin, 225*f*

K as function of solute mole fraction
of HCA in DDAB vesicles
containing β -cyclodextrin, 224*f*

parameters for K equation, 218*f*
preparation of DDAB vesicles, 202,
204

relationship between DDAB vesicle
diameter and time, 207*f*

relationship between degree of
dissociation of counter-ion Br⁻ from
DDAB vesicles and temperature,
214*f*

relationship between K at infinite
dilution and temperature, 210*f*

relationship between P of fluorescence
from ANS in DDAB vesicles and
total solute concentration for
benzoic acid and HCA, 221*f*

solubilization equilibrium constant, K,
204, 206

solute concentration dependence of K,
206

stability of DDAB vesicles, 204

temperature dependence of K's at
infinite dilution, 209

temperature dependence of vesicular solubilization, 206, 209, 212, 216
 values of K 's at infinite dilution for PEA in different vesicles and micelles, 223 f
 vesicle diameter dependence of K 's, 216–220
 vesicle diameter dependence of vesicular solubilization, 216–220

Vesicles

affecting kinetics of complex formation, 149, 152
 curved bilayer membranes, 201
 reducing mobility of solubilized extractant, 152, 153 f
 surfactant aggregates, 4, 9
 surfactant-based colloidal particles and investigated parameter, 140, 142 f
 use as substitute for micelles, 201–202

Vesicular solubilization

comparing solubilizing ability of didodecyl dimethyl ammonium bromide (DDAB) vesicles with other surfactant micelles, 222
 effect of β -cyclodextrin in internal aqueous phase on, 222–226
 effect of DDAB heat group charge, 212, 216
 effect of fluidity of DDAB vesicle bilayer membrane on, 209, 212
 effect of vesicular hydration layer, 220–222
 temperature dependence of, 206, 209, 212, 216
 vesicle diameter dependence of, 216–220

See also Solubilization

Volatile organic compound separation from surfactants by pervaporation

application of pervaporation to surfactant solutions, 60–61
 background, 58–61

calculation of extracellular fraction of volatile organic compound (VOC), 68
 comparison of predicted to observed pervaporation performance, 71–72
 current uses of pervaporation, 60
 effect of temperature and surfactant concentration on vapor-liquid partitioning of 1,1,1-trichloroethane (TCA), 66 f
 extracellular fraction of TCA as function of temperature and surfactant concentration, 69 f
 extracellular fraction of VOC varies with nature of VOC and surfactant concentration, 70 f
 headspace method for determining Henry's law constants, 64, 68
 impact of surfactant on traditional pervaporation mass transport model, 68, 71
 impact of surfactants on removal of VOCs, 63–72
 magnitude of impact of surfactant on Henry's constant varied with type of VOC, 67 f
 motivation, 57–58
 performance of Environmental Protection Agency's National Risk Management Research Laboratory (EPA-NRMRL) pervaporation pilot unit, 62 f
 pervaporation theory, 61, 63
 pictorial representation of partitioning of VOC between surfactant micelles and extracellular region, 65 f
 qualitative illustration of effect of surfactants on VOC concentration in liquid boundary layer and at membrane surface, 73 f
 schematic diagram of proposed integrated field demonstration of surfactant remediation and recovery/reuse, 62 f

schematic of pervaporation cell and system, 62*f*

W

Wash deinking

deinking flexographic newsprint, 398–400

See also Deinking papers with water-based inks

Wastewater remediation

analysis of equilibrium dialysis experiments, 115–116

binding isotherms of F127 and *p*-cresol and corresponding hydrodynamic diameters for F127/*p*-cresol complexes, 116, 117*f*, 118

determining remediation efficiency of F127, 119

equilibrium dialysis experiments, 115

foulant *p*-cresol and Pluronic F127 samples, 115, 121

idealized remediation cycle for stimuli-responsive polymeric surfactant, 114

instrumentation, 115

normalized flux as function of time for ultrafiltration experiment, 120, 121*f*

rejection rates as function of concentration of cresol and F127, and temperature, 119*t*

rejection ratio and F127 concentration as function of time for ultrafiltration experiment, 119, 120*f*

Scatchard plot for F127/*p*-cresol system at 5°C, 118*f*

shear forces experienced by retentate within membrane lumen, 119

ultrafiltration experiments, 116

Water-based gravure inks

behavior in deinking processes, 396

See also Deinking papers with water-based inks

Water remediation

biotreatment, 92

liquid-liquid extraction, 92–93

steam or air stripping, 92

See also Block copolymer micelles for water remediation

Winsor Type I, oil-in-water, 17

Winsor Type II, water-in-oil, 17

Winsor Type III, middle phase microemulsions, 17

Winsor Type III microemulsion

flotation process, 9–10

success of mobilization process, 7

Z

Zirconia membranes. *See* Crossflow microfiltration behavior of surfactants